AD-A089 050 ADVISORY GROUP FOR AEROSPACE RESEARCH AND DEVELOPMENT--ETC F/G 14/2
CRYOGENIC WIND TUNNELS.(U)
JUL 80
UNCLASSIFIED AGARD-LS-111 NL

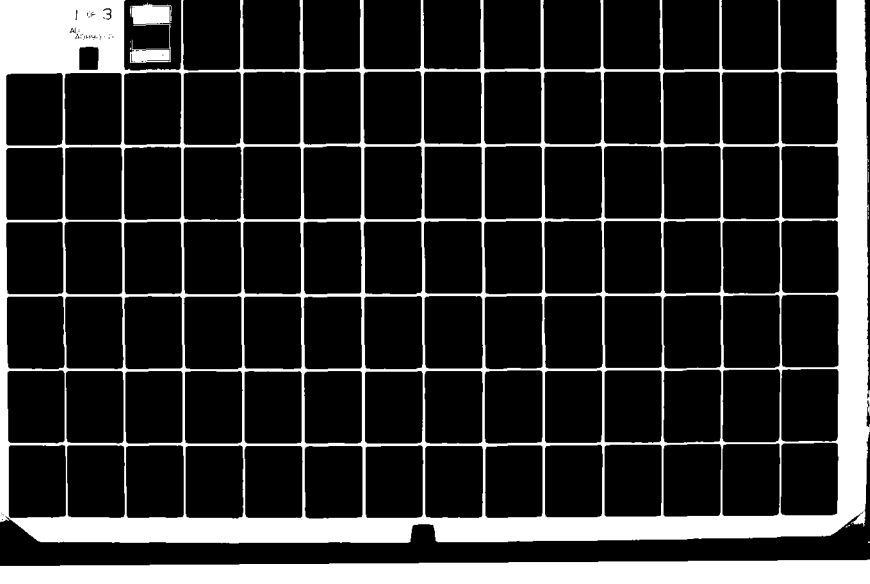

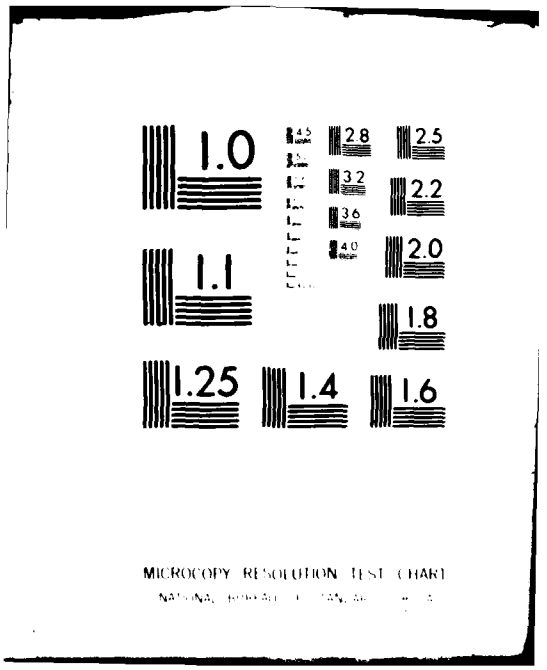
1.0
1.1
1.25
1.4
1.6
2.8
3.2
3.6
4.0
2.5
2.2
2.0
1.8
MICROCOPY RESOLUTION TEST CHART

LEVEL II

AGARD-LS-111

AGARD-LS-111

AGARD

ADVISORY GROUP FOR AEROSPACE RESEARCH & DEVELOPMENT

7 RUE ANCELLE 92200 NEUILLY SUR SEINE FRANCE

AGARD LECTURE SERIES No. 111

Cryogenic Wind Tunnels

NORTH ATLANTIC TREATY ORGANIZATION

DISTRIBUTION AND AVAILABILITY ON BACK COVER

NORTH ATLANTIC TREATY ORGANIZATION

ADVISORY GROUP FOR AEROSPACE RESEARCH AND DEVELOPMENT

(ORGANISATION DU TRAITE DE L'ATLANTIQUE NORD)

AGARD Lecture Series No.111

(6) CRYOGENIC WIND TUNNELS

The material in this publication was assembled to support a Lecture Series under the sponsorship of the Fluid Dynamics Panel, the Consultant and Exchange Programme of AGARD and the von Kármán Institute for Fluid Dynamics presented on: 19–23 May 1980 at the von Kármán Institute, Rhode-Saint-Genèse, Belgium and 27–30 May 1980 at NASA Langley Research Center, Virginia, USA.

THE MISSION OF AGARD

The mission of AGARD is to bring together the leading personalities of the NATO nations in the fields of science and technology relating to aerospace for the following purposes:

- Exchanging of scientific and technical information;
- Continuously stimulating advances in the aerospace sciences relevant to strengthening the common defence posture;
- Improving the co-operation among member nations in aerospace research and development;
- Providing scientific and technical advice and assistance to the North Atlantic Military Committee in the field of aerospace research and development;
- Rendering scientific and technical assistance, as requested, to other NATO bodies and to member nations in connection with research and development problems in the aerospace field;
- Providing assistance to member nations for the purpose of increasing their scientific and technical potential;
- Recommending effective ways for the member nations to use their research and development capabilities for the common benefit of the NATO community.

The highest authority within AGARD is the National Delegates Board consisting of officially appointed senior representatives from each member nation. The mission of AGARD is carried out through the Panels which are composed of experts appointed by the National Delegates, the Consultant and Exchange Programme and the Aerospace Applications Studies Programme. The results of AGARD work are reported to the member nations and the NATO Authorities through the AGARD series of publications of which this is one.

Participation in AGARD activities is by invitation only and is normally limited to citizens of the NATO nations.

Published July 1980

ISBN 92-835-1360-6

Printed by Technical Editing and Reproduction Ltd
Harford House, 7–9 Charlotte St, London, W1P 1HD

PREFACE

For aeronautical research the advantages of the cryogenic wind tunnel lie mainly in the practical attainment of full scale values of Reynolds number, and in the case of pressurised cryogenic tunnels the means to separate Mach and Reynolds number effects from aeroelastic effects.

This Lecture Series is designed for engineers, including those experienced with conventional wind tunnels, wishing to acquire in a concentrated form the principles and practice of cryogenic wind tunnels. The emphasis is on the unfamiliar facets of technology which must be applied, and on solutions to special problems which arise from the exploitation of a low temperature test gas. The Lectures provide up-to-date information on the aerodynamic and mechanical design of continuous and intermittent cryogenic wind tunnels and their models, and on techniques for controlling test parameters. Design information includes properties of materials, the storage and handling of cryogenic liquids, insulation systems for pipelines and tunnel circuits, and safety requirements. Solutions are included for the special requirements of instrumentation systems for plant, tunnel and model. The physical processes are described which determine the lower limits of operating temperature.

This Lecture Series is sponsored by the Fluid Dynamics Panel of AGARD and implemented by the von Kármán Institute.

M.J.GOODYER
Lecture Series Director

LIST OF SPEAKERS

Lecture Series Director: Dr M.J.Goodyer
Department of Aeronautics and Astronautics
The University of Southampton
Southampton SO9 5NH
Hampshire
UK

Mr J.D.Cadwell
Wind Tunnel Test and Development
Aerodynamics Subdivision
Douglas Aircraft Company
Mail Code 36–81
3855 Lakewood Boulevard
Long Beach, California 90846
USA

Dr R.M.Hall
Fluid Dynamics Branch
Subsonic-Transonic Aerodynamics Division
Mail Stop 287
NASA Langley Research Centre
Hampton, Virginia 23665
USA

Mr J.P.Hartzuiker
Technical Group
European Transonic Windtunnel – ETU
c/o National Aerospace Laboratory – NLR
Anthony Fokkerweg 2
1059 CM Amsterdam
The Netherlands

Mr W.B.Igoe
NASA Langley Research Center
Hampton, Virginia 23665
USA

Dr R.A.Kilgore
Fluid Dynamics Branch
Subsonic-Transonic Aerodynamics Division
Mail Stop 287
NASA Langley Research Center
Hampton, Virginia 23665
USA

Mr R.Michel
Aerothermodynamics Department
ONERA-CERT
2, Avenue Edouard Belin
B.P. No.4025
31055 Toulouse Cedex
France

Dr R.G.Scurlock
Institute of Cryogenics
The University of Southampton
Southampton SO9 5NH
Hampshire
UK

Dr D.A.Wigley
Department of Mechanical Engineering
The University of Southampton
Southampton SO9 5NH
Hampshire
UK

CONTENTS

THE PRINCIPLES AND APPLICATIONS OF CRYOGENIC WIND TUNNELS

by
M.J. GOODYER
Senior Lecturer
Department of Aeronautics and Astronautics
UNIVERSITY OF SOUTHAMPTON
Southampton SO9 5NH
England

SUMMARY

A description of the background to the emergence of the cryogenic wind tunnel leads to discussions of its advantages compared with other means for raising the values of test Reynolds number to full scale. An introduction to the basic aero- and thermodynamics of wind tunnel testing allows quantification of the advantages of low temperature in low speed and in transonic testing. Attention is drawn to secondary advantages unique to this tunnel, and to the potentials of unconventional test gases. Descriptions are included of current types and applications of cryogenic wind tunnels.

LIST OF SYMBOLS

ℓ	Size
M	Mach number
m	mean molecular weight
P	static pressure
R	Reynolds number
r_0	universal gas constant
T	static temperature
V	reference test velocity
γ	ratio of specific heats
μ	viscosity (dynamic, or coefficient of)
ρ	density

1. INTRODUCTION

The cryogenic wind tunnel has been under active development for only about eight years, but as a result of fairly intense and rewarding work on the part of the engineers involved, coupled with bold decision-making, large cryogenic wind tunnels are now emerging with more in the planning stage. Consequently, many more people are beginning to be involved with them in various capacities such as designers of tunnels and systems, or with experiments in the tunnels. This Lecture Series has been prepared with the aim of helping such people by concentrating on areas of new or unfamiliar technology. Lectures will cover:

basics of relevant aerothermodynamics;
aspects of cryogenic engineering and safety which are generally unfamiliar;
real gas effects, because these can determine suitable operating temperatures and gases;
current technology for tunnel control, model design, instrumentation;
descriptions of major cryogenic wind tunnel projects.

A bibliography is included as a convenient source of reference material.

Before dwelling on specific aspects of this type of tunnel a few background observations may be useful. The cryogenic wind tunnel was conceived at least 61 years ago as a means for, among other things, raising the Reynolds number of model tests. The 53-year gestation period is explained several ways. Dominating the earlier years would have been the difficulty of designing the large scale cryogenic plant. Later, during the 1940's when the bulk production of cryogenic liquids was common and the cryogenic tunnel feasible, aerodynamicists and wind tunnel engineers were preoccupied with the major problems of transonic and supersonic flight, and were content to address these problems in mostly conventional tunnels but at sub-full-scale values of Reynolds numbers. Throughout this period there will have been the inhibiting effect of a reluctance on the part of tunnel users to face whatever complication is implied by testing at low temperature.

A series of minor and major aerodynamic-based problems with several transonic aircraft projects, traced to disparity in Reynolds number, contributed in the 1960's to efforts on both sides of the Atlantic to begin the process of re-equipping with better wind tunnels. Proposals first centred on larger and more highly pressurised versions of conventional designs, but the high construction costs were still allowed to force the targeted Reynolds numbers to values below full scale, clearly an uneasy compromise. The cryogenic wind tunnel emerged in this environment, offering massive reductions of capital costs and therefore removing the need for compromise. Transonic aircraft aerodynamics were therefore a powerful stimulant to the development of the cryogenic wind tunnel, but the concept is now finding a broader application, including low speed aerodynamics.

While it is easily shown that cryogenic testing in tunnels of conventional size can eliminate disparity in Reynolds number as a source of discrepancy between model and full scale behaviour, we must not fall into the trap of assuming that from hereon all model data will be correct. Remaining are the many other potential sources of discrepancy: the effects of turbulence and noise, wall and model support interferences, model aeroelasticity, to identify just a few. We must, of course, continue with efforts to

improve the designs of tests and wind tunnels to reduce or eliminate these other sources of imperfection.

2. BASIC AEROTHERMODYNAMICS

2.1 Transonic testing

The influence of the properties of an ideal gas on test Reynolds number R can be seen by substituting the equation of state

$$\rho = \frac{Pm}{r_o T}$$

into the familiar expression for Reynolds number

$$R = \frac{\rho V \ell}{\mu}$$

giving

$$R = \frac{PmV\ell}{r_o \mu T} \qquad .. \qquad .. \qquad .. \qquad (1)$$

where P and T are static pressure and temperature respectively, m is the mean molecular weight of the gas, V its velocity and μ its viscosity at T. ℓ is the length scale and r_o the universal gas constant. For transonic testing the flow Mach number M is more significant than velocity. On substituting

$$V = M\sqrt{\frac{\gamma r_o T}{m}}$$

into (1) we get

$$R = \frac{PM\ell}{\mu}\sqrt{\frac{\gamma m}{r_o T}} \qquad .. \qquad .. \qquad .. \qquad (2)$$

where γ is the ratio of specific heats.

In the transonic testing of aircraft models we cannot use a gas with $\gamma \neq 1.4$ without introducing the unease of another compromise. Likewise the test must be at the correct Mach number, and therefore the only reasonable options for increasing Reynolds number are:

1. Choose a heavy diatomic gas, alternatively gas mixtures which together give $\gamma = 1.4$ and a high mean molecular weight.

2. Raise scale, hence ℓ.

3. Raise pressure.

4. Reduce temperature. The effect of reduced temperature is not only that due to the direct influence indicated by its appearance in equation (2) but also indirectly by its influence on viscosity. The viscosities of gases fall with falling temperature.

Some perspective on the nature of the problem facing the aeronautical testing community is required: the largest conventional wind tunnels are able to reach about one-tenth of the full-scale Reynolds number of a cruising transonic transport. The required factor in Reynolds number is therefore at least 10, depending on trends in the sizes of future aircraft.

The above options for increasing Reynolds number may be considered for use separately or in combination. Option 1 was investigated by Chapman[1] with the conclusions that the rewards from available mixtures were marginal. Options 2 and 3 were considered in combination for the large wind tunnel proposals of the 1960's. Capital costs increase particularly strongly with size, partly because of the influence of the cost of providing the tunnel drive power. It can be argued that drive power varies as $P\ell^2$, indicating the likelihood of a disproportionate increase in power with Reynolds number. Pressurised, intermittent wind tunnels were therefore also considered in order to reduce the investment in power. Such were the demands of economics that some proposed tunnels had very short run-times.

It was apparent that very few such facilities could ever be built, and inevitably there was a hesitation in deciding just which of the competing designs should be chosen. At this point in time (actually 1971) the fourth option, that of testing at low temperature, came under scrutiny at NASA Langley Research Center.

Figure 1 shows the influence of test temperature on Reynolds number. Two alternative diatomic gases are compared with air: nitrogen N_2 because it is relatively safe, inexpensive, and doubles as a convenient coolant; hydrogen H_2 because at the low temperatures available with this gas there are larger benefits in Reynolds number which should be weighed against any disadvantages.

The curve for nitrogen follows closely that for air at varying temperature. The maximum increase in Reynolds number in N_2 relative to conventional testing in air is a factor of about 6.5 at atmospheric pressure, where the test gas is at the saturation boundary. As the disparity in Reynolds number between conventional pressure tunnels and fullscale flight is a larger factor, most transonic cryogenic tunnel projects combine the benefits of low temperature with the practical limits of pressurisation. Secondary advantages can follow, as noted below. The minimum useable temperature increases with pressure and therefore the factor on Reynolds number due to reduced temperature is not

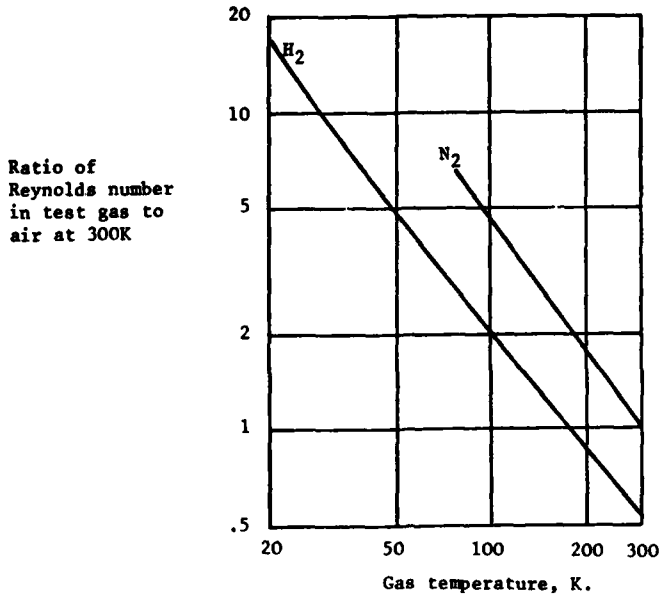

FIGURE 1. The influence of test gas and temperature on unit Reynolds number relative to air at 300K. Mach number and pressure are constant.

generally above about 5.

A change of test gas to hydrogen begins to show an advantage over conventional tunnels when the cryogenic hydrogen tunnel is cooled below about 180K, and advantages over the cryogenic nitrogen tunnel at temperatures below about 40K. At the available minimum temperature of about 20.3K the Reynolds number in H_2 is high enough to remove a need for pressurisation in some full scale testing. Naturally the implications of safety require consideration, as do real gas effects. Hydrogen could be used in a tunnel in either of two forms, parahydrogen or normal hydrogen. Theoretical studies of real gas effects for parahydrogen indicate the probability of unacceptable deviations of its behaviour at low temperature from that of air. An experimental verification, also a coverage of normal hydrogen, are required before this gas can be considered for use at transonic speeds.

In raising this issue early in the Lecture Series I aim to show that, as might be expected, the cryogenic tunnel in many ways is still in its infancy. While many engineering and aerodynamic options seem still to be open, teams involved with transonic cryogenic wind tunnels are for the time being concentrating on overcoming the problems of tunnel and model design, controls and instrumentation for use down to liquid air temperatures in tunnels which exhibit the minimum of unconventionality. Most probably this represents a fair compromise: there are advantages enough with this approach without the increased risk of technical failure which might be associated with more radical alternatives.

The tunnel drive powers required in transonic testing are high. Smelt discussed[2] the likelihood of drive power economy in low temperature testing. In comparisons between cryogenic nitrogen tunnels and conventional tunnels Kilgore[3] went further to show an overall economy in power even accounting for refrigeration. This may be regarded as a secondary advantage of the cryogenic tunnel, but is an example of the pleasant surprises that have emerged from time to time during the past eight years.

2.2 Low speed testing

The unit Reynolds number required in low speed testing to reach full scale depends among other things on the size of model. For economy reasons there is usually a requirement for the model to be small, but in aircraft testing there are manufacturing considerations limiting the minimum size. While there are many opinions on this minimum, a span of around 1m is taken here as representative. Full scale aircraft currently range in span up to about 70m; future designs might well be larger and therefore since model testing will include the evaluation of high lift devices the required unit Reynolds number in the tunnel is higher by about two orders of magnitude compared with a conventional atmospheric tunnel. There are parallels in the field of industrial aerodynamics particularly related to civil engineering which indicate the need for similar levels of unit Reynolds number.

In low speed testing several of the constraints may be lifted which apply at transonic speeds. A wide variety of gases may be considered; Mach number may be allowed to vary up to a level dictated by the onset of compressibility effects; the option is open of testing in a liquid.

An examination of the physical properties of liquids quickly leads to the conclusion that unless a very high dynamic pressure can be withstood by the model there is no argument based on Reynolds number for the use of a liquid test medium. Therefore we turn again to a consideration of gases - equation (1) applies. The achievement in a normal temperature tunnel, whatever its test gas, of up to two orders of

magnitude increase of unit Reynolds number is prohibitive in terms of cost or aerodynamic loads if tunnel size or pressure are raised. The situation is quite different, however, when operating temperature is reduced.

In the type of low speed testing where Mach number can be allowed to vary there is no point in adopting a constraint in Mach number when examining the effects of temperature. In some tunnels a more significant constraint will be fan speed. If temperature is reduced in such a low speed tunnel of fixed size and the test velocity V is assumed proportional to fan speed and is therefore limited to some maximum value, equation (1) simplifies to

$$R \propto \frac{1}{T\mu}$$

revealing a particularly powerful influence of temperature on Reynolds number in these circumstances. Figure 2 shows the ratio of the unit Reynolds number at test temperature T to unit Reynolds number at 300K with the same fan speed and gas.

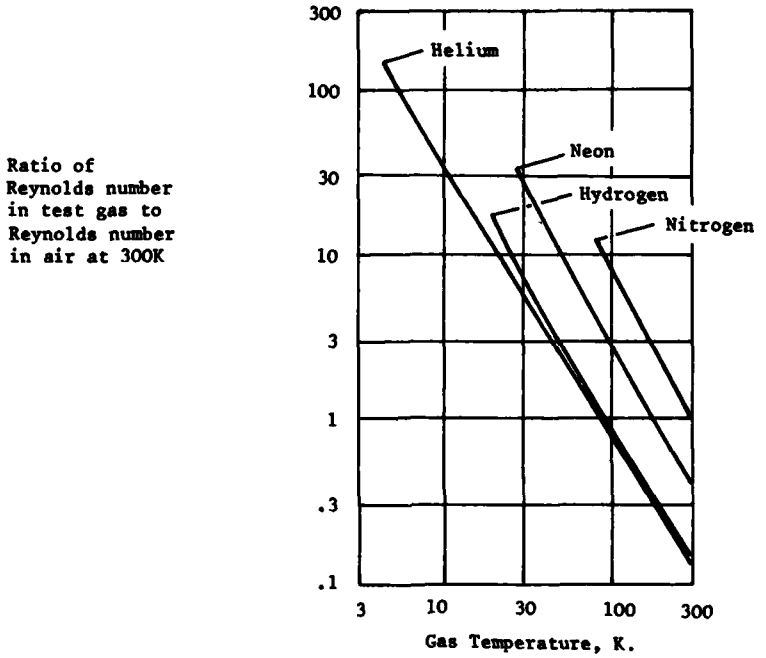

FIGURE 2. Low speed testing at constant fan speed. Effect of temperature and choice of gas on unit Reynolds number.

Of the gases considered, helium immediately appears the most attractive if the lowest temperatures can be employed, showing a Reynolds number increase of over 1,200 compared with normal temperature. Room temperature helium will develop a Reynolds number only just over 12% of that of air (at equal speed, etc.) mostly because of differences in density, but nevertheless the remaining factor of 150 between helium near its saturation boundary and air at 300K makes it a most attractive gas for use in low speed testing.

Changes of Mach number cannot always be ignored even at low speeds, notably with aircraft models. For example, it can be argued that Mach number should not be considered as a variable in tests on transport aircraft high lift devices: any increase over the take-off or approach values could lead to the appearance of compressibility effects, while a decrease is of no interest because of the need for high Reynolds number. In helium at its minimum temperature of 4.3K the flow Mach number is about 2.85 times higher than the Mach number in air at 300K and the same speed. Therefore in comparing Reynolds number in the cryogenic helium tunnel with normal temperature air, with equal Mach number flows the cryogenic helium tunnel promises a factor of 55 in unit Reynolds number over air at the same pressure. A cryogenic helium tunnel for a 1m span model can therefore provide full scale Reynolds number for present and future transports when operated in the one to two atmospheres pressure range. The same tunnel would also provide full scale Reynolds number flows over large civil engineering structures.

This discussion has highlighted the potential of helium, but the known low speed tunnels in fact use nitrogen as a test gas where the advantages in terms of Reynolds number, while more modest, are still useful. The curve on Figure 2 for Nitrogen shows that the cryogenic nitrogen tunnel will develop about 12 times the Reynolds number of normal temperature air at the same speed; at equal Mach numbers the factor reduces to about 6.5. Hydrogen or neon are other potential test gases for use at low temperatures. Their properties are compared with nitrogen and helium below:

Test Gas	Nitrogen	Neon	Hydrogen	Helium
R in gas at min. temperature / R in air at 300K				
at equal speeds	12.6	30.6	17.5	158
at equal Mach numbers	6.5	12	17.2	55
Minimum temperature, K	77.3	27	20.3	4.3

While this table shows the general tendency for rewards in terms of increased Reynolds number to increase with reduction of temperature, the choice of test gas will be influenced by variations in complexity and cost, not all of which are presently evaluated.

3. TYPES AND APPLICATIONS OF CRYOGENIC TUNNELS

The types of tunnel drive and test gas currently exploited in cryogenic wind tunnels include:

Drive	Test Gas
fan	nitrogen
induced flow	air/nitrogen mix
blowdown	air/nitrogen mix
blowdown	nitrogen
expansion tube	nitrogen

The usual refrigerant is evaporating liquid nitrogen except in the case of the expansion tube which is an intermittent tunnel drive which produces low temperature by the near-adiabatic expansion of the test gas. Other types of tunnel drives will undoubtedly be adopted.

Applications of cryogenic tunnels are varied. The smallest size, about 1cm across the test section, finds use in experimental studies of real gas effects and in the pilot evaluation of tunnel designs. Tunnels of order 10cm size of test section are used in pilot schemes but also for the development of instrumentation for larger tunnels. As an illustration, at my home institution, Southampton University, we have a 10cm low speed fan driven cryogenic nitrogen tunnel which has been used for:

development of a surface flow visualisation technique for cryogenic wind tunnels;
evaluation of a six component magnetic suspension system and force balance at cryogenic temperatures;
development of thin-film gauges for the detection of boundary layer transition on models in cryogenic tunnels

which serves to illustrate the usefulness of quite small tunnels, especially in these early, active years of the cryogenic wind tunnel. There is emerging also a need for a small cryogenic wind tunnel, perhaps of about the same size, for teaching purposes, to train tunnel operators in the art and science of tunnel control and management, and to expose young aerodynamicists to the versatility and potentials of the new wind tunnel technology.

The test section size band from about 0.3m to 3m covers the current range of wind tunnels offering near or full scale Reynolds numbers. In many cases these tunnels have been or are being constructed to satisfy the needs of transonic testing. Later in this Lecture Series we will hear descriptions of the main projects and therefore my remarks are confined to generalities. While their drives differ, the larger tunnels have certain common features, including the use of air and/or nitrogen as the test gas which restricts minimum operating temperature to around 80K to 120K depending on Mach number and pressure. To reach high Reynolds numbers they are designed to run at pressures up to several atmospheres.

Aircraft aerodynamicists are mainly concerned with the effects of Reynolds number and Mach number on performance. While conventional pressure tunnels can vary these numbers independently, there is a simultaneous variation of dynamic pressure which has its own influence on data through aeroelastic distortion of the model. The cryogenic pressure tunnel with its extra independent variable of temperature has the advantage that it can allow Reynolds and Mach number investigations at constant dynamic pressure and therefore nominally at constant load and distortion.

Adding to the attraction of testing at low temperature is an advantage in the dynamic testing of models. A common requirement is to match in the model tests some full-scale frequency parameter which varies inversely with gas velocity. The low gas velocities associated with low temperature testing allow a proportionate reduction in frequency of model motion, with consequent simplification in the construction of the model and its support.

Lastly, I will mention an unusual application of the cryogenic wind tunnel. This is to convective modelling at low speeds to obtain not only high levels of Reynolds number but also high levels of Grashof number. While Reynolds number increases by a factor of around 12 in nitrogen as temperature is reduced to the minimum, the maximum value of Grashof number rises by a factor of about 200! This, and the features described in the preceding two paragraphs, are good examples of the ways in which advantages of cryogenic testing have emerged additional to that originally envisaged, the increase of Reynolds number.

It is now my pleasure to hand over lecturing to the team of senior engineers which I have been most

fortunate in persuading to take part. These men have for many years been in the forefront of the development of the various facets of technology which have combined to create the cryogenic wind tunnel. That they have found time to prepare comprehensive lecture material in parallel with heavy professional duties makes me especially grateful. On your behalf I extend sincere thanks.

4. REFERENCES

1. Chapman, D.R. Some possibilities of using gas mixtures other than air in aerodynamic research. NACA TR-1259, 1956.

2. Smelt, R. Power economy in high speed wind tunnel by choice of working fluid and temperature. Report Aero 2081, Aug. 1945, Royal Aircraft Establishment, Farnborough, England.

3. Kilgore, R.A. The cryogenic wind tunnel for high Reynolds number testing. Ph.D. Thesis, Feb. 1974, University of Southampton, England.

CRYOGENIC ENGINEERING I

by Dr. R.G. Scurlock, Institute of Cryogenics, University of Southampton, U.K.

Abstract Basic properties of LIN, LOX and liquid air. Control of heat fluxes, insulation techniques and low loss storage.

1.1. Introduction

The purpose of this lecture is to introduce the concept of a liquid boiling under 1 atm pressure at a temperature which is well below the lowest naturally occurring temperatures (i.e. below -50°C or 223K) and below the region normally associated with refrigeration engineering.

Cryogenic wind tunnels require the use of cryogenic liquids, such as liquid nitrogen, in quantities ranging from 10 - 100 tonnes. These are relatively large quantities and are very much larger than those normally met with in cryogenic laboratories but smaller than commercial scales which range from 1000 to 100,000 tonnes. Care is therefore needed in extrapolating designs and operating techniques from those developed for handling laboratory-size quantities of a few litres or kilograms. The scale of use also means that safety precautions and safe operating procedures have to be rigorously maintained; much more so than with laboratory size quantities.

Cryogenic liquids are energy-intensive to produce and therefore expensive to use. Good housekeeping is therefore needed to make the maximum use of the available "cold." Ice or snow-covered patches on insulation, and white plumes of boil-off vapour, are specific indications of poor housekeeping techniques.

Apart from these considerations, cryogenic liquids are very easy to use and the technology for storage, for transport by road, rail or sea (or air), and for handling is well developed. A basic understanding of their differences from ambient temperature fluids like water and air will enable cryogenic liquids to be used with confidence.

1.2. Properties of Cryogenic Fluids

1.2(a) General

To obtain an overall picture, consider the main cryogenic fluids and some of their properties at their normal boiling points (under 1 atm pressure) in Table 1.

TABLE 1

The major cryogenic fluids and their boiling point properties

	T_M K	$T_{B.P.}$ K	T_C K	P_C atm	Density ρ_L kg m^{-3}	Latent heat of vaporisation kJ kg^{-1}	Expansion ratio vol. gas/vol. liqu. (at 15°C, 1 atm)
Helium		4.2	5.2	2.26	125	21.7	700
Hydrogen	16	20.3	33.3	12.8	71	450	789
Neon	24.6	27.1	44.5	26.9	1210	82.9	1340
Nitrogen	63.2	77.4	126	33.5	808	124	666
Air		Bubble pt 78.8 Dew pt 81.8	132	37.2	878	206	724
Argon	84.0	87.3	151	48.0	1400	158	784
Oxygen	54.8	90.2	155	50.1	1140	213	777
Methane	90.6	112	191	45.8	425	512	607
Ethane	89.9	185	305	48.2	550		401
Ethylene	104	169	283	50.9	568	486	476
Carbondioxide	195 (sublimation point)	195	304	72.9	-	-	-
Water	273	373	647	219	1000	2257	1800

Helium, hydrogen and neon are included for comparison purposes, but will no longer be considered. The main three of interest are oxygen, air and nitrogen in descending order of temperature. While their densities are close to that of water, their latent heats of vaporisation are considerably smaller. In all cases, the expansion ratio of gas produced from a given volume of liquid is about 700.

1.2 (b) Liquid Oxygen or LOX B.P. 90.2K

LOX has a density of 1.14 relative to water and has a latent heat of vaporisation almost twice that of liquid nitrogen. It is a bright blue liquid with strong paramagnetic properties. It is the most powerful oxidant known, and the particular hazards of handling LOX arise very largely from this fact. Substances, which do not burn in air, may burn fiercely or explosively in an oxygen rich atmosphere. Examples include plastics and synthetic polymers in solid, foam, woven or sheet form, lubricating oils and metal powders.

DO NOT think that the low temperature will prevent combustion, since the heats of combustion are at least 10 times the heat of vaporisation.

REMEMBER the standard test for oxygen compatibility is to drop a weight on to a test sample of the substance IMMERSED IN LOX.

DO APPRECIATE that oxygen-rich atmospheres will be a hazard with cryogenic wind-tunnels. (See below).

1.2 (c) Liquid Air Bubble-pt 78.8K Dew-pt 81.8K.

Liquid air, or more accurately condensed air, is a mixture of nitrogen and oxygen with a small percentage of argon. The mixture behaves like any other mixture in that the equilibrium composition of the vapour is higher in the low boiling point constituent (nitrogen) than the liquid.

As a direct result, the liquid will generally have an enhanced oxygen content. Moreover, as the liquid evaporates, (via a nitrogen rich vapour) the oxygen composition of the remaining liquid will rise continuously (Figure 1.) Thus the continual partial condensation and partial evaporation of liquid air collecting in an enclosure will produce an oxygen hazard.

Figure 1

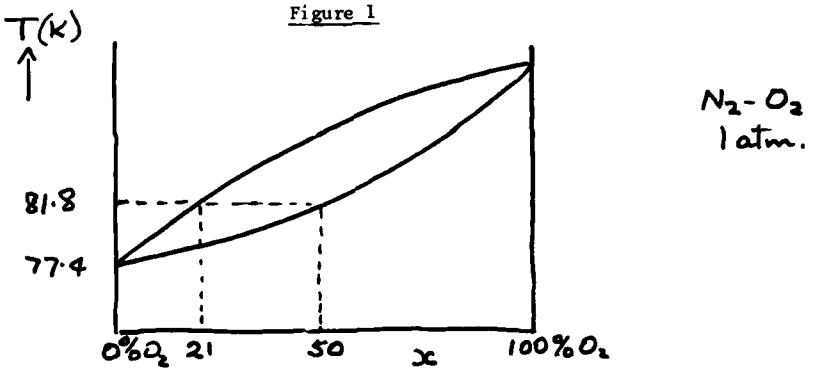

The condition for this to occur is the exposure of atmospheric air to a surface cooled to 81.8K or below by liquid nitrogen in a variety of conditions, including (i) the saturated liquid at pressures up to 2.2 atm absolute (ii) the sub-cooled or under-cooled liquid at higher pressures, and (iii) the exhaust liquid vapour or 2 phase mixture after throttle expansion from a temperature above 81.8K. The occurrence of air condensation can be checked visually, when access is possible. An uninsulated surface above 81.8K and in contact with atmospheric air is covered in frost. Below 81.8K the surface appears wet and the condensed liquid removes the frost.

If condensation of air is expected, an air-tight vapour barrier must be included in the insulation.

THE INADVERTENT PRODUCTION OF OXYGEN RICH LIQUID AIR is a hazard commonly met in the use of liquid nitrogen.

1.2 (d) Liquid Nitrogen or LIN B.P. 77.4K

LIN has a density of 0.808 relative to water and is a colourless mobile liquid with a low viscosity and low surface tension. The variation of some of the basic properties of the saturated liquid with temperature and pressure are given in Table 2.

TABLE 2

Properties of saturated liquid nitrogen

T K	Pressure atm	Density Kg m^{-3}	Viscosity μ Pa s.	Latent heat of vaporisation kJ kg^{-1}
70.0	0.38	837	220	208
77.4	1.00	808	160	199
80.0	1.34	792	140	195
90.0	3.55	746	110	180
100.0	7.70	691	80	162
110.0	14.52	621	60	135
120.0	24.81	526	-	94
126.0	33.3	311	- critical point	-

The density variation with temperature and pressure is very high. As a result, when LIN is pressurised by self-heating in a closed volume, the level of the liquid surface RISES. The liquid level is therefore not a good indicator of liquid quantity when the pressure is varying.

The viscosity of LIN is about twice that for water at 20°C. Frictional pipe losses are therefore relatively small and thermal effects leading to two-phase flow are much more important in the transfer of liquid nitrogen.

The surface tension of LIN is about 8 dyne cm^{-1} at 77.4K and decreases with increasing temperature to zero at 126K (the critical point).

While the latent heat of vaporisation at 1 atm is 199 kJ kg^{-1}, the sensible heat of the vapour between boiling point and ambient temperature is 231 kJ kg^{-1}. In other words, the "cold" contained in the vapour is approximately the same as the latent heat of the liquid.

Apart from oxygen and argon, which are completely miscible in liquid nitrogen, other gases with much higher boiling points can dissolve in LIN at significant levels. In particular, there are two which could be a nuisance in cryogenic wind-tunnels because they might not evaporate below 150K. They are CO_2 and water, which are believed to dissolve in LIN at levels up to 10 ppm.

1.2 (e) Production of liquid nitrogen

The composition of dry atmospheric air is:-

Constituent	% by volume	% by weight
Nitrogen	78.084	75.521
Oxygen	20.946	23.139
Argon	0.934	1.288
Carbon Dioxide	0.033	0.050
Rare gases	**ppm by volume**	**ppm by weight**
Neon	18.18	12.67
Helium	5.24	0.724
Krypton	1.14	0.295
Hydrogen	0.50	0.035

Air also contains variable quantities of:

Water vapour (up to 2.5% at 20°C)
Hydrocarbons including acetylene
Dust
Oil mist

The Cryogenic Separation of air into its constituents at high purity is achieved in the following steps:

1. The air is compressed in large multi-stage compressors with inter-stage water coolers.

2. The water and carbon dioxide are removed.

3. The dry compressed air is cooled by heat exchange with the outgoing gaseous products of nitrogen and oxygen.

4. The cold air is further cooled by expansion either isentropically through a turbine or piston expander, or isenthalpically through a throttle or Joule Thomson valve.

5. The cold mixture of saturated vapour and liquid air passes into a distillation column where separation takes place by fractional distillation.

6. The cold gaseous products are returned through heat exchangers to cool the incoming high pressure air. Not more than 10% of the products can be taken off in liquid form as LIN, LOX and liquid argon.

The cryogenic plant in which this separation process is achieved is called an Air Separation Unit or ASU. Liquid nitrogen purity levels of 99.999% are common.

If more liquid products are required, then additional liquefiers are added to the ASU. In all cases, the ASU is relatively inflexible and produces liquid products at a constant rate. The power costs to make liquid nitrogen are approximately 1 kW hr per kg of liquid and equal about 50% of the total production cost at the site of an ASU.

The problem with a large user like a cryogenic wind tunnel using an average of 20 tonnes/day is the need for 1MW of installed liquefier capacity to meet a single user's requirement.

There appear to be 3 alternatives for achieving a reliable cheap supply:

1. Tie in with a single producer planning additional liquid nitrogen making ASU capacity within easy reach by road or rail.

2. Persuade a producer to build a LIN making ASU adjacent to the tunnel - standard practice on a larger scale with industrial users.

3. Build a small ASU and LIN liquefier specifically for the tunnel.

Since the LIN market is expanding generally, alternatives 1 or 2 would be preferable. DO NOT EXPECT producers to be able to sell tonnage quantities of liquid nitrogen without adequate planning. In addition, do plan for ADEQUATE bulk storage of LIN, say to meet at least 7 days of variable demand by cryogenic wind-tunnel users.

1.3 Storage and Insulation techniques

1.3 (a) General criteria

Insulation is essential for the economical storage of cryogenic liquids. Correct insulation techniques can save a great deal of time and money.

Heat influxes through the insulation result in boil-off losses by evaporation at the liquid/vapour interface. Under equilibrium conditions, the boil-off is constant. However, non-equilibrium conditions, including those of cooldown, subcooling, superheating and stratification, may introduce non-steady boil-off.

Additional mechanical constraints apply to mobile containers, road and rail tankers etc. When partially filled, sloshing and surging present mechanical and thermal problems.

Since the production of cryogenic liquids is energy-intensive, poor storage and bad-handling techniques waste energy - an increasingly expensive exercise. Waste can be reduced in many ways by applying a little understanding, and not necessarily by the use of expensive capital investment.

1.3 (b) Sources of heat flux into storage containers

It is important to distinguish between heat fluxes through (A) the wetted and (B) the unwetted walls of the container. Heat fluxes (A) are absorbed by the latent heat of the liquid and lead to evaporation. Heat fluxes (B) may be absorbed by the sensible heat ΔH of the cold vapour. With good design, the latter may not contribute to the evaporation.

For LOX and LIN $\Delta H \simeq L_V$ where $\Delta H = \int_{bp}^{300} C_p \, dT$

A1 Conduction into liquid: Through insulation in space between inner and outer containers. Via mechanical supports of inner container, and pipework.

A2 Radiation into Liquid: Through insulation space and vapour space over liquid. Also along pipework. Vapours and liquids are transparent to infra-red radiation, and absorption takes places at solid surfaces.

A3 Convection into Liquid: Through insulation space when voids and large cells present. Although there is stratification in the vapour space, there is strong reverse flow in the centre of vapour columns carrying heat to the liquid surface.

B1 Conduction to unwetted walls: Through insulation space surrounding wall, and along wall material itself. Conduction in vapour is negligible.

B2 Radiation to unwetted walls: Same as A2.

B3 Convection to unwetted walls-Vapour Cooling: Strong natural convection boundary layer flow of vapour up the walls from the liquid ensures good cooling of the walls. This vapour-cooling effect is a bonus since it acts so as to reduce other heat fluxes.

Other sources can arise from thermally induced oscillations under both storage and transfer conditions.

1.3 (c) Reduction and control of heat fluxes

It is important to reduce all heat fluxes to the same order of magnitude. It is important to recognise that variation with scale is different for the various sources. Snow or ice on the outside of a cryogenic system is always an indication of poor insulation.

A1 Conduction: Reduced by use of correct type and thickness of insulation in the insulation space.

In general the one-dimensional heat conduction equation is:

$$Q = kA \frac{dT}{dx}$$

where the thermal conductivity k is a function of temperature k (T). The heat flow between temperatures T_1 and T_2 is then:

$$Q = \frac{A}{L} \int_{T_1}^{T_2} K dT$$

For standard conditions of temperature across the insulation, 300-77K, 300-20K etc., an effective mean thermal conductivity $\bar{k}$ can be defined using the above heat conduction equation by:

$$Q = \frac{A (T_1 - T_2)\bar{k}}{L}$$

$\bar{k}$ is then a measured value and contains ALL the contributions to the heat transfer through the insulation, solid conduction, gas conduction, radiation and so on.

A1 (a) Gas purged insulations at 1 atm: Table 3 gives a selection.

TABLE 3

Effective thermal conductivities between 300 and 77K

Material	Effective thermal conductivity with 1 atm nitrogen purge gas $Wm^{-1} K^{-1}$	Effective thermal conductivity evacuated $Wm^{-1} K^{-1}$	Oxygen Compatible
Expanded Perlite	$2.6 - 4.4 \times 10^{-2}$	0.95×10^{-3}	Yes
Silica Aerogel	1.9×10^{-2}	1.6×10^{-3}	Yes
Fibre glass	2.5×10^{-2}	1.7×10^{-3}	Yes
Foam Glass	5.2×10^{-2}		Yes
Balsa wood	4.9×10^{-2}		No
Expanded Polystyrene	2.4×10^{-2}		No
Polyurethane Foam	2.5×10^{-2}		No
Mineral Wool	$3.0 - 4.3 \times 10^{-2}$		Yes

The basic idea of gas-purged insulations is to reduce gas convection by the creation of small gas cells within a matrix of low conductivity solid fibres or foam walls. The lower limit is then determined by the thermal conductivity of the purge gas. For example, the conductivity of nitrogen at 1 atm is

$$1.0 \times 10^{-2} \text{ W m}^{-1} \text{ K}^{-1} \text{ at 100 K}$$

$$\text{rising to} \quad 2.5 \times 10^{-2} \text{ W m}^{-1} \text{ K}^{-1} \text{ at 300 K.}$$

Gas purging is necessary to avoid (1) the ingress of moisture and formation of ice-bridges as thermal shunts; (2) the condensation of O_2 rich liquid air from contact by atmospheric air with surfaces below 81.8K.

Gas purged insulations are used in cold boxes on ASU's and large static storage tanks greater than 3 m diameter. The use of vapour barriers and no purging is NOT ADEQUATE for commercial cryogenic insulations.

For a tank holding 1000 tons of LIN (diameter 13 m) with 0.2 m of Perlite, the heat flux is 16 kW, equivalent to a boil-off of 7 tonnes per day or 0.7%/day.

For a tank of 1.3 m radius holding 1 tonne, with the same thickness of Perlite, the boil-off will be 7.0%/day, which is not economical.

A1 (b) Evacuated powder insulations: By reducing the gas pressure to 0.1 Torr, the thermal conductivity of powder insulations may be reduced by a factor of 10 or more (see Table 3). The gas conduction has been removed. However, a penalty must be paid since the outer casing must now be vacuum tight and strong enough to withstand a collapsing pressure differential of 1 atm. Geometry is limited to cylinders, spheres and combinations for mechanical strength, and size is limited to about 3 m diameter. Thus for the above 1 tonne tank of 1.3 m radius, the boil-off with evacuated powder insulation will be 0.7%/day which is acceptable. Such tanks are used as customer storage tanks, and on road and rail tankers.

A1 (c) Evacuated multi-layer insulations (MLI or Superinsulation): The major heat flow through an evacuated insulation is radiation. For n thermally floating reflecting surfaces with emissivity ε the radiation heat transfer between parallel surfaces at temperatures T_1 and T_2 is given by:

$$\frac{Q}{A} = \frac{\varepsilon\sigma}{2(n+1)} (T_1^4 - T_2^4)$$

where $\sigma = 5.67\ 10^{-8}$ $Wm^{-2}K^{-4}$.

For standard conditions of temperature across the insulation, 293-77K, an effective mean thermal conductivity $\bar{K}$ can again be defined using the standard conductivity equation:

$$\frac{Q}{A} = \frac{\bar{K} (T_1 - T_2)}{t}$$

where t is the thickness of the insulation, NOT necessarily the width of the insulation space.

$$\text{Then } \bar{K} = \frac{\varepsilon\sigma (T_1^4 - T_2^4)\, t}{2 (n+1)(T_1 - T_2)} \quad \text{W m}^{-1} \text{ K}^{-1}$$

Inserting some figures, with $T_1 = 293$ K, $T_2 = 77$K, $\varepsilon = 0.02$ (as for aluminium) and $(n + 1)/t = 3000$ reflectors per metre,

$$\bar{K} = 6.5\ 10^{-6} \text{ W m}^{-1} \text{ K}^{-1}.$$

In practice, of course, there are other contributions to the heat flow via solid conduction etc. and the effective mean thermal conductivity can be expected to be higher. However, this simple calculation shows there is a lower limit to the effective conductivity of reflective insulants in the region of

$$10^{-5} \text{ W m}^{-1} \text{ K}^{-1}$$

which is 100 times lower than evacuated powders.

There are two ways of reducing radiative heat flow:

(1) by adding Al powder to powder insulants - opacified powders - which produce a reduction of 2 - 3 in conductivity;

(2) by abandoning the use of powders and using reflective sheets of Al foil or aluminised Mylar separated by insulating sheets of nylon net, fibre glass paper etc. with evacuation to 10^{-4} Torr in Multi-layer insulation or Superinsulation. Table 4 gives some typical values of mean thermal conductivity between 293 and 77 K.

TABLE 4

Multilayer insulations or Superinsulations

Type	Layers per cm	K 10^{-4} W m^{-1} K^{-1}
12 μ aluminium + 0.5 μ Fibre glass paper	31	0.34
12 μ aluminium + 12 μ Dexter paper	20	0.52
Aluminized Mylar film 12μ + 12 μ Dexter paper	9	2.0
Aluminium foil + 15μ nylon net	24	2.3
Linde SI4 Al foil + glass fibre paper	16-32	0.42
NRC2 Crinkled aluminized Mylar film 6μ	20	0.28
Southampton test 8.7μ Al foil + carbon loaded fibre glass paper	30	0.07-0.15
Aluminized Mylar film 12 μ + carbon loaded paper	30	0.26

It can be seen that at least 10 fold reduction in $\tilde{K}$ below that caused by evacuated powders can be achieved. More development is required in wrapping techniques etc. to achieve the lowest values of conductivity under commercial conditions. MLI can be used in small portable dewars and vessels up to 3 m diameter, and on transfer lines.

A2 Radiation:

Major source is radiation into liquid from warm upper parts of container, governed by:

$$\frac{Q}{A} = \frac{\epsilon_1 \epsilon_2}{\epsilon_2 + (1-\epsilon_2)\epsilon_1} \sigma \left(T_2^4 - T_1^4\right)$$

For 300K, the radiation peak is at 10 μ wavelength in the infra-red, and Q is 500 W m^{-2} for $\epsilon_1 = \epsilon_2 = 1$. Radiation heat fluxes are reduced by using vapour-cooled reflective radiation shields, or suspended decks in large tanks. Floating plastic ball blankets are also effective.

A3 Convection:

In general, density stratification acts so as to oppose vertical natural convection. In the absence of any heat flux, convection stability applies to both liquid and vapour. However, local heating changes the picture in a complex manner which we are only just beginning to understand. Convection in a cryogenic situation has many features common to convection in the atmosphere, and the latter is exceedingly complex.

Basically, local heating with upward convective flow at one point induces downward flow elsewhere in which the downward mass flux is related to the upward mass flux by the continuity equation:

Downward Mass Flux = Upward Mass Flux - Boil off mass flux.

Alternatively, there is a recirculating mass flux in addition to the boil-off. Studies show that the recirculation can greatly exceed the boil-off.

The downward mass flux may be distributed leading to small velocities, or localised with high local velocities. In both cases the downward mass flow will carry heat. In a tank of cryogenic liquid, two convective actions take place via heat flux through the tank walls:

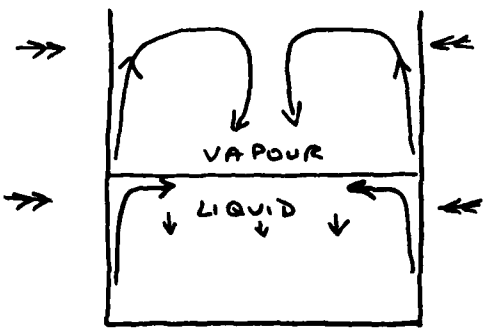

Figure 2

(1) In the vapour, there is intense boundary layer flow at the wall inducing reverse flow in the centre. The heat flux associated with this reverse flow is not understood.

(2) In the liquid, the heat flux through the wall is insufficient to produce local boiling. Heat is absorbed by a convective boundary layer flow to the surface, where evaporation from a superheated layer takes place.

B1 Conduction to Unwetted Walls:

Reduction through insulation space, in the same way as for A1. Low conductivity wall materials are required - stainless and Ni steels. Conduction down walls is reduced by natural vapour cooling effect, see B3.

B2 Radiation to Unwetted Walls:

Reduced by vapour-cooled reflective shields. To reduce "funneling" of radiation into liquid, walls should have high emissivity, i.e. black where they are adequately vapour cooled.

B3 Convection to unwetted Walls:

At any level in the ullage (vapour) space, the wall is always hotter than the vapour and injects heat into the vapour. The resulting natural convection boundary layer cools the wall and absorbs heat being conducted down the wall into the liquid. If the boil-off mass flux in the boundary layer is high enough, then all the heat in the wall is absorbed by the sensible heat of the vapour. No heat enters the liquid when the wall temperature gradient at the liquid surface is zero.

$$\text{i.e.} \qquad \left(\frac{\partial T}{\partial z}\right) \text{ liquid surface} = 0.$$

This condition can be met in practice by correct design. The boundary layer flow is quite different to that at ambient temperatures where the thickness δ varies as $\delta \sim z^{1/4}$. In the vertical temperature gradient pertaining to the cryogenic situation near the liquid surface

$$\delta \sim z$$

owing to rapid property variation with height. Consequently, the boundary layer is much thicker, up to 1 cm. This applies to the "developed stable stratified" region above a thin mixing region in contact with the liquid surface. In the upper part of the ullage space, the convective flow becomes unstable with internal oscillations, and the boundary layer becomes progressively thinner. This region is called the "unstable stratified" region.

The details of this convective flow have yet to be studied.

1.3(d) Storage Instabilities exhibited by boiling cryogenic liquids

(1) Irregular surface evaporation: This appears to be the normal mode of "boil-off". No boiling as such takes place, and the mass flux through the surface varies by $\pm$ 20-40% of the mean evaporation rate.

(2) Superheating and vapour explosions: After long periods of storage without disturbance, by transfers etc., it appears that surface evaporation can diminish, and a highly superheated surface layer is generated. Superheats of 40°K are required before homogeneous nucleation and explosive boiling are expected. This can occur in practice, or be reproduced in the laboratory. The pressure rises are considerable. Fortunately, cases reported appear to be limited to laboratory size containers.

(3) Rollover: In multi-component liquids, like LNG, evaporation of the volatile component occurs preferentially. The liquid remaining has a higher denisity, and in the absence of complete mixing, it is possible for the upper portion to become more dense than the lower portion. When this happens, the tank contents roll-over. The release of hydrostatic pressure head on the lower portion rising to the top creates "flashing" and a large quantity of vapour is released. On a small scale, a 5% flash can be controlled. On a large tank of 20,000 tons of liquid, the sudden evolution of 5% as vapour could be a disaster. Rollover is avoided by continuous mechanical mixing of tank contents.

(4) Assymetric thermosyphon: The convective recirculation described above has axial symmetry. If an off-axis symmetry is introduced, by for example tilting through a small angle of 10°, the recirculating mass flux can increase considerably. The heat flux into the liquid surface is increased, thereby increasing the boil-off and the possibility of the superheating effect.

(5) Narrow vertical channels: The boiling of cryogenic liquids in long vertical channels is particularly prone to oscillation. The oscillations invariably increase the boil-off.

1.3(e) Low Conductivity Supports

All storage vessels require mechanical supports for the inner insulated container in contact with the wetted portion. It is unusual for the insulation to have sufficient compressive strength to be load bearing.

If the tensile or compression strength of a material is σ and the required load is F, then the necessary cross-sectional area is $A = F/\sigma$. The heat conducted by the support of length L and mean conductivity $\bar{k}$ is

$$Q = \frac{\bar{k} A}{L} \Delta T = \frac{\bar{k}}{\sigma} \cdot \frac{F \Delta T}{L}$$

For Q to be as small as practicable, the value of $\frac{\bar{k}}{\sigma}$ should be as small as possible. Defining a figure of merit $m = \frac{\sigma}{\bar{k}}$, then for a good support material m should be as large as possible.

Table 5 shows comparative values which illustrate how the highest values of m are obtained with non-metals.

TABLE 5

Material	Ultimate tensile strength mega N/m^2	Yield stress mega N/m^2	Thermal conductivity $Wm^{-1}K^{-1}$	Figure of Merit
Metals				
Copper annealed		82.7	475	0.104
Brass	412		100	1.65
Aluminium 2024		379	81.3	2.80
Aluminium 7075	606	482	86.5	3.35
Stainless steel (annealed)		251	10.2	14.8
Titanium	825	586	15.8	22.1
35 Ni-50 Fe - 14 Cr Alloy	702		12.6	22.3
K Monel	up to 1,380	689	17.1	24.2
Hastelloy B		448	9.35	28.7
Stainless steel drawn wire		1,030	8.8	70.3
Titanium Alloy (4% Al - 4% Mn)		1,000	5.87	102
Inorganics				
Fibreglass	1,720		0.92	750
68% Fibreglass 32% Resin	378		0.36	420
Organics				
Nylon high tenacity	606	138	0.245	247
Terylene (high tenacity Polyester)	730	138	0.15	487
Fortisan 36	1,070		0.20	535
Araldite 6060	830		0.17	490

Notes: The figure of merit is calculated as follows:

$$m = \left(\frac{\text{Design stress in mega } N/m^2}{\text{Thermal conductivity in } W/m\,^{\circ}K} \right).$$

The Design stress is taken as 60% of yield stress or 40% of ultimate tensile strength for metals and inorganics, and 10% of ultimate tensile strength for organic materials.

Unfortunately, these high m materials may suffer from undesirable qualities such as brittleness at low temperatures, thermal contraction and jointing problems. Stainless and nickel steels are used in large plant, GRP is finding increasing use in road tankers and small vessels.

There are various geometrical tricks for achieving long conduction paths with adequate mechanical rigidity. Re-entrant supports and diagonally braced wires and struts are widely used.

In small containers and dewars the neck tube is the main support, and "bump-stops" are used to prevent excessive movement under handling conditions.

CRYOGENIC ENGINEERING II

by Dr. R.G. Scurlock, Institute of Cryogenics, University of Southampton, U.K.

Abstract

Thermal properties of commercial materials; Instrumentation, including thermometry pressure and flow; Avoidance of 2-phase flow conditions.

2.1 Some thermal properties of commercial materials

Table 1 gives a summary of three thermal properties for a wide range of commercial materials which are used in cryogenic plant.

The thermal conductivity values refer to ambient (293K) conditions.

The working figure of merit is calculated as the ratio of design stress to thermal conductivity, where the design stress is defined at the end of the previous lecture.

Fractional linear contractions are given at two temperatures, 80 and 150K respectively.

Important points to note are:

1. Different metals have differing linear contractions which are not negligible.
2. There is a large difference in contraction between metals and polymers.
3. Glass-reinforced plastic is now being widely used as a load-bearing "heat-break" material. Its linear contraction can be controlled by varying the filler/resin ratio.

Table 1

Material	$Wm^{-1}K^{-1}$ at 293K	Working figure of merit	Linear contraction $L/L_{293} \times 10^4$ T = 80K	150K
Copper	475	0.10	30.3	22.1
Brass	100	1.65	35.0	25.3
Aluminium 2024	81.3	2.80	39.0	29.4
7075	86.5	3.35	39.0	29.4
Stainless Steel	10.2	14.8	27.8	20.3
0.2% Carbon Steel	-	-	19.1	14.7
Invar	-	-	4.8	3.0
Titanium Alloy 4% Al. 4% Mn.	3.87	102	14.2	10.7
Constantan	23	-	24.7	18.3
Fibreglass	0.92	750	-	-
68% Fibreglass 32% Resin	0.36	420	20	15
Araldite 6060	0.17	490	94	71
Stycast 1850 GT	-	-	38	-
Nylon	0.24	247	125	95
Terylene	0.15	487	-	-
Polystyrene	0.04	-	131	93
Polyurethane foam	0.04	-	-	-
Teflon	-	-	193	160
Concrete	3.0	-	12-16	9-13

2.2 Instrumentation at Low Temperatures

The operation of any cryogenic plant entails the measurement and control of temperature, pressure, differential pressure, flow, level and composition. The design of the plant, and especially that of the cold box, must allow for the provision of suitable instrumentation. The signals obtained by the sensors have to be transmitted through the lagging via a suitable transducer to some kind of recording and control system. The inaccessibility of some of these sensors, the cyclic performance of the plant (including thermal and pressure cycling), the provision of projecting components, such as thermowells, add to design problems partly due to the increased probability of damage, and partly due to the increased thermal leakage. There exists also the complication of flashing liquids due to sudden pressure drop at liquid expansion valves and orifice plates.

2.3 Measurement of Temperature

2.3(a) General Points

Thermometers are generally required for (1) monitoring purposes when a precision of $\pm$ 5K may be adequate; and (2) accurate measurement when a precision of $\pm$ 0.1K or better is specified or required. The cost and operational problems of high precision thermometers is obviously considerably greater than those of monitors. The user has to decide at an early stage what precision is needed, and how many temperature measuring points are necessary for controlling the plant. Retrofitting of thermometers is expensive, and may be impossible, so it is wiser to request more than the required minimum at the design stage.

The sensor measures its own temperature. Hence it is important - indeed vitally important - to establish thermal equilibrium with its surroundings via good thermal contact.

There are two types of temperature scale: (1) empirical and (2) thermodynamic. The thermodynamic scale is visualised by a set of Carnot cycles (not very practicable) and is realised via the behaviour of an ideal gas. Hence the constant volume gas thermometer forms the primary instrument.

Gas thermometers are clumsy, slow and of relatively low accuracy and reproducibility. They are only suitable for fixed point determination. The defining fixed points, important in cryogenics above 50K are:-

Triple point of oxygen	54.361 K	
Boiling point of oxygen	90.188 K	
Triple point of water	273.160 K	(0.01°C)
Boiling point of water	373.150 K	(100°C)

2.3(b) The International Practical Temperature Scale (IPTS)

The low reproducibility of gas thermometers and the difficulty of using them, as well as the need for an international standard, led to the introduction of IPTS in 1927, with major revisions in 1948 and 1968.

IPTS is based on the thermodynamic temperature, T , the unit of which is the kelvin K; it is 1/273.16 of the thermodynamic temperature of the triple point of water. The Celsius temperature $t\,^{o}C$, is defined by $t = T - T_o$ where $T_o = 273.15$ K (ice point). Temperature differences are expressed either in K or in ^{o}C. (Normally, but not necessarily, K is used for temperatures below the ice point and ^{o}C above the ice point; this avoids negative values.)

IPTS - 68 was chosen such that the measured temperatures (T_{68} or t_{68}) closely approximate the thermodynamic ones within the limits of accuracy. Realisation of IPTS is made by means of specified standard instruments. For the cryogenic range, the standard instrument is the platinum resistance thermometer (13.81K to 630.74°C (freezing point of antimony)). It is relatively easy to use, and the reproducibility of this instrument is better than that of a gas thermometer.

Any other practical instrument is then calibrated against the standard, to an accuracy depending on precision required.

Among the wide variety of practical instruments in use, four types are of practical value in cryogenics. They are resistance thermometers, thermocouples, vapour pressure thermometers, and gas thermometers respectively.

2.3(c) Platinum resistance theremometers

This is the IPTS standard instrument, and is being increasingly widely used commercially for precision thermometry.

For industrial use, the sensor is a Pt-wire coil contained in one end of a stainless steel sheath of 5-8 mm. diam. and 75-250 mm. length. (Sometimes the sheath may be dispensed with. Instead of the coil the sensor may be a thin film of Pt mounted on a substrate.) For specification see BS 1904 (1964), DIN 43760 (1968) or ISO/ANSI equivalents. These standards are really out of date; they were drawn up before the introduction of IPTS-68, at a time when high purity platinum was not yet available. Standards will very likely be modified, but until this happens one works to existing specifications.

The definition of IPTS-68 is based on a resistance thermometer made of a high-purity Pt-coil (large temperature coefficient of resistance). The relation between R and t is given by empirical relations for the various ranges of temperature. There is no reason why these relations, truncated to meet the more modest needs of industrial thermometry, could not be used to define the industrial standards of IPTS-68.

The sensing element is a coil of wire of Pt of given resistance with 2, 3 or 4 leads depending on the use of the instrument (precision and associated circuitry).

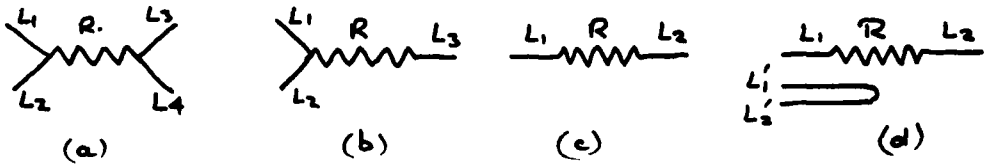

(a) For very high precision, influence of lead resistances L_1 to L_4 may be eliminated, or reduced to negligible proportions. Use a.c. or d.c. bridges, potentiometer, DVM with constant current supply, recorder. Also used industrially when R is small (either small coil or made of thick wire) where lead influence must be reduced anyway. The resistance measuring system or 'transmitter' is mounted close to the sensor, and may be used to convert temperature to an analogue current (e.g. 4-20 mA , d.c.); this technique avoids long runs of expensive thermometer leads.

(b) Precise, but hardly used nowadays. Operation only with special bridge (Mueller).

(c) If R is high (e.g. 500 Ω), the lead resistance can be neglected, and R can be determined in a simple bridge circuit. Not very precise.

(d) Use of separate compensating leads. Leads and compensating leads are inserted in opposite arms of a Wheatstone bridge in 1:1 ratio (Callendar-Griffiths bridge). Less accurate than (a).

Leads can be 100 m., or more, in length.

Sensing element requires current. There is then a self-heating i^2R effect. The larger i, the greater the sensitivity, but the larger is self-heating effect and the larger the temperature rise of sensor w.r.t. its surroundings. Usually one uses 1-2 mA depending on type. The larger current also gives a better signal/noise ratio.

TABLE 2

Tolerances of industrial Pt sensors according to BS1904 (1964):

	Temp. 90 K	170 K
Grade I (precision)	± 0.42 K	± 0.31 K
Grade II (industrial)	± 1.2 K	± 0.5 K

Errors are increased by transmission line and display or recording instrument.

For laboratory instruments, the precision may be better than 0.1 mK.

The response time of the laboratory instrument is about 0.5s, with DVM and good thermal contact. The response time of the industrial instrument with a 6 mm. sheathed sensor,if installed in a pocket, may be 7-10s.

On the whole, platinum resistance thermometers are very stable instruments (drift may be as high as 0.5 K/annum for industrial instruments; this can be corrected by frequent check of ice point resistance). The sensor is robust, but can be damaged by heavy vibration. Only strong magnetic fields will influence measurement. A.C. pick up can be rejected by suitable filters, but gross pick up of d.c. will influence readings.

2.3(d) Thermocouples

They were and probably still are the most popular means of measuring temperature in cryogenic plants because they are thought to be simple, robust and cheap. In fact, they are not very precise, not very sensitive, are difficult to use, and have a relatively large response time.

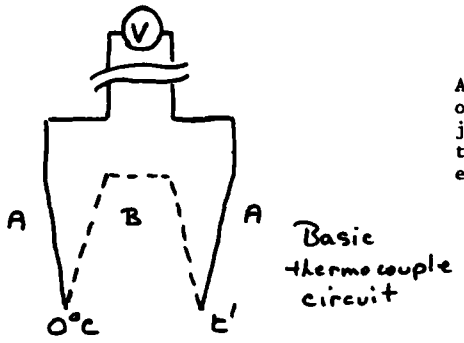

A thermocouple consists of two junctions of two dissimilar metals or alloys; one junction is maintained at a standard temperature (usually 0°C), the other is exposed to unknown temperature.

The couples suitable for cryogenic measurements are:

Type E:	Nickel-Chromium/Copper-Nickel (Chromel/Constantan)
Type J:	Iron/Copper-Nickel (Iron/Constantan)
Type K:	Nickel-Chromium/Nickel-Aluminium (Chromel/Alumel)
Type T:	Copper/Copper-Nickel (Copper/Constantan)

Type T is the most popular; for specification see BS 4937, Part 5 (1974) or ISO/ANSI equivalents.

Ideally, a thermocouple has a short response time, measures temperature at a point (junction of wires). In order to reduce thermal conduction, the wires have to be thin, and the junction has to be protected. For reliable operation, they should be electrically insulated from earth, and are encased in a mineral insulation within a stainless steel or cupronickel sheath. This sheathing increases the response time very considerably.

For correct measurements, the length/diameter ratio of the wires must be large, and again thin, usually fragile,wires are needed. Extension or compensating cables must match the thermocouple in composition. Alternatively, use isothermal box for both junctions.

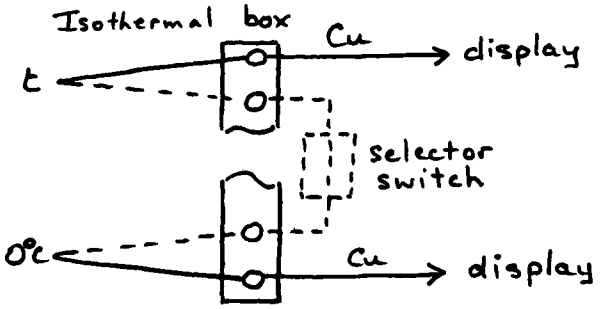

Good electrical insulation is also required between the wires. Inhomogeneities along the length of wire create thermal emf's, hence avoid large temperature gradients. Stray signals (e.g. earth loops) are major problems.

BS 4937 gives table of emf v. temperature.

These values are averages, and small variations exist for different couples. Calibration should be carried out in situ, which is hardly possible in a plant.

For industrial use, accuracies of 2-3 K are likely (sometimes worse, up to 6 K). Range from 70 K to well above room temperature (B.S. tables extend down to -270°C, but sensitivity drops off at low temperatures).

The simplest read-out is a direct deflection galvanometer, or current measuring device. For high sensitivity the leads should be kept short, but beware of changes in resistance. Usually a potentiometric indicator or recorder, or DVM (measurement of emf, independent of lead resistance) is more satisfactory, but more expensive. For industrial use, the cold junction is replaced by an automatic compensator for variations in reference temperature (e.g. ambient). Standard practise is to use an amplifier or transmitter near the measuring point, and relay the temperature signal as a standard 4 - 20 mA d.c. analogue current to the indicator or control point; this reduces long runs of compensating cable. The response time for a thin thermocouple directly in process stream, with DVM read out is about 0.5s. For a 6 mm. diameter sheathed thermocouple in a pocket a 2/3 change can take 4 - 10s.

The sensitivity of the type T thermocouple is $41\mu VK^{-1}$ at 300 K, decreasing to $16.5\mu VK^{-1}$ at 77 K.

2.3(e) Vapour pressure thermometers

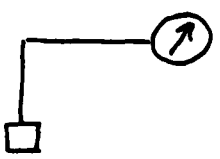

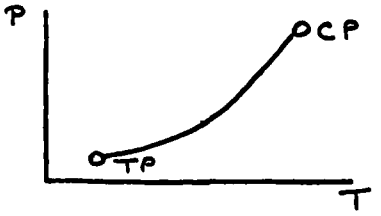

Very sensitive, because the bulb can be small, but limited in temperature range (Triple pt to Critical pt). The system is filled with gas at room temperature at a calculated pressure to ensure the measuring bulb will contain some liquid over the required temperature range. The vapour pressure is not a linear function of temperature, but may be used for control purposes.

There is a danger of cold spots, and the bulb must be at lowest temperature of system. Small leaks will ruin the system. The instrument has a very fast response due to its small size and the absence of a sheath. It is also useful where explosion hazards exist.

2.3(f) Gas Thermometer

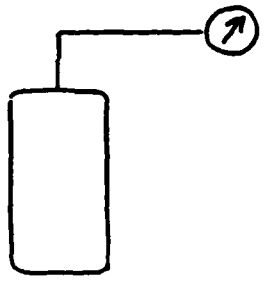

Measures $V = V(T)_p$ or $p = p(T)_V$; with an almost linear response. The gas should be non-condensing over the temperature range (hence use He, H_2 or Ne for 70 K upwards). Unlike the vapour-pressure thermometer, the gas thermometer requires a relatively large bulb. When filled with He, it can be made to operate over large temperature range (e.g. 5 - 300 K or more) with relatively low sensitivity, or over a narrow temperature range with higher sensitivity, again depending on size of bulb.

Response time depends on size of bulb, and geometry and size of dead volume. The latter also controls linearity of deflection. By suitable choice of gas, it can be made into a vapour pressure thermometer at the low temperature end of its range, but without the fast response of a purpose-built vapour pressure thermometer with its small bulb.

2.4 Pressure

On the whole, low temperature pressure measurements do not require special techniques. It is important to avoid cooling the pressure transmission line below the freezing point of the transmitting fluid. The indicator is usually a Bourdon gauge or recorder (helical pressure element) or electrical pressure transducer.

A versatile instrument is the differential pressure (DP) cell transmitter, coupled with either pneumatic or electronic transmission and control. It can be adapted for measurement of pressure, flow, density and level, and is used in antisurge control systems for compressors.

A modification is the differential vapour pressure (DVP) cell transmitter. It incorporates a sealed vapour pressure system filled with a reference fluid. The DVP cell can be used for continuous control of superheat, for example in the expanded gas coming from an expansion turbine to prevent condensation of vapour within the machine, or for the cryogenic wind-tunnel operating parameters. Differential vapour pressure cells can also be used to measure vapour pressure differences which, for binary fluids, are a measure of changes in composition.

2.5 Liquid Level

Level indicators serve to determine or control the head or quantity of liquid in a storage vessel or to maintain the head at a chosen level. All indicators are based on the generally large difference of a selected physical property across the liquid-vapour boundary, although this does not apply if the fluid is near the critical state. Level indicators can operate in three different ways: (1) as total content indicators measuring the quantity of liquid in the tank; (2) as point indicators (on-off type) sensing the level at some predetermined position; or (3) as variable level indicators, following the change in position of the level.

The properties employed depend on the nature of the liquid and the location, use and size of the tank. The simplest and probably most widely used indicator, apart from dip stick or dip tube, is the robust differential pressure gauge measuring the hydrostatic head of the liquid. Frequently this takes the form of a differential pressure cell transmitter. The disadvantage of this type of gauge is that it requires calibration for each liquid. More sophisticated indicators are based on the variation of resistance or capacitance; these are suitable for automatic control, although electrically conducting impurities which are always present, in spite of scrubbing, may spoil their performance.

Level indicators are subject to considerable errors due to a number of causes which should be appreciated before relying on the readings. Total content indicators will be in error due to the presence of the vapour, particularly at high pressures. The other types of gauges will be affected by boiling, splashing and wave motion of the liquid. They are especially unreliable in the early stages of filling a tank, particularly if the latter is at ambient temperature. The warm tank and associated piping cause the liquid to evaporate, resulting in high-speed fluid flow. Even when filling has been completed, boiling and turbulence may affect the reading for some time. Particular indicators include:

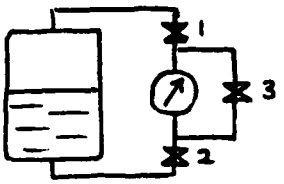

(1) Differential pressure gauge: 3 normally closed (open only when checking zero of gauge, when 1 and 2 have to be closed). Liquid in horizontal part of lower tube boils away (need for constriction), hence only vapour or gas near 2.

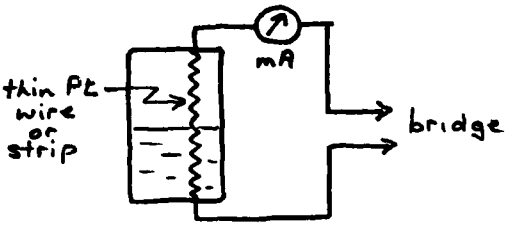

(2) Resistance gauge (hot wire):

Wire heated by passing current. Temperature of wire in liquid is lower than in vapour because of better heat transfer to liquid. Current should be kept low.

Calibration is necessary for each liquid, and the same liquid at different pressures via spot readings at particular levels.

(3) Carbon resistors: Placed at different heights to give a spot reading for each resistor. R increases with decreasing T.

(4) Resistance gauge with float: The float is electrically conducting, and is guided by two resistance wires. The float short-circuits the wires at various positions of liquid level, hence changing the resistance.

Calibration is needed for each liquid.

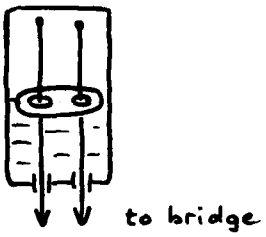

(5) Capacitance indicator: A parallel plate condenser extends over the whole length of the tank. The dielectric constant of the liquid differs from that of vapour; hence the capacitance is a function of liquid level.

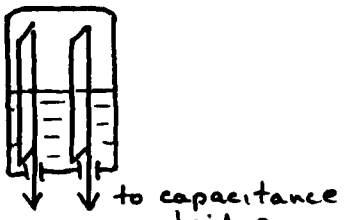

2.6 Flow

Measurement of flow is a difficult problem for low temperature fluids. This is due to the fact that the fluids are close to saturation conditions, so that the pressure drop through the flow meter must be kept small, to avoid 2-phase flow by flashing or condensation. This requirement reduces the possibility of accurate measurement. Furthermore, the length of the transfer pipes has to be kept to a minimum in order to reduce thermal leakage and associated problems like vaporisation. The instruments used are (i) the differential or flow-rate meters, and (ii) the integral or quantity-flow meters.

Flow-rate metering is normally based on a differential pressure measurement. Venturi meters have been used, but there is a tendency to induce cavitation for low inlet pressures. This can be avoided by temporarily raising the inlet pressure to a sufficiently high value, which at the same time provides for more accurate pressure drop measurements. This, however, cannot be done in many cases.

At present the most widely used type of meter is the orifice plate which suffers from the disadvantage of producing a relatively large pressure loss. This pressure loss is a function of the differential pressure and of the orifice ratio. The position of the vena contracta depends on the flow velocity of the fluid through the orifice as well as on the orifice ratio. The position of the pressure tappings for the measurement of the pressure difference (e.g. by a differential cell transmitter) therefore has to be carefully chosen to give meaningful results.

Turbine flow-meters are very promising, and are finding increasing popularity, but they have to be situated in a position where two-phase flow is impossible, and have to be calibrated for the fluid used.

There is a distinct lack of suitable quantity meters, whether for volume or for mass flow. The former is considered more accurate, but in order to convert to mass flow a knowledge of density is required. Large and intricate test rigs (e.g. at N.B.S., Colorado) have been built for the primary calibration of meters under laboratory conditions. The usual method in the field is to use a rate-flow meter to measure the volume rate of flow (e.g. turbine), and to integrate the readings over the time of flow. Errors may occur during conditions of fluctuating flow which prevent the setting up of thermal equilibrium.

A recent development, concerned with mass flow measurements for costing of liquid natural gas under fluctuating high pressures and temperatures, combines an orifice plate with differential pressure cell transmitters, density measuring cells, a scaling unit and a computer.

2.7 Leads to Low Temperature Instrument sensors

Considerable care and attention is needed to avoid spurious signals in electrical leads to and from sensors operating at low temperatures. At some point, the leads have to pass through the temperature gradient in the insulation of the cold-box before reaching a connector or terminal box at ambient temperatures outside the cold-box. This temperature gradient can lead to large thermo-electric effects (e.g. from inhomogeneities in the wires used) and ground loop signals, besides electromagnetic or electrostatic interference. Thermo-electric effects are a particular nuisance, because they are variable and non-reproducible.

The following suggestions are offered, bearing in mind that after installation access to leads, and the retrofitting of additional leads, may be difficult and expensive.

1. Use thermo-couple quality wire with braided screen or insulating metal sheath.

2. Do not earth the instrument sensor to the screen or to the cold-box frame.

3. Do not have joints in wires where there are temperature gradients.

4. All low temperature joints should be made with metal-to-metal contact to avoid thermo-electric effects associated with dissimilar metals and solders. Connectors should be designed so that contact pressure is maintained during thermal cycling.

5. Wires and their sheaths should not conduct heat through the insulation - they must be thin.

6. The wires must be kept free of moisture. Plastic insulation should remain non-hygroscopic, and the insulation of metal sheathed conductors should be completely dry prior to sealing, and remain dry during operation.

7. Wires should not be deformed in the cold area. Sharp bends should be avoided, and care taken that leads will not become stressed during the subsequent addition of insulation and after cooldown.

8. Do not use common return or ground leads.

9. Screens should be earthed at one end only, and nowhere else, to prevent ground loops being set up.

10. Remember that instrumentation problems are time-consuming, and some care, expense and forethought at the installation stage will provide considerable economies later.

PROPERTIES OF MATERIALS: THE PHYSICAL PROPERTIES OF METALS AND NON-METALS

by

D.A. Wigley,
Lecturer in Mechanical Engineering and Consultant to the Institute of Cryogenics
Engineering Faculty, The University of Southampton,
Southampton, SO9 5NH, England.

Summary

The requirements of a cryogenic wind tunnel project are considered in the context of the technology already developed for the storage and handling of large quantities of cryogenic fluids. Heat capacities are discussed in relation to the quantity of fluid evaporated during cooling and also to the thermal response time of the tunnel. The thermal conductivities of metals and non-metals are considered, particularly in the context of good conductors which are used to reduce thermal gradients, and poor conductors which can be used as insulants to minimise the heat flowing into the cold regions. Electrical conductivity is discussed particularly with reference to the high resistivity alloys used in strain gauges and heaters, together with brief reference to thermo-electric effects and possible use of superconducting magnets. Strong emphasis is placed on a discussion of the thermal contraction of materials at low temperatures and advice is given on how to avoid some of the more common problems caused by differential contraction. Some design data is included in the text and references are given to the major data compilations.

1. Introduction

Although the use of cryogenic techniques in the operation of wind tunnels is a relatively recent development, it is, I believe, important to set this against the background of the growth of cryogenics in the last few decades to a very large and efficient industry in its own right. Industrial and military requirements for the production of oxygen, nitrogen, hydrogen and natural gas in tonnage quantities have demanded solutions to the technical and economic problems involved in the liquifaction, transfer, transportation and storage of these liquified gases. The needs of high energy nuclear physics have nurtured the development of superconducting magnetic technology to a point where it is now virtually a routine procedure, while other projects such as magnetic levitation systems, superconducting power transmission, magneto-hydrodynamic power generation, infra-red detectors, superconducting memory devices, etc., have also contributed to an understanding of the many factors involved in the operation of equipment at low temperatures. Inevitably, a lot of unnecessary duplication and re-invention has taken place as these various projects have waxed and waned, but there is now a very large store of knowledge available to help those entering the field for the first time. *The message that I would like to bring home to you is that you should ADOPT as much of the existing technology as is possible and ADAPT it where necessary.* I would like to illustrate this theme by looking briefly at three different areas of a Cryogenic Wind Tunnel project in which I believe that this philosophy can be applied.

Firstly, let us consider the storage and transfer of the large quantities of liquid nitrogen needed to run a tunnel. In principle, this is virtually identical to the situation which exists in, for example, a large food freezing plant. The storage vessels, pumps, valves and control equipment, all serve the same purposes and there are, therefore, sound reasons for considering them as a commercial package once the relevant design specification has been established. Thus, for example, it should not matter whether 9% nickel steel, 304 stainless or 5083 aluminium is chosen for the construction of the LIN storage vessel as long as it is carried out by a technically competent organisation. In many respects the design and construction of the transfer line should also be a relatively simple commercial consideration once local constraints and requirements have been identified.

Secondly, in the design and construction of the tunnel itself it is necessary to bear in mind the extra constraints that cryogenic operation will introduce. For example:

- thin, light structures cool down more rapidly and evaporate less cryogenic fluid than do heavy sections, thus if a fast thermal response is required it is essential to minimise the thermal mass of the structure.
- insulation is necessary to cut down the heat inleak to the working space and hence the effective refrigeration power used. This insulation can be applied either internally or externally and the implications of this decision are manifested in considerations of the smooth profile of the inner liner in the first case and in the toughness of the pressure shell in the second.
- all materials contract to a greater or lesser extent when they are cooled and one of the most essential aspects of the successful design of cryogenic equipment lies in avoiding the problems that can be brought about by differential contraction caused by temperature gradients or the juxtaposition of dissimilar materials.

- some materials embrittle at low temperatures and it is of critical importance to select materials with strengths and toughnesses adequate for their intended duty. The failure of even a non-structural component could possibly cause damage further down the tunnel, or, at the very least, lead to the premature end of a test run.
- all materials used must be compatible with their working environment both internally and externally. Design must ensure the prevention of accidental condensation of liquid oxygen, particularly in the presence of hydrocarbon based polymers which are LOX incompatible.

Thirdly, it is important that designers and operators are aware of the differences that a low temperature environment will induce in a tunnel and its associated equipment as compared to conventional operation at ambient temperatures. Thus, certain aspects of the model suspension and force measuring systems will have to be reconsidered: for example:

- the materials used for constructing the sting assembly have to be very strong and stiff. In many alloys high strengths are associated with low toughnesses and as the strengths of all metals increase at low temperatures, it is essential to ensure that their toughness does not fall to unacceptably low levels: current state of the art technology seems to favour the various grades of maraging steel and the precipitation hardened forms of stainless steel for sting construction.
- if the force balance systems are to operate at ambient temperature in a cryogenic tunnel, heaters must be used to warm the appropriate regions. Low conductivity materials have to be used to provide the necessary heat breaks between warm and cold regions, while high conductivity inserts can even out unwanted temperature gradients.
- alternatively, if the whole system is to operate at low temperature it has to be possible to calibrate out the variations in the gauge constants brought about by changes in the electrical resistivity of the metallic films or wires. Soldered joints are best made with alloys containing antimony and adequate moisture proofing is essential.
- provision should be made for the removal of the model assembly from the test section without the need to warm up the whole tunnel. Furthermore, a cold model assembly should be allowed to warm up in an atmosphere of dry nitrogen if problems caused by moisture condensation and frost build-up are to be avoided.

Within the time available in this lecture series it is not possible to give a comprehensive and detailed exposition of all the information needed by designers for the construction and operation of a Cryogenic Wind Tunnel. Rather an attempt is made to give a broad outline of the principles involved in the selection and use of materials for low temperature applications and a limited amount of data has been included in graphical and tabular form to allow a designer to get a feel for the consepts involved. The references at the end of this paper can be used to identify the major sources of design data available on the properties of materials at low temperatures, and most of them are readily available through documentation centres in the U.S.A.

It is, however, necessary at this stage to point out that care needs to be exercised in the use of data taken from compilations and reference manuals because some properties are more "structure sensitive" than others. For example, the electrical and thermal conductivities, strength, ductility and toughness of materials are properties that are highly dependent on the microstructural and chemical condition of the material. In contrast, the specific heat, thermal expansion and elastic moduli are relatively unaffected by the presence of structural defects. Thus, although it is possible to apply the data taken from the literature for the structure-insensitive group of properties, it would be unwise, and even dangerous, to use uncritically the values given for the defect sensitive properties. These should be used for guidance only and if at all possible, they should be backed up by data obtained experimentally on material obtained from the suppliers of the batch of material to be used: in the absence of such experimental verification, generous safety margins should be applied to the literature data.

Although it is not possible to separate the mechanical and physical properties of materials it is convenient to do so for the purposes of this paper, and we will consider first the physical properties. The materials for which data has been given are those that might be utilised in the construction of a cryogenic wind tunnel and its associated equipment, and data has been limited to the temperature range 300K-80K for conciseness and on the assumption that lower temperatures are unlikely to be appropriate for this project.

2. Heat Capacity

Information on the heat capacity or specific heat of materials used in the construction of cryogenic equipment is necessary in order to calculate the amount of energy that has to be supplied for cool-down to the operating temperature. Materials with the highest heat capacities require the largest cooling power and this has to be supplied by the latent heat of the evaporating liquid or by the sensible heat of the cold gas. For structures which have to undergo frequent cooling and warming cycles, it is important to minimise the total heat capacity or thermal mass to achieve both low cool-down losses of refrigerant and also short cooling times: for equipment that rarely warms up once it has cooled, low heat capacities are not so important. For heat-balance calculations it is, in fact, the enthalpy,

$$H = \int Cp \, dT$$

which is of most direct use and in Table 1 tabulated values of the enthalpy relative to

Table 1. Specific heat, C_p, and Enthalpy, $H-H_o$, of selected solids at low temperatures*

Material	Specific heat, C_p, (J/kg K) and Enthalpy, $H-H_o$, (J/g) at temperatures indicated (K)													
	300		240		200		160		120		90		70	
	C_p	$H-H_o$	C_p	$H-H_o$	C_p	$H-H_o$	C_p	$H-H_o$	C_p	$H-H_o$	C_p	$H-H_o$	C_p	$H-H_o$
Aluminium	902	170	849	118	797	85	713	54	580	28	422	13	287	6
Chromium	450	79	419	53	385	37	332	22	249	10	161	4	93	2
Copper	386	80	371	57	356	42	332	28	288	16	232	8	173	4
Alpha iron	447	81	415	55	384	39	339	25	267	12	186	6	121	2
Gamma iron	-	-	-	-	470	51	427	33	345	17	255	8	180	4
Lead	130	33	127	26	125	21	123	16	120	11	116	7	112	5
Magnesium	1021	207	975	147	932	108	862	72	741	40	586	20	430	10
Nickel	445	82	410	57	383	41	342	26	278	14	204	6	139	3
Titanium	522	101	493	71	465	52	422	34	352	18	267	9	189	4
Silica glass	738	118	629	76	544	53	446	33	331	17	236	9	172	5
PTFE	1021	-	853	108	741	76	598	49	457	28	350	16	274	9
Graphite	716	89	535	51	414	32	296	18	188	8	118	4	77	2
Ice (at 273.15K)	2100	-	1860	234	1570	165	1290	108	1030	62	801	34	627	20
Natural rubber	1020	295	853	223	741	(128)	598	81	457	47	350	27	274	16
*Polyethylene	-	-	1430	166	1170	114	971	72	778	37	619	16	496	5
Constantan	410	79	380	56	362	41	333	27	279	15	213	7	153	3
Monel	430	81	400	57	370	41	340	27	280	14	210	7	150	3

* Enthalpy is referred to 60K not OK.

+ Data from NBS Monograph 21. (Ref.6)

absolute zero,

$$H - H_o = \int_o^T Cp\ dT$$

are given together with the specific heat at constant pressure, Cp, for a range of metals and non-metals. As may be seen the specific heats of all materials drop off at low temperatures eventually to become zero at OK, and the very low values found at hydrogen and helium temperatures can cause large temperature differences to be set up by small heat-inleaks. At liquid nitrogen temperatures and above, these effects are, however, not so severe.

The specific heat at constant volume, C_v, of crystalline materials is given by the Debye relationship

$$C_v = a\ D\ (\theta_D/T)$$

where a is a constant, D is the Debye function and θ_D is the Debye characteristic temperature. Values of θ_D are available in the literature for most crystalline solids, tabulated values of the function a $D(\theta/T)$ are given in many works, e.g. Gopal (20) and thus the variation of specific heat with temperature may be readily evaluated. The difference between C_v and C_p are so small that in practice values of C_v can be used without significant loss of accuracy. Furthermore, although large amounts of cold work may cause a slight decrease in heat capacity, for practical purposes specific heats are largely unaffected by the normal range of conditions found in metals. The specific heats of alloys at room temperature are given approximately by the Kopp-Neuman rule of mixtures in which the specific heat of a metallic solution is given by the sum of the products of specific heat and molar fraction for each constituent element, i.e. C_p mixture$=\Sigma$ Cpi Mi. Although the rule gets less applicable at low temperatures, in the absence of alternative data it gives an acceptable first approximation. Furthermore, it is worth noting that the lattice structure has a strong influence on specific heats as illustrated by the observation that the measured specific heat of f.c.c. austenitic stainless steels are closer to those calculated for γ iron than those measured on the b.c.c. α iron.

The heat capacities of non-crystalline and amorphous materials cannot be described by the Debye theory and there is, therefore, no satisfactory alternative to measured values for materials such as glass and amorphous ceramics, as well as all polymers, elastomers, composites and adhesives. When considered on a unit mass basis most of these materials have high heat capacities compared to metals, but this discrepancy is reduced considerably if they are considered on a unit volume basis.

The materials whose specific heats are given in Table 1 include those most likely to be used for the construction of a cryogenic wind tunnel and in this context it is interesting to note that a tunnel constructed of 9% nickel steel would require significantly less refrigerant than would an aluminium alloy tunnel because of the lower specific heat of 9% nickel steel.

3. Thermal Conductivity

Conduction of heat in solids takes place through the vibration of their lattice atoms and, in the case of metals, by the movement of their conduction electrons. Any mechanism which makes these processes more difficult lowers the thermal conductivity of the material and hence high conductivities are found in pure, strain free, large grain or single crystal metals and non-metals, while low conductivities are associated with impure, stressed, amorphous or microcrystalline structures. As it is difficult, if not impossible, to recognise these different conditions by looking at the surface of a material, and as the physical and mechanical history of a sample is rarely well documented, great uncertainties can arise in using thermal conductivity data from the literature. However, in many cases, conductivities at one extreme or the other are required - for example, very low conductivities where heat breaks are required to reduce heat in-leaks, or very high conductivities to minimise thermal gradients. Reference to Fig.1 will show that, in general, good conductors are materials of high purity and in an annealed state, while bad conductors are either alloys with many components and complex microstructures, or non-metals with amorphous or microcrystalline structures. Still lower conductivities may be obtained by increasing the number of interfaces crossed by the heat flux - for

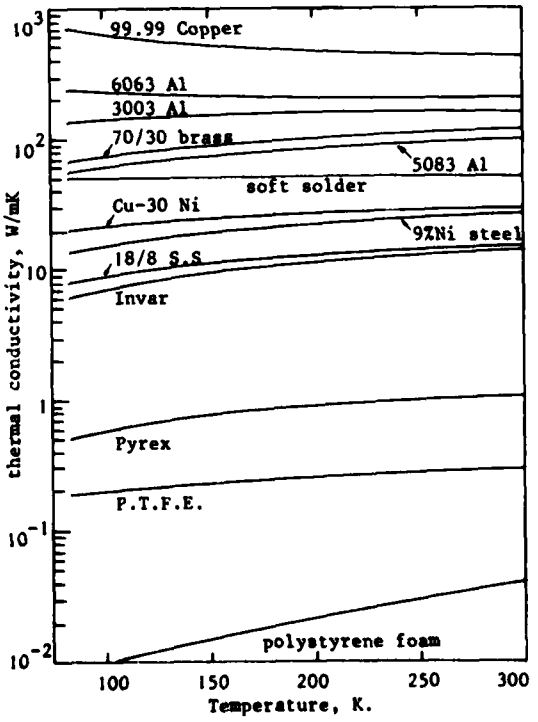

Fig.1 Thermal conductivity

example, stacks of stainless steel discs may be used for compressively loaded, thermally-insulating supports, while the combination of many fine glass filaments with a thermo-setting plastic matrix (G.R.P.) gives a material with the highest known ratio of tensile at compressive strength to thermal conductivity. The use of G.R.P. supports to separate the inner and outer skins of modern vessels for storing cryogenic liquids is, in a large measure, responsible for the low boil-off rates currently achieved.

It should, however, be noted that although the amorphous or microcrystalline structures of most non-metals make them very efficient thermal insulators, it also makes them very brittle, especially in the bulk form and they can be excessively prone to thermal shock if cooled rapidly. Furthermore variations in their density, structure and processing history can change their thermal conductivities by about an order of magnitude as well as causing considerable anisotropy, so care has to be taken in extracting suitable values from the literature.

Finally, many non-metallic materials used for thermal insulation at low temperatures are in the form of finely divided powders, fibres, films or foams and their low conductivities arise not only from the inherent low conductivity of the material, but even more so, from the poor thermal contact between adjacent particles or layers. Further improvements can be achieved by removing the gas from between the layers and so cutting down convection losses either by pumping or by use of a chemical getter, while in the most effective systems of all, the super insulants, thin metallic films intercept the infra-red radiation and so reduce the third natural source of heat in-leak.

In the case of insulating foams, it is important to appreciate the rôle played by the gas or vapour trapped in the cells. If the blowing gas has high boiling and melting points it may be possible to solidify this gas at low temperatures and so cut down convection within the cells and thus improve its insulation value. In contrast, if the cells are not completely closed, gas or vapour may permeate from the warm to the cold faces. Not only will this lower the efficiency of the insulation but permeation of water vapour will break down the cell structure by a cyclic freeze-thaw action. An even more serious problem can be caused by the permeation of air through imperfect foam insulation surrounding liquid nitrogen cooled surfaces as this can lead to the preferential condensation of liquid oxygen and the creation of a potential fire hazard. The solution to both of these problems is to provide an efficient vapour barrier on the warm side of the foam to prevent the ingress of gas or vapour, and this also helps to minimise ageing problems.

Closed cell foams are widely used for the thermal insulation of liquid nitrogen and and other cryogenic systems. They are relatively cheap, efficient and easy to apply, some being foamed in situ. Other types of foam, particularly the extruded type of polystyrene slabstock, have good load bearing characteristics - in general the strongest foams having the highest densities and the highest conductivities. Data on the effective thermal conductivity of some of the major cryogenic insulation systems is given in the paper by Dr. Scurlock.

4. Thermal Expansion

This is probably the most important of the physical properties because the stresses set up in components by differential thermal expansion can very easily cause severe distortion, or at worst, failure. At least three different expressions may be found in the literature and confusion can arise if they are not clearly understood;

a) the coefficient of linear (thermal) expansion, sometimes also called the instantaneous thermal expansion,

$$\alpha = \frac{1}{L}\frac{dL}{dT}, \ K^{-1}$$

b) the mean thermal expansion =

$$\frac{1}{L293}\frac{(L - L293)}{(T - 293)}, \ K^{-1}$$

c) the total linear contraction relative to 293K, sometimes called the linear thermal expansion is given by

$$\frac{L - L293}{L293},$$

Of these three functions, the total linear contraction relative to 293K is the most generally useful and it is shown as a function of temperature in Fig.2 and

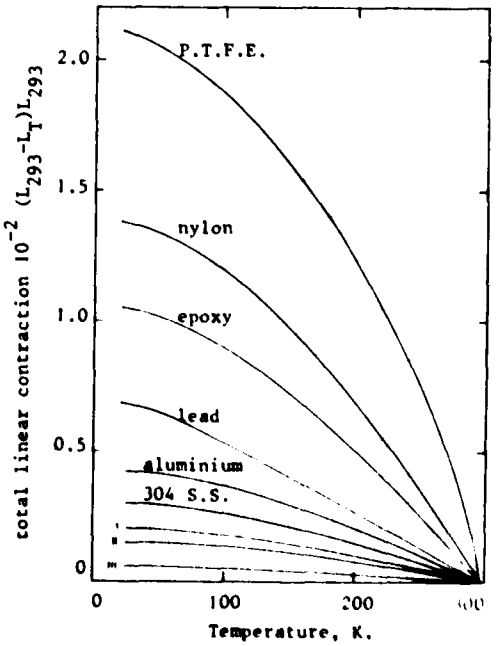

Fig.2 Total linear contraction

legend (i) 0.2% carbon steel, (ii) titanium, (iii) Invar, Pyrex

Table 2. Total linear contraction as a function of temperature*

Material	Linear contraction, $10^{-5}(L_{293}-L_T)/L_{293}$, at indicated temperature, T, (K)									
	273	260	240	220	200	180	160	120	90	70
Aluminium	45	75	118	160	201	240	277	343	381	399
Copper	33	55	87	118	149	179	208	260	293	310
Iron (b.c.c.)	23	38	60	82	102	122	140	170	185	192
Lead	58	96	152	208	263	318	372	477	552	601
Magnesium	50	83	132	180	227	273	316	393	441	466
Nickel	25	41	65	88	111	132	152	187	206	216
Titanium	16	27	43	58	73	87	101	125	139	145
Alpha brass (65 Cu-35 Zn)	37	62	98	134	169	204	237	299	339	360
Berylium Copper	35	57	90	121	151	179	206	255	287	304
Constantan	27	45	72	98	124	148	172	214	240	253
Invar	5.2	8.6	14	18	23	29	34	43	49	51
Inconel	25	41	65	89	112	194	154	191	211	221
Monel	27	45	71	96	121	144	167	206	230	241
0.2% C Steel	23	38	60	81	101	120	138	170	187	195
9% Ni Steel	24	39	58	78	98	117	134	163	183	193
Types 304 & 316 S/Steel	31	51	81	110	138	165	191	239	270	285
Type 310 S/Steel	29	47	75	101	127	152	176	218	246	-
Titanium RC-130-B (4 Mn, 4Al)	28	46	71	95	117	137	155	187	208	218
Pyrex	6.2	10.2	16	22	27	32	37	46	52	55
Borosilicate Crown BSC-1	15	25	39	53	67	80	92	114	128	-
Silica glass	0.8	1.3	1.8	2.2	2.4	2.3	2.1	0.9	-0.7	-2.1
Ice ($10^{-5}(L_{273}-L_T)/L_{273}$)	0	70	171	261	341	411	471	562	603	-
Araldite Type 501	122	199	308	410	505	594	676	819	908	960
Glass reinforced polyester	27	45	72	98	123	148	172	215	241	255
PCTFE, KelF	134	214	324	424	517	604	686	834	932	992
Perspex	136	220	335	441	540	632	717	869	966	1021
Nylon	161	265	412	548	673	789	896	1088	1211	1278
PTFE, Teflon	500	645	855	1050	1240	1400	1540	1760	1890	1965
Hard Rubber (90 Shore A2)	256	364	501	625	736	834	942	1069	1152	1196
Silicone Rubber	256	441	721	996	1246	1466	1656	1951	2117	2198
Polythene	359	594	919	1199	1439	1639	1814	2089	2240	2318
Cloth reinforced phenolic (// cloth axial)	43	70	108	143	176	207	236	288	320	337

* Data from NBS Monograph 29. (Ref.7)

Table 2. It is immediately apparent from Fig.2 that the total linear contraction at liquid nitrogen temperature varies from about 0.05% for Invar and pyrex glass to over 2% for some thermosetting resins, and it is not surprising, therefore, that problems can arise when materials are used together without adequate forethought. Problems can, in practice, usually be resolved into two basic categories:

i) those in which only one type of material is involved and where differential contraction is a result of temperature gradients

ii) those in which the same temperature gradient is applied across two or more materials of different expansion coefficient.

Considering first the case of dissimilar materials, a common mercury in glass thermometer uses the large difference in expansion coefficients between the two components, but no stresses are set up as the mercury is free to move inside the glass tube (Fig.3a). In contrast, a bi-metallic strip consists of two metals firmly fixed together, and when the temperature decreases the free end moves towards the side containing the metal with the higher expansion coefficient (Fig.3b). If the end were not free to move the metal with the higher expansion coefficient would be put into tension and the other metal into compression (Fig.3c). An idea of the forces that can be set up by contraction in dissimilar metals can be obtained by considering the hypothetical arrangement illustrated in Fig.3d, in which co-axial copper and steel pipes joined at both ends are cooled to 80°K. Table 2 shows tha the total linear contraction of copper is 302 x 10^{-5}, while that of a 0.2% carbon steel is 192 x 10^{-5}, a difference of 110 x 10^{-5} or just over 0.1%. Thus the differential strain is slightly larger than that considered to give the 0.1% proof stress, which in copper at 80°K is about 88MPa. If the joint between the two metals were a soft lead-tin solder it would have to yield and flow in order to accommodate this degree of mismatch. Most solders can, in fact, accommodate these strains as long as they do not embrittle: the correct choice of soldering alloys is discussed in White (25) and Hoare et al (26).

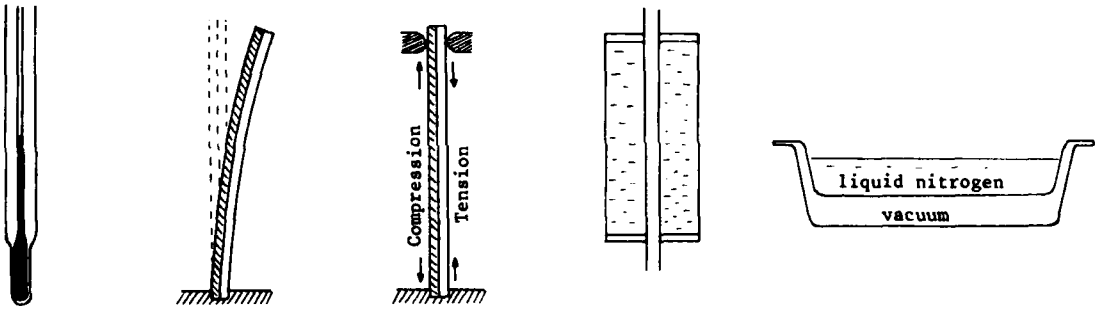

3(a) Mercury in glass thermometer

3(b) Bimetallic strip unconstrained

3(c) Bimetallic strip constrained

3(d) Dissimilar metals at same temperature

3(g) Similar metals at different temperatures

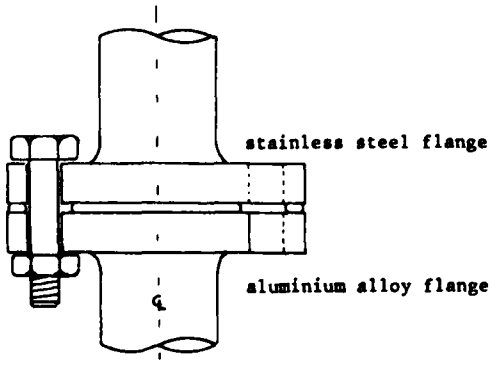

3(e) Flanged joint between dissimilar metals

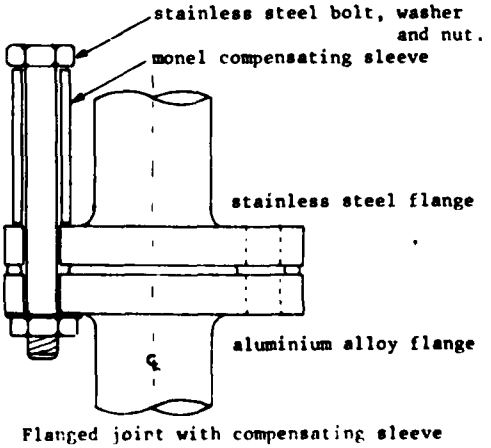

3(f) Flanged joint with compensating sleeve

Fig.3. Problems caused by differential thermal contraction

A further example of mismatched materials is illustrated in Fig.3e by a flanged joint between aluminium alloy and stainless steel pipes. Aluminium alloys contract more than stainless steels and if an aluminium alloy bolt were used its loading would be increased as it contracted more rapidly than the stainless steel flange. It is possible that the bolt might in fact fail on cooling: if not it would yield and stretch so that on warming to room temperature it would now be too long to compress the gasket adequately and a room temperature leak would be created. The use of a stainless steel bolt would also cause problems because on cooling it would contract less rapidly than the aluminium flange and so be unable to keep the same compressive stress on the gasket - the likely outcome being a low temperature leak which would then seal itself up when the joint were rewarmed to ambient temperature. This type of low temperature leak will be recognised by those with cryogenic experience and these low temperature leaks are some of the worst time wasters and blood pressure inflators known!

One elegant solution to this problem is shown in Fig.3f. A long stainless steel bolt passes through the centre of a Monel compensating sleeve as well as through the two flanges, the length of the Monel sleeve being calculated to compensate exactly for the lower contraction in the bolt. Reference to Table 2 shows that the total linear contractions at 80K relative to 293K are 391 x 10^{-5} for aluminium, 236 for Monel and 285 for type 304 stainless respectively, hence the difference between the stainless bolt and aluminium flange is 106 x 10^{-5} and that between stainless and Monel 49 x 10^{-5}. If the aluminium flange were 10mm thick a Monel sleeve 10 x 106/49, i.e. 21.6mm long would be needed for exact compensation. The same principle may be used for joints between 9% nickel steel and aluminium alloy flanges by using an Invar (Nilo 36) sleeve to compensate for the contraction in the 9% Ni steel bolt.

Returning to the case where temperature differences can cause problems even when the material is the same, Fig.3g shows schematically a situation in which co-axial, thermally insulated vessels are joined at their extremities. In reality this arrangement had been constructed to clamp around the outside of an oil filled high voltage cable so that the oil dielectric could be frozen to allow a repair to be carried out. The vessels were made of mild steel, welded at their perimeters and with the space between the two shells evacuated because the designer thought this would improve the insulation and reduce the amount of liquid nitrogen needed. On cool down the vessels shattered and the unfortunate designer retired to seek advice. In this case the total linear contraction of the inner shell at 80°K would have been 192 x 10^{-5} m/m relative to the outer shell which remained at ambient temperature. This strain was too large to be accommodated by the mild steel which, as we shall see later, was not only below its ductile-brittle transition, but in all probability embrittled by the welding used in its fabrication.

We noted earlier the very low contraction of Invar relative to that of most materials used to construct cryogenic equipment, a characteristic brought about by its large positive magnetostruction that approximately cancels out the normal thermal contraction. This low thermal contraction has been utilised in a number of cryogenic applications. For example, the tankers used to transport liquid natural gas across the atlantic are of an insulated double skin construction in which the inner liners and anti-slosh baffles are made from Invar. Of even more interest is the fact that the LNG transfer lines at Arzew that run from the storage tanks for about one mile to the loading jetties are also made of Invar. Expansion joints have to be built into long lengths of cryogenic transfer line and in this case the extra cost of Invar relative to, say, 304 stainless steel was more than offset by the savings that accrued from being able to instal fewer expansion joints.

It was therefore with interest that, while reading the now classic paper on Cryogenic Wind Tunnels by Kilgore, Goodyear, Adcock and Davenport, that I noted in their report that gaps up to about 12.7mm wide opened up around the tunnel circuit at the lowest operating temperatures. A moments consideration will show that with any insulated tunnel the inner shell must contract relative to the outer: the use of Invar for the inner liner of an internally insulated tunnel would minimise the contraction involved and hence the complexity of the joints necessary to maintain a smooth inner profile.

Persuing the thought of double-skinned insulated structures further, it is worth pointing out that this type of structure is widely used in the construction of insulated cold stores as it provides a strong, stiff insulating panel which can be used in load bearing applications. One small problem is, however, that if the skins are fully bonded - the inner will contract relative to the outer when cooled and cause thermal bowing of the panel which increases as the square of the panel length! The moral for cryogenic wind tunnel designers is to think how the strains or stresses set up by the contraction of the inner skin can be relived without causing bowing or cracking of the liner. Indeed the whole question of fits and clearances at low temperatures has to be kept very much in mind. Most of us are familiar with the practice of heating a gear wheel before placing it onto a shaft so that it will shrink to a tight fit on cooling. Some will also be aware that the same operation is sometimes carried out by cooling the shaft with liquid nitrogen prior to fitting the gear so that the required fit is obtained when the shaft expands on rewarming to room temperature. These examples should be remembered when constructing models, balances or other fittings where there are close fits and small clearances. On cooling these clearances could either decrease and cause a seizure or increase and lead to looseness and possible leakage. This can also manifest itself in changes in the clamping force applied to models which could decrease on cooling and allow the model to vibrate loose, or increase and possibly cause damage. Reference to Fig.2 or Table 2 will remind us that these problems are likely to be

particularly severe where non-metallic materials are involved as their total linear contractions are so large.

It is, at this stage, worth reiterating the comment made earlier about thermal shock. We have now seen that most non-metals have low thermal conductivities and high expansion coefficients, and we will find later that many of them also become embrittled at low temperatures. We thus have a combination of the 3 factors that lead to thermal shock and they are particularly severe if the materials are present in thick sections and/or cool-down rates are high. Nevertheless, brittle materials can be used safely at low temperatures if enough care is taken. For example liquid hydrogen bubble chambers have plate glass windows for viewing ports which are cooled at about a few degrees K per day to prevent thermal shock. In the case of viewing ports for cryogenic wind tunnels, it is probably much better to follow the practice adopted in the prototype NASA tunnel of adopting quadruple glazing as this not only minimises thermal shock but it cuts down the heat loss and prevents condensation on the outer skin.

Finally, two further points on finding data on the low temperature expansion coefficients of materials. Firstly, physics text books show that for crystalline materials there is a close relationship between the expansion coefficient, α. and the specific heat at constant volume, C_V. It is often quoted in the form

$$\alpha_T/\alpha_{293} \simeq C_{vT}/C_{v293} \simeq C_{pT}/C_{p293}$$

and thus it may be used to give approximate values for α_T if α_{293} and the specific heats are known. If measured values of C_p are available direct substitution is possible: if only the characteristic temperature θ_D is known calculation is somewhat more laborious.

Secondly, we have noted already the difference between the very high contractions shown by polymeric materials, in particular thermosetting resins, and the very low values given by ceramics and glasses. This discrepancy can in fact be used to tailor make adhesives that can match the total linear contraction of any particular metal and hence be used to form adhesive joints that are not excessively prone to cracking due to differential contraction. Ground up powders of pyrex, silica glass, carbon and other ceramics are used as fillers and to a first approximation the expansion coefficient of the resultant composite should be given by the rule of mixtures:-

$$\alpha_{mixture} = (\alpha_{resin} \times \text{vol } \%_{resin}) + (\alpha \text{ filler} \times \text{vol } \% \text{ filler})$$

A trial and error approach using filler volume fractions spread around the predicted value usually gives the required result.

5. Electrical and Magnetic Properties

The electrical resistivity of metals is one of the properties most sensitive to the physical and chemical purity of the sample. Mattheissens rule states that,

$$\rho = \rho_o + \rho(T)$$

where ρ_o, the "residual" resistivity caused by the scattering of conduction electrons by lattice defects and chemical impurities is temperature independent, and $\rho(T)$, the "ideal" resistivity caused by the scattering of electrons by lattice vibrations is a strong function of temperature which becomes vanishing small as the temperature tends towards absolute zero. This need concern us little but for the fact that simple measurement of the resistance ratio ρ_{293}/ρ_4 gives an excellent indication of the effective purity of supposedly pure metals, and, furthermore as the same electronic mechanisms are responsible for the thermal conductivity of pure metals at low temperatures, it also enables information to be obtained about their relative thermal conductivities. Resistivities of pure metals can be below 10^{-11} Ω m at 4K compared with typical room temperature resistivities of $\simeq 10^{-7}$ Ω m, while in complex alloys such as Constantan the resistivity changes only marginally from $\simeq 4.9 \times 10^{-6}$ Ω m at 300K to $4.6 \times 10^{-6}\Omega$ m at 4°K. This is highly relevant to a cryogenic wind tunnel project as the strain gauges widely used as the sensing elements in force balances are made from Constantan, Advance, Karma, Evanohm, Stabilohm, etc. and the less their resistivity varies between room and liquid nitrogen temperatures the easier it is to compensate the gauge factors accordingly.

In his paper on instrumentation, Dr. Scurlock discusses in detail the use of thermo-couples for temperature sensors. It should, however, be noted that the thermo electric emfs set up when dissimilar metals are subjected to a temperature gradient can also cause severe problems by creating undesirable thermal emfs in strain gauge and other measuring circuits. Great care has to be taken to prevent such stray emfs from interfering with the actual voltages generated by the stress-induced resistance changes in the strain gauges, "tricks of the trade" relevant in this case include the use of thermal-free solders, pairing of leads so that they induce equal and opposite emfs in a thermal gradient and generally trying to make joints under conditions where temperature variations are minimised. Semi-conductor strain gauges which are also sometimes used for force measurements are, in general, less prone to problems with thermal emfs but more sensitive to variations in gauge factor with temperature.

Finally, it is worth mentioning briefly the phenomena of superconductivity - the property possessed by some metals in which their resistance becomes un-measurably small

below their superconducting transition temperatures. Once virtually a laboratory curiosity in low temperature physics departments, this phenomena has given rise to the development of highly sophisticated high field magnet systems which generate magnetic fields undreamt of using conventional magnetic systems which would have required multi megawatts of electric power and vast amounts of cooling water to operate. The relevance to a cryogenic wind tunnel project lies in the possible future development of sting-free, magnetic suspension systems for models which would probably require the use of superconducting magnet technology to create the fields required. This possibility should be kept in mind when considering the selection of materials for construction of the tunnel and model systems, as the presence of ferromagnetic materials in regions of high magnetic flux can lead to the development of very strong, unwanted magnetically induced forces.

Sources of information and references

1. National Bureau of Standards, Thermophysical Properties Division, Boulder, Colorado 80303, U.S.A. : location of the NBS Data Centre, the best source of information on the mechanical and physical properties of materials and fluids at low temperatures. Services offered include a current awareness service and list of publications as well as the NBS Monographs and other publications listed below.
2. Cryogenic Materials Data Handbook, Technical document report ML-TDR-280 (1964 and supplement 1966), NBS, Boulder.
3. LNG Materials and Fluids Users Manual (1977 & supplements), Users Manual of property data in graphical format available from NBS, Boulder.
4. NBS Monographs that follow are sold by the Superintendent of Documents, U.S. Government Printing Office, Washington, D.C. 20402, U.S.A.
5. Monograph 13 Mechanical properties of structural materials at low temperatures (1960).
6. Monograph 21 Specific heats and enthalpies of technical solids at low temperatures (1960).
7. Monograph 29 Thermal expansion of technical solids at low temperatures (1961).
8. Monograph 63 Tensile and impact properties of selected materials from 20K to 300K (1963).
9. Monograph 101 Low temperature mechanical properties of copper and selected copper alloys (1967).
10. Monograph 111 Technology of liquid helium (1968).
11. Monograph 131 Thermal conductivity of solids at room temperature and below (1973).
12. Materials Properties Data Book, Vol. 1 & 2, NERVA Program Report 2275, Aerojet Nuclear Systems Co., Sacramento, Calif. (1970).
13. Handbook on Materials for Superconducting Machinery, Metals and Ceramics Information Centre, Battelle, Columbus, Ohio (1977).
14. Proceedings of the Cryogenic Engineering Conferences. Advances in Cryogenic Engineering (Ref.15) are the proceedings of the conference held every other year in America, International Cryogenics Engineering (Ref.16) are the proceedings of the International Conferences held in the years between the American Conferences.
15. Timmerhaus, K.D., Ed. Advances in Cryogenic Engineering, Plenum Press, New York, latest volume No.24 (1978).
16. International Cryogenic Engineering. IPC Science & Technology Press, Guildford, Surrey, latest volume ICEC.7, (1978).
17. Mendelssohn, K., and Timmerhaus, K.D., Eds., International Cryogenics Monograph Series, Plenum Press, New York. Titles include:
18. Wigley, D.A., Mechanical Properties of Materials at Low Temperatures (1971).
19. Meaden, G.T., Electrical Resistance of Metals (1965).
20. Gopal, E.S.R., Specific Heats at Low Temperatures (1966).
21. Zabetakis, M.G., Safety with Cryogenic Fluids (1967).
22. Croft, A.J., Cryogenic Laboratory Equipment (1970).
23. Cryogenics, a monthly journal published by IPC Science & Technology Press, Guildford, Surrey.
24. Journal of Low Temperature Physics, published quarterly by Plenum Press, New York.
25. White, G.K., Experimental Techniques in Low Temperature Physics, 3rd Ed., Clarendon Press, Oxford (1979).
26. Hoare, F.E., Jackson, L.C., and Kurti, N. Experimental Cryophysics, Butterworths, London, (1961).

REAL-GAS EFFECTS I - SIMULATION OF IDEAL GAS FLOW BY CRYOGENIC NITROGEN AND OTHER SELECTED GASES

Robert M. Hall
Aeronautical Research Scientist
NASA Langley Research Center
Hampton, Virginia 23665 USA

SUMMARY

The thermodynamic properties of nitrogen gas do not thermodynamically approximate an ideal, diatomic gas at cryogenic temperatures. Choice of a suitable equation of state to model its behavior is discussed and the equation of Beattie and Bridgeman is selected as best meeting the needs for cryogenic wind tunnel use. The real-gas behavior of nitrogen gas is compared to an ideal, diatomic gas for the following flow processes: isentropic expansions, normal shocks, boundary layers, and shock wave-boundary layer interactions. The only differences in predicted pressure ratio between nitrogen and an ideal gas that may limit the minimum operating temperatures of transonic cryogenic wind tunnels seem to occur at total pressures approaching 9 atmospheres and total temperatures 10 K below the corresponding saturation temperature, where the differences approach 1 percent for both isentropic expansions and normal shocks. Several alternative cryogenic test gases - air, helium, and hydrogen - are also analyzed. Differences in air from an ideal, diatomic gas are similar in magnitude to those of nitrogen and should present no difficulty. However, differences for helium and hydrogen are over an order of magnitude greater than those for nitrogen or air. It is concluded that helium and hydrogen would not approximate the compressible flow of an ideal, diatomic gas.

1. INTRODUCTION

Cryogenic wind tunnels under normal conditions should be operated at the lowest possible total temperature in order to maximize Reynolds number capability for a given tunnel total pressure or to minimize costs for operating at a fixed Reynolds number. This important realization is readily seen in figure 1, which shows for nitrogen gas both unit Reynolds number and drive power required relative to their values at a total temperature of 322 K as a function of total temperature for a constant total pressure. Not only is Reynolds number increasing as the temperature decreases, but its rate of increase is growing as well. Obviously, if one wants to maximize Reynolds number capability and is limited by total pressure capability, then it is desirable to operate as cold as possible to move up the steep portion of the curve. For operation at some Reynolds number below the maximum capability of the tunnel, being able to test as cold as possible maximizes the amount of Reynolds number gained by temperature reduction and minimizes the use of pressure to achieve the desired test Reynolds number. If pressure can be minimized, drive power, which is proportional to pressure, will be minimized due to both the reduced pressure and due to the trend of power reduction at the lower temperatures seen in figure 1. Operation at a reduced pressure also, of course, reduces the model loads which eases the balance, sting, and model stress problems. The minimum operating temperatures are, however, limited by the low-temperature behavior of the test gas. At some temperature, either the test gas begins to condense or its equation of state is such that it does not properly simulate the nearly ideal-gas behavior of air encountered in flight.

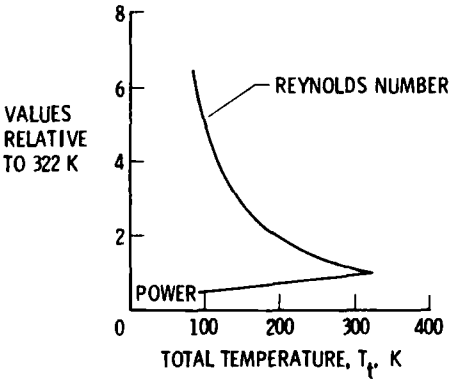

Figure 1.- Effect of temperature reduction on unit Reynolds number and drive power for a free-stream Mach number of 1.0 and a total pressure of 1 atm. Nitrogen gas.

The present report examines the real-gas behavior of cryogenic gases while the companion report, "Real-Gas Effects II - Influence of Condensation on Minimum Operating Temperatures of Cryogenic Wind Tunnels," examines the evaporation and condensation problems involved in cryogenic tunnels. Both papers concentrate on nitrogen as a test gas. In examining the real-gas behavior the present paper reviews the reasons to suspect non-ideal behavior of nitrogen, summarizes and compares the predictions of the possible equations of state that one may choose to model nitrogen gas, highlights the real-gas behavior of nitrogen for a variety of flow processes, and then briefly examines air, helium, and hydrogen as alternate cryogenic gases. The calculations discussed usually include examples at total pressures up to 9 atmospheres (atm), which approximates the high pressure capability of the National Transonic Facility currently under construction in the United States, and at total temperatures down to, or below, saturation values.

2. REAL-GAS PROPERTIES OF NITROGEN

The necessity of examining the real-gas behavior of nitrogen gas at the low temperatures is obvious after graphing the compressibility factor, Z, defined by

$$Z = \frac{pv}{RT} \tag{1}$$

and the ratio of specific heats, γ, defined as

$$\gamma = \frac{c_p}{c_v} \tag{2}$$

where p is pressure, T is temperature, v is specific volume, R is specific gas constant, and c_p and c_v are the specific heats at constant pressure and volume. The values of Z and γ as a function of temperature are shown by the line labelled "Jacobsen, Standard" in figures 2 and 3. The remaining lines in this figure will be explained later. As seen in both of these figures, significant departures occur in both Z and γ from the values associated with a thermally perfect ($Z = 1.0$) and a calorically perfect ($\gamma = 1.4$) diatomic gas at a pressure of 5 atm as the temperature decreases. Since the goal of testing in a cryogenic tunnel is to simulate flight through the atmosphere where $Z \simeq 1.0$ and $\gamma \simeq 1.4$, figures 2 and 3 would suggest that a complete real-gas analysis of nitrogen simulating various types of flows would be appropriate to ensure proper performance of nitrogen as a test gas down to some specified minimum operating temperature.

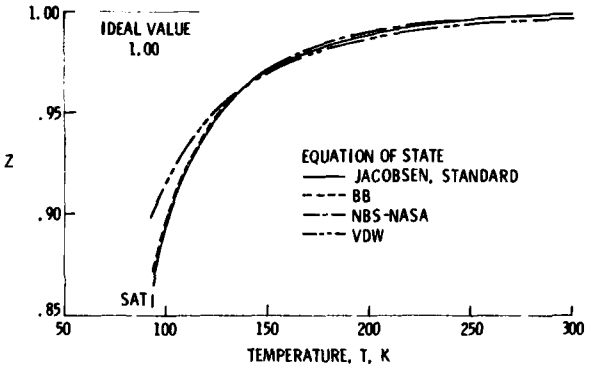

Figure 2.- Compressibility, Z, for nitrogen gas at $p = 5$ atm. "SAT" denotes saturation temperature. The Jacobsen line is taken to be the accepted value.

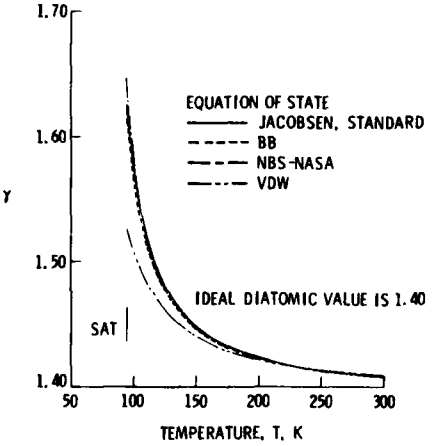

Figure 3.- Ratio of specific heats, γ, for nitrogen gas at $p = 5$ atm. "SAT" denotes saturation temperature. The Jacobsen line is taken to be the accepted value.

3. EQUATIONS OF STATE

Before a complete analysis of nitrogen gas, or alternate gases, can be performed, one must be able to characterize the behavior of that gas. The mathematical form of that description is called an equation of state and usually takes a form similar to

$$p = f(v,T) \tag{3}$$

where f is some arbitrary function. The next several paragraphs will summarize the various equations of state that are typically used to describe gases.

The simplest and most widely used equation of state in fluid mechanics is the ideal equation of state represented by

$$pv = RT. \tag{4}$$

The basic assumptions are that the gas molecules do not attract each other and that the molecules themselves do not have any finite volume. The compressibility factor, Z, is obviously constant and equal to 1.0 and the gas is consequently thermally perfect. That Z does not equal 1.0 and that γ does not equal 1.4 over the temperature range for nitrogen demonstrates the inability of the ideal equation of state to properly predict the thermodynamic properties for nitrogen at low temperatures. However, as will be developed later in this paper, this will not necessarily affect the ability of nitrogen to simulate the flow processes of an ideal, diatomic gase with $Z = 1.0$ and $\gamma = 1.4$.

Since the ideal equation of state does not adequately represent Z or γ at the low temperatures, an improved equation might be obtained by correcting for the assumptions

in the ideal equation. The two main assumptions of the ideal-gas equation of state are that the molecules do not attract each other and that the molecules themselves take up no volume, so the first step to improve the equation would be to incorporate the physical realities of attraction and finite volume in a more advanced equation of state. This was done successfully by J. D. van der Waals in 1873, as described in detail by Glasstone in reference 1. The effect of attraction between molecules is to introduce a positive correction to measured gas pressure, and the effect of the finite volume of the molecules is to introduce a negative correction for specific volume. Consequently, the van der Waals equation of state is written as

$$(p + \frac{a_1}{v^2})(v - b_1) = RT \tag{5}$$

where a_1 and b_1 are constants. Equation (5) will be referred to as the VDW equation in the rest of this report. While the VDW equation represented a substantial improvement in the ability to model gases, further equation of state development has continued until the present.

While the remaining equations of state to be discussed here are much more complicated than the VDW equation, there are some underlying physical reasons - as was the case for the VDW equation - or underlying mathematical reasons for the forms chosen by the authors of the equations. In 1927, Beattie and Bridgeman came up with an equation of state that has proved to be very useful and surprisingly accurate. The general form of the Beattie-Bridgeman equation (to be referred to as the BB equation) is given by

$$p = \frac{RT(1 - \varepsilon)}{v^2}(v + B) - \frac{A}{v^2} \tag{6}$$

where

$$A = A_o(1 - \frac{a}{v})$$

$$B = B_o(1 - \frac{b}{v})$$

$$\varepsilon = \frac{c}{vT^3}$$

and where A_o, a, B_o, b, c are constants that are tabulated in reference 2 for many different gases. The values for nitrogen are given below after conversion to SI units:

$$A_o = 173.60\ N \cdot m^4/kg^2$$

$$a = .0009342\ m^3/kg$$

$$B_o = .001801\ m^3/kg$$

$$b = -.000247\ m^3/kg$$

$$c = 1499.\ m^3K^3/kg$$

One of the most complicated equations of state developed specifically for nitrogen was that reported by Jacobsen in reference 3. He used a 32 term equation that describes both liquid and gaseous phases of nitrogen. The form of Jacobsen's equation can be found in reference 4 as well, which is an extremely valuable reference because it contains tabular values of, or equations for, liquid properties such as thermal conductivity, viscosity, and surface tension.

Because of the complexity and the wide range of applicability of Jacobsen's equation - with pressures to 10,000 atm and temperatures from 65 K to 2,000 K - Langley Research Center contracted with the National Bureau of Standards to construct an optimized virial equation of state which would focus on pressures only up to 10 atm and temperatures only up to 300 K. Furthermore, the equation of state was to calculate only gaseous phase properties of nitrogen. Full details of this work are included in reference 5. The form of this optimized virial equation of state is

$$p = RT\rho(1 + B\rho + C\rho^2) \tag{7}$$

where

$$B = \sum_{j=1}^{7} B_j T^{(3-j)/2}$$

$$C = \sum_{j=1}^{5} C_j T^{(1-j)/2}$$

and ρ is density. Values for the B_j and C_j can be found in reference 5 and this equation of state will be referred to as the NBS-NASA equation. This virial equation of state is the last equation to be considered in the comparisons to follow.

To compare the predictions of the different equations of state for flow problems, expressions for enthalpy, H, entropy, S, heat capacities, and sound speed, W, are required. A very helpful article which discusses the calculation of these and other thermodynamic properties is given in reference 6. The following equations are taken from that reference with the exception of the expression for c_p, which contains a typographical error in reference 6:

$$H = H^*_{T_o} + {}_T\int_0^\rho \left[\frac{p}{\rho^2} - \frac{T}{\rho^2}\left(\frac{\partial p}{\partial T}\right)_\rho\right] d\rho + \frac{(p - \rho RT)}{\rho} + {}_p\int_{T_o}^{T} c_p^o \, dT \tag{8}$$

$$S = S^*_{T_o} + {}_p\int_{T_o}^{T} \frac{c_p^o}{T} \, dT - R\ln(\rho RT/p_o) + {}_T\int_0^\rho \left[\frac{R}{\rho} - \frac{1}{\rho^2}\left(\frac{\partial p}{\partial T}\right)_\rho\right] d\rho \tag{9}$$

$$c_v = c_v^o - {}_T\int_0^\rho \frac{T}{\rho^2}\left(\frac{\partial^2 p}{\partial T^2}\right)_\rho d\rho \tag{10}$$

$$c_p = c_v + T\left(\frac{\partial p}{\partial T}\right)_\rho^2 \Bigg/ \left[\rho^2\left(\frac{\partial p}{\partial \rho}\right)_T\right] \tag{11}$$

$$W = \left[\left(\frac{c_p}{c_v}\right)\left(\frac{\partial p}{\partial \rho}\right)_T\right]^{1/2} \tag{12}$$

where $H^*_{T_o}$ and $S^*_{T_o}$ are reference values of enthalpy and entropy, p_o is a reference pressure, T_o is a reference temperature, and c_p^o and c_v^o represent zero-pressure values of specific heats. While most gases approach ideal-gas behavior at zero pressure, that is,

$$c_p^o = \frac{\gamma R}{\gamma - 1} \tag{13}$$

$$c_v^o = c_p^o - R \tag{14}$$

this should be verified for a gas of interest if high accuracy is desired. In reference 3, an eight term expression is used to approximate c_p^o for nitrogen. Our experience at Langley Research Center does not seem to warrant this for nitrogen but oxygen may be a borderline case. Also, absolute values for the constants $H^*_{T_o}$ and $S^*_{T_o}$ are not important for fluid mechanics problems because one is usually dealing only in terms of differences in H or S, not absolute values.

In making comparisons between the performance of the different equations of state, only nitrogen gas will be considered. The eight term expression for c_p^o is used in Jacobsen's formulation while the ideal value of $c_p^o = 3.5R$ from Eq. (13) will be used in the formulations for the BB, VDW, and NBS-NASA equations of state.

The comparisons of predicted nitrogen-gas thermodynamic properties for Z, γ, and c_p are shown respectively in figures 2, 3, and 4 for a value of pressure of 5 atm. In all of the graphs there is good agreement between the Jacobsen, BB, and the NBS-NASA equations, while the VDW equation does not seem to perform as well. In the United States, Jacobsen's formulation has been accepted as the best general description for nitrogen so it is labeled as the standard in the figures and is used for judging the other equations. That VDW is inaccurate is not surprising because of its simplicity; however, it does a good job of indicating the basic departures from the ideal values of $Z = 1.0$, $\gamma = 1.4$, and $c_p = 3.5R$.

While Jacobsen is usually considered the standard by which to compare other equations, figures 2, 3, and 4 can be used to get an idea of the possible uncertainties that may exist in the formulations of BB, NBS-NASA, and even Jacobsen by comparing the predictions of these three equations. From figure 4, for example, at saturation temperature there appears to be a difference of about 8 percent in the three predicted values of c_p. The large uncertainty in heat capacities is addressed at some length in reference 5 and the claim is made that the heat capacities predicted by the NBS-NASA equation will be accurate to within 2 percent and therefore must be more accurate than the BB or Jacobsen equations. In the work at Langley we have not been able to determine which formulation does give the most accurate heat capacities and generally consider the uncertainty in c_p to be that due to the total spread in values, or about 8 percent for c_p.

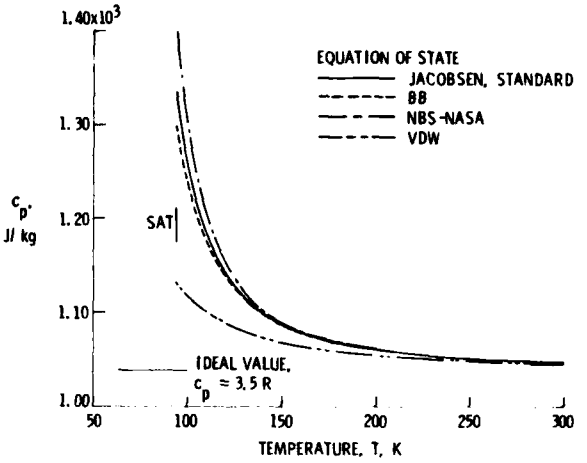

Figure 4.- Specific heat at constant pressure, c_p, for nitrogen gas at p = 5 atm. "SAT" denotes saturation temperature. The Jacobsen line is taken to be the accepted value.

The remainder of the comparison between the equations of state will involve the simulation of an isentropic expansion to a Mach number, M, of 1.5. The data will be presented in a fashion similar to that used by Adcock in his real-gas studies performed early in the Langley cryogenic wind tunnel program (ref. 7), where the ratio of the real-gas prediction of an expansion quantity such as p/p_t is divided by its ideal value predicted by a thermally (Z = 1.0) and calorically (γ = 1.4) perfect gas. The predictions of pressure, temperature, and density are shown in figures 5(a), 5(b), and 5(c) for isentropic expansions with total pressure, p_t, equal to 9.0 atm and for total temperatures, T_t, from 300 K down to saturation temperature for nitrogen gas. Once again, the VDW equation does not agree very well with the Jacobsen formulation. An interesting observation in all three of these figures is the good agreement between the BB and the Jacobsen formulations. The maximum differences over the temperature range between their respective real over ideal ratios are summarized below for both the 9 atm example shown in figure 5 and for a 1 atm case not shown:

p_t	$\frac{p}{p_t}$	$\frac{T}{T_t}$	$\frac{\rho}{\rho_t}$
1	.0001	.0002	.0002
9	.0003	.0002	.0014

The only difference of any magnitude occurs at p_t = 9 atm for the density ratio, where the difference is .0014, or 0.14 percent. Consequently, the BB formulation should be an excellent approximation to the very complex Jacobsen formulation over the temperature and pressure ranges of interest to cryogenic wind tunnels, which is a conclusion also reached by Wagner and Schmidt in reference 8. The new NBS-NASA and Jacobsen equations, however, do not compare as well. The maximum differences between their respective pressure, temperature, and density ratios are summarized next:

p_t	$\frac{p}{p_t}$	$\frac{T}{T_t}$	$\frac{\rho}{\rho_t}$
1	.0006	.0007	.0002
9	.0011	.0041	.0013

The largest differences here are in the temperature ratio. The NBS-NASA equation predicts noticeably smaller temperature deviations of up to 0.41 percent for the 9 atm example seen in figure 5(b).

The BB equation of state appears to be the best choice for an equation of state because it is still relatively simple - it has only five arbitrary constants - and compares very favorably with the complete Jacobsen formulation. An advantage of the BB equation over Jacobsen's in wind tunnel data reduction is that the BB equation is a gas-only description of nitrogen. Consequently, no special arrangements are needed in data reduction if local temperatures fall below the vapor-pressure temperature. The NBS-NASA equation of state may prove to be a more accurate description of the gas than the Jacobsen or BB equation, but this is not known yet. While it was derived using sound speed data unavailable to either Beattie and Bridgeman or Jacobsen, it is not obvious that the NBS-NASA equation actually fits this new sound speed data any better than the previous formulations, as seen in reference 5. Because of this uncertainty and the added complexity of the NBS-NASA equation, the BB equation is preferred. The VDW equation is a big improvement over the ideal equation of state, but does not seem to warrant serious attention because the BB equation can be employed just about as easily as the VDW equation.

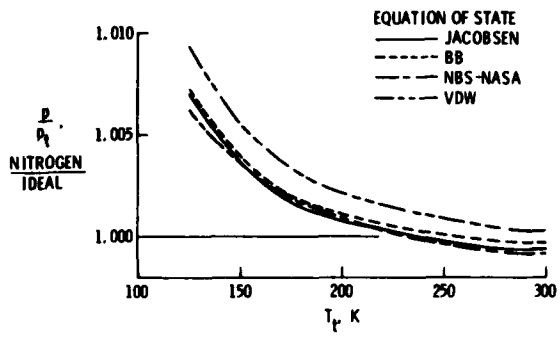

(a) Pressure

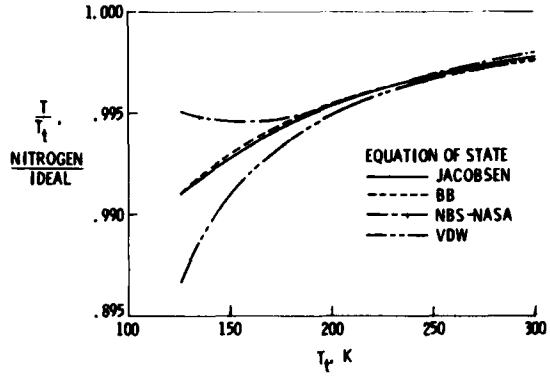

(b) Temperature

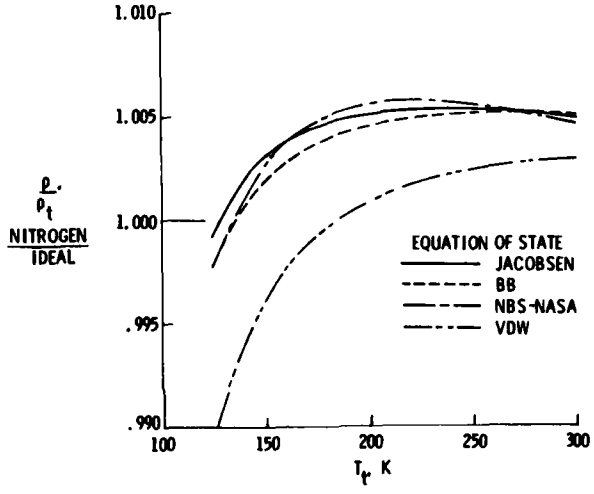

(c) Density

Figure 5.- Isentropic expansion ratios for nitrogen expanded to $M = 1.5$ at $p_t = 9.0$ atm. Ratios normalized by those of an ideal, diatomic gas.

4. HYBRID REAL-IDEAL CALCULATIONS

Many different investigators have done quick analyses of real-gas effects by substituting real-gas values of some parameter such as γ into equations derived on the assumption of a constant value of γ. While this is perhaps a natural first step in understanding real-gas effects, it is incorrect because equations such as that for the pressure ratio in an ideal isentropic expansion,

$$\frac{p}{p_t} = \left(1 + \frac{\gamma - 1}{2} M^2\right)^{-\frac{\gamma}{\gamma-1}} \tag{15}$$

are derived by assuming that the gas is thermally and calorically perfect. If the gas is not calorically perfect and c_p, c_v, and γ are functions of temperature, then Eq. (15) simply does not apply. In fact, any predictions of the magnitude of real-gas effects using real-gas values of parameters substituted into ideal equations are not simply incorrect but can be very misleading as seen in figure 6 taken from reference 7. In the figure it is seen that substituting the real-gas value of γ at 8 atm and 120 K, $\gamma = 1.565$, into Eq. (15) leads to a predicted pressure deviation of 6.2 percent at $M = 1.4$ instead of the actual departure, which is in the opposite direction, of about 0.7 percent.

5. MAGNITUDE OF REAL-GAS EFFECTS FOR NITROGEN

With the knowledge that the Beattie-Bridgeman (BB) equation of state agrees very well with the Jacobsen formulation, we will now focus on the magnitude of deviation of nitrogen from the behavior of an ideal, diatomic gas with $Z = 1.0$ and $\gamma = 1.4$. The

calculations shown are done with either the Jacobsen formulation or with the BB equation, depending primarily on who did the calculations and when. The type of flow processes examined include isentropic expansions, normal shocks, boundary layers, and shock wave-boundary layer interactions.

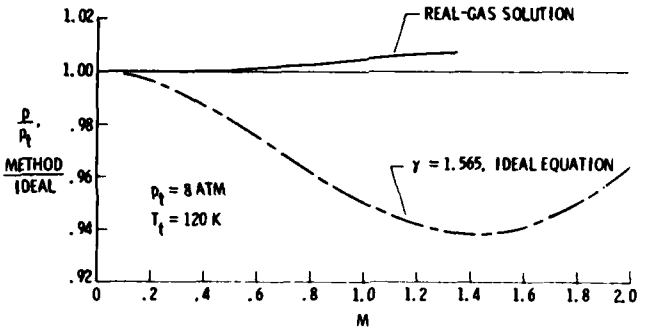

Figure 6.- Pressure ratios for isentropic flow in nitrogen as determined by various methods, relative to ideal, diatomic gas values with $\gamma = 1.4$. (Adcock, ref. 7).

The examination of isentropic flow expansions is carried out with the BB equation of state and assuming, as mentioned earlier, ideal values for the zero pressure heat capacities, c_p^o and c_v^o. Three total pressure values are considered - 1, 5, and 9 atm - and total temperatures are varied from 300 K down to temperatures below saturation temperature. The actual minimum temperatures shown are calculated based on the prediction of the onset of condensation effects due to homogeneous nucleation as reported by Sivier in reference 9. These minimum temperatures represent a lower temperature limit since the flow at any temperature lower would be likely to have undergone spontaneous nucleation and would not be very useful as a test gas. The entire subject of minimum operating temperature limits due to the onset of condensation effects will be discussed in detail in the paper entitled "Real-Gas Effects II - Influence of Condensation on Minimum Operating Temperatures of Cryogenic Wind Tunnels."

As in the previous section, the real expansion ratios of pressure, temperature, and density will be normalized by the comparable ideal expansion values. These three ratios are shown in figure 7 as a function of total temperature at total pressures of 1, 5, and 9 atm for isentropic expansions to M = 1.5. The pressure ratios show that departures up to 0.72 percent occur at the saturation temperature (labeled "SAT"), and can approach 1 percent at the total temperature (labeled "ONSET") corresponding to the

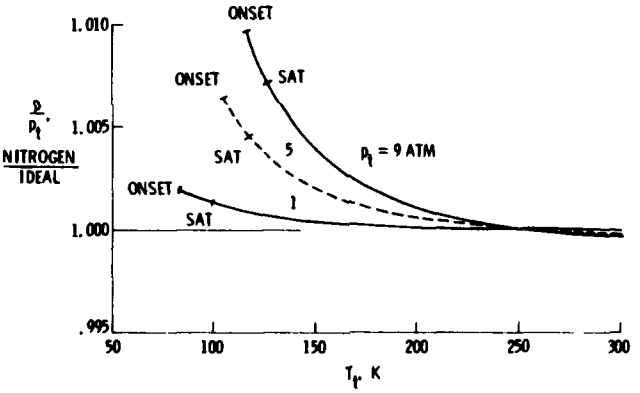

(a) Pressure

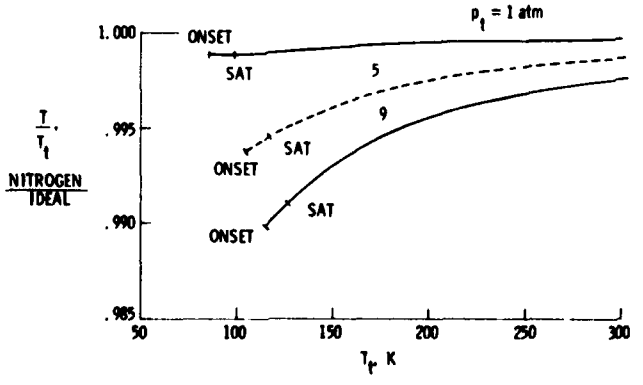

(b) Temperature

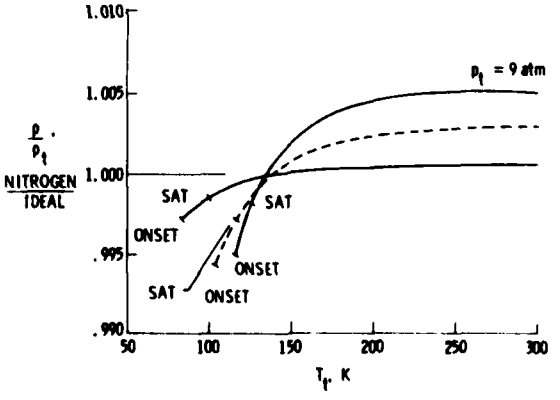

(c) Density

Figure 7.- Isentropic expansion ratios for nitrogen expanded to M = 1.5 using BB equation of state. "SAT" marks saturation temperature and "ONSET" marks possible onset of condensation effects.

possible onset of homogeneous nucleation. The deviations at the lower pressures of 5 and 1 atm deviate at most 0.64 and 0.19 percent before the onset of nucleation. Very similar magnitudes of deviations at low temperatures are shown for the temperature ratios in figure 7(b); however, deviations at 300 K are up to 0.25 percent for the 9 atm case and 0.13 percent for the 5 atm case. The density expansion ratios are shown in figure 7(c) and display somewhat different behavior than the pressure or temperature ratios. First, deviations for the 9 and 5 atm ratios at 300 K are 0.50 and 0.29 percent, respectively, and second, deviations at the low temperature boundary do not smoothly increase with pressure. At the temperatures predicted for the onset of homogeneous nucleation, density effects for the 1, 5, and 9 atm lines are respectively 0.28, 0.58, and 0.51 percent.

The deviations from the ideal, diatomic values for isentropic expansions do not appear to be of a magnitude to be of concern except perhaps at the 9 atm case when attempting to run below the saturation temperature. At these conditions pressure deviations can run as high as 1 percent and a data correction procedure may be appropriate in conjunction with a real-gas formulation. A more complete description of the isentropic expansion process is included in reference 7 by Adcock. Since the Jacobsen formulation gives liquid properties at supercooled values of pressure and temperature, Adcock's study was limited to temperatures above those for saturation.

The next flow process to be discussed is that of real-gas nitrogen passing through a normal shock. In this example, ratios of various quantities across the shock will be given as normalized by the shock flow of an ideal, diatomic gas with $Z = 1.0$ and $\gamma = 1.4$. The figures are taken from reference 7 by Adcock and show effects down to the appropriate saturation temperature. Adcock utilized the Jacobsen formulation to make these normal shock calculations. Upstream and downstream quantities are subscripted respectively by "1" and "2."

The differences in static pressure, temperature, and density ratios are shown in figure 8 for an upstream total pressure of 8 atm, upstream total temperatures from 300 K down to saturation temperature, and upstream Mach numbers, M_1, of 1.4, 1.7, and 2.0. (While not shown here, Adcock includes further figures showing that the effects of pressure are roughly proportional to the operating pressure. In other words, effects at 4 atm would be approximately half of those shown in the present example of 8 atm.) As seen in figure 8(a), $M_1 = 1.7$ gives the greatest deviations in pressure ratio between real and ideal flow - a value of 0.56 percent at saturation temperature. The deviations in static temperature ratio are seen in figure 8(b) to reach 0.52 percent at $M_1 = 2.0$ while deviations in static density ratios reach a maximum of 0.38 percent at 250 K for $M_1 = 2.0$.

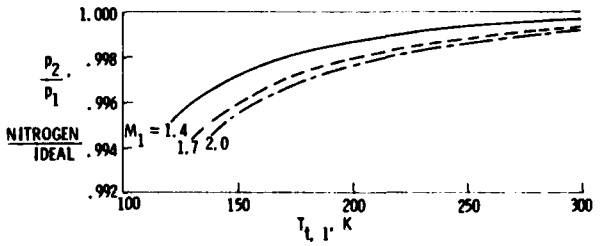

(a) Pressure

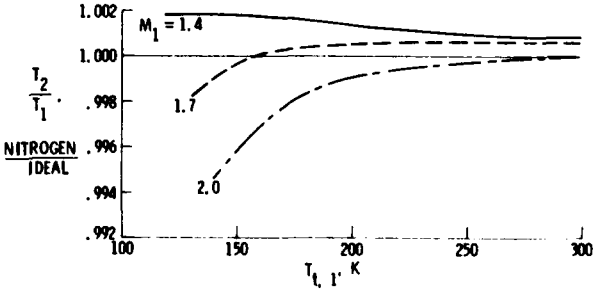

(b) Temperature

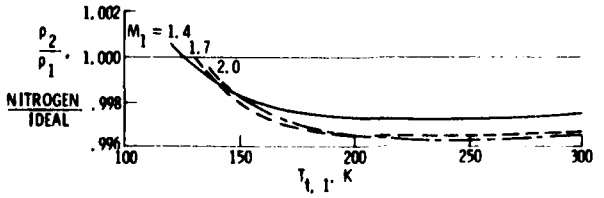

(c) Density

Figure 8.- Static ratios across a normal shock in nitrogen gas for various upstream Mach numbers, M_1. p_t = 8 atm. (Adcock, ref. 7).

The ratios of total pressure, temperature, and density across the normal shock are shown in figure 9 for the same upstream Mach numbers and total pressure of 8 atm. The maximum deviation of 0.22 percent for total pressure ratio occurs at about 275 K for the $M_1 = 2.0$ example. The maximum total temperature ratio departure is about 1.38 percent at saturation temperature for $M_1 = 2.0$. A maximum deviation in the total density ratio occurs near room temperature for $M_1 = 2.0$ and is 0.33 percent.

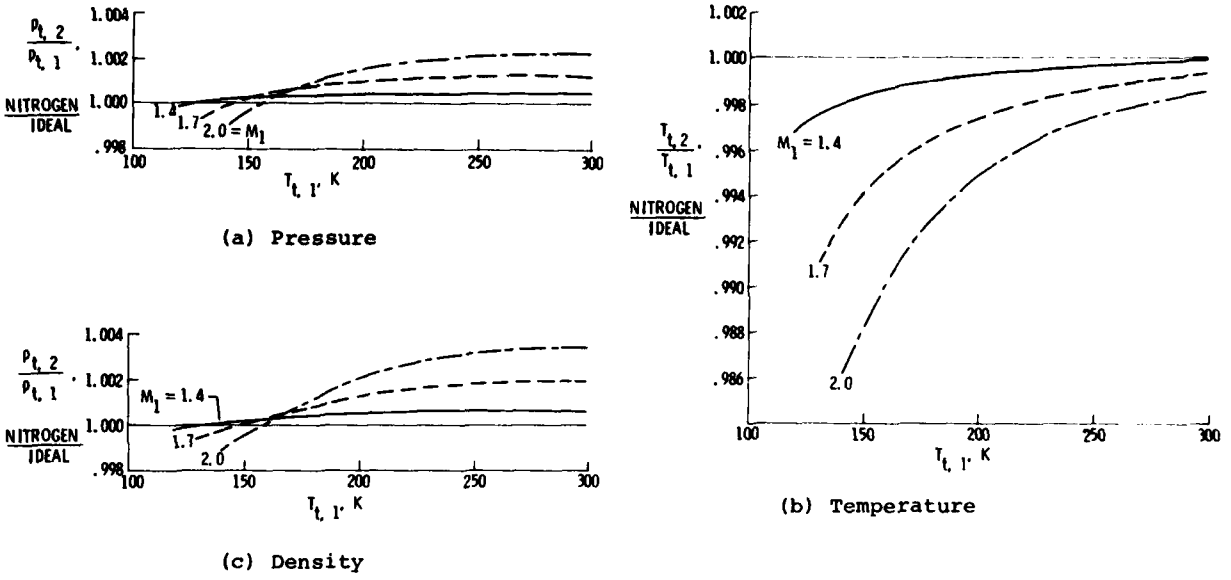

Figure 9.- Total ratios across a normal shock in nitrogen gas for various upstream Mach numbers, M_1. p_t = 8 atm. (Adcock, ref. 7).

The last figure in this series is figure 10 and shows the ratio of the real to ideal values for downstream Mach number, M_2, as a function of total temperature for an upstream Mach number, M_1, of 2.0 and a total pressure of 10 atm. The departure from the ideal value is seen to be less than 0.08 percent.

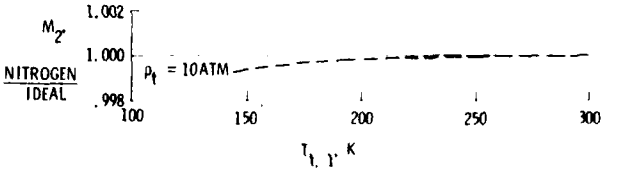

Figure 10.- Mach number downstream, M_2, of normal shock in nitrogen gas. M_1 = 2.0, p_t = 8 atm. (Adcock, ref. 7).

Nitrogen gas appears to give a good simulation of normal shock flow. Deviations in the static pressure ratio are seen in figure 8(a) to reach 0.58 percent at the saturation temperature for a value of total pressure equal to 8 atm. If operation at 9 atm and at temperatures 10 K below saturation (corresponding to the predicted onset of homogeneous nucleation) is desired, this deviation could go up to about 0.9 percent. The departures in static temperature are of the same magnitude as pressure while departures in static density appear to be less. The departures of the ratios of total pressure and density are not significant, but there are relatively large differences in the ratio of total temperatures. A difference in this quantity is not considered significant for most data of interest. None of the above differences appear to influence the downstream value of Mach number.

An additional comment should also be made before leaving normal shock flows. In showing real-gas effects for shock flows, some have chosen to calculate

$$\% \text{ Deviation} = \frac{\rho_{2_{real}} - \rho_{2_{ideal}}}{\rho_{2_{ideal}}} \qquad (16)$$

for given static values of upstream pressure, p_1, and temperature, T_1. The problem with this approach is that by specifying p_1 and T_1 for both the ideal and real cases, very different values of ρ_1 will be required because of the compressibility, Z, of nitrogen shown in figure 2. For example, for an upstream static condition of 5 atm and 120 K, figure 2 shows a difference in density, ρ_1, of 6 percent between the ideal-gas value and the Jacobsen value. Consequently, even if the ρ_2/ρ_1 ratios for the ideal and real shock flows were identical, Eq. (16) would still suggest a difference of 6 percent. Instead of being an indicator of the real-gas behavior of nitrogen through a shock, equations like number (16) may just be showing the influence of a parameter such as compressibility.

The next major flow problem discussed is that of boundary layer simulation over a flat plate. This section will draw from work by Adcock and Johnson in reference 10 that utilizes the Jacobsen formulation. As Adcock and Johnson mention, in boundary layer calculations not only is the equation of state important, but the expression for viscosity is important also. The expression for the viscosity of nitrogen used at the Langley Research Center comes from reference 4 and includes a total of nine constants in a low-density term and seven additional constants in what is called a dense-fluid contribution.

(The equation and accompanying constants are also described and discussed by Adcock in reference 7.) The real-gas parameters summarized in this report include displacement thickness, δ^*, boundary layer thickness, δ, skin friction, c_f, and boundary-layer momentum thickness, θ, for laminar and turbulent adiabatic boundary layers. Also shown will be the real to ideal ratios for static quantities such as T, H, and ρ.

The parameters δ^*, δ, c_f, and θ for laminar, adiabatic boundary layers on a flat plate are summarized in figure 11 and are shown normalized by values calculated for an ideal, diatomic gas obeying Sutherland's formula for viscosity. Figure 11(a) shows these parameters as a function of total pressure, and surprisingly, the maximum deviation in δ^* from the ideal case occurs at the lowest total pressure. This unexpected result is explained in detail by Adcock and Johnson and is the result of compensating real-gas effects between the thermal and caloric imperfections of the nitrogen gas and the change with increasing pressure in the slope of viscosity as a function of temperature. (This observation was made earlier by Wagner and Schmidt in reference 8.) The same four parameters are shown as a function of M_∞ in figure 11(b). In this case, effects generally grow with increasing M_∞. The deviation for δ^* is seen to be 1.34 percent for $M_\infty = 2.0$, $p_t = 9.0$ atm, and $T_t = 150.0$ K. Similar results are found in figure 12 for the turbulent, adiabatic boundary layer on a flat plate except that the magnitudes of the deviations are generally less than those for the laminar boundary layer.

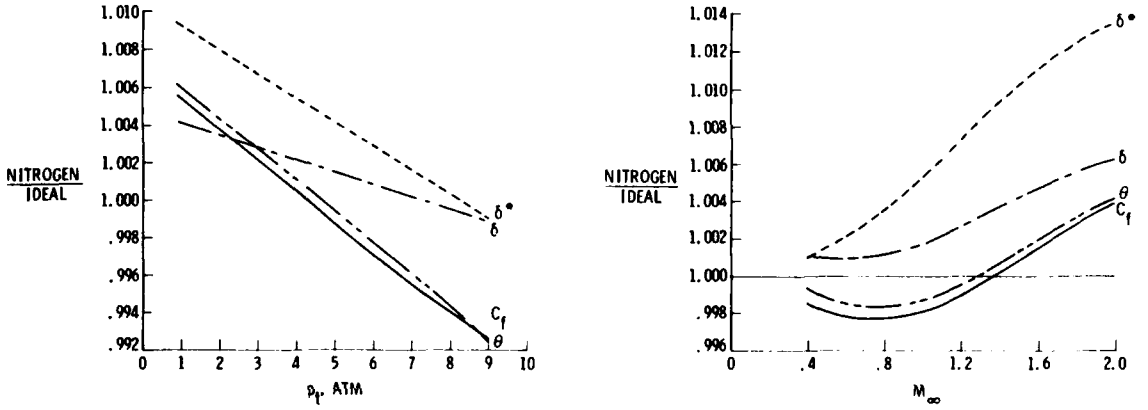

(a) As a function of p_t, $M_\infty = 0.85$, $T_t = 120$ K.

(b) As a function of M_∞, $p_t = 9$ atm, $T_t = 150$ K.

Figure 11.- Relative values of parameters for adiabatic, laminar boundary layers on a flat plate for nitrogen gas. (Adcock and Johnson, ref. 10).

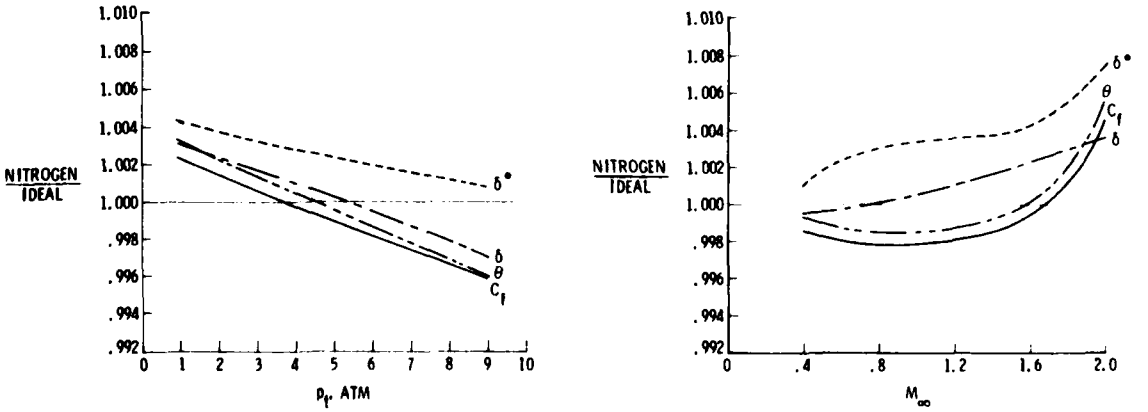

(a) As a function of p_t, $M_\infty = 0.85$, $T_t = 120$ K.

(b) As a function of M_∞, $p_t = 9$ atm, $T_t = 150$ K.

Figure 12.- Relative values of parameters for adiabatic, turbulent boundary layers on a flat plate for nitrogen gas. (Adcock and Johnson, ref. 10).

Next, ratios of static quantities will be summarized for both the laminar and turbulent boundary layer profiles. The results for the laminar boundary layer are shown in figure 13(a). The velocity ratios are not shown because the agreement is so good the ratio does not differ from the value 1.0 to the scale of this plot. The only large deviation, 2 percent, occurs for static temperature but does not appear to be of consequence according to Adcock and Johnson. The similar plot for the turbulent

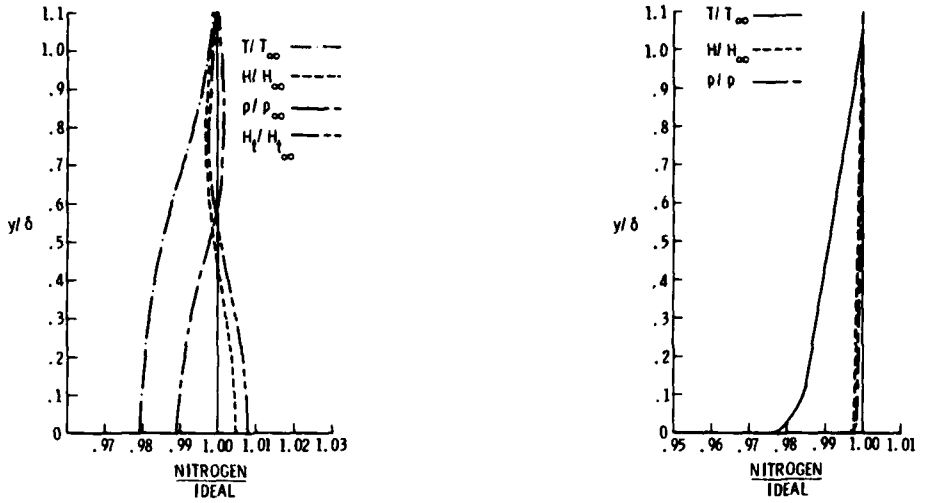

(a) Laminar

(b) Turbulent

Figure 13.- Relative adiabatic profiles for nitrogen gas flow over a flat plate. $M_\infty = 0.85$, $p_t = 9$ atm, $T_t = 120$ K, $R_x = 140 \times 10^6$. (Adcock and Johnson, ref. 10).

boundary layer is shown in figure 13(b). The agreement here is generally better than in the laminar case except for the temperature ratio. In this figure, velocity and total enthalpy are not plotted because of their excellent agreement with ideal values. Again, Adcock and Johnson found no significance to the temperature differences. None of the differences described for the flat plate work seem significant enough for concern about adequate boundary layer simulation.

The last analysis will consider the real-gas behavior of nitrogen in a shock wave-laminar boundary layer interaction problem. The results to be presented have been calculated by Wagner and Schmidt in reference 8 using the BB equation of state for nitrogen gas and a numerical program with a fine mesh description of the boundary layer region and a coarse mesh for the outer inviscid flow field. As a demonstration of the accuracy of the program, results using an ideal equation of state are compared to experimental data of Hakkinen and others (ref. 11) in figures 14 and 15 for an incident shock angle, ζ, of 32.6°. Real-gas calculations are made for upstream static conditions of $p_\infty = 1$ bar and $T_\infty = 78$ K, where 1 bar = 0.987 atm. The static conditions are at the saturation temperature for nitrogen and correspond to total conditions of 7.7 atm and 140 K. As shown in figure 14, the magnitude of differences between the ideal and real values of p/p_∞ is less than 0.4 percent and would seem to be quite acceptable given the total conditions of 7.7 atm and 140 K. It is interesting to note, as Wagner and Schmidt do, that the pressure deviations in the boundary layers (shown by the shaded area) correspond to the deviations of static pressure in the outer, inviscid flow (shown by the dotted line). The wall shear stress and the calculated differences are shown in figure 15. The maximum differences in wall shear stress seem to be on the order of 5 percent although it is not clear how much of that number is due to numerical scatter. (Further work on skin friction to reduce the numerical scatter may be desirable.) Given the good pressure agreement and fair agreement in skin friction, this flow process should not pose a problem for cryogenic nitrogen.

The study of cryogenic nitrogen as a wind tunnel test gas has indicated the following results. As shown by both the isentropic expansion analyses and the normal shock analyses, the only condition at which pressure ratios depart by more than 0.5 percent are at pressures greater than 5 atm combined with temperatures near or below saturation temperatures. With a total pressure of 9 atm and total temperatures below saturation, the pressure ratios may be in error by about a percent. If accuracies greater than this are required, either the temperatures below saturation will have to be avoided at high pressures or procedures will have to be devised to correct the data. The boundary layer analyses also show effects in displacement thickness as large as 1.34 percent for $p_t = 9$ atm and $M = 2.0$. At low temperatures and high pressures, the Reynolds number should be very large and the size of boundary layers about test models should be small compared to the thickness of the model. Consequently, the change in displacement thickness of 1.34 percent may not significantly affect the data because of the small size of the boundary layer to begin with. The differences of 2 percent in temperature profile through the boundary layer do not seem to affect other quantities and are not considered significant. The shock wave - laminar boundary layer analysis of Wagner and Schmidt shows only small pressure differences due to the real-gas nature of nitrogen. While they do show possible differences in c_f of about 5 percent, given the uncertainty in the magnitude of numerical scatter in this calculation and given the uncertainty in measuring c_f in the wind tunnel, any differences in c_f may never be apparent. Further analysis, nevertheless, of the differences in c_f may be worthwhile to verify the magnitude found by Wagner and Schmidt.

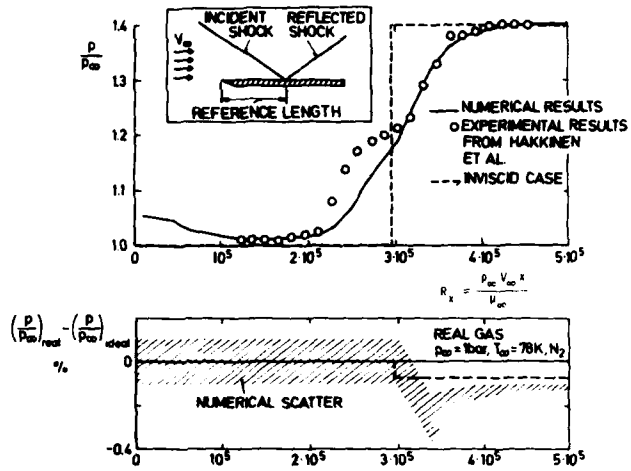

Figure 14.- Pressure distribution for shock wave and boundary layer interaction, $R_x = 2.96 \times 10^5$, $M_\infty = 2.0$, $\zeta = 32.6^o$. (Wagner and Schmidt, ref. 8, reprinted with permission of AIAA.)

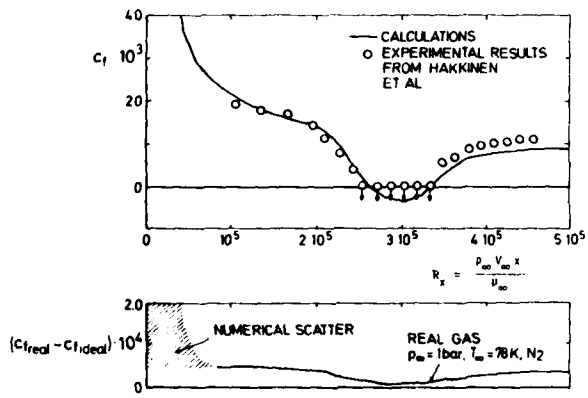

Figure 15.- Wall shear stress for shock wave and boundary layer interaction, $R_x = 2.96 \times 10^5$, $M_\infty = 2.0$, $\zeta = 32.6^o$. (Wagner and Schmidt, ref. 8, reprinted with permission of AIAA.)

6. ALTERNATE CRYOGENIC GASES

While the greatest attention has been on nitrogen as a test gas for transonic cryogenic tunnels, other gases are either being used or have been considered as alternatives. Cryogenic blowdown facilities such as those of McDonnell-Douglas in California cool dry air down to cryogenic temperatures by injecting an almost equal mass of liquid nitrogen and, consequently, test with an air-nitrogen mixture. To get an idea of the possible behavior of this mixture, an isentropic expansion will be modeled with a Beattie-Bridgeman (BB) equation of state supplied with appropriate constants for air. Further interest has also surfaced from time to time in using alternate gases that have significantly lower liquefaction temperatures than nitrogen in order to be able to test at larger unit Reynolds number. Helium and hydrogen are gases that come to mind because at 1 atm helium boils at 4.3 K and hydrogen at 20.4 K. Helium will also be examined using a BB equation of state, but because of some thermodynamic anomalies to be explained later, the BB equation of state for hydrogen would probably not be appropriate for describing cryogenic tunnel use of hydrogen. However, this report will draw upon work by Haut reported in reference 12 to describe the simulation properties of hydrogen.

The first alternate gas to be discussed is air. Since air is approximately 80 percent nitrogen, the two gases would be expected to have very similar properties. To see whether this is true or not, the isentropic expansion ratios of pressure, temperature and density will be normalized to the ideal diatomic values ($Z = 1.0$ and $\gamma = 1.4$) in a manner similar to figure 7. The constants used in the BB equation of state for air are found in reference 2 and are repeated below in SI units:

A_o = 168.01 $N \cdot m^4/kg^2$

a = .0006893 m^3/kg

B_o = .001646 m^3/kg

b = -.0003930 m^3/kg

c = 1549. m^3K^3/kg

The corresponding graphs for air are shown in figure 16, where the values are plotted from 300 K down to saturation temperature. As seen by comparing figures 16 to 7, there are only very small differences in pressure ratios between the real-gas performance of nitrogen and air. In fact, for a total pressure of 9 atm and a total temperature of 135 K, air departs from an ideal gas by 0.74 percent while nitrogen departs by 0.65 percent. Similarly when comparing the temperature or density ratios, there are again only small differences between nitrogen and air. The air results are plotted only down to saturation temperatures because, as explained in the companion report, air is not expected to undergo much cooling below saturation before the predicted onset of condensation effects. On the basis of this brief examination of isentropic expansions, air would indeed be an acceptable cryogenic test gas although it does show slightly more deviation than nitrogen at a given total temperature. Consequently, a tunnel using half air and half evaporated liquid nitrogen should experience no difficulties because the real-gas deviations should be somewhere between those predicted for pure nitrogen and those predicted for air. (The reason nitrogen is preferred over air for continuous flow, fan-driven tunnels injecting a liquid cryogen for cooling is the availability of liquid nitrogen, the safety of using liquid nitrogen over using liquid air, and the lower saturation temperatures associated with pure nitrogen.)

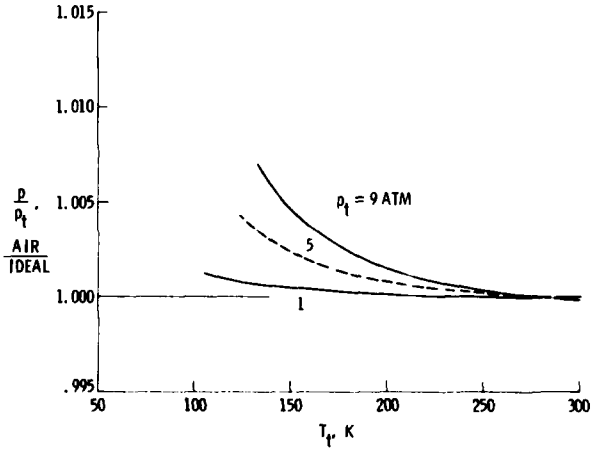

(a) Pressure

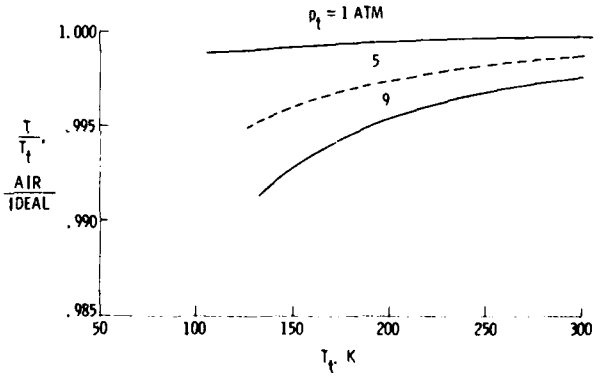

(b) Temperature

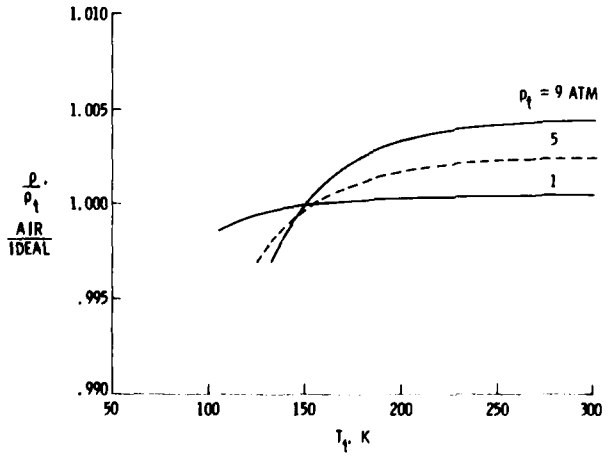

(c) Density

Figure 16.- Isentropic expansion ratios for air expanded to M = 1.5 using BB equation of state.

As a first candidate for cryogenic operation at temperatures much colder than is possible for nitrogen, helium is examined by using the following constants from reference 2 in the BB equation:

$$A_o = 2.79\ N \cdot m^4/kg^2$$

$$a = 0.002136\ m^3/kg$$

$$B_o = 0.0004998\ m^3/kg$$

$$b = 0.\ m^3/kg$$

$$c = 1.43\ m^3K^3/kg$$

The specific gas constant is taken to be 2077.3 J/(kg·K). The results of the analysis are shown in figure 17, which shows pressure, temperature, and density ratios as a function of Mach number, M, for two sets of total conditions. The first set is for a total pressure of 1 atm and a total temperature of 300 K, where helium acts like an ideal monatomic gas with $\gamma = 1.67$. The second set is for a total pressure of 9 atm and a total temperature of 30 K and should be indicative of pressure and temperature effects. As is easily seen in all three ratios, the differences in helium due to increased pressure or reduced temperature are insignificant compared to the fundamental differences between monatomic helium and an ideal, diatomic gas with $\gamma = 1.40$. The pressure ratio differs from an ideal, diatomic value by 6 percent at $M = 2.0$ after passing through a maximum deviation of about 10 percent at $M = 1.4$, while the temperature and density ratios are in error by about 23 percent at $M = 2.0$. These deviations are over an order of magnitude larger than those calculated for nitrogen or air. In addition, since the pressure ratio is in error by more than 1 percent at $M = 0.3$, the usefulness of using helium as a transonic test gas would have to be seriously questioned. There may be applications for helium, nevertheless, in very low speed flow that is sometimes appropriate for industrial aerodynamics.

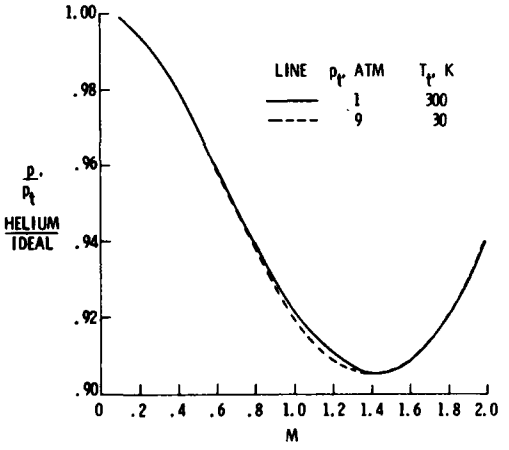

(a) Pressure

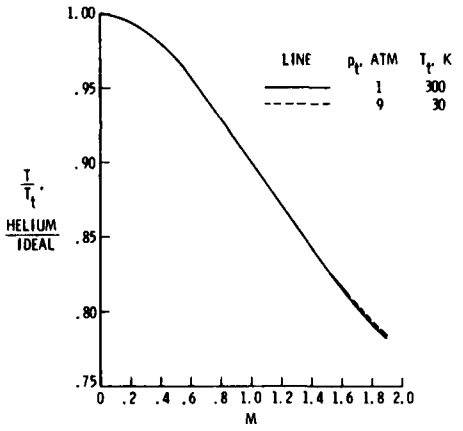

(b) Temperature

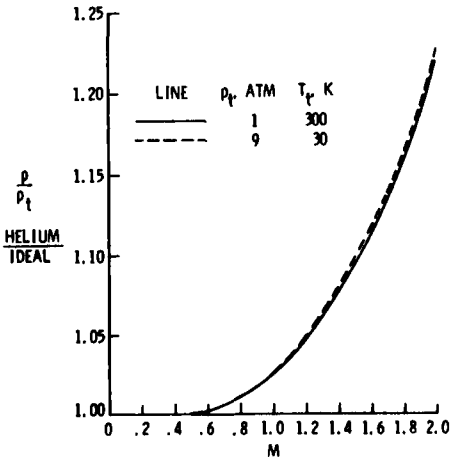

(c) Density

Figure 17.- Isentropic expansion ratios for helium as a function of M using BB equation of state. Ratios normalized by those of an ideal, diatomic gas.

Since helium does not appear to be useful as a transonic test gas, attention may be turned to hydrogen because of its low boiling temperature compared to nitrogen and because hydrogen, too, is diatomic. Unfortunately, the BB constants available in the literature would probably give an incorrect description of hydrogen as used in cryogenic tunnels because the constants as found in reference 2 are probably for orthohydrogen, which is the equilibrium state for ambient temperature hydrogen gas. In most cryogenic concepts, the test gas is formed by evaporation from the liquid state, which for hydrogen with its nuclear spin anomaly corresponds to parahydrogen. Consequently, as used in wind tunnels, hydrogen would be in the parahydrogen form with its antiparallel spins as explained in detail by Haut in reference 12. The equation of state used by Haut was of a polynomial interpolation form. Using this equation of state he simulated various flow processes, of which the isentropic expansion results will be summarized herein. The pressure, temperature, and density ratios for an expansion to $M = 1.0$ are shown in figure 18. As is readily apparent, parahydrogen does not appear to give a good simulation of ideal, diatomic flow. The deviations in pressure ratio are approximately 8 percent at low temperatures, deviations in temperature ratio are about 10 percent, and deviations in density are somewhat less with a value of about 4 percent. As in the case of helium, there may be applications for hydrogen in industrial aerodynamics, but anyone interested is urged to study reference 12, with particular attention to power requirements and safety considerations.

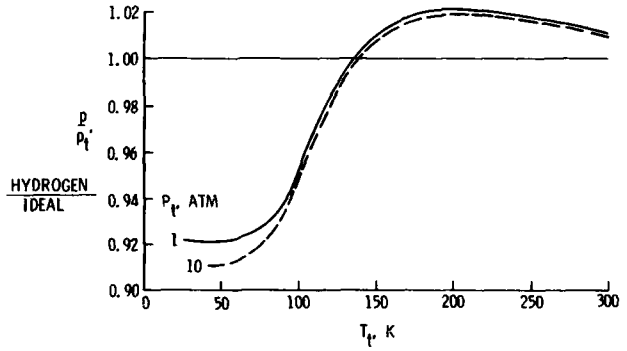

(a) Pressure

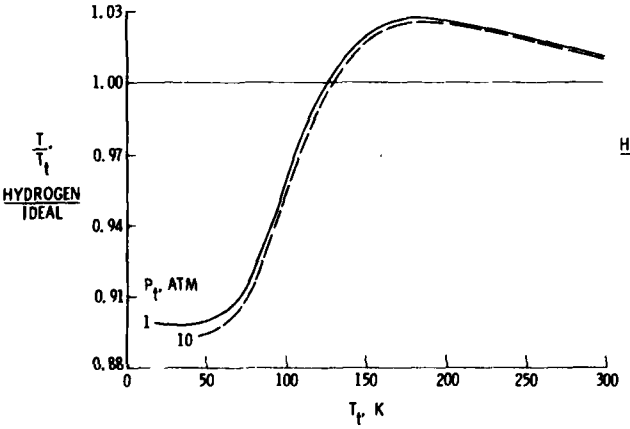

(b) Temperature

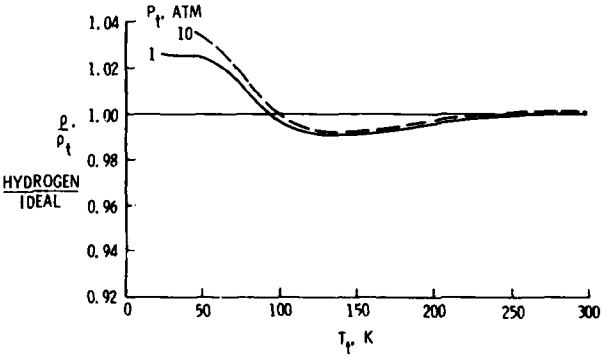

(c) Density

Figure 18.- Isentropic expansion ratios for parahydrogen expanded to $M = 1.0$. (Haut, ref. 12).

In this brief discussion of alternative cryogenic gases other than nitrogen, it appears that air (or an air-nitrogen mixture) will be a satisfactory cryogenic test gas on the basis of isentropic expansion analysis. Perhaps more analysis of air to include a look at normal shocks and boundary layer behavior would put to rest any questions that may remain about this test gas. It appears that both helium and parahydrogen will not be good test gases for compressible flow. Both of these gases exhibit large deviations from the isentropic flow of an ideal, diatomic gas with $Z = 1.0$ and $\gamma = 1.4$.

7. CONCLUSIONS

It is necessary to be aware that nitrogen gas, as well as other possible test gases, does depart from ideal values for thermodynamic properties such as compressibility, Z, and ratio of specific heats, γ, at low temperatures. However, as shown in this paper and

the reports referenced, the deviations in Z and γ do not necessarily impact on the ability of nitrogen gas to simulate flow of an ideal, diatomic gas with $Z = 1.0$ and $\gamma = 1.4$. In order to examine the simulation qualities of nitrogen, it is necessary to do a complete real-gas analysis. Substituting real values of Z or γ into ideal equations derived with the assumption that Z or γ are constant is incorrect. When a complete real-gas analysis is done for nitrogen gas, only small deviations are seen between nitrogen gas and an ideal, diatomic gas for isentropic expansions, normal shocks, boundary layers, and shock wave-boundary layer interactions. In fact, the only minimum operating temperature restriction that these real-gas effects may impose occurs at operating total pressures of about 9 atm, where the pressure ratio deviations can go as large as 1 percent if the total temperature is taken to be 10 K below the saturation temperature. If this magnitude of deviation is too large, the total temperatures at pressures close to 9 atm may have to be restricted to be at or above the saturation temperature.

Alternate gases have also been briefly investigated. Air appears to be almost as good as nitrogen in simulating an ideal, diatomic gas; consequently, minimum operating temperatures should not be limited by the behavior of gaseous air except, as in the case of nitrogen, perhaps at total pressures approaching 9 atm and at saturation temperatures. On the other hand, helium and parahydrogen do not satisfactorily simulate compressible ideal, diatomic flow. They would not make good transonic test gases.

8. REFERENCES

1. Samuel Glasstone, Textbook of Physical Chemistry, 2nd ed, New York, D. Van Nostrand Co., 1959, pp. 244-300.

2. James A. Beattie and Oscar C. Bridgeman, A New Equation of State for Fluids. II. Application of Helium, Neon, Argon, Hydrogen, Nitrogen, Oxygen, Air, and Methane. J. American Chem. Soc., Vol. 50, No. 12, Dec. 1928, pp. 3133-3138.

3. Richard T. Jacobsen, The Therodynamic Properties of Nitrogen From 65 K to 2000 K With Pressures to 10,000 Atmospheres, Ph.D. Thesis, Washington State Univ., 1972. (Available as NASA-CR 128526.)

4. R. T. Jacobsen, R. B. Stewart, R. D. McCarty, and H. J. M. Hanley, Thermophysical Properties of Nitrogen From the Fusion Line to 3500 R (1944 K) for Pressures to 150,000 psia (10 342 x 10^5 N/m^2), NBS Tech. Note 648, U. S. Dep. Com., Dec. 1973.

5. Ben Younglove and R. D. McCarty, Thermodynamic Properties of Nitrogen Gas Derived From Measurements of Sound Speed, NASA Reference Publication 1051, Dec. 1979.

6. R. D. McCarty, Determination of Thermodynamic Properties From the Experimental p-v-T Relationships, Experimental Thermodynamics. Volume 2 - Experimental Thermodynamics of Non-Reacting Fluids, Butterworth & Co., Ltd., c.1975, pp. 501-526.

7. Jerry B. Adcock, Real-Gas Effects Associated with One-Dimensional Transonic Flow of Cryogenic Nitrogen, NASA TN D-8274, Dec. 1976.

8. B. Wagner and W. Schmidt, Theoretical Investigations of Real Gas Effects in Cryogenic Wind Tunnels, AIAA Journal, Vol. 16, No. 6, June 1978, pp. 580-586.

9. Kenneth D. Sivier, Digital Computer Studies of Condensation in Expanding One-Component Flows, ARL 65-234, U. S. Air Force, Nov. 1965. (Available from DDC as AD 628 543.)

10. Jerry B. Adcock and Charles B. Johnson, A Theoretical Analysis of the Simulation of Boundary Layers in Cryogenic Nitrogen Wind Tunnels, NASA TP-1631, 1980.

11. R. J. Hakkinen, I. Greber, L. Trilling, and S. S. Abarbanel, Interaction of an Oblique Shock Wave with a Laminar Boundary Layer, NASA Memo 2-18-59W, 1959.

12. Richard C. Haut, Evaluation of Hydrogen as a Cryogenic Wind Tunnel Test Gas, NASA CR-145186, April 1977.

9. ACKNOWLEDGEMENTS

The author would like to thank his colleague at NASA-Langley Research Center, Mr. Jerry B. Adcock, for his very helpful discussions during the preparation of this text.

PROPERTIES OF MATERIALS:

THE EFFECT OF LOW TEMPERATURES ON THE STRENGTH AND TOUGHNESS OF MATERIALS

by

D.A. Wigley
Lecturer in Mechanical Engineering
and
Consultant to the Institute of Cryogenics
Engineering Faculty, The University of Southampton,
Southampton, SO9 5NH, England

Summary

The factors which influence the stiffness, strength and toughness of materials at low temperatures are considered in terms of the overriding design requirement that a load bearing structure must have adequate toughness at low temperatures and be compatible with its environment. The relative sensitivity of each major parameter to changes in the structure and purity of a material is discussed in the context of the degree of reliability that can be placed on data taken from the literature. Yield and plastic deformation are highly structure sensitive and the effect of crystal structure is discussed at length. Design data is given for copper-, nickel- and aluminium-based alloys, which together with Invar and the autenite stainless steels all have face-centred-cubic structures. The problems caused by the ductile-brittle transition in metals with body-centred-cubic structures are outlined, and the use of low alloy and nickel steels in the temperature range 300K - 70K is discussed. Fracture toughness is considered in the context of its use in promoting fail-safe design techniques under steady and alternating loads, and other relevant low temperature failure modes are also discussed.

The properties and use of non-metallic materials at low temperatures are considered with particular reference to their liability to embrittlement and thermal shock and also to the incompatibility of most hydrocarbon-based polymers with liquid oxygen. The use of polymers as adhesives, and in particular fluorocarbons such as P.T.F.E. for seals and gaskets is outlined together with an indication of their roles in the form of fibres, film and foams. Finally the properties of composites such as glass fibre reinforced plastics are discussed with a view to exploiting the very high ratios of strength to thermal conductivity that can be achieved from GRPs.

1. Introduction

One of the principal design requirements of any piece of equipment is that it should have adequate stiffness, strength and toughness to withstand safely any load or stress that may be applied to it. Operation at low temperatures effectively increases the requirement for adequate toughness at the operating temperature,as virtually all materials are both stiffer and stronger at low temperatures than an ambient. A load-bearing structure must, therefore, be able to cope with not only the static and dynamic stresses which can be predicted for normal operation, but also the thermal shocks it may be subjected to on cool down, the thermal stresses induced by differential expansion during warming and cooling cycles as well as the accidental overstresses or impact loads that it may receive in the presence of the scratches and dents it is liable to suffer during service.

Most materials are designed to operate within their elastic limits and typical stress and deflection formulae require the use of appropriate values for the elastic constants such as the Youngs, Shear and Bulk modulii as well as on occasions, Poissons ratio. Fortunately, the elastic constants are relatively insensitive to structure variations such as changes in grain size, the degree of cold working, heat treatment and small compositional variations etc., while decreasing the temperature in general increases Youngs modulus by about 10% between 300K and 80K. Accuracies greater than about 1% are rarely required in the calculations normally used to avoid buckling failure (elastic instability) or excessive elastic deformation (jamming) and thus values taken from the literature can be used with a reasonably high degree of confidence.

Yield and plastic deformation in metals are processes strongly influenced by their structure and condition to such an extent that accurate predictions are difficult and experimentally determined data invaluable. General classification of their properties is best started by considering their crystal structures, most metals and alloys having face-centred-cubic, body-centred-cubic or hexagonal-close-packed lattices. Of these the face-centred-cubic metals are greatly to be preferred for low temperature use as almost without exception their strengths, ductility and toughness all improve as the temperature falls, thus making them ideal for cryogenic applications. F.c.c. copper-, nickel-, and aluminium-based alloys, together with Invar and the austenitic stainless steels are, in fact, the metals most widely used for the construction of equipment operating below about 150K. Of the hexagonal-close-packed metals only magnesium and titanium are used in significant quantities below room temperature, the high specific

strengths offered by titanium alloys being particularly attractive for certain specialised applications in the aerospace industry.

It is the body-centred-cubic group of metals that offer the greatest challenge but which constitute the greatest risk as they almost all undergo a transition from ductile to brittle behaviour at some temperature, usually below ambient. Furthermore, small changes in their chemical composition, grain size, the degree of plastic constraint brought about by a notch or flaw, and even the rate at which a load is applied, can all have a marked effect on the delicate interrelationship between strength, toughness and the temperature at which the ductile-to-brittle transformation occurs. As, however, the economically irreplaceable ferritic steels have b.c.c. structures, their use at low temperatures cannot be precluded and it is necessary to define the temperature and stress limits to which a certain grade, thickness and condition of steel may be safely used. These limitations are traditionally laid down by codes of practice issued by independent bodies such as the American Society of Mechanical Engineers, government agencies such as the British Standards Institution, local or national Insurance agencies or even state regulatory authorities, and there are very few load bearing structures which can be built without conforming to one or more such codes. There is also, however, an increasing and very welcome tendency towards backing up these codes by a scientifically rigorous failure analysis based on the concepts of fracture mechanics - a study of the resistance offered by a material to the continued propagation of a crack nucleating in the vicinity of a sharp crack. Such analyses are also applicable to high strength alloys with f.c.c. and h.c.p. structures, as well as to the rate at which cracks propagate during fatigue and so constitute a powerful analytical technique which the aerospace industry in general was quick to develop and exploit.

Non-metallic materials have much more complex structures than metals and the amorphous and microcrystalline structures typically found in glasses and ceramics almost invariably make them brittle because they are unable to accommodate the plastic deformation needed to relieve the high stress concentrations which build up around small flaws. They are thus much stronger in compression than in tension but are rarely used in the bulk form even under compressive loadings because their poor thermal conductivities and consequent liability to thermal shock make them liable to shatter. However, in the finely divided form of fibres, powders, films, foams and expanded granules they are widely used for thermal and electrical insulation at low temperatures.

Polymeric materials can be divided basically into two structural categories; the thermoplastics and the thermosets. The long chain molecular structures of thermoplastics give them mechanical properties which are strongly dependent on the temperature and rate at which they are stressed. Furthermore, an increase in their intermolecular forces over a temperature range known as the glass transition, which may be above or below ambient, means that most thermoplastics undergo a reversible transition to a glass-brittle state in which they are unable to deform plastically. As their glass transition temperatures are all above 150°K there are no thermoplastics which exhibit any really significant degree of ductility below this temperature. It is, therefore, highly fortuitous that the molecular chain structure of polytetrafluoroethylene, and to a lesser extent, its cousin polychlorotrifluoroethylene, is such as to reduce the severity of their glass transitions and so give them a small, but nevertheless, usable measure of ductility even down to liquid helium temperatures. Add to this the bonus that these are among the few polymers to be fully compatible with liquid oxygen, it can be appreciated that these polymers are invaluable for use as gaskets and seals in cryogenic applications.

Thermosetting polymers have a network structure which renders them brittle and they are thus rarely used in the unfilled state. However, when combined with suitable fillers their toughness is greatly improved and phenolic-impregnated cloths and papers (such as Tufnol and Paxolin) are particularly useful for the fabrication of load-bearing, electrically-insulating fitments.

The remaining major group of materials of interest for low temperature applications are the high performance composites formed by the incorporation of glass or carbon fibres in matrices of thermosetting polymers. For most aerospace applications their attraction lies in their high specific strengths and stiffnesses, and these characteristics improve at low temperatures but not, perhaps, so markedly as those of metals. The major interest in glass-reinforced plastics for low temperature applications comes, as noted earlier, from their very high strength/thermal conductivity ratios which make them ideal for use as load-bearing, thermally-insulating supports.

Finally, it must be noted that the construction of equipment for cryogenic operation is subject to the same economic constraints as any other project and thus when selecting materials for low temperature use their total cost must be considered. For example, the expense of forming, joining, inspecting and, if necessary, refinishing must be added to basic material cost. Furthermore, cryogenic applications rarely demand the repeated purchase of sizeable quantities of material and hence the required sizes and sections of particular alloy grades are not always readily available, and the luxury of being able to obtain exactly the ideal choice of material from a technical point of view is not always achievable.

2. Elastic Properties of Metals

As noted earlier, the elastic properties of most metals are remarkably insensitive to changes in purity and structure and hence data taken from the literature can be used

Table 1. Elastic properties of alloys used in the construction of cryogenic equipment
(E = Youngs Modulus, G = Shear Modulus, K = Bulk Modulus, ν = Poissons Ratio)

Material	Property (Modulus in GPa)	Magnitude at indicated temperature, (K) 300	250	200	160	120	90	70
Aluminium type 5083-0 (annealed)	E	71.6	73.7	75.8	77.5	78.9	79.9	80.3
	G	26.85	27.65	28.5	29.2	29.85	30.25	30.45
	K	71.5	72.2	72.9	73.38	73.8	74.05	74.2
	ν	.3334	.3302	.3267	.3243	.3218	.3204	.3195
Aluminium type 6061-T6	E	70.2	71.8	72.5	74.8	76.1	76.8	77.3
	G	26.35	27.2	27.9	28.4	28.7	29.0	29.1
	K	72.15	72.85	73.5	73.95	74.3	74.55	74.7
	ν	.3383	.3362	.3340	.3322	.3302	.3285	.3277
Invar	E	152.5	146.7	142.7	140.1	139.6	140	140.6
	G	55.8	54.7	53.35	52.35	51.5	51.0	50.7
	K	110.9	110.5	111.2	112.0	113.2	114.2	114.8
	ν	.2845	.2865	.2925	.2970	.3015	.3050	.3075
Stainless Steel type 316	E	203.8	208.0	212.0	215.1	217.8	219.3	220.1
	G	78.5	80.3	81.9	83.2	84.5	85.1	85.5
	K	167.6	168.7	169.6	170.2	170.5	170.3	170.1
	ν	.2974	.2946	.2918	.2895	.2872	.2855	.2845
Stainless Steel type 310	E	183.7	187.0	190.3	192.9	195.5	196.9	197.9
	G	70.2	71.6	73.0	74.1	75.2	75.8	76.3
	K	159.2	160.3	161.2	162.0	162.5	162.6	162.6
	ν	.3075	.3054	.3032	.3013	.2995	.2982	.2972
Stainless Steel type 304	E	189.3	193.7	197.2	200.3	202.8	204.0	204.6
	G	73.5	75.2	76.7	78.0	79.0	79.6	80.2
	K	150.6	151.9	152.9	153.6	153.9	153.9	153.3
	ν	.2901	.2875	.2848	.2828	.2807	.2792	.2775
9% Nickel Steel	E	195	197.5	200	201.9	203.5	204.5	205
	G	73.8	74.8	75.9	76.7	77.3	77.8	78.1
	K	154.8	155.8	156.7	157.3	158.0	158.3	158.5
	ν	.2860	.2844	.2828	.2817	.2808	.2802	.2798
3½% Nickel Steel	E	203.7	206.4	209	211.1	212.9	214.1	214.6
	G	79.1	80.2	81.4	82.2	83.0	83.5	83.8
	K	159.8	161.0	162.1	162.9	163.7	164.2	164.4
	ν	.2823	.2807	.2794	.2785	.2775	.2768	.2763

with a high degree of confidence. In the absence of any measured values for sub-ambient temperatures, a useful rule of thumb is to allow an increase of about 0.04% per K decrease in temperature for the elastic moduli of most metals and alloys. This rule would give a 9% increase in modulus on cooling from 300K to 70K, which puts it near the middle of the range of 5-15% found for most alloys. Furthermore, the change in modulus is a smooth function of temperature except in those alloys which undergo a crystallographic or magnetic transformation in the range concerned. Some indication of the validity of this rule of thumb may be gained by comparison with the data given in Table 1 for the elastic constants of some of the alloys most commonly used for the construction of low temperature equipment.

The design problems created at ordinary temperatures by the relatively low moduli of aluminium alloys when compared to either austenitic or ferritic steels are also encountered at low temperatures where stiffness is important. For example, where shell bending is a significant design limitation, as in a column subjected to a lateral air flow loading. In such cases, the higher modulii offered by, for example, the austenitic stainless or 9% nickel steels would allow either stiffer structures for the same section or thinner sections for the same thickness.

3. Yield and Plastic Deformation in Metals and Alloys with Face-Centred-Cubic Crystal Structures

a) Copper and Nickel Based Alloys

These alloys were widely used in the early days of low temperature physics because of a combination of wide availability and ease of machining into the complex shapes needed, but above all because of the reliability with which soft and hard soldered leak-free joints could be made. In fact, in applications such as paired tube and high

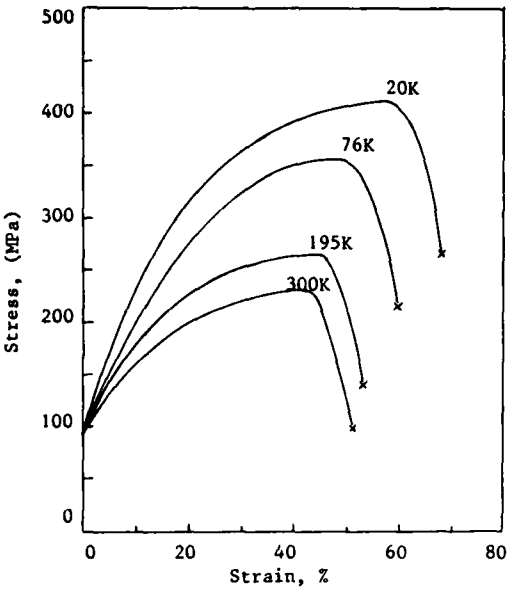

Fig.1 Stress-strain curves for O.F.H.C. copper tested at the indicated temperatures.

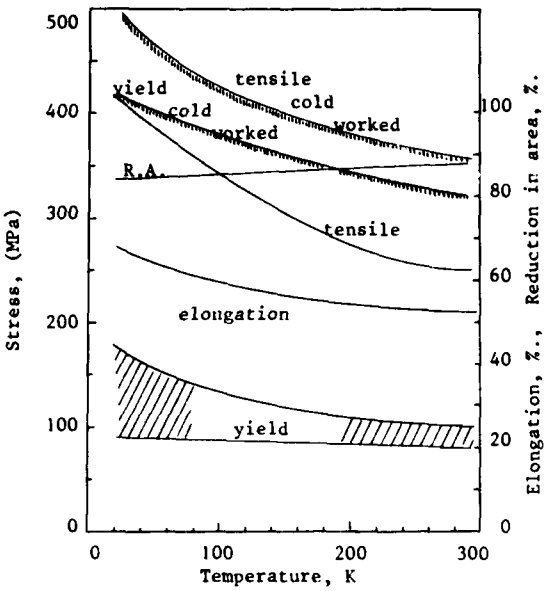

Fig.2 Effect of temperature on mechanical properties of annealed and cold worked copper

pressure heat exchangers where large numbers of joints have to be made, they are still the preferred material. In most cases, however, aluminium alloys and the austenitic stainless steels have replaced copper and nickel based alloys because of their relatively high cost. Nevertheless, it is instructive to start by considering the properties of copper because it demonstrates very clearly the basic characteristics of f.c.c. metals which make them so useful at low temperatures. In Fig.1 a series of engineering stress-strain curves are shown for oxygen-free high-conductivity copper tested at and below 300K. The following characteristic features should be noted.

i) Yield is a gradual process and the yield stress is relatively unaffected by changes in temperature.

ii) The strain hardening rate (slope of the stress-strain curve after yield), the ultimate tensile stress (maximum point in the curve) and the total plastic elongation all increase as the temperature falls. Thus the metal becomes both stronger and more ductile at low temperatures essentially because it is able to accommodate a greater degree of strain hardening before the onset of necking (plastic instability).

iii) The large drop oft in measured stress between the onset of necking and final failure is indicative of a large reduction in area and hence a very ductile type of fracture at all temperatures.

In Fig.2 this data is cross-plotted to illustrate more clearly how the major parameters vary with temperature. A band of values is given for the yield stress in order to represent the effects of impurity concentrations and residual stress levels normally found in commercially pure coppers, the purest samples having the lowest and least temperature-dependent yield stresses. Also shown in Fig.2 are the trends for samples which have been heavily cold worked and it can be seen that even in this condition the ultimate tensile stress increases more rapidly with decrease in temperature than does the yield stress. *It is this combination of increase in ductility and tensile strength, together with the relative temperature-insensitivity of the yield stress, that is the definitive characteristic of face-centred-cubic metals and alloys which makes them so eminantly suitable for use at low temperatures.*

As noted above the yield strength of commercially pure copper may be increased by work hardening but further gains can only be achieved by alloying. Copper-zinc alloys containing less than 39% Zn have an f.c.c. structure and these α-brasses are widely utilised for the construction of small cryogenic appliances, reference to the data given in Table 2 showing that the strengths and the ductilities of these alloys increase at low temperatures. Further improvements in strength can be achieved by cold working but only at the expense of a marked decrease in ductility at room temperature: even in the cold-worked state the ductility may be seen to improve at lower temperatures. Alloy concentrations in excess of 39% Zn give rise to α-β brass or Muntz metal which is

Table 2. Typical mechanical properties of some copper and nickel alloys.

Material and condition	Temperature (K)	Yield strength (MPa)	Tensile strength (MPa)	Elongation (%)	Reduction in area (%)	Impact energy (J)	Comments	Source
Oxygen-free, high-conductivity copper (annealed)	300 195 76	75 80 88	222 270 360	54 53 60	86 85 84	70.5 77 88	Charpy V (½ size)	NBS Monograph 63
70 Cu-30 Zn cartridge brass (annealed)	300 195 76	197 190 207	359 393 531	50 56 76	- - -	88 92 108	Izod	NBS Monograph 13
70 Cu-30 Zn cartridge brass (½ hard)	300 195 76	427 443 473	656 695 807	14 17 28	58 62 63	21 21 21	Charpy V	NBS Monograph 63
71 Cu-28 Zn-1 Sn Admiralty brass (annealed)	300 195 76	72 86 128	307 341 445	86 91 97	81 79 73	152 153 155	Charpy V	NBS Monograph 101
97.7 Cu-2 Be 0.3 Co, Beryllium copper (age-hardened)	300 195 76	1007 1117 1207	1296 1313 1482	6 7 9	- - -	7 8 9	Charpy V	NBS Monograph 13
70 Cu-30 Ni cupronickel (annealed)	300 195 76	128 152 221	400 469 617	46 49 52	68 70 69.5	157 155 155	Charpy V	NBS Monograph 101
Nickel, commercial purity (annealed)	300 195 76	103 124 138	421 483 621	45 44 60	≈65 ≈65 ≈75	126 117 117	Charpy V (½-size)	NBS Monograph 13
Inconel (20% cold drawn)	300 195 76	851 910 1038	905 988 1160	17 20 26	58 58 62	104 122 113	Charpy V	NBS Monograph 63
Monel (annealed)	300 195 76	193 207 331	524 586 779	50 45 65	- - -	292 297 293	Charpy V	NBS Monograph 13

stronger but less ductile than α-brass and may be used with care down to liquid nitrogen temperatures. Caution should be exercised if leaded free-cutting brasses are to be employed, especially if they are hard-soldered as this can lead to porosity and the liability to leakage.

Finally, it should be noted that the precipitation-hardened berylium coppers (and berylium brass) can exhibit very high strength characteristics while still retaining thermal conductivities not vastly inferior to that of some commercially pure coppers. This combination of high strength and conductivity make berylium copper extremely valuable for the construction of articles or inserts in which high heat fluxes are involved or where thermal gradients have to be kept to a minimum.

Commercially pure nickel is rarely found in low temperature applications but two of its alloys, Monel and Inconel are used where their excellent corrosion resistance, high strength and low thermal conductivities can justify their high costs. For example, in the petrochemical industry Monel valves are employed in situations where corrosive fluids are handled at high and low temperatures, but it is difficult to forsee such applications in a cryogenic wind tunnel project. Nevertheless, data for these alloys is included in Table 2 for completeness.

b) Aluminium and its Alloys

These now form a very important class of materials for low-temperature use and their relatively stable price and good availability suggest that their importance is likely to continue especially for shop-fabricated, volume-production applications.

Pure aluminium has high electrical and thermal conductivities and it has replaced copper in many instances where these characteristics are required. Its alloys are widely used where moderately high strengths combined with high toughness and low density are necessary, such as in road and rail transporters for liquid gases, as well as in static liquid storage tanks. Aluminium alloys may conveniently be divided into two groups according to the basic metallurgical strengthening mechanism involved: (1) the solution-hardened alloys, which are very ductile but only moderately strong in the annealed state (although their strengths can be improved by cold working), and (2) the precipitation-hardenable types, which can be heat treated to give considerably higher strengths.

Of the solution-hardened types, those containing manganese as the main alloying addition (3000 series) have only moderate strengths, but they are very ductile and hence easily formed. Type 3003 is used for tubes, bends, junctions, plate fin heat exchangers, tube plates and trays, as well as in distillation columns and many other applications. Their role in heat exchangers arises largely because they can be dip-brazed in molten salt baths using aluminium-silicon eutectic alloys. They can also be extruded and cut with roller cutters, characteristics which are advantageous for volume production. They can be cold-worked for higher strengths, but, as they are so often used in the welded or brazed condition where these advantages would be lost, it is more usual to use one of the higher-strength alloys where necessary.

The aluminium-magnesium alloys (5000 series) have higher strengths than the 3000 series and they are widely used for the construction of land-based storage tanks, road and rail transporters and for the primary containment of liquid natural gas in LNG ships. Type 5083 alloy is, in fact, the largest-tonnage alloy in cryogenic service largely due to its combination of moderately high strength with excellent weldability. Gas-metal-arc and tungsten-metal-arc systems have been used to weld plates up to 175mm thick even in the as-welded condition its full strength is retained thus giving it an advantage over the higher strength 2000 and 7000 heat-treatable alloys if post-weld heat treatment is not possible. Additional strength can be achieved in the 5000 series alloys by cold-rolling but the consequent loss of ductility is not always acceptable.

Aluminium-magnesium-silicon alloys (6000 series) have the lowest strengths of the heat-treatable types and, in general, they are the only ones used outside the aerospace industry. Type 6061 in the T6 condition is stronger than the 3003 and 5083 alloys but its strength in the as-welded condition drops below that of the solution hardened alloys. It is generally available in the forms of pipe, pipe fittings, extruded tubing and other shapes.

The aluminium-copper alloys (2000 series) have higher strengths than the Al-Mg-Si types but their toughness, especially their notch toughness, begins to fall seriously at low temperature and they are not widely used. Moreover, they are often considered to be less easy to weld reliably. Nevertheless welded Type 2014-T6 was employed in the construction of the liquid-oxygen and liquid-nitrogen fuel tanks for the Saturn V Rocket where its high strength/weight ratio proved advantageous.

Finally, the very-high-strength aluminium-zinc-magnesium alloys (7000 series) are rarely, if ever, used at low temperatures, especially below 77K, where they have very low notch toughness. These alloys in fact provide a convenient illustration of the fact that even though they have f.c.c. structures and fail by shear not cleavage, their strengths reach such high values at low temperatures that their toughness falls drastically. This point will be reconsidered briefly later.

The general relationship between temperature, alloy strength and ductility is summarized by the three families of stress-strain curves illustrated in Fig.3. As can be seen pure aluminium has low yield and tensile strengths but a high ductility at all temperatures. In the unhardened form its alloy has a moderately high yield stress and reasonable ductility, both of which increase at low temperatures. In the heat-treated form the yield strengths have increased enormously but the ductility has dropped to a low value at room temperature and is almost non-existent at 4K. Toughness tests would almost certainly reveal that in its heat-treated state this alloy would be unsuitable for use below room temperature.

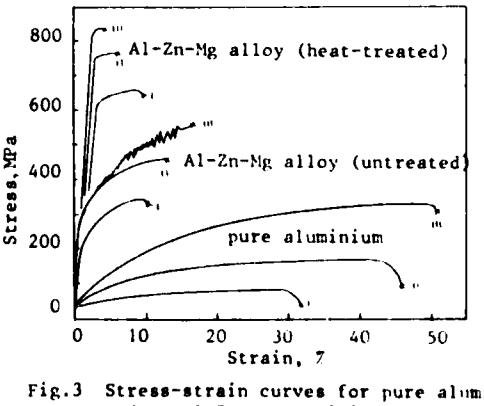

Fig.3 Stress-strain curves for pure aluminium and an Al-Zn-Mg aluminium alloy tested at i) 300K, ii) 78K and iii) 4K.

Aluminium and its alloys have a few drawbacks when compatibility is being considered. They are not suitable for use

Table 3. Typical mechanical properties of aluminium and some of its alloys.

Material and condition	Temperature (K)	Yield strength (MPa)	Tensile strength (MPa)	Elongation (%)	Reduction in area (%)	Impact Energy (J)	Comments	Source
Commercially pure aluminium BS1470-77 IC AAA 1100			annealed, O					
	300	48	93	46	88	31		NBS
	195	50	114	50	86	38	Charpy V	Monograph
	76	62	190	56	81	47	(½-size)	63
			half hard, H 14					
	300	110	124	20	-	98		NBS
	195	121	134	23	-	119	Charpy V	Monograph
	76	124	193	42	-	144		13
Al-1.5% Mn max. BS1470-77 N3 AAA 3003			annealed, O					
	300	41	108	43	81	-		NBS
	195	50	131	45	80	-	-	Monograph
	76	59	223	49	76	-		13
			full hard, H 18					
	300	184	210	9	34	-		NBS
	195	202	230	11	44	-		Monograph
	76	230	295	23	46	-		13
Al-2.8% Mg max. BS1470-77 N4 AAA 5052			annealed, O					
	300	99	201	33	72	136	Charpy V	NBS
	195	99	211	41	76	102	(material	Monograph
	76	116	309	50	69	75	in F. as-rolled, condition)	13
			half hard, H 34					
	300	183	238	10	-	-		NBS
	195	183	245	18	-	-	-	Monograph
	76	207	345	38	-	-		13
Al-3.9% Mg max. BS1470-77 N5 AAA 5154			annealed, O					
	300	118	243	29	66	133		NBS
	195	119	252	35	73	113	Charpy V	Monograph
	76	135	353	42	60	71		13
			quarter hard, H 32					
	300	231	303	12	-	-		NBS
	195	231	296	16	-	-	-	Monograph
	76	269	400	33	-	-		13
Al-4.9% Mg max. BS1470-77 N8 AAA 5083			annealed, O					
	300	150	313	23	35	-		NBS
	195	146	324	27	47	-	-	Monograph
	76	164	434	33	38	-		13
			strain hardened, H 113					
	300	281	343	15.5	29	-		NBS
	195	291	359	19	40	-	-	Monograph
	76	334	467	25	36	-		13
Al-1.2 Mg-0.8 Si BS1470-77 H 20 AAA 6061-T6			solution treated and artificially aged					
	300	270	306	18	56	22		NBS
	195	290	335	19.5	54	22	Charpy V	Monograph
	76	330	412	24.5	51	22		63

if alkalis may be present either as contaminants in the process fluids or for cleaning as in synthetic ammonia plants. Indeed, cross contamination by heavily polluted industrial or marine atmospheres has been shown to cause the premature failure of air separation equipment made from aluminium. Aluminium alloys have been safely used in conjunction with liquid oxygen (LOX) for many years, and it may be assumed that they are generally LOX compatible.

Table 4. The stability of some 300-series stainless steels (Data from International Nickel Co.)

Type	Intrinsic permeability at 300K (μ = 1)(H = 200 gauss) After cold rolling at 300 K		After thermal cycling to 77 K	Composition Ni (%)	Cr (%)	Other major additions (%)	Tensile strength after cold rolling (MPa)
310	0.005	(64% c.r.)	0.005	20.7	24.3	-	1328
316	0.01	(84% c.r.)	0.004-0.01	13.4	17.5	2.4 Mo	1338
347	3.12	(90% c.r.)	0.004-0.01	10.7	18.4	0.95 Nb	1493
321	8.4	(70% c.r.)	0.004-0.01	10.3	18.3	0.68 Ti	1388
304*	3.7	(84% c.r.)	1	10.7	19.0	-	2088
301	18.0	(55% c.r.)	large	7.8	17.6	-	1533

* The nickel content of this sample of 304 is higher than normal for the alloy.

even though laboratory tests show that under extreme conditions ignition can occur. The mechanical properties of a few selected aluminium alloys are given in Table 3.

c) Invar

We have already noted the unique thermal expansion characteristics of Invar, an iron - 36% nickel alloy sometimes known as Nilo 36: it is also relevant in this context as the presence of 36% nickel ensures that the alloy has a stable free-centred-cubic structure. It combines a moderately high strength with good ductility and toughness and it is readily welded using gas- and tungsten-metal-arc methods, if filler rods which prevent contamination by sulphur and selenium are utilised. The resultant welds have thermal and mechanical properties which match those of the parent metal. Invar is available in the product forms of plate, sheet, strip, bar and tube, as well as billets and forgings: for low-temperature applications it is normally used in the annealed condition. A brief summary of its mechanical properties is given in Table 5.

d) Austenitic Stainless Steels

This is one of the most important class of materials used in the construction of equipment for operation at low temperatures: examples cover a wide variety of applications including; small laboratory scale experiments and cryostats where thin walled tubes are used to minimise heat in-leaks, precision components such as shafts and rotors for pumps and turbines, large static and transportable vessels for the storage of cryogenic fluids such as helium, hydrogen, nitrogen and oxygen and the very high strength/weight fuel tanks used to contain liquified hydrogen and oxygen for space rockets. The face-centred-cubic gamma phase of iron is normally only stable at high temperatures, but the addition of alloying elements such as nickel, manganese, carbon and nitrogen suppresses the γ-α transformation and enables the austenitic γ phase to be retained to room temperature and below. The γ structure is, however, only metastable and under certain conditions of stressing and/or cooling a partial transformation to martensite can take place in some of the less highly alloyed steels such as type 304. Two martensitic phases are formed having h.c.p. and b.c.c. structures respectively, and it is the b.c.c. form which leads to an increase in strength but loss of toughness in the transformed state. Furthermore, b.c.c. martensite is ferromagnetic and its presence is a severe disadvantage in applications where magnetic fields are present. Finally, to make matters even worse, the transformation is accompanied by a volume expansion which can spoil the fit of accurately machined components such as shafts and flanges.

In general, the most stable steels are those with the highest nickel contents such as the 25-Cr 20-Ni type 310 wrought alloy and the analagous casting alloys CK20 and Kromarc-55 which have been used to cast large components for cryogenic bubble chambers. Typical mechanical properties for type 310 are given in Table 5 and it may be seen that its main disadvantage lies in its rather low yield strength of about 200 MPa at room temperature. If some loss of ductility can be tolerated this may, however, be raised to about 500 MPa by cold working without either a significant drop in toughness or transformation to martensite. Because of its high nickel content type 310 is more expensive than other 300 series stainless steels and it is somewhat more difficult to obtain in a wide range of product forms than the more popular alloys.

In most other 300 series austenitic stainless steels some degree of martensitic transformation may be induced by stressing or thermal cycling. The ferromagnetic nature of b.c.c. martensite allows its existence to be established very simply by the use of a small pocket magnet, while a somewhat more sophisticated, and hence expensive, variation on this theme uses a calibrated spring balance to measure the force required to remove a magnet from the surface of the sample. Some models even have the scale directly calibrated in % martensite and thus save the user the need to do any calculations!

In a series of experiments carried out by the International Nickel Company the magnetic permeability of a series of austenitic stainless steels was measured before and after cold rolling at 300°K and also after thermally cycling between 300K and 77K. The results of these experiments are shown in Table 4 and it can be seen that type 310 shows no transformation while type 301 is strongly effected by both treatments. The samples of 316, 321 and 347 show an increasing tendency to transform during cold rolling but they are relatively unaffected by thermal cycling. Type 304, one of the most widely available of all the austenitic stainless steels, has the greatest variability in its behaviour and Gunter and Read (14) have shown that small decreases in the carbon and nitrogen contents can be very harmful as both elements are strong austenite stabilisers. It is, therefore, worth noting that the recently developed *Hi-proof* grades of 304, 316 and 347 which contain 0.2% nitrogen to increase their yield strengths by about 70MPa, will also be very much more resistant to martensite transformation than the normal grades. In contrast the low carbon grades of 304 used to prevent weld decay will be *least resistant to martensitic transformation!* When the nitrogen bearing grades 304N, 316N and 347N become more readily available in the product forms required, they will offer probably the best combination of properties available for low temperature applications from any austenitic stainless steel and their use should be encouraged. Regrettably they are, at present, very difficult to obtain in small quantities and in forms other than sheet and plate.

A further point worth noting from the results of these experiments concerns the effect of thermal cycling. If the ferromagnetic nature of a partially martensitic 300 series steel is not a drawback for a particular application which demands good dimensional stability, it is possible to ensure that transformation is complete before final machining. This may be achieved by cycling repeatedly between 300K and 77K, if necessary taking measurements after each few cycles, until no further significant dimensional changes occur.

One problem often associated with austenitic stainless steels is weld decay, a tendency to intergranular cracking in a band situated about 5-10mm on either side of the weld zone. It is caused by the diffusion, at temperatures between 650 and 850°C, of uncombined carbon to form chromium carbides which deposit in the grain boundaries, "sensitise" them and seriously lower the impact resistance of the material at low temperatures. Furthermore, the chromium which forms the carbides has been taken from the region of the grains next to the grain boundaries, thus locally decreasing the chromium concentration to below the level necessary to provide a self repairing oxide film. Relatively mildly corrosive service conditions can then induce intergranular corrosion and failure sometime after the welded component has entered service. One traditional method of avoiding weld decay is to reduce the carbon content to less than 0.02% as in the L grades of 304 and 316 but, as noted earlier, this will make them more liable to martensitic transformation unless the nitrogen content is increased correspondingly. One other way of preventing weld decay is to add strong carbide formers such as niobium and titanium which combine preferentially with the excess carbon and thus stop it from depleting the chromium. There are, however, some disadvantages to this technique. The titanium stabilised type 321 steels can suffer from a problem known as "titanium streaking" if the titanium does not disperse evenly throughout the steel but instead concentrates in discrete particles. If these particles are of a size comparable to the thickness of the material, as may happen in the case of the thin walled tubes often used in cryostats, then porosity can develop. It is, therefore, prudent to inspect thin wall tubing using dye penetrant or other techniques before accepting delivery. Care has also to be taken when these steels are welded in order to ensure that the titanium is not oxidised and thereby rendered ineffective. Niobium is thus widely used to stabilise the welding consumables as it is less readily oxidised than titanium, and in the type 347 steels niobium is used as the stabilising agent itself. Apart from possible problems of "hot shortness" in thick sections of this material, it is entirely satisfactory for low temperature applications.

Thus to summarise briefly, the 300 series austenitic stainless steels offer a combination of reasonable strength and high toughness and they are readily available in a wide range of product forms. (Representative mechanical properties for some of the more important grades are given in Table 5). For applications such as valve bodies and pump casings, Alloy Casting Institute (ACI) types CF8 and CF8M are equivalent to the wrought alloy types 304 and 316 respectively.

e) Metals and alloys with hexagonal-close-packed crystal structures

The mechanical properties of these metals vary considerably at low temperatures: zinc is completely embrittled just below room temperature, while cadmium and indium retain their very high ductilities even at 4K (pure indium wire is sometimes used as a gasket to seal flanged and bolted joints at low temperatures).

The low density and good strength/weight ratio of magnesium alloys has led to their use at moderately low temperatures in aircraft components, but they are really only suitable for use as constructional materials at lower temperatures in applications where their notch sensitivity, low ductility, and poor impact strength can be tolerated. Typical mechanical properties for some magnesium alloys are given in Table 6. It is, however, titanium and its alloys with their very high strength/weight ratios that have excited the most interest for very low-temperature aerospace applications. Both yield and tensile stresses of titanium alloys rise rapidly at low temperatures, while their ductilities are strongly dependent on the concentration of interstitial impurities present. Oxygen in particular causes severe loss of ductility and toughness if present in concentrations in excess of approximately 0.12% and special ELI (extra low intersti-

Table 5. Typical mechanical properties of some austenitic stainless steels.

Material and condition	Temperature (K)	Yield strength (MPa)	Tensile strength (MPa)	Elongation (%)	Reduction in area (%)	Impact Energy (J)	Comments	Source
Invar, Nilo 36 (annealed)	300	290	510	27	-	300		LNG
	195	435	675	31	-	215	Charpy V	Materials
	77	650	935	30	-	-		& Fluids
Invar, Nilo 36 12-15% (cold drawn)	300	630	650	21	62	37		NBS
	195	725	790	29	60	33	Charpy V	Monograph
	77	920	1080	27	61	31		63
Stainless steel Type 310 (annealed)	300	220	580	59	71	95		NBS
	195	300	740	72	68	92	Charpy V	Monograph
	77	525	1080	68	50	68	(½ size)	63
Stainless steel Type 310 (cold drawn)	300	470	650	35	-	-		NBS
	195	550	780	50	-	-	-	Monograph
	77	800	1210	56	-	-		13
Stainless steel Type 304 (annealed)	300	241	641	65	83	217		NBS
	195	324	1089	55	77	163	Charpy V	Monograph
	77	427	1600	46	71	163		13.BSC†. USS‡.
Stainless steel Type 304 N (high proof)	300	315	590	51	75	61		BSC†
	195	459	1002	66	75	-	Charpy V	USS‡
	77	700	1557	47	63	27		
Stainless steel Type 316 (annealed)	300	241	586	74	-	168		NBS
	195	345	841	66	-	185		Monograph
	77	517	1269	58	-	166	Charpy V	13 BSC†
Stainless steel Type 316 N (high proof)	300	340	620	-	-	54	Charpy V	BSC†
	77	-	-	-	-	27		
Stainless steel Type 321 (0.4% Ti, annealed)	300	255	606	64	-	212		
	195	289	999	43	-	190	Charpy V	BSC†
	77	289	1517	36	-	133		USS‡
Stainless steel Type 347 (0.9% Nb, annealed)	300	248	627	50	74	-		
	195	260	931	51	70	-	-	USS‡
	77	295	1310	43	63	-		
Stainless steel Type 301 (extra hard)	300	1515	1660	15	35	-		NBS
	195	1520	1850	17	35	-	-	Monograph
	77	1870	2250	19	34	-		13

† British Steel Corporation

‡ United States Steel Inc.

Note: Data for some of the steels in Table 5 have been obtained from more than one source in an attempt to give as complete a picture as possible: they should therefore be treated with caution.

tial) grades which guarantee oxygen contents below this figure are now available for cryogenic applications. However, when welding these alloys, care must be taken to ensure that they do not become recontaminated and thereby embrittled.

There are basically three main types of titanium alloy. The α-stabilised h.c.p. grades such as Ti-5% Al-2.5% Sn are the safest for use down to 4K; one such alloy was in fact employed in the construction of the liquid-helium pressure vessels used in the Apollo spacecraft. The β-stabilised b.c.c. grades such as Ti-13% V-11% Cr-3% Al are rarely used below room temperature because they are too brittle, while the duplex α-β types such as Ti-6% Al-4% V are only considered safe down to 77K because of insufficient notch toughness below this temperature.

Table 6. The mechanical properties of some titanium and magnesium alloys.

Material and condition	Temperature (K)	Yield strength (MPa)	Tensile strength (MPa)	Elongation (%)	Reduction in area (%)	Impact Energy (J)	Comments	Source
ELI grade pure titanium (annealed)	300	441	538	22	-	24	Charpy V	NBS Monograph 13
	195	579	676	18	-	19		
	77	807	993	42	-	15		
Ti-5% Al-2.5% Sn α-stabilised h.c.p. (annealed)	300	875	925	19	44	24	Charpy V	NBS Monograph 63
	195	1038	1104	13.6	38.5	20		
	77	1380	1437	13.8	29.5	40		
Ti-6% Al-4% V duplex α-β (annealed)	300	951	1024	16.6	47	37	Charpy V	NBS Monograph 63
	195	1132	1199	13.9	42	31		
	77	1576	1642	10.2	41	21		
Ti-13% V-11% Cr-3% Al β-stabilised b.c.c. (solution treated)	300	946	946	26.5	56	26	Charpy V	NBS Monograph 63
	195	1261	1264	16.7	47	14		
	77	1885	1927	6.7	21	5		
Mg-3% Al-1% Zn ASTM B90 AZ31B wrought sheet (annealed, O)	300	145	248	26.0	-	7.6	Charpy V	NBS Monograph 13
	195	174	297	22.5	-	5.7		
	77	192	371	10.0	-	4.2		
Mg-3.2% Th-0.6% Zr ASTM B90 HK 31A wrought sheet (annealed, O)	300	124	197	36.5	-	5.7	Charpy V	NBS Monograph 13
	195	162	277	24.5	-	5.0		
	77	170	343	23.0	-	4.5		

f) Metals and alloys with body-centred-cubic crystal structures

As a general rule metals with b.c.c. crystal structures undergo a ductile brittle transition, this occurring at some temperature which may be above or below room temperature. There are a few exceptions, for example the alkali metals and β-brass remain ductile down to 4K, but for practical purposes the potentially brittle nature of b.c.c. metals at low temperatures puts a severe limitation on their use. However, they cannot be disregarded as they include the whole range of plain carbon, and low- and medium-alloy, steels which are economically irreplaceable for the construction of equipment operating at moderately low temperatures. *The basic philosophy behind their successful application lies in ensuring that they have adequate toughness at their minimum operating temperature for them to withstand not only their design stresses but also accidental impact and other overloads without failing in a brittle and catastrophic manner.*

In Fig.4 a series of stress-strain curves for a plain carbon steel tensile tested at a range of temperatures is shown, while in Fig.5 this data is cross-plotted to show how the yield stress, tensile stress, and elongation vary with temperature. From these figures it can be seen that the yield stress rises more rapidly than the tensile stress as the temperature drops. The stress-strain curves also show that the material loses its ability to work-harden and in consequence the elongation also decreases, slowly at first but much more rapidly over the temperature range where the yield and tensile stresses start to coincide. Thus the material undergoes a ductile-brittle transition over this temperature range, below about 75K for this sample.

The uniaxial tensile test is, however, not severe enough to simulate the more extreme conditions that the material may be subjected to in service. A better indication is given by impact tests such as the Charpy V-notch test which combines a high strain rate with the stress-raising effect of its sharp notch. Fig.6 shows the energy absorbed in a series of Charpy tests carried out on the same material as that used for the tensile tests whose results were shown in Figs. 4 and 5, together with the elongation values obtained from these tests. Although not measuring the same property characteristic as the tensile test, the increased severity of the impact test is immediately apparent in the shift of the tough-brittle transition to a temperature of the order of 200K higher than that of the ductile-brittle transition shown in the tensile test. It can be seen that this steel is in fact already undergoing its tough-brittle transformation at room temperature. The scatter shown in the value of the energy absorbed is characteristic of these tests and is due to the influence of small changes in composition, grain size, residual stress, notch-root sharpness, etc.

There are many factors which influence the toughness and the impact transition of a steel, the more important of which are its composition, structure, strength and thickness. From Figs. 5 and 6 it can be seen that the toughness transition coincides with an

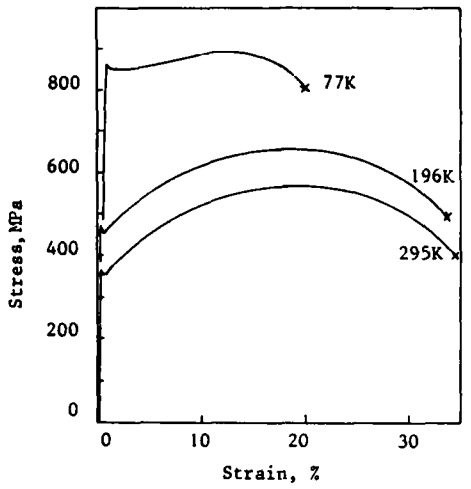

Fig.4 Stress-strain curves for 0.2% carbon steel at indicated test temperatures.

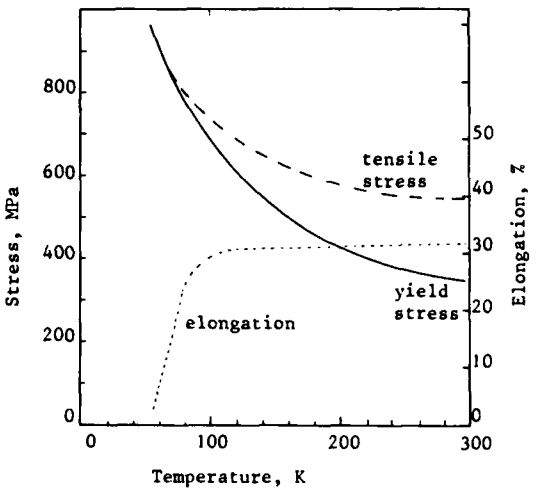

Fig.5 Data from Fig.4 cross-plotted to show variation of mechanical properties with temperature.

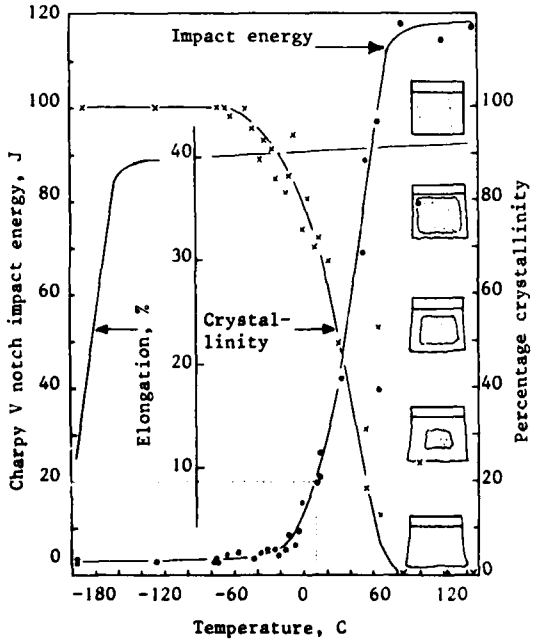

Fig.6 Impact energy, percentage crystallinity and elongation for a 0.2% carbon steel

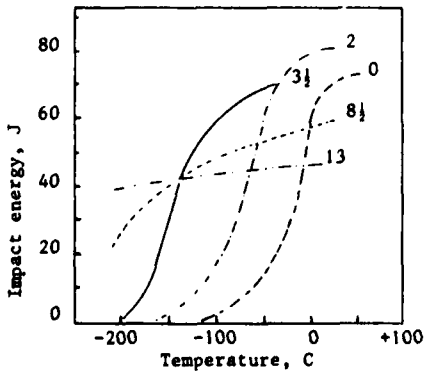

Fig.7 Impact energy transition curves for iron-nickel alloys of compositions shown

increase in yield strength caused by the fall in temperature. In general most metallurgical and other factors which strengthen the material, e.g. cold-work, increased alloy additions, precipitation hardening, etc., also lower its toughness. The only exception to this rule is the action of grain refinement as this increases *both* the strength *and* toughness. Indeed grain refinement is one of the most important methods of obtaining toughness in ferritic steels at low temperatures, and this is achieved principally by increasing the manganese concentration relative to that of the carbon, high Mn/C ratios giving finer grained structures. The degree to which the steel is deoxidised, or killed, by the addition of silicon and aluminium is also important, fully-killed steels being tougher, but more expensive, than semi-killed steels. Niobium and vanadium are also added to high grade steels to produce additional grain refinement, while careful control of the aluminium, nitrogen, and vanadium concentrations can lead not only to enhanced grain refinement but also to precipitation hardening by their resultant nitrides and carbides.

It is, however, the nickel-alloy steels that are most widely used at and below 220K, the beneficial effect of nickel being illustrated in the series of Charpy curves shown in Fig.7 for a range of nickel steels. In Britain 2¼, 3½, and 9% Ni steels are readily available and these grades adequately span most required temperature ranges. 2¼ per cent Ni steel is used down to 210K, particularly for equipment handling liquid propane at 230K, while 3½% Ni steel can be used down to 170K and is commonly specified for tanks, pipes, and other applications involving liquid ethylene, ethane, acetylene and carbon dioxide. It is, in fact, also often employed for higher-temperature applications because the additional safety margins given by its higher toughness compensate for its costing marginally more than 2¼% Ni steel. A 5% Ni steel is also used quite widely in Europe at temperatures down to 150K, particularly in the fabrication of welded vessels for the handling and storage of liquid ethylene.

The use of 9% Ni steel in thicknesses up to 50mm and at temperatures down to 73K

Table 7. Composition and basic mechanical properties of some constructional and pressure-vessel steels for plates used below room temperature.

Type and Condition	Designation	Composition C (%)	Mn (%)	Si (%)	Mo (%)	Nb (%)	Ni (%)	Cr (%)	Mechanical properties at 20°C Yield strength (MPa)	Tensile strength (MPa)	Elongation (gauge length $5.65\sqrt{S_o}$) (%)	Charpy V impact test temperature* (°C)
C-Mn semi-killed as rolled	BS 4360: grade 40C	0.22	1.6						260	400-480	25	0
	BS 4360: grade 43C	0.22	1.6						280	430-510	22	0
C-Mn-Nb semi-killed normalized	BS 4360: grade 40D	0.19	1.6			0.10			260	400-480	25	-20
	BS 4360: grade 43D	0.19	1.6			0.10			280	430-510	22	-20
	grade 50C	0.24	1.6	0-0.55		0.10			355	490-620	20	-15
C-Mn-Nb silicon killed normalized	BS 4360: grade 50D	0.22	1.6	0.1-0.55		0.10			355	490-620	20	-30
C-Mn silicon killed, fine grain, normalized	BS 4360: grade 40E	0.19	1.6	0.1-0.55					260	400-480	25	-50
	grade 43E	0.19	1.6	0.1-0.55					280	430-510	22	-50
	grade 55E	0.26	1.7	0-0.65		0.10			450	550-700	19	-50
Ni-Cr-Mo quenched and tempered	BSC QT 445 ASTM A517 Gd F (USS T1)	0.10-0.20	0.60-1.00	0.15-0.35	0.40-0.60		0.7-1.0	0.4-0.65	690	795-930	18	-45
2¼% Ni normalized	ASTM A203 Gd	0.17-0.23	0.70-0.80	0.15-0.30			2.1-2.5		255	450	25	-60
3½% Ni normalized and tempered	BS 1501/503 ASTM A203 Gd D	0.17-0.20	0.70-0.80	0.15-0.30			3.25-3.75		255	450	22	-100
9% Ni double normalized and tempered	BS 1501/509	0.13	0.90	0.13-0.32			8.40-9.60		515	690	22	-196
as welded with Ni-Cr-Fe (Inconel 92) electrodes	ASTM Code Case 1308 and A353								480	655		-196

* The impact test temperature is that laid down by the relevant standards for quality control purposes. This does not guarantee that the steel, especially if used in thick sections, will be completely satisfactory for use at low temperatures.

without post-weld heat treatment has been allowed since 1962 under ASME code case 1308. This steel is available in both (1) the quenched and tempered, and (2) the double normalized and tempered conditions, (1) having a marginally higher yield stress and lower ductility at room temperature: it is unusual in that post-weld heat treatment actually lowers its toughness and this treatment is therefore not recommended. It is the only ferritic steel permitted for use at liquid-nitrogen temperatures and it is economically competitive for the construction of large storage tanks for liquid nitrogen, oxygen, argon, and methane. Its high proof-stress/tensile-stress ratio gives it a distinct advantage if design on the basis of proof-stress codes such as BS5500 is permissible, but even when designing to tensile-stress codes it is still a very economical material. It is readily welded, but fillers with the same composition as the parent metal must not be used as such welds lack adequate toughness. Austenitic 25% Cr-20% Ni consumables give tough welds with expansion coefficients that match those of the parent metal, but whose strengths are lower, whereas the higher-strength Inconel types have mismatching expansion coefficients and this can cause high contraction stresses to be set up during thermal cycling. Thus neither type of electrode is ideal and furthermore their high cost detracts somewhat from the favourable economics offered by the parent metal. It should be noted that 9% Ni steel, like other high-tensile steels, is particularly prone to hydrogen embrittlement and thus precautions have to be taken to prevent hydrogen pick-up during welding or in service. Representative data for the properties of low alloy and nickel steels used at low temperatures are given in Table 7.

In our discussions of the toughness transition in b.c.c. metals and alloys we have used the change in energy absorbed in a Charpy impact test to illustrate the temperature range over which the transition occurs. It is, however, important to realise that, although impact testing is a valuable quality control technique, it does not give data that has any intrinsic meaning and which could be used for design calculations. In order to establish the temperature and stress limits at which any particular grade and thickness of material may safely be used, it is necessary to carry out an extensive series of large-scale tests in the as-received, as-welded and stress-relieved conditions on full-thickness plates. *Once valid correlations have been established between the toughness transitions shown by these tests and those obtained from Charpy specimens cut from the full-thickness plates, it is then possible to specify the appropriate values of test temperature and absorbed Charpy energy to be used for quality control purposes. It must be emphasised that these criteria are only valid for this particular grade of steel and that different energies and temperatures will be needed for other grades of steel.*

Thus, for example, the pioneering work of Pellini and his co-workers on brittle failure of the ship-plate steel used in the construction of the all-welded liberty ships made during the 1940's showed that if the plates absorbed a minimum of 15 ft.lb.(20J) at the operating temperature, failure in service was extremely unlikely and therefore this was an acceptable quality control for this material. Unfortunately, this led to the misconception that *any steel* that absorbed 15 ft.lb. at its operating temperature would be safe from brittle fracture in service. This is untrue and it is now usual to specify higher impact energy requirements for the stronger grades of steel. Thus BS.5500, Appendix D, calls for an energy of 40J for steels with tensile strengths above 450MPa, but only 27J for the lower strength grades. The effect of thickness is taken into account by requiring that specimens taken from thicker sections, where triaxial stresses will be greater and the toughness lower, should absorb the required energy at lower test temperatures than that used for thinner sections. Furthermore, as post-weld stress relief is so beneficial for most steels, impact test requirements are considerably less demanding for structures that have been heat-treated.

It is worth noting at this stage that examination of the fracture surface of a specimen broken in the tough-brittle transition range will show that it exhibits both crystalline (shiny) and shear (dull, fibrous) regions, the crystalline region being at the centre of the fracture surface. The relative proportions of these two areas change from 100% crystalline at low temperatures to 100% shear at high temperatures, this variation also being shown in Fig.6 together with a diagrammatic representation of the percentage crystallinity at five temperatures over the transition range. A fracture appearance transition temperature (FATT), defined on the basis of, say, 70 per cent crystallinity on the fracture surface of a Charpy V-notch test piece, is sometimes used as a guide to the likelihood of cleavage failure under service conditions, but for design purposes this criterion would need to be correlated with the results obtained using full-thickness plates. Care has to be taken to ensure that specimens prepared for Charpy tests are fully representative of the material. For example, the notches are always cut in the through-thickness direction for plates as this gives a more reliable result than would be obtained if the notches were cut in the (tougher) surface of the plate. Similarly, separate tests are normally carried out for samples cut both parallel to, and across, the rolling direction.

6. Fracture Toughness

In virtually all materials the presence of a notch or flaw has an embrittling effect due to a stress concentrating effect at the crack tip. Historically it was Griffith who first demonstrated the basic relationship between fracture stress and crack length in glass, but the modern techniques of Linear Elastic Fracture Mechanics owe their origins to the work of Irwin. It is possible to indicate in this lecture only the barest of outlines of this subject, in particular the influence of cryogenic temperatures on the basic parameter K_c, *the Fracture Toughness*. Thus the fundamental relationship of interest to us is:

$$\sigma_F = K_c/|\pi a + \tfrac{1}{2}(K_c/\sigma y)^2|^{\frac{1}{2}}$$

where σ_F is the fracture stress, K_c the fracture toughness, σy is the yield stress and a the crack length. Note particularly the term $(Kc/\sigma y)^2$. This gives an indication of the amount of plastic deformation that takes place in the material ahead of the advancing crack. If σy is small, $(Kc/\sigma y)^2$ is large and there is a large plastic zone ahead of the crack tip. Relatively large amounts of energy are absorbed in tearing through this zone and crack propagation is therefore made more difficult. In contrast, if σy is large $(Kc/\sigma y)^2$ is relatively small, the plastic zone size is small and little energy is absorbed by shear deformation.

We have already seen that lowering the temperature causes the yield stress, σy, of many alloys to increase rapidly and thus if Kc does not increase correspondingly, less energy will be involved in crack propagation and the material will be embrittled.

The elastic modulus of a material has a strong influence on its fracture mode and it is possible to divide materials roughly into high-medium- and low-strength types depending on their ratio of modulus/yield strength. This is shown in Table 8 together with the resultant strength ranges for steels, aluminium - and titanium alloys.

Table 8. Approximate classification of materials into high-, medium-, and low-strength types.

Classification	Approximate relationships	Steels	Stress (MPa) Al alloys	Ti alloys
High strength	$\sigma y > E/150$	$\sigma y > 1250$	$\sigma y > 420$	$\sigma y > 760$
Medium strength	$E/150 > \sigma y > E/300$	$1250 > \sigma y > 625$	$420 > \sigma y > 210$	$760 > \sigma y > 380$
Low strength	$\sigma y < E/300$	$\sigma y < 625$	$\sigma y < 210$	$\sigma y < 380$

High-strength materials fail in a low energy mode at all temperatures either by shear rupture or cleavage. Fracture toughness analyses are rigorously applicable for these materials and they provide the only reliable basis for fail-safe design. To use them safely the operating stress must at all times be kept below the fracture stress as determined by the size of the largest flaw that can remain undetected by the non-destructive testing technique being used.

Medium-strength materials usually have adequate fracture toughness at room temperature and fail in a shear mode which absorbs a reasonable amount of energy. However some grades of aluminium, titanium and steel show large increases in yield stress at low temperatures which can take them into the range covered by the definition of high-strength materials. Furthermore, their fracture toughness usually drops as an increasing proportion of their fracture mode changes over to a low-energy-absorbing shear mechanism and they become "notch-brittle". Fracture mechanics analyses should be used in these cases to check that serious embrittlement does not take place at the lower operating temperatures.

The only low strength materials liable to fail in a brittle mode are those, such as the ferritic steels, which undergo a shear to cleavage failure mode transition at low temperatures and these we have already discussed. The degree to which they are embrittled is determined by a combination of many factors which include the composition, plate thickness, strain rate, extent of crack like defects present, the level to which local stresses are increased at the crack tips and the application of post-weld stress relief. Linear elastic fracture mechanics does not apply strictly to low strength materials but General Yield Fracture Mechanics analyses have been developed to the level at which valid relationships have been established between critical Crack Opening Displacement (COD), δ_c, yield strain, ε_y, and the critical flaw size, a_{max}. Thus, at failure, a_{max} = constant x (δ_c/ε_y) = constant x $(K_c/\sigma_y)^2$.

One apparent drawback with fracture mechanics analyses is the variation of fracture toughness, K_c, with plate thickness, which means that a unique value of fracture toughness cannot be quoted for a given material. K_c falls off with increase in plate thickness becausethe triaxial stresses at the centre of the plate become relatively more important in thicker plates. For an infinitely thick plate it reaches a constant value, K_{Ic}, known as the plane strain fracture toughness, and it is this value which is usually found in data compilations. Its use for design calculations is therefore a conservative approach as thinner sections will have higher fracture toughnesses. However, a note of caution must be sounded here as the fracture toughness of a material can be altered significantly by the treatment it receives. In particular, welding has a strong adverse affect especially if post-weld heat-treatments are unsuitable or impracticable.

There are two particular aspects of the cryogenic wind tunnel project which I believe could benefit from a fracture mechanics approach to their design; the pressure shell and the model sting/balance system. COD tests have already been used to assess the toughness of welds made in 9% nickel steel for fabricating cryogenic storage tanks. Furthermore, it is possible to apply the concepts of fracture mechanics to whole structures

such as the pressure shell. For example it is possible to relate the sizes of the largest cracks present in a structure that has been proof loaded to a value higher than its operating stress, to the value of the proof load. Furthermore, it is possible to use crack growth data obtained on small scale laboratory specimens to predict the rate of crack growth in a periodically loaded structure such as the pressure shell, thereby enabling a value of proof test load to be chosen so as to eliminate the possibility of crack growth to a critical value during the service life of the vessel. A similar approach to fail-safe design relies on the so-called "leak-before-break" concept. If the shell has a wall thickness, t, choice of a material with a critical flaw size significantly in excess of the shell thickness, say $a_{crit} > 3t$, should ensure that an undetected flaw grows in a stable manner to become an easily-observed, through-thickness leak before it reaches the critical value for unstable propagation.

It is apparent from a study of the proceedings of the First International Symposium on Cryogenic Wind Tunnels, that the fracture toughness of materials used for sting construction is already under investigation. Table 9 includes data from a paper by Ferris (15) and comparison with Table 8 shows that the yield stresses of most of the candidate sting materials are high enough to rate them as high-strength materials. The data given in Table 9 is deliberately limited in extent and included only to illustrate the correct magnitude of the yield and toughness parameters for some of the materials likely to be used in the wind tunnel project. A number of reviews giving fracture toughness data at cryogenic temperatures are referenced at the end of this paper.

The significance of these values may be appreciated by recalling from the basic fracture mechanics relationship that the citical flaw size is a function of $(Kc/\sigma y)^2$. Thus a four-fold increase in fracture toughness is required from the stronger material to maintain the same critical crack size when comparing materials, one of which has a yield stress twice that of the other. If the yield stress of the stronger is three times that of the weaker its fracture toughness would have to increase by a factor of nine! Looked at in this light the apparently low values for the aluminium alloy are in fact more than adequate, while the figures for the highest strength steels are somewhat marginal.

Table 9. Toughness and strength data on some materials of construction.

Material	Strength at 300K (G Pa)		Fracture toughness (MPa $m^{\frac{1}{2}}$)		Charpy V (J)	
	Yield	Tensile	300K	77K	300	77
Maraging steel, type 200	1.46	1.49	143	-	49	38
Maraging steel, type 250	1.79	1.86	121	-	27	18
Maraging steel, type 300	2.01	2.06	110	-	34	15
HP 9-4-25	1.28	2.06	162	-	57	34
17-4 PH	1.21	1.31	-	-	27	4
9% Ni steel	0.52	0.69	155	155	-	-
Stainless, 316 annealed	0.24	0.59	370	570	168	166
Aluminium, 5083-0	0.15	0.31	30	44	-	-

7) Time-dependent failure

As has been shown, the fracture stress of a material is strongly influenced by the presence of cracks and flaws. There are three principal mechanisms by which such cracks may form or intensify during service: (1) fatigue, (2) corrosion (especially stress corrosion and corrosion-fatigue), and (3) hydrogen embrittlement. None of these is a specifically low-temperature phenomenon-indeed the fatigue lives of many metals increase considerably at low temperatures, while the rates at which most corrosion reactions take place drop rapidly as the temperature falls - rather they increase the probability of unstable failure under service conditions which would normally be considered satisfactory. Their effect is the result of one or more of the following factors:

(1) they lower the toughness of the material;

(2) they provide a mechanism whereby a crack may sharpen and thus increase the degree of stress concentration: and

(3) they allow a subcritical crack to grow at stresses below the gross yield stress until it reaches the critical length required for unstable propagation.

Fatigue

Fatigue failure occurs in materials subjected to cyclic or fluctuating stresses which may or may not be superimposed on static applied stresses. Failure under such loading

conditions can take place at stresses which are very much lower than the tensile or yield stresses even in materials which are normally considered to be tough and ductile. Fatigue must therefore be considered as a possible mode of failure in any piece of low-temperature equipment subjected to cyclic loading or vibration (for example pumps, motors, and turbines), or to periodic changes in pressure (transfer lines, storage vessels, and other process plant). The severity of the problem may be indicated by the estimate that about half the failures encountered in general engineering practice are caused by fatigue.

Thermal fatigue is of particular relevance to cryogenic plant, such failures having occurred in regenerators after a large number of temperature reversals, and in heat exchangers and other components after a relatively small number of warming and cooling cycles caused by plant shut-down. The basic cause of this type of fatigue is the high stresses and strains that can be set up during thermal cycling if temperature gradients are non-linear or if free expansion and contraction are restricted by external constraints. In this type of low-cycle, high-strain fatigue, small amounts of plastic deformation take place during each loading cycle and cumulatively lead to failure.

Fatigue tests carried out at low temperatures have shown that fatigue lives of most metals rise considerably as the temperature falls. It has already been stated that the tensile stresses of most metals increase as the temperature is lowered and it has been found that there is a strong correlation between fatigue strength and tensile strength; indeed experiments have shown that in some metals the ratio of the endurance limit at 10^5 cycles to the tensile stress is virtually independent of testing temperature.

Pre-existing flaws, notches, cracks, badly radiused corners and other surface defects have a strong influence on fatigue lives, causing them to drop sharply at all temperatures even in materials which are not normally considered to be notch sensitive. This is usually a result of the increase in stress intensity brought about by the sharp fatigue cracks and it is particularly severe in high-strength aluminium alloys, titanium, and stainless steels which are known to be notch sensitive.

As noted earlier, it is possible to apply the concepts of fracture toughness to crack growth under cyclicly applied stresses and many data compilations (e.g. [ ]) show the relationship between crack growth rate da/dN as a function of stress intensity factor range ΔK. Predicted component lives are then obtained by calculating how many cycles are required to increase the flaw size from its initial to critical value. In general, fatigue crack growth rates decrease at low temperatures for most metals normally used for the construction of cryogenic equipment. In contrast they increase for ferritic steels at temperatures below the ductile-brittle transition.

Corrosion fatigue can be a problem with some low temperature equipment particularly if it is frequently cycled between low and ambient temperatures. In the presence of even mildly corrosive environments large reductions in the endurance limits can occur even though the amount of metal corroded is negligible. Some aluminium alloys are especially prone to corrosion-fatigue, ordinary moist air causing some deterioration, while salt-laden atmospheres are particularly harmful. Premature failure has been known to occur in air separation plants located by the sea or near chemical plants and if such conditions are liable to be encountered it is necessary to apply a protective coating to the metal or to specify a material such as stainless steel, which is less susceptible to this type of failure.

Corrosion and embrittlement

These are two mechanisms by which failure can occur without warning long after the initial application of the stress and they can cause failure at low temperatures even though the actual corrosion or embrittlement is more likely to have taken place at or above room temperature. Stress-corrosion resulting from internal residual stresses is liable to occur in brass, aluminium, magnesium, titanium, and steel as well as some non-metals. It is usually prevented by annealing at a temperature high enough to remove the residual stresses without weakening the material. Hydrogen embrittlement is a particular problem in high-strength steels such as 9% Ni steel. The hydrogen is usually absorbed during pickling and plating processes or during welding, and, although the hydrogen can sometimes be removed from steels by baking at 350/^{o}C, it is better to prevent its initial pick-up where possible.

8) The effect of temperature on the mechanical properties of ceramics and glasses

As noted earlier these materials typically have amorphous structures and they are unable to deform plastically and relieve stress concentrations caused by microcracks in their surfaces. They fail in tension at relatively low stresses at all temperatures and their use in bulk form at low temperatures is limited. Glass Dewar flasks are however still used for storing small quantities of cryogenic fluids and large plate glass windows are employed as viewing ports in cryogenic bubble chambers. Careful thermal annealing to remove surface cracks and residual stresses is essential for these applications, while thick sections have to be cooled extremely slowly to avoid failure due to differential contraction or thermal shock. Ceramics and glasses are stronger in compression than in tension because the microcracks are propagated by tensile stresses and residual compressive stresses are often induced in the surfaces of glass plates to toughen them. In a similar manner concrete structures, which are also brittle in tension, can operate satisfactorily at low temperatures if kept in compression and large liquid-natural-gas storage tanks have been constructed in which the concrete is maintained in compression by steel reinforcing rods placed in tension around the warmer outside of the tank. For smaller

Table 10. Glass transition and LOX compatibility of some common polymers.

Common name	Synonyms or trade names	State at room† temperature	Glass transition temperature, Tg(K)	LOX compatibility	Comments
Natural rubber	Cis-1, 4-polyisoprene, NR	E	203	No	Crystallizes rapidly below room temperature
Butadiene rubber	'High-cis' polybutadiene, BR	E	173-203	No	Low temperature resilience of solution and emulsion polymerized BR better than NR
Styrene/butadiene rubber	Buna S, SBR	E	215-235	No	Low temperature resilience falls off with increase in styrene content, not as good as NR
Nitrile rubbers	Acrylonitrile/butadiene copolymer, Buna N, NBR	E	221-248	No	Low temperature resilience falls off with increase in acrylonitrile content, not as good as NR
Carboxylated nitrile latex	Hycar	E	<173	No	Terpolymer with improved low temperature properties
Chloroprene rubbers	Neoprene	E	230-243	No	Excellent resistance to most oils, greases and halogenated hydrocarbon refrigerants; cloth-inserted sheeting best for gaskets
Ethylene/propylene rubber		E	215-221	No	Good low temperature flexibility and abrasion resistance
Butyl rubber	Isobutylene/isoprene copolymer	E	210	No	Low temperature resilience inferior to NR; cloth-inserted sheeting best for gaskets
Polysulphide rubber	Thiokol ST	E	223	Moderate	Outstanding solvent and oil resistance but poor strength
Polyurethane rubber		E	203-238	Moderate	Can be formulated as an elastomer, coating, or adhesive
Silicone rubbers	Polydimethylsiloxane	E	150-160	Moderate	Good chemical and oxidation resistance but high cost; most suitable true elastomer for low temperature use
Fluoro-rubbers (i) vinylidene fluoride/hexafluoropropylene copolymers	Fluorel Viton A	E	220-250	Good	Oil resistant, chemically inert, good oxidation resistance
(ii) Nitroso rubber		E	222	Good	Incombustible in gaseous oxygen
Polytetrafluoroethylene	PTFE, TFE, Teflon	TP	400(Tg) 160(tgg)	Complete	Expensive but irreplaceable for low-temperature service; fabricated by cold pressing and sintering
Fluorinated ethylene/propylene copolymers	FEP	TP	-	Complete	Can be moulded and extruded, better impact strength than PTFE
Polychlorotrifluoroethylene	PCTFE, Kel-F	TP	490(approx)	Complete	Less ductile but tougher than PTFE at very low temperatures
Polyvinylidene fluoride	PVDF, Kynar	TP	230(approx)	Good	Stronger and tougher than PTFE or PCTFE at low temperatures; allows thinner and more flexible seals
Polyvinyl fluoride	PVF, Tedlar	TP	-	Good	Widely used as barrier layer film; good flexibility at low temperatures

Continued

Common name	Synonyms or trade names	State at room temperature †	Glass transition temperature, Tg(K)	LOX compatibility	Comments
Polyethylene terephthalate	Mylar,Terylene	TP	340	Moderate	Widely used as film or fibre, strong and tough down to very low temperatures
Polyimide	H film, Kapton	TP	-	Moderate	Originally developed for superior high-temperature performance; good flexibility at low temperatures
Polyamide	Nylons, (hexamethylene adipamide = Nylon 6.6)	TP	323	No	Widely used as engineering plastics at room temperature; embrittles at lower temperatures
Polyethylene	(low-density LDPE)	TP	153-173	No	Retains excellent toughness to below 200K but very high thermal contraction
Ethylene/vinyl-acetate copolymers	EVA	TP	<200	No	Retain flexibility and toughness down to approx. 200K. Crosslinked by ionic bonds to increase toughness flexible down to <200K.
Ionomers	Surlyn A	TP	<180	No	
Polypropylene	PP	TP	255	No	Stronger than polyethylene at room temperature but embrittles at moderately low temperatures
Polyvinylchloride	PVC	TP	360(approx)	No	Rigid PVC embrittles at approx. 240K but plasticized PVC flexible down to 220K

†E=elastomer; TP=thermoplastic

scale applications such as the floors of loading bays for cryogenic liquid road tankers it has been found that high-aluminous cements such as Ciment Fondue are much more resistant to shattering by thermal shock than is ordinary Portland cement.

9) The effect of temperature on the structure and properties of thermoplastics and thermosetting polymers

The mechanical properties of thermoplastics are very dependent on the temperature and rate at which they are loaded, these characteristics being a direct consequence of the long-chain molecular structure of thermoplastics and elastomers. (Elastomers are basically lightly cross-linked thermoplastics which are able to undergo large amounts of reversible deformation at room temperature because their molecular chains vibrate and move freely). As the temperature falls the interchain bonding forces effectively strengthen, and chain movement becomes more difficult until at the glass transition, T_g, it ceases. As can be seen from Fig.8 there is a large increase in the elastic modulus during this transition, which occurs over a temperature range of about 10-50 °C somewhere between ½ and 2/3 of the melting point. Below this transition the material is effectively an organic glass; it is very brittle and it is no longer able to respond to dynamic stresses. Indeed, as may also be seen from Fig.8, an increase in the frequency of a cyclicly applied load can alsc cause a change from rubbery to glassy behaviour in a thermoplastics material, a tenfold increase in frequency (or strain rate) being equivalent to a 10 K drop in temperature. Furthermore, the damping capacity of the material is at a maximum midway through the glass-rubber transition and hence for critical applications the damping capacity of a component could be optimized by the choice of a thermoplastics material with the appropriate glass-transition temperature.

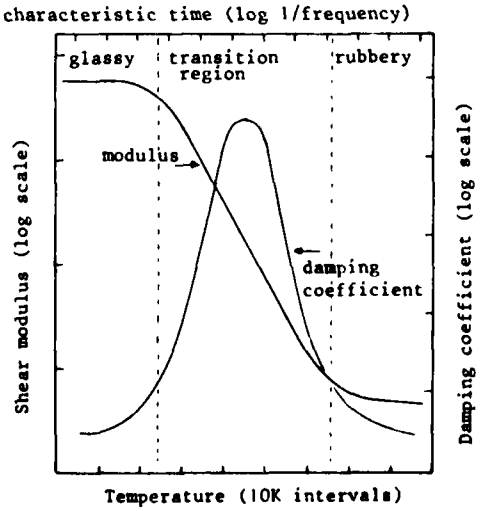

Fig.8 Shear modulus and damping coefficient of a typical polymer as a function of temperature and frequency.

Any polymer which is solid at room temperature (300 K) will be below its glass transition at 150 K and hence it will be incapable of forming a seal capable of responding to a dynamic load. (Seal designs suitable for carrying static loads at low temperatures will be considered further later). Depending on the type of loading cycle, the lowest useable working temperature of an elastomeric material is about 10-30 K above its glass-transition temperature, and in Table 10 values of T_g are given for several elastomers and thermoplastics of interest for cryogenic applications.

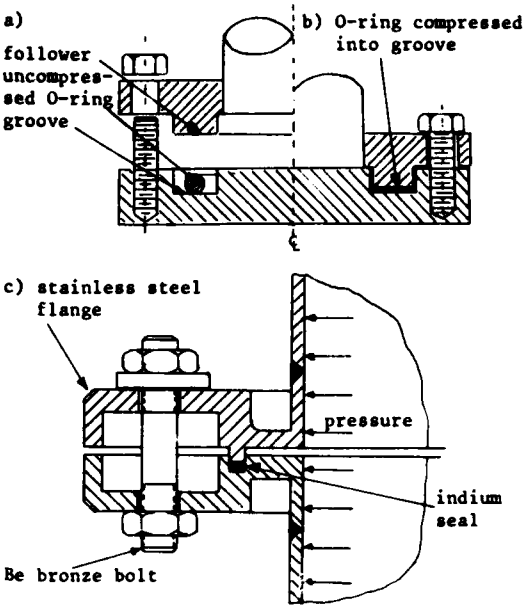

Fig.9 Two designs of demountable cryogenic seal
a) & b) after Weitzel et al (29)
c) after Solyanko et al (30)

The problem becomes even more complicated if these materials are needed in applications where liquid oxygen (LOX) is present, as virtually all hydrocarbon-based polymers are incompatible with LOX and burn violently in its presence. The polysulphides, silicones and fluorosilicones are more LOX compatible, but it is only the fluorocarbons that are completely satisfactory in this respect. The LOX compatibility of selected polymers is given in Table 10.

Temperature, strain rate and the degree of stress concentration are together responsible for determining whether or not a given thermoplastics material will be tough or brittle when stressed. If conditions are such that the polymer chains are able to flow past each other and allow deformation, the material will tend to be tough; if chain movement is severely restricted it will be more likely to fail in a brittle manner. Brittle failure will, in general, occur more frequently at low temperatures, high strain rates, and large stress concentrations caused either by the applied loading system or set up during manufacture. In this context low temperatures and high strain rates are essentially those which cause the working range of the material to lie in the glass-rubber transition as discussed above.

Fabrication techniques can have a strong influence on the toughness of thermoplastics components, particularly their sensitivity to notches and flaws. For example, considerable preferred orientation occurs during injection moulding or extrusion, with the polymer chains tending to lie along the flow direction. In consequence the material is usually much tougher when a notch lies perpendicular, and the applied stress is parallel to the flow direction than it is when the notch is parallel, and the applied stress is perpendicular to the preferred orientation. Furthermore the toughness falls markedly if the processing temperature drops below, or rises above, the optimum working range; also, the rate at which a component cools affects its degree of crystallinity, lower cooling rates giving increased crystallinity and in general decreased toughness. Batch to batch variation in the average molecular weight of the polymer can also affect the toughness of the resultant mouldings.

Good design also plays an important role in ensuring toughness, as thin sections of a component have better impact resistance than thick sections and thermal shock is more of a problem in thicker regions. Abrupt changes in section and sharp corners should also be avoided as they lead to unnecessarily high stress concentrations; better designs would have gradually varying thickness and generously radiused corners.

Fluorocarbons and their use as seals.

The fluorocarbon family of polymers, polytetrafluoroethylene (PTFE, TFE, Teflon), the fluorinated ethylene/propylene copolymers (FEP), and polychlorotrifluoroethylene (PCTFE, Kel-F), are excellent electrical insulators almost completely inert to most chemicals and solvents, useable for long periods at high temperatures, and also possessing valuable non-stick and low-friction characteristics. Furthermore, they are the only materials which retain any measureable ductility ($\simeq 1\%$) down to 4 K. This is a result of their unique molecular structure in which crystallites are formed having a tight spiral formation of fluorine and chlorine groups which are unable to pack closely together, thus preventing the material from having a strong glass transition. Although these materials are not elastomers, their ability to undergo enough plastic deformation to form a satisfactory seal makes them invaluable for use at temperatures down to 4K. They do however suffer from a tendency to cold flow under continuous load, and seals are thus liable to leak unless the load can be increased to compensate for the cold flow. Filled-PTFE compositions have been developed to overcome this problem, glass-fibre being most commonly used for O-rings and gaskets, while graphite, bronze and other powders are also used for bearing applications. Glass fibre improves the tensile and compressive properties of the materials while the PTFE gives it sufficient ductility to accommodate plastically the strains developed. Furthermore, the thermal contraction of the compo-

site is reduced from the high value characteristic of unfilled PTFE so that the expansion of the composite is more compatible with that of metals, thus making joint design easier. Two possible designs of flanged joint are shown in Fig.9.

Correctly designed fittings are important if leak-tight joints are to be made at low temperatures. As long as no dynamic stresses are involved, satisfactory seals can be ontained from elastomers, although they are below their glass transition. In order to achieve this aim, very large compressive strains are imposed at room temperature so that the elastomer is able to exert sufficient force to offset the decrease in load which accompanies the contraction taking place as it goes through its glass transition. The most satisfactory results are obtained using confined compression designs in which a follower on one flange squeezes the O-ring into the bottom of a matching groove in the face of the other flange, as well as into the clearance space between groove and follower. O-rings are typically compressed by about 80% of their original diameter and are not normally reuseable. Confined compression designs are also to be preferred with fluorocarbon seals because they minimise the deleterious effects of cold flow.

Polymeric materials of particular interest for cryogenic applications.

There are many applications in which metal-metal, metal-plastics or plastic-plastics adhesive joints are advantageous. For example brackets, clips, and other attachments can be bonded to pressure vessels without creating the stress raisers that would otherwise be caused by welding or other conventional techniques, while corrosion-free joints between dissimilar metals can be obtained if their surfaces are kept apart by the non-conducting adhesive. At room temperature, adhesives are usually able to deform sufficiently for any stress concentrations to be relieved, but at low temperatures their higher moduli make this much less likely and contraction and other stresses have to be minimized. The key to the successful development of structural adhesives lies in the use of fillers that match the expansion coefficients of the adhesives as closely as possible to those of the substrate and the adherant, as well as redistributing thermal stresses throughout the adhesive instead of concentrating them at the adhesive-substrate interface. Even so the thermal conductivities of most adhesives are low, and temperature differentials between them and metal substrates can cause failure from thermal shock if the glue line is not kept as thin as possible. One way of achieving this is to use a 'structure' or 'carrier' between adherant and substrate. This is usually a thin layer of glass-fibre mat which allows the adhesive to penetrate and wet the filaments, thus forming an even bond line as well as reducing the differential contraction between adhesive and adherant. It also has the further advantage of reducing creep at ambient temperature in adhesives such as the polyurethane pastes, which in other respects are among the most successful adhesives for low-temperature applications. Other types include the epoxy-nylons, nitrile modified phenolics, epoxy-phenolics, and fluorocarbon-epoxy-polyamides.

Particularly valuable for the electrical insulation of wires and the thermal insulation of flexible cryogenic pipelines and other non-rigid applications are fibres and thin films of polymers such as Terylene (Mylar), whose extreme thinness allows them to be bent around very small radii without exceeding their elastic limit in spite of the fact that they are potentially brittle from being below their glass transition. This characteristic was exploited in the construction of the positive-expulsion bladders used in the fuel tanks of the Saturn rocket which were made of multilayers of Mylar segments glued together to form flexible, gas-tight enclosures which could be inflated and deflated through many cycles. Mylar films have also been used to form vapour barriers for filament-wound glass-fibre fuel tanks, and foam insulation, while when aluminized they also form the basis of the superinsulation systems used to lag liquid helium and hydrogen storage vessels. Such film is often crinkled to reduce interlayer contact to a minimum by alternating crinkled and plane sheets, or alternatively they may be separated by woven Terylene or nylon netting.

Motors, turbines, pumps, and other machines are often required to operate at low temperatures, sometimes while totally immersed in a cryogenic fluid such as liquid oxygen, nitrogen, or natural gas. Organic fluid lubricants are normally unsuitable because they freeze, contaminate the fluid, or are LOX incompatible, while graphite and molybdenum disulphide solid lubricants fail to work satisfactorily in the absence of the moisture and oxygen which give the films their self-repairing characteristics. PTFE composites filled with graphite, bronze, or glass fibre are the only materials satisfactory for these applications, PTFE filled with a minority of graphite and bronze powder (Glacier DQ) being particularly suitable. Furthermore, it is essential to ensure good heat dissipation from a low-temperature bearing: in some designs it is possible to accomplish this by circulating the process fluid through the bearing itself, in others the use of bronze rather than steel shafts leads to lower wear rates due to the higher thermal conductivity of bronze.

It is important in this context to reiterate the warning given in lecture 1, that fits and clearances can vary on cooling due to differential expansion between the various materials used in constructing a bearing. For example the clearances necessary for correct operation at low temperatures may be insufficient at higher temperatures and rapid wear could occur if the machine were operated before they had fully cooled to their design temperature.

Thermosetting plastics

Thermosetting resins are typically small molecular units which are extensively crosslinked by primary bonds to form a three-dimensional molecular network. This structure gives rigid and strong, but inherently brittle, materials whose properties are not

so noticeably time- or temperature-dependent once they are fully cured. They are effectively organic glasses, like thermo-plastics well below their glass-transition temperature. Furthermore, as a result of a combination of their high coefficients of thermal expansion and their low thermal conductivities they have poor resistance to thermal shock and they are liable to craze if cooled rapidly to low temperatures. These factors impose severe limitations on their use in the unmodified state and they are almost invariably used in conjunction with suitable fillers such as powders or fibres. Most fillers have low expansion coefficients and so help to lower those of the resins to match them to common metals and alloys. Graphite and metallic flakes can improve the thermal and electrical conductivities of resins, while most fibrous fillers significantly increase their toughness. Cloth fabrics, paper, and other fibrous materials can be impregnated with resin and cured to form composites such as Tufnol, which are strong, tough, dimensionally stable, easily machined by conventional techniques, and available in the form of bar, rod, tube, and sheet. Furthermore, the good electrical-insulating characteristics of this material are not adversely affected by low temperatures as long as condensation is avoided during warm-up and cool-down.

10) Composite materials

Glass fibres are the most widely used reinforcement for load-bearing composites and, despite the inherently brittle natures of both fibres and thermo-setting resin, the resultant composites are strong and tough and remain so at low temperatures. Their toughness results from their heterogeneous structure which ensures that a crack nucleated in one fibre is slowed down or deflected by the matrix so that it does not lead directly to failure in adjacent fibres, thus ensuring that failure is progressive and energy absorbing and not brittle as in the bulk material.

As the reinforcing fibres are stronger and stiffer than the matrix, they support the greater part of the applied load and the strength of the composite is determined by the length, orientation, and concentration of the fibres, 50-60 per cent of fibres by volume being typical maximum concentrations unless filament-winding techniques are used. Tensile strengths of 270-420 MPa are typical of room-temperature values and these increase gradually to about 480-700 MPa at 77 K but then remain more or less constant down to 4 K. Their moduli are less temperature dependent, increasing by about 10-20 per cent on cooling from 300 K to 20 K, while their toughness as measured by impact or notched tensile tests shows little significant variation over this temperature range. These are quite high strengths by most standards, and when the low density of glass-fibre-reinforced plastics (GRP) is taken into consideration it can be seen that their specific strengths are extremely high - hence the interest in their use for fuel tanks and other structures in aerospace applications. Representative values of the mechanical properties of some fibre-reinforced composites are given in Table 11.

Glass-fibre reinforced composites do, however, have several drawbacks. Static fatigue, which is a characteristic failure mode in bulk glass and unreinforced thermoplastics, can also occur in GRPs if moisture is able to penetrate the fibre matrix interface, although this failure mechanism does not operate if the composite is maintained at low temperatures. A more serious difficulty lies in the highly anisotropic nature of their mechanical properties, reinforcement being much more efficient in a direction parallel to the fibres than perpendicular to them. Cross-plying the laminations allows two-dimensional reinforcement, but strengths and moduli are reduced to one-third of those attainable parallel to the fibres, while three-dimensional reinforcement lowers strengths and modulii to one sixth of their parallel value.

Tensile tests carried out on cross-ply laminated sheet specimens show a change from a high initial modulus to a lower secondary modulus at a load equivalent to about 13-15 per cent of their respective ultimate load-carrying capacities. If the specimens are examined at this stage they can be seen to be full of microcracks and the material is now porous and unable to retain vapour or liquids. The root of this difficulty lies in the failure of the bond at the fibre-matrix interface in those fibres that have a large stress component resolved perpendicular to the fibres, as this bond has a strength of about 12-15 per cent of that parallel to the fibres. Hence the material has become porous long before it has developed its full potential strength and this is a serious drawback for applications such as filament-wound GRP fuel tanks. Attempts have been made to line such vessels with thin plastic films such as Mylar, but severe problems are encountered as a result of differential expansion between the liner and the GRP, which usually causes decohesion. More success has been achieved by electroplating a thin layer of nickel inside the tanks as this is sufficiently ductile to yield and deform to remain adherent to the GRP wall. This technique has also the added benefit that the liner can be applied after all the side tubes and flanges have been bonded to the tank. Vacuum-tight joints between GRPs and metals are not easy to achieve and some of the earlier attempts at using GRP for the inner vessel of vacuum-insulated liquid-nitrogen storage vessels were unsuccessful because of the failure of the metal-GRP bond at the neck. Nevertheless once this problem was overcome the use of GRP neck tubes allowed very efficient storage Dewar flasts to be made because of the extremely low thermal conductivity of GRPs. As noted in lecture 4 , GRPs have the highest ratio of strength/thermal conductivity of any material used in cryogenic equipment and their use for load-bearing, thermally insulating supports is increasing both for tensile and compressive-loading configurations.

Finally, the recently developed carbon-fibre-reinforced plastics (CFRPs) are also suitable for use at low temperatures, although neither their strengths nor modulii increase by more than a few per cent on cooling from room temperature to 77 K and below.

Table 11. Typical mechanical properties of some fibre-reinforced composites.

Material and condition		Tempe-rature (K)	Tensile strength (MPa)	Tensile modulus (GPa)	Elonga-tion %	Flexural strength (MPa)	Flexural modulus (GPa)	Shear strength (MPa)	Comp-ressive strength (MPa)	Source
Filament-wound S/HTS glass cloth Type 1581-epoxy resin Type E787 (68% V/V glass)	stress applied parallel to fibres	298	638	22.7	3.4	718	22.9	57	432	Landrock (1965)
		197	797	24.1	4.1	928	23.0	69	548	
		77	997	27.4	5.0	1177	27.0	93	712	
		20	950	29.4	4.8	1243	25.3	80	752	
	stress applied at 45° to fibres	298	226	10.3	>10.0	335	11.3	43	216	Landrock (1965)
		197	317	14.5	10.6	498	12.5	50	317	
		77	349	18.8	6.7	725	17.9	65	482	
		20	321	19.5	4.8	712	20.1	60	536	
Type 181 glass cloth-epoxy resin (average of 5 resins, % V/V glass not specified)		300	363	-	-	576	-	-	387	Landrock (1965)
		195	536	-	-	758	-	-	630	
		77	735	-	-	1091	-	-	792	
		20	753	-	-	1068	-	-	810	
Type 181 glass cloth-polyester resin (average of 4 resins, % V/V glass not specified)		300	323	-	-	494	-	-	191	Landrock (1965)
		195	443	-	-	597	-	-	302	
		77	621	-	-	676	-	-	397	
		20	633	-	-	693	-	-	387	
Type 181 glass cloth phenolic resin (average of 2 resins, % V/V glass not specified)		300	310	-	-	485	-	-	403	Landrock (1965)
		195	425	-	-	608	-	-	494	
		77	498	-	-	667	-	-	624	
		20	473	-	-	665	-	-	580	
RAE Type I. carbon fibre epoxy resin (30% V/V carbon		300	434	110	-	-	-	-	-	Wigley (1971)
		77	448	116	-	-	-	-	-	

They have much higher thermal and electrical conductivities than GRPs, which makes them less useful as materials for insulating supports, and it is only where their much higher modulii are advantageous that they are likely to be employed. For example, their higher moduli enable them to develop higher working stresses at low strains with the result that, although liable to failure of the fibre-matrix interface perpendicular to the applied stress when cross plied, highly stressed fuel tanks having much lower working strains can be made, thus minimizing the vapour-barrier problem.

Composites reinforced with glass, carbon, boron, and other fibres have been reviewed by Kasen (17) while many aspects of the properties of "non-metallic materials and composites at low temperatures" are covered in the proceedings of an I.C.M.C. Symposium of the same title (10).

Further sources of data and references (see also references at end of paper 4)

1. American Society for Testing and Materials (ASTM), Philadelphia, Pa., U.S.A. publishes Special Technical Publications, occasional issues such as those listed below being of cryogenic interest.
2. STP 302 Metallic materials for low temperature service (1961).
3. STP 381 Fracture toughness testing (1965).
4. STP 387 Behaviour of materials at cryogenic temperatures (1966).
5. STP 410 Plane strain crack toughness testing of high strength metallic materials (1966).
6. STP 544 Heat transmission measurements in thermal insulation (1974).
7. STP 556 Fatigue and fracture toughness - cryogenic behaviour (1974).
8. STP 576 Properties of materials for liquid natural gas tankage (1975).
9. Thermophysical properties of materials, Plenum, New York, Vol.1. Thermal Conductivity (1970), Vol.12 Thermal Expansion (1975).
10. Clark, A.F., Reed, R.P., and Hartwig, G., Eds. Nonmetallic materials and composites at low temperatures, Proc. ICMC Symp. (Munich, Germany, Jul.10,1978) Plenum, New York, (1979).
11. Low temperature and cryogenic steels, U.S. Steel International, Pittsburg, Pa. (1966).
12. Materials for cryogenic service; engineering properties of 3½, 5 and 9% nickel steels and 36% nickel-iron alloys, International Nickel Ltd., London, (1972).
13. Engineering properties of stainless steels. International Nickel Ltd., London, (1974).
14. Gunter, C.S. and Reed, R.P. in Timmerhaus, K.D. (Ed.) Advances in Cryogenic Engineering, 6, 565, (1961).
15. Ferris, J., Cryogenic Wind Tunnel Force Instrumentation, Proc. 1st Int. Symp. on Cryogenic Wind Tunnels, Southampton, England (1979).
16. LNG Materials and fluids users manual (1977 and supplements) NBS, Boulder.
17. Kasen, M.B., Cryogenics, 15, 327 and 701 (1975).
18. Vance, R.W., Ed. Advances in Cryogenic Technology, 4, (1972).
19. Proceedings of Gastech. 78, Gastech. Ltd., Rickmansworth, Herts., England. (1979).
20. Wigley, D.A., Materials for Low Temperature Use, Engineering Design Guide No.26, Design Council/Oxford University Press, (1978).
21. Haselden, G.G. (Ed.) Cryogenic Fundamentals, Academic Press, London, (1971).
22. Scott, R.B., Cryogenic Engineering, Van Nostrand, New York (1959).
23. Serafini, T.S., and Koenig, J.L. Cryogenic properties of polymers, Marcel Dekker, New York, (1968).
24. Vance, R.W. and Duke, W.M. Applied cryogenic engineering, Wiley, New York, (1962).
25. Conte, R.R. Elements de cryogenie, Masson et Cie, Paris (1970).
26. Codlin, E.M. Cryogenics and refrigeration; a bibliographical guide, Plenum Press, New York, (1968).
27. Barron, R. Cryogenic systems, McGraw-Hill, New York, (1966).
28. Landrock, A.H. Properties of plastics and related materials at cryogenic temperatures. PLASTEC Report No.20, CDC Accession No AD469126 (1965).
29. Weitzel, D.H., Robbins, R.F. and Bjorkland, W.R. Advances in cryogenic engineering, 6, 219, (1961).
30. Solyanko, V.F., Boiko, T.P. and Kudrgavtseva, K.A. Cryogenics, 19, 113, Feb.1979.

REAL GAS EFFECTS II - INFLUENCE OF CONDENSATION ON MINIMUM OPERATING TEMPERATURES OF CRYOGENIC WIND TUNNELS

Robert M. Hall
Aeronautical Research Scientist
NASA Langley Research Center
Hampton, Virginia 23665, USA

SUMMARY

Minimum operating temperatures of cryogenic wind tunnels are limited by real-gas effects. In particular, condensation effects are responsible for the minimum operating temperatures at total pressures up to about 9 atmospheres. The present paper reviews the two primary modes of condensation - homogeneous nucleation and heterogeneous nucleation - and the conditions with which either may limit minimum operating temperatures. Previous hypersonic and supersonic condensation data are reviewed as are data taken in the nitrogen-gas, Langley 0.3-Meter Transonic Cryogenic Tunnel. Analysis of data in the 0.3-m tunnel suggests that the onset of homogeneous nucleation may be approximated by an analysis by Sivier and that the onset of heterogeneous nucleation is only apparent just below free-stream saturation. Extension of the results from the 0.3-m tunnel to other nitrogen-gas cryogenic tunnels is discussed and is shown to depend on length scales, purity of the liquid nitrogen injected for cooling, number of particulates in the flow, and the extent to which the injected liquid nitrogen is evaporated. On the basis of previous data, hybrid air-nitrogen tunnels are expected to realize little, if any, supercooling.

1. INTRODUCTION

Cryogenic wind tunnels under normal conditions should be operated at the lowest possible total temperature in order to maximize Reynolds number capability for a given tunnel total pressure or to minimize costs for operating at a fixed Reynolds number. This important realization is readily seen in figure 1, which shows for nitrogen gas both unit Reynolds number and drive power required relative to their values at a total temperature of 322 K as a function of total temperature for a constant total pressure. Not only is Reynolds number increasing as the temperature decreases, but its rate of increase is growing as well. Obviously, if one wants to maximize Reynolds number capability and is limited by total pressure capability, then it is desirable to operate as cold as possible to move up the steep portion of the curve. For operation at some Reynolds number below the maximum capability of the tunnel, being able to test as cold as possible maximizes the amount of Reynolds number gained by temperature reduction and minimizes the use of pressure to achieve the desired test Reynolds number. If pressure can be minimized, drive power--which is proportional to pressure--will be minimized as a result of both the reduced pressure and the trend of power reduction at the lower temperatures seen in figure 1. Operation at a reduced pressure also, of course, reduces the model loads and eases the balance, sting, and model stress problems.

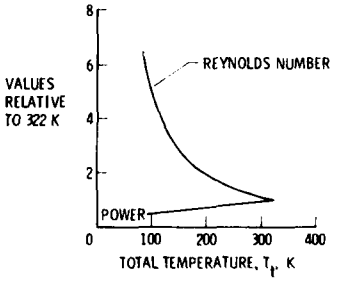

Figure 1.- Effect of temperature reduction on unit Reynolds number and drive power for $M_\infty = 1.0$ and $p_t = 1.0$ atm.

The minimum operating temperatures, however, are limited by the low-temperature behavior of the test gas. At some temperature, either the test gas begins to experience condensation effects or its equation of state will be such that the gas ceases to simulate the nearly ideal-gas behavior of air encountered in flight. The present report examines the condensation aspects of minimum operating temperatures associated with cryogenic wind tunnels, while the companion report entitled "Real Gas Effects I - Simulation of Ideal-Gas Flow by Cryogenic Nitrogen and Other Selected Gases" examines the real-gas behavior of nitrogen gas and other alternative cryogenic gases. As is reported in the companion report, nitrogen gas will adequately simulate the flow of an ideal, diatomic gas except possibly when attempting to run at or below saturation temperatures for total pressures approaching 9 atm. Consequently, it appears that for total pressures below 9 atm the onset of condensation effects will be the limiting factor with regard to the minimum operating temperatures.

The present report will review the two modes of condensation that can affect the minimum operating temperatures of cryogenic wind tunnels, review pertinent experimental evidence relevant to both types of condensation including data taken in the Langley 0.3-Meter Transonic Cryogenic Tunnel (TCT), and discuss the factors involved in predicting minimum operating temperatures in cryogenic tunnels other than the 0.3-m TCT. The main focus of this paper will be on pure nitrogen as the test gas, although some comments will be directed to tunnels that use an air-nitrogen mixture.

2. CONDENSATION CONCERNS IN WIND TUNNELS - PAST AND PRESENT

That condensation plays an important role in determining the wind-tunnel operating envelope is not unique to cryogenic wind tunnels. Interplay between wind-tunnel development and condensation phenomena first began in 1935 at the Volta conference (see reference 1). A schlieren photograph of a so-called "X" shock was shown at that conference by Prandtl and the resulting investigation determined that the phenomenon was associated with condensation of water vapor and led to the installation of dryers in supersonic wind-tunnel circuits. Again, during the development of hypersonic tunnels in the late 1940's and 1950's, condensation was a key concern as it established the minimum temperature to which the stagnation chamber would have to be heated in order to avoid condensation of the test gas itself in the test section. Once again during the 1970's, these same condensation considerations reappeared when nitrogen-gas cryogenic wind tunnels were being designed and built.

While condensation in nitrogen gas was examined during the studies concerning hypersonic wind tunnels, several differences exist between the situation in hypersonic tunnels and the present situation in transonic cryogenic wind tunnels. First, in the hypersonic tunnels, onset would typically occur in a static pressure range below 0.01 atm, whereas in transonic cryogenic tunnels onset may occur at static pressures on the order of 1 atm or more. At the higher static pressures of the transonic cryogenic tunnels, the rate of growth of droplets can be significantly higher than at the lower pressures. Furthermore, the residence times in the test section of transonic cryogenic tunnels are much longer than in the hypersonic tunnels because of both the reduced test-section velocities and, for many cryogenic tunnels, increased test-section sizes. For example, test-section residence time in the National Transonic Facility (NTF), described in reference 2, may be on the order of 0.05 sec, whereas a typical residence time in hypersonic tunnels is on the order of 10^{-4} or 10^{-3} sec. The longer residence times may allow sufficient condensation to occur on impurities in the cryogenic tunnels to affect the flow, whereas the small amount of growth that could take place during the short time in hypersonic tunnels would render the presence of an equal number of impurities unimportant. Because of these differences between the cryogenic and hypersonic tunnels, the necessity for a new investigation of condensation effects soon became apparent.

3. FORMATION OF HOMOGENEOUS NUCLEATION IN REGIONS OF HIGH LOCAL MACH NUMBER

An investigation of condensation in cryogenic wind tunnels must examine effects resulting both from the gas forming its own nucleation sites - homogeneous nucleation - and from droplet growth occurring on pre-existing seed particles - heterogeneous nucleation. The probability of homogeneous nucleation will be greatest for test situations in which high maximum local Mach numbers, $M_{L,max}$, occur over the model. To understand homogeneous nucleation, the insights of classical liquid droplet theory will be discussed as well as the shortcomings of the theory. As an example of classical liquid droplet theory, the work of Sivier in reference 3 will then be highlighted and used for comparison during the rest of this report.

If homogeneous nucleation could take place as soon as the flow became saturated, the minimum operating temperatures would be determined by the saturation temperatures corresponding to $M_{L,max}$ over the model. The saturation temperatures for values of $M_{L,max}$ of 1.0, 1.5, and 2.0 are shown in figure 2 for nitrogen as a function of p_t. The M = 0, or reservoir, saturation line is also shown for reference. This line represents the lowest possible operating temperature useful in cryogenic tunnels cooled by injecting liquid nitrogen, because at lower temperatures the injected liquid would be unable to evaporate and would fill the tunnel with liquid. Given the dramatic increase in Reynolds number, R, at the low temperatures in figure 1, being able to operate below saturation temperatures would result in significant increases in R, particularly at the higher values of $M_{L,max}$.

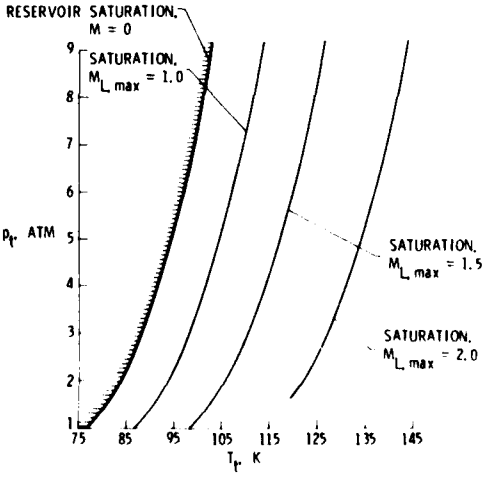

Figure 2.- Minimum operating temperatures for various values of $M_{L,max}$ if condensation effects occurred at nitrogen saturation temperatures.

Before explaining why operation below saturation temperatures should be possible prior to the onset of homogeneous nucleation, it is convenient to define two measures of how far the flow has progressed beyond saturation, which occurs when the flow isentrope reaches the vapor-pressure curve. One measure is called the supersaturation ratio, S, defined by

$$S = \frac{p}{p_\infty(T)} \qquad (1)$$

where $p_\infty(T)$ is the saturated vapor pressure for a plane surface of liquid at the gas static temperature, T. Another measure of how far below the vapor-pressure curve the flow has progressed is the supercooling, ΔT, defined as

$$\Delta T = T_s - T \tag{2}$$

where T_s is the saturation temperature at which the expansion isentrope crosses the vapor-pressure curve. Figure 3 illustrates such an expansion beyond the vapor-pressure curve and shows both S and ΔT for point 1 along the isentrope.

3.1 Classical Liquid Droplet Theory

The reason that it is usually safe to assume that homogeneous nucleation will not necessarily occur before the flow is supersaturated ($S > 1$) is that an energy barrier does exist to the formation of liquid droplets by the gas, which is the key mechanism of homogeneous nucleation. As explained in reference 4, the "classical" energy of formation of a drop has a maximum at some critical droplet radius, r_c, as seen in figure 4.

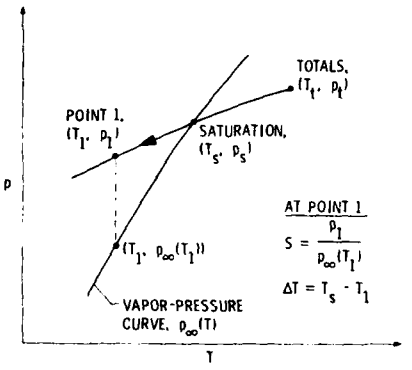

Figure 3.- Supersaturation ratio, S, and supercooling, ΔT, at a point 1 along an expansion isentrope beginning at T_t and p_t.

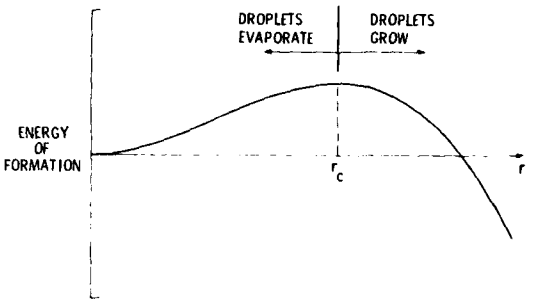

Figure 4.- Energy of formation of a classical liquid droplet.

All droplets with radius, r, less than r_c will tend to evaporate while all droplets with $r > r_c$ will be stable and will grow. The value of r_c will depend on the flow supersaturation ratio and is given in reference 5 in a form convenient for SI units as

$$r_c = \frac{2\sigma_\ell \rho}{\rho_\ell p \ln S} \tag{3}$$

where ρ and p are the vapor density and pressure, and where σ_ℓ and ρ_ℓ are the liquid values of surface tension and density. At saturation $S = 1$ and $r_c = \infty$, however, r_c decreases as S increases, and the more likely it becomes that random collisions of gas molecules will result in a growing droplet with $r > r_c$.

At some value of S, r_c will become small enough that random collisions of the molecules will result in a finite rate of production of stable, growing droplets. Again referring to reference 5, this rate of droplet formation, I, in units of droplets formed per second per kilogram of the gas, can be expressed as

$$I = \frac{\rho}{\rho_\ell} \sqrt{\frac{2\sigma_\ell}{\pi m_m^3}} \exp\left(-\frac{4\pi r_c^2 \sigma_\ell}{3kT}\right) \tag{4}$$

where m_m is the mass of one molecule, k is the Boltzmann constant, and T is the gas temperature. Substituting Eq. (3) into Eq. (4) gives

$$I = \frac{\rho}{\rho_\ell} \sqrt{\frac{2\sigma_\ell}{\pi m_m^3}} \exp\left(-\frac{16\pi \sigma_\ell^3 \rho^2}{3kT\rho_\ell^2 p^2 \ln^2 S}\right). \tag{5}$$

The dominant exponential term is proportional to σ_ℓ^3 as well as the inverse of $\ln^2 S$. The value of σ_ℓ is uncertain because the critical droplet sizes often correspond to clusters of 20 molecules or less. It is questionable if the planar value of macroscopic

surface tension even applies to such small clusters. Several researchers have proposed corrections to σ_ℓ, one of which was reported by Tolman in reference 6. The value of S is extremely important in Eq. (5) because it is responsible, to a large extent, for the dramatic increase in I as the gas proceeds along a supersaturated isentrope, which can be seen in Table I for an isentropic expansion from reservoir conditions of $p_t = 4.76$ atm and $T_t = 109.0$ K to a Mach number of 1.7. For this example, the flow crosses the saturation curve at $M = 1.26$.

TABLE I.- DROPLET FORMATION RATE ALONG AN ISENTROPE

M, Mach	I, Droplet Formation/(kg·sec)
1.50	3×10^{-28}
1.60	3×10^{-5}
1.70	4×10^{5}

3.2 Difficulties with the Classical Theory

There are, however, some theoretical problems with the classical liquid droplet theory. First, there is the uncertainty in the value of σ_ℓ to be used for the small droplets. The method of Tolman to correct for this small radius takes the form

$$\sigma_\ell = \frac{\sigma_\infty}{1 + \frac{D_T}{r}} \tag{6}$$

where σ_∞ is the macroscopic value of surface tension for an infinite plane surface and D_T is a dimension closely related to the intermolecular distance in the liquid droplet. Consequently, the value of σ_ℓ from Eq. (6) would be used in Eqs. (4) and (5) instead of the macroscopic, planar values. The next problem with the classical value of I for application to cryogenic wind tunnels, in which the test gas itself condenses, is that the droplets will not be at the same temperature as the surrounding gas because there is no carrier gas present which can carry the latent heat away from the growing droplets. Thus, a further correction can be made to I for cryogenic tunnels and can be expressed, as in reference 7, as

$$I_{noniso} = \Gamma_{noniso} I_{iso} \tag{7}$$

where the subscript "noniso" denotes nonisothermal temperature conditions (cryogenic tunnels) and "iso" denotes isothermal conditions (carrier gas present). The factor Γ_{noniso} is the correction for I_{iso}, the isothermal rate of production of droplets as given in Eq. (5). Details of Γ_{noniso} may be found in reference 7.

Theorists also disagree on how to incorporate into I the fact that the small droplets themselves behave like large molecules and have translational and rotational energy states, which are disregarded in the classical liquid droplet theory. In general, this further correction may also take the form (ref. 7)

$$I_{stat} = \Gamma_{stat} I_{class} \tag{8}$$

where the subscript "stat" denotes the statistical mechanics expression necessary to incorporate the energy states of the droplet and "class" denotes the classical formulation as in Eq. (7) or (5).

[illegible] in the condensation field, such as Wegener at Yale University, advo- [illegible] and Γ_{stat} together into a single Γ_{emp} and then adjusting Γ_{emp} [illegible] appropriate data, as was done, for example, in reference 8. [illegible] corrected planar value of σ_ℓ in his equations for I and allows [illegible] for that term also. Further calculations then proceed [illegible]

[illegible] Sivier

[illegible] the classical nucleation theory, it [illegible] problems. During an investigation in [illegible] comparable to Eq. (4) for I to [illegible] he did not incorporate [illegible] into his expression [illegible] for a [illegible] there have also [illegible] expansion [illegible]

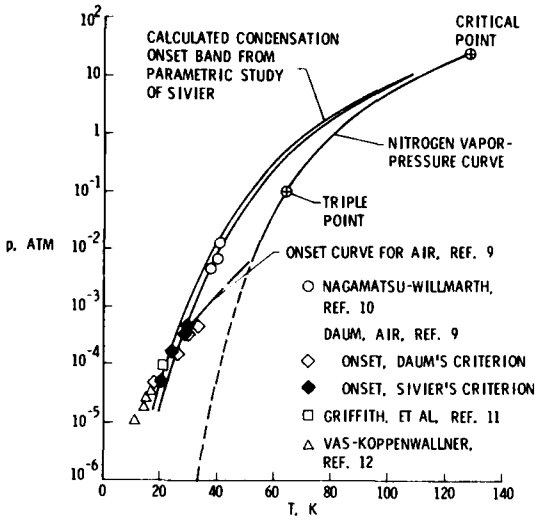

Figure 5.- Onset band of homogeneous nucleation as predicted for nitrogen by Sivier in reference 3. Experimental comparisons shown are examples used by Sivier.

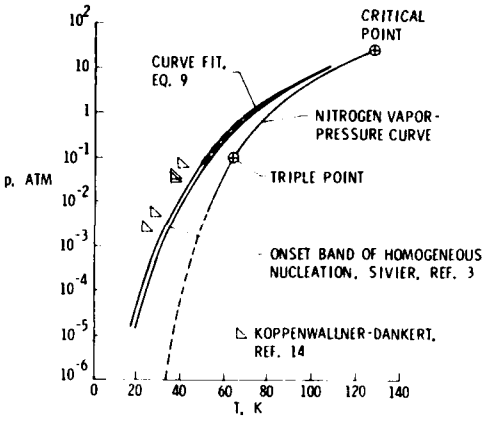

Figure 6.- Comparisons of Sivier's onset band for homogeneous nucleation effects to Eq. (9), dotted line, and to data from reference 14.

between the two curves encompassing Sivier's parametric study is not large compared to the magnitude of the distance to the vapor-pressure curve. Thus, to a good approximation in the 50 to 90 K temperature range, his onset values have been approximated in the Langley study by a single curve fit,

$$\frac{1}{T_e} = 0.01461 - 0.004962 \log_{10} p + 0.0001959 (\log_{10} p)^2 \qquad (9)$$

where T_e is the predicted static temperature at which homogeneous nucleation effects will be detected for a given value of static pressure, p. Equation (9) is compared to Sivier's onset band in figure 6 for static temperatures from 50 to 90 K. During this report, Eq. (9) will be used in conjunction with the isentropic flow equations to calculate the total conditions, p_t and T_t, corresponding to homogeneous nucleation effects at values of p and T_e when the flow has been expanded isentropically to some Mach number, M, usually $M_{L,max}$.

As shown in figure 5, Sivier compares his computational predictions to data from references 9, 10, 11 and 12. Nitrogen data are presented by references 10, 11 and 12 and are shown to agree quite well with his predicted onset conditions. (Isentropic expansions cross the vapor-pressure curve from right to left as seen in figure 3.) The air data presented by reference 9 are also of interest because cryogenic blowdown tunnels using a mixture of air and nitrogen may experience similar amounts of supercooling. At static pressures below 10^{-3} atm, air undergoes onset at conditions similar to nitrogen; however, as seen by the line labelled "Onset curve for air" in figure 5, the amount of supercooling to be expected above 10^{-3} atm begins to decrease until it is negligible above 10^{-2} atm. As explained by Daum and Gyarmathy in reference 13, at pressures above 10^{-3} atm the carbon dioxide and water vapor components condense out at higher temperature and form very large numbers of clusters that serve as seed nuclei for both nitrogen and oxygen. These large numbers of seed particles permit condensation to occur almost as soon as the flow is saturated and lead to the conclusion that the hybrid air-nitrogen cryogenic tunnels may not realize supercooling of any significant extent.

Nitrogen data in addition to those used by Sivier in his comparisons are available. In 1979 Koppenwallner and Dankert published nitrogen condensation data in reference 14, and a figure from that report is reproduced here as figure 7, which shows their onset conditions for free-jet expansions with a total pressure of 3 atm and a range of total temperatures. Taking their reported values for the onset of condensation for the examples in figure 7, their experimental values for onset are compared to Sivier's lines in figure 6. Koppenwallner and Dankert show significantly more supercooling before the onset of effects in their free jet than predicted by Sivier. On the other hand, in 1959 Goglia reported in reference 15 results taken with 95 percent pure nitrogen. His results are compared to Eq. (9) in figure 8, and as is seen, he found less supercooling in his nozzle flow than predicted by Sivier. It is logical to suspect that his low value of supercooling may have been due to the low purity of his nitrogen. However, this possibility was recognized by Goglia, and consequently he conducted a few tests with high-purity nitrogen (>99.995 percent) and found no difference from the data for 95 percent nitrogen. While neither reference 14 nor reference 15 agrees exactly with Sivier's predictions, they both at least follow his trend with pressure.

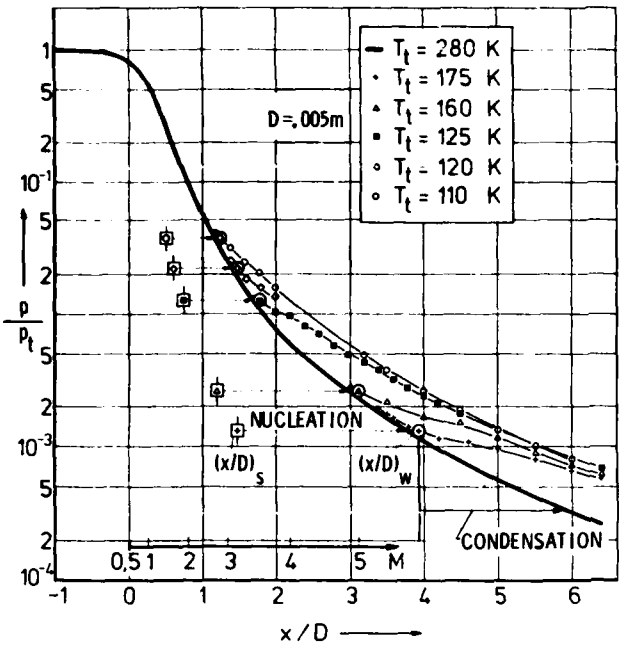

Figure 7.- Effects of homogeneous nucleation on static pressures along a free jet for p_t = 3 atm. D is orifice diameter. Subscript "s" is for conditions at saturation and "w" is for conditions at onset (Koppenwallner and Dankert, ref. 14).

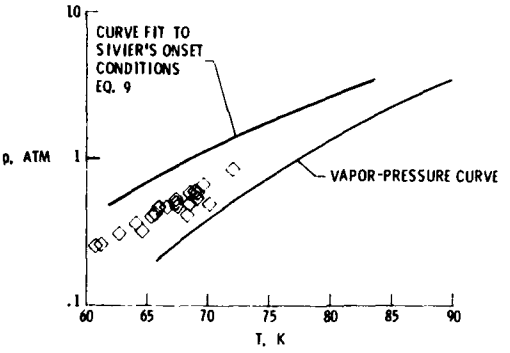

Figure 8.- Data (symbols) for onset of homogeneous nucleation as determined by Goglia in reference 15 compared to Eq. (9).

3.4 Predicted Onset of Homogeneous Nucleation Effects

Because of the agreement between Sivier's calculations for the predicted onset of homogeneous nucleation effects and at least the trends of the existing data, Sivier's onset of effects as represented by Eq. (9) will be used to give an estimate of operating temperatures that would mark the onset of homogeneous nucleation. At the beginning of this section, saturation curves were shown in figure 2 that would designate minimum operating temperatures in nitrogen-gas, cryogenic wind tunnels if no supersaturation took place before the onset of homogeneous nucleation. The comparable operating temperatures are redrawn in figure 9 assuming that the curve fit to Sivier's onset conditions, Eq. (9), adequately represents those static temperatures at which the onset of homogeneous nucleation will occur. Comparing figures 2 and 9, it is obvious that the lower operating temperatures predicted before the onset of homogeneous nucleation would lead to significant increases in Reynolds number capability at a given total pressure. In fact, typical percentage increases in R obtained by running with $M_\infty = 1.0$ at the operating temperatures as predicted using Eq. (9) over the values of R at the same p_t but at the higher saturation temperature are listed in the following Table II.

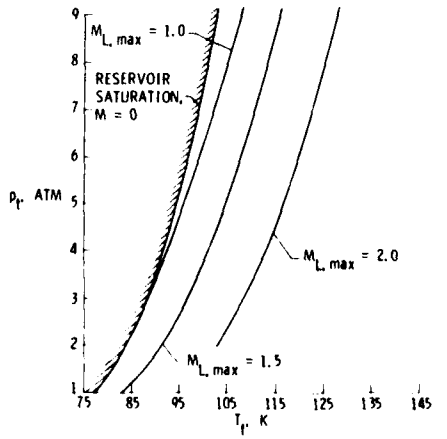

Figure 9.- Operating temperatures at the predicted onset of homogeneous nucleation according to Eq. (9) for various values of $M_{L,max}$. Nitrogen gas.

TABLE II.- PERCENTAGE INCREASES IN R OVER VALUES AT SATURATION WHEN RUNNING WITH TEMPERATURES AT WHICH HOMOGENEOUS NUCLEATION IS PREDICTED TO OCCUR BY EQ. (9). $M_\infty = 1.0$.

	PERCENTAGE INCREASES IN R FOR VALUES OF $M_{L,max}$ OF		
p_t, atm	1.0	1.5	2
1	-	27	32
5	14	18	23
9	8	14	19

Again, the $M = 0$ saturation line is shown in figure 9 as the absolute minimum operating temperature for cryogenic tunnels because of the method of injecting liquid for cooling, even if the analysis predicted lower total temperatures before the onset of homogeneous nucleation. For this reason the percentage increase in R in Table II for $p_t = 1$ atm and $M_{L,max} = 1.0$ is not given.

The operating temperatures at which homogeneous nucleation is predicted to occur, as shown in figure 9, do not necessarily form the minimum operating temperature limits for cryogenic wind tunnels. If, for example, the local Mach number over the airfoil is not very high ($M_{L,max} < 1.5$), then effects due to heterogeneous nucleation upstream of the model on pre-existing seed particles may affect the test-section flow at a higher temperature than that at which homogeneous nucleation is predicted over the airfoil. It is even possible that in situations when large numbers of pre-existing seed particles are present or large-chord airfoils are being tested, condensate growth on pre-existing seed particles in the region of high local Mach number flow over an airfoil may locally affect the data at temperatures above those corresponding to homogeneous nucleation. Consequently, the lines in figure 9 only apply to prediction of the onset of homogeneous nucleation; there may be condensation effects at higher temperatures due to pre-existing seed particles in the flow.

4. SOURCES OF SEED PARTICLES IN CRYOGENIC TUNNELS

As seen in the previous section, there is usually a significant amount of supercooling possible before the onset of homogeneous nucleation. The other mode of condensation, heterogeneous nucleation, can take place when there are pre-existing seed particles - perhaps liquid or solid - in the flow. With existing seed particles available as surfaces on which the nitrogen gas can condense, there is no energy barrier to overcome before phase transition can take place because there are already particles on which growth can occur. Consequently, the condensation process can proceed as soon as the saturation line is crossed. Fortunately for the user of cryogenic tunnels, either a large number of impurity sites or a long residence time is usually required for heterogeneous nucleation to influence the flow. The number of nucleating sites in fan-driven cryogenic wind tunnels due to dust or dirt is not expected to be unusually large compared to conventional tunnels. In fact, the tunnels are being continuously purged by evaporated liquid nitrogen and are expected to be as free of solid or liquid impurities as the injected liquid nitrogen is itself. However, at some low tunnel temperatures, the liquid nitrogen injected to cool the tunnel will not evaporate completely before being convected to the test section. At whatever temperature this occurs, there can be a very large increase in the number of seed particles in the test section on which condensation can occur.

4.1 Seed Particles Generated at the Liquid Nitrogen Injection Station

The first step in understanding the liquid nitrogen injection problem is to characterize the distribution of droplet sizes immediately downstream of the injection station. Many different theories are available to describe this process and some are reported in references 16 to 18. The distribution that has been used in calculations at Langley is a modified version of the Nukiyama-Tanasawa distribution.

Nukiyama and Tanasawa published a series of reports (ref. 18) on droplet atomization in 1938. By analyzing empirical results, they were able to formulate expressions to predict the volume to surface mean droplet diameter, D_{32}, and a size distribution about that mean. Their formula for D_{32} in their system of units is given by

$$D_{32} = \frac{585}{w_r}\sqrt{\frac{\sigma_\ell}{\rho_\ell}} + 597\left(\frac{\mu_\ell}{\sqrt{\sigma_\ell \rho_\ell}}\right)^{0.45}\left(1000\,\frac{Q_\ell}{Q}\right)^{1.5} \qquad (10)$$

where D_{32} is in micrometers; w_r is the relative velocity between the liquid and the gas in meters per second; σ_ℓ, ρ_ℓ, and μ_ℓ are the liquid values of surface tension, density, and viscosity in cgs units; and Q_ℓ/Q is the ratio of volume of liquid injected to volume of gas flowing. For the droplet size distribution function they arrived at the following equation:

$$\frac{dn}{n} = 0.5b^3D^2 \exp(-bD)\, dD \tag{11}$$

where n is the total number of droplets per second and dn is the number of droplets in the size range dD per second. The constant b is empirically found to be

$$b = \frac{5}{D_{32}} \tag{12}$$

In reference 16, Ingebo and Foster suggest a refinement to Eq. (11) by placing an empirically determined upper limit to the droplet size. Ingebo and Foster use the following expression for the maximum droplet diameter:

$$D_{max} = 22.3\, d_o \left(\frac{\sigma_\ell\, \mu_\ell}{\rho\rho_\ell d_o^2 w_r^3}\right)^{0.29} \tag{13}$$

where d_o is the diameter of the injection orifice. A typical example of a droplet size distribution calculated for the Langley 0.3-m TCT using Eqs. (10) through (13) is shown in figure 10 for the following conditions: $M_\infty = 0.35$, $p_t = 4.0$ atm, $T_t = 96$ K, $T_\ell = 80$ K, a percent of liquid mass injected to mass of gas flow of 1.57, and a Mach number at the injection point, M_{inj}, of 0.20. The actual numbers in each size category, Δn, are based on a test-section cross-sectional area of about 0.1 m^2. The liquid temperature, T_ℓ, is taken to be 80 K during injection because that is the temperature at which the liquid nitrogen is normally stored and pumped into the tunnel. For this example $D_{32} = 54$ μm and $D_{max} = 94$ μm. Both of these values are very large diameters when compared to typical diameters of 0.1 μm or 0.01 μm for droplets resulting from homogeneous nucleation.

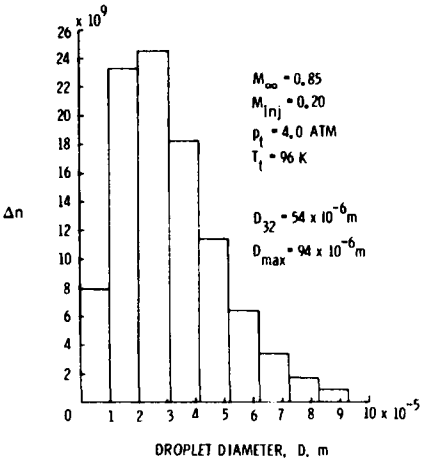

Figure 10.- Droplet distribution as predicted by Nukiyama-Tanasawa for conditions in the 0.3-m TCT. Percent of liquid injected to test-section mass flow is 1.57 percent.

The attractiveness of the Nukiyama-Tanasawa formulation is that it models both the process wherein the liquid nitrogen is shattered by the aerodynamic forces resulting from the difference in velocity between the liquid and the gas, and the process of recombination of the atomized droplets due to random collisions when a large amount of liquid is being injected. Atomization is represented by the first term on the right side of Eq. (10) and recombination is represented by the second term. The recombination term does not represent a significant increase in D_{32} for a continuous-flow, fan-driven tunnel, in which the percentage of liquid mass injected is only about 1.5 percent of the total mass flow. On the other hand, for blowdown tunnels that add nearly an equal mass of liquid to the gas flowing past the injection station, recombination can be an important term. Another observation from Eq. (10) is that to minimize the size of D_{32}, it is desirable to inject the liquid at a station in the tunnel where the value of relative velocity, w_r, between the injected liquid and the gas is as large as practical.

4.2 Interaction of the Liquid Nitrogen Seed Particles with the Tunnel Circuit

Once the initial droplet size distribution can be calculated, the progress of the droplets as they proceed in the tunnel circuit can be described. This progress is related to the type and location of flow obstacles in the circuit, and the Langley 0.3-m TCT will be used as an example for the present discussion. The TCT is shown in schematic form in figure 11 and presents a series of obstacles to droplets: corners with turning vanes, a drive fan, and anti-turbulence screens. Droplets being convected by the gas past these obstacles may impact on them and then may return to the flow with different sizes. In other words, each obstacle has the potential of changing the droplet size distribution. Consequently, to adequately describe the flow of gas and droplets past a flow obstacle such as a set of turning vanes, two questions must be answered. First, it must be possible to predict what percentage of the incoming droplets actually impact on the obstacle. The percentage will, of course, vary with the size of the droplet - the larger droplets in the distribution will not be able to avoid an obstacle as easily as the smaller droplets. An excellent review of determining these percentages for a variety of obstacles is found in reference 19. Second, it must be possible to determine what happens to the liquid from the droplets that do impact on these surfaces. In applications such as steam turbines, droplets are found to wet the surface of the obstacles (turbine blades, for example) and then

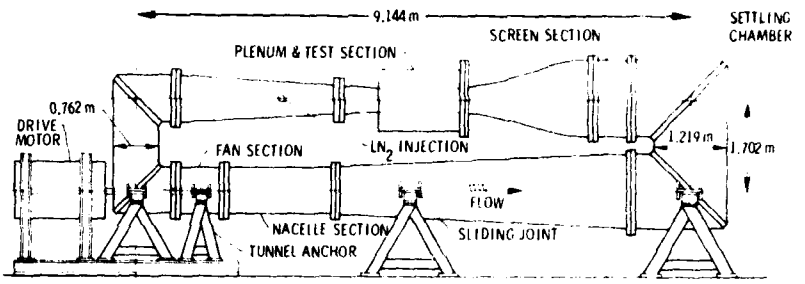

Figure 11.- Schematic of Langley 0.3-Meter Transonic Cryogenic Tunnel (TCT).

stream to the trailing edge, at which point they are sheared off the obstacle by aerodynamic forces and broken up again. The size at which these droplets come off appears to be related to the Weber number, We, which is defined in reference 20 to be

$$We = \frac{\rho w_r^2 D}{\sigma_\ell} \tag{14}$$

where w_r is again the relative velocity between the droplets and the gas, D is the droplet diameter, and ρ is the gas density. By substituting a "critical" value of Weber number, We_{cr}, into Eq. (14), a value of the maximum stable droplet size can be calculated. Any droplets larger will be broken up by the aerodynamic forces as they are sheared off the obstacle. The value of $We_{cr} = 20$ is given in reference 20 as a good approximation in steam turbines and may also apply to cryogenic application within the uncertainties in characterizing w_r around these obstacles. Reference 21 deals with We_{cr} in detail.

In cryogenic wind tunnels, however, the temperature of the flow near the surfaces of the obstacles will be above the boiling temperature of the droplets because the total temperature of the tunnel must always be kept above the reservoir saturation, or boiling, temperature to avoid filling the tunnel with liquid nitrogen. Because of the temperature recovery in the boundary layer, all wall surfaces in the tunnel will initially see gas temperatures above the droplet boiling temperature. When droplets begin impacting on the obstacles, they may either boil on these "hot" surfaces or they may wet the surfaces and not actively boil. In the former case the re-entrained droplets may have a significantly smaller diameter than predicted by Eq. (14) with $We_{cr} = 20$, whereas in the latter case $We_{cr} = 20$ may adequately predict the droplet sizes being shed off the obstacles. Further work needs to be done in this area to properly predict the interaction between the droplets and the flow obstacles so that correct mathematical modelling of the droplet progress around the tunnel can be assured.

Aside from questions of whether obstacles will boil the droplets, two aspects of Eq. (14) can be very important in determining whether the shed droplets will be small or large. First, while the pressure of the tunnel has very little effect on D_{32}, as seen in Eq. (10), the tunnel pressure does affect the size of droplets being shed off the flow obstacles as predicted by Eq. (14). Since for a given T, the value of ρ for the gas is proportional to p, the predicted mean diameter of the droplet being generated by liquid shedding off an obstacle will be inversely proportional to pressure. Consequently, droplets being generated from the flow past an obstacle should be smaller for high-pressure operation than for low-pressure operation. Second, the relative velocity of the gas past the obstacle is also very important in determining the re-entrained droplet size. In slow portions of the tunnel such as the settling chamber, very large droplets may be shed off the screens because of the small values of w_r.

4.3 Seed Particles from the Injected Liquid Itself

A further source of seed particles in the test section in addition to possible unevaporated droplets may be particulates in the liquid nitrogen itself. With the specifications used in NASA procurement, the liquid nitrogen is allowed to have 1 mg of particulates per liter of liquid. These particulates may be dust in the air being liquefied or may be added inadvertently to the liquid nitrogen during some stage of the manufacturing process. While gas samples taken from the 0.3-m TCT have not shown any particulates, the tests were not designed to detect particles of 1 μm in diameter.

4.4 Summary

To summarize, several different sources of seed particles do exist for cryogenic tunnels. There may be dirt or debris left after model changes, there may be particulates in the liquid nitrogen injected into the tunnel for cooling, and there may be a large number of unevaporated liquid droplets from the liquid nitrogen injection process reaching the test section. As of this time, the droplet evaporation problem is not well characterized because of the uncertainties in the interaction between the droplets and the flow obstacles. Nevertheless, as will be discussed in a following section, it has been experimentally

determined that unevaporated injected liquid does not reach the test section of the 0.3-m TCT in sufficient numbers at temperatures above free-stream saturation to cause condensation effects.

5. LIQUID DROPLETS - EFFECTS, GROWTH, AND DETECTION

Now that the two primary modes of condensation - homogeneous and heterogeneous nucleation - have been described, it is appropriate to discuss how liquid droplets disturb the thermodynamics of the flow and how to detect their presence. The primary effect of droplets growing (or evaporating) is the addition (or removal) of heat. For example, while the static pressure is slightly decreased during condensation because of the transfer of gas molecules to the denser liquid state, this is a small effect compared to the latent heat being released into the flow by the phase change. The extent to which condensation influences the flow depends on the amount of mass condensed and the resulting amount of latent heat released.

Describing droplet growth depends on a variety of flow circumstances. First, if the droplet is small compared to the mean-free path of the gas molecules, the droplet is considered to be in free-molecular flow and the growth equation must reflect this. If the droplet is large compared to the mean-free path, then the equation must reflect continuum processes. Whether the condensing gas is pure or mixed with a "carrier" gas can determine whether heat transfer or mass transfer limits the rate of droplet growth. Also, if the droplet is at a different velocity than the gas, the growth equations must be modified to take into consideration the movement of the droplet. Droplet growth is discussed in references 5, 22, and 23 for the range of conditions but will be specialized in the following discussion to the case of continuum flow with a one-component gas, which is appropriate for evaporating the droplets resulting from injected liquid nitrogen in both nitrogen and air-nitrogen cryogenic tunnels.

An equation for droplet growth in a continuum environment with no carrier gas is given in reference 22 along with expressions for droplet acceleration. The expression given for the droplet growth rate is

$$\frac{dr}{dt} = \frac{-\lambda_m (T - T_\ell) Nu}{2\rho_\ell L r} \tag{15}$$

where r is droplet radius, λ_m is the mean value of thermal conductivity of the gas at the saturation (droplet) temperature and at the gas temperature, L is the latent heat, and Nu is Nusselt number, which is defined as

$$Nu = 2(1 + 0.28\, R_d^{1/2} Pr^{1/3}) \frac{\ln (1 + B)}{B}$$

with

$$R_d = \frac{2\rho w_r r}{\mu}$$

$$Pr = \frac{\mu c_p}{\lambda}$$

$$B = \frac{c_p (T - T_\ell)}{L}$$

In the above equations, ρ is vapor density, w_r is the difference in velocity between the droplet and the gas, μ is the gas viscosity, λ is the gas thermal conductivity, R_d is droplet Reynolds number, Pr is Prandtl number, and c_p is the gas specific heat at constant pressure. (In reference 22, there is a typographical error in the equation corresponding to Eq. (15).) Equation (15) shows that growth rate in continuum flow is inversely proportional to size.

To detect the presence of condensation or unevaporated liquid droplets, one may examine either indirect evidence such as static or total pressure measurements or direct evidence such as that provided by light scattering systems. Pressure instrumentation has traditionally been available to the experimentalist in the form of static pressure orifices either in the tunnel sidewalls or model and in the form of total pressure probes. Both methods have been used to detect condensation in conventional tunnels, as reported in reference 1, and in cryogenic tunnels, as reported in references 24 and 25. Two notes of caution are appropriate for total pressure probes. First, in supersonic flow the detached bow shock may re-evaporate condensate and give a misleading measurement. Second, if large droplets with diameters greater than about 50 μm are in the flow, their presence in the flow will not be detected by total pressure probes constructed with tubing less than 0.01 m in diameter because the droplets will not be brought to rest in front of the probe even for flow velocities as low as 10 m/sec.

Light scattering can be used as a means of looking directly for condensation and has been used in this capacity since the earliest condensation experiments in the late 1800's. Many references can be cited as giving examples of detecting onset by light scattering, but reference 26 is particularly useful because in that report onset of condensation detected by light scattering is compared to onset detected by pressure measurements and both methods are found to be equally sensitive in determining the onset. Both pressure measurements and a simple light scattering system have been used in experiments in the 0.3-m TCT at Langley.

6. RESULTS OF EXPERIMENTS IN THE LANGLEY 0.3-METER TRANSONIC CRYOGENIC TUNNEL

With the need to verify Sivier's analysis and to provide more information about droplet evaporation, Langley has been in a unique position to gather experimental data with the availability of the fan-driven, 0.3-Meter Transonic Cryogenic Tunnel (TCT). The condensation studies in the 0.3-m TCT have primarily involved a 0.137-m chord NACA 0012-64 airfoil mounted in the octagonal, three-dimensional test section; total pressure probes mounted at different longitudinal positions along the same octagonal test section; and a 0.152-m chord British NPL-9510 airfoil mounted in the two-dimensional test section. The first two studies utilized pressure data while visual detection was used in the NPL-9510 studies.

6.1 NACA 0012-64 Airfoil Studies

The NACA 0012-64 airfoil studies involved taking static pressure data along the airfoil surface, as reported in reference 24. The cross section of the airfoil is shown in figure 12, and a typical pressure coefficient, C_p, distribution is seen in figure 13 for $M_\infty = 0.85$ and a chord Reynolds number, R_c, equal to 38×10^6. The airfoil was fixed at a zero angle of attack, α, for the entire test program. The method of determining the onset of condensation effects was to control the tunnel so that M_∞ and R_c were held constant while the total temperature was decreased below the saturation temperatures corresponding to $M_{L,max}$ and M_∞. Because both M_∞ and R_c were held constant, any difference in pressure coefficient could be attributed to low-temperature effects, which were assumed to be due to condensation. The procedure of following a "path" of constant M_∞ and R_c could be repeated at various values of R_c to span the operating envelope as was done for the $M_\infty = 0.85$ test. This is seen in figure 14, which also shows the appropriate saturation temperatures for $M_{L,max}$ and M_∞. Along each path of constant R_c, graphs showing differences in pressure coefficient as a function of total temperature were analyzed for each pressure orifice over the airfoil and used in the determination of the onset of condensation effects. Total temperatures and pressures at which effects were first detected for the $M_\infty = 0.85$ test are shown in figure 15. Similar tests were also made for $M_\infty = 0.75$ and 0.95.

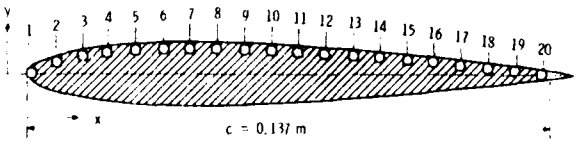

Figure 12.- Two-dimensional NACA 0012-64 airfoil with orifices spaced at 5 percent-chord intervals.

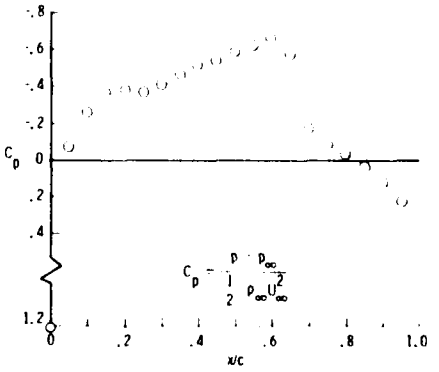

Figure 13.- Pressure coefficient, C_p, distribution without condensation effects for the NACA 0012-64 airfoil with $M_\infty = 0.85$, $R_c = 38 \times 10^6$, and $\alpha = 0^\circ$.

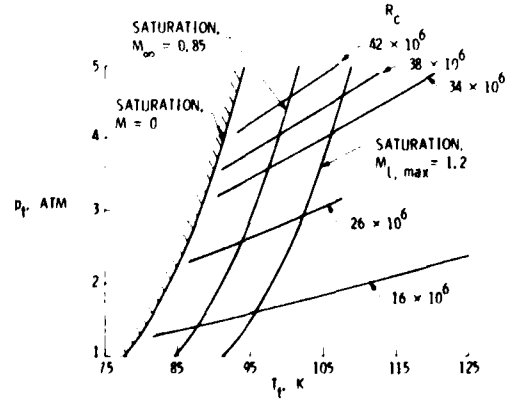

Figure 14.- Paths of constant R_c for the test of the NACA 0012-64 airfoil at $M_\infty = 0.85$.

Supercooling is a traditional manner of presenting data on the onset of condensation and is used in figures 16(a) and 16(b) to analyze the onset of pressure effects for the NACA 0012-64 airfoil test, assuming that either the local or free-stream conditions are the important parameter. In other words, for the calculation of supercooling in figure 16(a), the maximum local Mach number over the airfoil is assumed to be the relevant velocity with which to solve for T and then ΔT in Eq. (2). For figure 16(b), M_∞ is assumed to be the pertinent velocity for determining supercooling. A comparison of figures 16(a) and 16(b) shows that the results correlate much more closely with supercooling based on M_∞. Thus, the onset of effects in the pressure distribution would appear to be originating in the free-stream and not necessarily over the model. Furthermore, as reported in reference 24, effects over the airfoil do not necessarily occur first in the region of high local Mach number over the airfoil, where homogeneous nucleation would be expected to occur first. Consequently, heterogeneous nucleation seems to be the most likely cause.

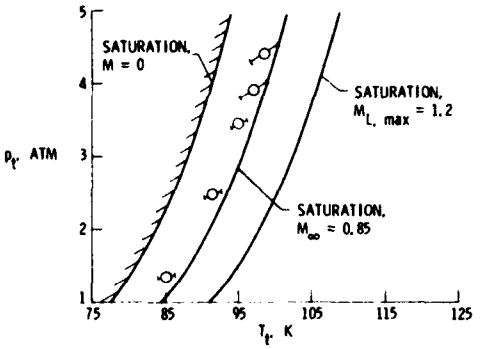

Figure 15.- Onset of condensation effects for test at $M_\infty = 0.85$. Error bars indicate possible experimental error. NACA 0012-64 airfoil.

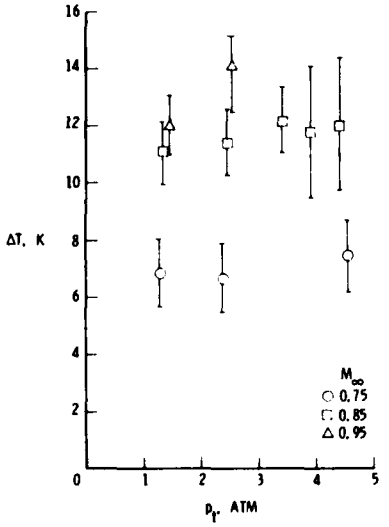

(a) Supercooling based on $M_{L,max}$

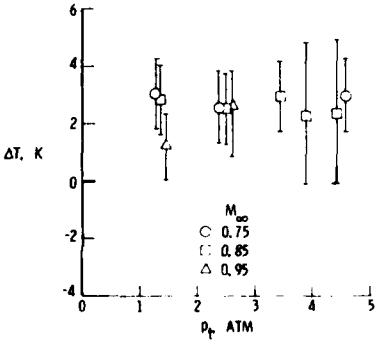

(b) Supercooling based on M_∞

Figure 16.- Supercooling for NACA 0012-64 airfoil tests. Error bars indicate possible experimental error.

6.2 Total Pressure Probe Studies

That the onset of effects for the NACA 0012-64 airfoil were the result of heterogeneous nucleation on some existing seed particles present in the test section was substantiated by the total pressure results reported in reference 25. During these experiments a similar test procedure was followed except that the airfoil was removed from the tunnel and total pressure probes were installed along the length of the octagonal test section, as seen in figure 17. Without the airfoil present, the probes could only measure what was occurring in the free-stream flow itself. Supercooling calculated by using M_∞ as the relevant velocity in Eq. (2) is given for the probes in figure 18, which shows results similar to those for the airfoil in figure 16(b). Again, the evidence of heterogeneous nucleation occurring on seed particles in the free stream seems clear.

6.3 Need for Higher Local Mach Numbers

Since heterogeneous nucleation effects were the apparent cause of the onset of condensation in the tests with the NACA 0012-64 airfoil, heterogeneous effects form the minimum operating temperature limits for those test conditions. Consequently, the operating temperatures at which homogeneous effects would have occurred over the airfoil must have been lower than those at which heterogeneous nucleation occurred on seed particles upstream of the model. Sivier's predicted operating temperatures, as described by Eq. (9), at which

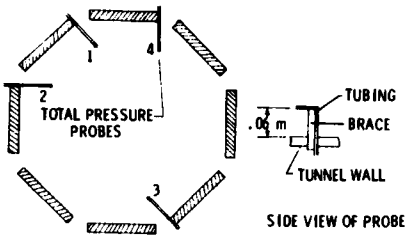

CROSS-SECTIONAL VIEW OF THE PROBES IN THE TEST SECTION LOOKING DOWNSTREAM

PROBE	DISTANCE DOWNSTREAM
1	0.33m
2	0.49
3	0.65
4	0.81

Figure 17.- Description and placement of total pressure probes in the three-dimensional, octagonal test section.

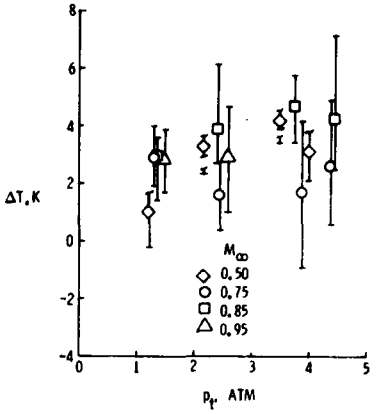

Figure 18.- Supercooling for total pressure probes based on M_∞.

homogeneous nucleation would have occurred for the NACA 0012-64 airfoil at $M_\infty = 0.85$ and $M_{L,max} = 1.20$ are shown in figure 19. Indeed, as seen in the figure, the predicted onset of homogeneous nucleation would have occurred at lower temperatures than those at which growth on pre-existing seed particles was detected. In other words, for these conditions of relatively low maximum local Mach number, $M_{L,max} = 1.20$, the supercooling over the airfoil was not sufficient to trigger homogeneous nucleation at the temperatures corresponding to the onset of effects due to heterogeneous nucleation. While figure 19 is not a quantitative check of Eq. (9), it does appear that Sivier's calculations are consistent with the experimental results. In order to check Eq. (9) quantitatively, tests were required that would incorporate much higher local Mach numbers than free-stream Mach numbers in order to move the $M_{L,max}$ saturation curve to higher temperatures and to move the predicted onset of homogeneous nucleation to temperatures higher than free-stream saturation, where growth can occur on pre-existing seed particles in the test-section flow itself.

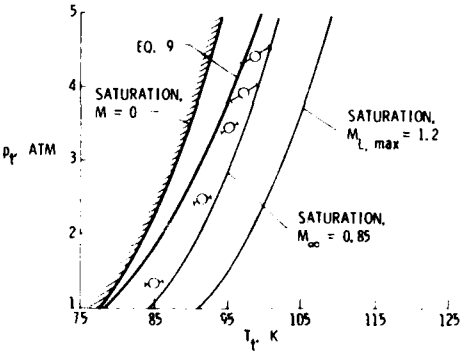

Figure 19.- Comparison between prediction of homogeneous nucleation, Eq. (9), and effects attributed to heterogeneous nucleation for the test of the NACA 0012-64 airfoil at $M_\infty = 0.85$.

6.4 NPL-9510 Airfoil Studies

To satisfy this need for higher local Mach numbers over an airfoil, a recent series of experiments was completed on a 0.152-m British airfoil, the NPL-9510. While no pressure data have been studied yet for condensation effects, one of the methods of detecting condensation during the experiment was a simple light scattering system which could visually detect condensation in the form of fog either over the airfoil or in the test-section flow itself. A 25-watt arc lamp was placed outside the field of view in one of the schlieren boxes mounted on the two-dimensional test section of the 0.3-m TCT and a video camera was placed at the exit pupil of the opposite schlieren box. The schlieren system was not operating and the knife edge was removed. The airfoil was mounted in a set of D-window turntables, as shown in figure 20. It is important to notice that the view of the flow over the top of the airfoil was limited by the 0.012-m placement of the airfoil chord line below the field of vision. The airfoil was tested at angles of attack, α, of -2°, 0°, and 6° for $M_\infty = 0.75$; at $\alpha = 0^\circ$ and 4° for $M_\infty = 0.55$; and at $\alpha = 0^\circ$ for $M_\infty = 0.85$. Video recordings were made which showed whether any fog was apparent locally over the airfoil and whether any fog was present upstream of the airfoil in the test section. Static

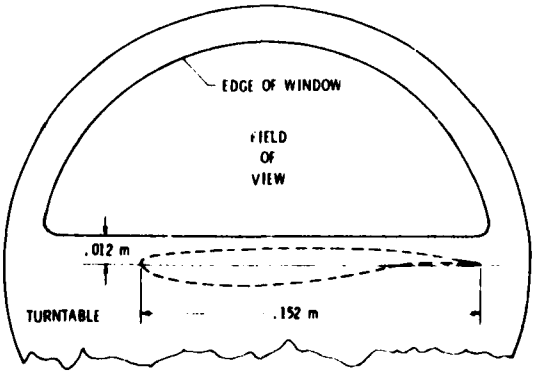

Figure 20.- Field of view over the NPL-9510 airfoil mounted in the D-window turntables.

pressure measurements were taken over the airfoil to determine the maximum local Mach number, $M_{L,max}$, so that the corresponding saturation temperatures would be known.

The use of visual means to detect the appearance of fog permitted distinguishing between fog occurring locally over the airfoil and fog occurring in the free stream itself. Furthermore, an additional distinction was made in the appearance of fog in the test-section flow. When fog first appeared, it was very light and intermittent in nature. At total temperatures 1 or 2 K lower, the test-section fog became brighter and steadier in nature.

6.4.1 Detection of Fog Locally Over NPL-9510 Airfoil

The results for the test with $M_\infty = 0.75$ and $\alpha = 6^\circ$ are shown in figure 21(a). For these conditions, $M_{L,max}$ is equal to 1.70. Also shown in this figure is the predicted onset of homogeneous nucleation as calculated by using Eq. (9) and assuming that $M_{L,max} = 1.70$ is the Mach number at which condensation is detected. Equation (9) predicts the onset of homogeneous nucleation at temperatures far above free-stream saturation, and the agreement between Eq. (9) and the detection of local fog over the airfoil (represented by circles in figure 21) appears good in both magnitude and trend. However, as seen in figure 20, the field of view above the airfoil does not extend down to the airfoil surface and it is not known, therefore, if the experimental setup is really able to detect condensation at $M_{L,max}$. If, for example, only velocity regions of $M = 1.50$ are visible in the field of view, then a new predicted onset of effects would have to be drawn using Eq. (9) and $M = 1.50$. This new line would be displaced to the left of the present line shown in figure 21(a), and this new prediction for the onset of homogeneous nucleation might suggest that homogeneous nucleation is occurring at higher temperatures than predicted by the Sivier analysis.

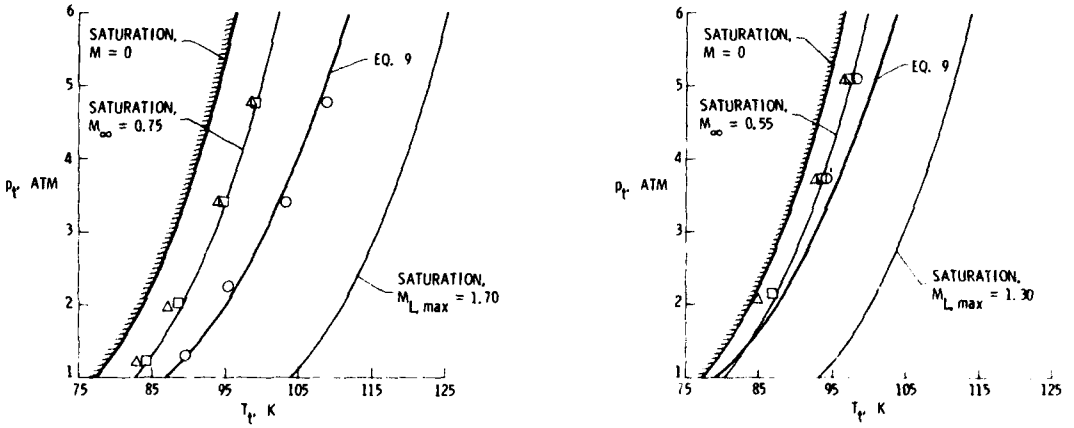

(a) $M_\infty = 0.75$, $\alpha = 6^\circ$, and $M_{L,max} = 1.70$ (b) $M_\infty = 0.55$, $\alpha = 4^\circ$, and $M_{L,max} = 1.30$

Figure 21.- Onset of nucleation effects for the NPL-9510 airfoil shown as follows: local by circles, intermittent by squares, and steady by triangles. Predicted onset of homogeneous nucleation effects is given by Eq. (9) for the respective values of $M_{L,max}$.

The results for $M_\infty = 0.55$ and $\alpha = 4^\circ$ are summarized in figure 21(b). In this case $M_{L,max} = 1.30$ and the agreement between the predicted onset of homogeneous nucleation and the data for local onset is not as good as shown in figure 21(a). It appears that more supercooling occurs locally than is predicted by Eq. (9). In fact, during the 2-atm run, fog was detected in the free-stream flow before any could be seen locally over the airfoil. This extra supercooling may again be the result of the limited view of the model. The high local Mach number region in the pressure distribution for $M_\infty = 0.55$ and $\alpha = 4^\circ$ is limited to a small region near the leading edge of the airfoil, as seen in figure 22(a). It is just this region that is 0.012 m below the field of view of the D-windows. The high local Mach number region in the distribution for $M_\infty = 0.75$ and $\alpha = 6^\circ$ shown in figure 22(b) is not as limited chordwise and is not as close to the leading edge. One would expect a larger region of high Mach numbers over the airfoil for $M_\infty = 0.75$ than for $M_\infty = 0.55$ and consequently more visibility of the high local Mach numbers through the D-windows. This would explain the better agreement between Eq. (9) and the data for $M_\infty = 0.75$ than for $M_\infty = 0.55$. Nevertheless, because of the limited field of view in the tests at both $M_\infty = 0.55$ and 0.75, the actual temperatures at which local onset occurs are uncertain and may possibly be above the temperatures corresponding to Eq. (9) in figure 21.

Additional data beyond the present visual detection in a limited field of view over the airfoil are required for conclusive verification of the predicted onset of homogeneous nucleation according to Eq. (9). If effects are occurring at temperatures above those predicted by Eq. (9), either the Sivier analysis may be predicting too much supercooling before homogeneous nucleation or heterogeneous nucleation may be occurring locally over the airfoil at temperatures above those corresponding to homogeneous nucleation. At the present

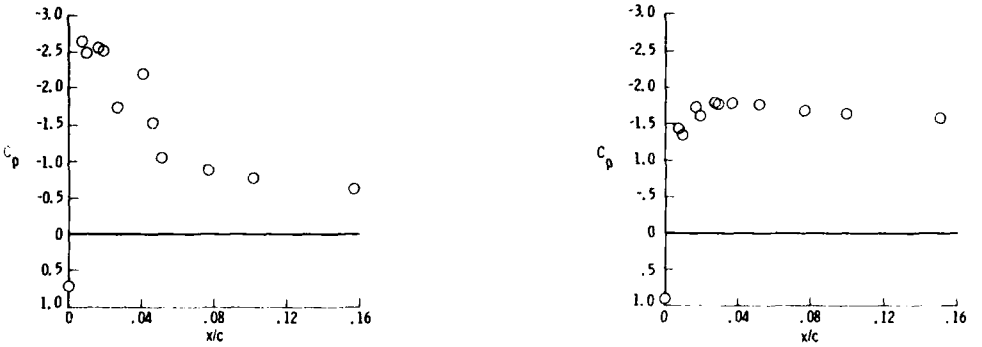

(a) $M_\infty = 0.55$, $\alpha = 4^o$, and $R_C = 20.2 \times 10^6$ (b) $M_\infty = 0.75$, $\alpha = 6^o$, and $R_C = 22.5 \times 10^6$

Figure 22.- Pressure distributions near the leading edge of the NPL-9510 airfoil.

time, however, because of the general agreement between the detection of local fog over the NPL-9510 airfoil and both the trend and magnitude of effects as predicted by Eq. (9), it will be assumed that the effects were the result of homogeneous nucleation and that Eq. (9) is at least a rough approximation to the onset of homogeneous nucleation effects.

6.4.2 Detection of Fog in Test Section

It is interesting to notice in figure 21 that the temperatures corresponding to intermittent fog in the test section (represented by squares) coincide with free-stream saturation temperatures, while the temperatures at which the steady, more dense fog is observed (triangles) are lower by 1 or 2 K. A closer look at intermittent fog onsets for all the data taken in the NPL-9510 tests is given in figure 23, which shows the supercooling below free-stream saturation at the detection of intermittent fog. The agreement between temperatures for detection of thir intermittent fog in the test section and free-stream saturation temperature ($\Delta T = 0$) is surprisingly good. Apparently, there are seed particles in the flow that are ready to serve as nucleating sites as soon as the free-stream saturation temperature is reached. Supercooling below free-stream saturation at the onset of steady, denser fog is seen in figure 24. Similarity between the supercooling for the NACA 0012-64 airfoil, for the total pressure experiments, and for the steady fog tests with the NPL-9510 airfoil is apparent when comparing figures 16(b), 18, and 24. The onset of measurable pressure effects seems to correspond to the steady fog seen in the test section in the NPL-9510 experiment, as might be expected. What makes this correspondence surprising is that the NACA 0012-64 airfoil and total pressure data were taken in the 0.3-m tunnel with the three-dimensional, octagonal test-section leg in place, while the NPL-9510 airfoil was tested with the two-dimensional test-section leg in place. The three-dimensional test section had about 25 percent less cross-sectional area and required correspondingly smaller amounts of power and rates of liquid nitrogen injection.

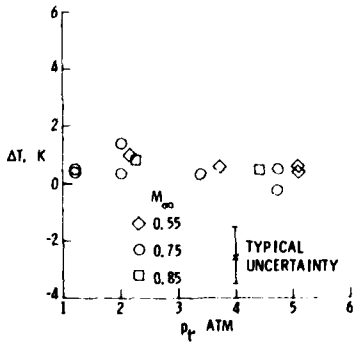

Figure 23.- Supercooling based on M_∞ at the onset of intermittent fog in the test section during the NPL-9510 airfoil tests.

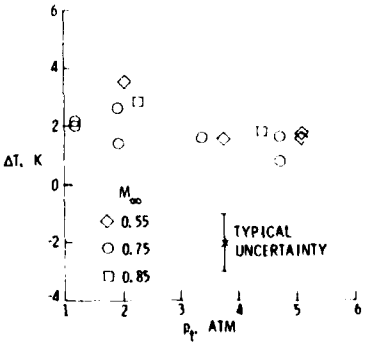

Figure 24.- Supercooling based on M_∞ at the onset of steady fog in the test section during the NPL-9510 airfoil tests.

6.5 Source of the Seed Particles

For two reasons, it would seem that unevaporated droplets resulting from the liquid nitrogen injection process were not the cause of the onset of heterogeneous nucleation observed in any of the three studies. First, if unevaporated droplets were the cause, total pressure would influence the amount of supercooling from the free-stream because droplets injected into the tunnel are expected to strike one or more of the various flow obstacles and lead to new droplets being generated by the flow obstacles. These new droplets should be significantly smaller at the higher pressures, according to Eq. (14), and should evaporate much more readily. Even without obstacles in the flow, droplets

would evaporate more quickly at the higher pressures because latent heat, λ, decreases with increasing pressure (see Eq. (15)). Thus, it would be expected that more supercooling would be realized with increasing pressure if the liquid injection were the source of seeds for heterogeneous nucleation. However, no more supercooling was observed at the higher pressures than at the lower pressures. Second, if unevaporated droplets were the cause of effects, a more likely candidate for onset correlation would be some temperature increment above the reservoir (M = 0) saturation temperature rather than correlation with free-stream saturation temperature. The flow in the return portion of the tunnel, where the geometric area is large compared to the area in the test section, is not very sensitive to M_∞; therefore, more reason exists for the droplets being swept around the tunnel to correlate with reservoir rather than free-stream saturation temperature. Any correlation with the free-stream saturation temperature must be either very coincidental or very complex, indeed, if unevaporated droplets are causing the onset of effects.

If the seed particles do not result from unevaporated liquid nitrogen droplets from the injection process, then dust or some other particulates must be the source of the nucleating sites. These particulates may come from the liquid nitrogen itself, as mentioned in the section on sources of seed particles. A note of caution, however, is appropriate. While the liquid nitrogen injection process does not appear to be the source of seed particles in the above experiments in the 0.3-m TCT, it should always be considered as a possibly large source of seeds. At some temperature approaching the reservoir (M = 0) saturation temperature, there simply will not be enough temperature difference between the gas and the liquid to evaporate the droplets formed during injection. During the tests in the 0.3-m TCT, this temperature was apparently below the temperature at which particulates could serve as nucleating sites in the free stream itself.

6.6 Summary

To summarize the experimental results in the 0.3-m TCT, growth on pre-existing seed particles in the test-section flow upstream of the airfoil triggered the onset of condensation effects during the NACA 0012-64 airfoil tests, a result substantiated by later total pressure measurements. Homogeneous nucleation did not occur because not enough supercooling was present in the regions of maximum local Mach number over the airfoil at the temperatures corresponding to the detection of heterogeneous effects. With the relatively high local Mach numbers during the experiments with the NPL-9510 airfoil, fog was detected locally over the airfoil at temperatures higher than the free-stream saturation temperature. While the experiment did not permit visual detection of fog close to the airfoil surface, the agreement between the data and Eq. (9) seems to imply that homogeneous nucleation was the source of condensation effects over the airfoil. Consequently, the minimum operating temperatures corresponding to the onset of condensation effects in the 0.3-m TCT appear to be determined by either homogeneous effects occurring locally over the test model (dependent on the magnitude of $M_{L,max}$) or by heterogeneous effects occurring upstream of the model in the free stream itself (dependent on M_∞).

7. MINIMUM OPERATING TEMPERATURE LIMITATIONS DUE TO ONSET OF CONDENSATION EFFECTS

While the minimum operating temperatures at which condensation effects would occur in the 0.3-m TCT are predictable, there are a number of tunnel factors that may influence the onset of either homogeneous or heterogeneous nucleation in other cryogenic wind tunnels. These factors include length effects, purity of the injected liquid nitrogen, number of particulates in the flow, and number of unevaporated liquid nitrogen droplets reaching the test section. The present section will first outline the brief procedure for determining minimum operating temperatures in the 0.3-m TCT and will then discuss how these minimum operating temperatures may be influenced by differences in tunnels.

7.1 Minimum Operating Temperatures in the 0.3-m TCT

The 0.3-m TCT operating temperature should be kept high enough to avoid the onset of condensation from either homogeneous or heterogeneous nucleation. As described in the previous section, condensation effects detected locally over the NPL-9510 airfoil (see fig. 21) seem to follow the trend and general location of Sivier's predicted onset of homogeneous nucleation, as characterized by Eq. (9). For this reason the effects are tentatively assumed to be the result of homogeneous nucleation and not the result of heterogeneous nucleation. The NPL-9510 results, however, are not a conclusive check on Eq. (9) because of an experimental limitation which did not allow detection of effects close to the airfoil surface. Nevertheless, until further data are available, Eq. (9) seems to be the best estimate for the operating temperatures at which the onset of homogeneous nucleation can be expected.

A second operating temperature boundary in the 0.3-m TCT may be imposed by heterogeneous nucleation. During the tests of the NPL-9510 airfoil, the NACA 0012-64 airfoil, and the total pressure probes, condensation from heterogeneous nucleation in the free stream was detected at temperatures corresponding to free-stream saturation or just below. Consequently, a prudent lower limit to operating temperatures before the onset of heterogeneous effects would be the free-stream saturation temperature for the test under consideration. Thus, to predict the minimum operating temperature for tests in the 0.3-m TCT, one must compare the temperature predictions of Eq. (9) for an assumed value of $M_{L,max}$ to the free-stream saturation temperature. Whichever is higher should be taken as the minimum operating temperature. To predict the minimum operating temperatures in other tunnels, it

it is necessary to review the influences of various factors on both homogeneous and heterogeneous nucleation.

7.2 Influence of Length Effects

The first factor to be considered is the effect of increased tunnel size compared to the 0.3-m TCT. The onset of homogeneous nucleation should not change appreciably even if models in the larger tunnel have characteristic lengths larger than the 0.137-m and 0.152-m airfoils of the present study. For comparable supercooling before the onset of homogeneous effects, doubling the length of the 0.152-m NPL-9510 airfoil should require a reduction of droplet formation rate, I, to compensate for the increased residence time over the airfoil during which droplets can form and grow. Suppose, as a first guess, that I must be halved in value to compensate for doubling the length. The magnitude of I, however, is so sensitive to supersaturation ratio, S, that only a small increase in T_t can halve I. For the example given in Table I, where $p_t = 4.76$ atm and $T_t = 109.0$ K, at the expansion Mach number of 1.70, $I = 4 \times 10^5$ droplets/(kg·sec). By increasing T_t to just 109.1 K, I drops to 2×10^5 at M = 1.70. While the onset of homogeneous nucleation effects involves growth in addition to just I and a larger reduction in I than a factor of 2 may be necessary, it does not appear that doubling the length scale should impact noticeably on the total temperatures at which the onset of homogeneous nucleation occurs.

The influence of increasing length scale on the onset of heterogeneous effects, however, may potentially be more detrimental. The effect of doubling the length scale on heterogeneous nucleation can be determined by examining the droplet growth equation, Eq. (15), and remembering that T is gas static temperature and T_ℓ is droplet temperature, which will be very close to saturation temperature for the gas static pressure, p. Separating variables and integrating over the time interval from t_o to t_1, during which time r has gone from r_o to r_1, gives

$$r_1^2 - r_o^2 = \frac{-\lambda_m (T - T_\ell) Nu (t_1 - t_o)}{\rho_\ell L} \tag{16}$$

Assuming that the onset of heterogeneous effects in both tunnels occurs when the presumed equal number of droplets in each has grown from r_o to the same value of r_1, then the right side of Eq. (16) would have to be equal in value for the two cases. Assuming the parameters such as λ_m, Nu, ρ_ℓ, L to be the same, then equal growth on the seed particles will occur in the two cases if

$$(T - T_\ell)(t_1 - t_o)\big|_A = (T - T_\ell)(t_1 - t_o)\big|_B \tag{17}$$

where conditions at A represent the 0.3-m TCT and conditions at B represent the larger tunnel. Since the residence time $(t_1 - t_o)_B$ in the larger tunnel will be twice that in the 0.3-m TCT, $(T - T_\ell)_B$ may be only half the value in the 0.3-m TCT. While $(T - T_\ell)$ is not strictly the same as supercooling, it is a similar measure of how far below the vapor-pressure curve the flow has progressed. For effects being generated in the test-section flow upstream of the model, Eq. (17) is not a serious limitation. For example, instead of pressure instrumentation detecting the onset of heterogeneous nucleation at a value of supercooling 2 K below free-stream saturation, only a supercooling of 1 K would be expected. Since operation just above free-stream saturation is recommended anyway to avoid heterogeneous effects in the free stream itself, this would not impact on predicted minimum operating temperatures.

However, heterogeneous nucleation may impose severe restrictions in areas of high local Mach number over the test model when doubling length scales. It must be remembered that growth on seed particles occurs as soon as the flow is saturated. For flows in regions of high local Mach number, it is simply a question of whether enough seed particles exist and have enough time to grow sufficiently to affect the flow. While it is assumed that during the NPL-9510 tests the local fog was the result of homogeneous nucleation effects, suppose the local onset temperatures may have been close to the temperatures at which heterogeneous effects could have occurred locally. Then, Eq. (17) would suggest that only about half the supercooling over the 0.152-m NPL-9510 airfoil might be realized if the length of the airfoil were doubled while holding all other parameters constant. Thus, the local onset of effects for the larger airfoil could possibly be halfway between the present data for local onset of effects and the saturation curve corresponding to $M_{L,max} = 1.70$ in figure 21(a). Consequently, the greatest danger of increased heterogeneous nucleation is not in increased effects upstream of the models but in the regions of high local Mach numbers over the test models. In these regions, the amounts of supercooling observed during the 0.3-m TCT tests before the onset of homogeneous nucleation could be appreciably reduced if heterogeneous effects increased enough, by virtue of increased length scales, to cause effects in these regions at temperatures above those predicted for the onset of homogeneous nucleation.

7.3 Influence of the Purity of the Injected Liquid Nitrogen

The next influence to be discussed is the purity of the injected liquid nitrogen. As reported by Arthur and Nagamatsu in reference 27, certain impurities in nitrogen can significantly reduce the amount of supercooling realized before the onset of condensation

AD-A089 050 ADVISORY GROUP FOR AEROSPACE RESEARCH AND DEVELOPMENT--ETC F/G 14/2
CRYOGENIC WIND TUNNELS.(U)
JUL 80
UNCLASSIFIED AGARD-LS-111 NL

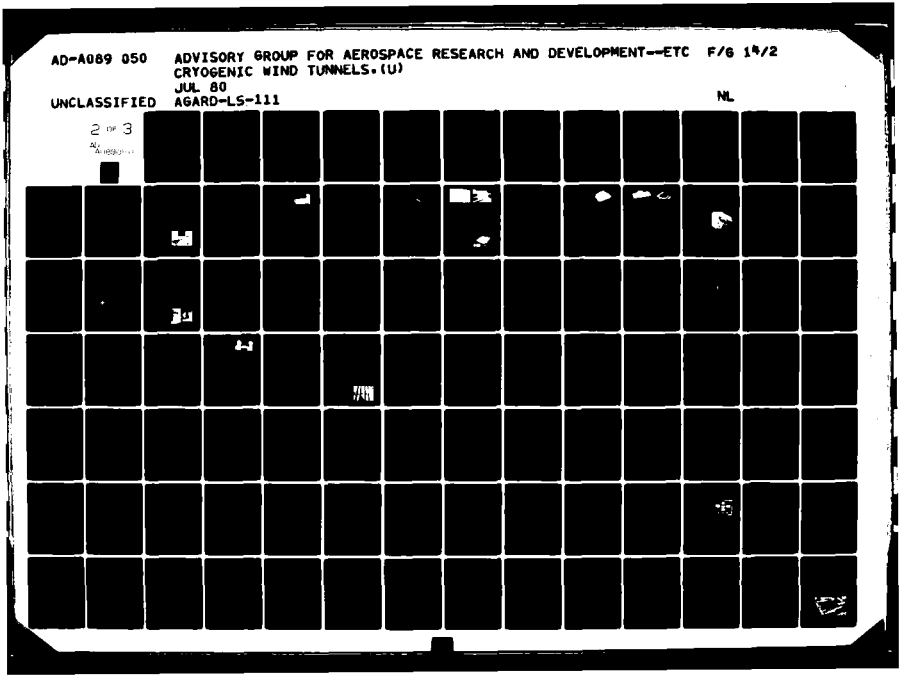

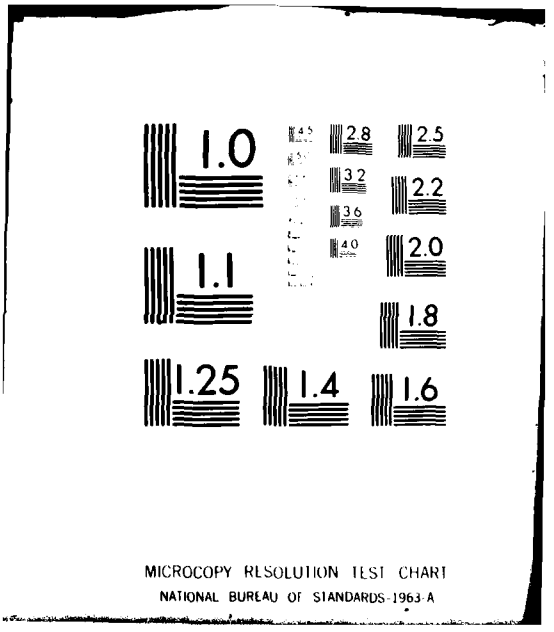
1.0
1.1
1.25
1.4
1.6
1.8
2.0
2.2
2.5
2.8
3.2
3.6
4.0
MICROCOPY RESOLUTION TEST CHART
NATIONAL BUREAU OF STANDARDS-1963-A

effects. Water vapor and carbon dioxide, in particular, are detrimental because these impurities may pre-condense and create nucleating sites for heterogeneous nucleation of the nitrogen. In other words, while not necessarily affecting homogeneous nucleation, these impurities may permit an early onset of heterogeneous nucleation because of the additional nucleating sites they create. In fact, Arthur and Nagamatsu report decreases in the supercooling before the onset of condensation in their nozzle with gaseous impurity levels as small as 0.0095 percent by volume for water vapor and 0.033 percent by volume for carbon dioxide.

7.4 Influence of the Number of Particulates

A third possible difference in tunnels may be in the number density of particulates in the flow resulting from either dirt or debris left in the tunnel or from solid or liquid impurities in the injected liquid nitrogen itself. The onset of homogeneous nucleation should not be affected by an increased number of particulates; however, increased effects of heterogeneous nucleation may preempt the occurrence of homogeneous nucleation, as in the increased-length situation. To correlate the onset of heterogeneous effects both in the 0.3-m TCT, case A, and in the second tunnel with a larger number of particulates, case B, it will be assumed that the total growth of condensate mass, Δm, is the same for similar operating conditions, since the resulting equal amounts of latent heat released into the flow would have caused equal changes in the thermodynamics. Thus, at onset,

$$\Delta m_A = \Delta m_B \tag{18}$$

but

$$\Delta m_A = n_A \int_{r_o}^{r_A} \rho_\ell 4\pi r^2 dr \tag{19}$$

and

$$\Delta m_B = n_B \int_{r_o}^{r_B} \rho_\ell 4\pi r^2 dr \tag{20}$$

where r_A and r_B are the respective radii at onset of effects and n_A and n_B are the respective number densities of particulates. It is also assumed that the growth begins on particles of equal radius, r_o. Equations (18) to (20) can be solved to give

$$r_B^3 = \frac{n_A r_A^3 + (n_B - n_A) r_o^3}{n_B} \tag{21}$$

Equation (21) in conjunction with Eq. (16) can be used to estimate the differences in $(T - T_\ell)$ to be expected at onset between case B and case A, which is assumed to be the 0.3-m TCT. Suppose the number density in case B, n_B, is twice that of case A, n_A. Equation (21) becomes

$$r_B^3 = \frac{r_A^3 + r_o^3}{2} \tag{22}$$

As can be seen with Eq. (22), the greatest difference between r_A and r_B occurs when r_o is small compared to r_A. Assuming $r_o = 0$, then $r_B = 0.79 r_A$, and Eq. (16) becomes

$$r_1^2 = \frac{-\lambda_m (T - T_\ell) Nu (t_1 - t_o)}{\rho_\ell L}$$

where r_1 is either r_A or r_B. Since the residence time, $(t_1 - t_o)$, is the same for cases A and B and all the other parameters are the same except for $(T - T_\ell)$,

$$\frac{(T - T_\ell)_B}{(T - T_\ell)_A} = \frac{r_B^2}{r_A^2}$$

or for the present example,

$$(T - T_\ell)_B = 0.62\ (T - T_\ell)_A$$

Consequently, it would be expected that only around 60 percent of the supercooling seen in the 0.3-m TCT tests before the onset of heterogeneous nucleation would be possible if the number density of particulates were doubled. Again, the greatest limitations due to increased heterogeneous effects could occur in regions of high local Mach number over the test model.

7.5 Influence of the Liquid Nitrogen Evaporation

The last difference between tunnels to be considered is the efficiency at which the injected liquid nitrogen is evaporated. Suppose another tunnel is not able to evaporate its injected liquid nitrogen as efficiently as the 0.3-m TCT. Then it is quite possible to have a sufficient number of seed particles in the test section to trigger the onset of heterogeneous effects both upstream of the model and locally over the model at temperatures above free-stream saturation. One distinction between seeds due to particulates, as described in the previous paragraph, and seeds due to unevaporated liquid nitrogen is that the number density of seeds due to unevaporated liquid nitrogen will be a strong function of tunnel temperature, whereas the number density of particulate seeds is expected to be relatively constant over the temperature range.

7.6 Summary

To summarize, an approximate procedure is available, on the basis of analysis and experiment, to predict minimum operating temperatures in the 0.3-m TCT. In predicting the onset of condensation effects in other tunnels, a number of factors can influence the minimum operating temperatures; these factors include length effects, purity of the injected liquid nitrogen, number of particulates in the flow, and the evaporation efficiency of the liquid nitrogen injection process. None of these factors are expected to impact very much on the temperatures at which the onset of homogeneous nucleation may occur. However, nearly all these influences can intensify heterogeneous nucleation effects in the free stream and can possibly trigger the onset of heterogeneous nucleation effects in regions of high local Mach numbers at temperatures higher than those corresponding to the predicted onset of homogeneous nucleation.

8. CONCLUDING REMARKS

Minimum operating temperatures of cryogenic wind tunnels are limited by real-gas effects. Either the test gas ceases to simulate the nearly ideal, diatomic behavior of the atmosphere or condensation effects begin to disturb the flow in the test section. As seen in the companion report in this lecture series, nitrogen or air as test gases will very adequately simulate ideal-gas behavior for temperatures well below saturation at operating total pressures up to about 9 atmospheres. Consequently, minimum operating temperatures over most tunnel operating envelopes will be fixed by condensation effects, which may result from either of two condensation processes.

The first process is homogeneous nucleation and will typically be responsible for minimum operating temperature limitations during tests in which the local Mach numbers over a model are high compared to the free-stream Mach numbers. From preliminary observations, an analysis by Sivier seems to approximate the onset of homogeneous nucleation in the Langley 0.3-Meter Transonic Cryogenic Tunnel. Since the differences in the onset of homogeneous nucleation effects are expected to be minimal in going from one tunnel to another, whether the same magnitude of supercooling in regions of high local Mach number will be seen in other tunnels will depend more on the second condensation process.

Heterogeneous nucleation, the second process, occurs when droplet growth takes place on pre-existing seed particles. These seed particles are generally the result of either particulates in the flow or unevaporated liquid nitrogen droplets from the injection process reaching the test section. During tests in the 0.3-m tunnel, heterogeneous nucleation in the test-section flow was observed at or below free-stream saturation temperature. Heterogeneous nucleation effects were not detected locally in regions of high local Mach number over the airfoils at temperatures higher than those predicted for the onset of homogeneous nucleation. Whether other tunnels will be able to test without the onset of heterogeneous effects in regions of high local Mach number will depend on length scales, purity of the injected liquid nitrogen, the number of particulates in the flow, and whether the injected liquid nitrogen used for cooling is adequately atomized and evaporated.

While no new experimental data are reported concerning minimum operating temperatures in hybrid air-nitrogen blowdown tunnels, previous air condensation data in hypersonic tunnels suggest that relatively little, if any, supercooling will be possible.

9. REFERENCES

1. P. P. Wegener and L. M. Mack, Condensation in Supersonic and Hypersonic Wind Tunnels, Advances in Applied Mechanics, Volume V, H. L. Dryden and Th. von Karman, eds., Academic Press, 1958, pp. 307-447.

2. R. A. Kilgore, J. B. Adcock, W. B. Igoe, and R. M. Hall, Full-Scale Aircraft Simulation with Cryogenic Tunnels and Status of the National Transonic Facility, Presented at the First International Symposium on Cryogenic Wind Tunnels, University of Southampton, England, April 1979.

3. K. D. Sivier, Digital Computer Studies of Condensation in Expanding One-Component Flows, ARL 65-234, U.S. Air Force, Nov. 1965. (Available from DTIC as AD 628 543.)

4. F. F. Abraham, Homogeneous Nucleation Theory - The Pretransition Theory of Vapor Condensation, New York, Academic Press, 1974, pp. 1-8.

5. G. Gyarmathy, Condensation in Flowing Steam, Two-Phase Steam Flow in Turbines and Separators, M. J. Moore and C. H. Sieverding, eds., Washington, Hemisphere Publishing Corporation, 1976, pp. 156-177.

6. R. C. Tolman, The Effect of Droplet Size on Surface Tension, J. Chem. Phys., Vol. 17, No. 3, March 1949, pp. 333-337.

7. B. J. C. Wu, Computer Programs for Calculating Condensation Rate in Steady, Adiabatic Expansions in Supersonic Nozzles, Dept. of Engr. and Appl. Sci., Yale University, 1974, pp. 13-16. (Available from DTIC as AD 775 257.)

8. P. P. Wegener and B. J. C. Wu, Homogeneous and Binary Nucleation: New Experimental Results and Comparison with Theory, Faraday Discussions of the Chemical Society, No. 61 Precipitation, 1976, pp. 77-82.

9. F. L. Daum, Air Condensation in a Hypersonic Wind Tunnel, AIAA Journal, Vol. 1, No. 5, May 1963, pp. 1043-1046.

10. H. T. Nagamatsu and W. W. Willmarth, Condensation of Nitrogen in a Hypersonic Nozzle, GALCIT Hypersonic Wind Tunnel Memorandum No. 6, Calif. Inst. of Tech., Jan. 1952.

11. B. J. Griffith, H. E. Deskins, and H. R. Little, Condensation in Hotshot Tunnels, Arnold Engineering Development Center Report AEDC-TDR-64-35, Feb. 1964.

12. I. E. Vas and G. Koppenwallner, The Princeton University High Pressure Hypersonic Nitrogen Tunnel N-3, (Princeton U. Gas Dynamics Lab Report 690), U.S. Air Force, AFOSR 64-1422, July 1964.

13. F. L. Daum and G. Gyarmathy, Condensation of Air and Nitrogen in Hypersonic Wind Tunnels, AIAA Journal, Vol. 6, No. 3, March 1968, pp. 458-465.

14. G. Koppenwallner and C. Dankert, The Homogeneous Nitrogen Condensation in Expansion Flows with ETW-Relevant Stagnation Conditions, Presented at the First International Symposium on Cryogenic Wind Tunnels, University of Southampton, England, April 1979.

15. G. L. Goglia, Limit of Supersaturation of Nitrogen Vapor Expanding in a Nozzle, Ph.D. Diss., Univ. of Michigan, 1959.

16. R. D. Ingebo and H. H. Foster, Drop-Size Distribution for Crosscurrent Breakup of Liquid Jets in Airstreams. NACA TN-4087, 1957.

17. J. P. Longwell, Combustion of Liquid Fuels, Sect. J, Combustion of Liquids and Solids, Part Four, Combustion Processes, Vol. II, High Speed Aerodynamics and Jet Propulsion, B. Lewis, R. N. Pease, and H. S. Taylor, eds., Princeton University Press, 1956, pp. 407-415.

18. S. Nukiyama and Y. Tanasawa (E. Hope, transl.), Experiments on the Atomization of Liquids in an Air Stream. Reports 1 to 6, Defense Research Board, Canada 1950, pp. 14-32.

19. M. N. Golovin and A. A. Putnam, Inertial Impaction on Single Elements, Indust. and Engr. Chem. Fundamentals, Vol. 1, No. 4, Nov. 1962, pp. 264-273.

20. G. Gyarmathy, Basic Notions, Two-Phase Steam Flow in Turbines and Separators, M. J. Moore and C. H. Sieverding, eds., Washington, Hemisphere Publishing Corporation, 1976, p. 49.

21. M. P. Anisimova and E. V. Stekolschikov, Deformational Breakup of Drops in a Gas Stream, Power Engineering - Academy of Sci. of the USSR, (Allerton Press, N.Y.), Vol. 15, No. 3, 1977, pp. 126-133.

22. J. Luneau, N. Rochas, and C. Kirrmann, Preliminary Study of the Injection Process of LN_2 in a Cryogenic Wind Tunnel, Presented at the First International Symposium on Cryogenic Wind Tunnels, University of Southampton, England, April 1979.

23. R. M. Hall and S. A. Kramer, A Review of "At Rest" Droplet Growth Equations for Condensing Nitrogen in Transonic Cryogenic Wind Tunnels, NASA TM-78821, Jan. 1979.

24. R. M. Hall, Onset of Condensation Effects with a NACA 0012-64 Airfoil Tested in the Langley 0.3-Meter Transonic Cryogenic Tunnel, NASA TP-1385, April 1979.

25. R. M. Hall, Onset of Condensation Effects as Detected by Total Pressure Probes in the Langley 0.3-Meter Transonic Cryogenic Tunnel, NASA TM-80072, May 1979.

26. C. A. Moses and G. D. Stein, On the Growth of Steam Droplets Formed in a Laval Nozzle Using Both Static Pressure and Light Scattering Measurements, Presented at the 1977 Joint Applied Mechanics, Fluids Engineering and Bioengineering Conference (ASME), Yale University, June 15-17, 1977.

27. P. D. Arthur and H. T. Nagamatsu, Effects of Impurities on the Supersaturation of Nitrogen in a Hypersonic Nozzle, GALCIT Hypersonic Wind Tunnel Memorandum No. 7, Calif. Inst. of Tech., March 1952.

10. ACKNOWLEDGEMENT

The author would like to thank his NASA-Langley Research Center colleague, Mr. Paul B. Gooderum, for his assistance during the experiments with the NPL-9510 airfoil.

CRYOGENIC ENGINEERING III

by Dr. R.G. Scurlock, Institute of Cryogenics, University of Southampton, U.K.

Abstract Handling and transfer of LIN. Cooldown and thermal cycling problems. Safety, including asphyxia, cold burns, explosion and fire hazards.

3.1 General points on liquid nitrogen

For adiabatic flow, with no heat in-leak, the behaviour of single phase liquid nitrogen is well-defined in terms of viscosity, density, mass velocity, etc., just like ambient temperature fluids. Conventional correlations via dimensionless parameters, such as Nusselt and Reynolds numbers, friction factors, etc., can be used.

However, the behaviour is not well-defined under a number of conditions which lead to 2-phase flow as a result of partial vaporisation of the liquid. Whenever possible, 2-phase flow should be avoided for a number of reasons:

(a) the mass flow capacity of a transfer line is severely reduced;

(b) pumps may cavitate with a fall-off in throughput, or fail to prime and overheat;

(c) transient or continuous oscillations may cause mechanical damage.

The liquid will generally be close to saturation when partial vaporisation and 2-phase conditions will arise from two basic causes: (i) pressure reduction; and (ii) heating.

Figure 1

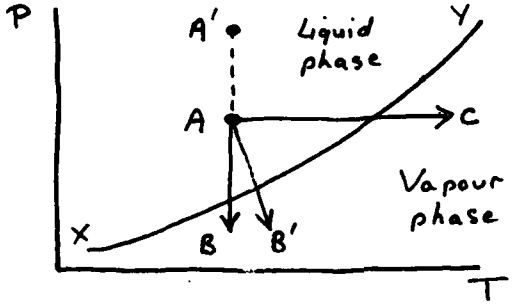

This is illustrated in Figure 1, where the liquid has a thermodynamic state A close to the saturation vapour pressure line XY. The liquid is in a slightly under-cooled or sub-cooled state, and its state can cross XY by two paths:

(i) along AB (or strictly AB^1) by a reduction in pressure;

(ii) along AC by the addition of heat.

In practice, both paths should be avoided; at the same time, adequate under-cooling of the liquid must be provided by pressurising along AA^1.

There are two particular difficulties which may occur. Firstly, the density of LIN varies considerably with temperature, and it is possible for stratification to occur with saturated liquid above sub-cooled liquid in a storage tank. Mixing of the two layers is almost non-existent.

Secondly, during removal of liquid from a tank, the pressure above the liquid will NOT be maintained by evaporation of the liquid. It is necessary to back-fill the ullage space with nitrogen gas, not only to maintain pressure, but also to prevent a negative, collapsing pressure differential being produced when the tank is insulated by gas purged insulation at 1 atm.

3.2 Transfer Techniques

A positive ΔP is needed for transfer, and can be created in a number of ways:

(1) Pressurising by external use of a non-condensing gas. For example, helium is used for pressurising oxygen and hydrogen space rocket tanks.

(2) Pressurising by external use of same gas. The introduction of warm nitrogen gas into the ullage space will rapidly raise the pressure. Some condensation at the liquid surface takes place so as to form a thin layer of saturated liquid. Stratification prevents this layer mixing with the rest, and little further condensation of the inlet gas will take place. This technique is convenient for laboratory systems, but not for larger scales.

(3) Heating by: (a) normal heat flux through the insulation;

(b) the use of a pressure raising coil or vaporiser mounted in a pipe between bottom and top of the tank (VI vessels only).

(4) Mechanical pumps, which can be submerged for LIN, but definitely not for LOX. Like any liquid pump, the Net Positive Suction Head (NPSH) of the pump is an additional requirement to be met by the thermodynamic state of the sub-cooled LIN. Clearly, the fluid state must not cross the saturation line, particularly in the pump inlet passages. If it does, then cavitation will cause the pump to stall. The problem can be countered by the use of an inducer - an Archimedean screw on the suction side of the pump impellor.

3.3 Cryogenic Pumps

Pumps for use with LIN are very similar to those used in other industries, and most of the hydraulic design details are based on water. In 1955, the National Bureau of Standards investigated the characteristics of a number of pumps used for LOX and LIN. Basically, it was found that, providing the liquid was undercooled, the pump performance characteristics were very similar to those for water; the liquid capacity for a given head was only 5-10% lower than the capacity for water; the maximum head at zero delivery was also about 5-10% lower.

Whereas hydraulically, cryogenic pumps are similar to water pumps, there the similarity ends. The cryogenic pump has to incorporate a number of design features to enable it to operate safely with minimum maintenance, under poor environmental conditions of frost and moisture, with a heat break between motor and impeller for an externally mounted pump, and cryogenic liquid shaft seals.

Two particular types of pump to be met are:

(a) Single stage external centrifugal;

(b) Multi-stage submerged centrifugal.

3.4(a) Single stage external centrifugal pump

Commercially available models of this pump are suitable for the range 50 psig (3.4 bar) to 450 psig. (31 bar) and 20 gpm (1.5 litre per second) to 250 gpm (20 litres per second).

The pump is mounted as close as possible to the liquid bulk storage, and a particular example fed with a standard 3-phase 440v 50Hz power supply operates at a synchronous speed of 3,000 rpm to give pressures of 50 to 100 psig (3.4-6.8 bar), and a liquid throughput of 250 gpm (20 litres per second). A cross-section of this type of pump is shown in Figure 2.

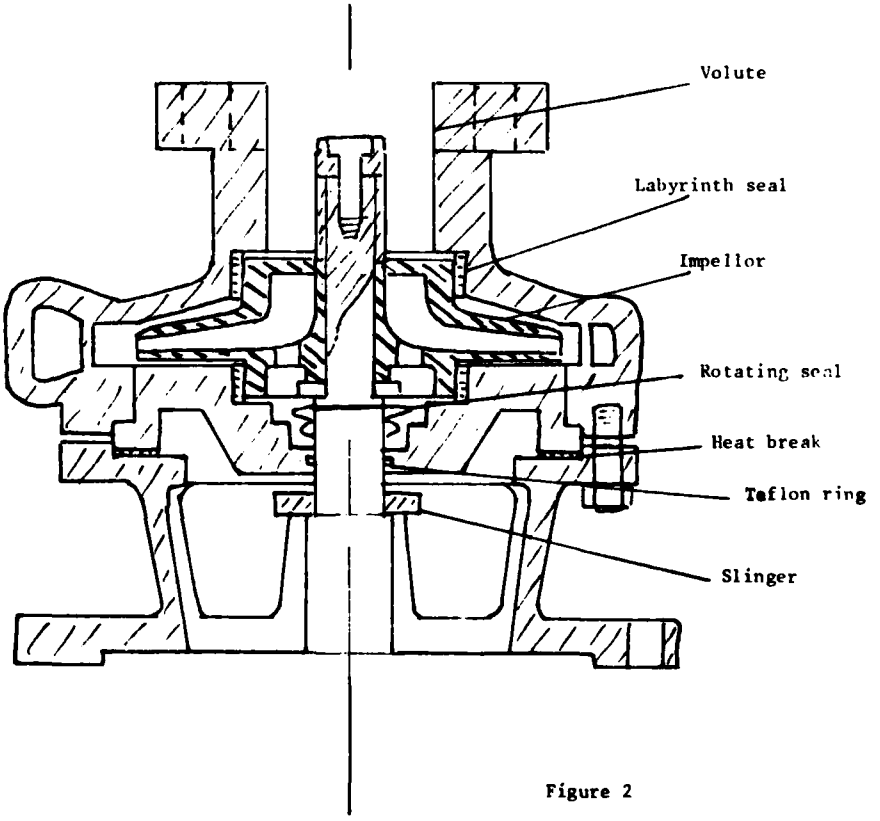

Figure 2

3.4(b) Multi-stage submerged centrifugal pump

The multi-stage pump is capable of much greater pressures for the same diameter and speed of rotation. For any stage, the pressure head varies as the square of the speed of rotation and as the square of the impellor diameter. To keep pump speed and impellor diameters to manageable proportions, multi-staging is used, with impellors mounted on the same shaft.

A submerged pump is usually driven via an extension shaft passing through the insulation to an externally mounted synchronous motor. The use of totally submerged motor plus impellor is attractive, and large Carter pumps are widely used for pumping LNG at large throughputs but relatively low pressures. The use of smaller totally submerged multi-stage pumps has fallen into disuse through a variety of development problems.

The submerged pump with external drive has a number of advantages over the externally mounted pump, namely:

(a) during its operational life it is constantly cold. It is immediately available for operation, since cooling is not required.

(b) priming does not constitute a problem. The NPSH is related entirely to the flow characteristic of the inlet to the impellor, and is consequently very small.

(c) a rotating liquid seal is not required at the cold end of the shaft. A rotating gas seal is, however, necessary to prevent leakage from the tank. Since this is not normally subjected to cryogenic temperatures, the operating conditions are less stringent.

(d) in the submerged environment, it is possible to design a centrifugal pump to operate against a completely closed delivery valve. Normally, under cryogenic conditions, if the delivery valve is closed vapour quickly forms and the pump loses prime. By arranging a controlled liquid bleed back into the tank, gas leaking and consequent loss of prime is prevented, while the pump is maintained at liquid temperature with the delivery valve closed.

3.5 Insulation of transfer lines

The degree of insulation depends on the duty cycle. It should be borne in mind that for intermittent use, more liquid may be lost in cooling down the insulation of a well insulated line, than with no insulation at all. This argument applies particularly to the flexible hose connections used for filling storage tanks from road or rail tankers.

Two types of insulation are in common use:
(1) Polyurethane foam with external vapour barrier.
(2) Evacuated multi-layer insulation with its low loss capability and low thermal capacity.

All transfer lines should be as short as possible and should be made up from the minimum number of long straight runs. A small number of 90% bends will enable the thermal contraction to be absorbed without severe stressing.

3.6 Cooldown

The rate of cooldown of a line or vessel is dictated by
(1) the thermal mass to be cooled and
(2) natural or forced convective heat transfer.

In general, cooldown cannot be accelerated by high pressures and high liquid mass velocities. The generation of vast white plumes of cold vapour during cooldown is a sign of excessive use of liquid nitrogen. REMEMBER that during cooldown, the available cold in the vapour is just as important as the latent heat of vaporisation of the liquid. Let the cooldown process take place naturally without forcing the pace.

The cooldown of a long transfer line by admitting liquid nitrogen from one end is a surprisingly long process. The velocity of the liquid front (Figure 3)

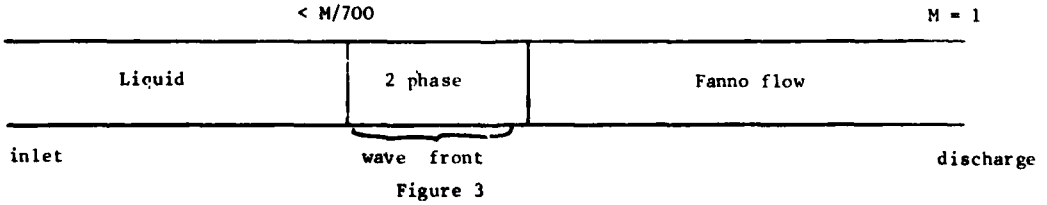

Figure 3

is dictated entirely by the Fanno-flow of ambient temperature vapour ahead of the front, and a choking condition near the vapour discharge end. Vapour is generated by
(1) cooling the thermal mass of the line and
(2) absorbing the heat in-leak into the cold section.

3.7 Typical Layout for Storage and Pumped Delivery

Figure 4 is a schematic diagram of a typical control system for handling liquid nitrogen.

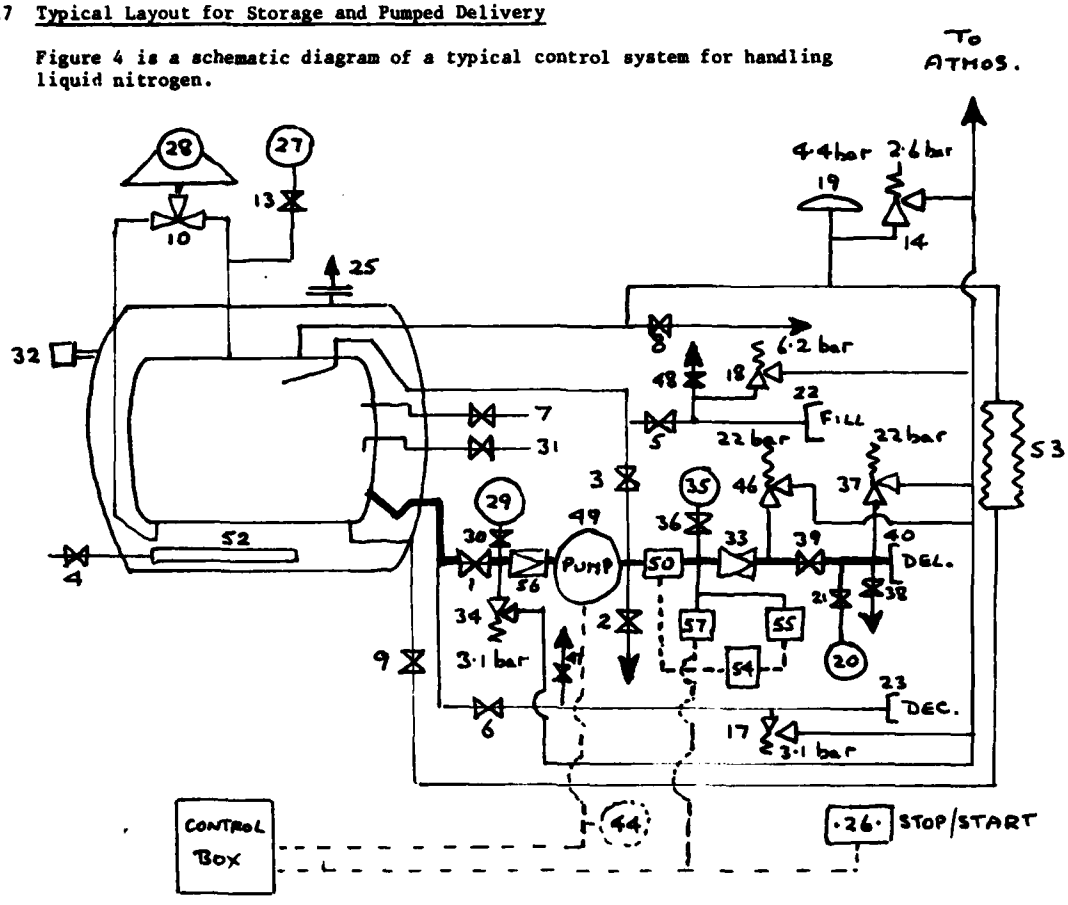

Figure 4.

1. Pump suction valve
2. Pump vent to atmos.
3. Recycle valve.
4. Vacuum valve
5. Top fill valve
6. Decant valve
7. Trycock valve
8. Main vent valve
9. Pressure raising valve
10. Contents gauge valve
13. Pressure guage isolating valve
14. Vessel safety valve
17. Decant Hose safety valve
18. Top fill Hose safety valve
19. Bursting disc
20. Back Pressure gauge
21. Back Pressure gauge valve
22. Top fill line coupling
23. Decant line coupling
24. Vent valve coupling
25. Blow-off plate valve
26. Pump start-stop unit
27. Liquid pressure gauge
28. Liquid level contents gauge
29. Pump suction pressure gauge
30. Pump suction guage isolating valve
31. Analysis valve
32. Vacuum reading connection
33. Non-return valve
34. Pump suction safety valve
35. Pump delivery pressure gauge
36. Pump delivery gauge isolating valve
37. Delivery line safety valve
38. Delivery line vent valve
39. Pump delivery valve
40. Delivery line coupling
44. Ammeter
46. Delivery line safety valve
47. Decant line vent valve.
48. Topfill hose vent valve
49. Cryogenic pump and motor
50. Turbine or Flow meter
52. Vacuum filter
53. Pressure raising coil
54. Flow counter unit
55. Metering pressure switch
56. Pump suction filter
57. Off prime pressure switch

3.8 Zero delivery

In this extreme case, the cooldown process stops and the liquid front becomes stationary when the line is long and has high thermal mass and poor insulation. Zero delivery can be countered by the use of cooldown vapour vents along the line which are closed in succession.

3.9 Pressure surges during start-up

Rapid opening of liquid control valves leading into warm lines must be avoided. Pressure oscillations with peak pressures exceeding the delivery pressure may lead to flow reversal and damage to pumps and meters. Gate and globe valves are preferred. Flap valves should be avoided. Electromagnetically controlled valves must open and close over $\sim$ 10 seconds. Emergency stop and vent valves should also act slowly.

3.10 Thermal cycling

Any cooldown or warming up procedure results in temperature gradients being produced in the walls of vessels, tanks, lines and fittings. These temperature gradients are very much larger than those met in high temperature plant like furnaces or boilers, being in the range 0.1 to 100 K mm^{-1}; and they induce severe stressing. Under repeated cooldowns or local cyclic temperature changes produced by LIN flow controllers, the repeated induced thermal stresses may lead to mechanical failure in a variety of ways.

The sudden appearance of a "cold" leak after a period of operation is an all-too-common experience. Leaks must be rectified immediately before further damage occurs. Should a leak develop, the plant must be depressurised and warm-up commenced as soon as possible. At the same time, the exact location of the leak should be established when the plant is cold. In many cases, this will be easier than when the plant is at ambient temperature.

REMEMBER that failures arising from thermal cycling can be prevented by
(1) avoiding thermal cycling altogether and
(2) changing temperatures slowly so as to avoid inducing high stress levels.

3.11 Safety

The major problem with safety in the operation of cryogenic plant and the handling of cryogenic liquids is the lack of safety codes of practice. A guide to good practice is provided by the Cryogenics Safety Manual of the British Cryogenics Council, but this publication is not mandatory.

Although non-toxic and non-flammable, liquid nitrogen has particular properties which give rise to some, perhaps unexpected, hazards:

1. Asphyxiation: Multiple fatalities can occur because the victims are unable to escape or to attract attention. When the oxygen concentration in inhaled air is reduced from 20% to 10%, there is a serious hazard from asphyxiation.

   In sudden and acute asphyxia, such as that produced by inhaling pure nitrogen gas, unconsciousness is immediate. You will fall as if struck down by a blow on the head, and you may die in a few minutes.

   In gradual asphyxia, such as that produced by a gradual and unnoticed reduction in oxygen content from 20% to 10%, the victim may be wholly unaware that anything is wrong until his legs give way, leaving him unable to stand, crawl to safety, or shout for help. You will die quite painlessly; if you are rescued and resuscitated, your brain may be permanently damaged.

   A cryogenic wind-tunnel will generate large quantities of nitrogen gas. All vents must be at an adequate height above buildings. The accidental spillage of liquid nitrogen and the venting of nitrogen gas in enclosed experimental areas must be anticipated by the use of adequate ventilation. All personnel must be made aware of the insidious danger of asphyxiation.

2. Cold burns: Liquid nitrogen or cold nitrogen vapour will produce effects on the skin similar to burns. They will vary in severity with temperature and the time of exposure.

   Naked or insufficiently protected parts of the body coming into contact with uninsulated pipes or vessels will stick fast by virtue of the freezing of available moisture, and the flesh will be torn in removal. The wearing of wet clothes should be avoided.

   Cold burns can be avoided by the use of suitable protective clothing, including asbestos gloves, boots, overalls and face shields or goggles. The first-aid treatment for cold burns is rapid thawing with cold, not hot, water.

3. Physical Explosion: If liquid nitrogen becomes sealed off in a section of transfer line, or any closed vessel, and is left to evaporate and warm up, then a pressure of up to 600 atm can be generated. This pressure is much greater than the likely bursting pressure, and a physical explosion will occur. Clearly, such events can be avoided by correct operation of valves in transfer lines and so on. On the other hand, lines can block through the condensation of water from the atmosphere and its subsequent collection and freezing as a plug in the exit of a vent.

It is therefore advisable to have bursting discs or other pressure relief devices installed in sections of liquid lines.

Vacuum spaces must also have bursting discs fitted as a standard protection. Failure of the inner vessel and leakage of liquid nitrogen into the vacuum space will inevitably lead to a physical explosion. DO NOT risk using evacuated vessels or dewars with faulty or no bursting discs.

4. Fire: Fire results through the co-incidence of:

1. Flammable material
2. Oxidant

and 3. Ignition source.

A fire hazard exists when two of the above three occur together.

A fire hazard occurs with liquid nitrogen, when oxygen-rich liquid air is produced by condensation of air on surfaces cooled by liquid nitrogen below 81.8K.

Oxygen-rich air contains 40-50% oxygen, and is a powerful oxidant. If it collects in insulating material such as polyurethane foam, a serious fire hazard exists.

Air-tight vapour barriers and/or nitrogen gas purging must be used to prevent the condensation of liquid air inside insulations.

3.12 Other safety factors

Accidents with cryogenic liquids tend to follow a chain reaction of events. For example, a small leak leads to a physical explosion; a subsequent fire then leads to the collapse of a storage tank. These chain reactions should be anticipated by preventative safety measures.

Finally, all safety procedures must be observed by all personnel all the time. A major problem is familiarity breeding contempt of safety rules.

3.13 General References for further information

Barron R., Cryogenic Systems (1966) McGraw Hill.

Haselden G.G., Cryogenic Fundamentals (1971) Academic Press.

White G.K. Experimental Techniques in Low-Temperature Physics 3rd ed. (1979) Oxford Univ.Press.

Zabetakis M.G., Safety with Cryogenic Fluids (1967) Plenum Press.

MODEL DESIGN AND INSTRUMENTATION EXPERIENCES WITH CONTINUOUS-FLOW CRYOGENIC TUNNELS

Robert A. Kilgore
NASA - Langley Research Center
Hampton, VA 23665, U.S.A.

SUMMARY

The development of wind tunnels that can be operated at cryogenic temperatures has placed several new demands on our ability to build and instrument wind tunnel models. Some of the experiences at the NASA Langley Research Center relative to the design and instrumentation of models for continuous-flow cryogenic wind tunnels are reviewed in this lecture.

SYMBOLS

$\bar{c}$	Mean geometric chord
c_f	Local skin friction coefficient, $\frac{\text{local skin friction}}{q_\infty}$
Δc_p	Orifice induced pressure error, $\frac{\text{measured pressure - correct pressure}}{q_\infty}$
C_B	Buffet coefficient, $\frac{\text{unsteady wing root bending}}{q_\infty S\bar{c}}$
C_D	Drag coefficient, $\frac{\text{drag}}{q_\infty S}$
C_L	Lift coefficient, $\frac{\text{lift}}{q_\infty S}$
C_m	Pitching-moment coefficient, $\frac{\text{pitching moment}}{q_\infty S\bar{c}}$
d	Orifice diameter
f	Frequency
h	Burr height
k_a	Acceptable roughness height
K_T	Buffet bridge sensitivity
M	Mach number
q	Dynamic pressure
$R_{\bar{c}}$	Reynolds number based on $\bar{c}$
R_d	Reynolds number based on d
S	Reference area
V	Velocity
α	Angle of attack
δ^*	Boundary layer displacement thickness
λ	Linear coefficient of thermal expansion
ν	Kinematic viscosity

Subscripts

t	Stagnation value
∞	Free-stream value

Abbreviations

%	Percent
2-D	Two dimensional
3-D	Three dimensional
LN_2	Liquid nitrogen
NRT	Nickle resistance thermometer
NTF	National Transonic Facility
TCT	0.3-m transonic cryogenic tunnel

1. INTRODUCTION

It is well known to anyone familiar with wind tunnels that the successful testing of a model is usually a combination of science, art, and good luck. The recent addition of the very low operating temperatures associated with the cryogenic wind tunnel concept requires that we take a new look at model testing technology. Of the many details that must be considered by the test engineer, this lecture will attempt to cover only two: model design and model instrumentation. Further restriction of the scope of this lecture is made possible by strict adherence to the "Aims of the Course" which state that the emphasis of the lectures should be on the unfamiliar aspects of technology which must be applied, and on solutions to special problems which arise from the exploitation of low temperatures.

Therefore, I will not attempt to review in this lecture those aspects of model design and instrumentation that are accepted as standard practice for ambient temperature tunnels.

The various methods that we now use to build and instrument wind tunnel models have evolved slowly since the first simple flat-plate models were built and tested by Wenham in 1870. Many of the problems we face today were not present in the early years of wind tunnel testing when tunnels operated at low speeds and at ambient pressure and temperature. In 1920, in order to increase the test Reynolds number, Munk build a low-speed wind tunnel designed to operate at a pressure of 20 atmospheres. By testing 0.1-scale models at 0.5 flight velocities, Munk realized full-scale values of Reynolds number at dynamic pressures only five times greater than experienced at one atmosphere rather than 10 times as would have been the case had he matched flight velocity and tested at 10 atmospheres. Nevertheless, the introduction of higher dynamic pressures made it necessary to modify many of the existing practices in order to successfully realize the benefits of increased Reynolds number. As aircraft became more refined and increased in speed, the resultant need to increase the speed of wind tunnels resulted in increased model loads and support interference effects which caused yet further changes to be made in how tests were conducted. In testing 3-D models, for example, it became necessary to use internal strain-gage balances in place of external balances connected to the model by struts or wires.

Today, we again find ourselves in the position of modifying, adapting, or changing our traditional wind tunnel techniques in order to utilize fully the tremendous increase in Reynolds number and the other research benefits offered by a pressurized cryogenic wind tunnel. Particularly pertinent to this lecture is the benefit of cryogenic operation that provides a large reduction in model loads for a given Reynolds number. Successful utilization of this important benefit requires, however, the consideration of other effects of the wide temperature range. Just as we were able to successfully accommodate increases in tunnel operating pressure and speed, we find that we are able, in most cases, to successfully accommodate the decrease in operating temperature required for the cryogenic tunnel. Personnel at the Langley Research Center have had experience in operating cryogenic wind tunnels since 1972. Our initial experience was with a small low-speed atmospheric fan-driven tunnel.[1] Based on the experience and confidence gained with the low-speed tunnel, a larger fan-driven tunnel capable of being pressurized and operated at transonic speeds was built and put into operation during 1973.[2] This pilot transonic pressurized cryogenic tunnel, now known as the Langley 0.3-m transonic cryogenic tunnel (TCT), has been used since August of 1973 to validate cryogenic nitrogen as a transonic test gas, develop cryogenic tunnel model construction, instrumentation, and testing techniques, determine possible operating limits set by condensation or other real-gas effects, study various tunnel control schemes, and gain practical experience in the operation of a cryogenic nitrogen-gas transonic wind tunnel.[3-5] In addition, it has been used for a variety of aerodynamic tests that could take advantage of either the high unit Reynolds number or the extremely wide range of Reynolds number available.

Along with the experimental work with the low-speed and transonic cryogenic tunnels, there was a parallel theoretical study of the real-gas effects resulting from operating a tunnel using nitrogen gas at cryogenic temperatures.[6] These studies, described in previous lectures, combined with the experimental verification of the cryogenic tunnel concept at transonic speeds in the 0.3-m TCT, had a far reaching effect. A direct and most significant effect was the decision in 1975 to build a single large transonic cryogenic tunnel to meet the high Reynolds number testing needs of the United States. Implementation of this decision is evidenced by the construction at Langley, now well underway, of the National Transonic Facility (NTF), which will be described in detail in a subsequent lecture.

As would be expected, in 8 years of using cryogenic tunnels, we have experienced both successes and failures in our efforts to build, instrument, and test models. The purpose of this lecture is to review some of our experiences, both good and bad, in the hope that such information will be useful to others wishing to exploit the research advantages offered by the cryogenic wind tunnel.

It should be noted that the use of trade names does not imply endorsement by NASA or the U.S. Government. Further, the views expressed herein are those of the author and do not necessarily represent the views of NASA.

2. THE ENVIRONMENT IN A CONTINUOUS-FLOW CRYOGENIC TUNNEL

In order to properly set the stage for a discussion of model design and instrumentation for continuous-flow cryogenic tunnels, it is necessary to examine in some detail the environment to be found in such tunnels. The mode of operation of the Langley 0.3-m TCT, as well as the range of test conditions over which it can be operated, can be taken as typical of continuous-flow transonic cryogenic tunnels and will therefore be used to illustrate several essential points.

Listed in the following table are the test conditions available in a typical ambient temperature continuous-flow transonic tunnel, the Langley 8-ft transonic pressure tunnel (TPT), and the 0.3-m TCT.

	8-ft TPT	0.3-m TCT
T_t, K	320	78 - 340
p_t, atm	0.25 - 2	1 - 6.1
M_∞	0.2 - 1.2	0.1 - 0.9
q_∞, atm	0.007 - 0.54	0.007 - 2.0
R/m, max	14×10^6	390×10^6

The most obvious differences between the two tunnels is the very wide range of operating temperatures, the higher maximum dynamic pressure, and the extremely large value of unit Reynolds number available in the cryogenic tunnel. These differences give rise to many, if not all, of the practical problems of building and instrumenting models for testing in cryogenic tunnels to be discussed in later portions of this lecture. In making comparisons such as this, it must be kept in mind that the high dynamic pressures in the cryogenic tunnel is a result of using increased pressure to provide even greater Reynolds number increases than offered by reduced temperature alone and to provide the unique operating envelopes that allow separation of aeroelastic, viscous, and compressibility effects.

2.1 Operating Envelope

The operating envelope of the 0.3-m TCT at a constant free-stream Mach number can serve to illustrate graphically the wide range of conditions available in a pressurized cryogenic wind tunnel. As shown in Figure 1, the envelope of dynamic pressure versus Reynolds number is bounded on the left by the maximum operating temperature line of 340 K and on the right by the minimum operating temperature boundary which, as discussed in a previous lecture, is set by the saturation boundary of the test gas under free-stream conditions. The lower boundary is set by the minimum operating pressure of 1 atm while the upper boundary is set by the 6.1 atm pressure limit of the tunnel pressure shell.

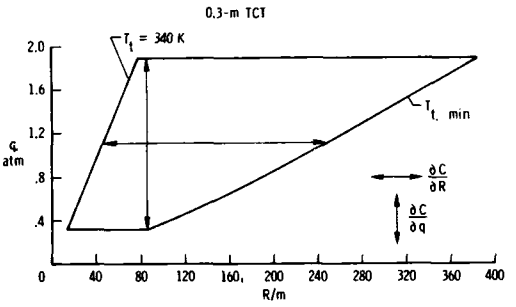

Fig. 1 Constant Mach number operating envelope.

If the 0.3-m TCT were an ordinary ambient temperature pressure tunnel, for all practical purposes the entire operating envelope at a constant Mach number would be represented by the single 340 K line of constant temperature. In such a tunnel, only the effects of dynamic pressure, and the relatively modest changes in Reynolds number, need to be taken into account in the design and instrumentation of models.

However, having temperature as a completely independent variable transforms a single operating line into an operating envelope. In addition to the extremely high test Reynolds number capability, the advantages of having such an envelope are the ability, as indicated in Figure 1, to perform either pure Reynolds number studies, pure aeroelastic studies, or achieve various combinations of loading and Reynolds number in order to more nearly match some desired flight shape - Reynolds number combination.

One of the primary advantages of the cryogenic tunnel concept is the fact that the large increase in Reynolds number is obtained with no increase in the inertia force and that the model loads are greatly reduced relative to the ambient temperature condition for the same Reynolds number. However, as previously mentioned, the fact that the operating temperature can be varied over such a wide range cannot be ignored when we consider the design and instrumentation of models for such a tunnel. Furthermore, as will be discussed in more detail later, the high Reynolds numbers result in very thin boundary layers on the models which can impose severe model surface finish and pressure orifice size requirements. However, it must be noted that these particular problems are no more severe when a given value of Reynolds number is achieved by using cryogenic temperatures than when the same value of Reynolds number is achieved by increasing the operating pressure. In fact, experience has shown that the extremely high pressures required in an ambient temperature tunnel in order to match the Reynolds number achieved in a moderately pressurized cryogenic tunnel give rise to a host of non-trivial problems, the most obvious being the high model stresses brought about by the much higher dynamic pressure.

2.2 Variation of Temperature with Time

As contrasted to intermittent flow cryogenic tunnels, the changes in temperature are generally very gradual in continuous-flow cryogenic tunnels. As a consequence, problems related to thermal stresses or non-adiabatic wall conditions are either reduced or completely avoided. Stream and tunnel wall temperatures recorded during a typical run in the externally insulated 0.3-m TCT are shown in Figure 2 to illustrate the way in which temperature is varied during the pre-run cooldown, during the testing period, and during the post-run warm-up. It should be noted that data are being taken during the testing period only when the stream temperature has stabilized to a constant value.

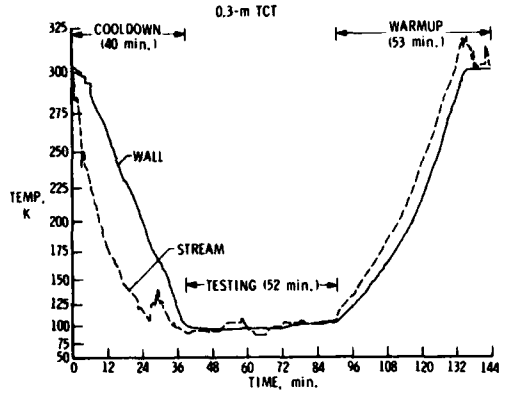

Fig. 2 Stream and wall temperature vs. time.

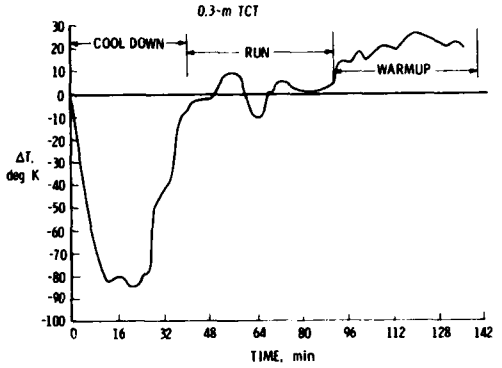

Fig. 3 Temperature difference between stream and wall vs. time.

The difference between the stream and wall temperatures are shown in Figure 3. The wall temperature responds much more slowly to changes in stream temperature than would a typical model under the same conditions due to the fact that the tunnel wall has more thermal inertia and is in contact with the stream only on one side as contrasted to a model which is completely surrounded by the high velocity stream. Even under these less than ideal conditions, the wall temperature differed from the stream temperature by no more than ±10 K° when data were being taken. Unfortunately, no experimental data have yet been recorded of model temperature response to changes in stream temperature. However, based on unrecorded observation as well as on calculations made by Johnson,[7] the time required for a typical model to reach near adiabatic conditions following a step change in stream temperature is very short, typically in the order of 10 to 20 seconds. The point to be noted is that there is no need for any special precooling of the model in a continuous-flow cryogenic tunnel in order to insure adiabatic wall conditions. The very nature of a continuous-flow cryogenic tunnel demands that changes in stream temperature be made rather slowly, thus assuring quasi-adiabatic conditions at all times.

3. MODEL DESIGN

The wide range of operating temperature discussed in the previous section as well as the high pressure capability available in many cryogenic tunnels are obviously two of the most important factors to be considered in the design of models for cryogenic tunnels. However, there are several other factors which must also be taken into account. For example, continuous flow tunnels, whether or not cryogenic, generally require greater factors of safety in the model design than do intermittent tunnels. Thus, for a given model loading, there should be a wider choice of materials and construction methods available for use in building models for intermittent tunnels. This simple fact should not be overlooked. Perhaps the most important point to be made regarding model design is that there are very few general rules which can be or should be applied. Every model design exercise needs to take into account not only such obvious things as factors of safety but also such things as the changing physical properties of the model material with changing temperature. The increased strength of a material at cryogenic temperature may be just what it takes to realize an acceptable model design. Such benefits of cryogenic operation are free and should be exploited.

This portion of the lecture will address some of the aerodynamic aspects of the design, construction, and testing of models for continuous-flow cryogenic tunnels.

3.1 Aerodynamic Considerations

The high Reynolds number capability of cryogenic tunnels, such as the 0.3-m TCT and the NTF, give rise to very thin boundary layers over the models. This fact, combined with the requirement for high quality test data from these tunnels, has prompted personnel at the Langley Research Center to re-examine some of the aerodynamic considerations related to model surface definition, particularly in the areas of fabrication tolerance, model surface finish, and orifice induced pressure errors. Each of these areas is briefly reviewed in the following sections. In addition, some of the planned and on-going programs that relate directly to the aerodynamic aspects to be considered in building models for the high Reynolds number testing range of cryogenic tunnels will be described.

3.1.1 Fabrication Tolerance

Fabrication tolerances, in contrast to surface finish, are probably more critically dependent on compressibility effects than on Reynolds number effects. It might be expected, therefore, that the fabrication tolerances required for accurate data in the new high Reynolds number tunnels will not differ appreciably from current transonic models. Unfortunately, fabrication tolerance requirements for models to be tested at

transonic speeds are very difficult to determine because of the extreme accuracies that are needed to properly define the effects of fabrication tolerance either by experimental investigations or analytical studies using modern transonic theoretical methods. There seems to be no published guidelines on the specification of fabrication tolerances. It appears that fabrication tolerance for models to be tested at transonic speeds is based on past experience and the accuracy of the delivered model is very much a function of the ability of the model maker and the accuracy of the machines he uses. Since, for supercritical flow conditions, model tolerance can have a major influence on both data accuracy and model costs, it is highly desirable to develop improved techniques for defining the tolerance required. The same care should be exercised in defining model fabrication tolerance for any transonic model regardless of its projected test Reynolds number. In keeping with the aims of this lecture series, there will be no further discussion of model fabrication tolerance in this lecture since the use of cryogenic temperatures per se is expected to have at most only a second order effect through its influence on the choice of model materials or manufacturing methods.

3.1.2 Model Surface Roughness

An overly rough surface finish on a model can lead to many problems with respect to boundary layer transition, separation, skin-friction drag, and shock location. Although all of these are important, I will focus on but one area; the effect of model surface finish on skin friction.

Drag estimates for full-scale aircraft are made by adding the aircraft manufacturing roughness drag to the drag measured on an "aerodynamically smooth" wind-tunnel model. Therefore, any skin friction increases associated with the wind-tunnel model due to surface roughness are undesirable. Surface roughness problems are dependent on Reynolds number due to fact that as the boundary layer becomes thinner with increasing Reynolds number, the acceptable surface roughness height (the maximum roughness height which results in no skin friction penalty) decreases.[8-10]

In most high Reynolds number transonic tests it is desirable to have a model surface finish that on its own will produce no measurable aerodynamic effect. The data in Figure 4 show the variation of acceptable roughness height k_a in a zero pressure gradient turbulent boundary layer as a function of Reynolds number $R_{\bar{c}}$ where $\bar{c}$ is taken as 0.20 m, a value representative of a transport model sized for the NTF. Shown on Figure 4 for reference are the maximum NTF Reynolds number, the Boeing 747 cruise Reynolds number and the maximum Reynolds number for current tunnels. At a given Reynolds number, any roughness height falling below the acceptable roughness curve will produce no skin friction penalty. The shaded band on Figure 4 is the range of typically specified and achievable surface finishes for current transonic models. The current specified model surface finishes appear to be compatible with a significant part of the NTF Reynolds number range. However, as is noted on the figure, the acceptable roughness curve is for a surface with uniformly distributed three-dimensional particles affixed to it. As can be seen in the photographs in Figure 5, the surface of a typical model does not resemble a smooth surface with distributed particle roughness. Because of this fact, an experimental program is planned to determine the equivalent distributed particle roughness for typical NTF model surfaces. In order to carry out this experimental program, a good definition of the topography of a typical NTF model surface is needed.

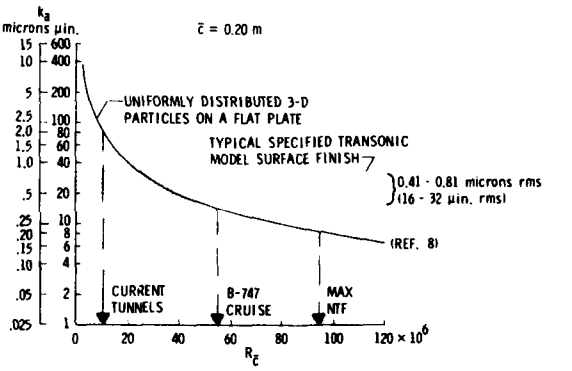

Fig. 4 Acceptable surface roughness vs $R_{\bar{c}}$.

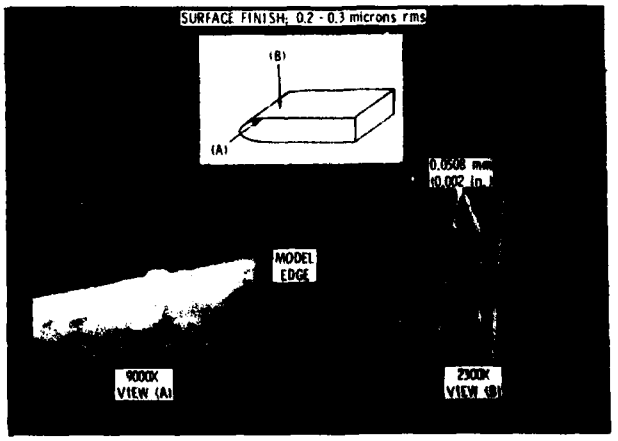

Fig. 5 Electron micrographs of typical NTF model surface.

The instrumentation which is almost universally used in model shops to measure surface roughness is the stylus profilometer. However, there are at least two potential problems associated with the stylus profilometer. As shown in Figure 6, problems can arise when the roughness slope is too steep or the roughness frequency is too high. The resolution of the stylus profilometer is directly related to the size of the stylus, which typically has a radius of 2.5 microns (100 μin). There are no published data to indicate that a stylus profilometer can accurately determine the topography of surfaces typical of NTF models. It is planned, therefore, that the U.S. National Bureau

of Standards (NBS) will compare the topography of a surface typical of NTF models as measured by a stylus profilometer and by a stereo scanning electron microscope in order to determine if, in fact, the stylus profilometer is adequate or if other methods of determining the surface finish must be used.

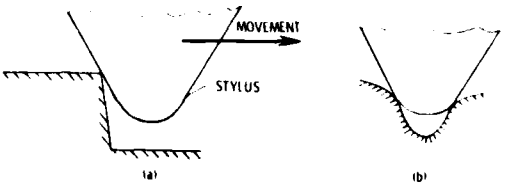

Fig. 6 Potential problems with stylus profilometer.

In addition to the two potential problems just discussed, the stylus profilometer has great difficulty measuring the finish on highly curved surfaces similar to the leading edge of a wing. The leading edge of a wing is, of course, the region where the boundary layer is thinnest and thus the region where the local skin friction is most sensitive to surface roughness. Thus, it is highly desirable to have the capability of measuring surface finish over the leading edge. Towards this end the NBS will endeavor to develop a light scattering system to measure the finish accurately on surfaces with high curvature.

3.1.3 Orifice Induced Pressure Error

It has been known for some years that there is an orifice induced pressure error associated with static pressure measurements. In general, however, the boundary layer displacement thickness δ^* is large compared to the orifice diameter for models being tested in the Reynolds number range of conventional (ambient temperature) tunnels. Under these conditions, the static pressure error due to the finite size of the orifice is small and is usually neglected as insignificant relative to other sources of error. At a sufficiently high test Reynolds number, the boundary layer thickness on the model can become very small compared to the orifice diameter. Under these conditions the orifice induced pressure error may not be negligible.

When the static pressure in a flow field is measured by a pressure orifice, the stream line curvature can change in the vicinity of the orifice and eddies can be set up inside the orifice resulting in the static pressure measurement being higher than the true value.[11-15]

An additional orifice induced error can result from orifice imperfections. Although there are several types of orifice imperfections, experimental data[12] exist only for a burr around the orifice. A burr can produce flow separation in the orifice causing additional streamline deflection. Some other types of orifice imperfection which can produce pressure error are out-of-round orifices, particles in the orifice, and orifices with their longitudinal axis not normal to the model surface.

Figure 7 presents a compilation of experimental results[11-13] for orifice induced pressure error of "perfect" (absence of imperfection) orifices. It can be shown from local dynamical similarity considerations that

$$\frac{\Delta c_p}{c_f} = f\left(R_d \sqrt{\frac{c_f}{2}}\right)$$

therefore, orifice induced pressure error is generally presented as $\Delta c_p/c_f$ versus $R_d\sqrt{\frac{c_f}{2}}$. The largest values of d/δ^* (orifice diameter/boundary layer displacement thickness) for which test results are shown in Figure 7 is 4.0. Using the data of Reference 13, the variation of pressure error, Δc_p, with Reynolds number, $R_{\bar{c}}$ for three orifice diameters, 0.508 mm, 0.254 mm, and 0.127 mm are shown in Figure 8 where the local skin friction coefficient is taken as 0.0022 and the mean chord is taken as 0.20 m. For reference, the maximum NTF Reynolds number, the Boeing 747 cruise Reynolds number, and the maximum Reynolds number available in current ambient temperature tunnels are also shown on Figure 8. From these data it may appear that a 0.127 mm orifice is satisfactory for the complete range of NTF Reynolds numbers since the maximum error is only 0.008. However, the data in Figure 8 are limited to $d/\delta^* \leq 4$. As the leading edge is approached, d/δ^* can be of the order of 100 and erroneous conclusions may be drawn regarding the level of the orifice induced pressure error if only these data are considered. Therefore, a test program is underway to extend the type of data shown in Figure 8 to higher values of d/δ^*.

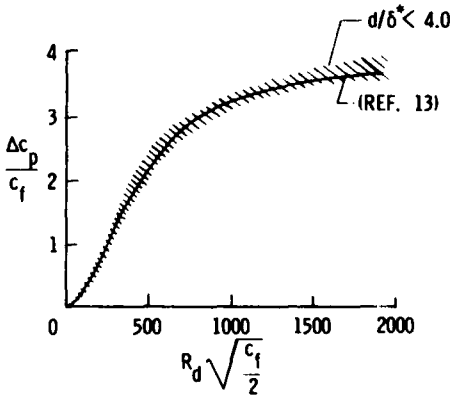

Fig. 7 Compilation of test results for orifice induced pressure error.

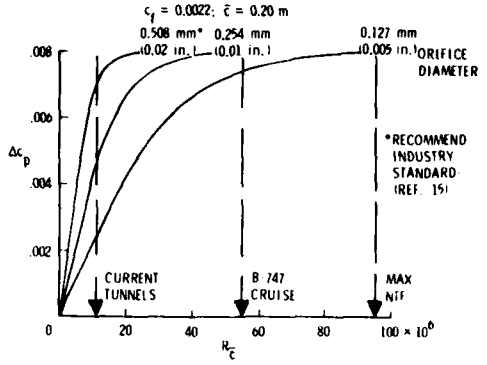

Fig. 8 Orifice induced pressure error vs. $R_{\bar{c}}$.

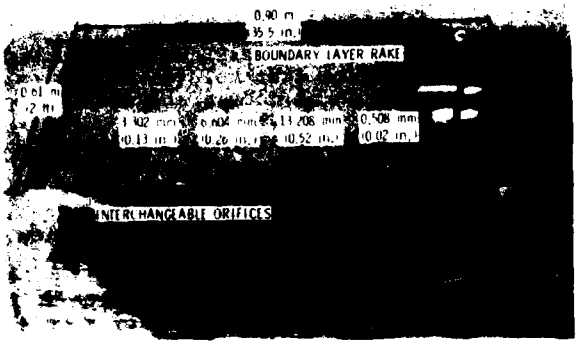

Fig. 9 Model setup for orifice studies.

Figure 9 is a photograph of the flat plate model to be used in this test program; the interchangeable orifices have diameters of 3.30 mm, 6.60 mm, and 13.21 mm. The reference orifice diameter is 0.51 mm. Only one of the interchangeable orifices will be in the plate at a time and the unused orifice locations will be filled with solid plugs. Since this plate will be tested at low Reynolds number in the Langley 7- x 10-foot wind tunnel, the orifices were scaled up in size so that a wide range of d/δ^* could be attained. The complete orifice, including the plumbing, has been scaled up for these tests. Local values of skin friction and δ^* will be obtained from a boundary layer survey.

Figure 10 shows the envelope of d/δ^* variation with Reynolds number for a 0.51 mm diameter orifice on an NTF model attainable with the present hardware. Although the maximum value of d/δ^* encountered in the leading edge region of an NTF wing may be in excess of 100, these data will extend the data base far enough to allow judgement on whether the data may be extrapolated safely to the desired values of d/δ^*. The d/δ^* range covered in this test will be adequate to directly assess the orifice induced pressure error for a large majority of the orifices on NTF models.

As can be seen in Figure 11, burr heights of 1/42 the orifice diameter can increase the hole error by a factor of approximately five. Thus, it is highly desirable to fabricate orifices that have the hole imperfections minimized. Reference 15 outlines a routine for fabricating high quality orifices with the final step calling for close visual and stylus profilometer inspection of each orifice.

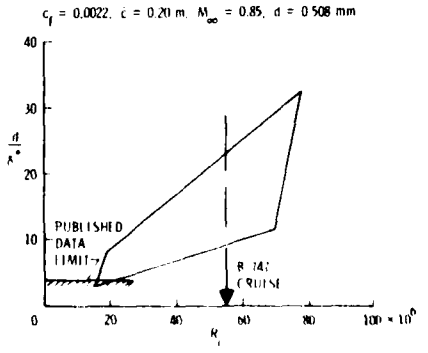

Fig. 10 Envelope of current pressure error experiment.

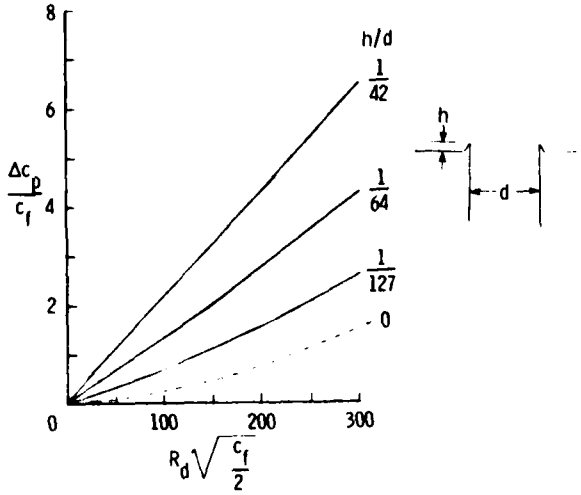

Fig. 11 Effect of hole imperfection on pressure error.

3.2 Experience

3.2.1 Choice of Material

One of the problems in designing models for the 0.3-m TCT has been the tendency to discard, too readily, the materials used heretofore to build models for ambient temperature tunnels in favor of more exotic materials. Change for the sake of change can, and has, lead to a series of problems ranging from delays in the procurement of seldom used materials to models being ruined during manufacture because the builder is not familiar with the machining or welding characteristics of the new material. In general, one should use the unfamiliar only when the familiar is proven inadequate for the job.

In designing models or other devices for use in cryogenic wind tunnels, it is extremely important to know how the materials used in their construction behave over the range of operating temperatures. Previous lectures in this series have described how the mechanical and physical properties of materials vary with temperature and no further details on that subject are needed in this lecture. Based on experience at Langley in building three cryogenic tunnels, numerous models, and several pieces of equipment used in association with the tunnels, we have gained, through failures as well as successes, some practical experience that relates to the suitability of a wide variety of materials for use in the construction of models and other pieces of equipment for cryogenic wind tunnels.

Materials that have been successfully used at Langley are listed in Figure 12 to illustrate the wide range available for use in the construction of models. The choice for a given application obviously depends upon such things as the type of tunnel, loads, surface finish requirement, and all of the other factors that are considered in the design of models for ambient temperature tunnels. There is, however, the very important additional requirement that the material have acceptable mechanical and physical characteristics at cryogenic temperatures.

IRONS & STEELS	PLASTICS
CARBON STEEL	PLEXIGLAS
AUSTENITIC STAINLESS STEEL	LEXAN
AGE-HARDENABLE STAINLESS	SYNTHANE
	NYLON
	TEFLON
NONFERROUS METALS	ADHESIVES & FILLERS
ALUMINUM ALLOYS	PLASTIC PADDING, TYPE HARD
BRASS	CREST (391 A & B)
COPPER	DEVCON
	DEVCON F, DEVCON ST
	RTV-102
WOOD PRODUCTS	MISC.
WOOD	QUARTZ
LAMINATED WOOD	GLASS
PLYWOOD	SOLDER

Fig. 12 Materials used successfully in cryogenic tunnels.

The linear coefficient of thermal expansion λ, is one of the more important properties to be considered when building models or other pieces of equipment to be used in a cryogenic tunnel. Either as a result of misdesign or misadventure, we have experienced several failures when materials having different values of λ were used in combination. One of the first failures attributed to this cause was a component of an angle-of-attack drive system used in the 3-D test section of the 0.3-m TCT. The system had a threaded brass rod fitted to a threaded bracket made from 347 stainless steel. The good fit at room temperature became a binding fit at cryogenic temperatures which caused the brass rod to fail in torsion.[4]

Another early failure in the 0.3-m TCT occurred when we attempted to hold several pieces of a stainless steel calibration strut together with brass bolts. The bolts failed in tension when the tunnel was cooled to cryogenic temperatures. Fortunately the larger pieces of the strut were stopped by the turning vanes downstream of the test section. Portions of each of the brass bolts managed to pass through the fan section without doing any serious damage.

Recognition of the problems that can arise when materials of different thermal expansion characteristics are combined has eliminated, hopefully, failures from this source. However, in the case of airfoil testing in the 0.3-m TCT, the aluminum of the test section walls and turntables, the glass of the windows in the turntables, and the steel models all have different values of λ. This gives rise to some serious design problems in trying to achieve precision fits between these components over the entire temperature range of the tunnel. Problems such as this do not arise with 3-D models where, at least in theory, a single material can be used for the entire model and there is no problem of interfacing the model with the turntables.

In addition to complicating model design, the fact that materials change dimension with temperature must also be taken into account in the data reduction process. For example, when operating at 115 K, a given linear dimension of a model made from 17-4 PH is reduced by approximately 0.2% from its room temperature value. Thus, C_D and C_L, which are nondimensionalized with respect to linear dimension squared, will be in error by approximately 0.4% while C_m, which is nondimensionalized with respect to linear dimension cubed, will be in error by approximately 0.6% if the data taken at 115 K is reduced by using values of S and $\bar{c}$ determined at 293 K (68° F). Such a correction is significant and should be taken into account in the data reduction process. Even greater corrections would be required for models made of aluminum or other materials having larger values of λ than 17-4 PH.

3.2.2 Models for the Low-Speed Tunnel

The first models to be built specifically for use in a cryogenic tunnel were those built to be tested in the Langley 7" x 11" low-speed cryogenic tunnel. These models were very simple in design and, due to the low speed and atmospheric pressure, were not subjected to large loads. Only three models were built and tested in the low-speed tunnel.

Cylindrical Model.- The first, and simplest of the three, was made from a cylindrical piece of brass stock 2.54 cm in diameter. The hollow cylinder spanned the test section and was fitted with a single pressure orifice and a single thermocouple. The experience with this model indicated that there was no fundamental problem of measuring either pressures or temperatures over the wide temperature range of a cryogenic wind tunnel.

Flat-Plate Model.- The second model was only a bit more complex. It consisted of a flat plate of aluminum alloy which spanned the test section, had a rounded leading-edge, a single static pressure orifice, and a simple fixture for holding a pitot tube in the free stream above the plate and a Preston tube against the surface near the leading edge of the plate in the laminar portion of the boundary layer. The test made with this model over a Reynolds number range gave the first experimental confirmation that cryogenic gaseous nitrogen is a valid test medium.[16]

Delta-Wing Model.- The third model to be built for the low-speed tunnel was a simple sharp leading-edge 74° delta-wing which was used in conjunction with the evaluation of a sting-mounted internal strain-gage balance to be described later. A photograph of the model, balance, and supporting sting is presented in Figure 13. The wings and fuselage were made of a single piece of mahogany which was fitted to a simple steel cylinder which in turn was fitted to the balance. The wood was filled and painted with several coats of lacquer enamel in order to produce a reasonably smooth surface.

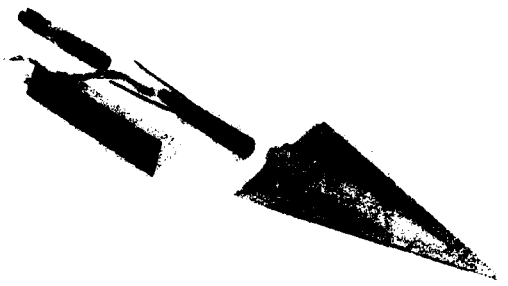

Fig. 13 Delta-wing model, balance, and sting used in low-speed tunnel.

That these first cryogenic wind tunnel models were successful should not be surprising in view of their simple design and the low loads to which they were subjected. However, as crude as they were, collectively they demonstrated the ability to build models that could be used in a cryogenic wind tunnel for force tests and pressure tests, therefore covering the requirements for the vast majority of wind tunnel models.

3.2.3 Models for the 0.3-m TCT

There have been many models built to be tested in the 0.3-m TCT. A few of these will be described in this portion of the lecture in order to illustrate some of the construction techniques that have worked and to call attention to some of the problems that can arise.

NACA 0012-64 Airfoil.- The first model to be built for the 0.3-m TCT was a modified NACA 0012-64 airfoil having a 13.72 cm chord. The airfoil spanned the original octagonal test section of the 0.3-m TCT and was fastened to the walls in such a way that incidence could be varied. This model is of some historical significance in that pressure tests made with it provided the first experimental confirmation in compressible flow that gaseous nitrogen at cryogenic temperatures behaves in the manner very close to that of a perfect gas and that Reynolds number obtained by reducing temperature is fully equivalent to Reynolds number obtained by increasing pressure.[17] Because of the comparative nature of the tests, surface finish and orifice size requirements were of no particular concern for this model. The pressure tubes were simply soldered into grooves cut into the model and the surface finished and the orifices drilled just as would be done for a model to be tested in an ambient temperature low-Reynolds number tunnel.

Two problems developed with this model. The most serious was the breaking of the pressure tubes where they entered the ends of the model. This problem was caused by the tubes becoming brittle as they were soldered to the model. The second problem developed after a trailing edge orifice was added to the airfoil by using an electric discharge milling process that involved immersing the model in an oil bath. The oil seeped into minute voids around the solder and reappeared as not-so-small drops on the model surface which froze in place as the tunnel and model were cooled to cryogenic temperatures. Because of their proximity to the pressure orifices the frozen drops of oil greatly affected the pressure data. It took a thorough cleaning in solvent using an ultrasonic cleaner to eliminate the problem with the frozen drops of oil.

Boattail Models.- Two very successful series of models were built in the shops at Langley and tested in the 0.3-m TCT by Reubush[18] to determine the drag on isolated boattails and on boattails in the presence of a simple wing.

The models used in the isolated boattail tests are shown in Figure 14. There were a total of six models: four short models (20.32 cm from the nose to the start of the boattail) having different boattail geometries and two long models (40.64 cm) which duplicated the boattail geometries of two of the short models. These models were all sting mounted with the diameter of the sting being equal to the model base diameter. Thus in this case the sting was used to advantage to simulate the geometry of a jet exhaust plume for a nozzle operating at its design point. This series of isolated boattail models was constructed of cast aluminum with stainless-steel pressure tubes cast as an integral part of the model. The tubes were placed in a sand mold in the proper position, the aluminum poured, and the model machined to the desired contour. Each of the models has 30 pressure orifices in three rows of 10 orifices each. Although it would have been desirable to have all of the orifices in one row, the fact that the models are only 2.54 cm in diameter combined with the number of orifices precluded this possibility.

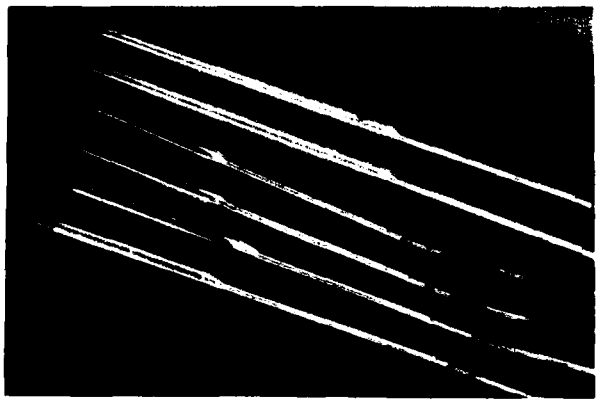

Fig. 14 Boattail nacelle models.

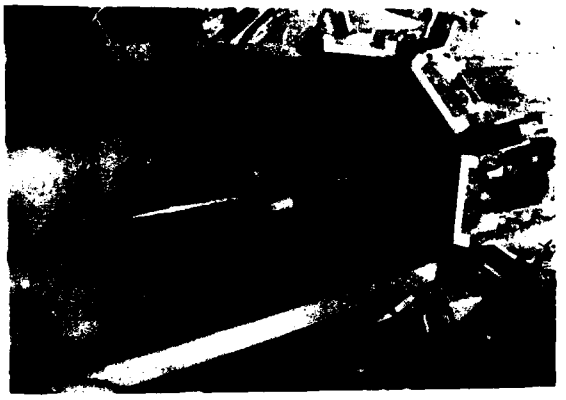

Fig. 15 Boattail nacelle model with wing in 0.3-m TCT.

The models used in the wing-body tests duplicated the forebody and boattail geometry of two of the short isolated boattail models. Construction of these models differed slightly from that of the isolated boattail models in that each of the models was cast around both the pressure tubes and a stainless steel sting. By using this method, it was possible to fit each of these models with 50 pressure orifices in five rows of 10 orifices each. Provision was made for the mounting of a 10.16 cm span 60° delta wing at 0° incidence on the top of each of the models in one of three positions. Figure 15 is a photograph of one of the wing-body models mounted in the 0.3-m TCT.

Delta-Wing Models.- A set of four simple delta wing models were made to be used in evaluation tests of a three component internal strain-gage balance to be described later in this lecture. Each of the models has a 75° leading edge sweep. Two of the models were machined from 17-4 PH stainless steel which was heat treated to conditions H 1150-M. With this heat treatment, 17-4 PH can be used at temperatures as low as 77 K. One of the steel models has a sharp leading edge and one has a rounded leading edge. Not knowing exactly what to expect with respect to heat transfer through the metal models, we hedged our bets by building a duplicate set of models out of glass fiber reinforced plastic.

Although some tests were made using one of the plastic models, the final balance evaluation was made using the sharp leading edge steel model. Due to the nature of the glass fiber reinforced plastic, it was impossible to make the surfaces of the plastic models as smooth as would be desired. Except for this single problem, these simple delta-wing models have proven to be satisfactory in every respect.

Airfoil Models for the 2-D Test Section.- Two of the main factors that must be considered in designing and building airfoil models for testing in the 2-D test section of the 0.3-m TCT have been discussed previously in this lecture. These are the requirements of surface finish and orifice size dictated by the high test Reynolds number and the requirements of acceptable material properties at cryogenic temperatures dictated by the operating temperature of the tunnel.

The requirement for a very smooth surface finish precludes the use of the simpler model construction techniques such as the "potting" of the pressure tubes in the airfoil surface as was done for the NACA 0012-64 airfoil described previously which was tested as a "proof-of-concept" airfoil in the 3-D test section of the 0.3-m TCT. In order to provide the surface finish required for testing at high Reynolds number it is necessary to use considerably more complex methods of model construction.

One method, which has been used successfully to build airfoil models for both ambient temperature pressure tunnels and the 0.3-m TCT, is illustrated in Figure 16. In this method, a void is machined through one surface into the interior of the model to allow for the routing of the pressure tubes. After the tubes and orifices are installed, an accurately machined mating plate, also equipped with tubes and orifices, is used to cover the void and thus produce a complete airfoil model. If only a chordwise row of orifices is desired on the model, the shape of the void and covering plate can be very simple. Several models having only one row of chordwise orifices have been successfully built using this method. However, if spanwise orifices are also desired on the model, the shape of the void and the covering plate becomes much more complex, as can be seen in the photograph.

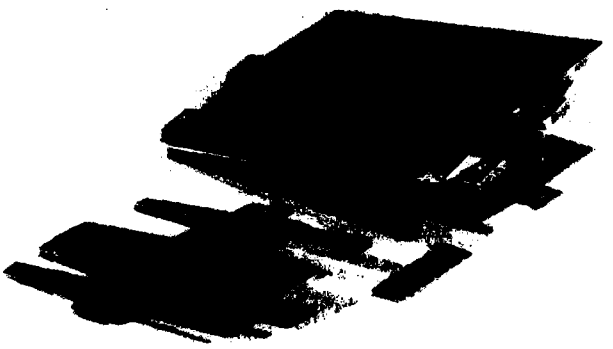

Fig. 16 Airfoil model with complex void and cover.

Several complications have been encountered in our attempts to use this more complex model design. The first problem is in the attachment of the cover plate. Electron beam welding has been attempted. However, the relatively long lengths of weld tend to warp the model and, in one case, the welds actually cracked due to internal stresses. Furnace brazing is being attempted but many of the materials suitable for models to be tested at high pressures in the cryogenic environment do not braze well.

A second problem encountered on two models being built by this method is not fundamental in nature but nevertheless real and is an example of the unexpected difficulties that can arise. The cover is intended to fit against a ledge machined in the main portion of the model. This is done in order to keep the beam of electrons from passing through the joint between the two pieces and burning holes in the pressure tubes. On two of the models, one of which is shown in Figure 16, the ledge is missing on both sides just where the tubes are taken from the model. Because of the missing ledge, over 50% of the tubes were cut or punctured during the electron beam welding process.

When successful, this type of model construction requires between 1000 and 1500 manhours which results in very high model costs considering the relatively small size of the airfoil models required for the 0.3-m TCT.

Casting airfoil models with the pressure tubes in the mold has also been attempted but has been unsuccessful to date due to voids in the casting. Beryllium-copper alloy has been used as the casting metal using stainless steel pressure tubing. Both centrifugal and vacuum casting have been used in an attempt to eliminate the voids in the casting. In addition to the problem of voids, another serious problem has been the breaking of the bond between the steel pressure rubes and beryllium-copper alloy after thermal cycling, thus producing discontinuities in the model surface in the worst possible locations. Further work is being done in an attempt to develop a successful casting technique.

3.3 Development Work

Much of the model design and construction technology presently being used for ambient temperature tunnels can be applied directly to the design and construction of models for cryogenic tunnels. However over the last few years a number of problems have become apparent during our attempts to design and build airfoil models for testing in the 20 cm by 60 cm 2-D test section of the 0.3-m TCT. For example, for a number of reasons, the actual cost of making airfoil models for the 0.3-m TCT by the traditional techniques almost always exceeds the estimated, budgeted cost. Furthermore, most of the traditional techniques require skilled craftsmen and model makers who are increasingly in short supply. This fact, along with some design related problems, has resulted in a very high percentage of unsatisfactory models being delivered. In addition, the traditional techniques of making airfoil models frequently do not allow defects such as plugged tubes, leaks, cracks, etc., to be detected until after the time consuming, and therefore expensive, final contour machining of the model. One additional problem with many of the existing methods of model construction is the inability to produce a "standard" orifice geometry. The need for a standard orifice arises from the fact that details of the plumbing near the orifice can influence the pressure reading. The geometry of the orifice must be known before applying any corrections to the pressure readings due to orifice induced errors.

From the engineering and research viewpoints, the existing techniques of making airfoil models also require excessive volume within the model to allow for the connection and routing of pressure tubing. In addition to the obvious problem of reducing the strength of the model, the presence of a large void within the model poses a potential problem due to uneven heat transfer during temperature changes with attendant problems of model distortion and the nonuniform approach of the model surface to adiabatic wall conditions.

For any model, whether it is to be tested at ambient or cryogenic temperatures, the existing airfoil model construction techniques often unduly limit the researcher in his selection as to size, location, and number of pressure orifices. Also, small highly loaded thin airfoils, that is, airfoils having a maximum thickness of less than about 6% chord, are beyond the present state-of-the-art. All of the above factors, along with the intuitive feeling that there had to be a better way, provided the impetus for the development efforts related to airfoil model construction techniques described in the following section.

3.3.1 Initial Efforts

Flame-Spray Coating.- In an initial attempt to develop an airfoil model construction technique which avoids many of the problems listed above, a small block of 17-4 PH was fitted with pressure tubes let into grooves machined into the surface of the block. The block and the tubes were then covered with an overcoating of metal using an oxyacetylene torch flame-spraying process. Even after being ground to a "smooth" finish, the surface of the sample was much too rough to be used on a wind-tunnel model. Further development work undoubtedly would have improved on the surface finish obtainable by using this technique. However, this technique was not pursued further at the time because other techniques looked more promising.

Channel and Cover.- A second approach was tried which eliminated both the tubing and the metal overcoating at the expense of a more complicated groove or channel which had to be machined into the model surface. As shown schematically in Figure 17, a covering strip was fitted into the stepped channel and brazed in place, the orifice drilled, and the surface machined and polished. This method of model construction provides a

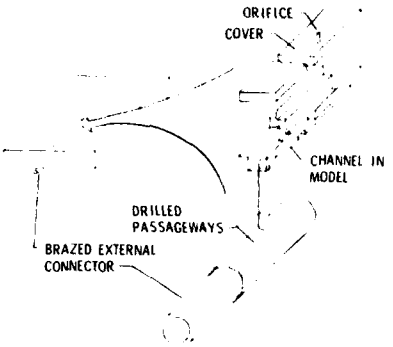

Fig. 17 Channel and cover method.

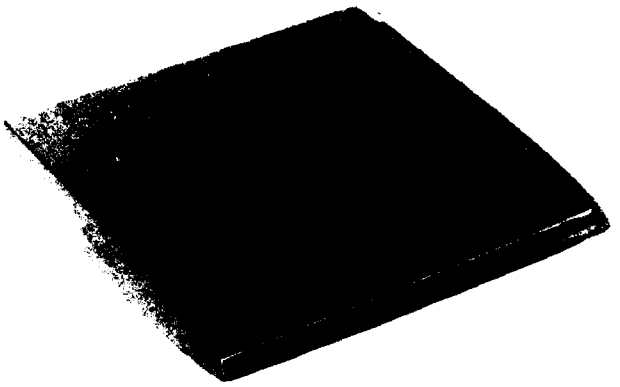

Fig. 18 Thin-skin method.

smooth, strong surface and provides an easy method of getting the pressure tubing from the model. However, there are obvious difficulties in applying this technique on anything other than simple airfoil models.

Thin Skin.- A third approach is shown in the photograph of Figure 18 where a family of simple channels has been cut into the surface of a test specimen in preparation for covering the surface with a thin metal sheet. Based on our experience, this technique appears to be a difficult one to master and seems applicable only to simple, single curvature surfaces, thus ruling out its use for most applications on three-dimensional models. Also, it is not obvious how to use this technique at the trailing edge of a very thin wing.

There are two advantages inherent to all ~~three of these~~ approaches. They do not weaken the model to any great extent and they ~~provide~~ a thin and relatively uniform surface for ~~pressure~~ orifice drilling. This last feature is important since, when drilling very small orifices, the depth usually cannot exceed a few hole diameters. Although exceptions to this can be found, model builders are not willing to guarantee the success of models covered with "exceptional" pressure orifices. Obviously, the next step is to develop a method that eliminates the problems and retains the advantages of these early efforts.

3.3.2 Present Effort

The approach being investigated at present is to make the model from a number of blocks, plates, or sheets of metal joined together in a manner appropriate to the desired model. The concept of pressure channels, rather than tubing, is retained. However, the pressure channels are now located in the interior of the model at the interface between the laminated sections. The pressure channels required for this method are relatively simple and, in various samples, have been machined, scribed, or chemically milled into the surface. The chemical milling process allows very complex patterns to be realized quite simply in a manner similar to the photoreduction process commonly used in the manufacture of printed circuits.

Access from the pressure channels to the surface of the model is accomplished by drilling a hole, roughly the same diameter as the channel width, to near the intended airfoil surface from the back side and meeting this hole with a smaller hole drilled from the surface side of the airfoil. In the case of laminated blocks, the channels can be carried around the edge of a block and go directly to the surface. This latter method is conceptually very attractive in that no drilling is required to produce an orifice and the size of the orifice, in principle, can be as small as desired. After joining the separate pieces together, the final assembly is machined to the desired model shape.

A copper plating brazing technique is presently preferred for laminating the blocks. Although the copper flows very freely and any excess copper results in clogged pressure channels, careful attention to the amount of copper plated onto the blocks has eliminated this problem. As would be done for actual model construction, pressure tests are made on each sample, prior to any final machining, to detect any leaking or blocked channels or any cross-leakage between channels.

The various steps taken in the construction of a sample airfoil model by this technique are shown in Figures 19 and 20. In Figure 19, the blocks are shown after they have been machined flat, the pressure channels cut, and the orifice passages drilled nearly to the intended airfoil surface. A trough has been machined along the path of the pressure orifices from the airfoil surface side of the block with the bottom of the trough only slightly above the final model surface, thus creating a relatively thin surface to be drilled through for the orifices. In the sample shown, small holes have been drilled normal to the final airfoil surface. The blocks were then copper plated and brazed together. The final machined-to-shape form is shown in Figure 20.

Fig. 19 Blocks for airfoil model using brazing method.

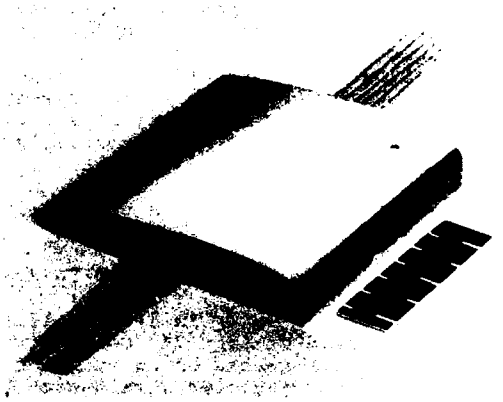

Fig. 20 Airfoil model made by brazing method.

4. MODEL INSTRUMENTATION

In another lecture in this series, the instrumentation used for the calibration and control of the Langley 0.3-m TCT is described. As explained in that lecture, problems with instrumentation that arise as a result of the extremes in the temperature environment of a cryogenic tunnel are best avoided by thermal isolation of the instrumentation, if at all possible. In many cases this can be accomplished by locating the instrumentation in the ambient temperature environment outside the tunnel or, if a particular instrument must be located in the tunnel, packaging it in a heated, insulated container. In the case of model instrumentation, however, thermal isolation is more difficult or, at times, impossible. Some of our experiences related to the instrumentation of models in continuous-flow cryogenic tunnels are described in the following sections.

4.1 Strain-Gage Balances

The majority of wind tunnel tests are "force-tests" aimed at determining the aerodynamic forces and moments acting on the model. Force tests in ambient temperature tunnels are usually made by supporting the model in the test section on a sting-mounted internal strain-gage balance. Because of the importance of this type of testing, tests were undertaken to determine if it would be possible to use either existing or especially designed strain-gage balances for force tests in cryogenic tunnels or whether some other approach, such as the use of magnetic suspension and balance systems, would be required. Obviously, the problems that might arise with strain-gage balances in a cryogenic tunnel would be completely avoided if it were possible to replace the strain-gage balance and the supporting sting with a system of electromagnetic coils exterior to the test section capable of performing the required functions of model support and force and moment measurement. It should be noted that a six-component magnetic suspension and balance system has been used successfully in combination with the relatively small (10 cm x 10 cm test section) low-speed cryogenic wind tunnel at the University of Southampton.[19] However, the use of internal strain-gage balances will continue to be standard practice for measuring forces and moments until magnetic suspension and balance systems can be scaled up both in size and load capacity and made fail-safe in their operation.

Work related to the use of internal strain-gage balances in cryogenic tunnels is underway at research centers on both sides of the Atlantic.[20-23] Because of the problems with strain-gage balances related to the wide range of operating temperatures available in cryogenic tunnels, much of the present research is aimed at finding ways to eliminate the effects of temperature on balance output.

The three design options being studied for thermal control of balances are shown in Figure 21. When the option of no thermal control is selected, it is likely that an extensive balance calibration will be required. In addition, in the absence of thermal control, it is uncertain how much time must be allowed between the changing of test conditions and the taking of data.

The other extreme of thermal control is the option which keeps the bulk of the balance at a constant temperature near ambient (≈300 K) and eliminates any temperature gradients within the balance. In theory, this option of full thermal control can eliminate the need for extensive balance calibration as well as reduce to zero the time between changing test conditions and taking data. The potential advantages of full thermal control are achieved only by having a more complex balance equipped with heaters, sensors, insulators, shields, etc.

The in-between option is to eliminate the temperature gradients while allowing the bulk temperature of the balance to follow the stream temperature. This option is not very attractive, since it still requires the complexity of the fully controlled balance and does not completely eliminate the problems of the unheated balance.

Three internal strain-gage balances have been tested at Langley under actual cryogenic tunnel conditions. The first was an existing off-the-shelf water-jacketed balance which was tested in the low-speed cryogenic tunnel. In addition, two electrically heated balances were especially designed and built for use in the 0.3-m TCT. Some of the details of the design and use of these balances are given in the following sections.

4.1.1 Water-Jacketed Balance

Early in 1972, a 11.4 cm span sharp leading-edge 74° delta-wing model (see 3.2.2) was tested on an existing three component water-jacketed strain-gage balance in the Langley 7" x 11" low-speed cryogenic tunnel. Since the purpose of the test was to investigate any possible adverse effects of temperature on the measuring techniques rather than the effects of Reynolds number on the model, a sharp leading-edge 74° delta-wing model was chosen since it is known that, except for the usual effects of friction drag, the aerodynamic characteristics of this shape are relatively insensitive to changes in Reynolds number. A photograph of the model, balance, and supporting sting is shown in Figure 13 (see 3.2.2). The strain-gage elements of the balance were heated and protected from the cryogenic environment by a water jacket through which ordinary tap water at approximately 294 K (+70° F) was circulated at a flow rate of about 1 kg per minute.

The test set-up in the low-speed tunnel was very simple, as can be seen in Figure 22. This photograph, taken with the plastic top and side walls of the test section removed, shows the model mounted to the balance on the very simple angle of attack mechanism with the balance leads and water tubes trailing down the test section. It was noted during low temperature testing that the Tygon tubes, exposed as they were to the stream, became hard and spring like. However, the insulating properties of the tubing are such that the temperature of the water being circulated through the tubes dropped only about 4 K° between inlet and exit to the tunnel.

	THERMAL CONTROL		
	NONE	ELIMINATE GRADIENTS	FULL-CONSTANT TEMPERATURE NO GRADIENTS
●HEATERS	NO	YES	YES
●INSULATORS	NO	?	YES
●SHIELDS	NO	?	YES
●TEMP. SENSORS	YES	YES	YES
●COMPLEXITY (HEATERS, ETC.)	SIMPLE	MODERATE	DIFFICULT
●CALIBRATION	EXTENSIVE (?)	MODERATE	SIMPLE
	K / T	K / T	K / T
●TIME BETWEEN DATA POINTS	?	?	SHORT

Fig. 21 Design options for strain-gage balances.

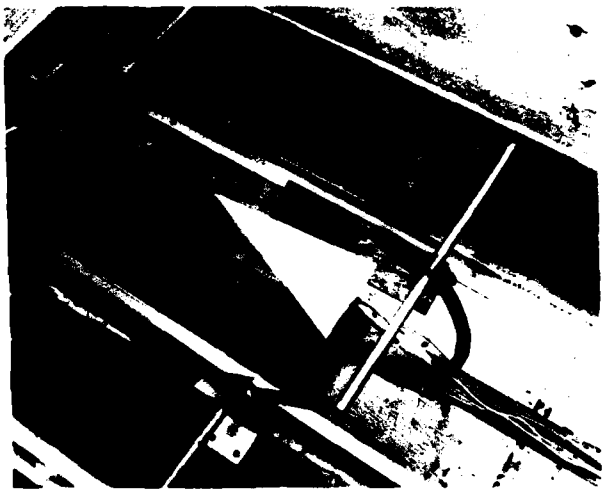

Fig. 22 Low-speed test set-up.

The most serious practical problem to develop with this test set-up was the result of alga which apparently grew rapidly within the system when water was not being circulated through the balance. The tubes became clogged allowing the water in the jacket to freeze which, in turn, split the seams between the jacket and the balance. This experience contributed to our decision to use electrically heated balances in future tests.

Some of the aerodynamic test results are shown in Figure 23 as the variation of C_m, C_L, and C_D with α for various test conditions. As can be seen, there is generally good agreement between the data obtained at stagnation temperatures from 322 K (+120° F) to 111 K (-260° F). Based on these results, we concluded that conventional strain-gage balances can be used for model testing in a cryogenic tunnel and that a satisfactory arrangement is to maintain the balance at ambient temperatures by heating.[16]

4.1.2 HRC - 1

A three component electrically heated balance, identified as HRC - 1 (High Reynolds number Cryogenic - 1), was designed and built especially for testing the previously described delta-wing models (see 3.2.3) in the 0.3-m TCT. Details of the balance design and the testing program have been reported[4] and only the main points will be reviewed herein.

The one piece balance was machined from 17-4 PH stainless steel (vacuum remelt) which was heat treated to condition H 925. With this heat treatment 17-4 PH can be used under nonimpact conditions at LN_2 temperatures. That it could not be subjected to impact loading without damage was dramatically demonstrated during post-test calibrations with the balance at cryogenic temperatures. A weight hanger slipped and the balance was

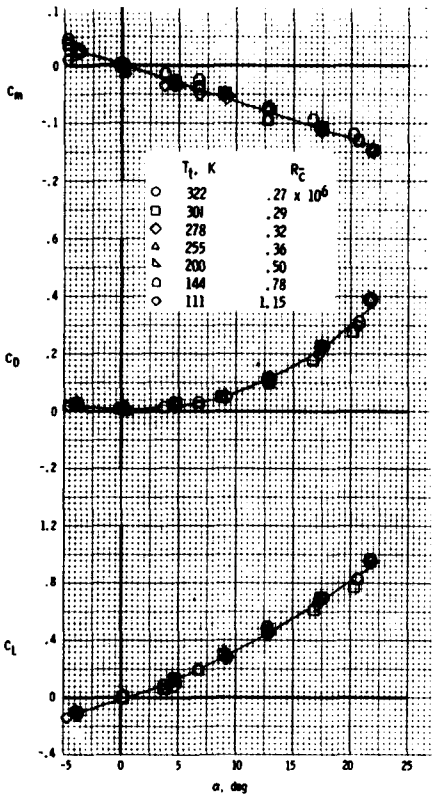

Fig. 23 Low-speed results, water jacketed balance.

destroyed. HRC - 1 must therefore be referred to in the past tense. HRC - 1 was designed to have the following load limits:

Normal force. . . . . 890 N (200 lbf)

Axial force . . . . . 89 N (20 lbf)

Pitching moment . . . . . .27.1 N-m (20 ft/lbf)

At ambient temperature (≈300 K) the balance accuracy was approximately ±0.5% of the design load for all components. The balance was modulus compensated for ΔT = 55 K (100° F) and temperature compensated to ±0.5% for ΔT = 55 K (100° F).

HRC - 1 was originally fitted with two 30 ohm resistance-wire heaters and two 50 ohm nickle resistance thermometer (NRT) temperature sensors. The temperature of the balance at or near a given heater was determined by the resistance of the NRT. In theory the temperature of the balance at an NRT was held constant by an automatic temperature controller which could vary the current through the heater in direct proportion to changes of resistance of the NRT with changes in temperature. Theoretically, only two heaters should be needed to hold the temperature of a balance constant and insure zero temperature gradient across the balance; one heater located at each end of the gaged portion of the balance. Thermal insulators made from glass-cloth reinforced epoxy were placed between the model and the balance and between the balance and the supporting sting in an attempt to reduce to an insignificant amount the conduction of heat from the balance to the stream through either the model or the sting.

The balance was first tested at cryogenic temperatures in conjunction with one of the plastic models previously described. During the tunnel cool-down process the balance temperature tended to follow the stream temperature and the desired balance temperature of 322 K could not be maintained at either the front or rear heater locations even with 100 watts supplied to each of the heaters. Details of the many modifications made to the balance in order to achieve successful operation are given in the appendix of Reference 4. The balance as modified is shown in the sketch presented as Figure 24. As can be seen, the balance

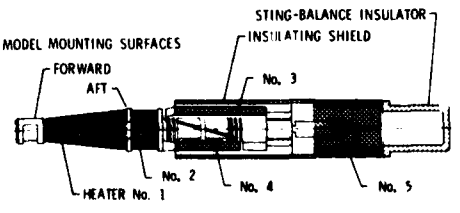

Fig. 24 Sketch of modified balance HRC - 1.

heater configuration is considerably more complex than the simple concept of two heaters. In addition to a second heater at the front of the balance, heaters were added to each side of the axial-force measuring portion of the balance.

In addition to the changes made to the balance, a simple cylindrical extension was added to the sharp leading edge delta-wing model in order to reduce the effects of the cold gas of the stream being circulated over the balance at the rear of the model. Such an extension would, of course, in no way affect any hot-cold comparisons and, in fact, would not be expected to have a significant aerodynamic effect since it lies entirely in the wake of the basic delta-wing model. Additional justification for such a modification to the model in a development program such as this exists in the fact that the rear portion of a typical internal strain-gage balance is usually 8 or 10 sting diameters inside the model rather than projecting beyond the base of the model as was the case with the original model-balance combination.

During the subsequent wind-tunnel tests using the modified balance and model, the automatic heater controllers were able to hold the balance temperature constant at the heater locations under all test conditions. However, thermocouples located at various points on the balance away from the heaters indicated the surface temperature of the balance was not being held constant but in fact was as much as 20 K lower than the desired set-point temperature being maintained at the heater locations. The effect of the observed temperature differences on the balance surface did not, however, show up as a zero shift in any of the components of the balance. Because of the nature of the instrumentation being used, it was not possible to get accurate values of the steady-state power supplied to the heaters. However, it was possible to determine that the steady-state power never exceeded 10 watts for the front heater (No. 2) or 30 watts for the rear heater (No. 5).

The use of heater No. 1 at the extreme forward end of the balance was found to be optional. When in use, it would dissipate at most about 10 watts which reduced by 2 or 3 watts the amount of power dissipated by heater No. 2. Whether or not heater No. 1 was used did not affect the ability to hold the balance temperature constant across the gage section of the balance.

As determined by thermocouples located on the surface of the balance, the use of heaters No. 3 and 4 resulted in a slightly more uniform distribution of temperature across the pitching-moment and normal-force measuring section at the rear of the balance. Unfortunately, no attempt was made to determine if the 5 watts or so dissipated by each of these heaters was critical to the successful performance of the balance or if, in fact, stable zeros for the various components would have been obtained without using heaters No. 3 and 4. In spite of the lack of experimental confirmation that the side heaters (Nos. 3 and 4) are redundant, it is very likely that they were at best only marginally beneficial. Therefore, based on the experience with this balance, it appears that strain-gage balances could be designed with only two heaters (theoretically the minimum number), one on either side of the gaged portion of the balance.

The choice of material for balance construction is another area where some improvement is perhaps possible. In general, the avoidance of a temperature gradient across the gaged portion of the balance is made more difficult if the balance is made from a relatively poor thermal conductor such as 17-4 PH. An obvious improvement in balance design, from the point of view of uniformity of temperature, can be realized if a material of high thermal conductivity, such as beryllium copper, can be used in making the balance. (Beryllium copper has roughly 10 times the thermal conductivity of 17-4 PH at room temperature.)

The heat input to this balance seemed remarkably small for such extreme tunnel conditions. Although some concern has been expressed as to the effect of heat flux through the model surface from a heated balance, such a modest heat flux through the model from the front heaters would not be expected to modify in any way the nature of the flow over the model.

An example of the results obtained on the delta-wing model using the HRC - 1 balance are presented in Figure 25 which shows the variation of C_m, C_D, and C_L with α at both ambient and cryogenic temperatures for a Mach number of 0.80. The circular symbols indicate experimental results obtained at a stagnation pressure of 4.60 atm and at a stagnation temperature of 301 K. The square symbols are data taken at a stagnation pressure of 1.20 atm and at a stagnation temperature of 114 K. With both sets of data, flagged symbols are used to indicate repeat data point. The Reynolds number, based on mean geometric chord, was 8.5×10^6 for the two sets of data. As can be seen, there is reasonably good agreement between the experimental results

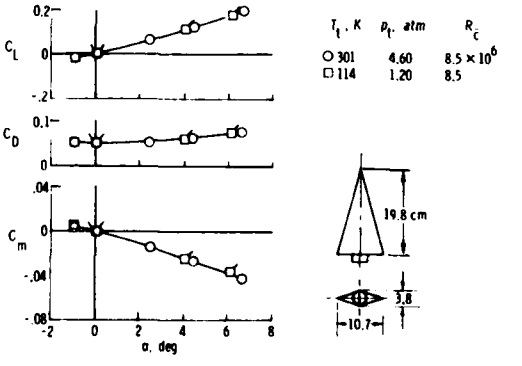

Fig. 25 Delta-wing results, heated balance HRC - 1. $M_\infty = 0.80$

obtained at ambient and cryogenic temperatures. The results of these tests provided additional evidence that cryogenic nitrogen is a valid test gas even under conditions of separated and reattached (vortex) flow.

Toward the end of these tests, an attempt was made to determine if accurate aerodynamic data could be obtained if the balance temperature was held at some temperature less than ambient or, in the extreme case, was uncontrolled and allowed to follow stream temperature during cryogenic operation of the tunnel. By stopping the tunnel drive fan after tunnel temperature had been established and the model and balance allowed to come to temperature equilibrium with the stream, it was possible to take a "wind-off" zero reading and thus, hopefully, eliminate this potential source of error from the aerodynamic data. Unfortunately, the sensor used for control of heater No. 5 failed as the balance temperature was being reduced to 105 K (-100° F) so that only a limited amount of data were obtained.

The results are shown in Figure 26 where C_m, C_D, and C_L are compared for constant test conditions (M_∞ = 0.80, p_t = 1.2 atm, T_t = 114 K) for balance temperatures of 310 K (+100° F), 255 K (0° F), and 114 K (-255° F).

Surprisingly good agreement between the data taken at the different balance temperatures was obtained for the drag component. The agreement is not so good for the lift component where there appears to be a shift in zero that was not taken into account by the cold wind-off zero. Although the model and balance were allowed to soak for several minutes at each new value of T_t with the fan running in an attempt to insure uniform balance temperatures, the apparent zero shift is probably due to changing temperature gradients across the balance with time. The pitching moment component shows poor agreement with a constant offset at the higher angles of attack. Here, again, there appears to be changing zero with time due to temperature gradients across the balance.

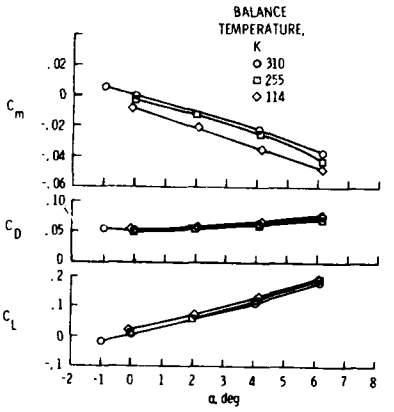

Fig. 26 Delta-wing results, heated and unheated balance HRC - 1.

As previously mentioned, HRC - 1 was broken following these tests, thus preventing further modification and retesting. Based on the rather limited tests with HRC - 1 it appeared that the concept of keeping the balance at ambient temperatures (≈300 K) during tests at cryogenic temperatures was a fundamentally sound approach. However, it was also concluded that the concept of allowing balance temperature to vary with stagnation temperature should be investigated further since the absence of heaters and insulators on the balance would make possible a reduction in balance diameter for a given load capacity. The decision was therefore made to build a new balance in order to continue these studies. The resulting balance, HRC - 2, is now described.

4.1.3 HRC - 2

The strain-gage balance evaluations in the 0.3-m TCT are but a part of a larger balance program at Langley aimed at insuring the availability of suitable balances when the NTF becomes operational in 1982. As a part of the larger program, the Force and Strain Instrumentation Section at Langley has been involved in a comprehensive strain-gage balance evaluation and development effort. The basic elements that make up a strain-gage balance, including the material used in its construction, the strain gages, adhesives, solders, wires, and moistureproofing, have been evaluated over a wide range of temperatures in an attempt to select those materials and techniques that minimize the effects of the cryogenic environment on strain-gage output when compared to its output at room temperature. Details of this research effort have been reported by Ferris.[22] The brief description presented herein draws freely on her paper.

Based on considerations of impact strength at cryogenic temperature, heat treatment requirements, and availability, Maraging 200 steel was chosen as the material for use in building HRC - 2. A Karma (K-alloy) SK-11 strain gage was made especially to Langley specifications for use with the Maraging 200 steel. This gage has a self-temperature compensation factor of 11 which minimizes the apparent strain output over the entire range of operating temperatures. It also has a change in gage factor which tends to counter the changes in the modulus of the Maraging 200 steel with temperature.

Identified as acceptable during the testing were a commercially available epoxy-based adhesive and a solder containing a small amount of silver. The use of silver-plated copper wire with Teflon insulation was also found to be acceptable. However, it was discovered during tests of connectors for cryogenic use that a non-trivial thermocouple effect was present on one lead. This discovery indicates that it may be necessary to check all wiring junctions for thermocouple effects that could introduce errors in the balance output.

Tests of various moistureproofing compounds were also made. During these tests, it was discovered that the compound which had been used with the HRC - 1 balance gave rise to very erratic gage output at temperatures below 275 K. Thus, the use of this moistureproofing compound is the most likely cause of the large zero shifts with temperature experienced with that balance. No moistureproofing compound has been found that does not have some effect on apparent strain when applied over the strain-gage grid, although some were found that were much better than the standard ones previously used. While research is continuing in this area, the rubber-based moistureproofing compound is being applied only to exposed terminals and wiring.

The HRC - 2 balance was fabricated and gaged in accordance with the information obtained from the testing and evaluation program. The balance and the delta-wing model used in the 0.3-m TCT tests are shown in the photograph of Figure 27. Details of the pretest calibration of the balance are given in Reference 22. Some of the preliminary test results have also been reported by Ferris in Reference 23.

A sample of the preliminary data obtained at $M_\infty = 0.5$ for various test conditions is shown in Figure 28 where C_m, C_D, and C_L are shown as functions of α. Data were taken at cryogenic temperatures both with the balance electrically heated to 300 K and with the balance allowed to stabilize thermally at the ambient temperature. This particular sample of data is for the electrically heated case at 200 K and 110 K compared with the standard "room temperature" run at 300 K. The balance did have a bakelite convection shield surrounding the balance proper to minimize heat loss. The procedure used in taking the wind-off zero point was to stabilize the tunnel parameters and the balance temperatures with the wind-on at the appropriate test condition and then rapidly reduce tunnel fan speed to zero to take the wind-off data points. The runs made at cryogenic temperature without the heaters operating were corrected for the change in sensitivity with temperature, but the same procedure outlined above was used for wind-off zeros. The particular model used for these tests loaded the balance to about 85 percent of the design loads at 300 K for normal force and pitching moment, but only loaded the axial force to about 20 percent of its design load at $M_\infty = 0.5$. The agreement between the data obtained at the three test conditions is generally good. Details of these tests and a discussion of some of the difficulties encountered are given in Reference 23. Based on a preliminary analysis of all of these data, it is apparent that more development work is needed relative to thermal control and/or temperature compensation to further increase the accuracy and reduce the complexity of internal strain-gage balances intended for use in cryogenic wind tunnels. A recent investigation at Langley by personnel of the Force and Strain Instrumentation Section strongly suggests that it may be possible to fully temperature compensate a balance over the entire operating range of cryogenic tunnels and thereby eliminate any requirement for thermal control of the balance.

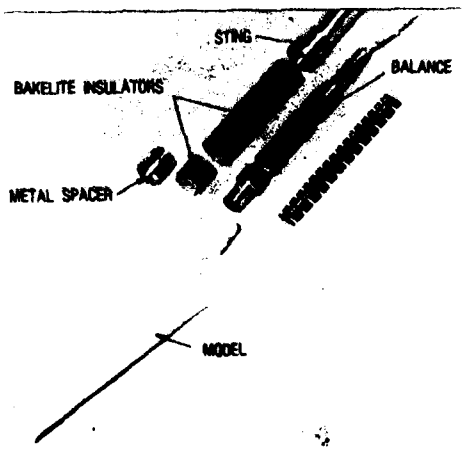

Fig. 27 HRC - 2 balance and model.

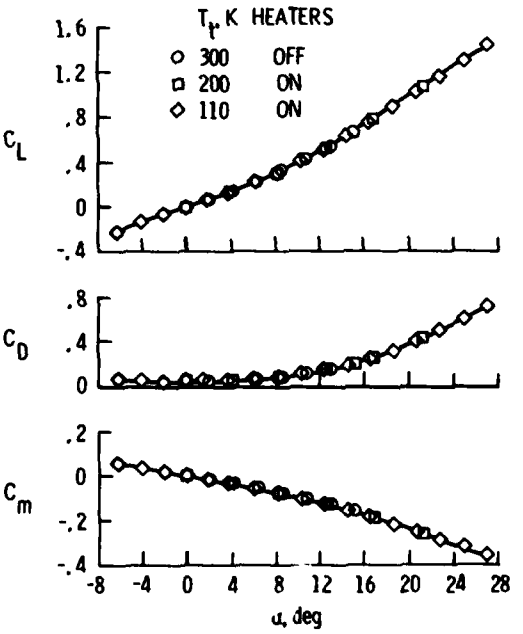

Fig. 28 Preliminary results, HRC-2.

4.2 Buffet Model Instrumentation

The development of buffet research techniques suitable for use in cryogenic wind tunnels is but one of a number of studies at the Langley Research Center being made in preparation for aerodynamic research in the NTF. Buffet, defined as the structural response of the aircraft to the aerodynamic excitation produced by separated flows, is dependent on Reynolds number. Thus the NTF, with its wide range of test conditions, offers a unique opportunity for research in this area.

The purpose of the present effort in the 0.3-m TCT is to evaluate at cryogenic temperatures an existing buffet testing technique that can be used to detect the onset as well as the severity of buffet. Once a suitable technique is demonstrated, it will be used in combination with the unique capability of the 0.3-m TCT to study the effect of Reynolds number on buffet at constant model shape and to study the effect of aeroelastic distortion on buffet at constant Reynolds number.

For this development program, two semispan buffet models, suggested by Mabey,[24] have been built and instrumented. Planform views of the two models are shown in Figure 29. The slender delta wing is known to be relatively insensitive to Reynolds number and was therefore chosen to provide a baseline model for tests to demonstrate the test technique. The zero sweep airfoil model has an NPL 9510 section known to be very sensitive to Reynolds number which makes it a suitable model for demonstrating the effect of Reynolds number on buffet. An end view of the 2-D test section of the 0.3-m TCT is shown on the left side of Figure 29. The semispan buffet models were cantilevered from the turntable in the sidewall of the test section. It is recognized that there are wall-interference effects with this mounting scheme. However, in developing test techniques suitable for cryogenic tunnels, wall interference effects are of no concern since the validity of the technique is determined by comparing results obtained at ambient temperatures with results obtained at cryogenic temperatures, both obtained at the same values of Mach number and Reynolds number.

The measurement of unsteady root bending moment is generally accepted as the most consistent and reliable method of assessing buffet onset and, with suitable methods, also provides information on buffet intensity. For the models used for these tests, the root bending moment is measured by using strain-gage bridges. The bridges were calibrated in an environmental chamber from ambient to cryogenic temperatures to determine the effect of temperature on sensitivity. A calibration obtained for the delta-wing model is shown in Figure 30. The rather large change in sensitivity with temperature was the result of the strain gages not being well matched to the aluminum alloy used for this model. Such a cablibration curve of sensitivity as a function of temperature was used in reducing the data.

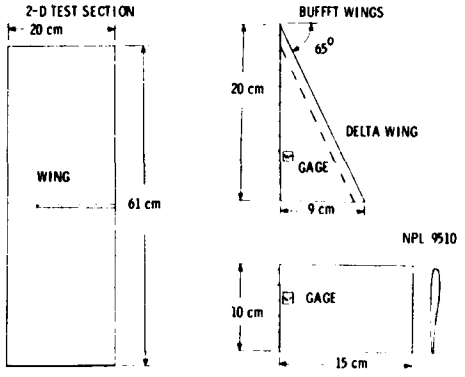

Fig. 29 Buffet models and 2-D test section.

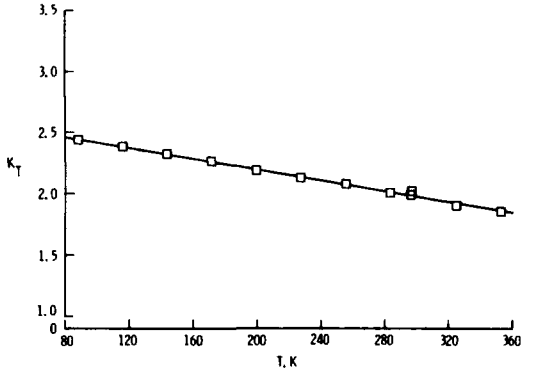

Fig. 30 Delta-wing buffet model calibration.

Photographs of the two buffet models are shown in Figure 31. The view of the delta-wing model is looking down on the model with the slotted floor of the 2-D test section in the background. The NPL 9510 airfoil is seen mounted inverted on the turntable in a removable portion of the sidewall.

The test envelope for the delta-wing model for $M_\infty = 0.35$ is shown in Figure 32 where R/m is plotted as a function of the reduced-frequency parameter $f\bar{c}/V_\infty$. The symbols indicate the actual test conditions where α sweeps were made. This envelope also illustrates the large increase in reduced frequency associated with the reduced speed of sound at low temperatures.

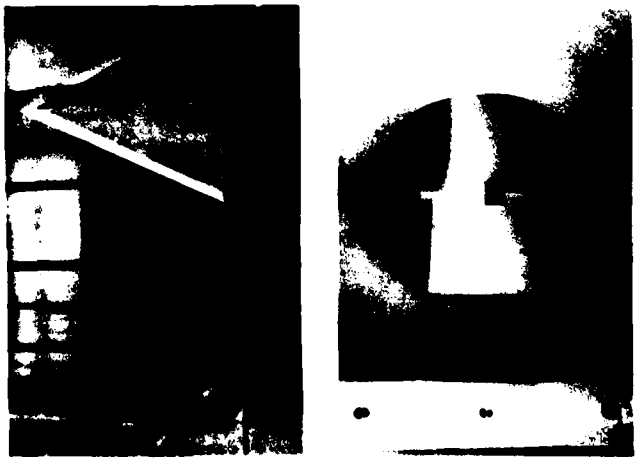

Fig. 31 Photographs of buffet models.

This effect provides increased levels of aerodynamic damping in relation to structural damping which makes possible increased accuracy in extracting the aerodynamic damping. The ability to vary the reduced frequency at constant values of R and M_∞ is also of interest.

A sample of the on-line buffet data for the delta-wing model is shown in Figure 33. The buffet coefficient C_B is the nondimensionalized average integrated value of the time-varying portion of the root bending moment. The data obtained at the same value of reduced frequency at 300 K and at 110 K shows good agreement in terms of the angle of attack for buffet onset as well as in terms of the variation of C_B with α following buffet onset. In addition, the onset angle of attack agrees well with that predicted by the method of Wentz for vortex breakdown at the trailing edge.

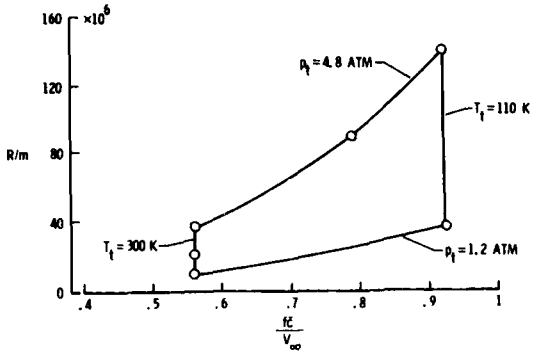

Fig. 32 Test envelope for delta-wing buffet model.

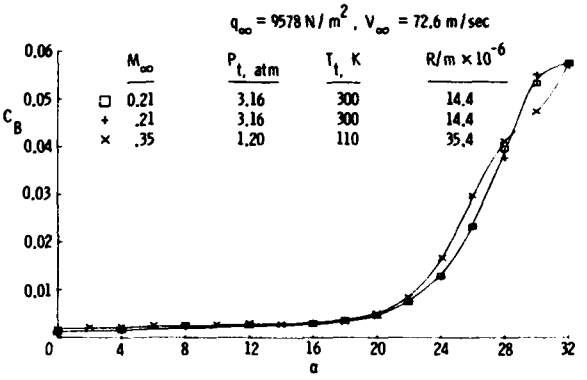

Fig. 33 Buffet data for delta-wing model.

A sample of the on-line buffet data for the NPL 9510 wing model is shown in Figure 34. These data clearly show the increase in buffet onset at the higher Reynolds number.

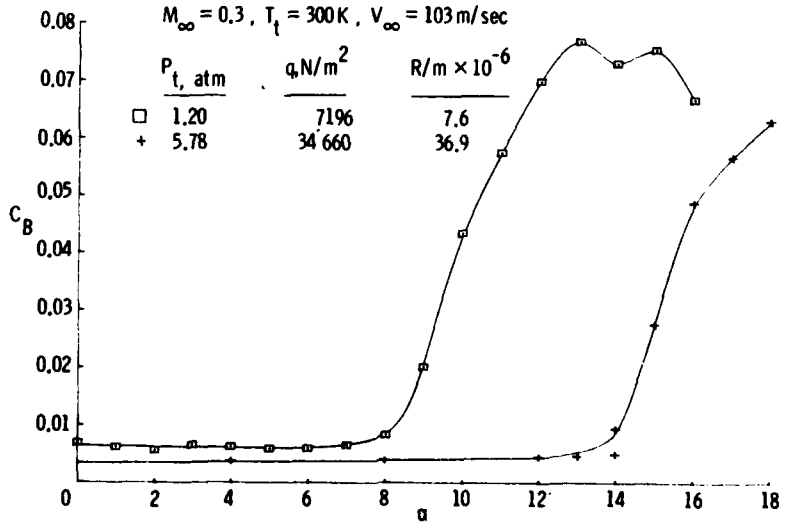

Fig. 34 Buffet data for NPL-9510 airfoil.

The data from these tests are currently in the process of being reduced and analyzed. However, based on the preliminary on-line data, such as shown here, we believe that the present technique can be used successfully for buffet tests in cryogenic wind tunnels.

4.3 Pressure Measurement

In making pressure measurements on models, we have not attempted to use pressure transducers inside the cryogenic tunnels. As explained in more detail in lecture No. 11 of this series, at the 0.3-m TCT all of the model pressures are measured using transducers mounted outside the tunnel in the ambient temperature and pressure environment.

An electronically scanned pressure (ESP)[25] measuring technique using multisensor modules has been selected for making pressure measurements on models in the NTF. Because the sensor modules will not operate properly at cryogenic temperatures, they will be housed in especially designed temperature controlled containers within the model. Evaluation testing of an EPS system in the 0.3-m TCT is scheduled for later this year in order to determine if the required accuracy can be realized over the wide ranges of pressure and temperature to be used in the NTF.

5. CONCLUSIONS

Some of the experiences at the NASA Langley Research Center relative to the design and instrumentation of models for continuous-flow cryogenic wind tunnels have been reviewed in this lecture. The main conclusions to be drawn from our experience at Langley are:

1. The very thin boundary layers at high unit Reynolds numbers force more attention to be given to the details of model surface finish and, in the case of pressure models, pressure orifice induced errors.

2. The measurement of model surface finish to the accuracy required for tests at high unit Reynolds numbers is difficult, if not impossible, using existing techniques.

3. A wide range of materials have been successfully used for building models and other devices for use in cryogenic tunnels.

4. A common source of trouble with models and other devices used in cryogenic tunnels is the practice of combining materials having different rates of thermal expansion.

5. A simple method for building airfoil models has been developed which offers many advantages over methods previously used. By brazing together two or more grooved sheets of metal it is possible to greatly increase the number of pressure orifices while reducing the volume within the model required for the pressure plumbing.

6. Internal strain-gage balances for use in cryogenic tunnels can be built that will have the required accuracy under steady-state conditions. Continued development is needed relative to thermal control and/or temperature compensation to further increase the accuracy and reduce the complexity of the balances.

7. A buffet testing technique has been successfully demonstrated at cryogenic temperatures using two simple semispan buffet models in the 0.3-m TCT.

6. REFERENCES

1. Goodyer, Michael J.; and Kilgore, Robert A.: The High Reynolds Number Cryogenic Wind Tunnel. AIAA Paper No. 72-995, September 1972.

2. Kilgore, Robert A.: Design Features and Operational Characteristic of the Langley Pilot Transonic Cryogenic Tunnel. NASA TM X-72012, 1974.

3. Ray, Edward J.; Kilgore, Robert A.; Adcock, Jerry B.; and Davenport, Edwin E.: Analysis of Validation Tests of the Langley Pilot Transonic Cryogenic Tunnel. NASA TN D-7828, 1975.

4. Kilgore, Robert A.; and Davenport, Edwin E.: Static Force Tests of a Sharp Leading Edge Delta-Wing Model at Ambient and Cryogenic Temperatures with a Description of the Apparatus Employed. NASA TM X-73901, June 1976.

5. Balakrishna, S.: Modeling and Control of a LN_2 - GN_2 Operated Cryogenic Closed Circuit Wind Tunnel. Paper No. 23, First International Symposium on Cryogenic Wind Tunnels. Southampton, England, 3-5 April 1979.

6. Adcock, Jerry B.: Real-Gas Effects Associated with One-Dimensional Transonic Flow of Cryogenic Nitrogen. NASA TN D-8274, 1976.

7. Johnson, Charles B.: A Study of Non-Adiabatic Boundary - Layer Stabilization Time in a Cryogenic Tunnel for Typical Wing and Fuselage Models. AIAA Paper No. 80-0417, March 1980.

8. Schlichting, H.: Boundary Layer Theory, McGraw-Hill Book Company, Inc., New York, New York, 1951.

9. Hoerner, S. F.: Fluid-Dynamic Drag. Published by author. 1965.

10. Clutter, Darwin W.: Charts for Determining Skin-Friction Coefficients on Smooth and on Rough Flat Plates at Mach Numbers up to 5.0 With and Without Heat Transfer. Report No. ES 29074, Douglas Aircraft Company, Inc., 1959.

11. Rainbird, W. J.: Errors in Measurement of Mean Static Pressure of a Moving Fluid Due to Pressure Holes. Canada, National Research Council, Division of Mechanical Engineering and National Aeronautical Establishment, Quarterly Bulletin, no. 3, 1967, pp. 55-89.

12. Shaw, R.: The Influence of Hole Dimensions on Static Pressure Measurements. J. Fluid. Mech., Vol. 7, Cambridge University Press, London, England, January - April 1960, pp. 550-564.

13. Franklin, R. E.; and Wallace, J. M.: Absolute Measurements of Static-Hole Error Using Flush Transducers, J. Fluid. Mech. Vol. 42, part 1, pp. 33-48, 1970.

14. Rayle, R. E.: Influence of Orifice Geometry on Static Pressure Measurements. S.M. Thesis - MIT, 1959.

15. Reed, T. D.; Pope, T. C.; and Cooksey, J. M.: Calibration of Transonic and Supersonic Wind Tunnels. NASA CR-2920, November 1977.

16. Kilgore, Robert A.; Goodyer, Michael J.; Adcock, Jerry B.; and Davenport, Edwin E.: The Cryogenic Wind-Tunnel Concept for High Reynolds Number Testing. NASA TN D-7762, November 1974.

17. Polhamus, E. C.; Kilgore, R. A.; Adcock, J. B.; and Ray, E. J.: The Langley Cryogenic High Reynolds Number Wind-Tunnel Program. Astronaut. and Aeronaut., Vol. 12, No. 10, October 1974, pp. 30-40.

18. Reubush, David E.: The Effect of Reynolds Number on the Boattail Drag of Two Wing-Body Configurations. AIAA Paper No. 75-1294, September - October 1975.

19. Goodyer, M. J.: Cryogenic Wind Tunnel Activities at the University of Southampton. NASA CR-159144, September 1979.

20. Bazin, Maurice; and Dubois, Maurice: Balance and Sting Design for Cryogenic Wind Tunnels. Paper No. 2, First International Symposium on Cryogenic Wind Tunnels, Southampton, England, April 3-5, 1979.

21. Krogmann, Paul; and Lorenz-Meyer, Wolfgang: Design and Testing of an Unheated Strain-Gauge Balance Element for Cryogenic Temperatures. Paper No. 3, First International Symposium on Cryogenic Wind Tunnels, Southampton, England, April 3-5, 1979.

22. Ferris, Alice T.: Cryogenic Wind Tunnel Force Instrumentation. Paper No. 32, First International Symposium on Cryogenic Wind Tunnels, Southampton, England, April 3-5, 1979.

23. Ferris, Alice T.: Cryogenic Wind Tunnel Force Instrumentation. Paper No. 19 in Cryogenic Technology, proceedings of a conference held at Langley Research Center, Hampton, VA, November 27-29, 1979. NASA CP-2122, pp. 299-315.

24. Mabey, Dannie G.: Some Remarks on Dynamic Aeroelastic Model Tests in Cryogenic Wind Tunnels. Transcript of an informal lecture and discussion. NASA CR-145029, 1975.

25. Juanarena, D. B.: A Multiport Sensor and Measurement System for Aerospace Pressure Measurements. ISA 25th International Instrumentation Symposium, May 1979.

7. ACKNOWLEDGEMENTS

The author is grateful to NASA for permission to give this lecture and to his colleagues at the Langley Research Center who have assisted in its preparation. Special thanks is due to Mr. Pierce L. Lawing for his contributions relative to the development of model construction techniques, to Mr. Blair B. Gloss for his contributions relative to the aerodynamic considerations of model design and construction, to Mr. Richmond P. Boyden for his contributions relative to internal strain-gage balances and buffet testing technique, and to Ms. Alice T. Ferris of the Force and Strain Instrumentation Section for her contributions relative to the testing and evaluation of the HRC - 2 balance as well as helpful discussions on other aspects of balance design and application.

MODEL DESIGN AND INSTRUMENTATION FOR INTERMITTENT CRYOGENIC WIND TUNNELS

by
J. D. Cadwell
Branch Chief
Wind Tunnel Test and Development
Aerodynamics Subdivision
Douglas Aircraft Company
McDonnell Douglas Corporation
3855 Lakewood Blvd.
Long Beach, Ca. 90846
USA

SUMMARY

The design and instrumentation of a model for an intermittent cryogenic wind tunnel is discussed. The model requirements including tolerances and data accuracy are noted. The mechanical design of the wing and the considerations for material to be used are discussed as well as the instrumentation that is to be installed in the wing. The design of the fuselage center section, the six component balance installation with heaters, and the heater for the balance-to-sting adapter is reviewed. The design of the aft fuselage and empennage, and the fuselage nose including the instrumentation package to be housed in the fuselage nose compartment is shown. The model conditioning that is required to obtain acceptable data, prevent frost buildup on the model after it has been cooled, and reheating the model to make model configuration changes is also discussed. The material used in this report is the result of work directed toward the design and instrumentation of a verification model to be used to checkout the operation of the modified Douglas Aircraft Company four-foot trisonic tunnel (4-TWT) to a cryogenic facility.

INTRODUCTION

The late 1950's and the early 1960's is the time period when the blowdown wind tunnel made its appearance, in the United States and Europe, as a relatively low cost ground simulation facility that could be utilized to aid in the development of aerospace systems. Most of the facilities included the tri-sonic capabilities of subsonic, transonic, and supersonic speeds that covered a Mach range from 0.5 to 5.0.

The blowdown facility proved to be an excellent tool in developing low aspect ratio aircraft as well as missile and space systems. The high pressure air storage supply provides the energy to conduct aerodynamic tests at significant Reynolds numbers for short operating periods up to 30 seconds. A typical operating envelope for a blowdown tunnel is shown below in Figure 1.

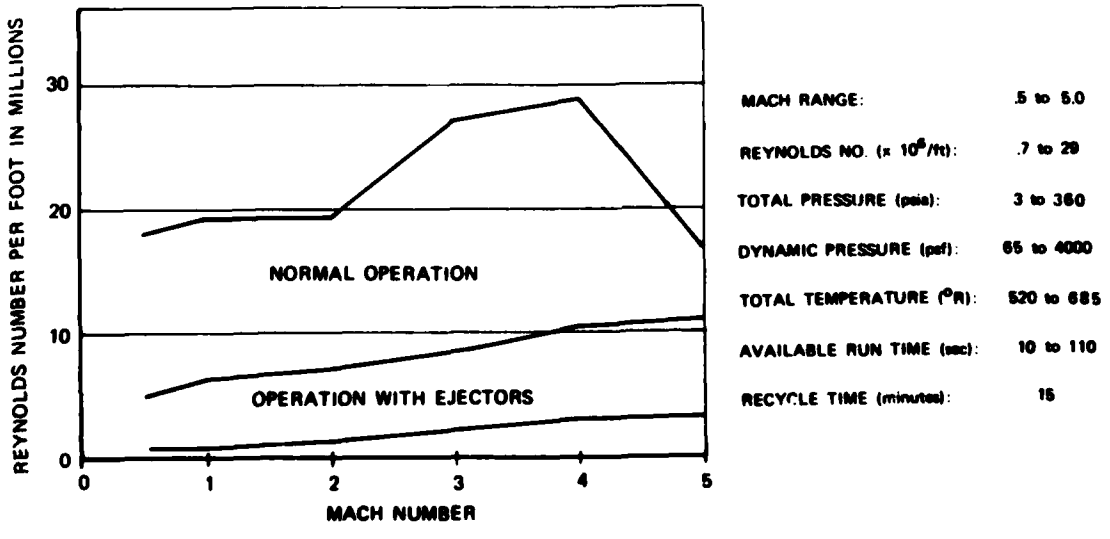

FIGURE 1 DOUGLAS AIRCRAFT 4-TWT OPERATING ENVELOPE

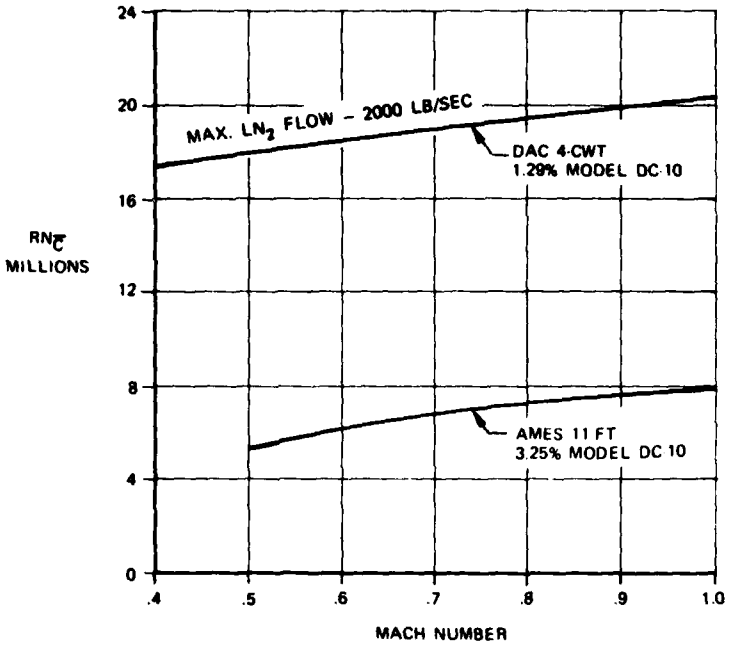

FIGURE 2. REYNOLDS NUMBER COMPARISON

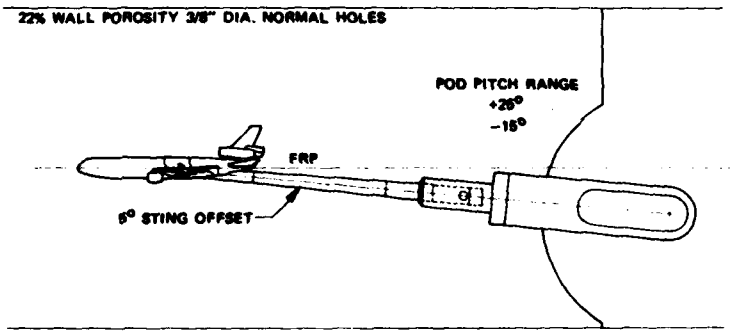

FIGURE 3. DC-10 MODEL INSTALLATION IN 4-CWT

TOLERANCES

LIFTING SURFACES	± 0.0015 IN.	4 MICROINCH (R_A) FINISH
NONLIFTING SURFACES	± 0.005 IN.	8 MICROINCH (R_A) FINISH
ANGULAR MEASUREMENTS	± 0.025 DEG.	

DATA COEFFICIENT ACCURACY

LIFT AND SIDE FORCE	± 0.001
DRAG	± 0.00015
PITCHING MOMENT	± 0.002
ROLL AND YAWING MOMENT	± 0.0005

FIGURE 4. 4-CWT MODEL TOLERANCES AND DATA ACCURACY

With the exception of the Rockwell International seven-foot tunnel the majority of the blowdown type tunnels were considered too small for testing high aspect ratio transport configurations. Models for a four-foot blowdown would be only 36% of one sized for the NASA Ames 11-foot tunnel and would require 2.75 times the Ames dynamic pressure at non cryogenic temperatures in order to obtain a comparable Reynolds number on the smaller model. The risks associated with the smaller model, that did not offer an increase in Reynolds number, were considered too great to commit transport design development tests to the small blowdown wind tunnel. These tunnels were used for component tests such as inlets, and nacelle and pylon studies.

The use of the small blowdown tunnel for high aspect ratio transport configurations was not seriously considered until NASA proved the cryogenic concept in 1972 and reported in reference 1 the possibility of using the cryogenic principle in a blowdown wind tunnel. The payoff of the small blowdown tunnel operating at cryogenic temperatures is shown in Figure 2.

The fact that a model tested in a four-foot tunnel at cryogenic temperatures and moderate dynamic pressures of 2100 pounds per square foot would have three times the chord Reynolds number of an eleven-foot tunnel indicated that the design and instrumentation of the small model should be reviewed in the light of the advanced technology of today as compared to that of 20 years ago. The purpose of this report therefore is to discuss the design and instrumentation of a model for a cryogenic blowdown wind tunnel. The model to be described is a 1.29% scale model of the DC-10-30 but the information should be applicable to all models to be tested in a cryogenic environment.

MODEL REQUIREMENTS

There are many ways that a model can be supported in a high subsonic Mach number wind tunnel. The type model support that will be discussed in this report is a conventional aft sting with an internal six-component balance as shown in Figure 3.

The information presented would be applicable to blade support arrangements that utilize an internal six-component balance but twin sting balance arrangements would require a re-evaluation of the techniques.

The model should be capable of a buildup starting with the fuselage alone and adding wing, empennage, and nacelles and pylons. The model must operate in a temperature range from 540°R down to 180°R at a maximum dynamic pressure of 2150 psf over a Mach number range from 0.5 to 1.0. The tolerances required and the data accuracy are shown in Figure 4.

The indicated surface finish tolerances are conservative, and reflect concern for eliminating as far as possible extraneous perturbations to the model boundary layer, even those short of outright "tripping" in testing conducted with natural transition.

Planform and profile sketches of the model and pertinent model geometric data are shown below in Figure 5.

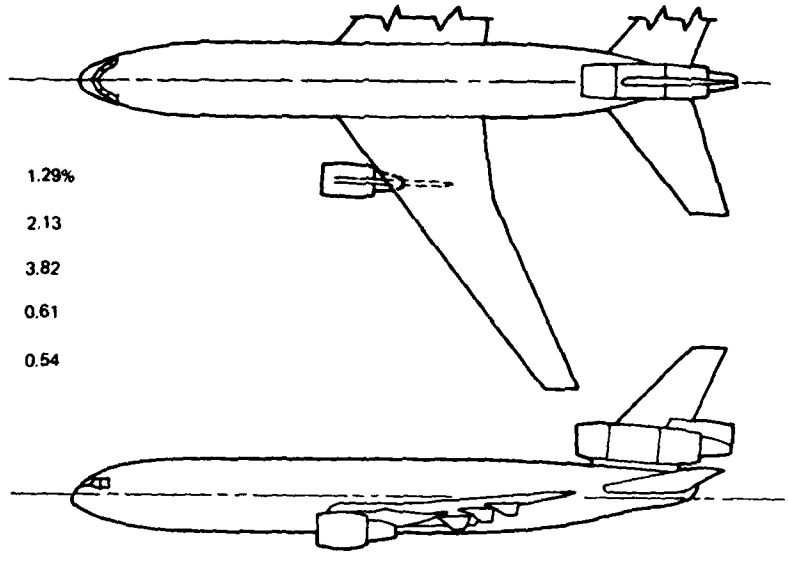

MODEL SCALE	1.29%
WING SPAN (FT)	2.13
MEAN AERO CHORD (IN.)	3.82
WING AREA (FT^2)	0.61
% BLOCKAGE	0.54

FIGURE 5. SKETCH OF DC-10 MODEL AND GEOMETRIC DATA

WING

The wing will be machined as one piece after a tongue and groove joint has been machined into the wing for ease of installing pressure, temperature, and boundary layer transition instrumentation. The wing material has not been finalized but we have established two materials that we feel are acceptable. Our first choice would be a stainless steel, specifically ARMCO PH 13-8 MO - condition H1150M. The one problem that this material has with regard to the blowdown tunnel operation where model pre-cooling is required is low thermal conductivity. The criteria for temperature differential between the model and the recovery temperature have not been finalized but in order to meet the drag repeatability requirement the heat transfer beween the model and the air-stream must be minimized. This may require an elaborate pre-cooling system which will be discussed later, but the use of a highly thermally conductive material would minimize temperature variations within the model and a less elaborate model pre-cooling sysem could be utilized. The alternate material that is being considered with high thermal conductivity is Berylco 25, temper A 1/2AT beryllium copper. A comparison of the two materials is shown in Figure 6. As can be seen the major differences between the stainless steel and the beryllium copper are the Modulus of Elasticity (E), the Charpy Impact Strength,(CIS), and the thermal conductivity. It should be noted however that the CIS value of 15 to 20 shown in Figure 6 has not been obtained in samples tested. A value of nine is the highest obtained to date where the specimen was over aged in the heat treat process.

	STAINLESS STEEL (ARMCO PH 13-8 Mo, CONDITION H 1150 M)	BERYLLIUM COPPER (BERYLCO 25, TEMPER A -1/2 AT)
ULTIMATE TENSILE STRENGTH (10^3 PSI)	175	200
MODULUS OF ELASTICITY (10^6 PSI)	29	18.4
MODULUS OF RIGIDITY (10^6 PSI)	11	7
CHARPY IMPACT STRENGTH (FT - LB)	60	15 20
COEFFICIENT OF THERMAL EXPANSION (10^{-6} INCH/INCH ^oF)	4 0	6 0
SPECIFIC HEAT (BTU/LB ^oF)	0.10	0 09
THERMAL CONDUCTIVITY (BTU/HR FT ^oF)	8	62 75

FIGURE 6 COMPARISON OF MATERIAL PROPERTIES AT 180°R (100°K)

The one-third lower E value is not a major concern since it would actually be a closer represenation of the model wing twist as compared to the full scale airplane as the lift on the wing is changed. The Langley Research Center of NASA has established a Charpy Impact Strength of 25 Ft-Lbs for their Pathfinder I model although they consider Inconel 718 as marginally acceptable with a Charpy of 20 at a temperature of 140°R, Reference 2. The low Charpy of nine indicated earlier for beryllium copper is a definite concern but the potential of a uniform model temperature distribution dictates that a more quantitative assessment of a lower than desired Charpy impact strength criteria must be obtained. If the beryllium copper is the final selection for the wing material, nacelles and pylons, much of the fuselage, and the empennage would also be fabricated from the same material. The high conductivity that makes beryllium copper an attractive solution to temperature gradient problems introduces new concerns regarding pressure tube installation, appropriate crack and hole filler material, and other necessary model fabrication techniques.

A study has been initiated to look at the possibility of fabricating the wing and possibly the whole model out of composites. If the thermal conductivity is low enough it would eliminate the need to pre-cool the model as well as the transient protection system discussed in the paper on control of pressure, temperature, and Mach number in a blowdown-to-atmosphere cryogenic wind tunnel.

Instrumentatio in the wing will include up to 256 surface pressures, upwards of 50 thermocouples if the wing is stainless steel or 20 if beryllium copper is used, and either hot film gages, or dynamic pressure transducers for detecting the boundary layer transition point. The complete instrumentation package is considered quite soft at this point pending results of several test technique development programs that are currently underway and will be reported on in the lecture describing the progress of the Douglas Aircraft Company four-foot cryogenic tunnel modification.

In order to ease the installation of the instrumentation the leading edge will be removed during the fabrication phase but will be semi permanently installed once the instrumentation is in place and checked out. The pressure orifices will be installed in the top surface on the left wing panel and in the bottom surface in the right wing panel with several correlate orifices in each panel to establish the repeatability of data between each panel. The wing panels will have spanwise internal passages behind the tongue and groove joint and chordwise channels that feed into the spanwise passage for routing the wing instrumentation leads into the fuselage for connection to the appropriate transducers. Figure 7 shows the layout of the wing with typical cutouts for the routing of instrumentation leads.

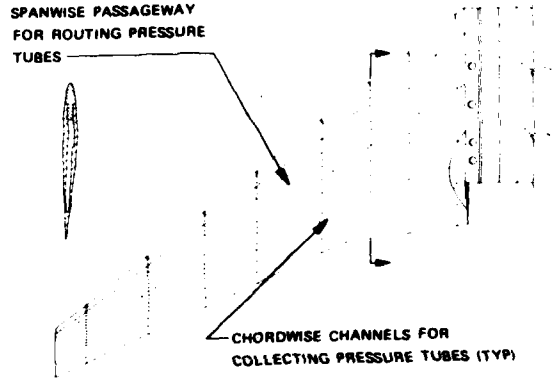

FIGURE 7. WING PRESSURE INSTRUMENTATION

FUSELAGE CENTER SECTION

The fuselage center section is conventional for a high speed transport model. It provides a housing for the balance assembly, including heater and insulator if the balance is to be heated, and is the structure used for attaching the wing and carrying the wing loads into the balance. Rigidity is of primary importance. The material therefore should be a durable material such as stainless steel PH13-8MO. Passageways should be provided in the center fuselage for routing instrumentation leads from the fuselage nose (instrumentation compartment) to the sting access hole.

BALANCE & STING

The primary question to be answered with regard to the balance is whether to use existing balances with heaters and operate at normal temperature or design new balances that can operate at cryogenic temperatures. The advantage of an unheated balance is that there is no heat input to dissipate except for the heat transfer from a warm sting into the balance, in the case of a blowdown tunnel, which may establish the requirement for pre-cooling the sting as well as the model.

Heating existing multi element balances appears attractive, at least for near term uses, since the balance characteristics with regard to accuracy and capability are known and the heat can be applied for the full extent of the balance outer shell. The heat path to the inner rod is only through flexures and active balance components and this cannot compensate for the heat transfer from the sting to the inner rod. An additional requirement therefore is to provide a sting heater that will stabilize the inner rod temperature and prevent heat flow from the cold sting, that has been cooled during the pre-cooling cycle and during the actual blowdown from aerodynamic heating, to the balance inner rod.

The sting and other structural components of the model are designed to a factor of safety of three based on the yield stress. An acceptable sting material is 13-8 stainless steel which has a yield stress of 145,000 psi at 180°R. The critical sting design parameter that must be satisfied is sting divergence, the ratio of balance plus sting deflections per unit load, which must be equal to or less than 0.5.

BALANCE & STING HEATERS & CONTROLLERS

The balance could be installed in the fuselage center section as shown in Figure 8. This figure also shows the attachment of the wing to the balance housing or fuselage center section core.

The balance should be installed in a beryllium copper heater sleeve which is grooved in order to imbed the balance heaters in the sleeve. The beryllium copper should insure a uniform temperature distribution along the length of the balance. Two heaters, one forward and one aft, should provide flexibility to minimize gradients along the balance, particularly in the inner rod. Thermocouples, forward and aft, on the balance inner rod or those on the heater grid should be evaluated as the monitor temperatures for the balance heater controllers. Figure 9 shows the balance heater sleeve and Figure 10 shows the flat pattern layout of the balance heaters and the heater specifications.

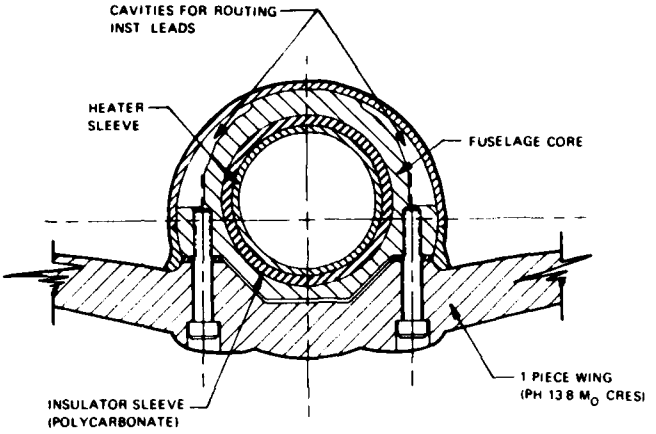

FIGURE 8. DC-10 MODEL FUSELAGE CROSS SECTION

HEATER SPEC
- WIRE-INCONEL
- INSULATION SILICON RUBBER COATED GLASS CLOTH
- RESISTANCE - 57Ω
- OUTPUT 849 WATTS AT 220 VOC

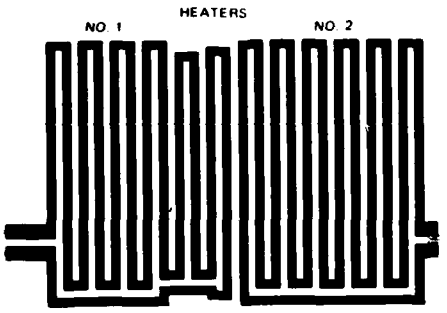

FIGURE 9. FLAT PATTERN LAYOUT OF BALANCE HEATERS

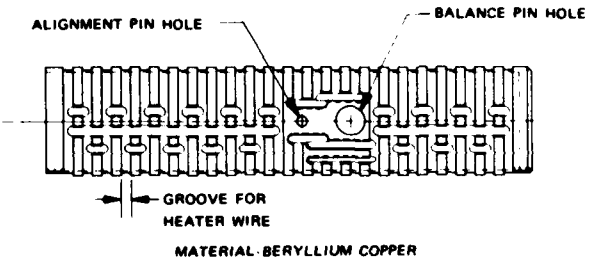

FIGURE 10. BALANCE HEATER SLEEVE

The sting to balance heater can be the same electrical design as the balance heaters but may differ depending upon the sting-balance interface configuration. The standard sting geometry used at Douglas Aircraft for transport models requires a dog-leg in the sting as shown in Figure 11.

The sting enters the fuselage at an angle that attempts to minimize the sting angle with respect to the fuselage reference plane while keeping the sting axis as far as possible from the horizontal tail mounting trunnion. This normally turns out to be an angle of five or six degrees. This angle and the desire to orient the balance at an angle that is near zero when the model is at a cruise condition dictate the requirement for a dog-leg in the sting inside the model.

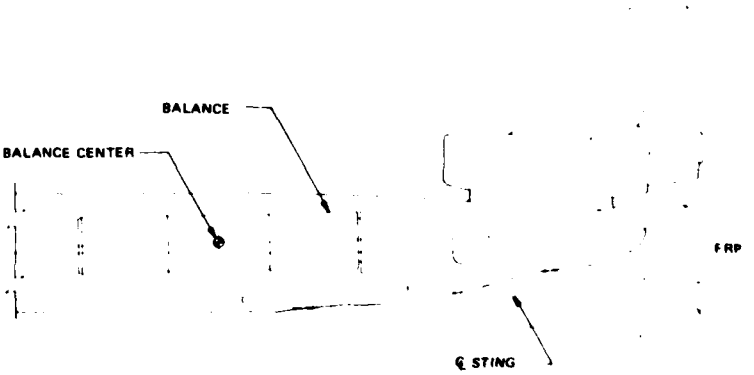

FIGURE 11. DC-10 MODEL AND STING FOR 4-CWT

The sting to balance adapter heater attempts to keep the cold sting from cooling the balance inner rod. The heater assembly is wrapped around the outside of the sting taper joint and the dog-leg portion of the sting structure. A flat pattern layout of the sting to balance heater is shown in Figure 12.

Each of the three heaters has a set point proportional controller that provides full output power when the control temperature sensor is more than 1.5°F below the set point falling to zero output when the control temperature is at or above the set point.

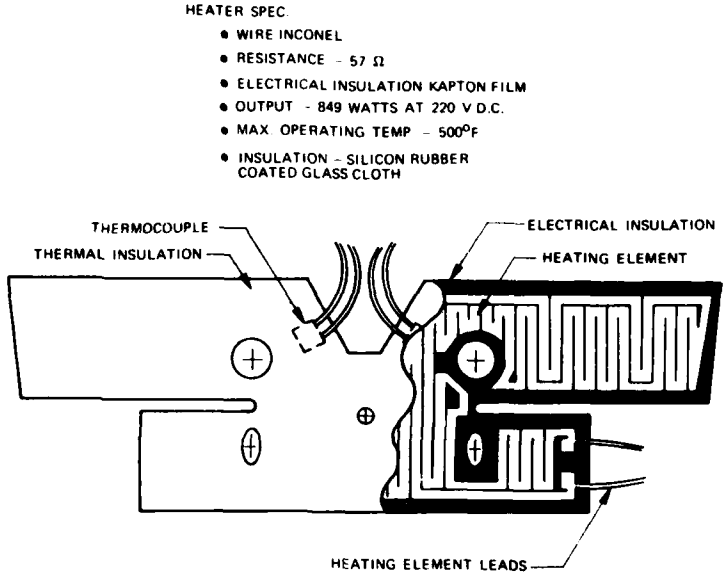

FIGURE 12. FLAT PATTERN LAYOUT OF STING HEATER

The flow around a dog-leg sting and aft fuselage produces a pressure variation in the sting cavity that should be corrected to a common level. The standard procedure is to determine the pressure differential between the measured cavity and the calculated free stream static pressures and correct the normal and axial forces and pitching moment as shown below in Figure 13.

$$\Delta \text{ NORMAL FORCE} = \sum_{i=1}^{n} (P_i - P_\infty)\, A_i \cos\theta$$

$$\Delta \text{ AXIAL FORCE} = \sum_{i=1}^{n} (P_i - P_\infty)\, A_i \sin\theta$$

$$\Delta \text{ PITCHING MOMENT} = \sum_{i=1}^{n} [\, (P_i - P_\infty)\, (A_i \cos\theta\, Y_i + A_i \sin\theta\, Z_i)\,]$$

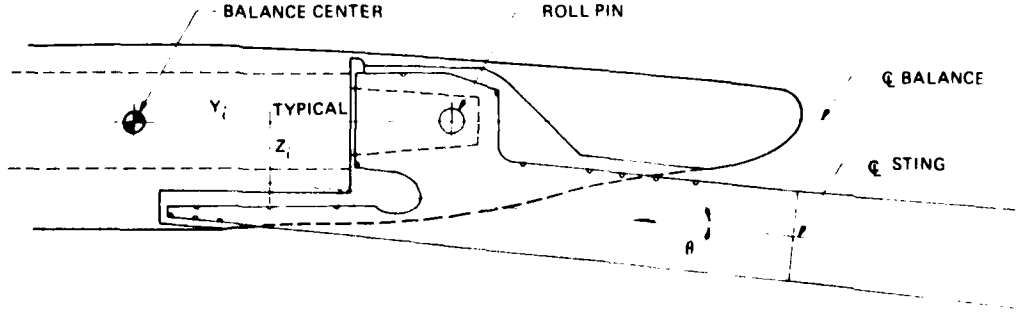

FIGURE 13 STING CAVITY CORRECTION

AFT FUSELAGE & EMPENNAGE

The aft fuselage of a model to be tested at cryogenic temperatures should not differ from one to be tested at conventional temperatures. If an aft dog-leg sting is used to support the model it is not necessary to distort the aft fuselage. The aft fuselage shape would represent the aircraft configuration except for the cutout to provide access for the sting. If a straight sting is used the aft fuselage generally requires distorting to make room for the sting and structure for the horizontal and vertical tails. The aft fuselage incorporates the structure to transmit the empennage loads into the balance housing and requires a high degree of rigidity. The material used in fabricating the aft fuselage therefore would be a high strength cryogenically compatible stainless steel or beryllium copper or made of composites.

FUSELAGE NOSE

The fuselage nose in addition to providing the forward fuselage aerodynamic shape, also houses pressure transducers, and temperature and transition detection system multiplexers. In order to maximize the internal volume and provide insulation for the instrumentation package the fuselage nose can be made of fiberglass since the aerodynamic loads are relatively low, and bonded to a titanium connector ring for attaching to the fuselage center section. Titanium is used to minimize the heat transfer from the fuselage center section to the nose.

INSTRUMENTATION PACKAGE

The instrumentation in the fuselage nose consists of pressure transducers and multiplexers for thermocouples and boundary layer transition detectors. There are two candidates that can satisfy the desired pressure instrumentation. One is a rotary pressure valve that scans 36 pressures at a rate of 5 ports per second. This requires the use of the pitch pause technique. That is, the model is pitched to an angle of attack and during a pause the model pressures are read-out as the valve rotates a common transducer into individual pressure ports. This system is very reliable but is time consumming. A new approach that uses semi-conductor gages has individual transducers for each pressure port that are switched electronically rather than mechanically. This approach allows continuous sweep data to be taken at a rate that is set by the response time from the orifice to the transducer. A one to two degree per second sweep rate would be slow enough to meet the response time criteria but fast enough to complete angle of attack sweeps at several Mach numbers. Both systems require heaters to protect the units from the hostile environment as well as to minimize errors that result from zero shifts or sensitivity changes due to temperature variations.

The installation of the electronic pressure sensor modules in a model sized for a four-foot blowdown wind tunnel is shown in Figure 14.

The modules are attached to an epoxy/fiberglass support that is cantilever mounted from the fuselage centerbody. The epoxy/fiberglass support should minimize the heat transfer from the balance housing to the pressure sensor modules. The modules are oriented with the transducers at the top and bottom in sets of four. A copper heat sink is placed next to the transducer modules on the top and bottom of the two units and a heater assembly is attached to the copper plates. Hypodermic tubing from the orifices are routed to the connector plate on the modules where a short segment of plastic tubing is used to complete the connections to the transducers.

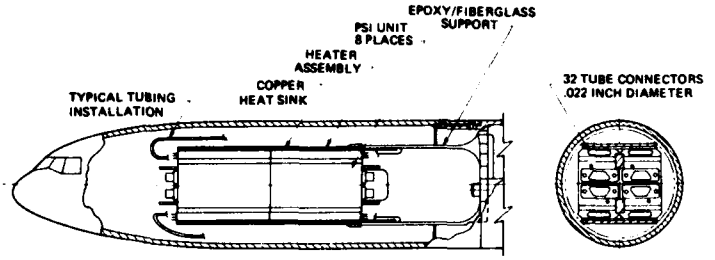

FIGURE 14. ELECTRONIC PRESSURE SENSOR MODULES WITH HEATERS

Two thermocouple multiplexers can be installed on the epoxy/fiberglass structure. Each multiplexer can be connected to 48 thermocouples and transmit their output to the data acquisition system. The multiplexer is approximately 1 1/2 inches square and 0.1 inches thick. The multiplexers are required to minimize the number of electrical leads required to bridge between the model and the sting.

Output from instrumentation to detect boundary layer transition, hot film gages or dynamic pressure transducers, will be routed to multiplexers located in the fuselage nose for transmission to the data acquisition system.

MODEL CONDITIONING

The requirement that the model be at the adiabatic wall temperature before valid data can be taken establishes the need to pre-cool the model before the start of a run in a cryogenic blowdown wind tunnel since the short run time would be insuficient to cool the model as can be done in a continuous flow tunnel. Even if it could be shown to be technically feasible the liquid nitrogen cost would prohibit the procedure. The preferred pre-cooling method is to either enclose the model in a cold box outside the test section and inject the model into the tunnel once the flow has been established or to house the model in position in the test section inside clam-shells that can be retracted once the flow is established.

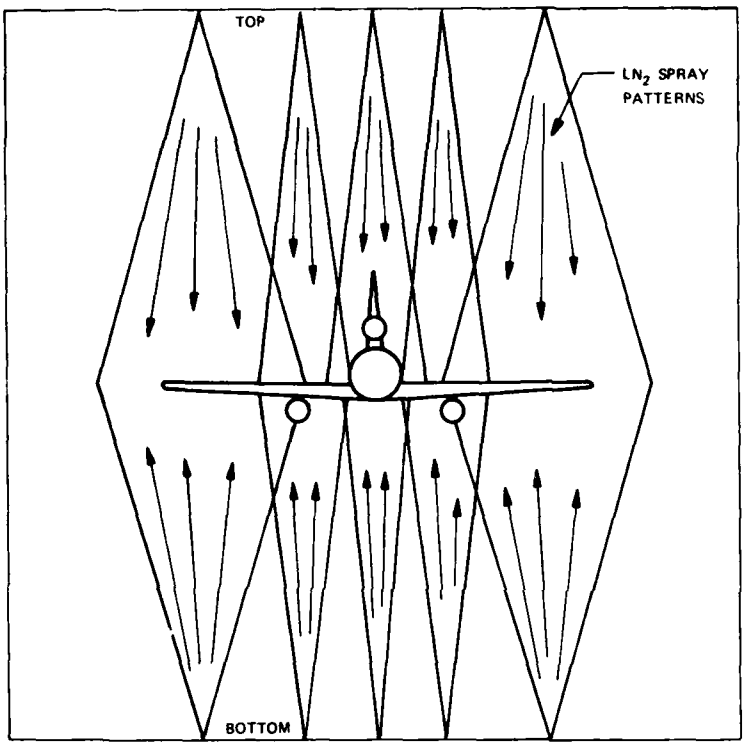

FIGURE 15. MODEL PRE-COOLING FOR WING AND WING NACELLES AND PYLONS

The mechanical complexities with either of the arrangements discussed above prompted the look at a simpler pre-cooling system, shown in Figure 15, that sprays the model with liquid nitrogen until the desired model temperature is achieved. Difficulty in obtaining a uniform temperature distribution in the model and exposing the model to warm air during the starting process are disadvantages to this approach. However, the cost factor which is considerable necessitates a thorough checkout of this system.

When a blow has been completed the model will be very close to the operating temperature and will collect frost if exposed to an environment that has any moisture content. The "clean room" approach is possibly the best method to keep moisture from collecting not only on the model but also on the tunnel itself. This can be accomplished by maintaining a slight positive pressure, with very dry air, in the area that encloses the tunnel circuit. This procedure would satisfy the condition where the same configuration is to be tested at several Mach numbers.

If it is necessary to make a configuration change to the model it is necessary to reheat the model to room temperature. This can be accomplished by ducting hot air from the tunnel high pressure air system before going through the compressor aftercoolers.

REFEENCES

1. R. A. Kilgore, M. J. Goodyear, J. B. Adcock, E. E. Davenport — The Cryogenic Concept For High Reynolds Number Testing. NASA-TN-D-7762, Nov. 1974.

2. C. M. Hudson — Material Selection For The Pathfinder I Model. Paper No. 28 Cryogenic Technology Conference NASA Langley Research Center Nov. 27-29, 1979.

SELECTION AND APPLICATION OF INSTRUMENTATION FOR CALIBRATION AND CONTROL OF A CONTINUOUS-FLOW CRYOGENIC TUNNEL

by
Robert A. Kilgore
NASA - Langley Research Center
Hampton, Virginia 23665
U.S.A.

SUMMARY

This lecture describes those aspects of selection and application of calibration and control instrumentation that are influenced by the extremes in the temperature environment to be found in cryogenic tunnels. A description is given of the instrumentation and data acquisition system used in the Langley 0.3-m transonic cryogenic tunnel along with typical calibration data obtained in a 20- by 60-cm two-dimensional test section.

SYMBOLS

c	Chord of airfoil
M	Mach number
p	Pressure
q	Dynamic pressure
R	Reynolds number
T	Temperature
$\bar{T}_t$	Mean value of stagnation temperature
V	Velocity

Subscripts

l	Local value
ref	Reference
t	Stagnation value
∞	Free-stream value

Abbreviations

GN_2	Gaseous nitrogen
LN_2	Liquid nitrogen
%	Percent
2-D	Two dimensional

1. INTRODUCTION

The need for increased capability in terms of Reynolds number has been recognized since the earliest days of testing sub-scale models in wind tunnels. The need has been especially acute at transonic speeds where, because of the large power requirements of transonic tunnels, economic forces have dictated the use of relatively small tunnels.

In considering the various ways of increasing Reynolds number that have been tried or proposed for transonic tunnels, cooling the test gas to cryogenic temperatures (150 K or less) appears to be the best solution in terms of model, balance, and sting loads, as well as capital and operating cost.[1] In addition, having temperature as an independent test variable offers some new and unique aerodynamic testing capabilities which, in some instances, may be of equal importance with the ability to achieve full-scale Reynolds number.[2]

Personnel at the NASA Langley Research Center have been studying the application of the cryogenic wind tunnel concept to various types of high Reynolds number transonic tunnels since the autumn of 1971 and, through extensive theoretical and experimental studies, have successfully demonstrated both the validity and practicality of the concept.[3-5]

There is, however, a price to be paid for the many advantages offered by a cryogenic wind tunnel. The price is added complexity in both the design and operation of the tunnel. Compared to an ambient temperature tunnel, the wide range of operating temperatures available in a cryogenic tunnel results in added complexity in such areas as model design and instrumentation, tunnel control, and the instrumentation used for tunnel calibration and control. Some of these areas have been or will be covered in other lectures of this series. This lecture deals with the single area of instrumentation and associated equipment used in the calibration and control of cryogenic continuous-flow transonic pressure tunnels. Specifically, this lecture addresses those aspects of instrumentation selection and application that are influenced by the extremes in the temperature environment to be found in cryogenic tunnels. The calibration and control instrumentation used

in the Langley 0.3-m transonic cryogenic tunnel is described and examples of tunnel calibration data obtained in a 20- by 60-cm two-dimensional test section are given.

It should be noted that the use of trade names in this lecture in no way implies endorsement or recommendation by the U.S. government.

2. INSTRUMENTATION SELECTION

In general, the process of selecting instrumentation for the calibration and control of a continuous-flow transonic pressure tunnel capable of being operated at cryogenic temperatures is no different from the process that would be followed for a similar tunnel that operates only at ambient temperatures. The steps to be taken are: (1) determine the accuracy requirements for the test parameters of Mach number M_∞, Reynolds number R, dynamic pressure q_∞, and velocity V_∞; (2) calculate the sensitivity of the test parameters to the uncertainties in the test conditions of total pressure p_t, static pressure p, and total temperature T_t; and finally, (3) select instrumentation which will meet the accuracy requirements.

2.1 Accuracy Requirements for M_∞, R, q_∞, and V_∞

The accuracy requirements of the test parameters will vary in a given tunnel depending upon the type of aerodynamic test to be performed. For most transonic applications an accuracy in M_∞ of ±0.002 and accuracies in R and q_∞ of better than ±0.5% of reading are required. This accuracy requirement for Mach number can probably be relaxed for low-speed testing. However, larger variations in Mach number can cause significant changes in shock wave location at the higher transonic speeds. The accuracy requirements of R and q_∞ are independent of tunnel speed. In some applications, such as dynamic-stability testing, V_∞ is an important test parameter which must be determined. Here again, an accuracy of better than ±0.5% of reading is usually required.

2.2 Allowable Error in Pressure and Temperature Measurements

None of the test parameters - M_∞, R, q_∞, or V_∞ - can be measured directly with conventional instruments. However, all are functionally related to three quantities that can be measured directly, namely, stagnation pressure p_t, static pressure p, and stagnation temperature T_t. It then becomes necessary to determine the sensitivity of M_∞, R, q_∞, and V_∞ to the inaccuracies in the measured values of p_t, p, and T_t. Once this has been accomplished, the required accuracy for a given test parameter can be expressed in terms of the required accuracy for the pressure and temperature measuring instruments.

2.2.1 Allowable Error in Pressure Measurement

Calculations have been made to determine the allowable error in the measurement of stagnation pressure p_t for fixed errors in M_∞ and q_∞.[6] The results of these calculations are shown in Figure 1 as a function of M_∞. For an allowable error in M_∞ of ±0.002 and q_∞ of ±0.5% of reading, p_t must be measured to an accuracy of about ±0.25% of reading at the higher Mach numbers and to better than ±0.1% of reading at the lower Mach numbers. The sensitivity of M_∞ to errors in static pressure is the same as for stagnation pressure, but q_∞ is less sensitive, especially at the higher Mach numbers. It should be noted, however, that these are maximum errors for a single measurement. If the error analysis is based on most probable error or on standard deviation, the required instrumentation accuracy is not as great.

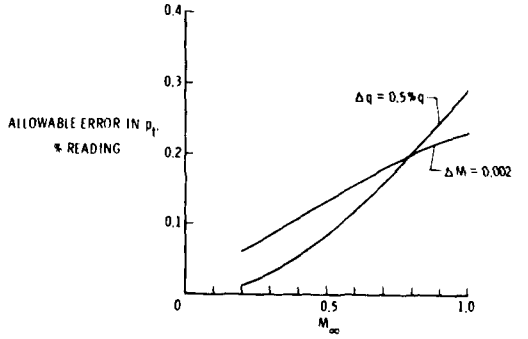

Figure 1.- Allowable error in p_t for fixed error in M_∞ and q_∞.

2.2.2 Allowable Error in Temperature Measurement

Calculations have also been made to determine the required accuracy of stagnation temperature T_t, necessary to have measurements of V_∞ and R accurate to ±0.5% of reading. Results of these calculations, in terms of allowable temperature error, are presented in Figure 2. Of the two parameters, R is the most sensitive to temperature, requiring an accuracy of about ±1 K at ambient temperatures and about ±0.3 K at cryogenic temperatures.

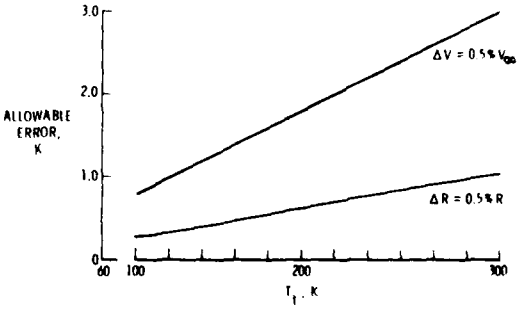

Figure 2.- Allowable error in T_t for 0.5 percent in R and V_∞.

This is one area in which the accuracy requirements for instrumentation for a cryogenic tunnel are more severe than for an ambient temperature tunnel.

2.3 Other Considerations

The final step in the selection process is one of choosing from the available instrumentation that which will meet the accuracy requirements. However, other factors, such as the range of the test variable, response time, compatibility with the test environment, and cost and budget constraints, must also be considered.

2.3.1 Accuracy of Available Instrumentation

2.3.1.1 Pressure Instrumentation

The accuracy of three types of commercially available pressure transducers as a function of percent load are shown in Figure 3. Typical "high accuracy" strain-gage devices have an accuracy of about 0.25% of full scale. When converted to percent of reading, this increases to about 1% at 25% of full-scale load. Variable capacitance transducers have a quoted accuracy of 0.25% of reading throughout the load range but their cost is at least an order of magnitude greater than a strain-gage device. The quartz bourdon tube transducer is by far the most accurate, although it costs about 50% more than the variable capacitance transducers.

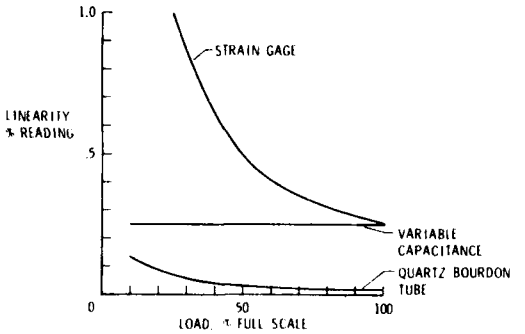

Figure 3.- Accuracy of pressure instrumentation.

Because pressure instrumentation accuracy on the order of 0.1% is required to give the desired accuracy in Mach number and dynamic pressure, the quartz bourdon tube instrument has been selected for the primary tunnel pressure instrumentation for both the 0.3-m TCT and the National Transonic Facility (NTF), the large transonic cryogenic tunnel now under construction at Langley and the subject of a separate lecture later in this series. The quartz bourdon tube instrument is also used as the primary pressure instrumentation in other pressure tunnels at Langley. Unfortunately, the quartz bourdon tube pressure instrument has a response time that is generally much too slow for use with automatic tunnel control systems. Thus, as will be discussed in more detail later, less accurate but more responsive pressure instrumentation is used to provide the inputs to these systems.

2.3.1.2 Temperature Instrumentation

Two general types of temperature measurement devices are available for use at cryogenic temperature. These are resistance devices, such as the platinum resistance thermometer (PRT), and thermocouples, both of which are being used in the 0.3-m TCT. As shown on Figure 4, the PRT has an accuracy of ±0.25 K which meets the accuracy requirement for measuring T_t. However, it also has a very slow response time, varying from 10 to 100 seconds, depending upon its design and size. Again, as was the case for the pressure instrumentation, the high accuracy devices do not have adequate response time for use in automated tunnel control systems. Thermocouples, which have accuracies varying from ±0.5 K to ±2 K, depending upon the temperature range, have response times which vary from about 0.1 to 20 seconds. This response time is a function of both the wire diameter and the type of thermocouple (bare wire, shielded, etc.), and for unshielded thermocouples in the smaller wire diameters, the response times are compatible with automatic tunnel temperature control systems.

- RESISTANCE DEVICES
  - PLATINUM RESISTANCE THERMOMETER (PRT)
  - ACCURACY ± 0.25 K
  - RESPONSE TIME 10 - 100 SECONDS
- THERMOCOUPLES
  - ACCURACY ± 0.5 K TO ± 2 K
  - RESPONSE TIME 0.1 - 20 SECONDS

Figure 4.- Temperature transducers suitable for cryogenic tunnels.

One disadvantage of thermocouples is their very low voltage output, being on the order of a few millivolts. Another disadvantage with thermocouples is due to the fact that the net voltage output is a function not only of the base metals of the two wires but also of any material inhomogeneities which produce a parasitic voltage if located in a temperature gradient. Inhomogeneities in the wire can be produced by either a variation in the chemical composition along its length or by mechanical strain such as a kink.

The presence of defects such as these can be detected by testing lengths of thermocouple wire in a temperature gradient by using a device, such as shown in Figure 5, which runs the wire through a liquid nitrogen bath and records the voltage output resulting from the temperature gradient. However, the effects of inhomogeneities cannot be readily corrected. Typical results obtained at Langley by Germain on three types of thermocouple wire in the test apparatus shown in figure 5 are presented in Figure 6. The voltage spikes for the type E (Chromel vs. Constantan) and K (Chromel vs. Alumel) thermocouples are typical of those recorded throughout the length of wire tested whereas the spike for the type T (Copper vs. Constantan) thermocouple was the only one found in that sample of material.

Figure 5.- Homogeneity test rig.

Based on these results and on company literature, it appears that having one wire of pure copper makes it easier to control the overall chemical composition of type T thermocouples than either types E or K which have both wires of alloyed metal. For these reasons, type T thermocouples are being used in the 0.3-m TCT and have been selected for use in the NTF. An additional practical advantage of the type T thermocouple is that it is available in a "premium quality" wire which has a good (±1%) match to published voltage standards at cryogenic temperatures. None of the other types are so available. Our experience over the years has been that only the type T "premium" thermocouple remains within the ±1% band at cryogenic temperatures.

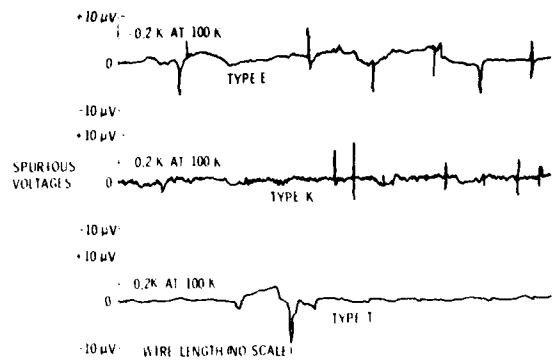

Figure 6.- Typical homogeneity test results.

The standard limits of error for commercial premium grade type T thermocouple wire are presented in Figure 7 as a function of temperature. These results, obtained at Langley by Edwards and Stewart from a calibration of four selected thermocouples, show their error to be only about one-half of the limit of error specification, with the largest error occurring in the cryogenic temperature region. Using calibration data such as these can increase the accuracy of a thermocouple reading, but it must be remembered that the effect of inhomogeneity cannot be accounted for.

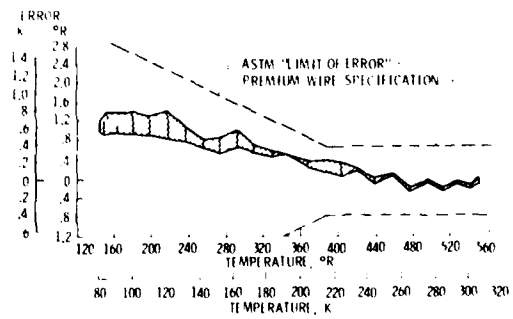

Figure 7.- Calibration of type T thermocouples.

2.3.2 Range of Test Variables

In the selection of instrumentation to meet the required accuracy, the range of the variable to be measured can be a major factor. For example, a liquid column manometer is a very accurate device for pressure measurement. However, if the pressure level exceeds two atmospheres or so, the height of the liquid column makes it impractical to use a manometer. The range of test conditions for both the 0.3-m TCT and the NTF are shown in Figure 8 to illustrate the ranges to be encountered in these tunnels as well as to indicate the ranges likely to be encountered in other transonic cryogenic tunnels. The largest difference to be noted between these two tunnels is in stagnation pressure where the maximum pressure in the NTF is about 50 percent greater than in the 0.3-m TCT. The differences in Mach number do not affect the selection of instrumentation to any great extent.

	0.3 m TCT		NTF	
MACH NUMBER, M_∞	0.1	0.9	0.2	1.2
STAGNATION TEMPERATURE, T_t, K	78	340	78	339
STAGNATION PRESSURE, p_t, atm	1.0	6.12	1.0	8.85
STATIC PRESSURE, p, atm	0.5	6.12	0.5	8.85

Figure 8.- Range of test conditions.

2.3.3 Response Time

Because of the relatively high cost of operation of high Reynolds number tunnels, fast response times are desirable for all instrumentations. Response time is especially important when an instrument is used to provide an input signal to an automatic closed-loop tunnel control system. For example, the tunnel control system inputs for the 0.3-m TCT come from instruments with as short a response time as practical, at the sacrifice of some accuracy. Separate dedicated instrumentation, which is less responsive but more accurate than that used with the tunnel controls, is used to give highly reliable readings of the test variables p_t, p, and T_t. Details of this particular instrumentation as well as further discussion of response times are given in subsequent portions of this lecture.

3. INSTRUMENTATION USED IN THE 0.3-m TCT

In the 0.3-m TCT, the practice of isolating instrumentation from the cryogenic environment has been adopted when possible. With the obvious exception of temperature transducers, most instrumentation is located exterior to the tunnel pressure shell, thus completely avoiding problems related to temperature variation. If a device must be located in the cryogenic environment, it is enclosed in an insulated container which is maintained automatically at approximately 300 K by using a thermostatically controlled electric heater. Devices such as slidewire potentiometers, digital shaft encoders, and pressure scanning valves have been successfully operated within the tunnel pressure shell in this manner. However, with each of these systems there are heaters, thermostats, wires, electrical connections, electrical feedthroughs, and power supplies which add to the complexity of the system and, inevitably, reduce its reliability. On many occasions, run time in the 0.3-m TCT has been lost due to the failure of one of these simple support devices rather than due to any failure in the instrument itself. Based on our experience with the 0.3-m TCT, we must conclude that it is best to locate electronic equipment exterior to the tunnel in an ambient temperature and pressure environment if at all practical.

Some details of the instrumentation presently being used in the 0.3-m TCT are now described.

3.1 Pressure Instrumentation

For two-dimensional airfoil tests, the 0.3-m TCT is equipped to obtain static-pressure measurements on the airfoil surface, total head measurements in the airfoil wake, and static pressures on the test section sidewalls, floor, and ceiling. Static-pressure taps are also located throughout the tunnel circuit to obtain information on the performance of the contraction and diffuser sections, fan pressure rise, and pressure losses across various elements of the tunnel circuit. To measure the pressures for such a large number of points, a scanning valve system capable of operating ten 48-port scanning valves is used. Because of the large changes in dynamic pressure of the tunnel over its operational range (a factor of about 75) conventional strain-gage pressure transducers are not used. Instead, we use commercially available high-precision capacitive potentiometer-type pressure transducers.[7]

The pressure transducers are mounted in instrument racks adjacent to the test section in order to reduce response time. To provide increased accuracy, the transducers are mounted on thermostatically controlled heater bases to maintain a constant temperature and on "shock" mounts to reduce possible vibration effects. The electrical outputs from the transducers are connected to individual signal conditioners located in the tunnel control room. The signal conditioners are autoranging and have seven ranges available. As a result of the autoranging capability, the analog electrical output to the data acquisition system is kept at a high level even though the pressure transducer may be operating at the low end of its range.

Pressure transducers with a maximum range of 6.8 atm are available for model and tunnel wall pressure. More sensitive transducers, having a maximum range of 1.36 atm, are available for pressure measurements in the airfoil wake. The transducers have an accuracy of ±0.25% of reading from -25% to 100% of full scale. At present about 35 pressure transducers are available. However, the system is being expanded and 125 pressure channels will be available in early 1981.

To determine M_∞ to an accuracy of ±0.001, it is necessary to use instrumentation that is much more accurate than the capacitance potentiometer type pressure transducer. As a result, the commercially available quartz bourdon tube type of pressure gage previously described is used for the measurement of p_t, p, and the reference pressure used on other differential pressure transducers. This system has an accuracy of about 0.01% of full scale at low pressures to about 0.02% of full scale at the high end of its range.

3.2 Temperature Instrumentation

The characteristics of both thermocouples and platinum resistance thermometer (PRT) temperature sensors have been previously described. Based on response time, accuracy, and to some extent cost, it has been necessary to use both thermocouples and PRT's in the 0.3-m TCT.

Type T thermocouples are used for a fixed temperature survey rig located in the settling chamber of the tunnel. In this application, we are trying to determine the distribution of temperature and the absolute level is relatively unimportant. The various thermocouples on the rig are made from the same roll of wire and care was taken to avoid kinking the wire or introducing other possible sources of error into the system.

In addition, type T thermocouples are used in the test-section—plenum area to monitor temperature differences during and immediately after tunnel cooldown in order to avoid taking aerodynamic data with the relatively thick test section walls distorted due to thermal gradients. Although the amount of thermally induced distortion is small, even small changes in test section area have a major effect on the longitudinal distribution of M_∞ at the higher values of M_∞.

As previously mentioned, because of the need for rapid response time, the type T thermocouple is also used as the temperature sensor for the closed-loop automatic temperature control system. In this application, the rapid response requirement has been achieved at the expense of accuracy.

The reference temperature for the thermocouples is provided by a commercially available "ice point" junction which automatically maintains the reference junction at 273.2 K ± 0.025 K.

The values of T_t which are used to calculate the tunnel parameters are obtained from PRT's located just downstream of the screen section. As previously discussed, the higher accuracy requirements for T_t have been achieved at some sacrifice in response time by using PRT's. Although the long response times of the PRT's would introduce problems if they were used in the automatic temperature control system, the nature of the testing in the 0.3-m TCT is such that sufficient time is available for the PRT's to come to equilibrium with the stream before temperature readings are required for the accurate determination of T_t.

3.3 Mass-Flow Measurement and Control Instrumentation

One special instrumentation requirement for the 0.3-m TCT is associated with the two-dimensional test section sidewall boundary layer removal system. The requirements for this system are to remove from 1% to 4% of the test section mass flow through porous plates in the test section sidewalls and to measure and control the removal rate to within 1% of the desired set point. With the large operational range of the 0.3-m TCT, the ratio of maximum to minimum removal rate is about 140 to 1. This range of mass-flow control and its measurement to the required accuracy is well beyond the capability of conventional mass-flow control and measurement devices.

Two commercially available (Process Systems Incorporated) microprocessor controlled 11 bit digital valves have been selected to meet these requirements since they have the ability to handle both the control and measurement functions. These digital valves are similar to those presently being used at the 0.3-m TCT for the control of LN_2 injection into the tunnel and the control of GN_2 exhaust from the tunnel. (The concept of digital valves and their principle of operation is contained in a lecture to be given later in this series which describes the control system of the 0.3-m TCT.) Although the 11 bit valve does not give the desired 1% of reading accuracy over the entire mass-flow range, it gives the desired accuracy over the most important portion of the operating envelope. The two digital valves and their associated control microprocessor are currently under construction and should be operational at the tunnel in late 1980.

3.4 Traversing Wake-Survey Probe

A vertical traversing probe system is located on the left sidewall of the two-dimensional test section downstream of the turntable. The mechanism has a traversing range of 25.4 cm. The distance between the airfoil and the centerline of the probe support can be varied with the probe capable of being located either at tunnel station 26.0 cm or at tunnel station 31.1 cm. The probe is driven by an electric stepper motor and can operate at speeds from about 0.25 cm/sec to about 15 cm/sec. The stroke and speed can be remotely controlled from the operator's panel in the control room. Although the primary purpose of this system is to survey the total pressures in airfoil wakes by using a pitot-tube survey rake, the probe can be equipped with other types of instruments such as thermocouples or hot wires. Figure 9 is a general view of the two-dimensional test section which shows an airfoil in place and the present pitot-tube survey rake located in its most forward position in the test section. For this configuration, the pitot tubes are located 0.88 chord downstream of the airfoil trailing edge.

Figure 9.- View of 2-D test section showing airfoil and survey rake.

Details of the multitube pitot probe are shown in Figure 10. Three disc type static probes as well as six pitot probes are mounted on the assembly. Tunnel sidewall static-pressure taps are also provided in the plane of the pitot probes for use in the determination of the airfoil drag coefficient. Individual transducers are used for each tube on the probe assembly in order to keep pressure response time low. The vertical position of the probe is recorded on the data acquisition system using the output from a digital shaft encoder geared to the probe drive mechanism.

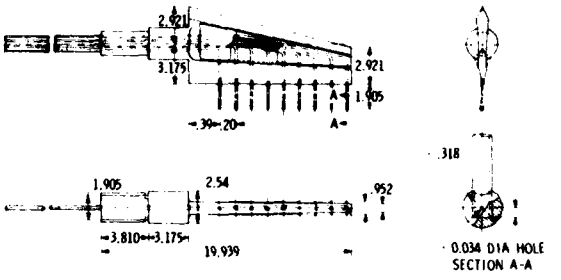

Figure 10.- Details of wake survey probe.

3.5 Flow-Quality Instrumentation

During the calibration of a wind tunnel it is highly desirable to obtain information on the flow quality as well as on the Mach number distribution. The flow quality is generally determined by measurements of sound pressure level and velocity fluctuations in the different planes.

The sound pressure level can be measured by the use of piezoelectric transducers. One such device has been used in the test section of the 0.3-m TCT at Mach numbers up to 0.9 for stagnation pressures to 5 atm.[5] During these tests, T_t was varied from ambient to near liquid nitrogen temperatures. Because this particular transducer has a sensitivity to temperature of about 0.05% per 1 K, it must be calibrated dynamically throughout its operational temperature range if accurate measurements are required. This type of calibration is difficult to obtain and little has been done to date.

Velocity and temperature fluctuations can be measured by using hot wire probes. To date, hot wires of 5 micron diameter and a length-to-diameter ratio of about 250 have been successfully used in the 0.3-m TCT only to Mach numbers of about 0.1 for stagnation pressures up to 5 atm under cryogenic temperature conditions. Further tests are planned in the near future using 3.8 micron diameter wire at higher Mach numbers. The limit to which hot wire probes may be used has not yet been determined.

Laser doppler velocimeter (LDV) systems can also be used to determine fluctuating velocities in a tunnel of this type. A simple LDV setup is currently being prepared to make preliminary tunnel empty measurements. The requirements for seeding particles and, hopefully, resolution to any problems that might arise as a result of cryogenic operation of the tunnel are expected to be obtained during these preliminary tests.

4. 0.3-m TCT DATA ACQUISITION SYSTEM

Data from the 0.3-m transonic cryogenic tunnel are recorded on magnetic tape at the Langley central data recording system. This system, which was installed in the late 1950's, serves several wind tunnels and other test facilities on a time-share basis. A total of 99 analog channels of recording capability are available at the tunnel with a maximum range of 100 mV and a resolution of 1 part in 10,000. In a continuous mode, all data channels can be scanned at a sample rate of 20 per second while in a single scan mode the maximum rate is about 4 scans per second. All analog data are filtered with a 4 Hz low pass filter.

A small computer is used to sequence the data acquisition system, provide timing input signals for the scanning-valve drive system, provide real-time visual displays and plots, and control the angle-of-attack and wake-survey-probe drive systems. The computer is programmed to allow the recording of from one to nine single frames of data for each port on the scanning valves. The time between each frame of data and the dwell time on the port before the first frame of data is taken are both variable inputs.

All inputs to the computer are made through a teletype keyboard. An X-Y plotter is used to produce real-time plots of pressure distribution over the airfoil and total head loss through the airfoil wake. Other real-time displays include digital readouts of Mach number and Reynolds number. Angle-of-attack and wake-survey-probe drive commands are also entered through the teletype and are transmitted through the computer to the respective drive system.

The wake-survey drive can operate in either of two modes. In the first or manual mode, the initial and final location of the probe in the tunnel as well as the number of steps between are the input parameters. In the second or automatic mode, the computer determines the upper and lower boundaries of the airfoil wake automatically by first making a continuous sweep of the survey probe through the tunnel before the data recording sequence begins. The wake-survey probe is synchronized with the scanning valves so that the probe is moved to a different vertical location each time the scanning valves are advanced to a new port. If more survey probe points are desired than scanning valve ports, the probe will continue on its traverse after the scanning valves have reached their last port.

5. TYPICAL CALIBRATION RESULTS FROM THE 0.3-m TCT

A sketch of the Langley 0.3-m TCT is presented in Figure 11. In this view the flow is clockwise. An array of thermocouples is located at the upstream end of the screen section to measure vertical and lateral temperature distributions. The primary pressure and temperature sensors are located in the contraction section, just downstream of the screen section. Details of the plenum and 2-D test section of the 0.3-m TCT are shown in Figure 12. Pressure taps are located in longitudinal rows

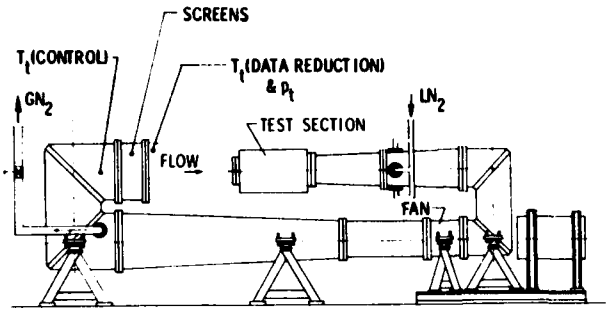

Figure 11.- Sketch of Langley 0.3-m TCT.

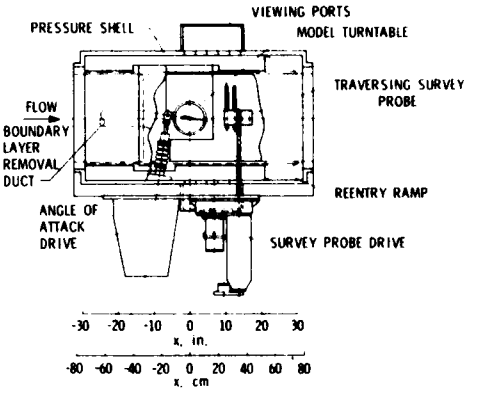

Figure 12.- Sketch of two-dimensional test section.

along the centerline of both top and bottom slotted walls and along the centerline of one solid sidewall. Both left and right turntables are also instrumented with pressure taps for tunnel empty calibration purposes. The reference static pressure is measured on a manifold which connects four orifices, two on each sidewall located as far upstream of the turntable as practical.

5.1 Mach Number Distribution

Typical results of the longitudinal distribution of local Mach number along the centerline of the top slotted wall are presented in Figure 13. This distribution is for a stagnation pressure of 3.1 atm and a stagnation temperature of 105 K. The top and bottom slotted walls were diverged about 0.5° from the centerline whereas the two solid sidewalls were parallel to the centerline. The data show that for Mach numbers below about 0.75, the distribution is relatively uniform to about 50 cm downstream of the center of the turntable where the speed begins to drop off. This location roughly corresponds to the location in the test section where the slots begin to open rapidly. At higher Mach numbers, a negative gradient is observed, indicating the walls were diverged slightly more than necessary.

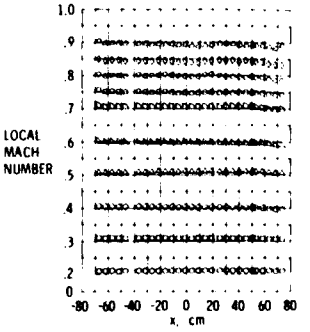

Figure 13.- Typical local Mach number distribution along top slotted wall.

Figure 14 shows the local Mach number distribution on one of the model turntables for the same conditions of 3.1 atm and 105 K. As shown on the sketch, there are 5 rows of pressure taps on the turntable, two horizontal, two diagonal, and one vertical, numbered 1 through 5. This figure again shows the longitudinal gradient in rows 1 through 4, but the data from row 5 indicate essentially no vertical gradient.

The test section Mach number M_∞ has been defined based on the average of the 36 pressure taps located on the turntable. The calibration factor ΔM is defined as the difference between the calculated reference Mach number M_{ref}, and the test section Mach number M_∞. A plot of the calibration factor

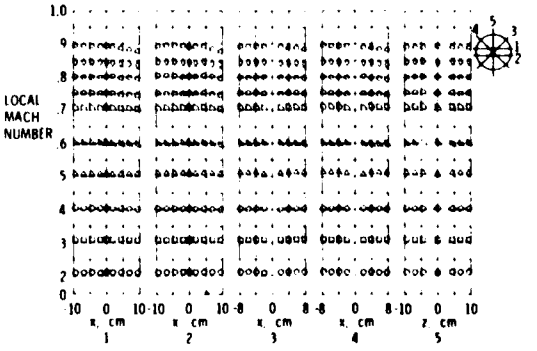

Figure 14.- Typical local Mach number distribution on model turntable.

is presented in Figure 15 as a function of M_{ref}. Data are presented for four stagnation pressures and at three stagnation temperatures at each pressure. These values of temperature and pressure include combinations which are close to the operational extremes of the tunnel. Although a large increase in the calibration factor occurs at Mach numbers above approximately 0.75, due to the previously discussed longitudinal gradient, it should be noted that there is little effect of temperature and pressure on the calibration factor. The scatter of the data is generally within an error band of about 0.001 which, it should be noted, is within the accuracy of the test instrumentation.

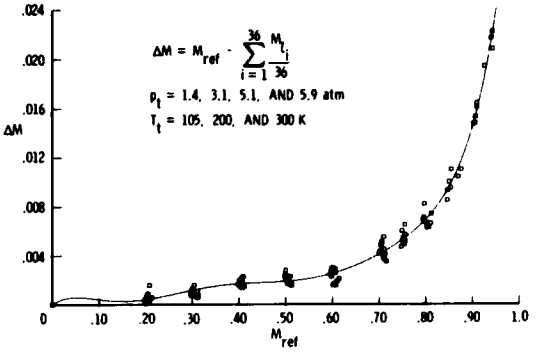

Figure 15.- Mach number calibration for two-dimensional test section.

5.2 Temperature Distribution

A typical lateral temperature distribution in the screen section of the tunnel is presented in Figure 16 for a Mach number of 0.70 and a stagnation pressure of 5.9 atmospheres. As shown on the figure, there are eight radial rows of instrumentation with three thermocouples on each row, spaced equidistant between the centerline and the wall. There is also a single thermocouple located on the centerline. Each temperature shown on the figure is the average of 185 readings of the thermocouple during a time span of 72 seconds. During this time, the tunnel was at a steady state condition and pressure data were being obtained using scanning valves. For this case, which is near the maximum Reynolds number capability of the tunnel, the average of the 25 thermocouples is 105.9 K and the standard deviation, σ, is 0.20 K. As mentioned previously, the absolute value of this temperature may be slightly in error due to the accuracy of the thermocouple wire, but the differential temperatures should be reliable.

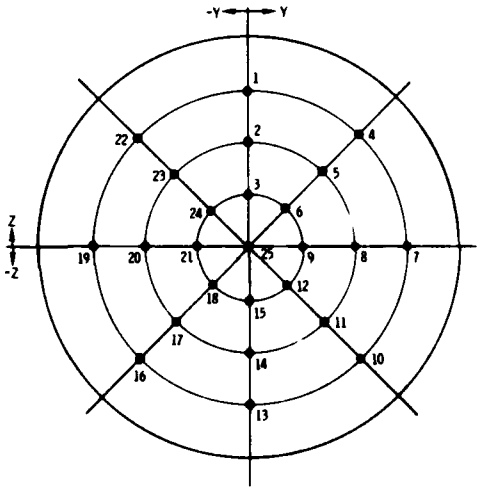

T_1	106.0 K	T_{10}	105.8 K	T_{19}	105.7 K
T_2	106.0	T_{11}	106.0	T_{20}	105.7
T_3	106.2	T_{12}	105.9	T_{21}	105.8
T_4	106.1	T_{13}	105.7	T_{22}	105.8
T_5	106.0	T_{14}	105.7	T_{23}	105.6
T_6	106.2	T_{15}	105.8	T_{24}	106.0
T_7	106.0	T_{16}	105.4	T_{25}	105.9
T_8	106.0	T_{17}	106.0		
T_9	106.2	T_{18}	105.6		

Figure 16.- Typical lateral temperature distribution.

Data such as presented in Figure 16 have been obtained throughout the operational range of the tunnel during the tunnel empty calibration process. Results, in the form of standard deviation, are presented in Figure 17 for selected Mach numbers at three different stagnation temperatures and for near minimum and maximum stagnation pressures. The results show that the variations in standard deviation of stagnation temperature in the screen section of the tunnel are less than about 0.5 K and that the results do not vary in any systematic way with either Mach number or stagnation temperature. The value of the deviation does, however, tend to be lower at the higher stagnation pressure.

	T_t, K					
	105		200		300	
	P_t, atm					
M_∞	1.4	5.9	1.4	5.9	1.4	5.9
0.20	0.51 K	0.16 K	0.49 K	0.23 K	0.12 K	0.05 K
.30	.43	.16	.50	.15	.13	.09
.40	.38	.14	.41	.12	.11	.12
.50	.31	.19	.50	.13	.24	.24
.60	.27	.21	.41	.16	.19	.31
.70	.21	.20	.35	.21	.50	.30
.80	.18	.18	.27	.19	---	---
.90	.17	---	.37	---	---	---

Figure 17.- Standard deviation of stagnation temperature survey.

6. CONCLUSIONS

Some of the aspects of selecting and using instrumentation for the calibration and control of continuous-flow cryogenic wind tunnels have been discussed and examples of instrumentation used in the Langley 0.3-m TCT have been given in this lecture. In addition, typical calibration results from the 0.3-m TCT have been described. The main conclusions to be drawn from our experience at Langley are:

(1) Adequate pressure and temperature instrumentation is commercially available to meet the requirements for calibration and control of continuous-flow cryogenic wind tunnels.

(2) The response time of high accuracy instrumentation is usually much too slow for use with automatic tunnel control systems. Thus, it may be necessary to use one set of less accurate but highly responsive instrumentation for control purposes and a separate set of highly accurate but less responsive instrumentation for the determination of the test conditions.

(3) Thermal isolation of the instrumentation from the cryogenic environment is the best way of avoiding problems related to temperature variation. However, the ancillary equipment needed for thermal isolation inevitably results in reduced reliability.

(4) Conventional flow-quality instrumentation, such as hot-wire probes, has yet to be used successfully except at extremely low speeds in the 0.3-m TCT.

(5) The use of a piezoelectric transducer to measure sound pressure levels has been demonstrated. However, because these transducers are sensitive to changes in temperature and are exposed to the cryogenic environment, they must be dynamically calibrated over the entire operational temperature range of the tunnel if high accuracy measurements are desired.

(6) For applications such as sidewall boundary layer removal systems, measuring and controlling mass flow can be realized to any desired degree of accuracy by using commercially available "digital" valves.

7. REFERENCES

1. Kilgore, Robert A.: Development of the Cryogenic Tunnel Concept and Application to the U.S. National Transonic Facility. Paper No. 2 in AGARD-AG-240, "Towards New Transonic Windtunnels." Nov. 1979, pp. 2-1 to 2-27.

2. Polhamus, E. C.; Kilgore, R. A.; Adcock, J. B.; and Ray, E. J.: The Langley Cryogenic High Reynolds Number Wind-Tunnel Program. Astronaut. & Aeronaut., Vol. 12, No. 10, Oct. 1974, pp. 30-40.

3. Goodyer, M. J.; and Kilgore, R. A.: The High Reynolds Number Cryogenic Wind Tunnel. AIAA Paper 72-995, 7th Aerodynamic Testing Conference, Palo Alto, Calif., Sept. 1972. Also, AIAA Journal, Vol. 11, No. 5, May 1973, pp. 613-619.

4. Adcock, Jerry B.; Kilgore, Robert A.; and Ray, Edward J.: Cryogenic Nitrogen as a Transonic Wind-Tunnel Test Gas. AIAA Paper 75-143, Jan. 1975.

5. Ray, Edward J.; Kilgore, Robert A.; and Adcock, Jerry B.: Analysis of Validation Tests of the Langley Pilot Transonic Cryogenic Tunnel. NASA TN D-7828, 1975.

6. Reed, T. D.; Pope, T. C.; and Cooksey, J. M.: Calibration of Transonic and Supersonic Wind Tunnels. NASA CR 2920, Nov. 1977.

7. Bynum, D. S.; Ledford, R. L.; and Smotherman, W. E.: Wind Tunnel Pressure Measuring Techniques. AGARD-AG-145-70, Dec. 1970, pp. 13-16.

8. ACKNOWLEDGEMENT

The author is grateful to NASA for permission to present this lecture and to his colleagues at the Langley Research Center for their assistance in its preparation. The author is also grateful to Mr. E. F. Germain of our Instrument Research Division for providing much of the information relative to thermocouple selection. Mr. C. L. Ladson is deserving of very special thanks, not only for his contributions to the technical content of this lecture but also for his major contribution towards producing this written version.

CALIBRATION OF A BLOWDOWN-TO-ATMOSPHERE CRYOGENIC WIND TUNNEL

by
J. D. Cadwell
Branch Chief
Wind Tunnel Test & Development
Aerodynamics Subdivision
Douglas Aircraft Company
McDonnell Douglas Corporation
3855 Lakewood Blvd.
Long Beach, Ca. 90846
USA

SUMMARY

Calibration of short duration cryogenic wind tunnels pose difficulties and requirements beyond those already present in the calibration either of conventional short run time facilities or of cryogenic continuous tunnels. The requirements and instrumentation for calibration of a transonic blowdown-to-atmosphere cryogenic wind tunnel are described, with emphasis on those aspects differing from the calibration of similar non-cryogenic tunnels. Reference is made to the literature for detailed descriptions of conventional calibration practices which remain applicable for cryogenic blowdown tunnels.

INTRODUCTION

The existing Douglas Aircraft Company four-foot trisonic wind tunnel has been calibrated on several occasions when significant changes were made to the tunnel that were considered to have an effect on the existing calibration. The modification of the present tunnel to convert the facility to one capable of operation at cryogenic temperatures is significant enough without the cryogenic consideration to warrant a tunnel calibration. The operation at the very cold temperatures however adds another dimension to the calibration of a wind tunnel. Although the calibration will cover the entire speed range capability of the tunnel this lecture will be restricted to the Mach number range that is possible with the transonic cart where cryogenic operation substantially increases the Reynolds number over that obtained at conventional non-cryogenic temperatures. It is interesting to note that the advantages of the cryogenic operation diminish rapidly as the Mach number increases and the static temperature decreases to the point where heat must be applied to prevent liquefaction of oxygen and nitrogen, the predominant gases that make up the mixture that we call air.

The scope of this lecture therefore is to present the requirements and problems associated with the calibration of intermittent cryogenic transonic wind tunnels and the methods that we consider best suited to carry out the various tasks. The emphasis is placed on those aspects of the calibration of the cryogenic tunnel that differ from the facility that operates today at temperatures that are considered ambient for a particular location. The literature, in particular Reed, et al. (Reference 1), is an invaluable guide to the calibration of conventional transonic wind tunnels and is frequently referred to in this presentation.

The short run time of the blowdown tunnel, which made it possible to modify to a cryogenic facility, does not allow thermal equilibrium to be established over either the tunnel wall or the model by merely operating the tunnel. The lack of thermal equilibrium can cause changes to the boundary layer flow along the walls that can change the tunnel calibration as a function of time during a blowdown and also as a function of the wall temperature at the start of a blowdown. The sensitivity of the flow to this potential buoyancy correction will be addressed during the course of the calibration.

Thermal non-equilibrium of the model itself also leads to undesireable aerodynamic effects. Discussion of this important problem is beyond the scope of this presentation, but a basic appreciation of the subject may be gained from Reference 2.

It is important to keep in mind with respect to the cryogenic blowdown tunnel that more questions than answers will remain until the facility is actually put into operation and the checkout and calibration are underway. The general test plan for the calibration of the Douglas Aircraft cryogenic tunnel, that will hopefully provide positive answers to the many questions, will be reviewed. The final phase of the calibration will be to obtain the data necessary to describe the flow conditions so that the necessary calibration factors can be determined, to assess the stability of the various parameters during a blowdown, and to determine the repeatability of the test conditions from a random selection of repeat blowdowns throughout the calibration.

THE FLOW PARAMETERS AND FLOW QUALITY

A test condition in a transonic wind tunnel is defined by three flow parameters. The first two are dimensionless similarity parameters, namely Mach number and Reynolds number. The third parameter, dynamic pressure or "q", is used to reduce measured aerodynamic data into coefficient form, but on its absolute value also depends the state of aeroelastic deformation and thus to a measureable degree the aerodynamic characteristics of a model. Therefore, dynamic pressure is important as well as the true similarity parameters of Mach and Reynolds numbers in defining a test point. It is the unique characteristic of the cryogenic wind tunnel that all three of these parameters can be varied independently through its ability of changing total temperature T_T.

These three flow parameters are defined by the following relations:

Mach number $M \equiv \frac{V}{a}$

Reynolds number $Re \equiv \frac{\rho V L}{\mu}$

Dynamic pressure $q \equiv \frac{\rho V^2}{2}$

Substitution and manipulation lead to the expressions used to compute these parameters using basic measured flow quantities:

$$M = \left\{ 5 \left| \left(\frac{P_T}{P_\infty} \right)^{2/7} - 1 \right| \right\}^{1/2}$$

$$R_e = 2.29 \times 10^6 \frac{P_\infty M}{T_T^2} (1+.2M)^2 \left(\frac{T_T}{1+.2M^2} \right) L$$

$$q = \frac{\gamma}{2} M^2 P_\infty$$

where

a	= sound speed
P_T	= total pressure head in settling chamber
L	= characteristic length
P_∞	= test section freestream static pressure
T_T	= stagnation temperature
V	= velocity
γ	= ratio of specific heats C_p/C_r *
μ	= coefficient of viscosity
ρ	= gas density

*Ideal gas assumptions, in particular that of $\gamma = 1.4$, have been found generally applicable at transonic cryogenic wind tunnel conditions. See References 3 and 4.

The measured quantities used to compute these test parameters are seen to be settling chamber total pressure P_T, test section freestream static pressure P_∞, and test section stagnation temperature T_T. The objectives of the calibration are to determine the calibration factors that will allow the test parameters to be reset without the special calibration equipment in place and to establish the level of uncertainty in the test conditions inferred from these reference measurements.

To be complete, calibration must include the determination of the nonuniformity in space and the unsteadiness in time of the flow. The levels of flow nonuniformity and unsteadiness are usually grouped together under the term "flow quality". These amount to disturbances which, in ways not all yet clearly understood, compromise the fidelity of the simulation. The greater the nonuniformities and unsteadiness in the flow, the worse the flow quality. Evaluation of flow quality includes consideration of the distribution of static pressure (and therefore of Mach number) and of total temperature in the clear test section, as well as of flow angularity, temperature spottiness, small scale velocity fluctuations (turbulence), and pressure fluctuations (acoustic noise). The special problem of time dependency of the buoyancy correction to be made on measured model drag must also be considered.

STATIC AND TOTAL PRESSURE

For purposes of establishing test conditions in transonic tunnels, the static pressure reference is most conveniently and commonly measured in the plenum chamber of ventilated test sections and is related to freestream static pressure through the calibration. The calibration is best accomplished by means of a long, so-called "survey pipe" extending from the settling chamber through the test section. See Reference 1 for a detailed discussion of the procedure as applied to conventional tunnels. The method is also directly applicable to blowdown cryogenic tunnels, though with the added requirement that thermal contraction be accounted for in the installation. Figure 1 presents a layout of the static pipe to be used in the calibration of the Douglas four-foot cryogenic wind tunnel.

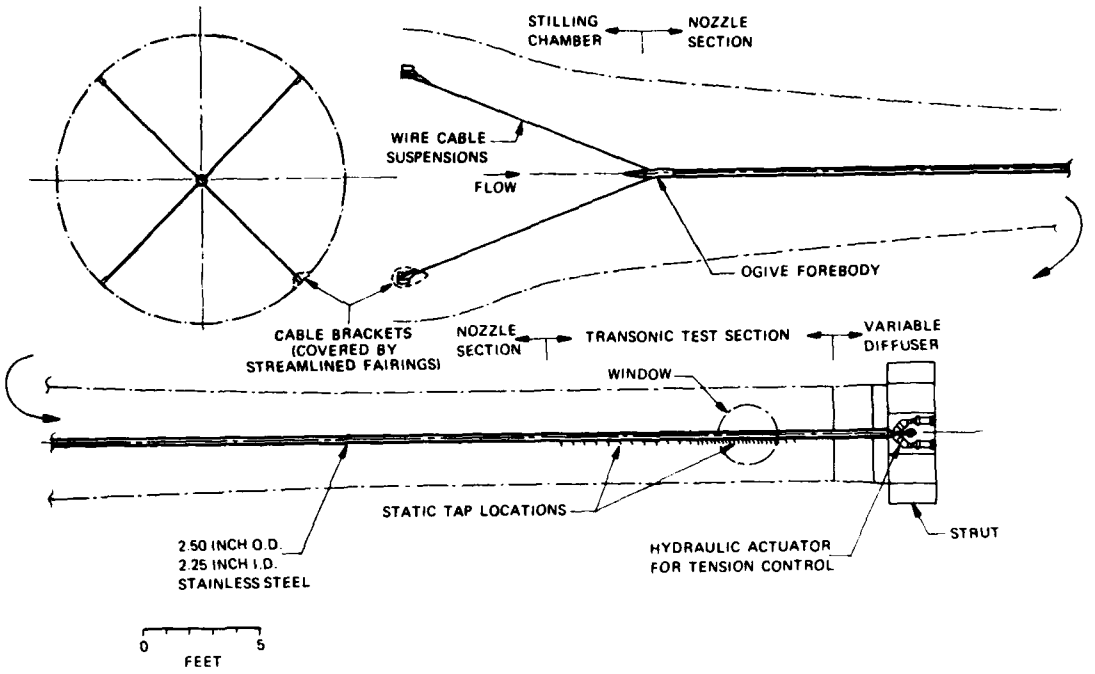

FIGURE 1. CALIBRATION STATIC SURVEY PIPE INSTALLATION IN 4-CWT

Changes in freestream static pressure are equivalent to changes in Mach number. It should be obvious that variations of this type in the region of a model are very important aspects of flow quality and must be accounted for in calibration. Indeed, respondents to a survey conducted by the authors of Reference 1 indicated that static pressure variations across the test section are often larger than the longitudinal variations on the centerline as measured by a static survey pipe. Thus, off-axis static pressure measurements seem highly desireable. The discussion of moveable static pressure probes found in Reference 1 is both very adequate and directly applicable to short run time cryogenic tunnels, so no more time will be devoted to the subject here.

The measurement and calibration of settling chamber total pressure in a cryogenic blowdown transonic tunnel also do not differ from those in a conventional facility. Again, see Reference 1 for a discussion of conventional practices. Care must be taken to avoid local influences of the flow fields associated with the injection of liquid nitrogen, if present.

TOTAL TEMPERATURE

Measurement of total temperature is required in routine wind tunnel operation to define the test Reynolds number. For this purpose total temperature is usually monitored in the stilling chamber, where velocities are low, using a high-recovery or even a simple bare thermocouple junction. Blowdown tunnels require rapid response sensors, as total temperature may change rapidly. Constant Reynolds number testing in blowdown tunnels therefore requires a continuous measurement of total temperature as an input to an automatic total pressure/temperature control system. In conventional transonic blowdown facilities the tunnel flow is usually assumed to be isentropic so that stilling chamber conditions are used to define the test Reynolds number. According to a survey conducted by Reed, et al., few conventional tunnels have been calibrated for temperature gradients which may exist along and across the flow in the test section itself.

In the case of a cryogenic blowdown tunnel, however, neither the assumption of uniform test section conditions nor that of the adequacy of measured stilling chamber conditions to define average test section conditions may be warranted. The means of producing cryogenic flow that has been adopted in currently operating cryogenic blowdown tunnel designs is direct injection of liquid nitrogen into the circuit at some point downstream of the main control valve. Mixing of the air and evaporated LN_2 may not be perfectly uniform within the stilling chamber, and therefore total temperature measurements made at points within the stilling chamber may not accurately represent the average total temperature in the test section. The differences may be expected to be repeatable, though, and can be accounted for in calibration by correlation with measured test section total temperatures.

It is very important to note that the specific method of LN_2 injection may give rise to nonuniformities in total temperature across the test section. Experience in the Douglas Aircraft one-foot blowdown cryogenic tunnel has indicated that temperature gradients produced in the LN_2 injection spray pattern do persist downstream through perforated plates and screens to the test section and are repeatable.

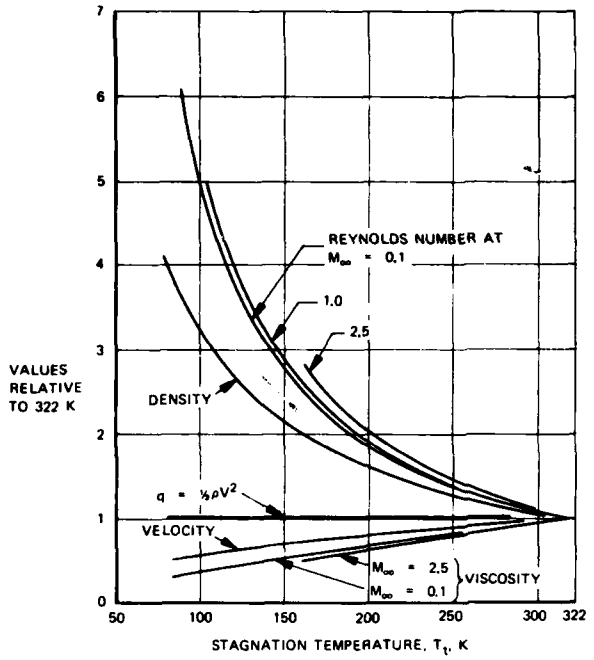

FIGURE 2 – VARIATION OF TEST SECTION FLOW PARAMETERS RELATIVE TO VALUES AT 322 K WITH STAGNATION TEMPERATURE IN AIR. CONSTANT VALUES OF STAGNATION PRESSURE, TUNNEL SIZE, AND MACH NUMBER. (FROM REFERENCE 5)

TYPICAL BARE WIRE PROBE

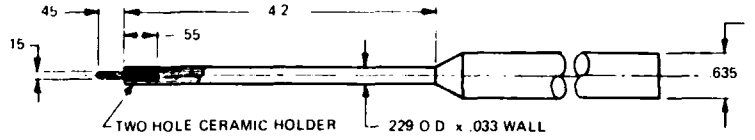

ALL DIMENSIONS IN CENTIMETERS

AEDC PWT 16T PROBE (REF. 7)

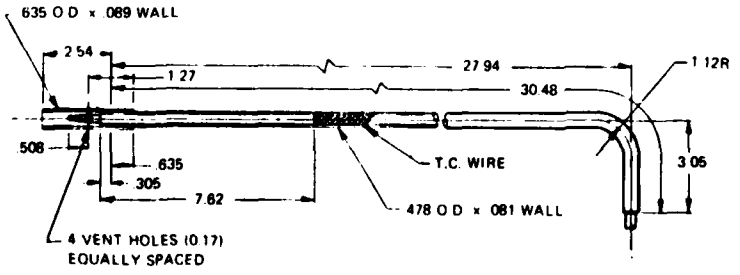

FIGURE 3 TOTAL TEMPERATURE PROBES

Variations of total temperature across the test section must be evaluated in calibration of a blowdown cryogenic facility. Serious effort must be made to achieve the best resolution possible in the test section temperature surveys. As may be seen in Figure 2, from Reference 5, Reynolds number becomes a strong function of total temperature as the temperature is reduced to the low absolute values typical of cryogenic test conditions. This means that only a few degrees variation in time or space may result in significant variations in test Reynolds number over all or part of a model. This is especially of concern, for example, in the case of configurations featuring modern supercritical airfoils, for which the shock/boundary layer interaction, not at present adequately predictable through calculation, is known to be very sensitive to Reynolds number.

A traversing probe or rake offers the most flexibility of placement in making temperature surveys, but traversing during a run does not permit observation of variations of temperature with time. Grids of thermocouples statically mounted for purposes of calibration at desired stations in the tunnel are the preferred method of surveying temperature uniformity and slow-period unsteadiness (Refs. 6 and 7). These grids may be supplemented by a moveable probe in regions where more detail is desired. Successful total temperature probe designs are presented in Figure 3, and the required calibration of probe recovery factor for Mach and Reynolds number effects is described in Reference 8.

The importance of small scale, high frequency fluctuations of freestream total temperature in cryogenic wind tunnels is still a matter of speculation, and to our knowledge has not yet been discussed in the literature. Enthalpy fluctuations with typical scales comparable to those of the energy-containing turbulent eddies can result from imperfect mixing and evaporation of injected liquid nitrogen. Associated density fluctuations will cause fluctuations in the momentum flux of the flow: this is itself not true turbulence, but its effects on the simulation are similar and as such are at least partly understood. It is hoped that scalar fluctuations in the temperature itself will have no important effects on boundary layer transition and separation processes through the resulting unsteadiness in fluid viscosity as long as these fluctuations are "small" relative to the mean total temperature, but no "acceptable" level has yet been established.

At this early point in our experience with transonic cryogenic testing probably all one can do is work to achieve the lowest attainable level of temperature fluctuations in the test section freestream, and document the amplitude and spectral characteristics as a part of the tunnel calibration. As more cryogenic facilities of all kinds come into operation, interfacility comparisons of temperature unsteadiness and test data may lead to insights comparable to those gained relatively recently into the significance of turbulence and noise as contributions to the aerodynamic characteristics of a model.

Flow temperature fluctuations can in principle be measured by means of a hot-wire probe operated in the constant current mode. Probes with ultra-fine wires for high frequency response are available. Unfortunately, more rugged hot-film probes do not offer satisfactory frequency response when operated in this mode, so that the notoriously high mortality rate of very fragile wire probes apparently must be accepted. On the other hand, only a relatively small number of measurements may be required to adequately document test section total temperature fluctuations.

FLOW ANGULARITY

Flow angularity, or deviation of freestream streamlines from the direction parallel to the tunnel centerline, is a nonuniformity which can result in very troublesome variations in flow incidence angle over a model and as such is an important aspect of flow quality. Calibration of wind tunnels of all types must include definition of flow angularity within the test section, and corrective action must be taken if it is found to be excessive.

Measurements of flow angularity in the test sections of transonic tunnels are normally made by means of a variety of probes, termed yawmeters. They fall into three general categories: (1) pressure probes, (2) force models, (3) hot wire/hot film probes. Reference 1 contains a guide to the use of these probes. In recent years laser doppler velocimetry has been used in a few cases for flow angularity calibration purposes, but application of this class of non-intrusive technique for calibration is not yet widespread. This probably should not be surprising, considering the relative expense and difficulty of setting up and operating laser doppler systems at a time when most tunnels do not have such equipment already installed for aerodynamic test measurements.*

All flow angularity calibration methods using a physical probe supported in the test section provide measurement of the incident angle of the local flow with respect to some reference direction associated with the yawmeter itself. Therefore, the accuracy of these techniques is ultimately limited by the uncertainty in the orientation of this yawmeter axis relative to the test section centerline. It is this requirement for accurate orientation of the yawmeter that poses a problem in the case of a blowdown or intermittent cryogenic facility.

The difficulty is associated with the thermal strains that may arise in the probe and especially in its support system during runs of short duration in which these structures may be exposed to very strong nonuniform cooling from the cryogenic flow. Experiments at the Douglas Aerophysics Laboratory have indicated that angular deflections arising from thermal strains are not necessarily repeatable or easily correlated. Furthermore, experiments carried out with the sting support system of the Douglas four-foot blowdown cryogenic wind tunnel have shown that even if a yawmeter and its entire support system were to be precooled to preclude thermal deformations during a run, the cold support system at its new equilibrium temperature can be expected to deflect from its attitude at room temperature. This effective zero shift also does not appear strictly repeatable and must be measured directly, but the details of the effect probably would be peculiar to each individual installation. We note in passing that attempts to correct for aeroelastic deflection of the probe/support system are complicated in cryogenic facilities by the dependence of the elastic modulus on material temperature, which may not be uniform.

It must also be pointed out that precooling to equilibrium of an entire support system may not be possible in many facilities. Likewise, combinations of heating and insulation to maintain support systems for models or flow angularity probes at uniform, predetermined temperatures may not be practical in the face of the always conflicting requirements for minimum blockage yet maximum strength.

These thermally induced deflection phenomena, collectively dubbed the "hot dog" effect at Douglas, are expected to introduce unacceptably large uncertainties into conventional flow angularity measurements in at least most short run time cryogenic tunnels, and have in fact also led to abandonment of indirect approaches to determination of the angle of attack of sting mounted models in the Douglas four-foot cryogenic tunnel.

We suggest two alternative methods for flow angularity measurement. First is a sting mounted yawmeter consisting of a cylindrical centerbody, cruciform flat plate wings and small internal force balance, as described in Reference 1, but also incorporating a means of directly measuring the angular orientation of the probe itself relative to a fixed reference, such as accelerometers or an optical two-component angle of attack system. Secondly, of course, the non-intrusive laser methods deserve consideration.

TURBULENCE AND NOISE

The importance of effects of turbulence and acoustic noise on the quality of transonic flow simulations is generally recognized and has lately been receiving increased attention. References 9 and 10 contain important discussions of the significance of flow quality and of recent insights into its characterization.

---

*The laser transit anemometer (LTA), in particular the system recently introduced by Spectron Development Laboratories of Costa Mesa, California, offers an interesting alternative to laser doppler systems, with relatively simple set-up and operation.

The usual sources of flow disturbances present in conventional transonic intermittent/blowdown tunnels are also present in their cryogenic counterparts, together with at least one important additional source: injection of liquid nitrogen into the flow. As alluded to in the previous section, imperfect mixing and evaporation of injected LN_2 can result in fluctuations of density, and thus in momentum flux, through fluctuations in total temperature. Note especially that temperature spottiness upstream of the contraction will contribute directly to an increase in the streamwise (u) component of freestream unsteadiness in the test section.

The hot wire anemometer is the accepted means of measuring turbulence in isothermal low speed flows, but its use in high speed flows, most especially in the transonic regime, is very complicated and is rarely undertaken. Unfortunately, the transonic blowdown cryogenic wind tunnel may represent the most difficult measurement environment possible from the viewpoint of hot wire anemometry.* The addition of unknown temperature fluctuations forces one to use procedures such as those of References 12 and 13, which involve operation of the wire at a series of overheat ratios, if results more detailed or quantitative than an order of magnitude indication of turbulence level are desired. These procedures require very detailed calibrations of their own, and their application within the constraint of the limited run time available in blowdown tunnels would seem difficult at best.

Thus, the use of hot wire anemometry for turbulence measurements in transonic blowdown cryogenic tunnels does not seem practical. If the fluctuating temperature level as inferred from constant current low overheat ratio hot wire measurements is "reasonably small" or spectrally distinct from the true velocity fluctuations, a reasonable estimate of turbulence levels might be obtainable by relatively straightforward constant temperature mode measurements. Of course, care need be exercised in interpreting and applying such measurements.

Laser anenometer measurements, on the other hand, avoid all of these difficulties, and are applicable regardless of temperature fluctuation level. Remembering, too, that laser methods also avoid the special difficulties of flow angularity measurement in cryogenic tunnels, the suggestion is strong that laser anemometers will prove to be very useful calibration tools for these new facilities in spite of their relative expense and complexity.

The measurement of test section pressure fluctuations (noise) in transonic blowdown cryogenic tunnels does not fundamentally differ from the problem in conventional tunnels, except for possible environmental difficulties for transducers due to low temperatures. There is at present no clear consensus regarding the correct or most appropriate method of making these measurements. The discussion of the subject in Reference 1, including consideration of standard models such as the AEDC transition cone, is entirely applicable. The approach that will be adopted in calibration of the Douglas four-foot cryogenic tunnel is that of surveys of fluctuating pitot pressure, using a probe similar to that of Figure 4, supplemented by test section wall fluctuating static pressure measurements.

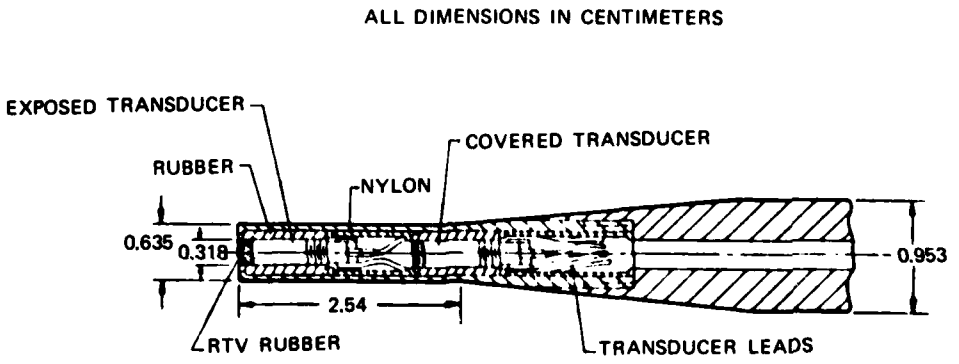

FIGURE 4. SMALL PIEZOELECTRIC DYNAMIC PRESSURE PROBE (REF. 1)

*Work at Douglas and at ONERA (Ref. 11) has demonstrated that at least some common commercially available hot film probe designs do not survive in cryogenic flow conditions, probably due to differential thermal contraction between the film and the substrate, whereas common hot wire probes seem to have no mechanical difficulties in cryogenic flows beyond those they have in room temperature flows.

BUOYANCY CORRECTION

In conventional transonic tunnel operations, the test section walls are either set at one "optimum" divergence angle or are adjusted according to a fixed schedule related to test section conditions through calibration. This procedure is based on the assumption, which is justified in conventional tunnels, that the wall boundary layer displacement thickness distribution and the resulting buoyant force increment on the model is repeatable if not actually constant over all test conditions.

The displacement thickness of a turbulent boundary layer and in particular its rate of growth is strongly influenced by heat transfer between the boundary layer and the wall. While conditions at the walls of a conventional blowdown tunnel are more or less repeatable even if not strictly adiabatic because temperature is in effect a dependent variable, this will not be true in a cryogenic blowdown tunnel, in which total temperature of the flow is itself an independent variable. As was pointed out by J. E. Green in Reference 2, this makes buoyancy correction a function of the test temperature, a situation which would by itself greatly compound the problem of calibrating the effect even if it were repeatable. However, the effect is not expected to be strictly repeatable since the tunnel wall temperature and thus the heat transfer rate will change during the course of a cryogenic run, the entire tunnel structure will change in average temperature over a series of runs, and the test section walls in the vicinity of the model may be subjected to varying amounts of cooling as the model is precooled prior to a run, depending on the method used.

Accounting for this effect with its complicated dependencies by simple calibration does not seem practical. It may of course be entirely eliminated by either precooling the entire tunnel circuit to achieve the adiabatic wall condition or by implementing fully adaptive test section walls. Neither of these approaches seems practical, either, though the second alternative is certainly attractive for its own sake. One may hope to find a simple correlation between the magnitude of the effect and some easily measured parameters, such as the difference between two longitudinally spaced wall static pressures, which would allow satisfactory correction. At worst it may be necessary to include direct surveys of the test section boundary layer in the routine set of tunnel parameters recorded in a run.

It must be appreciated that the magnitude of this effect is potentially large. Green has estimated, for the case of a square test section with solid walls adjusted for zero longitudinal pressure gradient at adiabatic conditions, that measurement of model drag coefficient to an accuracy of .0001 (one "drag count") by means of an internal force balance requires that

$$\frac{\Delta T}{T_T} < 0.2\ (1-M^2)$$

where ΔT is the difference between the wall temperature and its adiabatic value. One can see this suggests that at transonic Mach numbers the tunnel walls should be within only a few percent of adiabatic recovery temperature. While this result cannot be expected to be very accurate for the realistic case of slotted or perforated transonic test section walls, it does point out the necessity of evaluating this effect in the calibration of blowdown cryogenic wind tunnels. The seriousness of the effect and what, if any, measures are to be adopted to account for it will depend on the operational procedures, structural characteristics, and data accuracy requirements of each individual tunnel.

It should also be noted that the effect is not only common to all blowdown and intermittent cryogenic facilities, but will even be encoutered in continuous cryogenic tunnels following step changes in total temperature.

CHECKOUT OF DAC 4-CWT

The completion of the design, fabrication, and assembly of the tunnel signifies the start of the checkout phase of the tunnel which will be followed by the calibration and then the verification of the modified tunnel.

The checkout of the tunnel discussed here assumes that all of those checks that could have been made without actually blowing air have been completed and we are to a point where we are ready to make blowdown checkouts.

The first checkout will be to verify that the control of the tunnel flow is operating properly at normal "un-cooled" temperatures. Subsystems such as the plenum auxiliary suction system and the ejectors must operate as they had before the modification. New systems such as the steam injector and the tunnel purge system can be operated and checked out with ambient temperature runs.

When all of the elements of the tunnel operation have been verified as working properly at the normal operating temperatures the checkout of the systems that vary and control the temperature down to 180° Rankine will be investigated. A cursory check of the temperature distribution will be made with several thermocouples attached to the support strut that will hold the downstream end of the calibration pipe when it is installed for the tunnel calibration phase.

The checkout of the tunnel at cryogenic temperatures will verify the satisfactory operation of all systems throughout the Mach number and temperature ranges including a check of the exhaust plume control, liquid nitrogen injection system, and temperature stabilization. The temperature of the primary structure will also be observed.

CALIBRATION OF DAC 4-CWT

The hardware of the Douglas Aircraft 4-CWT between the storage tanks and the test section is considerably different than the 4-TWT that was in operation up to 1976. The conrol valve, the injection chamber, the perforated plate in the wide angle diffuser, the acoustic straightener vanes, and the honeycomb are all new. In addition to the new hardware, the added feature of being able to operate the tunnel down to 180° Rankine substantially increases the performance envelope of the facility. The primary purpose of the calibration will be to determine for the expanded operating envelope the Mach number distribution in the test section and the plenum chamber calibration factor, required to set Mach number during future test programs when the static pipe will not be installed in the tunnel. The instrumented static pressure pipe discussed earlier will be installed to obtain the tunnel centerline Mach number distributions. In addition, a sidewall strip with several static pressure orifices will be installed to obtain correlation data between tunnel centerline and the test section wall. The sidewall data will provide useful information regarding Mach number distributions in the test section without re-installing the centerline static pipe.

The static survey pipe will be removed when adequate Mach number distributions are obtained and the support strut and pod will be installed. A thermocouple rake will be attached to the pod and the temperature distribution in the test section will be determined. At this point the temperature distribution should be reasonably good since it will be tuned to a first order approximation during the checkout phase of the tunnel. Final tuning and documentation of the temperature distribution will be accomplished with the thermocouple rake during this phase of the calibration.

Pitot and yaw head probes will be installed in the test section after the thermocouple rake is removed and flow angularity measurements will be made using a four-hole yaw probe assembly. An integrated vertical flow angularity measurement will be made when the DC-10 model is tested in upright and inverted attitudes during the verification test program.

In addition to the Mach calibration, and determining the temperature distribution and flow angularity a fourth measure of the quality of the tunnel flow is the magnitude and frequency of the flow fluctuations. During the checkout and calibration phases, dynamic pressure data will be obtained from transducers installed in the walls of the settling chamber and test section.

Boundary layer rakes will be installed along the walls of the test section in order to determine the variations in displacement thickness for correlation with the Mach number distributions as effected by the heat transfer from the warm wall to the cold air stream as a run progresses.

Other instrumentation that are being discussed for inclusion in the calibration are as follows:

a) A fixed thermocouple grid in the test section to provide a complete temperature distribution as well as an indication of the slow period unsteadiness.

b) Constant-current hot-wire probes to be mounted on a rake to evaluate temperature spottiness.

c) Constant-temperature hot-wire probes on a rake to attempt to evaluate the turbulence level in the test section.

d) Fluctuating pitot pressure probes to be correlated with test section and settling chamber wall microphones in order to evaluate pressure fluctuations or noise in the test section.

Although there is considerable laser work being applied to fluid mechanic problems at Douglas Aircraft there are no firm plans to apply this technology to the cryogenic tunnel at this time. It is recognized, however, that the application of laser technology to flow angularity and turbulence measurements in the cryogenic tunnel will be a natural outgrowth of the work that is being applied to conventional wind tunnels.

CONCLUDING REMARKS

In conclusion, we state the obvious: a fundamental requirement for accurate test data is accurate and complete knowledge of the test conditions. Nevertheless, it is a sad fact, well known to the operators of many important wind tunnel facilities, that calibration often has not received the full attention, time, and resources it requires. Certainly in the case of high Reynolds number cryogenic tunnels of all types, with all their special problems and requirements and in the face of demand for better data accuracy, it is imperative that accurate and comprehensive calibration (along with the associated concern of high flow quality) receive both thoughtful attention and high priority if the promise of greatly improved full scale performance prediction is to be realized. It is hoped that this presentation has pointed out at least some of the potential pitfalls to be faced.

REFERENCES

1. T.D. Reed, T.C. Pope, J.M. Cooksey — Calibration of transonic and supersonic wind tunnels. NASA Contractor Report 2920 (1977)

2. J.E. Green, D.J. Weeks, P.G. Pugh — Heat transfer to model or test section as a source of spurious aerodynamic effects in transonic wind tunnels. Paper No. 26 in Proceedings of First International Symposium on Cryogenic Wind Tunnels (1979)

3. R.A. Kilgore, J.B. Adcock, E.J. Ray — Flight simulation characteristics of the Langley high Reynolds number cryogenic transonic tunnel. AIAA Paper No. 74-80 (1974)

4. B. Wagner, W. Schmidt — Theoretical investigations of real gas effects in cryogenic wind tunnels. Dornier-System G.m.b.H. Theoretical Aerodynamics Group (1976)

5. R.A. Kilgore, M.J. Goodyer, J.B. Adcock, E.E. Davenport — The cryogenic wind-tunnel concept for high Reynolds number testing. NASA TN D-7762 (1974)

6. R.A. Kilgore — Design features and operational characteristics of the Langley pilot transonic cryogenic wind tunnel. NASA TM X-72012 (1974)

7. G.D. Robson — Test section temperature calibration of the AEDC PWT 16-ft transonic tunnel at stagnation temperatures from -30 to 30°F. AEDC-TR-69-2 (1969)

8. T.M. Stickney — Recovery and time response characteristics of six thermocouple probes in subsonic and supersonic flow. NACA TN 3455 (1955)

9. J.P. Hartzvicker, P.G. Pugh, W. Lorenz-Meyer, G. E. Fasso — On the flow quality necessary for the large European high-Reynolds-number transonic tunnel LEHRT. AGARD-R-644 (1976)

10. D.G. Mabey — Flow unsteadiness and model vibration in wind tunnels at subsonic and transonic speeds. R.A.E. C.P. No. 1155 (1971)

11. F. Liousse, P. Calvet, A. Giovannini — Experimental study of thermoresistive sensors under cryogenic conditions. Paper No. 4 in Proceedings of the First International Symposium on Cryogenic Wind tunnels (1979)

12. C.C. Horstman, W.C. Rose — Hot wire anemometry in transonic flow. NASA TM X-62,495 (1975)

13. W.C. Rose, E.P. McDaid — Turbulence measurement in transonic flow. Proceedings of AIAA 9th Aerodynamic Testing Conference, pp. 267-271. (1976)

ACKNOWLEDGEMENTS

The major thrust and research for this lecture was accomplished by a fellow co-worker at the Douglas Aircraft Company, Mr. Michael F. Fancher, who is preparing a Douglas paper on this important subject of calibrating a cryogenic wind tunnel. I am truly grateful that this work was available and could be included in this lecture series on cryogenic wind tunnels.

THE DEVELOPMENT OF A CRYOGENIC WIND TUNNEL DRIVEN BY INDUCTION : FLOW CONTROL AND INSTRUMENTATION STUDIES IN A PILOT FACILITY AT ONERA/CERT

R. Michel
Chief, Aerothermodynamics Department
ONERA, Centre d'Etudes et de Recherches de Toulouse
31055 - TOULOUSE, FRANCE

SUMMARY

A new solution for an intermittent cryogenic wind tunnel, using high pressure air as a driving gas and nitrogen as cooler, is being studied at the ONERA Toulouse Research Center. The contemplated application is the cryogenization of the transonic injector driven tunnel T2, the project of which is presented in a second lecture.

The experimental studies have been carried out till now on a pilot unit, a pressurised return circuit wind tunnel with a 10 x 10 cm test section which is about the 1/4th scale of T2.

Systematic investigations on the various problems related with the control and optimization of short cryogenic runs of an I.D.T. as well as with experimental techniques, have been carried out and are summarized in this paper.

RESUME

Une solution nouvelle de soufflerie cryogénique à rafales, utilisant l'air à haute pression comme gaz moteur et l'azote liquide comme réfrigérant, est étudiée depuis quelque temps au Centre de Recherches de l'ONERA à Toulouse. L'application envisagée est la cryogénisation de la soufflerie transsonique à induction T2 dont le projet est présenté dans une deuxième communication.

Les études expérimentales ont été menées jusqu'ici sur une installation pilote ayant un circuit à retour pressurisé ; avec une veine d'essai de 10 x 10 cm de section, elle représente sensiblement l'échelle 1/4 de la soufflerie T2.

Des recherches systématiques sur les différents problèmes liés au contrôle et à l'optimisation d'une soufflerie à induction fonctionnant par rafales cryogéniques, aussi bien qu'aux techniques expérimentales, y ont été effectuées et sont présentées dans cet article.

1. INTRODUCTION

Among various European projects for a transonic wind tunnel in which should be attained or approached the flight Reynolds numbers, ONERA proposed a few years ago a project for an induction driven tunnel. We then built an adjusted the injector driven transonic wind tunnel T2, which is operating since 1975 at the Toulouse Research Center. With a test section of 40 x 40 cm and a pressure which can reach 5 bars, it is about the 10th scale model of the Large European High Reynolds Number Tunnel project proposed at that time by ONERA.

A very different solution is considered now, which consists in increasing the Reynolds number by means of an important diminution of the flow temperature. The interest of the crogenic wind tunnel is of course to obtain high Reynolds numbers in quite smaller test sections. Its inconvenience is that the cooling of whole circuit and test section walls as well as models may bring serious technological problems.

In order to avoid or reduce these problems, a simple idea was to combine a cryogenic test with an induction one, in the hope that the short duration of the flow would give a diminution of the temperature in the walls superficial part, whereas most part of their thickness remained at ambient or nearly ambient temperature.

The contemplated application is a cryogenization of the T2 wind tunnel in which could be obtained already interesting values of the Reynolds number.

Systematic investigations carried out on a pilot facility have shown the interest and the feasibility of such a solution. The main results or conclusions obtained in the study of various problems related with a short cryogenic run operating of an injector driven tunnel, are reviewed under a summarized form in the following paragraphs.

2. THE CRYOGENIC INJECTOR DRIVEN TUNNEL CONCEPT

2.1. Theory of Ejectors ; Influence of Driving Gas Temperature

The injector driven wind tunnel uses the principle of injecting high-pressure air to drive the air-stream in the tunnel. It includes a supersonic ejector, supplied by a source of compressed air, and placed within the flow at a convenient location downstream of the testing chamber. The jet (j) emitted by the ejector mixes with the driven flow (1) in a mixing chamber, from where both flows emerge in a theoretically uniform state (m).

The basic equations for the conservation of mass, dynalpy and energy in stationary conditions are given in figure 1.

The flows are assumed to be uniform, losses due to wall friction being included in the over-all evaluation ; p_i and T_i are respectively the total pressure and total temperature ; the increase from p_{i1} to p_{im} has to compensate the total pressure loss of the tunnel circuit.

By making use of the isentropic flow relations, these equations can be reduced to a system involving 8 unkwowns ; for example, if the characteristic parameters of the injected and induced flow are given :

$\lambda = 1/\mu$: area ratio

M_1 : induced flow Mach number

M_j : injected flow Mach number

p_{ij}/p_{i1} : total pressure ratio

T_{ij}/T_{i1} : total temperature ratio

One can deduce the other four parameters defining the drive system efficiency :

q_1/q_j : mass flow ratio

p_{im}/p_{i1} : pressure ratio provided by the drive system

T_{im}/T_{i1} : temperature ratio

M_m : uniform flow Mach number after mixing

A thorough discussion of the performances of an injector drive system based on the previous equations and parameters has been previously presented by P. Carrière[1]. It was so possible to choose, among numerous configurations, a reasonable compromise between the desired high efficiency and the aerodynamical or technological problems.

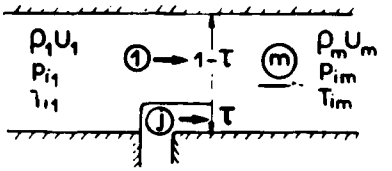

$$(1-\tau)\rho_1 U_1 + \tau \rho_j U_j = \rho_m U_m$$

$$(1-\tau)(p+\rho U^2)_1 + \tau (p+\rho U^2)_j = (p+\rho U^2)_m$$

$$(1-\tau)\rho_1 U_1 T_{i1} + \tau \rho_j U_j T_{ij} = \rho_m U_m T_{im}$$

FIG. 1 : THEORY OF EJECTORS : BASIC EQUATIONS

For T2 as well as for its pilot rig T'2, the driven flow Mach number in nominal conditions (Mach number 0.9 in the test section) has been choosen to be $M_1 = 0.6$, the jet Mach number being $M_j = 1.6$.

A area ratio λ from 20 to 30 gave a satisfactorily compromise for a good efficiency of the entrainment and a sufficiently moderate pressure ratio p_{ij}/p_{i1}.

In the case of a cryogenic operating, an additional and very important parameter is the difference between temperatures of the driven and the injected flow, or their ratio $t = T_{ij}/T_{i1}$.

In a first configuration, we tried to get a cryogenic flow in T'2, by injecting through the first corner vanes, a driving fluid previously cooled down to 100°K. Such a test did not give satisfactory results, not only for temperature in the test section, but also for the entrainment mass flow rate, quite lower to the one we had at room temperature induction.

Such a loss of performance can be easily explained if we consider in the ejector's theory equations the influence of the temperature ratio.

Figure 2a, shows the results obtained by solving these equations, as concerns the pressure ratio provided by the drive system as function of the mass flow rates ratio, at different values of the jet to driven flow temperature ratio. It is obvious that the provided total pressure increases appreciably with the injection temperature.

Figure 2b, gives the influence of the temperature upon the jet to driven flow pressure and mass flow ratios, required to compensate a 10 % total loss (a conservative value for a test section Mach number of the order of 0.9). It is clear that the flow rates ratio increases considerably with the temperature ratio, while jet total pressure remains practically constant.

2.2. The Pilot Wind Tunnel T'2 and its Operating Method

A diagram of T'2 wind tunnel is shown in figure 3 ; it allows to underline the main characteristics hold in our injector driven tunnel solution.

A first characteristic aspect is that the driving injection is provided through the trailing edges of the two vanes of the first corner, after the test section ; so the injection involves 2 jets which rapidly mix with the induced flow ; the injection Mach number is $M_j = 1.6$; the area ratio between the mixing cross section and the injector exit section is $\lambda = 20$.

Another typical aspect is that the flow removal is located just upstream of the injector ; taking advantage of the pressure level in the wind tunnel, it is simply performed through the porous walls of a rectangular cross section duct, acting as a diffusor after the test section. So the injector has to drive only the difference between the mass flow in the test section and the removed mass flow.

The test section, 0.1 x 0.1 m^2 dimensions, equiped with solid walls for the tests we present, and a sonic second throat on the rear of the test section gives about 0.8 Mach number.

The favourable influence of a jet temperature superior to that of the driven flow dictated the operating method for the cryogenic functionning ; it consists in having as usual the driving gas induction process at room temperature, then cooling the flow with a quick supply of liquid nitrogen in the return circuit.

The diagram of such device is also shown in figure 3. It includes a liquid nitrogen tank, with regulated pressure insuring the required rate ; this tank supplies an injection device which was made in a first configuration of two tubes perforated with many holes placed perpendicularly one to the other in the return circuit section.

The second main aspect of the cryogenic adaptation is that, contrarily to the continuously running cryogenic wind tunnel for which there can be an external insulation, an internal insulation appeared preferable very soon. For the short flow duration considered a thin insulating layer appeared as sufficient to ensure a good thermal protection.We simply lined the inside of the circuit, as well as the four test sections walls with a 3mm thick cork layer

The efficiency of an internal thermal insulation can be shown by means of even approximate calculation of the aerodynamic heat flux transmission inside the material forming the wall. We therefore established a heat transfer calculation method using the equations of radial heat transmission through a wall submitted to a quickly decreasing temperature flow on its internal side.

An example of the results obtained by this calculation is shown on figure 4. Two configurations are considered :

- Test section (M = 0.8) : aluminium wall 15mm thick lined with a 3mm cork layer,
- second throat (M = 1) : non-insulated steel wall, 15mm thick.

For the test section, the very small conductibility of the insulating material gives rise to considerable temperature gradients in its thickness ; temperature at cork metal junction does not change practically, whereas temperature on the internal walls comes quickly to a value near the flow one. Within the running time of the order of 30 seconds to be considered, we have in fact a regime of heat transfer sufficiently low for the boundary layer to be near adiabatic conditions.

For the non-insulated throat, the whole wall suffers an appreciable cooling but the internal wall temperature remains a lot higher than the flow one. We then record a quite considerable heat flux indicating therefore a very important thermal loss.

Despite the simplicity of the experimental device, we very quickly obtained results showing that it is possible to get temperatures to 100°K and below. It seemed reasonable to aim at a stagnation temperature of 120°K for a Mach number, 0.8 in the test section.

In figure 5, we therefore present an example of variation, in time, of stagnation temperature measured during the flow in the test section. We also give the liquid nitrogen mass flow necessary for the test.

The wind tunnel being started with a room temperature induction, the instant t = 0 corresponds with the liquid nitrogen injection. Immediately we observe a quick decrease of the temperature, which comes to 120°K in 6 to 8 seconds. It is to be noted that "this settling time" could be reduced by increasing the nitrogen flow during the initial period.

Figure 5 also shows the variation of the total pressure and Mach number as well as the injected flow rate and flow rate in the test section.

It can be seen that the total pressure, settled first at 1.8 bars, increases with the nitrogen liquid injection to 2.2 bars, then decreases a little during the flow "said settled".

The Mach number does not vary much during the nitrogen liquid injection and quickly becomes constant.

The driving jet mass flow, determined by the p_{ij} pressure imposed, remains constant, whereas the mass flow in the test section is almost doubled. This confirms therefore the increase of performance that brings the increase of the jet to driven flow temperatures ratio.

3. MEASUREMENT TECHNIQUES

Various measurement techniques have had to be implemented for qualifying as precisely and completely as possible our cryogenic flows characteristics, and for preparing the experimental studies to develop in cryogenic facilities.

They are concerned not only with permanent flows, established in pressure and temperature, but also with unsteady phenomenons, occuring obviously in the tunnel starting process, or more generally with transient flows which can appear in cryogenic wind tunnels when changing the test conditions.

3.1. Temperature Measurements

The platinium resistances which represent a precise mean for measuring temperatures have obviously a response time much too long for our purposes ; they have been used only in particular conditions, mainly as a control of other temperature measurement techniques.

Cupper-Constantan thermocouples with 1/10 to 2/10 mm diameter wires have been used for measuring the total temperature in established regime ; we must underline that special cares and a somewhat long time have had to be spent for their calibration and adjustment.

Thin foil thermocouples have proved to have sufficiently short response time for measuring temperature in some transient flows, notably to obtain a good determination of the temperature evolution during the starting process.

In order to control the frequency bandwidth of these thermocouples a spectral analysis of the thermal turbulence at the entrance of the test section has been performed with each of them.

By comparison with cold wire results a cut frequency situated between 3 and 10 hertz is clearly observed in the spectra (figure 6), depending on the size of the sensitive element.

The coldwire technique, allowing measurements at several hundred hertz, finally appeared as the only way for measuring temperature fluctuations, and was used also for studying the temperature front propagation in the dynamic tests reported thereafter.

3.2. - Pressure Measurements

Breafly speaking, two methods have been developped for pressure measurements.

The simplest one was to measure only the average pressure, with a bandwidth of a few hertz, by mean of a pitot probe and a transducer working at ambient temperature.

We also tested fast response time Kulite transducers in cryogenic environment, and observed a satisfactory behaviour (figure 7). In static calibration, they present a good linearity of the outpout tension as function of pressure for all temperatures. The sensitivity increases at low temperature, but is sufficiently well defined to permit a valuable pressure measurement when the transducer temperature is known.

Kulite transducers measuring the pressure at the test section walls, have been tested also dynamically in the natural pressure fluctuations of the cryogenic flow (figure 7). In a first device, a very small volume between the flow and the transducer sensitive element let this one work at low temperature. In a second mounting a more important cavity is involved and the sensitive element remains at a practically ambient temperature.

It can be observed on figure 7, that the frequency answer strongly depends on the size of the cavity.

4. EXPERIMENTAL DEVELOPMENTS AND VALIDATIONS

Systematic investigations on various problems related with control and optimization of the short cryogenic runs operating of an Injector Driven Tunnel, have been carried out with the pilot facility T'2, having especially in view to determine the best solutions for a cryogenic adaptation of the wind-tunnel T2.

The main points can be summarized under the following headings :

4.1. Liquid Nitrogen Supply Studies

Two types of liquid nitrogen injection system could be chosen : either a pump system drawing nitrogen directly from a storage tank and pushing it into the tunnel, or a pressurised tank system regulated by a supply pressure.

The second solution having been taken up for its greatest simplicity, the danger was a priori that a loss of efficiency could be produced by the storage at high pressure, due to the increase of temperature and diminution of latent heat which are obvious if we consider the diagram enthalpy-temperature of nitrogen at equilibrium.

In fact, a number of measurements made in the injection device showed that the change of liquid state to higher pressures is a slow and non homogeneous phenomenon. It could be verified for example, that the pressure rise produced in the tank by the vaporisation due to wall heat transfer is not at all accompanied by an increase of the temperature which stays in fact well below the equilibrium value.

Therefore the pressurised nitrogen injection appeared as a very convenient solution, the only condition being that the pressurization is done in a reasonably short time.

4.2. Tunnel Capabilities. Nitrogen Consumption

Most of the tests have been done at nominal conditions involving a test section Mach number of the order of 0.8, a total pressure around 2 bars, and a total temperature of 100 to 120°K.

The preliminary tests of which an example was shown on figure 5, gave a first order of magnitude of the mass flow rates necessary to drive the air flow.

The driving jet mass flow which remains constant during the whole run was about 0.8 kg/s, while the nitrogen mass flow was about 1 kg/s. The exhaust rate in established flow is the sum of the two mass-flow rates.

The test section mass flow is around 4 kg/s at ambient temperature operating ; it is almost doubled when the liquid nitrogen is injected, this confirming the important increase of the entrainment ratio q_1/q_j.

Various adjustment tests, carried out notably in the aim of reducing the nitrogen consumption, confirmed the strong influence of thermal insulation. In the preliminary tests, only a partial internal insulation was available, the collector, the second throat, the corners vanes having not yet been insulated.

It is seen on figure 8 that a complete insulation brought a noticeable gain on the nitrogen consumption. Moreover the total thermal loss of the circuit remains much more constant during the run, this avoiding or facilitating the nitrogen mass flow regulation necessary to have a constant temperature.

A few tests at different temperatures have been carried out also, and have shown that it is easy to establish the flow at various temperature levels, between 100 to 120°K and ambient.

The curve on figure 8 gives the test section to nitrogen flow rates ratio as function of the total temperature : it is of the order of 10 at nominal operating, T_i = 120°K.

4.3. Flow Quality : Influence of Nitrogen Injection

The studies carried out in T'2 have shown particularly that the nitrogen injectors configuration and their location in the aerodynamic circuit, are very important parameters, influencing considerably the uniformity and the quality of the flow in the test section.

4.3.1. Test Section Flow Uniformity

At the beginning, we used a liquid nitrogen injector simply constituted of two tubes perforated with many holes, and placed perpendicularly one to the other in the middle part of the low-velocity return circuit. This did not give satisfactory results as concerns the test section flow in which noticeable transverse temperature gradients were registered, and an effect of gravity of the liquid nitrogen droplets produced at injection was suspected.

This gravity effect could be effectively pointed out by special tests, in which we used two spray nozzles welded onto an horizontal stainless steel tube where the direction of the nitrogen spray could be adjusted. This is shown in figure 9 where is also presented the vertical temperature gradient measured in the test section for various angles given to the injection spray bar ; as it can be seen the influence is very important and the temperature uniformity does not correspond with the zero angle.

This led to an adaptation of the injection tubes for which the suppression of the lower branch, and a convenient distribution of the holes finally permitted to obtain, as shown in figure 9, a reasonably good transverse uniformity of temperature.

4.3.2. Temperature and Pressure Fluctuations

The nitrogen injectors configuration also proved to have a considerable influence on the flow characteristics fluctuations.

Using the cold wire technique, temperature fluctuations have been measured at the exit of the stilling chamber and for a few tests in the test section flow.

Examples of results are shown in figure 10.

With the first injection configuration (A), important fluctuations were registered, the total temperature fluctuating of several degrees aroundits means value. Complementary measurement made along the circuit, between the injection section and the stilling chamber, showed in evidence the direct effect of nitrogen vaporisation on this temperature fluctuation.

A second configuration (B) was carried into effect in the aim of avoiding vaporisation effects to be yet experienced in the test section by improving the vaporisation process at injection and by increasing the distance between nitrogen injection and test sections. It consists in a peripherical LN2 injection, performed by a series of spray nozzles, at located at the exit of the mixing chamber which follows the driving air injection corner.

It can be seen on figure 10 that this second configuration led to a much lower temperature fluctuation.

Using the fast response time Kulite transducers, pressure fluctuations and their spectra in a large frequency bandwidth have been also measured, at the test section wall. Very encouraging results were obtained, showing in fact that the fluctuation and the spectrum measured in cryogenic operating are practically identical with those observed at ambient temperature.

4.4. Dynamic Tests Related with Cryogenic Wind Tunnels Controls

A series of experiments on unsteady cryogenic flows have been carried out in the pilot facility T'2.

On one hand, it was obviously very important to collect experimental results on the tunnel behaviour in order to define the transfer functions of a cryogenic IDT circuit, for validly designing the control system to be used in flow regulation.

On the other hand, it appeared that the facility was able more generally to give interesting experimental informations for controlling transfer functions and mathematical models used to simulate the dynamics of cryogenic wind tunnels.

Related with the problem of changing test conditions and predicting transient times between test points in the European Cryogenic wind tunnel, E.T.W., we have been led to perform an experimental study on the effect of a variation of the liquid nitrogen mass flow, on flow pressure and temperature as well as on wall heat transfer.

The most important observations, of which an example is given in figure 11, concerned the flow temperature.

In this example, a quick and important change of the nitrogen flow rate is produced by closing and re-opening the liquid nitrogen tank valve for a short time (less than the time taken by the flow to cover the circuit length, τ = 0,5s).

It is observed clearly that a temperature front is created, which propagates in the circuit about at the stream velocity. It seems to diffuse longitudinally, the amplitude decreasing sensibly as function of time and distance along the circuit.

5. THEORETICAL STUDIES : PREDICTION METHODS

Parallelaly to the experimental studies, it has been proved very useful to establish methods of calculation which permit to have a theoretical estimation of the flow characteristics, in order to predict, therefore to optimize the cryogenic operating of the Injector Driven Tunnel.

A first and very important problem is concerned with thermal losses on which depends to a large extent the nitrogen consumption. We therefore established and applied systematically calculations methods using the unstationary equations for radial heat transmission through a wall submitted on its internal side to a quickly varying temperature flow.

The convective heat transfer was formulated with the hypothesis of a turbulent boundary layer. The main practical problem in fact remained to know what are exactly the thermal characteristics of the materials.

Joined to the flow calculation methods presented thereafter, these heat transfer calculations led to a good prediction of liquid nitrogen consumption, as it can be seen by comparison with experiments in figure 8.

Special efforts have been paid moreover to establish calculations methods which permit to predict the flow characteristics, in transient operating as well as in established conditions. We briefly present the principle of two methods of which the basic equations are given in figure 12.

The first one is an exact unstationary method, using the hypothesis of one-dimensional flow, and based on the resolution of the three unstationary equations describing the evolution of mass flow, dynalpy and energy. Its interest is to give the evolution of the flow characteristics, pressure, temperature, mass flow, as function of time and distance along the circuit ; it has been used especially in the analyzis of the dynamic tests results.

The second method is a global "pseudo-stationary computation" for which the preceding equations are integrated along the circuit length. Very simple and easy to use, it gives only the mean values of pressure, mass flow, temperature, as function of time, and cannot simulate the propagation along the tunnel.

A typical cryogenic run is compared in figure 13 with the global computation ; it shows a very reasonable agreement for temperature and pressure for the starting process as well as for the established flow.

Figure 14 comes back to the dynamic tests involving a change in Nitrogen flow rate ; it shows that the unstationary method leads to a fairly good representation of the temperature front propagation.

REFERENCES

1. Carrière P. — *The Injector Driven Tunnel.* AGARD Lecture Series on Large Transonic Wind Tunnels ; AGARD Report R-600, 1973.

2. Michel R., Faulmann D. — *Preliminary Tests in a Cryogenic Transonic Wind Tunnel Driven by Induction.* SUPERSONIC TUNNEL ASSOCIATION, El Secundo (Calif. U.S.A.) 17-18 April 1978.

3. Blanchard A., Faulmann D. — *Progress Report on a Cryogenic Transonic Wind Tunnel Driven by Induction.* First International Symposium, CRYOGENIC WIND TUNNELS, Southampton (G.B.) 3-5 April 1979.

4. Mignosi A., Archambaud J.P. — *Prediction of Thermal Losses and Transient Flows in a Cryogenic Wind Tunnel.* First International Symposium, CRYOGENIC WIND TUNNELS, Southampton (G.B.) 3-5 April 1979.

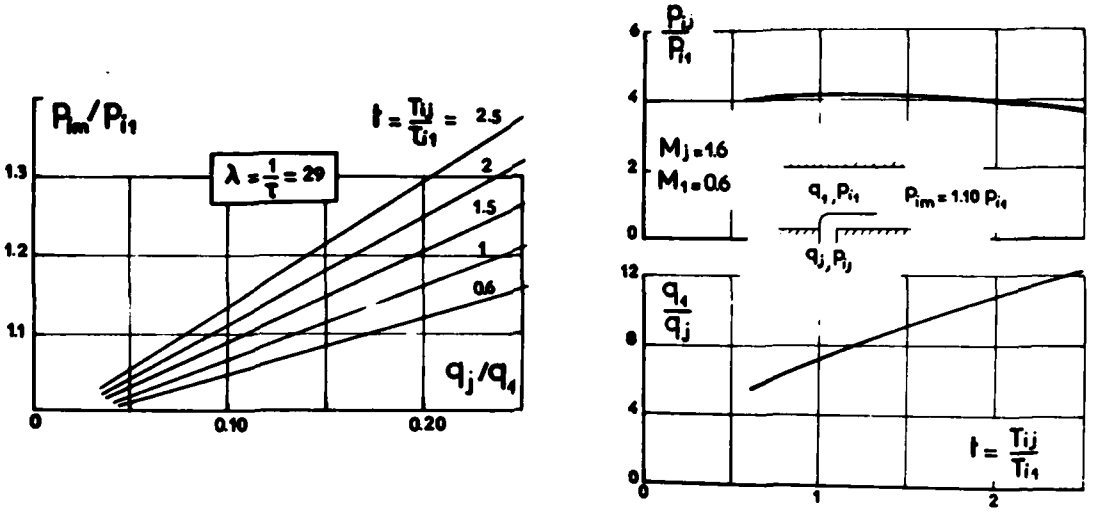

a) : Pressure ratio as function of Mass flow rate.

b) : Driving gas total pressure and entrainment flow rate for a pressure ratio 1.10.

FIG. 2 : THEORY OF EJECTORS : INFLUENCE OF THE DRIVING GAS TEMPERATURE.

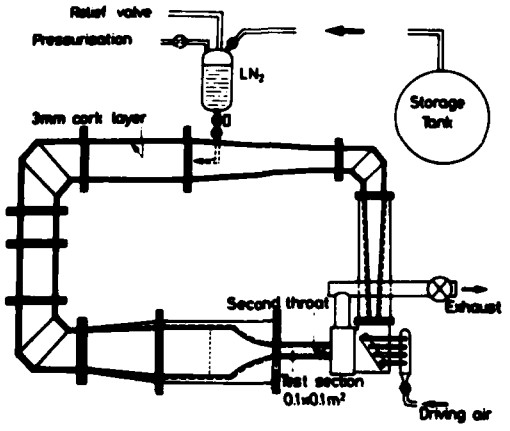

FIG. 3 : PILOT WIND TUNNEL T'2 AND CRYOGENIC ADAPTATION.

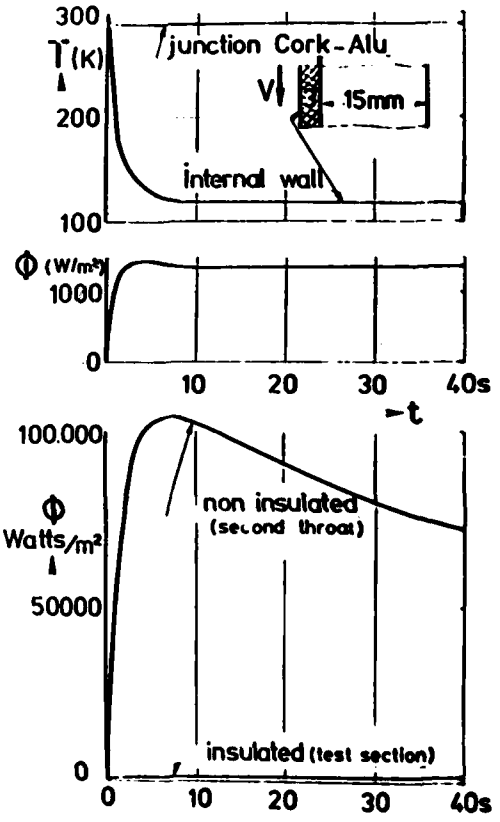

FIG. 4 : EFFICIENCY OF INTERNAL THERMAL INSULATION.

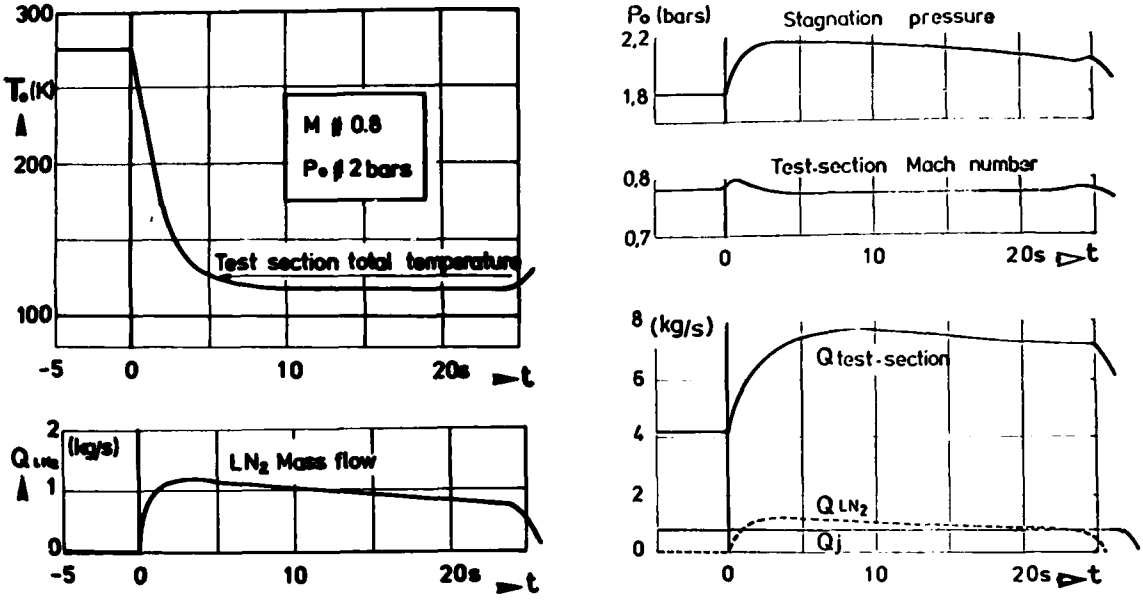

FIG. 5 : FLOW ESTABLISHMENT AND MASS-FLOW RATES FOR A TYPICAL CRYOGENIC RUN IN THE T'2 WIND-TUNNEL.

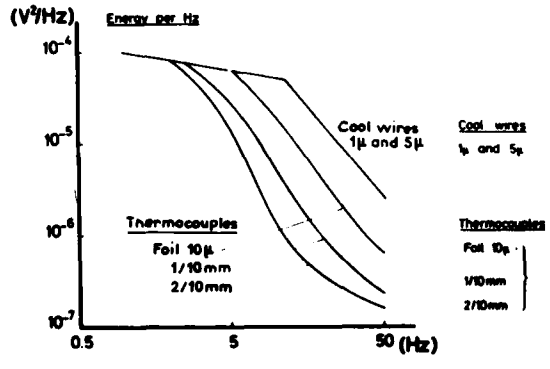

FIG. 6 : THERMOCOUPLES RESPONSE-TIME.

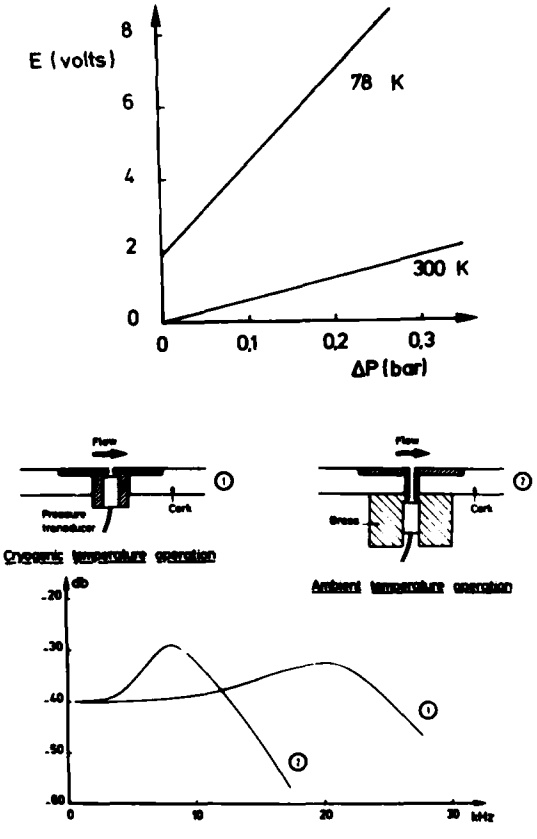

FIG. 7 : CALIBRATION OF KULITE PRESSURE TRANSDUCERS.

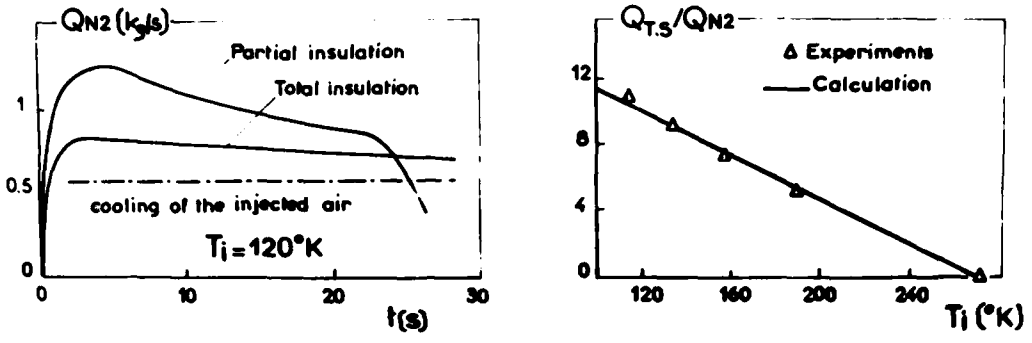

a) : Effect of thermal insulation upon Nitrogen consumption (T_i = 120°K, p_i = 2 bars).

b) : Nitrogen consumption as function of the flow temperature.

FIG. 8 : TUNNEL PERFORMANCES : LIQUID NITROGEN CONSUMPTION.

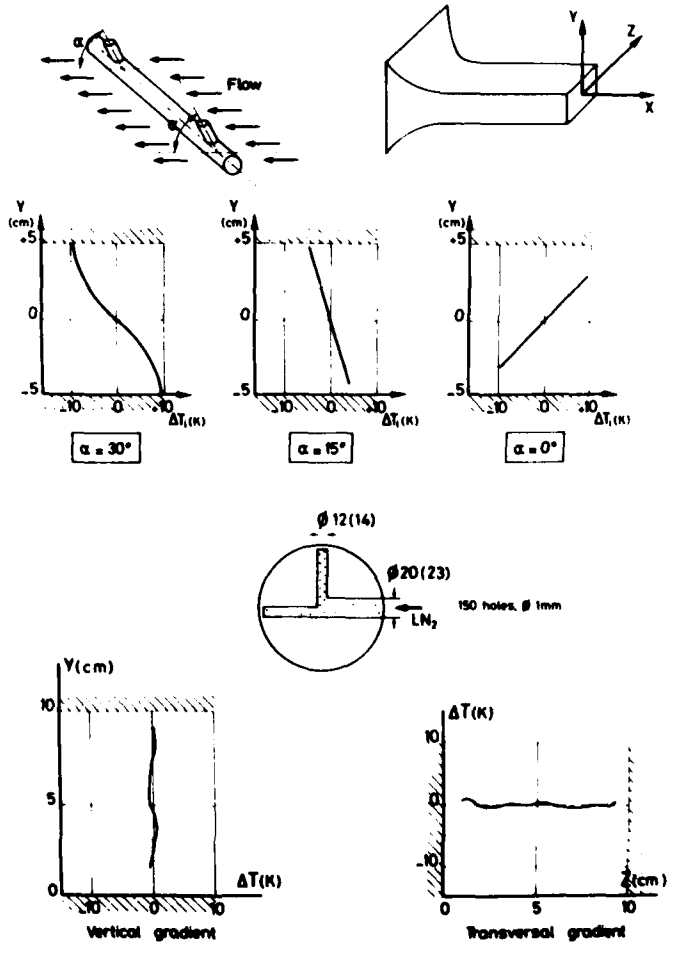

FIG. 9 : INFLUENCE OF LN2 INJECTION UPON THE TEMPERATURE GRADIENT IN THE TEST SECTION.

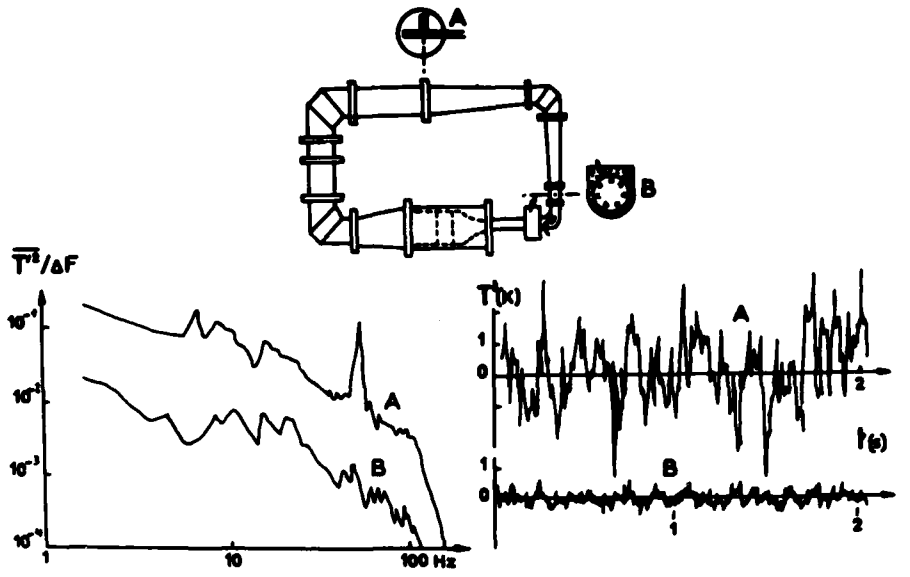

FIG. 10 : FLOW QUALITIES : INFLUENCE OF LN2 INJECTION UPON TEMPERATURE FLUCTUATIONS IN THE STILLING CHAMBER.

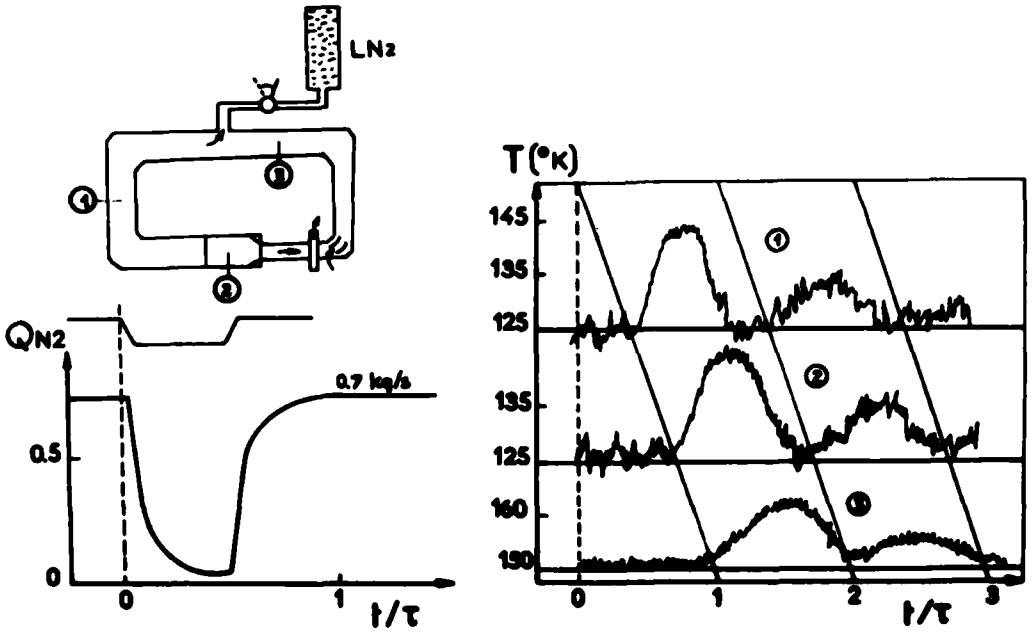

FIG. 11 : DYNAMIC TESTS (NITROGEN MASS FLOW VARIATION).

Mono dimensional equations :

Mass : $\frac{\partial(\rho\omega)}{\partial t} + \frac{\partial}{\partial x}(\rho u\omega) = m'$

Dynalpy : $\frac{\partial}{\partial t}(\rho u\omega) + [(p+\rho u^2)\omega] = p\frac{\partial \omega}{\partial x} + j' - f'$

Energy : $\frac{\partial}{\partial t}(\rho h_t \omega) + \frac{\partial}{\partial x}(\rho u \omega h_t) = \frac{\partial}{\partial t}(p\omega) + \varphi'$

ω circuit aera ; m' : mass flow injection per meter ; φ' : heat transfer per meter
j' dynalpy injection per meter , f' : drag losses per meter

Integrated equations :

Mass : $L\omega_0 \frac{dPm}{dt} = q_j + q_{N2} - q_e$

Energy : $\frac{L\omega_0}{\gamma - 1}\frac{dPm}{dt} = q_j h_j + q_{N2} h_{N2} - q_e h_e + \Phi$

Dynalpy or sonic throat :

$$\begin{cases} L\frac{dqm}{dt} = J - F \\ q_v = A_c \left[\sqrt{\frac{\gamma}{R}} \frac{M_c}{(1+\frac{\gamma-1}{2}M_c^2)^{\frac{\gamma+1}{2(\gamma-1)}}}\right] \frac{Pm}{\sqrt{Tm}} \end{cases}$$

FIG. 12 : BASIC EQUATIONS FOR UNSTATIONARY AND PSEUDO-STATIONARY METHODS OF CALCULATION FOR TRANSIENT FLOWS.

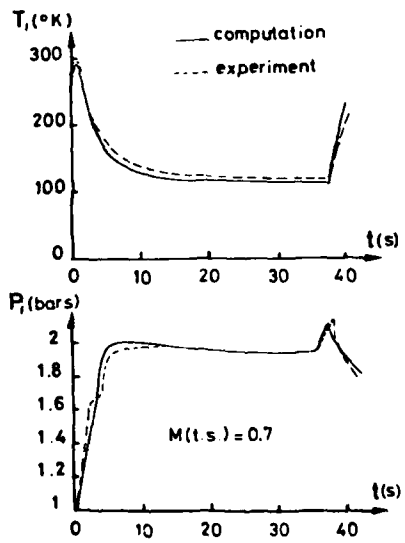

FIG. 13 : COMPARISON OF COMPUTED AND EXPERIMENTAL RUN IN T'2.

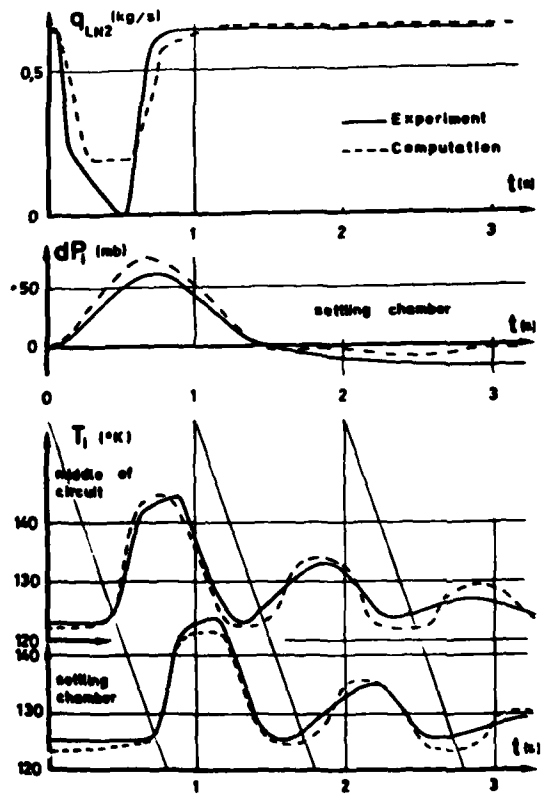

FIG. 14 : COMPUTATION OF FLOW RE-ESTABLISHMENT AFTER A SHORT STOP OF LN2 INJECTION.

EXPERIENCE IN THE CONTROL OF A CONTINUOUS FLOW CRYOGENIC TUNNEL

Robert A. Kilgore
NASA-Langley Research Center
Hampton, Virginia 23665, U.S.A.

SUMMARY

The concept of using liquid nitrogen to cool the test gas of a wind tunnel to cryogenic temperatures has lead to the successful achievement of very high Reynolds number flows in relatively small transonic tunnels. The economical operation of liquid nitrogen cooled cryogenic tunnels is critically dependent on fast and accurate control of the tunnel variables. In this lecture, the control problem of a continuous flow fan driven cryogenic tunnel has been addressed, firstly by developing a lumped multivariable mathematical model of a tunnel and validating the model by reconciling the responses of the Langley 0.3-m transonic cryogenic tunnel to the responses of the mathematical model on a simulator. Finally, the development of laws for the closed loop control of the tunnel pressure and temperature and the successful implementation of a control system for the 0.3-m transonic cryogenic tunnel based on these laws are presented. An accuracy of ±0.25 K in temperature and ±0.017 atm in pressure in the tunnel contrcl has been achieved.

LIST OF SYMBOLS

A	area, m^2 or percent
c_m	specific heat of metal, J/(kg·K)
c_p	specific heat of gas at constant pressure, J/(kg·K)
c_v	specific heat of gas at constant volume, J/(kg·K)
D	circuit loss factor
e	exponential
E	energy, J
h	enthalpy, J/kg
K	gain, or temperature, K
$\dot{m}$	mass-flow rate, kg/sec
M	Mach number
M	mass, kg
N	fan speed, rpm
p	pressure, atm
$\dot{Q}$	heat flow, J/sec
r	pressure ratio
s	Laplacian mathematical operator
t	time, sec
T	temperature, K
u	specific internal energy, J/kg
U	internal energy, J
V	volume, m^3
y	heat transfer coefficient, J/(m^2 K·sec)
Z	thermal impedance (m^2 K·sec)/J
α,β	cooling capacities of liquid nitrogen and gaseous nitrogen, J/kg
γ	ratio of specific heats
η	fan efficiency
θ	thermal mass, J/K
τ	transport time lag, sec

Subscripts and Superscripts

a	acoustic
c	tunnel circuit
F	fan
G	gas
i	insulation
L	liquid
m	metal
set	set point value
S	static
$*$	test section

The use of a dot over a quantity denotes the derivative of the quantity with respect to time, $\frac{d}{dt}$.

Controller Terms

ET	temperature loop error, K
ST	temperature loop set point, K
KT	temperature loop gain
AL	liquid nitrogen valve area, percent
PT,IT,DT	temperature PID controller gains
QDF	fan power, kW
KL	liquid nitrogen valve gain, kg/sec
KB	bias
TGR	temperature gradient, K/sec
LLT	liquid nitrogen limit, percent
FF	feed forward
Ep	pressure loop error, atm
Sp	pressure loop set point, atm
Kp	pressure loop gain
AG,A1,A2	Gaseous nitrogen bleed valve area, percent
Pp,Ip,Dp	Pressure PID controller gains
p_s	test section static pressure, atm

1. INTRODUCTION

Historically, capital and operating costs have tended to keep transonic wind tunnels small, while the many problems encountered at high pressures have tended to keep operating pressures low. The net result has been that existing (ambient temperature) tunnels operate at Reynolds numbers which are, in general, far too low to insure proper simulation of the flow experienced in flight, particularly with regard to shock—boundary-layer interactions encountered on modern high subsonic and transonic aircraft.

Of the various ways of increasing Reynolds number that have been tried or proposed for transonic tunnels, cooling the test gas to cryogenic temperatures (150 K or lower) appears to be the best solution in terms of model, balance, and sting loads, as well as capital and operating cost (Ref. 1). Personnel at the NASA Langley Research Center have been studying the application of the cryogenic wind tunnel concept to various types of high Reynolds number transonic tunnels since the autumn of 1971 and, through extensive theoretical and experimental studies, have successfully demonstrated both the validity and practicality of the concept. As a result of this work, the first major transonic tunnel especially designed to take full advantage of cryogenic operation is now under construction at the Langley Research Center. This tunnel, the U. S. National Transonic Facility (NTF), will provide an order of magnitude increase in Reynolds number capability over existing tunnels in the United States when it becomes operational in 1982.

It can be shown that for equal test Reynolds numbers and any arbitrary maximum operating pressure, a cryogenic tunnel uses less total energy, and therefore costs less to operate, than an ambient temperature tunnel doing the same amount of testing. Even so, the operation of large cryogenic tunnels will be very expensive in absolute terms. For example, the NTF, when operating at its maximum Reynolds number of 120×10^6 at transonic speeds, will use liquid nitrogen at the rate of approximately 450 kg/sec (1000 lb/sec). Although the average LN_2 usage rate in the NTF will be much less than 450 kg/sec, it is still highly desirable, if not essential, that the tunnel be operated in an efficient manner in order to minimize liquid nitrogen consumption.

The economical and efficient operation of a cryogenic wind tunnel is critically dependent on fast and accurate control of the tunnel variables and, hence, the tunnel control system. This has been recognized at the Langley Research Center and studies have been undertaken by two teams to enunciate the problem of cryogenic tunnel controls and to obtain control strategies to realize fast, accurate, and economical control of the Langley 0.3-m transonic cryogenic tunnel (TCT) and the NTF.

The first phase of the cryogenic tunnel process control consists of understanding the physical processes occurring in the cryogenic tunnel through appropriate thermo and fluid dynamical analysis, and obtaining a control compatible model of the tunnel process which relates the tunnel variables to the tunnel control inputs.

A fan-driven closed-circuit cryogenic nitrogen wind tunnel can be looked upon as a thermodynamical system wherein the tunnel resident nitrogen gas mass, while in motion over the streamlined walls of the tunnel geometry, interacts with the walls of the tunnel (metal and/or insulation) and the control inputs, viz., liquid nitrogen injected into the tunnel, warmer gaseous nitrogen bleed flow out of the tunnel, and fan induced compression and wall friction heating. This thermofluid dynamical interaction occurs both in the space of the tunnel and in time. Any efforts at deriving a control compatible unsteady model of a cryogenic tunnel aims at describing this physical process in its entirety. In view of the complexity of the spatial and temporal unsteady thermodynamic interaction of the tunnel resident gas with the walls of the tunnel and the various control inputs, different approaches with various degrees of simplification can be taken to obtain an appropriate model of the cryogenic tunnel.

In the case of the NTF modeling, the approach taken has been to solve the unsteady duct flow equations for the full length of the tunnel by invoking the one-dimensional duct flow laws of momentum, continuity, and energy. Two methods of resolving the unsteady

spatial flow are being used. In the first method, the tunnel has been discretized into a finite number of cylindrical segments, and the various duct flow equations have been set up for each segment by allowing appropriate transit time for the segment boundary conditions. In the second method, the continuous spatial problem is being solved. Both techniques require considerable computational time. In either case, the cryogenic tunnel model is implicitly contained in the software and provides dynamical solutions to a given set of tunnel conditions and disturbances.

In developing the mathematical model of the 0.3-m transonic cryogenic tunnel, a third approach has been taken. This approach consists of determining the average dynamical state of the tunnel gas by considering the tunnel to be an autonomous pressure vessel wherein ideal mixing of the mass-energy control inputs occur. This average dynamical state of the tunnel gas is superimposed on the steady state spatial profile of the tunnel states, which in turn is obtained by the duct flow equations of continuity, momentum, and energy. Appropriate transport time delays are superimposed on the various control inputs to account for temperature transport delay. However, mixing is assumed to be total within one circuit time. The justification for separating the dynamical response to average state, and static profile to duct flow is by observing that the system has maximum stored energy in the metal of the tunnel structure followed by the internal energy of the mass of gas resident in the tunnel. The kinetic energy of the tunnel flow, which contributes to the spatial unsteady flow, can be noted as being, at its maximum, only 0.75 percent of the internal energy of the gas. Hence, the kinetic energy of the tunnel flow has been ignored.

Such an analysis leads to an explicit mathematical model of the cryogenic tunnel, whose parameters are the tunnel geometrical constants such as surface area, volume, etc., the thermophysical properties of gaseous and liquid nitrogen, and the characteristics of the control elements. This approach for modeling fully accounts for all the mass and energy in the system; but truncates the system dynamics by suppressing the circuit modes and acoustic modes. Since these modes can be considered to be uncontrollable for the given degrees of input freedom, this lumped approach has been taken to be adequate.

It is the aim of this lecture to present details of the development of a lumped parameter multivariable model, the use of the model to develop an interactive real-time cryogenic tunnel simulator, the validation of the model, and the development of closed loop control laws and their performance with specific reference to the 0.3-m TCT at NASA Langley Research Center.

2. DEVELOPMENT OF MATHEMATICAL MODEL

2.1 Energy State Diagram

The internal energy associated with a finite volume of gas at a uniform pressure p and temperature T is the total energy associated with the gas at the molecular level and is a function of temperature as predicted by the third law of thermodynamics. At absolute zero, the internal energy and gas specific heat tend to zero. This can be expressed using the classical equation

$$U = \int_0^T c_v dT$$

where

$$c_v = \frac{dQ}{dt} \text{ at constant volume.}$$

The expression for the density of nitrogen gas can be used to estimate the mass of gas M_G for a given volume of gas V at pressure p and temperature T. The expression for M_G, from Reference 2, is

$$M_G = 338.90 \frac{p}{T} \left[1 + 250 \frac{p}{T^2}\right] \quad kg/m^3 \tag{1}$$

The internal energy associated with this volume of gas is

$$U = M_G \int_0^T c_v dT$$

Assuming $\int_0^T c_v dT = c_v T$ we have

$$U = 253.49\, p \left(1 + 250 \frac{p}{T^2}\right)\left(1 + 250 \frac{p^{0.7}}{T^2}\right) \quad kJ/m^3$$

Function fits for density and c_v in terms of p and T from Reference 2 have been used in the above expression.

The mass-energy relationship for a unit volume of gas is illustrated in Figure 1, which shows the internal energy of the gas U versus its mass M_G. The loci of constant temperature, isotherms, on the diagram are the lines of slope c_vT radiating from the origin. The loci of constant pressure, isobars, are the lines which generally run parallel to the x-axis. If the nitrogen gas were truly perfect statically, the isobars would be truly parallel to the mass axis. The real gas isobars have positive slope. The liquid-gas phase boundary runs near the 100 K isothermal line, and its true position has been ignored.

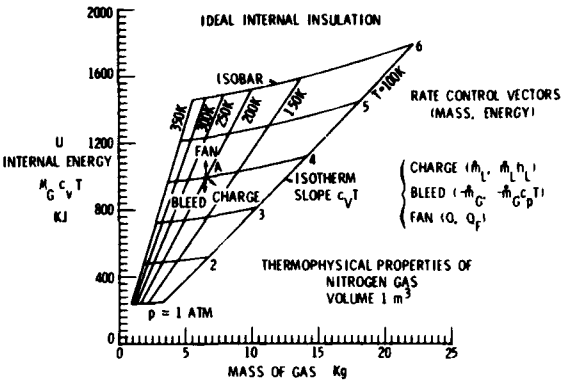

Fig. 1 Energy state diagram.

Consider a representative point A on the diagram, corresponding to a finite mass of gas at a known pressure and temperature in a 1-m^3 volume. If any extra gas mass or energy is added to this system, the point A appropriately shifts graphically to account for the new mass and energy state. In the case of the cryogenic wind tunnel, the three control inputs and the thermal leakage, either from the ambient conditions surrounding the tunnel or from the tunnel metal shell, change the energy state of the system by moving the point A to new coordinates of pressure and temperature. The addition of liquid nitrogen constitutes a reduction of energy by negative enthalpy $\dot{m}_L h_L$ and an increase of mass by $\dot{m}_L$. Bleeding of gas from the system similarly represents a reduction of energy by negative enthalpy $-\dot{m}_G h_G$, and a decrease of mass by $\dot{m}_G$. Heat release from the fan $\dot{Q}_F$ and heat released from the wall $-\dot{Q}_m$ are true energy inputs. All of these inputs can be represented as mass-energy rate vectors, and the sum of these control vectors provides the final state of system. This analysis can be carried out graphically by vector manipulation as shown in Figure 1. The same analysis can also be carried out analytically, by studying the open thermodynamic system.

2.2 Thermodynamic Model of a Closed Circuit, Cryogenic Pressure Tunnel

The cryogenic pressure tunnel can be considered as a thermally autonomous pressure vessel of volume V containing nitrogen gas of mass M_G at a uniform pressure p and temperature T. The vessel is assumed to be ideally insulated, insulation being external to the metal wall. This vessel is assumed to be opened to a liquid nitrogen source and a gas bleed valve which allow transfer of mass and associated enthalpy. The vessel is also assumed to be opened to a fan shaft which creates the necessary fluid flow and delivers the fan energy. Such a system is shown in schematic in Figure 2. The liquid nitrogen flow rate is taken to be $\dot{m}_L$ and occurs at a liquid pressure of p_L. The gas bleed valve allows flow of $\dot{m}_G$ out of the tunnel.

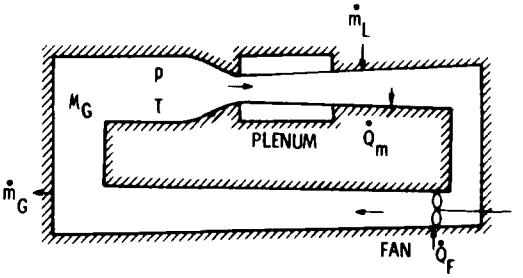

Fig. 2 Thermodynamic model of a closed circuit cryogenic pressure tunnel.

Assuming uniform mixing and ignoring the work done, the potential energy, and the kinetic energy, and invoking the first law of thermodynamics, we have

$$h_L = U_L + p_L V_L$$

$$h_G = U_G + p_G V_G$$

then

$$-\dot{Q}_m + \dot{Q}_F + \dot{m}_L h_L = \dot{m}_G h_G + \frac{dU}{dt}$$

where

$-\dot{Q}_m$ = rate of heat release from tunnel to gas, J/sec

$\dot{Q}_F$ = rate of heat release from fan, J/sec

U = internal energy = $M_G u$, J

u = specific internal energy, J/kg

$$-\dot{Q}_m + \dot{Q}_F + \dot{m}_L h_L = \dot{m}_G h_G + \frac{d}{dt}\left(M_G u\right) = \dot{m}_G h_G + u\frac{dM_G}{dt} + M_G\frac{du}{dt}$$

$$-\dot{Q}_m + \dot{Q}_F + \dot{m}_L h_L - \dot{m}_G h_G = u\left(\dot{m}_L - \dot{m}_G\right) + M_G\frac{du}{dT}\cdot\frac{dT}{dt}$$

which can be simplified to

$$\dot{m}_L\left(h_L - u\right) - \dot{m}_G\left(h_G - u\right) - \dot{Q}_m + \dot{Q}_F = M_G c_v\frac{dT}{dt}$$

For a perfect gas we have $u = c_v T$ and $h_G = c_p T$; hence

$$\dot{m}_L\left(h_L - c_v T\right) - \dot{m}_G\left(c_p - c_v\right)T - \dot{Q}_m + \dot{Q}_F = M_G c_v\frac{dT}{dt} \qquad (2)$$

The mass and energy crossing the boundary of the tunnel react with tunnel resident gas and changes its state. This interaction of the control vectors can be shown on an energy state diagram as the charge, bleed and fan mass-energy rate vectors. In order to run the tunnel at a steady gas state, the Mach dependent $\dot{Q}_F$ needs to be cancelled by the sum of the negative enthalpies from charge and bleed, which in themselves should create no mass change. By manipulating the magnitudes of these control vectors, either a balance condition can be obtained or the tunnel state moved along any desired path. Details of such a manipulation are given in Reference 2.

2.3 Role of Metal-Stored Energy in Cryogenic Tunnels

Cryogenic tunnel engineering design demands insulation of the cold test gas from the ambient to prevent heat gains and the associated energy waste. Since these tunnels are required to operate over a considerable pressure range, one to nine atmospheres, in the case of the NTF, the insulator shell must possess the ability to withstand internal pressure without leakage.

Most insulators are poor structural material, and storage of high-pressure compressible fluids in the shell demands perfect safety and conformity to appropriate pressure vessel code. These requirements dictate the use of structural metals suitable for use at cryogenic temperatures for the pressure vessel integrity. However, the location of the insulation of this vessel can be either internal or external. When the insulation used is external to the tunnel shell, the structural metal is exposed to cold gases and thermally interacts with the gas by releasing heat. Alternately, the insulation can be internal to the tunnel, thereby isolating the metal from cold gases. In the latter case, the need for very good surface finish on the insulator to obviate problems of boundary layer growth demands the use of thin, highly finished, metal panels. This is particularly true of the test section and contraction section wherein good aerodynamic contouring is required. Thus, engineering design of cryogenic tunnels dictates the use of a considerable amount of metal within the insulation shell.

When the insulator behaves ideally, the cryogenic tunnel can be looked upon as an autonomous thermodynamic system. The metal-stored energy then becomes a part of the tunnel thermal inertia and tunnel internal energy. The tunnel energy is now in the form of gas molecule motion and lattice vibration of metal molecules. Any gross temperature difference between gas and metal results in heat transfer between the two at the gas-wall boundary, and under steady-state conditions the metal and gas are at the same temperature. The magnitude of metal-stored energy can be estimated by studying the enthalpy and specific heat of metals. (See, for example, Ref. 3.)

2.3.1 Metal to Gas Heat Transfer

The mechanism of heat transfer in a tunnel is a surface phenomenon and is a complex function of the metal and gas properties such as thermal conductivity, specific heat, gas density, and gas viscosity. A numerical estimation of the heat transfer coefficient is now made based on constants validated by Bartz in Reference 4. Using equation (6) of Bartz's work and using his notation,

$$h = \left[\frac{C}{D^{0.2}}\left(\frac{\mu^{0.2}\,c_p}{Pr^{0.6}}\right)\left(\frac{P_g}{C^*}\right)^{0.8}\right]\left(\frac{A^*}{A}\right)^{0.9}\sigma$$

$$\sigma = \frac{1}{\left[\frac{1}{2}\frac{T_w}{T_o}\left(1 + 0.2M^2\right) + \frac{1}{2}\right]^{0.632}\left(1 + 0.2M^2\right)^{0.167}}$$

using constants of $w = 0.8$ and $C = 0.026$. This heat transfer coefficient has been validated at the nozzle of a rocket. A number of values of heat transfer coefficient Y_G were estimated using $Pr = 0.73$ and $C^* = 61.5\ T^{0.5}$ for various pressures, temperatures, and area ratios. This set of data was function fitted to obtain a simple heat transfer equation

$$Y_G = 8234\ p^{0.8}\ T^{-0.22}\ M\left(1 - 0.67M^{0.65}\right)\quad J/(m^2\ K{\cdot}sec) \tag{3}$$

This heat transfer coefficient Y_G provides the local forced convection heat transfer on a unit area of the tunnel metal-gas boundary and is a function of local pressure, temperature, and Mach number. It has been used by Balakrishna in Reference 2 to establish the overall heat flow rate.

The heat flow from the wall to the gas is not only a function of surface convection based Y_G, but also a function of wall thermal conductivity, wall thermal capacity, and wall leakage, if any. Consider a unit area of the tunnel wall thickness, starting from the gas boundary to the external tunnel face, as shown in Figure 3. This cross section consists of the tunnel metal wall and the insulation. The heat flow occurring under transient conditions can be obtained from a simple electrical analog. Here $1/R_G$ corresponds to the heat transfer coefficient Y_G associated with the turbulent boundary layer of the tunnel flow discussed previously. Further, $1/R_m$ corresponds to the thermal conductivity of the metal wall thickness and c_m corresponds to thermal capacity of that layer. By making some simplifications and combining the wall and gas heat transfer equations, the heat flow in a unit area of the tunnel wall on the basis of one-dimensional heat flow, is, for ideal insulation:

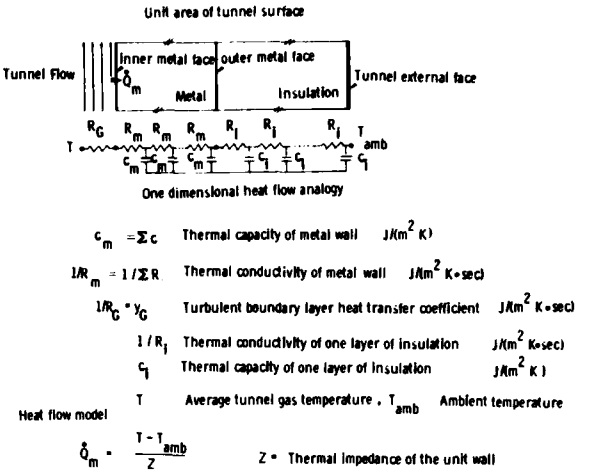

Fig. 3 Metal to gas heat transfer mechanism.

$$\dot{Q}_m = \frac{T}{Z} = \left[\frac{T\ c_m s\left(1 + \frac{R_m c_m s}{20}\right)}{1 + \left(\frac{R_m}{2} + R_G\right) c_m s}\right] \tag{4}$$

2.4 Temperature and Pressure Dynamics

The basic thermodynamic equation for determining the time rate of change of the internal energy of the gas is

$$\dot{E} = \frac{\partial}{\partial t}\left(M_G c_v T\right) = \int_{Surface} \dot{Q}_m + \dot{Q}_F + \dot{m}_L h_L - \dot{m}_G c_p T$$

with heat energy added to the gas being positive.

After mathematical manipulation, adding the transport delays involved in the measurements, and using the definitions $\dot{Q}_m = \frac{M_m c_m T s}{1 + t_m s}$, $\alpha = \left(c_p - c_v\right)T$, and $\beta = h_L - c_p T$ of Reference 3, the temperature dynamics of the tunnel can be written as

$$\frac{\partial T}{\partial t}\left(\frac{1 + t_G s}{1 + t_m s}\right) = \frac{\beta + \alpha}{\theta}\ \dot{m}_L e^{-\tau_L s}\ \frac{\alpha}{\theta} - \dot{m}_G e^{-\tau_G s} + \frac{\dot{Q}_F}{\theta}\ e^{-\tau_F s} \tag{5}$$

where $\theta = M_G c_v + M_m c_m$.

From the ideal gas law the pressure of a confined gas is proportional to the mass of the gas and its temperature, $p \propto M_G T$. After taking the appropriate derivatives and making substitutions, the time rate of change of pressure may be expressed as

$$\frac{\partial p}{\partial t} = \frac{p}{T}\ \frac{\partial T}{\partial t} + \frac{p}{M_G}\ \frac{\partial M_G}{\partial t}.$$

After substitution and manipulation, the pressure dynamics for the tunnel can be written

$$\dot{p} = \frac{\partial p}{\partial t} = \frac{p}{M_G}\dot{m}_L e^{-\tau_G s} - \frac{p}{M_G}\dot{m}_G e^{-\tau_G s} + \frac{p}{T}\dot{T} + DbMp\frac{\partial M}{\partial t} \tag{6}$$

where $b = 0.197\left(1 - \frac{7pM}{T}\right)$ for the 0.3-m TCT.

Equations (5) and (6) permit the description of the temperature and pressure response characteristics of the gas in the tunnel due to the tunnel control inputs.

2.5 Additional Relationships

Other important functional relationships necessary for modeling a fan driven cryogenic tunnel are given below. The specific constants of these relations for the 0.3-m TCT are also presented.

Mach number:

$$M = \frac{N}{K_m\sqrt{T}}\frac{e^{-\tau_a s}}{\left(1 + t_p s\right)} \tag{7}$$

where

t_p = the plenum time constant, τ_a = the acoustic time lag, and
$K_m = 600\ (1 - 0.3M)p^{-0.035}$ for the 0.3-m TCT.

Tunnel circuit time:

$$t_c = \frac{(0.0486)V}{A^*M\sqrt{T}}\left(1 + 250\frac{p}{T^2}\right)\left(1 + 0.2M^2\right)^3 \tag{8}$$

LN_2 flow rate:

$$\dot{m}_L = K_L A_L = 3.47\sqrt{p_L - p}\,A_L \quad \text{for} \quad 0 \le A_L \le 100\% \tag{9}$$

where 3.47 corresponds to the 0.3-m TCT liquid nitrogen injection valve.

GN_2 flow rate:

The mass flow out of a control valve can be expressed as

$$\dot{m}_G = C^*\sqrt{\frac{gC}{RT}}\rho A C_d$$

where C = speed of sound, ρ = density, g = gravitational constant. Assuming a $C^* = 0.7$ and a valve coefficient C_d of 8, for choked flow out of the valve we have,

$$\dot{m}_G = K_G\frac{p}{\sqrt{T}}A_G = 21.8\frac{p}{\sqrt{T}}A_G \quad \text{kg/sec for} \quad p > 1.5 \text{ atm} \quad \text{and} \quad 0 \le A_G \le 100\%. \tag{10a}$$

Wher the flow out of the valve is not choked we have,

$$\dot{m}_G = K_G\frac{p}{\sqrt{T}}A_G = \left[2 - \left(\frac{1.5}{p}\right)^{1.7}\right]21.8\frac{p}{\sqrt{T}}A_G \quad \text{kg/sec for} \quad 1 \le p \le 1.5 \text{ atm} \quad \text{and} \quad 0 \le A_G \le 100\%. \tag{10b}$$

The value 21.8 refers to the 0.3-m TCT gaseous nitrogen bleed valve.

Mass of gas in tunnel:

$$M_G = 338.9 \frac{pV}{T}\left[1 + 250\frac{p}{T^2}\right]\left[1 - 0.033\,M^{1.5}\right] \quad kg \tag{11}$$

Fan pressure ratio:

$$r = 1 + bM^2 \tag{12}$$

where, for the 0.3-m TCT, the experimentally determined expression for b is

$$b = 0.197\left(1 - \frac{7pM}{T}\right)$$

Metal enthalpy:

The 0.3-m TCT is constructed of 6061-T6 aluminum alloy. The energy stored in the metal is

$$h = 2.75T^2 - 0.0026T^3 \quad kJ/kg \tag{13}$$

Fan dynamics:

The fan speed control system for the 0.3-m TCT has a dynamic response characterized by

$$\frac{N}{N_{set}} = \frac{1}{0.2s^2 + 0.56s + 1} \tag{14}$$

Cooling capacities:

The cooling capacity of the liquid nitrogen and the cooling capacity of the gaseous nitrogen bleed can be expressed as

$$\beta = h_L - c_pT,\ \alpha = \left(c_p - c_v\right)T \quad kJ/kg \tag{15}$$

Fan heat:

The heat generated under isentropic compression in the fan is

$$\dot{Q}_F = \frac{K_F p^{1.3}\sqrt{T}}{\left[1 + 0.2M^2\right]^3} \quad kw \tag{16}$$

where

$$K_F = \frac{6965\ A^* c_p\ b}{\eta}\left[\frac{\gamma - 1}{\gamma}\right].$$

Using the above functional relationships between the tunnel variables and the control inputs, an explicit multivariable control model has been developed, and is shown in Figure 4. This non-linear three-input and three-output model has fairly strong off-diagonal terms pointing to considerable cross coupling between the control inputs and the tunnel variables. In the following section, this model has been used to develop a real time cryogenic tunnel simulator.

3. CRYOGENIC TUNNEL SIMULATION

The preceding set of expressions presented explain the total behavior of the cryogenic tunnel process. The time responses of this non-linear multivariable model are somewhat difficult to explicitly determine analytically. However, generation of the time responses of this model can be achieved by simulating the tunnel on a hybrid computer. The

Fig. 4 0.3-m TCT multivariable model.

development of such a hybrid simulator has been detailed in Reference 2. The digital part of the hybrid computer estimates the non-linear segments of the model and communicates these quantities to the analog computer which provides the real time dynamical solutions, the update rate being as high as 25 times a second. Manual control of the 0.3-m transonic cryogenic tunnel consists of a fan speed control rheostat, and liquid nitrogen injection valve and gaseous nitrogen exhaust valve control stations. Displays of Mach number, Reynolds number, temperature, pressure, and drive-fan speed are provided on the control panel for setting and maintaining test conditions. Other displays include liquid nitrogen pump pressure, fan drive motor power, and digital valve status indicator lights. A similar manual control panel and set of displays were developed for the hybrid computer simulation. Using the hybrid computer control panel, shown in Figure 5, operator inputs are made through potentiometers which control the (simulated) liquid and gaseous nitrogen valve openings and the fan speed. The digital displays permit realistic simulation of tunnel operation including operator imposition of constraints such as maximum cool down rates or metal to gas temperature differences.

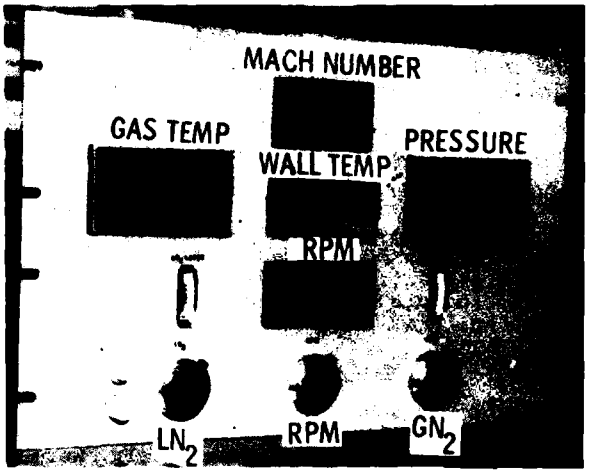

Fig. 5 Display and control panel for simulator.

In order to validate the model of the fan driven tunnel, experimental responses of the 0.3-m TCT for transient and quasi steady conditions are compared with the simulator generated responses for identical tests.

3.1 Transient Response Tests

The 0.3-m transonic cryogenic tunnel and its simulator were disturbed from their steady state equilibrium conditions with identical control input disturbances, in the form of a positive liquid nitrogen flow pulse, a positive gas bleed flow pulse and a negative fan speed pulse of about 3 seconds. The resultant responses of the 0.3-m TCT and its simulator are now compared, reconciled and correlated with explicit mathematical model terms. These responses are shown in Figure 6.

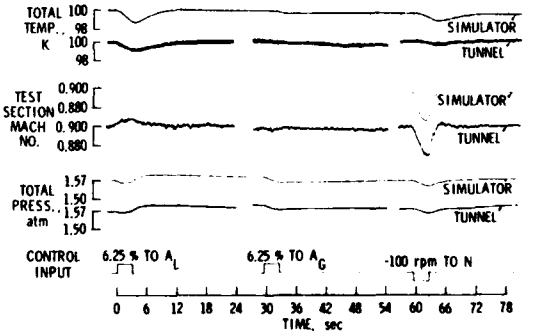

Fig. 6 Tunnel and simulator responses.

A positive liquid nitrogen flow pulse creates a negative total temperature pulse response in the tunnel gas which decays down to steady state value in time. The temperature response has a transport time delay of about $0.8\ t_c$ as expected. The peak amplitude of the temperature pulse, ΔT, can be related as $\Delta T \propto \frac{\beta}{\dot{M}_G c_v} \Delta\dot{Q}_L$. The tunnel test section Mach number demonstrates a positive pulse with a peak amplitude of ΔM. This change is caused by pressure ratio change in the fan at constant speed due to temperature. Since the fan is situated very near the liquid nitrogen input segment, no transport delay can be found. This change in Mach number can be related to ΔT as $\Delta M/M \propto -\Delta T/2T$. The tunnel total pressure response has a singular signature, typical of a cryogenic tunnel with large metal enthalpy. The tunnel pressure change is caused by the two opposing terms $\frac{P}{T}\dot{T}$ and $\frac{P}{\dot{M}_G}\Delta\dot{Q}_L$. The gas temperature rate $\dot{T}$ is maximum at the start of the pulse, but

gradually diminishes because of gradually increasing wall heat release. Thus, initially term $\frac{p}{T}\dot{T}$ is far greater than $\frac{p}{M_G}\Delta\dot{Q}_L$ creating a negative pressure movement. The diminishing $\frac{p}{T}\dot{T}$ falls below the value of $\frac{p}{M_G}\Delta\dot{Q}_L$ during the pulse period and the negative pressure movement stops and the pressure starts increasing. Beyond the pulse period the pressure continues to increase because of continued wall heat release.

These features of pressure, Mach number, and temperature, shown in Figure 6 for both the tunnel and the simulator, are seen to be in very good agreement. A gas bleed pulse to the tunnel when in equilibrium shows a weaker pulse response in tunnel temperature. This negative pulse amplitude ΔT is related to $\frac{\alpha}{M_G c_v}\Delta\dot{Q}_G$. The tunnel Mach number response to the gas bleed pulse occurs through temperature and since temperature response is very weak, there is negligible effect on tunnel Mach number. The response of total pressure to gas bleed pulse is the most dominant response, and the tunnel pressure falls. The amplitude of the tunnel pressure is related to $\frac{p}{M_G}\Delta\dot{Q}_G$. Both the tunnel and the simulator agree by behaving similarly.

The negative fan speed pulse of the tunnel results in reduced fan power. Since the tunnel cooling is not reduced, the tunnel total temperature shows a negative temperature response. The maximum ΔT corresponds to the function $\frac{\Delta\dot{Q}_F}{M_G c_v}$. The tunnel test section Mach number is also considerably affected by reduced fan pressure ratio. This Mach number amplitude can be related to fan speed by $\Delta M/M \simeq \Delta N/N$. Though temperature fall should induce a positive Mach change, the effect of fan speed is most dominant. The tunnel total pressure is somewhat weakly related to fan pressure ratio and shows a pressure drop pulse which is proportional to bMp.

3.2 Quasi-Steady-State Tests

In addition to the transient response test, studies on the cool down of the tunnel from ambient and warmup of the tunnel to ambient, using excess liquid nitrogen flow and excess fan heating respectively, were conducted in order to validate the long-term dynamics of the heat transfer model:

The basic energy equation of the cryogenic tunnel process is

$$M_G c_v \frac{dT}{dt} + c_v T\left(\dot{m}_L - \dot{m}_G\right) = \dot{Q}_F + \dot{m}_L h_L - \dot{m}_G c_p T - \int^{\text{Surface}} \dot{Q}_m$$

where

$$\int^{\text{Surface}} \dot{Q}_m = \frac{M_m c_m T_s}{1 + t_m s}\left(T - T_m\right)y$$

In order to prove this heat transfer model, time histories of average metal temperature T_m and gas temperature T were recorded for ordered energy input terms. Matches between temperature, metal to gas temperature difference, and time were sought for the tunnel and simulator quasi-steady-state responses.

3.2.1 Cool-Down Studies

The tunnel cool-down test consisted of starting with both the metal and gas at ambient temperature and running the tunnel with excess liquid nitrogen flow while the tunnel pressure and low fan speed were maintained constant.

Under these conditions $\dot{m}_L \simeq \dot{m}_G$ because of constant pressure and $\dot{Q}_F << \dot{m}_L\left(h_L - c_p T\right)$ because of low fan speed, then

$$M_G c_v \frac{dT}{dt} = -\int^{\text{Surface}} \dot{Q}_m + \dot{m}_L \beta$$

$$\dot{Q}_m = \left(T - T_m\right)y; \quad T_m = \frac{T}{1 + t_m s}$$

Both the tunnel and the simulator were balanced at equilibrium conditions of 290 K, 1.5 atm, and 1200 rpm. The liquid nitrogen supply pressure was maintained at 6 atm. The tunnel cooling was started by rapidly opening the liquid valve to 12.5 percent open, corresponding to about 1 kg/sec flow. The tunnel pressure was maintained at 1.5 atm throughout the cool down. Gradually the tunnel metal cooled down, and time histories of gas temperature, metal temperature at a forward diffuser leg location, and the test section Mach number were recorded. Figure 7 shows the time histories of tunnel gas and average metal temperature as the tunnel was cooled from 290 K to about 100 K in about 35 min. It may be noted that the simulator and tunnel temperature histories match reasonably well. An initial gas to metal temperature difference of about 65 K (at 290 K) and a final difference of 15 K (at 100 K) occur in both the tunnel and simulator. The simulator and tunnel temperatures agree to within 5 K over most of the cooling period except at the very end where the difference is 10 K. This can be attributed to heat gains through some uninsulated flanges and supports in the actual tunnel which make the cool-down process a bit slower. The Mach number time histories of the tunnel and the simulator during the cool down agreed to better than 0.005, starting from an initial value of 0.140 and ending with a value of 0.228. The total quantity of liquid nitrogen consumed for cool down from 290 K to 105 K was determined for both the tunnel and simulator. The tunnel value was 1825 kg against a simulated consumption of 1800 kg. Thus, a fairly good match between the tunnel and the model for a quasi-steady-state cool down confirmed the heat transfer modeling used.

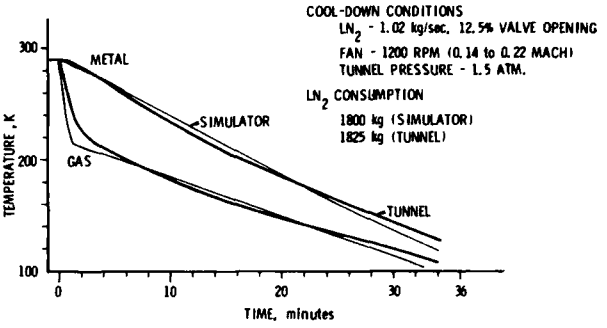

Fig. 7 Cooldown time histories.

3.2.2 Warmup Studies

The warmup tests for the 0.3-m TCT were started with a cold tunnel running at a fairly high Mach number. With the liquid nitrogen flow fully cut off and the tunnel pressure maintained constant, we have

$$\dot{m}_L \simeq \dot{m}_G = 0 \quad \text{and} \quad \dot{Q}_F >> \dot{m}_G c_p T$$

$$M_G c_v \frac{dT}{dt} \simeq \dot{Q}_F - \int_{\text{Surface}} \dot{Q}_m$$

where

$$\int \dot{Q}_m = \frac{M_m c_m T s}{1 + t_m s}$$

and

$$\dot{Q}_F = \frac{K_F \, p M^3 \sqrt{T}}{\left(1 + 0.2 \, M^2\right)^3}$$

For these studies, both the tunnel and the simulator were cooled to 100 K and operated at equilibrium conditions at a pressure of 2 atm and a Mach number of 0.6.

The warmup was started by cutting off the liquid nitrogen flow and maintaining pressure and Mach number constant by fine adjustment of the gas valve area and fan speed. Records of gas temperature and the average metal temperature were taken as functions of time. The warmup profile of the tunnel and the simulator at $M = 0.6$, $p = 2$ atm from 100 K to 300 K is shown in Figure 8. The metal to gas temperature differences agree very well. However, the physical tunnel shows an initial warmup rate lower than the simulator. This difference has been attributed to an initial tunnel pressure of slightly less than 2 atm. Subsequently, the tunnel and simulator warmup gradients match quite well. The metal to gas temperature difference in the tunnel and the simulator agree to within 2 K, indicating the adequacy of the heat transfer model. A detailed reconciliation of the 0.3-m TCT, its real time simulator and the mathematical model is available in Reference 2.

In summary, the cryogenic tunnel transient and quasi steady responses to various input commands are adequately described by the process equations derived from the first principles. These equations can now be used to develop closed loop control laws.

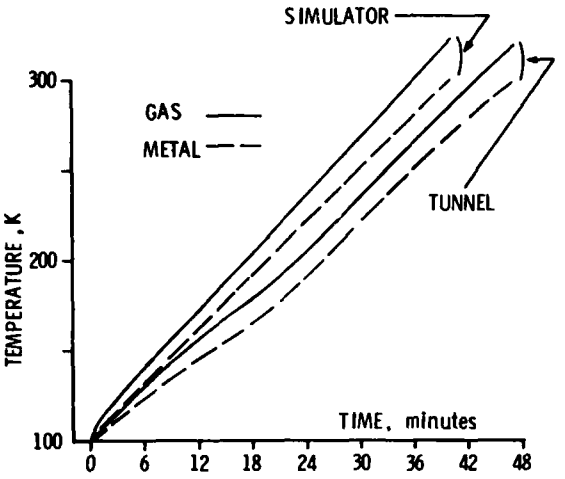

Fig. 8 Warmup time histories, M = 0.6, p = 2 atm.

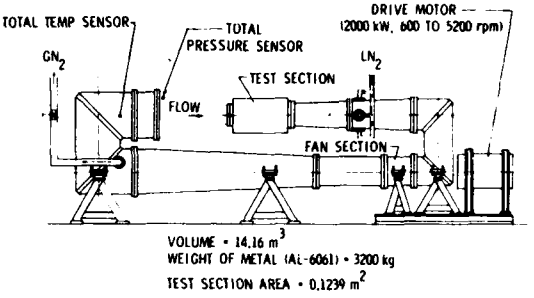

Fig. 9 Langley 0.3m TCT.

4. TUNNEL CONTROLS

The aim of tunnel control is to precisely and quickly regulate the tunnel variables of total temperature, test section Mach number, and total pressure, using the control inputs of liquid nitrogen mass flow, fan speed, and gaseous nitrogen bleed flow. In the case of the 0.3-m TCT, a control system performance of ±0.25 K in total temperature, ±0.017 atm in total pressure in the bandwidth of 2 to 3 radians/second is the goal. Figure 9 shows the 0.3-m TCT from a control viewpoint. Details of the design and operating characteristics of the 0.3-m TCT can be found in References 5 and 6. The following paragraphs describe some of the subsystems of the 0.3-m TCT that relate directly to tunnel control.

In order to control tunnel temperature, the liquid nitrogen injection valve area A_L must be dynamically varied by a control law in the presence of a steady liquid nitrogen supply pressure p_L. A liquid nitrogen valve, typically having a full area control speed of 1/2 second and a flow ranging to 1000, is considered adequate. In the case of the 0.3-m TCT, four digital control valves, each having a resolution of 1 in 1024 (a 10 bit valve) with binary weighted area and having the individual elements operated by solenoid valves, have been used. The advantages of digital valves are very fast response and perfect linearity. Because of precise area control, the digital valves can be used to accurately measure the flow rate of liquid nitrogen into the tunnel.

The tunnel total pressure can be controlled by dynamically varying the gaseous nitrogen bleed valve area A_G by an appropriate control law. Again, a fast response valve with a speed of 1/2 second for full area control and a range of about 1000 is considered necessary. In the case of the 0.3-m TCT, a digital valve with a resolution of 1/256 having binary weighted sonic nozzles controlled by pneumatically piloted solenoid actuators has been used. The range improvement of about 1/1000 is obtained by using two parallel valves with fixed and controlled bias opening for operation under conditions of high mass flows and low pressures.

The tunnel Mach number is controlled by fan speed control, wherein the fan is designed to operate away from the surgeline throughout the tunnel envelope. In the case of 0.3-m TCT, the fan speed control is obtained by controlling t[he] two pole induction motor by maintaining constant voltage/frequency ratio from a 5 to 1[.] Hz variable frequency voltage and power source. The fan speed is directly related to supply frequency.

The control law designs are briefly discussed in the following paragraphs. By assuming local linearity for small perturbation, and by ignoring the off-diagonal coupling terms of the mathematical model (see Fig. 4), single-input single-output (SISO) control laws are derived. Two control laws, one for tunnel total temperature control using liquid nitrogen mass flow control and the other for tunnel total pressure control using gaseous nitrogen bleed mass flow control, are discussed. Details of the development of these control laws are given in Reference 7.

4.1 Temperature Control

In Figure 10 the temperature control loop is shown which has been designed by [using] SISO root locus analysis. This has resulted in a non-linearly gain scheduled [control] law of the type $M\sqrt{p/T}$. However, because of strong interaction from the fan [as] can be seen in Figure 4, the control law uses feed forward of either the measured [fan] power. Secondly, in view of the non-linear behavior of the system, the [gains] are conditionally used based on an error magnitude dependent logic. Further,

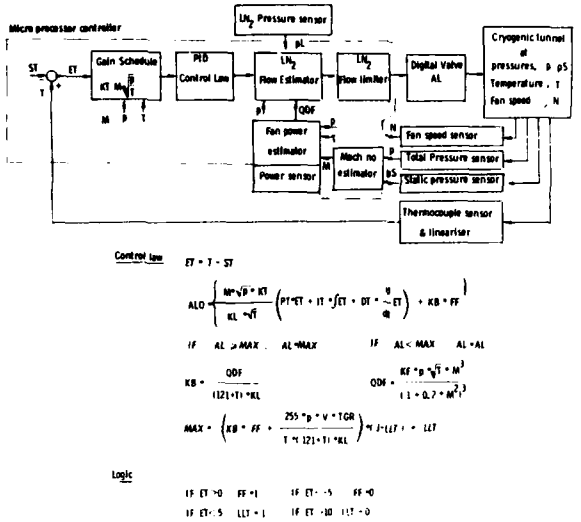

Fig. 10 Automatic temperature control scheme.

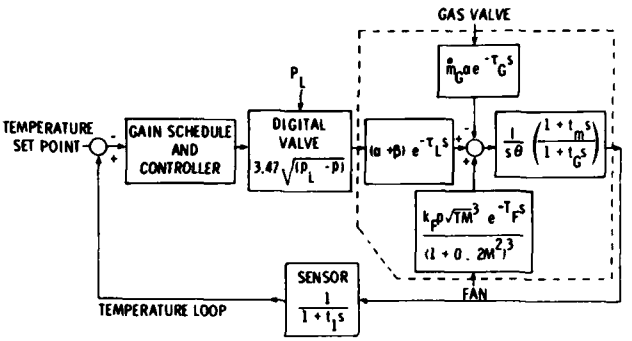

Fig. 11 Schematic of 0.3-m TCT temperature control.

to avoid rapid cooling rates for the tunnel walls, a limit has been placed on liquid flow rate which again is used with an error magnitude dependent logic. All of these features have been incorporated in the temperature control schematic shown in Figure 11.

4.2 Pressure Control

The tunnel pressure control schematic is shown in Figure 12, which has been designed using SISO root locus control analysis. This analysis has resulted in a non-linearly gain scheduled PID control law with a gain schedule of $1/(p\sqrt{T})$ for the total pressure loop. The tunnel pressure control law realization is shown in Figure 13. As can be seen, this scheme includes the logic for augmenting the digital valve area for low pressure runs by using existing analog valves.

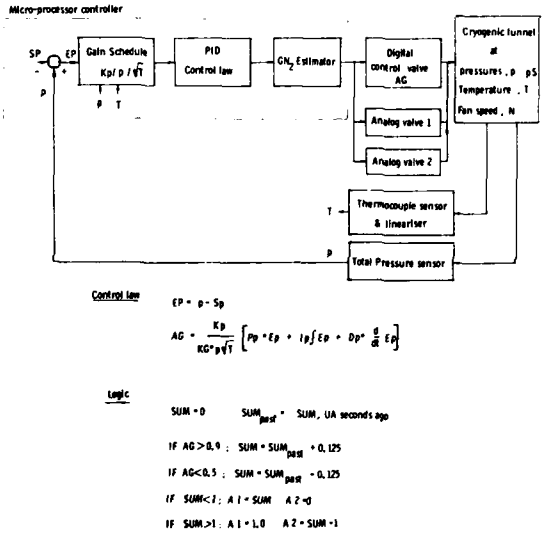

Fig. 12 Automatic pressure control scheme.

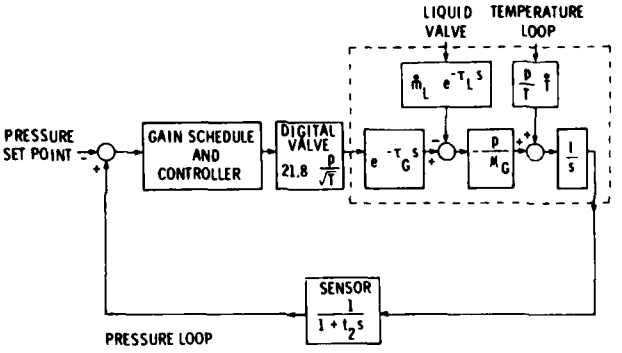

Fig. 13 Schematic of 0.3-m TCT pressure control.

4.3 Verification

These control laws, shown in Figures 11 and 13, were first proved on the tunnel simulator. The temperature and pressure loop performances on the simulator, for set point changes, are shown in Figures 14 and 15. Typically a settling time of about 20 seconds can be noted for each loop. It demonstrated the ability of SISO control laws to perform properly in the presence of cross coupling.

The control laws were then mechanized on a custom built microprocessor based controller working at 10 samples/sec. The microprocessor based controller has been successfully commissioned and proven for the total envelope of tunnel operation. The tunnel performance under closed loop control is very good and agrees well with the performance predicted by the simulator. In Figure 16, a typical cryogenic tunnel run is provided,

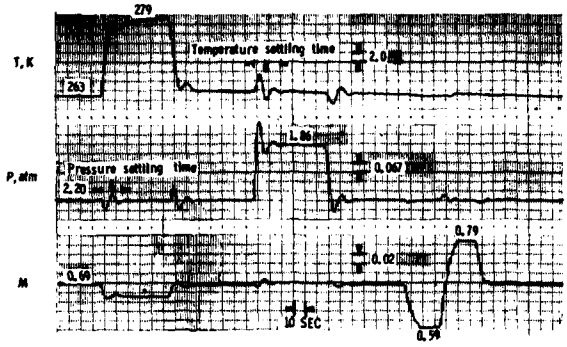

Fig. 14 Simulator closed-loop responses, high temperature.

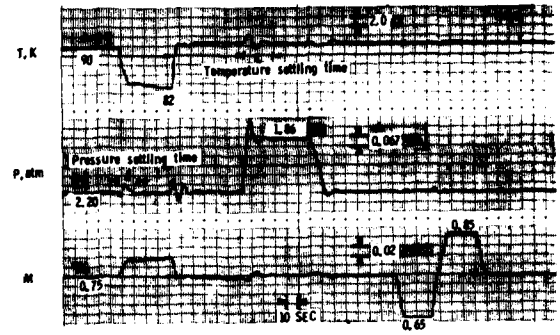

Fig. 15 Simulator closed-loop responses, low temperature.

which shows a cool down of the tunnel from 300 K to 100 K at a constant pressure of 2.1 atm. Once the tunnel temperature reaches 100 K the tunnel pressure is raised to 5.5 atm at constant temperature. Subsequently, a number of Mach number changes and angle of attack changes (from -8^{o} to 16^{o}) for a high blockage model were made while maintaining temperature and pressure at 100 K and 5.5 atm. The disturbances due to Mach number and angle of attack changes on the tunnel temperature and pressure have been successfully countered by the control system resulting in the rapid convergence of the tunnel conditions. Following each change in test condition, tunnel temperature recovered to within ±0.25 K in about 20 secs and pressure to within 0.017 atm (±0.25 psi) within 20 to 30 seconds. Despite the non-linearities and cross coupling in the cryogenic wind tunnel process, the control law designs based on simple SISO analysis have provided good accuracy and stability in the control of both total pressure and total temperature as well as greatly reducing the time taken to get from one set of test conditions to another under manual control.

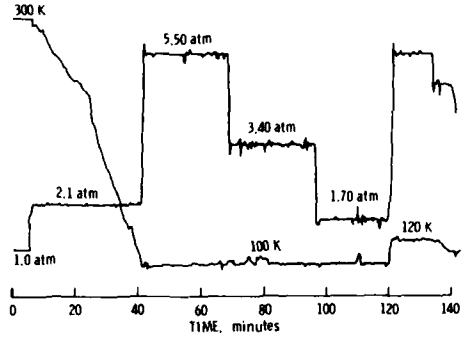

Fig. 16 Typical 0.3-m TCT test with closed-loop control of p and T.

5. FUTURE PLANS

Despite the demonstrated success of the control scheme described in the previous section, further improvements are planned. For example, one of the limitations on temperature and pressure control is caused by a lack of resolution within the existing controller of the analog to digital conversion of the temperature and pressure signals. The existing 10 bit converter is being changed to provide 16 bit resolution. This modification, along with some other minor changes, should result in improvement in temperature control from the present ±0.25 K to ±0.1 K and improvement in pressure control from the present ±0.017 atm to ±0.005 atm.

In addition, provision is being made for the automatic control of Mach number by closing the loop on fan speed in order to control the ratio of test section static pressure to total pressure.

The ultimate goal of the 0.3-m TCT control effort is to reduce the cost of operation of the tunnel while at the same time providing the needed degree of stability for the test conditions. Future work toward this goal will include refinements to the mathematical model by the use of identification techniques for more precisely determining the tunnel parameters and the development of some optimal control schemes in order to allow either energy or time minimization in the operation of the tunnel.

6. CONCLUDING REMARKS

In this lecture the efforts of synthesizing a control compatible mathematical model from first principles, and validation of the model by comparing experimental responses with mathematical model responses, and finally the design of a tunnel controller for the Langley 0.3-m TCT and its successful performance have been described.

It has been shown that, despite the non-linearities and cross coupling in the cryogenic wind tunnel process, control law designs based on simple single input-single output analysis

provide good accuracy and stability in the control of both total pressure and total temperature for the 0.3-m TCT. In addition, the use of automatic control schemes has greatly reduced the time previously required under manual control to change from one set of test conditions to another. Thus, the goals set for the 0.3-m TCT of efficient operation and stability in test conditions have been realized by the straightforward application of automatic control schemes.

Since no specific assumptions with respect to the dimensions of the 0.3-m TCT are made in the development described herein, it is expected that the methodology used for the 0.3-m TCT controls development would yield satisfactory results for other tunnels having different dimensions if they were otherwise similar to the 0.3-m TCT. In this case, "similar" implies having a closed circuit, being cooled by the direct injection of LN_2, and having roughly the same ratio of metal to gas enthalpies. Whether or not the approach used to develop the control schemes for the 0.3-m TCT can be generalized to other continuous-flow cryogenic tunnels remains to be demonstrated.

7. REFERENCES

1. Kilgore, R. A.; Goodyer, M. J.; Adcock, J. B. and Davenport, E. E.: The Cryogenic Wind Tunnel Concept for High Reynolds Number Testing. NASA TN D-7762, November 1974.

2. Balakrishna, S.: Synthesis of a Control Model for a Liquid Nitrogen Cooled, Close Circuit, Cryogenic Nitrogen Wind Tunnel and its Validation. Report from Old Dominion University Research Foundation on NASA sponsored project NSG-1503. NASA CR-162508, November 1979.

3. Corrucini, R. J.; and Gniewek, J. J.: NBS Monograph 21, October 1960.

4. Bartz, D. R.: A Simple Equation for Rapid Estimation of Rocket Nozzle Convective Heat Transfer Coefficients. Jet Propulsion, pp. 49-51, January 1957.

5. Kilgore, R. A.: Design Features and Operational Characteristics of the Langley 0.3-m Transonic Cryogenic Tunnel. NASA TN D-8304, December 1976.

6. Ray, E. J.: Review of Design and Operational Characteristics of the 0.3-meter Transonic Cryogenic Tunnel: Proceedings of the First International Symposium on Cryogenic Wind Tunnels, Paper 28, April 1979.

7. Balakrishna, S.: Automatic Control of a Liquid Nitrogen Cooled Closed Circuit Cryogenic Pressure Tunnel. Report from Old Dominion University Research Foundation on NASA sponsored project NSG-1503, March 1980 (under preparation).

8. ACKNOWLEDGEMENTS

The author is grateful to NASA for permission to present this lecture. He also wishes to thank his colleagues at the Langley Research Center whose willing assistance has made this lecture possible. In particular, he is indebted to Dr. S. Balakrishna and Mr. J. J. Thibodeaux, without whose efforts the successful control of 0.3-m TCT could not have been realized and upon whose work this paper is based.

THE CONTROL OF PRESSURE, TEMPERATURE AND MACH NUMBER IN A BLOWDOWN - TO - ATMOSPHERE CRYOGENIC WIND TUNNEL

by
J. D. Cadwell
Branch Chief
Wind Tunnel Test and Development
Aerodynamics Subdivision
Douglas Aircraft Company
McDonnell Douglas Corporation
3855 Lakewood Blvd.
Long Beach, Ca. 90846
USA

SUMMARY

The control system that was used in the Douglas Aircraft four-foot blowdown wind tunnel prior to the modification of the facility to a cryogenic operation is reviewed. The control requirements for a cryogenic blowdown tunnel and the Mach and Reynolds number controls are discussed. The proposed method to be used to control the temperature in the cryogenic tunnel is shown. The start of a blow sequence in a cryogenic blowdown tunnel and the detrimental effect that it has on a pre-cooled model is considered. A transient protection system, to be evaluated in the one-foot pilot tunnel, that will shield the model during the start of a run is shown. The conventional method of measuring model attitude by correcting the pod angle for sting and balance deflections is shown to be inadequate in a cryogenic blowdown tunnel and alternate methods that can be used are discussed.

INTRODUCTION

The Douglas Aircraft Company four-foot wind tunnel began operation in 1959 as a supersonic tunnel with a maximum Mach number of 5.0. A transonic cart became operational in March 1962 giving the facility a trisonic capability and was known as 4-TWT. Figure 1 illustrates the tunnel circuit and identifies the major operating components.

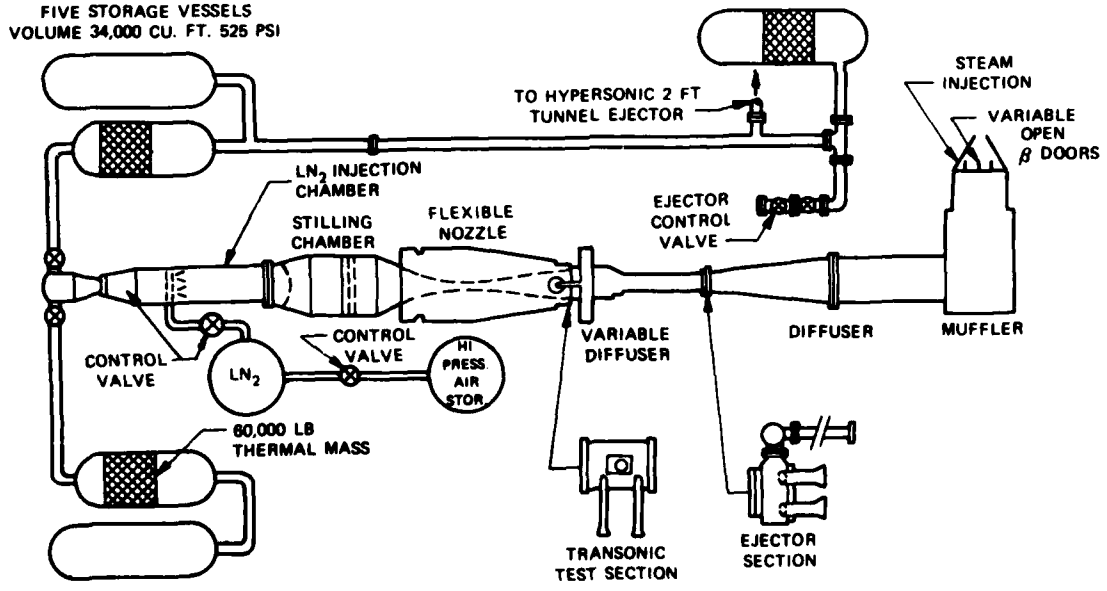

FIGURE 1. FOUR FOOT TRANSONIC WIND TUNNEL - MACH 0.5 TO 5

The original control system was built using conventional hydraulic and electrohydraulic devices driven by state-of-the-art vacuum tube electronics. The control equations for each controller were mechanized using analog computers. A control modernization program, initiated in 1972 to increase reliability of the electronics, improve maintainability, and improve run efficiency, is described in reference 1. The design approach was to a) replace vacuum tube electronics with state-of-the-art equipment based on solid-state technology, b) replace analog computers in each controller with one central digital computer which controls all systems, c) use a modular concept so that each controller is self contained, and d) use similar circuits, power supplies, amplifiers, etc. wherever possible to reduce spare parts requirements and enhance maintainability. The modernization program was completed in 1974 and is the system that was in operation when the tunnel was shut down in 1976 for the modification of the tunnel to operate at cryogenic temperatures. The following discussion will review the control system that was in operation when the modification was initiated and the additional controls required to maintain tunnel total temperature down to 180 degrees Rankine.

CONTROL REQUIREMENTS

The short run times of a blowdown wind tunnel make it imperative that a computer controlled control system be used to maximize the output of the tunnel. The cryogenic addition to the facility increases the performance envelope by a large factor which adds to the requirement for adequate control systems for all pertinent variables. Figure 2 illustrates the many control systems necessary to effect the necessary results from a cryogenic blowdown wind tunnel.

P_T = TOTAL PRESSURE
P_∞ = PLENUM PRESSURE (≈ FREESTREAM STATIC)
P_{TJ} = EJECTOR TOTAL JET PRESSURE

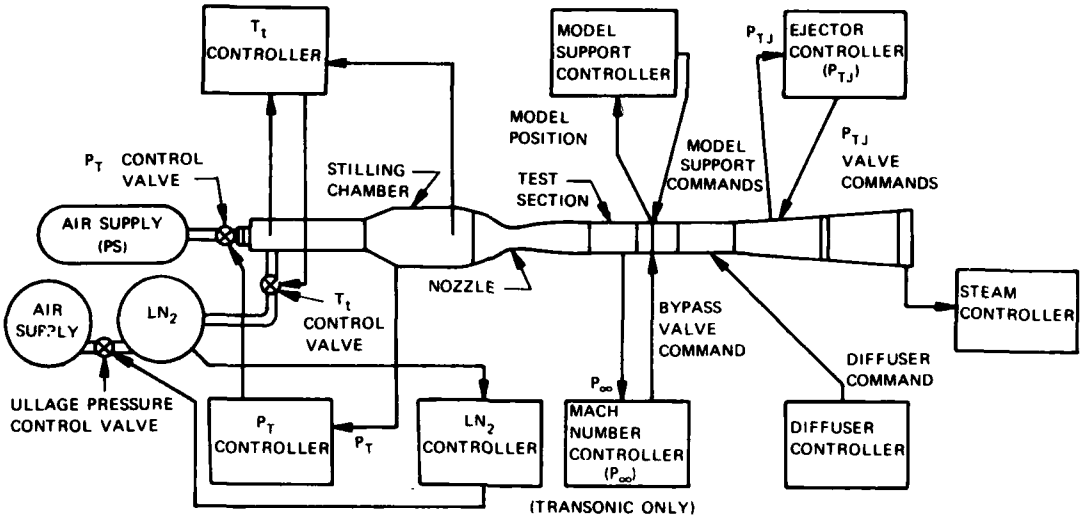

FIGURE 2. MAJOR CONTROL SYSTEMS IN THE 4-TWT

The 4-CWT control systems are listed as follows

Freestream Total Pressure
Transonic Plenum Bypass Valves (Mach >.7)
Variable Diffuser (Mach ≤.7)
Ejector Total Pressure
Transonic Plenum Auxiliary Suction System
Model Support - Pitch and Strut Position
Model Support - Roll Position
Temperature Control - Liquid Nitrogen Pressurization
Temperature Control - Liquid Nitrogen Flow
Pressure/Temperature Safety Interlocks
Auxiliary Air System (2000 PSI)

The PDP-11/34 computer, the decision maker and director of the control system in the 4-CWT, is configured with the following:

64K bytes memory
Two RK05 Disk Drives (2.5M bytes each)
Floating Point Processor
LA36 DEC Writer
Real Time Clock

The computer is dedicated to controlling the 4-CWT during a blowdown. The software system is executed every 32msec. During the 32msec the A/D converters (32 channels) are inputed and various control parameters are computed. The output through D/A converters is used to control (12) servo hydraulic systems of the 4-CWT. The software also monitors all safety parameters of the 4-CWT and will abort the blowdown in the event of a component failure.

The primary tunnel flow parameters and the accuracy desired for each is as follows:

Mach number ±.001
Reynolds number ±100,000

Mach number is a function of the tunnel total pressure and the free stream static pressure as related to the test section plenum chamber pressure. Reynolds number is a function of free stream static, Mach number, and the square root of the free stream static temperature. The control systems necessary to meet the basic flow conditions of Mach and Reynolds number are:

Tunnel total pressure and temperature
Free stream static pressure

In addition to the basic flow conditions, the model attitude must be controlled in pitch and yaw modes in order to obtain the aerodynamic characteristics of the configuration being tested.

There are also many interactive or auxiliary support systems that must function in order to permit a smooth and efficient tunnel operation. Included in this category are:

Safety interlocks for both pressure and temperature
Ejector total pressure
Exhaust cloud control
Model temperature control
Balance temperature control

Figure 3, is a flow chart which describes the overall control system and illustrates the interface between the PDP-11/34 computer/controller, and the 4-CWT control sub-systems. This particular system is well suited to the Douglas Aircraft four-foot wind tunnel. It is flexible, fast, and reliable. However, in order to perform as the design intends the system requires readily available software skills.

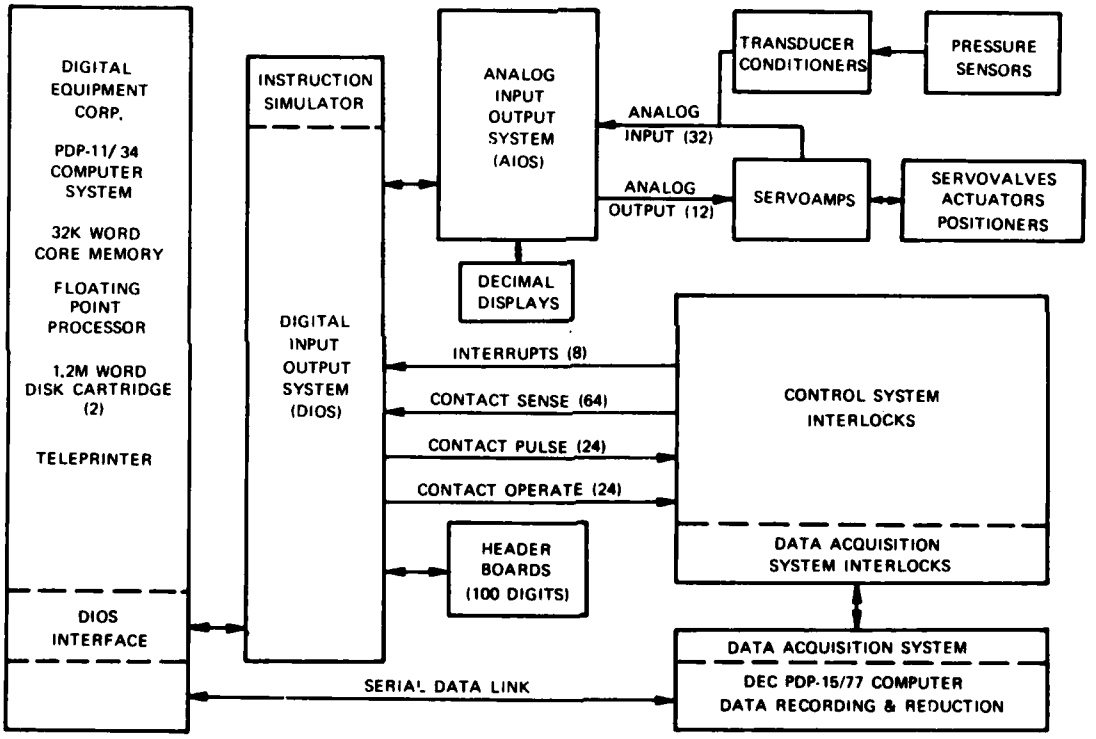

FIGURE 3. COMPUTER INTERFACE WITH 4-CWT CONTROL SYSTEM

MACH & REYNOLDS NUMBER CONTROLS

Prior to the cryogenic modification the tunnel Mach and Reynolds numbers were set by controlling the tunnel total and the free stream static or plenum chamber pressures. Heat sinks in the storage tanks helped stabilize the temperature of the air as the tank pressure decreased during a blow. This system will also be utilized during cryogenic operation by presenting the temperature control system with a steady initial temperature before the air from the tank is exposed to the liquid nitrogen injection system. It is anticipated that the tunnel total pressure control system will function in the cryogenic mode much as it had in the standard temperature operation except that the pressure will be influenced by the liquid nitrogen injection. In other words, the total pressure sensor in the stilling chamber will continue to seek the desired total pressure value regardless of whether circuit losses or changes in pressure due to cooling of the air by the liquid nitrogen are causing a disparity in the total pressure reading. The total pressure control system therefore is essentially the same for cryogenic or standard operations. Standard operation is when the tunnel is operated without the liquid nitrogen cooling system and the tunnel total temperature is basically the temperature in the storage tanks.

The tunnel total temperature will be sensed by a thermocouple in the settling chamber that has been correlated with the test section mean temperature. The basic temperature control will be to vary the valve opening in the liquid nitrogen supply line. The relatively long reaction time between the valve and the temperature monitoring point in the stilling chamber dictate that a temperature measurement near the injection station must be incorporated in the control equation for telegraphing to the control station in the settling chamber that corrective action to the temperature error has been taken and has been effective at the injection station.

The accurate control of the test temperature is a difficult problem because of the lag time between changes in LN_2 injection rate and the changing heat transfer from the tunnel circuit to the air stream. It takes from about one-half second at Mach 1.0 to one second at Mach 0.5 for the air stream to travel from the injection point to the sense point. If the sense point were moved closer to the injection location an error in magnitude would result because the difference between the upstream sensor and the stilling chamber sensor is not constant, i.e., on start-up the internal components are relatively warm and transfer heat to the air stream, as the run progresses, these components cool down and transfer less and less heat to the air stream. On closely coupled runs the initial temperature of components will not be the same. These characteristics combine to create a varying differential between the stilling chamber temperature and a temperature sensed immediately down stream of the injection station.

The proposed solution to this problem is to use two sensors for control. The stilling chamber temperature is sensed and compared to the set-point. The computer also determines the rate of change of the upstream sensor and must decide whether to affect a change in the injection rate. Corrective action is based on the error signal which is the sum of the error in set-point and the rate of change of the upstream sensor. The following examples illustrate how the system will operate:

1. The difference between set-point and stilling chamber temperature is zero and the rate of change of the upstream sensor is zero. The error signal is zero and no change is made.

2. There is a difference between set-point and stilling chamber temperature and there is a large rate of change in the upstream sensor. The computer would receive an error signal and take action to reduce the rate of change of the upstream sensor. The temperature control valve function is described by the following equation:

$$P_n = P_\ell + K_1 (\epsilon_n - \epsilon_\ell) + K_1 K_2 \epsilon_n \Delta T$$

where:

P_n	=	valve position command
P_ℓ	=	last valve position command
K_1	=	gain, f(MACH)
K_2	=	time constant, f(MACH)
K_3	=	gain, TBD
ΔT	=	program sample TIME = .032 seconds
ϵ_n	=	temperature error
	=	$T_{set} + [T_t + K_3 (T_{in} - T_{i\ell})]$
T_{in}	=	temperature near the injection station
$T_{i\ell}$	=	last temperature near the injection station
T_t	=	temperature in the stilling chamber
ϵ_ℓ	=	last temperature error

The Mach number or free stream static pressure is controlled below Mach = 0.73 by varying the area at the downstream throat section. This control is also utilized below Mach = 0.73 to keep the Mach number and the free stream static pressure constant as the losses in the test section increase, for instance, as the model angle of attack increases the effective critical area decreases which would allow the Mach number to decrease if corrective action was not taken. At Mach numbers above 0.73 this correction, as well as the basic Mach number control, is made by opening the by-pass valves between the plenum chamber and the diffuser.

TUNNEL START

The start of the tunnel for a cryogenic blow is very critical for the case where the model has been pre-cooled by the spray cooling technique, shown in Figures 4 and 5, and is not protected. It can be assumed that no liquid nitrogen will flow until the main tunnel control valve has opened. If the reverse were true, that is, if liquid nitrogen were allowed to flow before the tunnel control valve was opened, a pool of liquid nitrogen would collect along the bottom of the injection chamber and eventually flow into the stilling chamber. This pool would continue to evaporate during the course of a blow giving an unsteady temperature distribution in the test section. The assumption that no liquid nitrogen flows until the main control valve opens therefore is a realistic one that adds to the interaction problem that will exist between the pre-cooled model and the relatively warm stagnant air that is trapped between the main control valve and the test section.

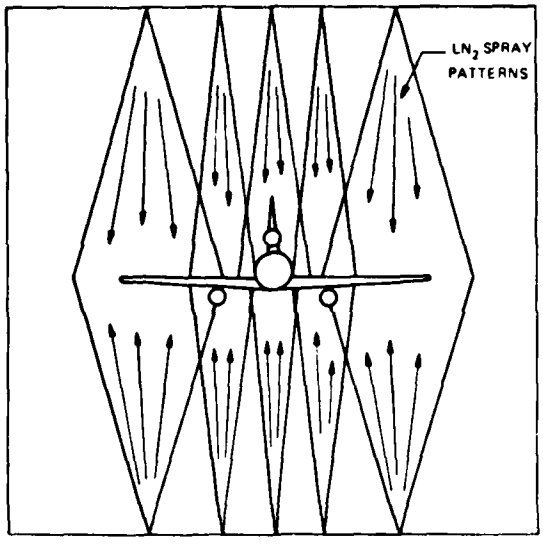

FIGURE 4. MODEL PRE-COOLING FOR WING, FUSELAGE, WING NACELLES AND PYLONS

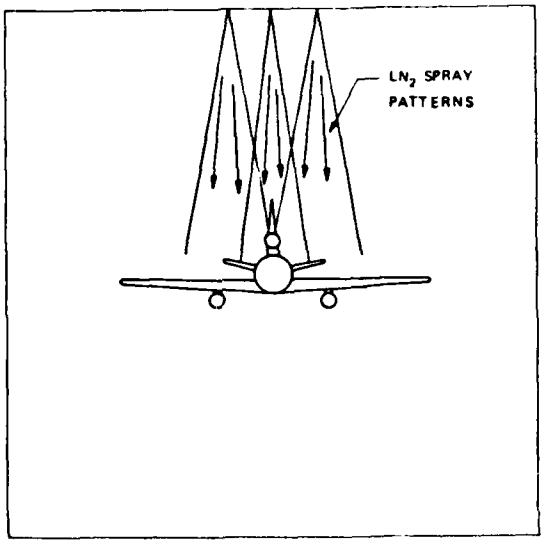

FIGURE 5. MODEL PRE-COOLING FOR EMPENNAGE AND AFT NACELLE AND PYLON

When the model pre-cooled temperature has been achieved, the spray is turned off, zero and calibrate information is taken, the tunnel starting sequence is initiated, and the tunnel total pressure and temperature reach equilibrium in the time shown below in Figure 6.

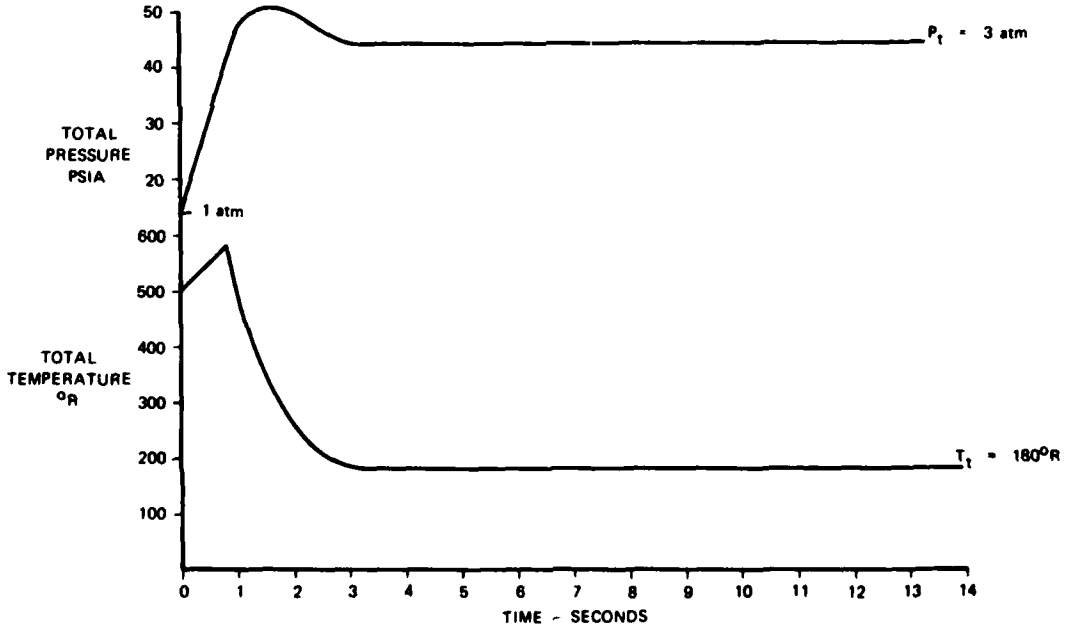

FIGURE 6 ESTIMATED CHARACTERISTICS OF 4-CWT STARTING TRANSIENT

During the starting process the pre-cooled model has been subjected to the trapped warm air described earlier for only a short time period, however, the aerodynamic heating virtually destroys the model pre-cooling as shown in Figure 7. Overcooling the model to a temperature near the boiling point of liquid nitrogen would not appreciably modify the time required for the model temperature to recover from the starting transient for a test at a tunnel total temperature of 180°R. This effect becomes less critical as the desired tunnel temperature is increased. However, the test conditions where the majority of blows will be made, will be at tunnel total temperatures that are as close to the saturation temperature as possible, in order to achieve the highest test Reynolds number. It is quite clear that some form of protection for the model, during the tunnel start, is required.

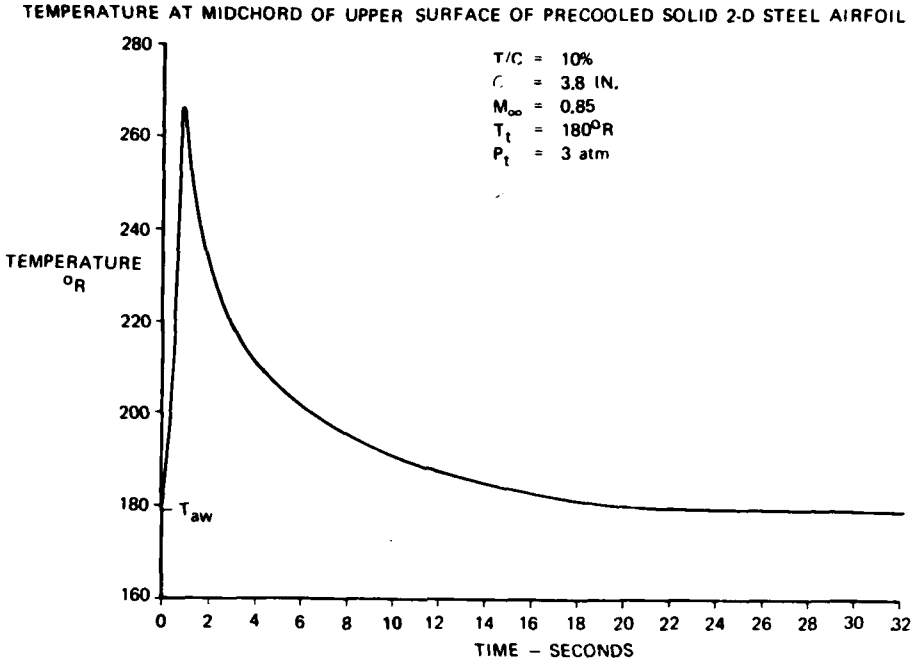

FIGURE 7. ESTIMATED MODEL SURFACE TEMPERATURE RESPONSE TO 4-CWT STARTING TRANSIENT

Sophisticated pre-cooling methods that could be used that would also protect the model during the tunnel starting process are a retractable model conditioning enclosure described as a clamshell and shown in Figure 8 or injecting the model into the tunnel from an enclosure that would pre-cool the model to the desired temperature. Each of the above methods would be operationally complicated, require considerable time to design, fabricate, and install, and would require a significant capital expenditure to incorporate into the facility. Undoubtedly, one of the above methods will be added to the facility in order to obtain quality data without expending excessive quantities of liquid nitrogen, unless the scheme to fabricate models with composite materials proves successful and eliminates the requirement to pre-cool the model as well as the need to protect the model during the starting transient. However, when the facility first operates with a pre-cooled model installed in the test section it must be protected from the tunnel starting transients in order to minimize the time required for the model to reach the desired adiabatic wall temperature.

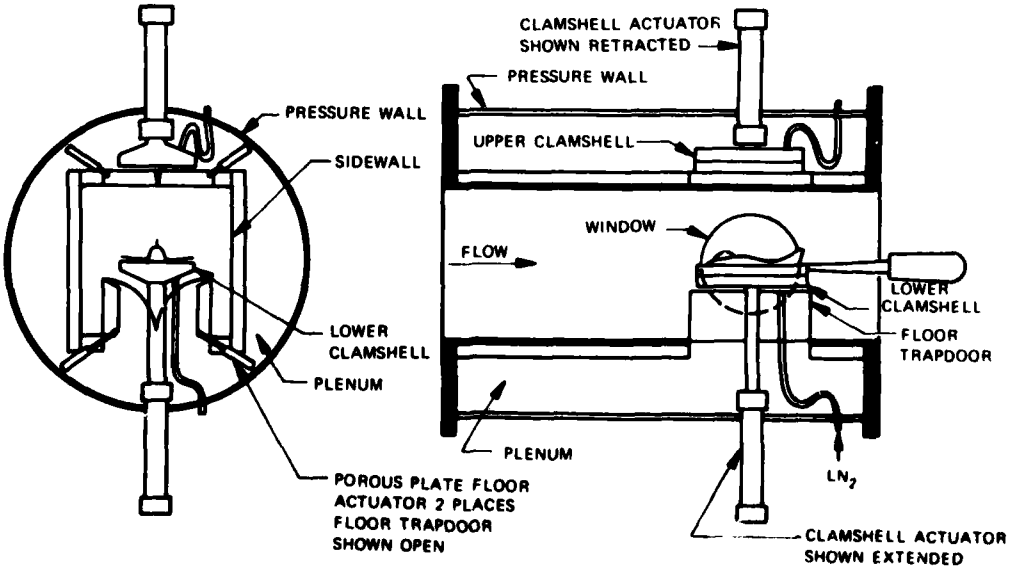

FIGURE 8 MODEL CLAMSHELL PRE-COOLING SYSTEM

TRANSIENT PROTECTIVE DEVICES

One method that is being evaluated in the one-foot cryogenic pilot tunnel, 1-CWT, is a wedge shield that will spray liquid nitrogen into the on-coming air stream as shown in Figure 9.

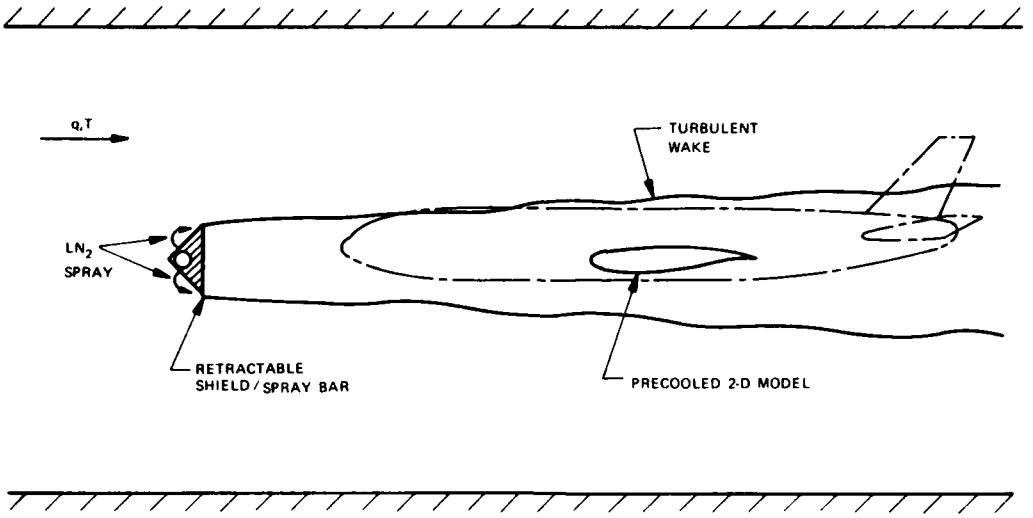

HEAT TRANSFER FROM WARM AIR PULSE TO COLD MODEL REDUCED BY
- o REDUCTION OF FLUID VELOCITY OVER MODEL
- o COOLING OF AIR FLOWING AROUND MODEL BY COLD SHIELD STRUCTURE (HEAT SINK)
- o FURTHER COOLING OF AIR AROUND MODEL BY LN_2 SPRAY FROM SHIELD

FIGURE 9. 2-D MODEL TRANSIENT PROTECTION CHECKOUT IN 1-CWT

The reaction of the air stream on the liquid nitrogen will be to break the liquid nitrogen into small droplets that will be carried back past the wedge and hopefully set-up a region of cold air that will surround the model. When the air stream becomes cooled by the tunnel liquid nitrogen injection system, the shield would be retracted out of the test section into the plenum chamber.

Another method being considered would utilize the translating capability of the tunnel support pod and move the model to the bottom test section wall. With the model near the wall, a section of the wall could be oriented to serve as a blast fence that would shield the model from the tunnel air stream as shown in Figure 10. The flow quality that the model would be exposed to with the wall section deflected must be evaluated. The flow at that point would undoubtedly be quite rough, but the flow field where the model is located should not have a significant dynamic pressure head.

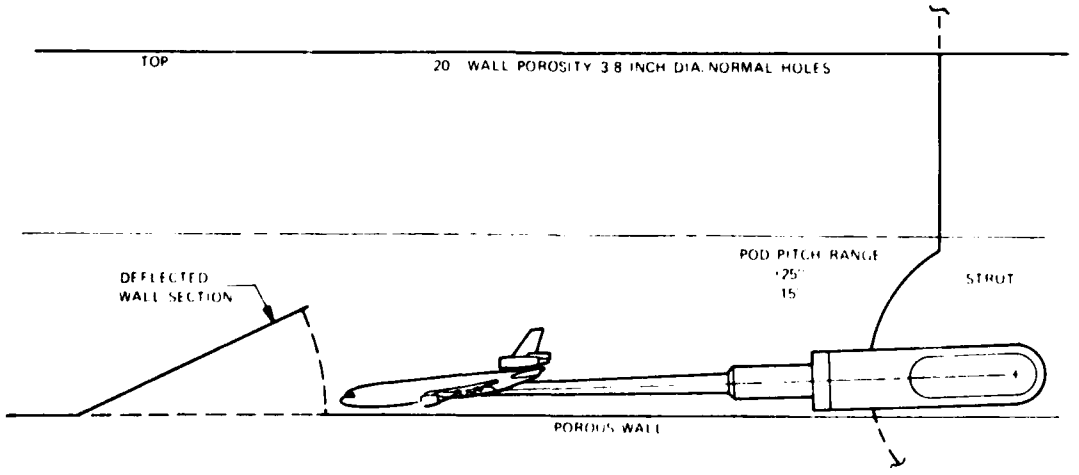

FIGURE 10 MODEL SHIELD DURING START USING DEFLECTED WALL SECTION

MODEL ATTITUDE CONTROL

The blowdown cryogenic wind tunnel further complicates the life of the test engineer who is trying to resolve the drag of a configuration from a body axis six-component strain gage balance. The aerodynamicist watches his career rise or fall by counting those elusive drag counts that depend on his knowing the angle of attack to a very close tolerance. For instance, an error in angle of 0.0115^{o} will represent a one count error in the drag coefficient, 0.0001, at a normal force coefficient of 0.5. Determining the angle within this close tolerance is very difficult under ideal conditions but under cryogenic blowdown conditions it is not possible using standard techniques. The technique normally used in conventional blowdown tunnels is to accurately measure the pod or sting angle where it is not effected by the load on the model and to deduce the true angle of the model by calibrating the change of angle due to the load and the load point on the model. Using this technique the angle can be resolved to $\pm.02^{o}$. Laboratory tests have shown that this procedure is not advisable where the heat transfer is not uniform along the sting or from top to bottom of the sting. The non-uniform cooling can give the sting a "hot dog" effect which is an order of magnitude greater than the desired accuracy and not repeatable.

The emphasis therefore is to develop an angle of attack system that will measure the model attitude directly. Accelerometers or dangleometers have been used in continuous flow tunnels with reasonable success - generally in the ± 0.02 to 0.03 degree repeatability. The damping characteristics can be set so that accurate angle information can be obtained. This is more difficult in a blowdown tunnel where the required damping characteristics increase the reaction time such that the system lag cannot accurately track the angle during the sweep technique used in a blowdown tunnel. Other solutions that must be considered are laser beams or other optical systems that can track the model attitude through its angle of attack range. In any case, the normal control system to be used for model attitude would be a sting or pod measurement while the system to determine the true model angle of attack would be used to resolve the body axis data into the desired aerodynamic coefficients.

REFERENCES

1. A. B. Smee; "MDAL 4-TWT Control Modernization Program". Presented at the 37th Semi-Annual Supersonic Association Meeting, Aberdeen Proving Ground, Maryland, May 4-5, 1972.

THE EUROPEAN TRANSONIC WINDTUNNEL ETW

by

J.P. Hartzuiker and R.J. North

Technical Group ETW
c/o National Aerospace Laboratory NLR
Anthony Fokkerweg 2
1059 CM AMSTERDAM
The Netherlands

SUMMARY

This lecture contains a progress report on the European Transonic Windtunnel ETW. The high-Reynolds-number transonic tunnel is described on the basis of preliminary design results.

Also the construction of a cryogenic pilot tunnel (PETW) and supporting programs on model design and instrumentation are discussed.

LIST OF SYMBOLS

$\bar{c}$	mean aerodynamic chord
M	Mach number
n	fan speed
p_o	total pressure
$\dot{q}$	mass flow
Re	Reynolds number
T_o	total temperature

1. INTRODUCTION

The Governments of France, the Federal Republic of Germany, the Netherlands and the United Kingdom are co-operating under a Memorandum of Understanding with the intention to build a transonic windtunnel for high Reynolds numbers.

This MoU covers the Preliminary Design of the European Transonic Windtunnel ETW. The windtunnel will be of the cryogenic type. Also included in the MoU is the construction of a scale model of the tunnel, the Pilot ETW (PETW). In parallel a program is performed on

model design and instrumentation under cryogenic conditions, in close co-operation with the national programs of the participating countries.

The present MoU covers the time period from early 1978 until mid 1981. The Preliminary Design of ETW has been finished and PETW is under construction. The Steering Committee ETW, consisting of members named by the respective Governments, has established an international Technical Group of 11 members. This Technical Group is situated at NLR, Amsterdam until the site of ETW has been chosen. The Group directs the contracts for Preliminary Design ETW, the design and construction of PETW as well as other contracts (special studies, model design, etc.).

A follow-up MoU is being prepared, covering a period of about 2 years in which the Final Design of ETW will be done.

This lecture summarizes the results of Preliminary Design of ETW, whereas short descriptions will be presented of PETW and the programs on model design and instrumentation.

2. ETW

2.1 General

The ETW will be a closed-circuit continuous transonic windtunnel. Liquid nitrogen will be injected to obtain the low working temperatures desired for testing at high Reynolds numbers. The advantages of working at low temperatures have been explained in earlier publications [1,2] and will not be repeated here.

The selection of a cryogenic windtunnel has been made on the basis of extensive engineering studies, which were reported earlier[2].

An artist's impression of ETW is presented in figure 1.

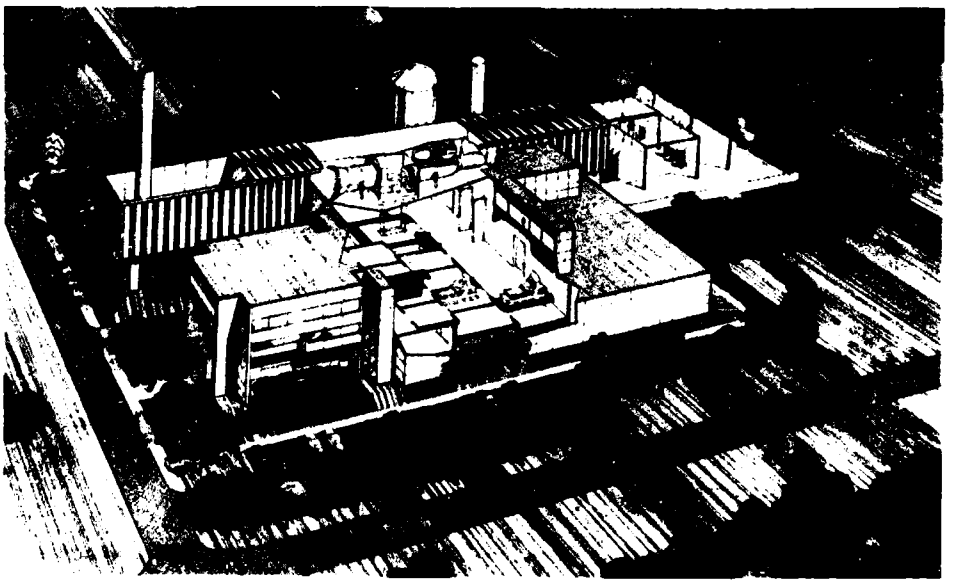

Fig. 1 - Artist's impression of ETW

AD-A089 050 ADVISORY GROUP FOR AEROSPACE RESEARCH AND DEVELOPMENT--ETC F/G 14/2
CRYOGENIC WIND TUNNELS.(U)
JUL 80
UNCLASSIFIED AGARD-LS-111 NL

3 OF 3

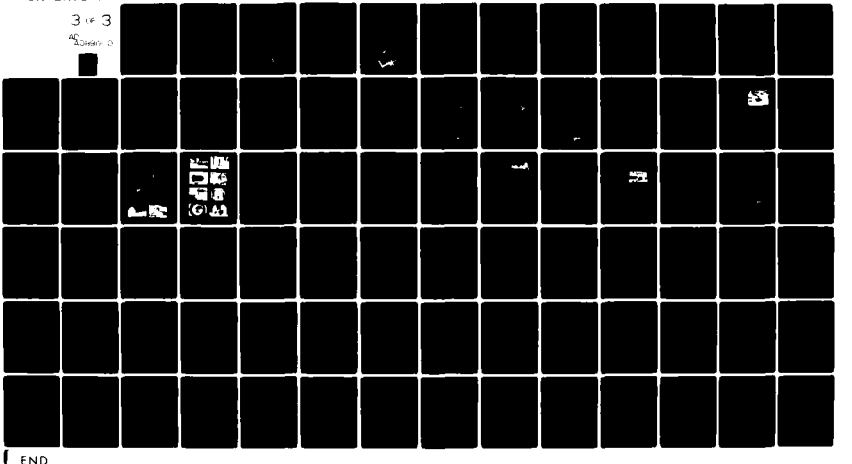

END
DATE FILMED
10-80
DTIC

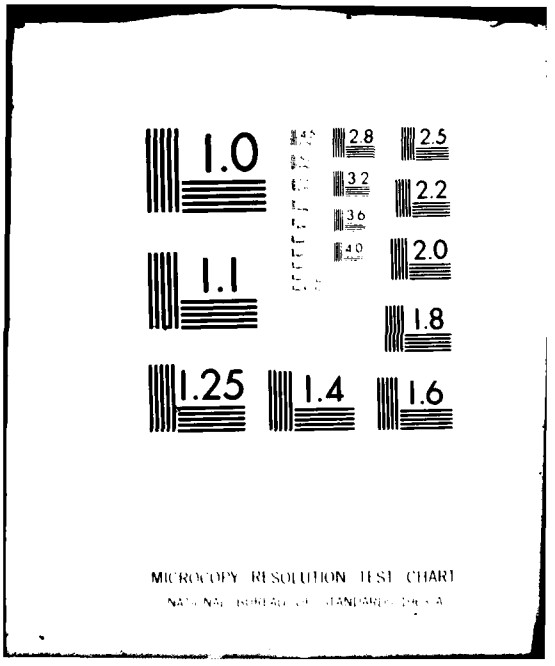
1.0
1.1
1.25
2.8
3.2
3.6
4.0
2.5
2.2
2.0
1.8
1.4
1.6
MICROCOPY RESOLUTION TEST CHART

2.2 Aerodynamics and performance considerations

2.2.1 Specifications

The principal requirements for ETW were laid down by the Large Windtunnels Working Group (LaWs) of the Fluid Dynamics Panel of AGARD in 1972[3] and 1974[4] following the philosophy that it should enable model tests to be made over a range of Reynolds numbers which, if not extending to full-scale, would permit extrapolation to flight conditions to be made with confidence. The Reynolds number (based on model mean aerodynamic chord) should be variable between 25 x 10^6 and 40 x 10^6 at the design point M = 0.9.

The maximum Mach number should be M = 1.35. After adoption of the cryogenic option in 1977[2] the ETW specifications were settled. The test section size of 1.95m x 1.65m was chosen as the minimum at which the required model detail can be adequately represented. This size was chosen to minimize capital investments.

Furthermore the conservative assumption was made that on the model local flow saturation would take place at a local flow Mach number of 1.7. This, together with the given test-section dimensions and the required Re = 40 x 10^6, leads to a maximum stagnation pressure of about 4.5 bars.

2.2.2 Performance

The operating envelope at design Mach number M = 0.9 is presented in figure 2.

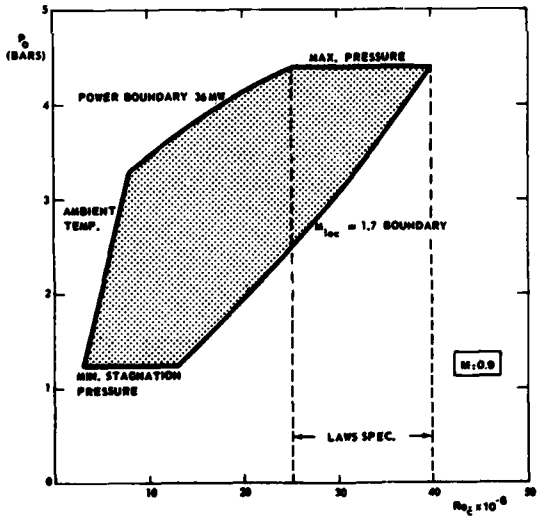

Fig. 2 - Operating envelope of ETW at design Mach number

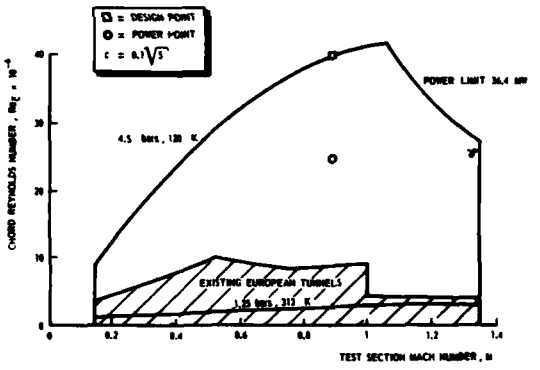

Fig. 3 - Reynolds number performance over the Mach number range

The maximum fan power is determined by Re = 25 x 10^6 and 4.5 bars to be about 36MW.

The off-design performance for ETW is shown in figure 3 for the Mach number range from M = 0.15 to 1.35. In the same figure a comparison with existing European facilities is made.

2.2.3 Productivity

The possible modes of operation have been considered in the light of productivity, nitrogen consumption and costs. A number of 5000 polars per year is foreseen, each of about 15 (force polars) to 60 seconds (pressure polars) duration. About 3 runs per day of approximately 10 minutes and 10 polars each are considered at about 2 hour intervals for model access, modification and re-installation.

2.2.4 Flow quality

ETW is meant to provide aerodynamic data at high Reynolds numbers of high standard in a relatively short running time. This implies that the flow quality has to be excellent. Quantitative requirements for turbulence and noise level as well as for pressure fluctuations have been defined in reference 5.

The free stream turbulence level should be less than 0.1%. In view of the concern about the influence of accoustical disturbances on boundary-layer transition and development a test section level noise of little more than that from a turbulent boundary layer on a flat plate should be aimed at.

The preliminary design had further been based on steady and unsteady uniformities in M of 0.001 for subsonic and 0.003 for supersonic operation respectively. The maximum deviation in temperature is 0.25K (all 2σ values).

2.2.5. Aerodynamic circuit

A circuit optimization study has been conducted[6] to define the most economic circuit configuration based on the combination of capital and operating costs consistent with the above flow quality, the defined test spectrum and the operational requirements. From this study the main circuit features were defined. In the course of preliminary design the first corner was opened up slightly and some diffusion was introduced in the first cross leg, in order to minimize losses in the 2nd corner (where a catch net is placed) and to obtain some contraction into the compressor. Figure 4 shows the present ETW circuit. A short description of the main circuit features follows.

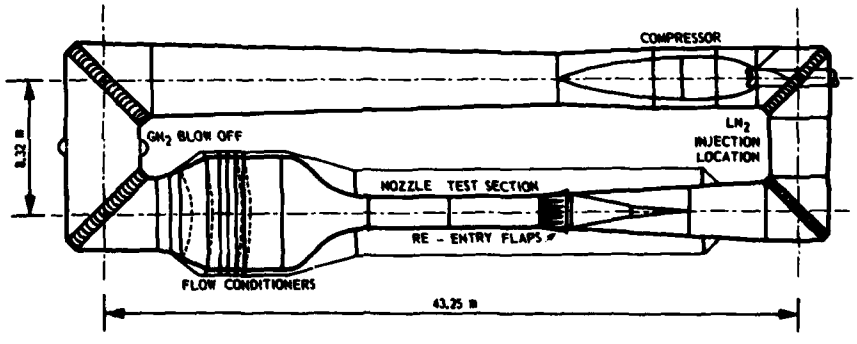

Fig. 4 - ETW aerodynamic circuit

The wide angle diffuser (AR = 2.4) has 2 conical segments and 2 spherically shaped filling screens. The honeycomb (L/D = 25) and 2 anti-turbulence screens are designed to meet, in connection with the contraction, the flow quality requirements of 0.1% turbulence level and maximum flow misalignment of 0.1° in the test section.

The total contraction ratio of 12 is obtained by a fixed 3-dimensional contraction and a 2-dimensional nozzle. The flexible nozzle is to assure good flow quality in the supersonic range up to M = 1.35.

The slot configuration in the test section selected consists of 6 slots on the floor and ceiling and 2 on each side wall with remotely controlled finger type re-entry flaps. Side wall divergence can be remotely set between 0 and 0.25°.

The high-speed diffuser design is chosen to be conservative to prevent separation under any extreme inlet disturbances caused by plenum re-entry flow and model wake.

An alternative high-speed diffuser with a variable geometry sonic throat is developed for use in place of the fixed geometry diffuser if deemed desirable for Mach number control and pressure fluctuation suppression for the regime $0.6 < M < 1.0$. A final decision on the diffuser choice will be done after testing both options in the scale model of ETW.

2.3 Design of components

2.3.1 Pressure shell and insulation

The pressure shell is formed by the plenum around the high-speed leg and by the rest of the aerodynamic circuit. The plenum contains a rectangular downward extension, the model access lock, which will be discussed later.

A drawing of the pressure shell is presented in figure 5. The shell will be of welded construction fabricated from austenitic stainless steel and will incorporate removable flange bolted sections at the compressor and at the screens.

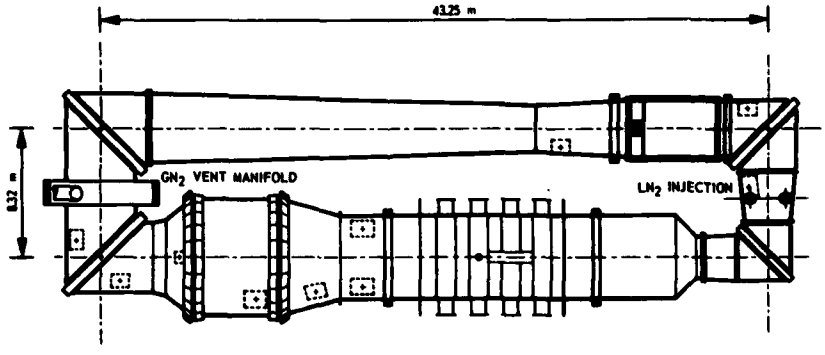

Fig. 5 - Pressure shell design

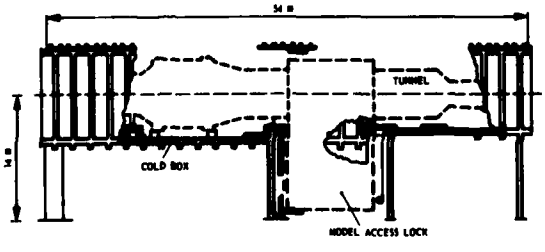

Fig. 6 - Cold box around the pressure shell

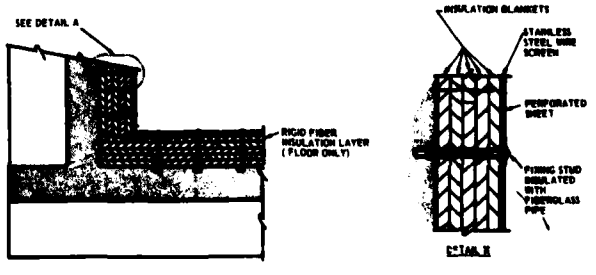

Fig. 7 - Details of insulation in cold box

The shell will be supported by spherically ended vertical struts, stabilised by 3 lateral guides and anchored at the fixed point of compressor thrust reaction.

The complete tunnel circuit will be contained within a reinforced concrete "cold box' which will incorporate a number of removable roof panels for access to major equipment (figure 6).

To achieve the necessary cryogenic environment for the pressure shell the 'cold box' will be lined with fibre glass insulation blankets to a total thickness of 0.4m (figure 7). The blankets will be covered with a fine mesh stainless steel wire screen and faced finally with perforated stainless steel sheet.

It should be noted that the floor area alone within the 'cold box' will incorporate a layer of rigid fibre to provide support for personnel during casual access.

A vapour barrier will be applied to the interior surfaces of the insulated concrete to provide protection against condensation. The severity of local cold spots where pressure shell supports and guides are to be secured will be minimised by the use of insulated bearing pads.

2.3.2 Test Section

The test section is 5.65m long. It is of rectangular section 1.95m wide and 1.65m high giving an area of $3.2m^2$.

Ventilation with slotted walls is used; with 6 slots in roof and floor, and 2 slots in each sidewall. The final wall open area ratio will be chosen during Final Design, but the design allows for a maximum area ratio of 12%.

Most models will be sting mounted, but provision is also made for floor-mounted half models. For sting supported models, a circular arc strut will be used giving a pitch angle range of -10° to $+25^{\circ}$(figure 8). However one of the interchangeable model carts is planned as a special purpose cart with a support strut giving a pitch range of -10° to $+35^{\circ}$.

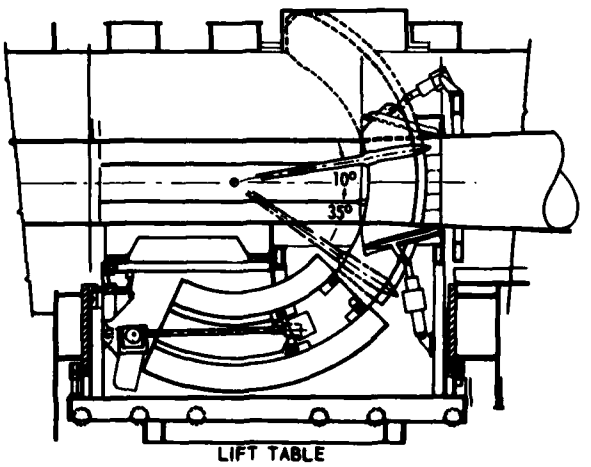

Fig. 8 - Typical model support

Testing will be possible in continuous sweep or pitch/pause mode, pitch rate being variable up to about 4 degrees/sec. Side slip will normally be obtained from a combination of pitch and roll, but a "double roll" sting to provide wings-level sideslip will be available for small incidence and side slip cases.

Finger type re-entry flaps at the rear of the slots will be used, starting at the strut leading edge station. It will be possible to trim the flaps remotely over a range of about 20°. At high sting incidences, part of the re-entry flap area in the floor has to retract to clear the sting and roll unit; this has led to some compromise in re-entry flap design at this point.

Sidewall angle is adjustable to allow for boundary layer blockage along the test section, and area blockage compensation for the support strut and roll unit is also built in to the sidewall profile.

2.3.3 Model access and handling

As mentioned earlier, the ETW productivity target, once the tunnel operational, is for 5000 test polars to be carried out per year using single shift working. Sophisticated model access and handling arrangements will be necessary to achieve this.

An interchangeable model cart system is planned. A cart will be removed from the tunnel to a safe human working environment for adjustments or changes to the model. To conserve nitrogen, it will be possible to keep the tunnel pressurized when the cart is removed. 4 carts are planned, 3 sting support carts and 1 half-model cart.

To reduce the number of mechanisms inside the tunnel and to compromise the structural continuity of the pressure shell as little as possible, an access concept was chosen with vertical cart insertion/removal and a single isolation valve in the plenum. Figure 9 shows the essential features of the system which requires a downward extension of the plenum underneath the test section, here referred to as the access lock. Removal and replacement of the cart through the roof of the plenum was also considered, but was not found to be as attractive. The carts consist of part of the test section floor and the complete model support.

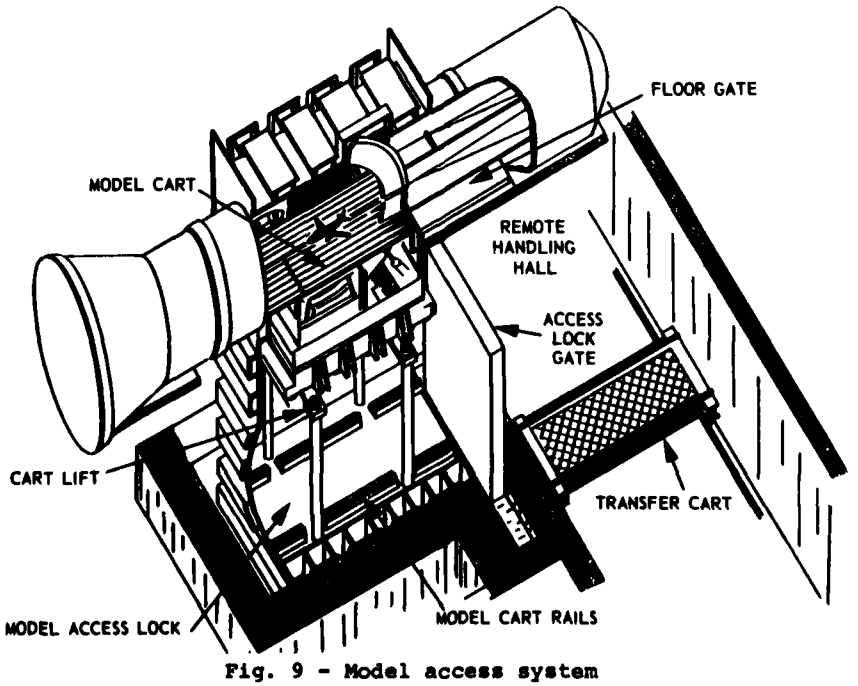

Fig. 9 - Model access system

The sequence of operations for cart removal is:

1. Model is pitched to full positive incidence, so that the top of the support will not foul the test section roof on removal.
2. Cart is lowered from the tunnel into the access lock.
3. Access lock is isolated from the rest of the tunnel circuit by a horizontal pressure door, which is stored in the plenum under the first diffuser when the tunnel is running.
4. Access lock is vented to ambient pressure.
5. Access lock vertical pressure door is opened.
6. Cart is driven out of the access lock on to a transfer cart.
7. Cart is carried to the desired location on the transfer cart.

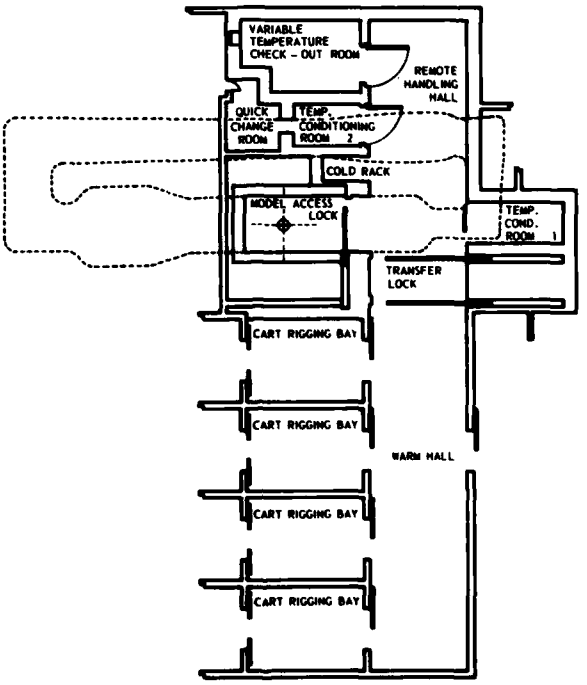

Fig. 10 - Model handling lay-out

Figure 10 shows the layout of the part of the ground floor of the building associated with model handling. The cart rigging bays and "warm hall" are regions of human access. The "remote handling hall" (RHH) will be a nitrogen area. The transfer lock provides environmental isolation between them. Air in the "warm hall" will be very dry at all times. There will be a changeover from ambient (i.e. moist) air to very dry air in a cart rigging bay a few hours before the cart is due to go into the RHH. This atmospheric control is intended to minimise any moisture contamination problems in model and cart when they are cooled. Carts are driven between the rigging area and the RHH on the transfer cart. Once in the RHH, the cart goes for cooldown into one of the "temperature conditioning rooms" (TCR's) or into the "variable temperature check-out room" (VTCR).

Adjustments or changes between runs to a sting mounted model can be accomplished in the "quick change room" (QCR) attached to the TCR (Figure 11). It is anticipated that the QCR will be used for routine changes or adjustments which might take an hour or so to complete. A breathable (dry air) atmosphere will be provided in the QCR before human entry. The model will be heated up, prior to being worked on, using an enclosure containing infrared lamps. After model work is complete and personnel have left, the cart is rolled back

into TCR 2 and the model is cooled down again with LN_2 spray mist. Critical model temperatures will be monitored during warm up and cool down.

Adjustments or changes to a half-model will take place in TCR 1 (Figure 12). It is expected that the warm up and cool down times for the half-model will be considerably longer than those for the sting mounted model.

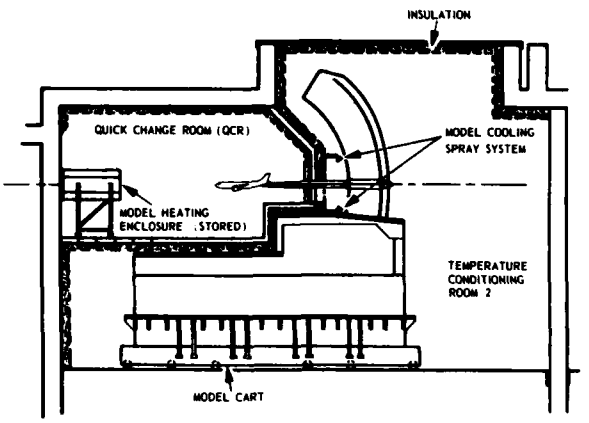

Fig. 11 - System for model configuration changes

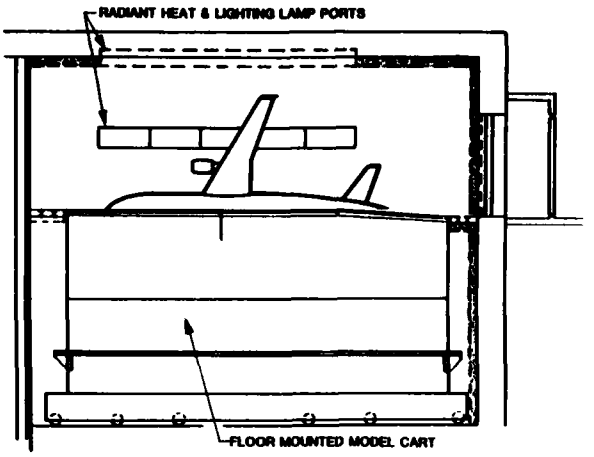

Fig. 12 - Half-model cart

In view of the probable complexity of the models and the high cost of tunnel operation, great efforts will have to be made to achieve reliable operation of all model and cart systems. This will be the main function of the variable temperature check-out room, where a complete pre-test check-out at any temperature will be possible. The VTCR can also be used simply for cart cooldown, if required.

A possible activity schedule during a testing day is presented in figure 13.

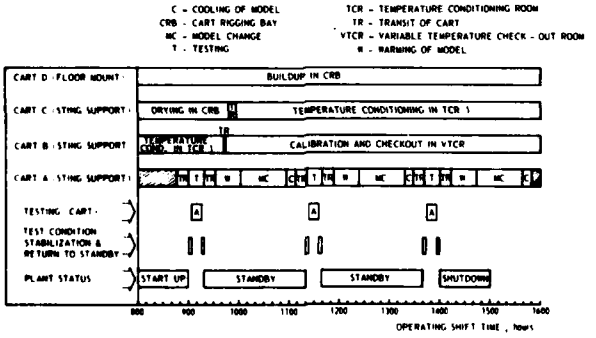

Fig. 13 - Typical operating sequence during testing day

2.3.4 Compressor and drive system

To overcome the circuit losses for the large Mach number range specified for ETW (up

to M = 1.35), the compressor has to provide pressure ratios as high as 1.42 in the cryogenic environment as well as at ambient temperatures. Efficiencies should be high as the losses are not only paid for in terms of compressor energy consumption but also in additional LN_2 use. These requirements present some difficulties for the aerodynamic and the mechanical design of the unit.

The size of ETW does not allow the compressor drive to be built into the nacelle. Therefore the compressor has been placed just downstream of the second corner to allow a short drive shaft penetrating the pressure shell and the cold box wall.

A layout of the compressor is presented in Figure 14. The compressor has two stages with inlet and outlet guide vanes, the inlet guide vanes being variable to provide full control for the compressor which is mainly speed controlled. A straddle bearing arrangement with the bearings installed in heated compartments, surrounded by the low temperature gaseous nitrogen, was chosen.

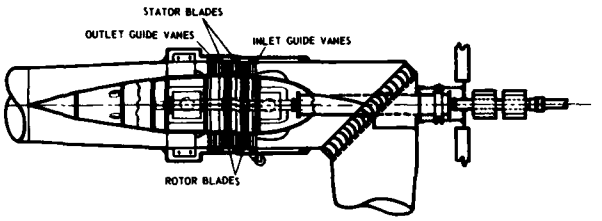

Fig. 14 - Compressor lay-out

The aerodynamic design of the compressor is a compromise. It was not possible to design for best efficiency at the most frequent high subsonic operating conditions of the tunnel and at the same time provide sufficient surge margin for the top Mach number conditions.

The blade profiles have a modified NASA 65A series thickness distribution with circular arc camber lines.

The drive system for the compressor has to provide a maximum power of about 37MW over the speed range from 650 to 1300 rpm, the lowest speed required being about 200 rpm.

The need to perform fast set point changes between tests to save LN_2, requires a 30% overtorque capability of the motor. A synchronous motor fed from a 50 Hz power source was recommended as a relatively simple and reliable prime mover.

However, actual energy prices at the site yet to be selected for ETW might lead to other solutions, including on-site power generation with a gas turbine.

2.3.5 Nitrogen systems

Liquid nitrogen will be used for cooling of the tunnel. Based on the required productivity and the expected test spectrum it is estimated that about 40.000 tonnes of LN_2 will be needed annually. A reservoir capacity of about 1200 tonnes is required.

A schematic of the LN_2 system is presented in Figure 15.

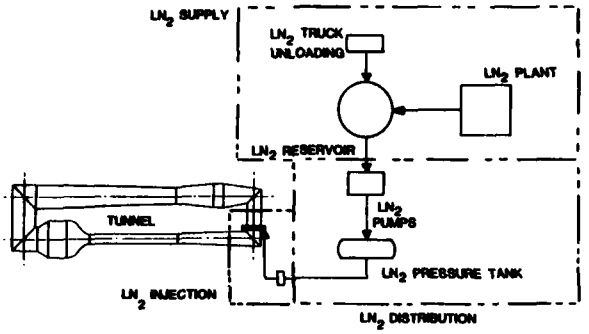

Fig. 15 - LN_2 system

An economic analysis has indicated that on-site production of LN_2 is the preferred solution. Such a LN_2 plant would need a capacity of about 120 tonnes per day.

The test requirements include significant transient flow rates in addition to steady-state requirements. A pressurized tank design is chosen, as indicated in Figure 16, to assure good control and reliability of LN_2 injection. A schematic of the LN_2 injection system is presented in Figure 17. The main injection control is by a digital valve with secondary nozzle unit selection by on-off valves.

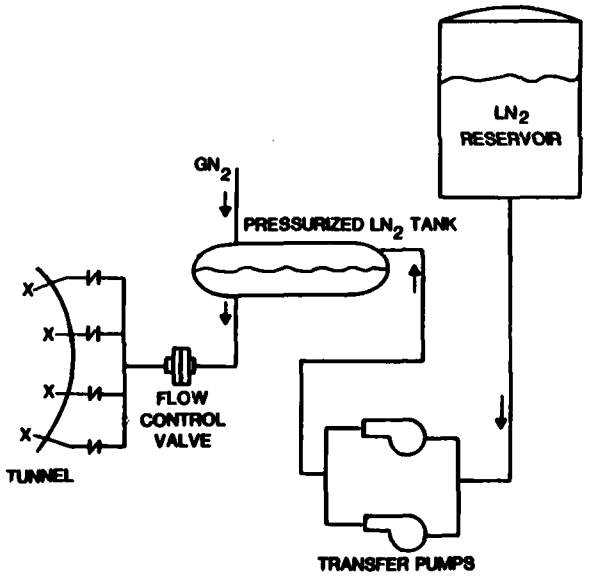

Fig. 16 - Pressurized LN_2 distribution system

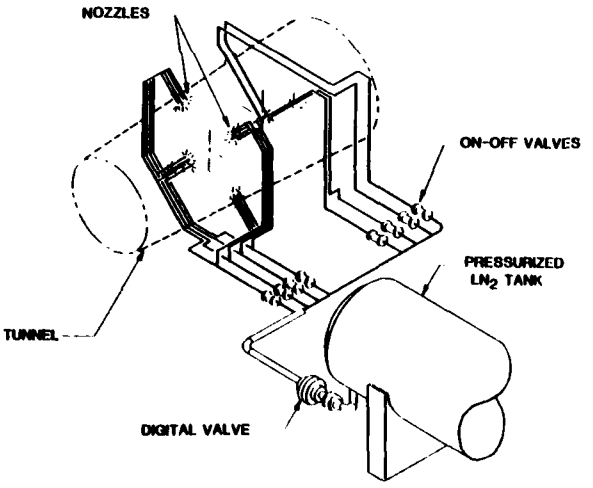

Fig. 17 - LN_2 injection system

Gaseous nitrogen will be blown off from the second cross leg, through a manifold surrounding the ducting. Via a silencer, the nitrogen is led into the exhaust stack where it is mixed with surrounding air. The mixing is forced by two fans and by an ejector system which draws outside air into the stack.

The mixture of GN_2 and air is blown into the atmosphere at an adequate velocity to prevent any safety and fogging hazards. The exhaust stack will be about 2.3 m in diameter; in the present design it is about 50 m high.

2.3.6. Control and data system

As mentioned above, large quantities of liquid nitrogen will be used to cool down the tunnel, as well as to compensate the heat input from the fan. The cost of nitrogen may represent from 30 to 50% of the total operating cost. An analysis of typical tunnel operation has indicated that test-related liquid nitrogen represents around 55% (about 40% for data acquisition and about 15% for starting, stopping and set-point changes). Figure 18 presents a breakdown of the LN_2 consumption for a typical yearly testing program. It illustrates the importance of maintaining set-point accuracy during data acquisition (Mach number, pressure and temperature control during a polar) and of minimizing liquid nitrogen consumption between set-points.

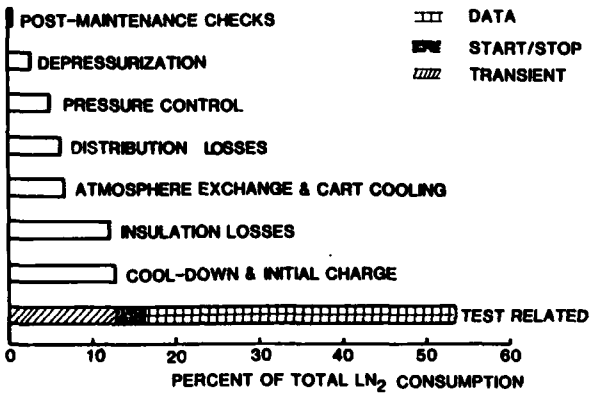

Fig. 18 - Annual LN_2 consumption

At an early stage of preliminary design it was decided to pursue a comprehensive control program with the following aims:

- study of the flow dynamics in the circuit,
- study of the feasibility of predictive control techniques for required set-point accuracy and minimisation of LN_2 consumption between set-points,
- preliminary selection of control hardware.

Concerning the flow dynamics study, the set-point conditions are controlled by LN_2 injection and GN_2 exhaust, by the fan operating condition, and by second throat and nozzle areas and they are affected by model attitude. It is clear that this is a highly coupled and non-linear system. A simplified model has been developed which has the following characteristics:

- three control volumes
- temperature propagation at the gas velocity
- heat transfer with the shell, the honeycomb and the model.

In order to validate the mathematical model developed, experiments were performed in several existing European windtunnels (fan changes, model attitude variations, second throat changes in the NLR High Speed Tunnel and in the DFVLR 1m x 1m tunnel, and LN_2 variations in the ONERA/CERT cryogenic induction tunnel, T'2). These experiments have shown that the simplified dynamic model predicts the low frequency behaviour of a closed-circuit tunnel in a satisfactory way.

Figure 19 illustrates the open-loop response of the test-section conditions to a continuous pitch polar, as calculated by the simplified model. The highly-coupled nature will require a sophisticated control system and in the course of preliminary design a predictive control technique was chosen for fast control of the facility.

Typical results of this technique are presented in figure 20, where it is shown that the set point conditions can be kept within the required tolerances, when the model is pitched, by the use of drag flaps behind the test section. Analysis of the results of applying the simplified model indicated that typical set-point changes (eg Δ M = 0.03, ΔT_o = 6K or Δp_o = 0,15 bar) can be achieved in about 4 circuit times (around 10 s at M = 0.9 and low temperatures). Figure 21 also illustrates the case for a change in total temperature of 6K.

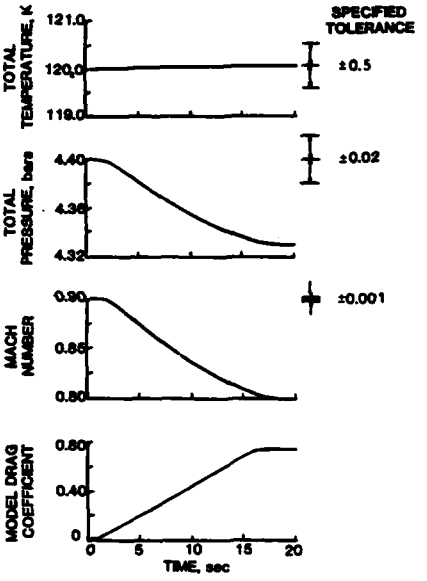

Fig. 19 - Open-loop response to continuous pitch polar (2 degrees per second)

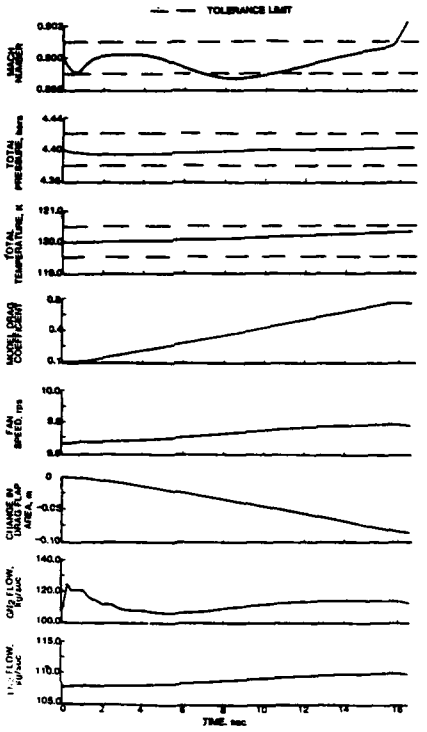

Fig. 20 - Closed-loop response to a continuous polar using drag flaps and fan speed for Mach number control

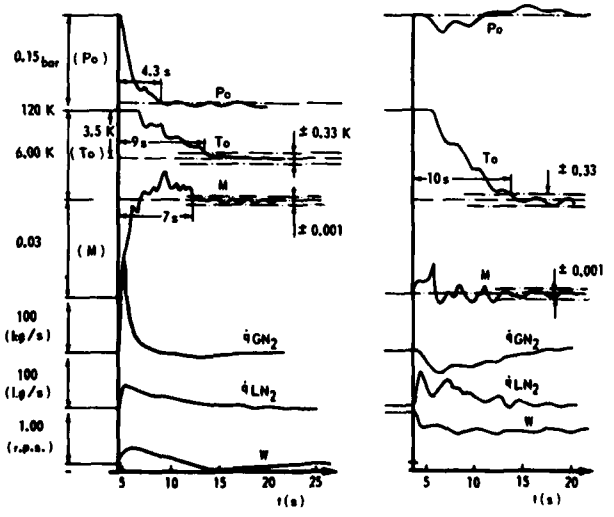

Fig. 21 - Set-point change (predictive control)

As the application of this model is limited to low frequencies due to the assumptions made, a general model with less restrictive assumptions is being constructed. It is intended to verify the settling time estimates from the simplified model, to check the high frequency stability of the tunnel and to get detailed predictions of the time history of flow parameters around the circuit (eg for the calculation of temperature stresses).

The conceptual design of the computer-based control and data system is a three-tier hierarchical network following the same general principles used for the RAE 5m Tunnel and the NASA NTF for the same reasons:

- the necessity for a versatile and flexible system adaptable in the light of changing user demands, technical developments, and locally-favoured design philosophies.
- the separation of functions so that design and development of both hardware and software each can proceed without interference with unimpeded access to the computer.
- the possibility of continued operation with some malfunction of parts of the system. As a corollary it would be possible to start with a basic system and expand it in the light of experience.
- the possibility of using optimum computer hardware, operating systems and programming languages for each function.
- the use of mini-and microcomputers for which the pace of technical development is faster than for larger machines and the cost of computing power less.

The control and data system, envisioned so far, will contain the following main items:

- a supervisory computer, managing all lower levels
- a control computation computer, calculating optimum trajectories for tunnel parameter control
- a control distribution computer, which routes commands to the individual controllers (M, p_o, etc.)
- a tunnel monitor computer, monitoring temperatures, stresses, etc.
- a model data and control processor, taking care of model control and acquisition of data from the data system on the model cart
- a data display computer

The data system will have to deal with the problem of the transmission of small signals from the model to the recording system. One solution might be to mount redundant data systems on board the cart and transmit the amplified signals, preferably in digital form, at volt levels. This would require substantial space on the cart which may not be available in practice: in this case remotely controlled means of disconnecting multiway cables must be developed.

Because of the brief run duration (several minutes) only a limited amount of online data processing will be necessary for the conduct of the test. However, some processing will be essential for safety purposes and it is possible that some intervention with the progress of test runs will be possible by the operators. It is to be expected that visual displays of raw and processed data will be widely exploited. Sufficient computing capacity will be provided for a complete preliminary processing of data acquired during a run within about 30 minutes afterwards.

3. PETW

A pilot tunnel for ETW is now under construction at NLR in Amsterdam (PETW). Final design was finished early 1980, and the tunnel is expected to become operational in 1981.

The main goals of PETW are:

- check of ETW design concerning aerodynamics and flow quality
- check of mathematical models which describe the dynamic behaviour of ETW (controls)
- experience in operation of a cryogenic windtunnel.

An artist's impression of PETW is presented in figure 22.

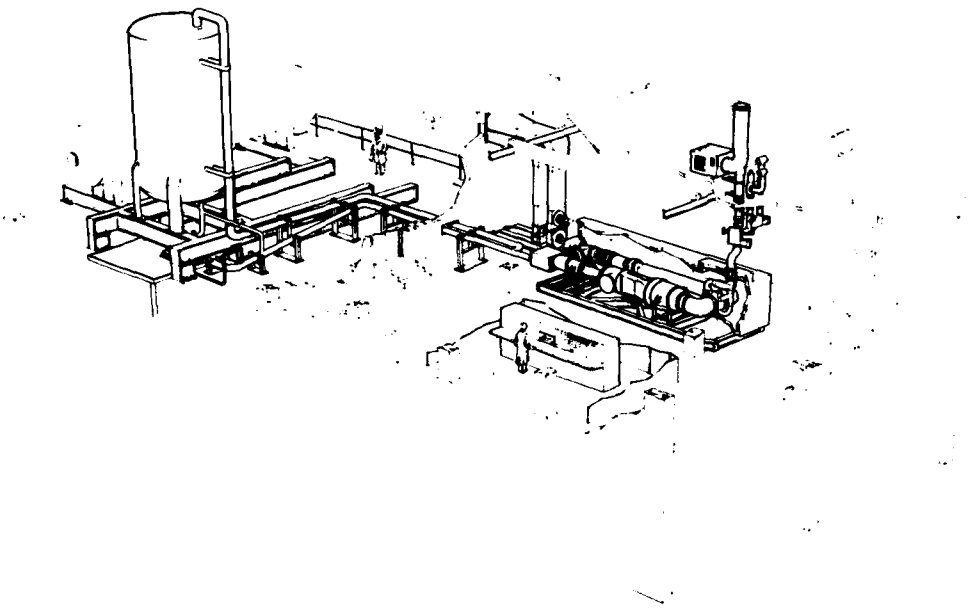

Fig. 22 - Artist's impression of PETW

The aerodynamic circuit of PETW is a scaled-down version of ETW (scale 1:7.2), it has the same operating range (as far as pressure, temperature and Mach number are concerned). Supersonic Mach numbers are generated by nozzle blocks instead of by a flexible nozzle. The high-speed diffuser can be replaced by a sonic throat, to study the effects on flow quality and on the dynamic behaviour of the circuit (controls).

Access to the test section is obtained by a large hatch (ø 0.7m) in the cylindrical plenum. The tunnel shell is made of an aluminium alloy.

The compressor is a fixed geometry two-stage fan, powered by a 1MW electrical motor. Maximum speed of the fan is about 9000 rpm.

The nitrogen system is sized for a maximum flow rate of 6 kg/s. LN_2 is stored in a reservoir with a capacity of about $15m^3$. Injection of LN_2 is either by pressurization of the tank or by a LN_2 pump. The injection system consists of 18 nozzles (3 nozzle types), arranged in 5 independent groups, in order to be able to cope with the large range in flow rate (0.07 up to 6 kg/s). Gaseous nitrogen blow-off is through a manifold in the second cross-leg. The nitrogen is released into atmosphere through a stack. To prevent safety and environmental problems, a heater (using natural gas) will be installed such that the nitrogen exhausts at ambient temperature.

The cold box, enclosing the tunnel (except in the test-section area) is made of removable panels, providing easy access to the structure. The cold box is purged with GN_2, kept at a pressure slightly higher than atmosphere. The test-section area is insulated by easily removable rigid foam, directly applied to the structure.

PETW will be, at least in the beginning, manually and remotely controlled from a control room adjacent to the tunnel.

4. MODELS AND INSTRUMENTATION

In comparison with present-day testing techniques, the design and construction of models and the instrumentation for ETW will present problems.

The problems for model design and construction are related to:
- the low temperatures,
- the wide temperature range and the rapid temperature changes,
- the extra internal space required for heated and insulated instrumentation,
- the smooth surface finish required because of the high Reynolds numbers,
- the relatively high dynamic pressures,
- the changes of shape at the rear of models which may be necessary to accommodate large diameter stings.

The principal problems of model measurements are as follows:
- force balances will either have to work over a wide range of temperatures and be insensitive to rapid temperature changes or be heated and insulated,
- pressure measurements will have to be made by electronically-scanned devices since conventional pneumatic scanning (Scanivalves) may be too slow for the desired productivity. It is assumed that internally-mounted pressure instrumentation will be heated and insulated.
- transducers which cannot be insulated and heated will pose special problems if it is necessary to measure steady as well as fluctuating components.

The above mentioned problems are actively studied in the USA in connection with NTF and the McDonnell-Douglas cryogenic tunnels. In Europe the problems are attacked under the ETW Cryogenic Technology program. The work is partly funded by ETW, and partly by the national programs of the participating nations. Studies are underway on the subjects of:
- materials
- model design and construction
- strain-gauge balances (heated and unheated)
- electronic pressure scanners

Also, the same program includes fundamental studies such as those related to minimum operating temperature.

The difficulties are well-known and it is intended that workable solutions will be found in the period before ETW is operational.

5. CONCLUDING REMARKS

Preparations are now being made for a new Memorandum of Understanding between the participating nations, which will cover the Final Design of ETW. After that construction can start, which will take approximately 4 years according to the present planning.

REFERENCES

1. R.A. Kilgore — Development of the cryogenic tunnel concept and application to the U.S. National Transonic Facility. Part 2 of "Towards New Transonic Windtunnels", AGARDograph-AG-240 (1979).

2. J.P. Hartzuiker, J. Christophe, W. Lorenz-Meyer, P.G. Pugh. — The cryogenic windtunnel; another option for the European transonic facility. Part 3 of "Towards New Transonic Windtunnels", AGARDograph-AG-240 (1979).

3. - — The need for large wind tunnels in Europe; Report of the Large Wind Tunnels Working Group. AGARD-AR-60 (1972).

4. - — The need for a large transonic windtunnel in Europe; Second report of the Large Wind Tunnels Working Group. AGARD-AR-70 (1974).

5. J.P. Hartzuiker, P.G. Pugh, W. Lorenz-Meyer, G.E. Fasso. — On the flow quality necessary for the large European high Reynolds number transonic windtunnel LEHRT. AGARD-R-644 (1976).

6. P.J.F. Clark, J.P. Morel. — Circuit optimization study for the European Transonic Windtunnel. Proceedings of the First International Symposium on Cryogenic Windtunnels, Paper 36. University of Southampton (1979).

CHARACTERISTICS AND STATUS OF THE U.S. NATIONAL TRANSONIC FACILITY

William B. Igoe
NASA Langley Research Center
Hampton, Virginia 23665, U.S.A.

SUMMARY

The U.S. National Transonic Facility, a major application of the cryogenic wind tunnel concept, is under construction at the NASA Langley Research Center and is scheduled to become operational in 1982. It will have a closed return fan-driven circuit with a 2.5 meter square slotted test section, be pressurized up to 8.85 atmospheres, and provide chord Reynolds numbers of 120 million based on a chord of 0.25 meter at transonic speeds using cold nitrogen as the test gas.

SYMBOLS

$\bar{c}$	wing mean geometric chord	Abbreviations	
M	Mach number		
p	pressure	IGV	inlet guide vane
q	dynamic pressure	GN_2	gaseous nitrogen
$R_{\bar{c}}$	Reynolds number based on $\bar{c}$	LN_2	liquid nitrogen
T	temperature	RPM	revolutions per minute
ΔT	temperature change		

Subscripts

L	local
min	minimum
t	stagnation conditions
∞	free stream

1. INTRODUCTION

The U.S. National Transonic Facility (NTF) is a transonic wind tunnel primarily intended to provide a high Reynolds number test capability for aerodynamic research and the development testing of commercial and military aircraft configurations. The NTF is a conventional closed circuit, single return fan-driven wind tunnel capable of continuous operation and capable of achieving a chord Reynolds number of 120 million at a Mach number of 1.0 by operating at elevated pressures and cryogenic temperatures.

The need for this high Reynolds number test capability became convincingly evident in the 1960's. In the U.S., it received early attention by Heppe et al.,[1] and subsequently by Howe,[2] Jones,[3] Lukasiewicz,[4] and others. International recognition of this testing requirement was shown at the AGARD Paris conference on Transonic Aerodynamics[5] in 1968 and more extensively later at the AGARD Göttingen conference on Facilities and Techniques[6] in 1971.

The emphasis here on Reynolds number or scale-related effects is not meant to downgrade the importance of other transonic testing deficiencies. For example, reduced or correctable boundary-induced and model-support-induced interferences, improved flow quality and accuracy of measurement, and more realistic propulsion simulation techniques are all important goals. However, as indicated by Howe,[2] even though proper simulation of Reynolds number effects will not solve all of the problems of disparity in wind tunnel test results, there are some problems that cannot be studied even with all available ingenuity, without such simulation.

Many different types of test facilities[6,7] were studied to see what type might best fulfill the testing requirements. These facilities ranged all the way from impulsively-driven flow facilities on the one hand to ground-track facilities and free-flight model testing on the other. Most of the concepts fell in the stored-energy, intermittent-flow category and were variations of the blowdown concept. These included Ludweig tube, piston, and injector driven wind tunnels. Although highly ingenious, these concepts were generally limited in their run-time, involved high dynamic pressures, or were costly to build and operate.

It was not until the cryogenic wind tunnel concept was successfully demonstrated at Langley in 1972[8] that the desired high Reynolds number test capability finally seemed within reach from a practical and economically acceptable viewpoint. This demonstration involved the development of a practical cooling system, integration of cryogenic technology into the tunnel design, and aerodynamic proof of concept tests. From a historical standpoint, it is interesting to note that the use of modest cooling was first proposed by Margoulis[9] in 1920 and that theoretical benefits of further temperature reduction was pointed out by Smelt[10] in 1945. In the U.S. this concept has evolved into what is now called the National Transonic Facility (NTF), a pressurized transonic wind tunnel with a

2.5 meter test section, located at the NASA Langley Research Center in Hampton, Virginia. In Europe, the AGARD countries of France, Germany, the Netherlands and the United Kingdom have jointly supported a similar initiative, designated as the Large European High-Reynolds-Number Transonic Windtunnel (ETW).

2. THE REYNOLDS NUMBER GAP

The magnitude of the gap in test Reynolds number between U.S. ground test facilities and flight is shown in Figure 1 for past, present, and projected future airplanes. This figure indicates that the disparity in Reynolds number between flight and existing U.S. wind tunnels might have widened to as much as an order of magnitude for the large airplanes foreseen for the future.

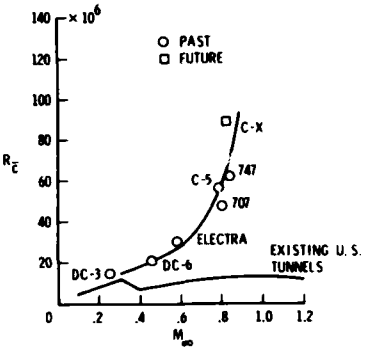

Fig.1 The growing Reynolds number gap.

The lack of high Reynolds number test capability has in the past reinforced the tendency towards conservatism in the design of aircraft. As a result of what may be excessive conservatism, the potential advances in performance and efficiency have not been fully realized. With increased emphasis on energy efficiency, new generations of aircraft will rely heavily on newly developed aerodynamic technologies which will be even more sensitive to Reynolds number effects than those of the past, and for which the consequences of excess conservatism will be even greater than before. Without new high Reynolds number facilities for adequate research and development, the new aircraft designs may be unable to take full advantage of the new technologies without running undue risks of performance guarantees not being met, or of major deficiencies or problem areas being encountered.

3. SIZING THE NTF

The sizing and performance requirements for the NTF were established by a subpanel to the U.S. National Aeronautics and Astronautics Coordinating Board as indicated by Nicks in Reference 11. The responsibility for both the aerodynamic and mechanical design was vested in a Project Office at the Langley Research Center with Robert R. Howell as the overall Project Manager and Linwood W. McKinney responsible for the aerodynamic design and performance.

The rationale behind the selection of the size, pressurization and performance requirements for the NTF has been discussed by Nicks.[11] In essence, the objective has been to achieve full-scale Reynolds numbers for the cruise or other design point, and to cover as much of the performance envelope as possible for current and future commercial and military aircraft, and aerospace vehicles.

An example of the kind of sizing studies that led to the selection of the NTF performance requirements is illustrated in Figure 2. The left side of the figure shows a flight envelope in terms of altitude versus Mach number for a large commercial airplane. Also shown are lines of constant Reynolds number and the cruise point. The boundaries are established at the bottom by sea level altitude, at the left by maximum lift, at the upper right by maximum power, and at the lower right by the structural limits of the airframe. When transferred to a Reynolds number versus Mach number plot on the right side of this figure, the flight envelope transfers to the dashed boundary where the bottom is the maximum lift limit, the left side is the sea-level limit, the top is the airframe structural limit, and the right side is the maximum power limit.

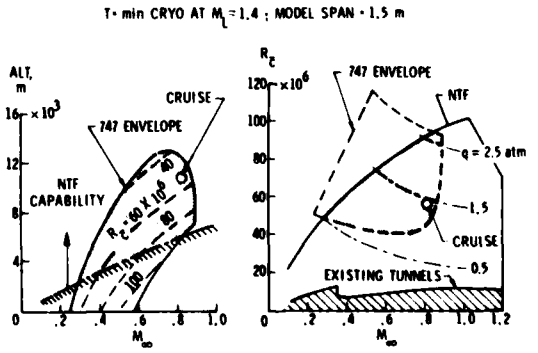

Fig. 2 Comparison of flight envelope of 747 airplane with NTF test envelope (from Reference 15).

Preliminary estimates of the wind tunnel Reynolds number performance envelopes were superimposed on the aircraft performance envelopes as shown in Figure 3 for different

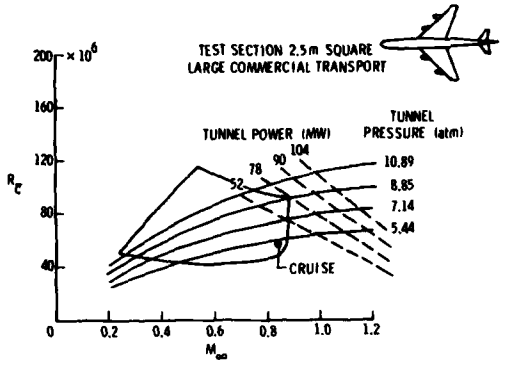

Fig. 3 Matching of aircraft and wind tunnel performance (after Reference 11).

values of tunnel pressure and maximum drive power. Similar plots were made for other aircraft configurations of interest as shown in Figure 4 where only a single value of pressure and power are shown for the wind tunnel performance estimates. On the basis of these and similar studies, the size, pressurization, and power requirements for the NTF were selected. The selection itself was, of course, a compromise, balancing maximum Reynolds number requirement, maximum usable dynamic pressure, and capital cost.

The sizing criteria mentioned above, combined with the constraints imposed by dynamic pressure and costs resulted in the performance and dimensional characteristics shown in Figure 5. In this figure, and in subsequent usage, the Reynolds number is based on a wing chord equal to one-tenth of the square-root of the cross-sectional area of the test section. The temperature range is established at the lower end by the liquefaction temperature of nitrogen at one atmosphere of approximately 78 K and at the upper end by a temperature limit of 339 K on structural materials used in the construction of the tunnel.

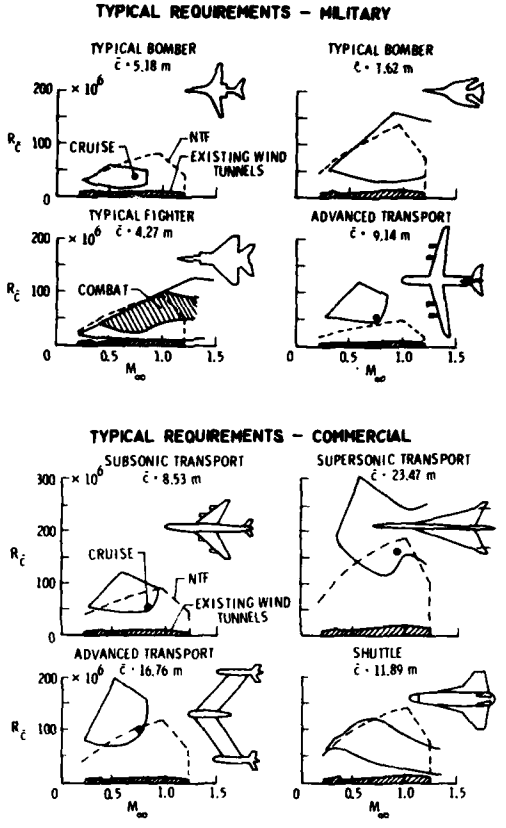

Fig. 4 Comparison of aircraft requirements with wind tunnel performance (from Reference 12).

MACH NUMBER	0.1 TO 1.2	
REYNOLDS NUMBER	3×10^6 TO 120×10^6 AT M = 1.0, $\bar{c}$ = 0.25 m	
PRESSURE	1 TO 8.85 ATM	
TEMPERATURE	78 K TO 339 K	
TEST GAS	NITROGEN, AIR	
TEST SECTION SIZE	2.5 m SQUARE	
LENGTH	7.62 m	
AREA	6.203 m^2	
CONTRACTION AREA RATIO	14.95 TO 1	
CIRCUIT LENGTH	151.5 m	
VOLUME	6512 m^3	
DRIVE POWER,	10 MINUTES	CONTINUOUS
INDUCTION MOTORS	49.2 MW	35.1 MW
SYNCHRONOUS MOTOR	44.8 MW	31.3 MW
TOTAL	96.0 MW	66.4 MW

Fig. 5 NTF geometry and performance characteristics (after Reference 16).

4. FACILITY DESCRIPTION

The NTF is, in most respects, a rather conventional wind tunnel with only a few unconventional features. References 12 through 18 present descriptions of the NTF as its characteristics have evolved during the design process. What follows is essentially a review of these previous publications, and borrows material freely from them.

By using the cryogenic approach to high Reynolds numbers, the NTF achieves its performance of near full-scale conditions at lower cost and at lower model loads than concepts based on ambient temperature operation. In addition, as shown in Reference 19, with temperature as a test variable, testing modes are possible in which, at a given Mach number, the dynamic pressure, and hence the model loads, can be kept constant while

Reynolds number is varied as illustrated in Figure 6; or in which the Reynolds number is kept constant while dynamic pressure is varied as illustrated in Figure 7; or in which the dynamic pressure and Reynolds number are kept constant while Mach number is varied as illustrated in Figure 8.

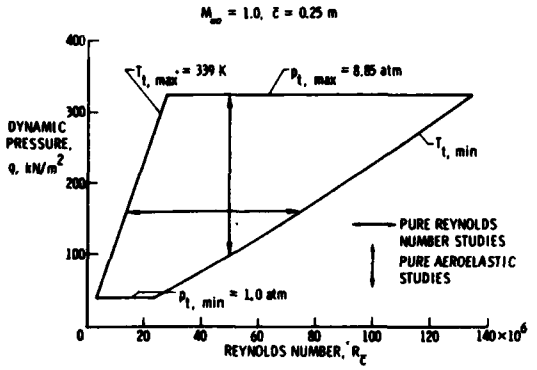

Fig. 6 Constant Mach number operating envelope.

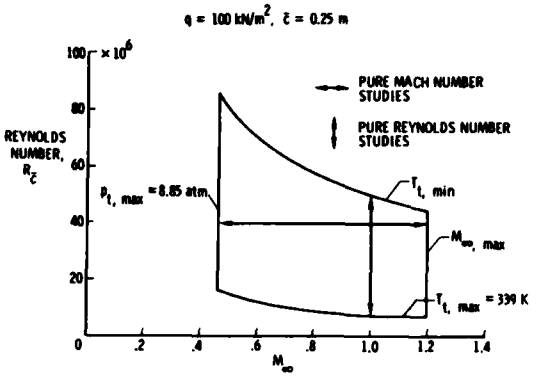

Fig. 7 Constant dynamic pressure operating envelope.

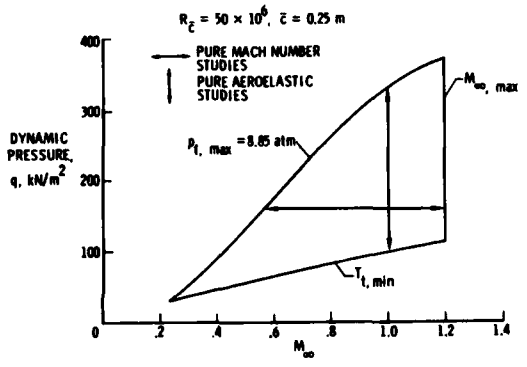

Fig. 8 Constant Reynolds number operating envelope.

4.1 General Arrangement

The circuit lines and overall dimensions of the NTF are shown in Figure 9. The tunnel circuit is about 61 m long and about 15 m wide between centerlines, giving a circuit length of about 152 m and an enclosed volume of about 6512 m^3. The NTF is being constructed on the site of the deactivated 4-foot supersonic pressure tunnel and will use some of the equipment from that tunnel including induction drive motors, drive control system, cooling towers, and the adjacent office building. The plane of the tunnel circuit is tilted about 9^o with the centerline of the fan being below the centerline of the test section. The fan and test section centerlines lie in horizontal planes, and the walls of the test section are oriented horizontally and vertically. The reason for the tilt was to accommodate the fan centerline positioning, and to minimize large below-grade excavation requirements in the test section - plenum region.

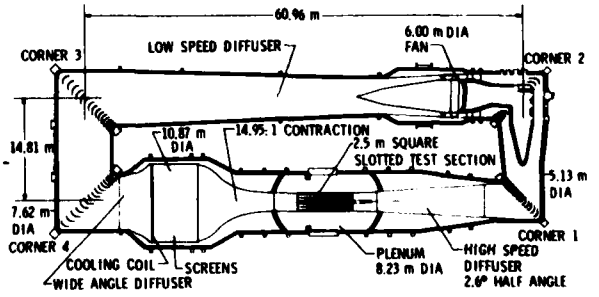

Fig. 9 Planview of NTF circuit (from Reference 18).

4.2 Thermal Insulation

Thermal insulation for the tunnel (shown shaded in Figure 9) is internal rather than external to the pressure shell. Being internal, the insulation shields the pressure shell from large temperature changes as the tunnel temperature is varied during the cryogenic mode of operation. Because the pressure shell with its large thermal inertia is not

directly involved in changes in gas temperature, liquid nitrogen consumption is reduced, and since thermal cycling of the pressure shell is avoided, its service life is also enhanced.

As can be seen in Figure 9, in the high speed portion of the tunnel, from corner number 4 to corner number 1, the insulation is completely isolated from the flow by the internal aerodynamic liner. In the remainder of the tunnel circuit, except for the fan shroud region, the insulation is separated from the flow stream by a relatively thin metal liner. For economy of fabrication, the liner plates are flat, leading to a polygonal (24 sided) cross section in those parts of the tunnel where these plates are installed.

The insulation itself is a closed-cell, high-density, rigid foam of modified polyurethane material. It is attached to the inside of the pressure shell in thicknesses varying from about 15 to 19 cm. It has excellent fire-retardant properties, an important feature for all materials used in a wind tunnel such as the NTF which can be highly pressurized with either air or nitrogen.

4.3 Principal Components

The principal components of the NTF circuit are shown in Figure 10. In the cryogenic mode of operation, nitrogen is used as the test gas, with cooling accomplished by the injection of liquid nitrogen directly into the tunnel circuit. The liquid nitrogen injection nozzles are located upstream of the fan nacelle. It has been shown by Adcock[20] that liquid nitrogen injection upstream of the fan results in lower power requirements and lower liquid nitrogen flow-rates compared to downstream injection. This location may also be favorable with respect to the complete evaporation of the injected liquid as well as with respect to the level of injection noise which reaches the test section. At ambient temperatures, either air or nitrogen can be used as the test gas with cooling accomplished by a conventional chilled-water heat exchanger inside the tunnel circuit.

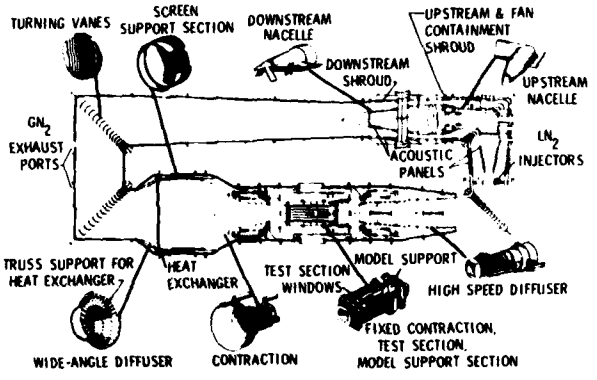

Fig. 10 Principal components of NTF circuit (after Reference 15).

The aerodynamic design of the NTF has been strongly influenced by the need for economy of operation. The cryogenic concept permits the achievement of high Reynolds numbers at relatively low energy consumption levels compared to other high Reynolds number ground test facility concepts. However, even for the cryogenic tunnel, the overall consumption of energy is high and must be carefully managed. The main item of energy consumption for the NTF in the cryogenic mode of operation is the energy required to produce the liquid nitrogen used for cooling.[13] To minimize the cost of nitrogen required to pressurize the tunnel and also to reduce the cost of the pressure shell, the volume of the NTF circuit was designed to be as small as practical.

The corners of the circuit are mitered to form 90° turns. The turning vanes in these corners have what is known as arithmetic progression spacing, introduced by Dimmock[21] for gas turbine research and used successfully in other wind tunnels.

4.3.1 Wide-Angle Diffuser

The wide-angle diffuser, shown in Figure 11, is located immediately upstream of the settling chamber and was designed in the manner described in Reference 22 to have a nearly constant static pressure along the walls. This desired pressure gradient, with its reduced tendency for boundary-layer separation, is obtained by proper curvature of the walls. The centrifugal force acting on the flow as it follows the curved wall contour is balanced by the stream pressure gradient as the flow is slowed due to the increased area of the wide-angle diffuser. At the downstream end, the flow direction must be returned toward the axial direction. In the NTF, the turning will be accomplished by the finned-tube heat exchanger which also supplies the downstream pressure loss of 3q to 5q required to prevent flow separation from the diffuser walls. The aerodynamic loads on the heat exchanger are supported by a truss with radial and annular

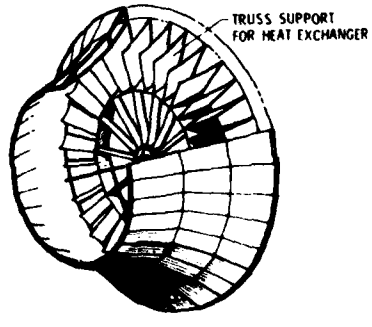

Fig. 11 NTF wide-angle diffuser.

elements located near the downstream end of the wide-angle diffuser. The annular elements have been shaped so as to conform to the flowfield curvature in the streamwise direction.

The wide-angle diffuser geometry is axially symmetrical, with an exit-to-inlet area ratio of 2.08. The length-to-inlet diameter ratio is 0.465, and the exit wall angle is about 61°. The use of a wide-angle diffuser upstream of the settling chamber allowed the return duct of the tunnel circuit to be kept to small diameter, but still permitted a large settling chamber and a high contraction ratio with its attendant benefits on tunnel flow quality.

4.3.2 Turbulence Damping Screens

The exit of the wide-angle diffuser is followed by a settling chamber about 5.8 m long. There are four turbulence damping screens in the settling chamber, spaced about 0.6 m apart with the last screen about 1.5 m from the start of the contraction. The four screens are each the same; square mesh wire cloth woven of approximately 0.8 mm diameter wires at a spacing of about 0.4 cm between wires, with a resulting porosity of about 0.65.

4.3.3 Contraction Section

The area ratio of the contraction is 14.95 to 1. It was designed to produce uniform flow at the throat under choked conditions, or in other words, to have an essentially straight sonic line. The prescribed area distribution for the contraction was calculated by a streamline curvature method (ref. 23) for axially symmetrical flow using the exact equations for an inviscid compressible flow.

The NTF contraction, shown in Figure 12, consists of three subsections. The first part is axially symmetrical with the prescribed area distribution matched exactly. The second section is a transition section where the cross-sectional shape changes from round to flat-sided with circular arc corner fillets. Here, the prescribed area distribution is matched only approximately. The third section is a continuation of the essentially square cross section with corner fillets. In this third subsection, the corner fillet shape changes from circular arc to flat about 2.8 m upstream of the test section.

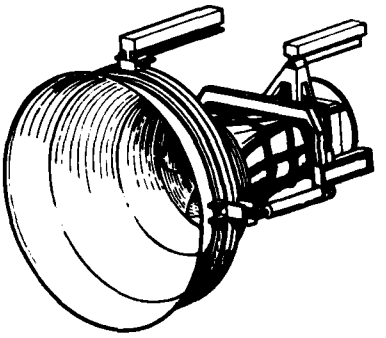

Fig. 12 NTF contraction section.

The length of the contraction is about 14.6 m. An upstream section of the contraction, about 11.8 m long, is a movable structure which can be detached from the rest of the contraction, and moved upstream within the pressure shell to permit deployment of one of two isolation valves which seal the test section and plenum from the rest of the circuit. The isolation valves permit access to the test section without depressurizing the entire tunnel circuit. The operation of this component of the model access system will be described subsequently.

4.3.4 Test Section

A plan view of the NTF test section is shown in Figure 13. The design of the NTF test section closely resembles that of the Langley 8-foot transonic pressure tunnel, especially in the flow reentry region at the downstream end of the test section. The cross section is nominally square, 2.5 m wide; with flat fillets at 45° angles in the corners resulting in a test section cross-sectional area of 6.203 m^2. There are six longitudinal slots in the horizontal (top and bottom) walls, and two in the vertical (side) walls. The length of the slotted region is approximately three test section widths. The vertical walls are parallel but the horizontal walls have flexures at the upstream end which permit variation in wall angle from about 0.5° converged to 1.0° diverged. The vertical walls have provision for three large windows for flow field observations. Smaller ports are located in both the vertical and horizontal walls for lighting and viewing.

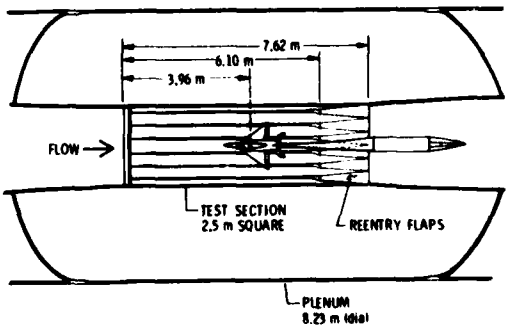

Fig. 13 Planview of NTF test section (after Reference 13).

Remotely adjustable reentry flaps are located at the downstream end of each slot, occupying the rear 20 percent of the length of each slot. The position of these flaps can be varied to control test section flow gradients and to minimize power consumption. The range of flap angle adjustment is from 4° toward the flow to 15° away from the flow on the horizontal walls, and from 0° to 15° away from the flow on the vertical walls.

4.3.5 Model Support Section

The model support section, located immediately downstream of the test section, is rectangular in cross section with corner fillets which are tapered in the streamwise direction. The vertical walls adjacent to the model support strut are indented to relieve strut blockage. The horizontal walls of this section are attached to flexures at their downstream end. The angle of inclination of the horizontal walls can be varied from 0° (walls parallel to tunnel centerline) to about 4.5° inward (leading edge toward flow). The offset vertical height between the horizontal test section walls and the model support section walls is variable from near zero offset to about 20 cm independently on the top and bottom walls. This offset vertical height can be varied as a function of Mach number to accommodate varying reentry flow requirements and thus to minimize tunnel power consumption.

Generally, test models will be sting supported from a circular arc strut permitting a pitch range of 30°, nominally -11° to 19° but this can be varied using offset sting supports. The pitch angle can be varied at rates up to 4° per second with capability for both pitch-pause and continuous sweep operation. The model roll angle range is ±180° at roll rates up to 10° per second. Sideslip angles are obtained from combinations of the pitch and roll. Wall-mounted half-span models can be accommodated in the test section for tests where large model sizes are required. These and other operational characteristics of the NTF are summarized in Figure 14.

MAXIMUM MODEL LOADS,	NORMAL	86.7 kN (19,500 LB)
	AXIAL	41.4 kN (9,356 LB)
	SIDE	44.5 kN (10,000 LB)
PITCH ANGLE RANGE		-11 DEG TO 19 DEG ACCURACY 0.01°
RATE		UP TO 4 DEG/SEC
ROLL ANGLE RANGE		± 180 DEG ACCURACY 0.03°
RATE		UP TO 10 DEG/SEC
ACCESS TIME TO MODEL		30 MIN
COOLDOWN/WARMUP TIME,	ΔT = 222 K	4.1 hr/5.9 hr
	ΔT = 48 K	NO TIME LIMIT

Fig. 14 NTF operational characteristics (after Reference 16).

4.3.6 Test Section Access

The test section and model support section are surrounded by a plenum 8.23 m in diameter. As can be seen in Figure 15, isolation valves are located at the upstream and downstream ends of the plenum. In order to deploy the isolation valves, with the flow at rest the contraction and high-speed diffuser are retracted upstream and downstream, respectively. The isolation valves are then remotely moved into the closed position and locked to the pressure bulkheads at either end of the plenum. With the valves in the closed position, the plenum and test section can be brought to atmospheric pressure. In this condition, the plenum and the test section access doors can be opened, and access tunnels can be inserted from both sides providing direct access to the model at ambient temperature and pressure conditions. A "room temperature" work environment can be maintained by fans which circulate air through the access tunnel, and heaters which are used to bring models to a temperature suitable for model work.

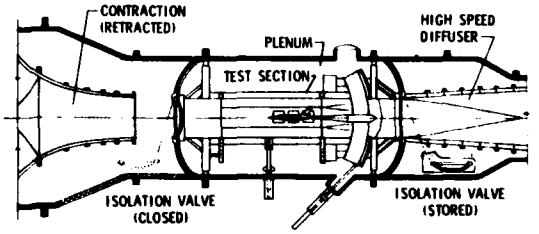

Fig. 15 NTF test section isolation system.

After model work is completed, the process is reversed. The access tunnels are withdrawn, the test section and plenum doors are closed, and the pressure is equalized across the isolation valves. The isolation valves are then remotely disengaged and moved to the stored position, the contraction and high-speed diffuser are returned to their operating positions, and the tunnel is readied for resumed operations.

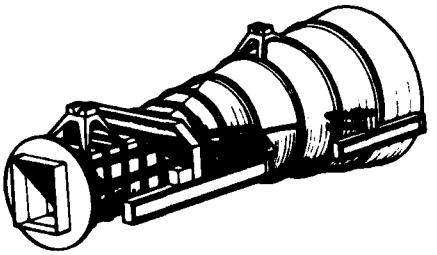

Fig. 16 NTF high-speed diffuser.

4.3.7 High-Speed Diffuser

The high-speed diffuser, shown in Figure 16, is located immediately downstream of the model support section. It consists of two sections, a three-stage transition

section and a conical section. The three stages of the transition section approximate the area distribution of a cone with a half-angle of about 2.6°, the same angle as the actual conical section. The transition cross-sectional shape progresses from a rectangular section with flat corner fillets to a fully round section in the three stages of nearly equal length. The flat corner fillets are faired out within the first stage of the transition. Except for these fillets, the shapes in the transition section consist of flat panels, joined at the corners of the cross section by quarter-round conical sections. The diffuser, including the model support section, has an overall area ratio of 2.92 to 1.

As noted earlier, the high-speed diffuser, like the contraction, is a movable structure. It can be detached from the model support section, and moved downstream within the pressure shell to permit deployment of the isolation valves.

4.3.8 Fan Drive System

The fan is located 8.85 m downstream of corner number 2. As shown in Figure 17, the upstream fan nacelle fairing is bent through that corner. The single-stage fan has 25 fixed-pitch blades with fan loading changed by 24 variable inlet guide vanes (IGV) upstream of the fan, or by variable rotational speed. There are 26 fixed downstream stators. The fan blades are fabricated of fiberglass reinforced plastic.

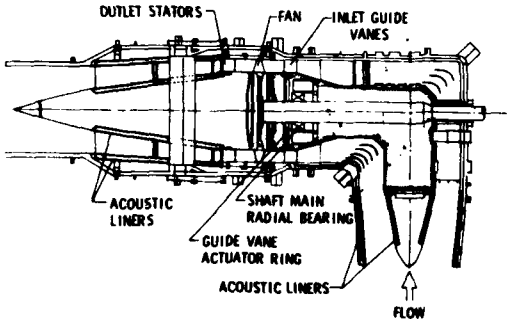

Fig. 17 NTF fan section assembly.

4.3.8.1 Acoustic Treatment

Acoustic panels are located in the fan nacelle and the adjacent tunnel walls at the nose and tail cone of the nacelle. These panels are intended to attenuate fan noise propagating upstream and downstream from the fan station. They use a dual Helmholtz resonator concept and are designed to provide about a 13 dB reduction of fan noise at the test section.

4.3.8.2 Drive Motors and Gear Box

The fan will be powered by two variable-speed wound rotor induction motors and a synchronous motor with 10-minute maximum power ratings of 49.2 MW and 44.8 MW, respectively. As shown in the upper part of Figure 18, the induction motors are coupled to the fan drive shaft through a two-speed gear box with gear ratios (motor to fan speed) of 835/360 in low gear and 835/600 in high gear. The purpose of the two-speed gear box is to provide a better match of the motor torque available to the fan torque required at different operating temperatures. The synchronous motor is in-line with the fan drive shaft and rotates at fan speed at all times.

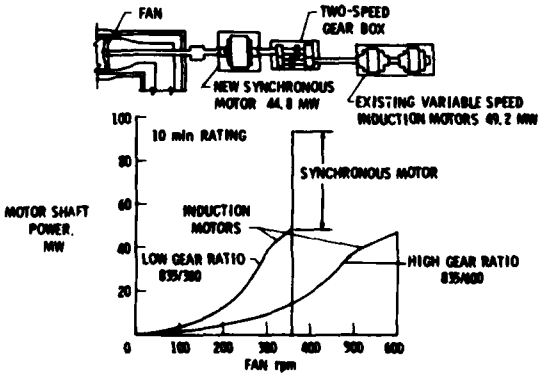

Fig. 18 NTF drive system power (after Reference 13).

The maximum (10-minute rating) shaft power available from the drive motor combination as a function of fan rotational speed is shown in the lower part of Figure 18 for both the high and the low gear ratios. The synchronous motor is operated at the fan shaft speed corresponding to the maximum speed of the induction motors in the low gear ratio, and is brought up to synchronous speed by the induction motors. The rotational speed of the induction motors is controllable within 1/4-percent over the entire range using a modified Kraemer drive control system.

Under high power conditions, when the power of both the induction and synchronous motors are required, the fan is rotated at the synchronous motor speed of 6 Hz (360 RPM), and tunnel speed control is accomplished by variation of the inlet guide vane angles. At lower power conditions where only the induction motor power is required, tunnel speed can be varied either by inlet guide vane angle variation or by motor rotational speed variation.

4.4 Performance

With the power characteristics shown in Figure 18, and tunnel pressure ratio and fan performance characteristics, the tunnel operating envelopes have been calculated by Gloss for a range of tunnel Mach numbers from 0.1 to 1.2. The envelope shown in Figure 19 for a Mach number of 1.0 is typical. The envelopes are in the form of stagnation pressure versus Reynolds number with lines of constant stagnation temperature superimposed. The maximum operating envelope is shown by the cross-hatched line. The boundaries on the figure are formed on the left by the maximum operating temperature or inlet guide vane limits, across the top by drive power or shell pressure limits, and on the right by permissible saturation conditions. Two saturation lines are shown, one for saturation conditions corresponding to a local Mach number of 1.4; the other for saturation at free-stream conditions. The lower power boundaries are for the induction motors alone in the low gear or high gear settings.

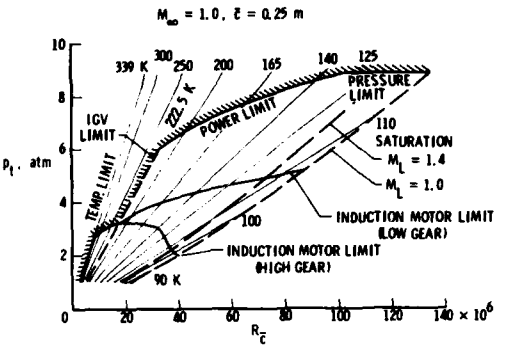

Fig. 19 NTF operating envelope for $\bar{c}$ = 0.25m and M_∞ = 1.0 (from Reference 16).

In general, the maximum Reynolds number occurs where the permissible saturation lines intersect either the shell pressure limit line (as is the case for Mach numbers from 0.1 to slightly above 1.0) or the maximum power limit (as is the case for higher Mach numbers up to 1.2). An envelope of maximum Reynolds number for the NTF is shown as a function of Mach number in Figure 20 for two saturation boundaries. The upper boundary is for saturation at free-stream conditions. Condensation studies by Hall described earlier in this lecture series have indicated that the onset of condensation effects may not be apparent until free-stream conditions are reached or even exceeded. A more conservative boundary corresponding to saturation conditions at a local Mach number 0.4 above the free-stream Mach number is also shown. With a representative wing chord length taken as 0.25 m, the conservative saturation boundary reaches a maximum Reynolds number based on chord of about 120 million at a Mach number of 1.0. The free-stream saturation boundary reaches a Reynolds number of about 135 million. It should be noted that the increase in Reynolds number from 120 to 135 million obtained by lowering the stream temperature closer to condensation conditions is achieved with no increase in dynamic pressure. At these peak Reynolds numbers, the dynamic pressure is about 3.35 atm for either boundary.

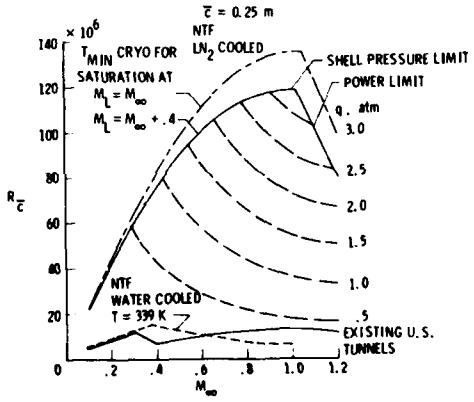

Fig. 20 NTF maximum Reynolds number (from Reference 16).

As indicated earlier, the NTF will be capable of operating in an ambient temperature mode using either air or nitrogen as the test gas with cooling accomplished by a conventional chilled-water heat exchanger. The cooling capacity of the heat exchanger corresponds to a power input of about 35 MW. With this heat duty, the maximum Reynolds number for the NTF in this mode of operation is as shown by the lower dashed line on Figure 20. In addition, the maximum Reynolds number for existing U.S. wind tunnels is also shown on the figure for comparison.

4.5 Tunnel Control

Because of the direct impact that the tunnel operating time has on the cost of operation, the control of the tunnel processes in changes of temperature, pressure, and Mach number assume major importance in the NTF. To minimize the cost of high Reynolds number testing, it is necessary to insure that the operating time interval required to obtain data is as small as possible.

The need for completely automatic control of the test conditions has been recognized and, as noted in a previous lecture in this series, work is underway to develop fast, accurate, and economical control of the NTF. The Langley 0.3-m transonic cryogenic tunnel (0.3-m TCT)[24,25] is being used to help refine some aspects of the mathematical model being developed for the NTF. In addition, experience with the automatic controls of the 0.3-m TCT gives confidence that the control requirements for the NTF can be achieved.

4.6 Problem Areas

As indicated by Howell,[18] there are certain technical areas connected with the design of the NTF which still have some unresolved aspects. These areas include the

tunnel operating constraints which may be imposed by thermal stresses, the performance of seals in a highly variable cryogenic environment, and the control of the tunnel flow processes. In all cases, the design of the tunnel has been made sufficiently adaptable so as to be capable of dealing with these aspects if the need should arise.

4.7 Status of Construction

The NTF has been under construction since March 1977 and is at present about 85 percent under contract.[18] As can be seen in the aerial view of the construction site shown in Figure 21, the construction of the pressure shell is well along towards a hydraulic pressure test date planned for August 1980. After completion of the hydro-test, the installation of the internal thermal insulation will proceed, along with other internal items which could not be installed prior to the hydro-test. The planned date for the completion of construction is the end of 1981, and operational readiness is scheduled for the fall of 1982.

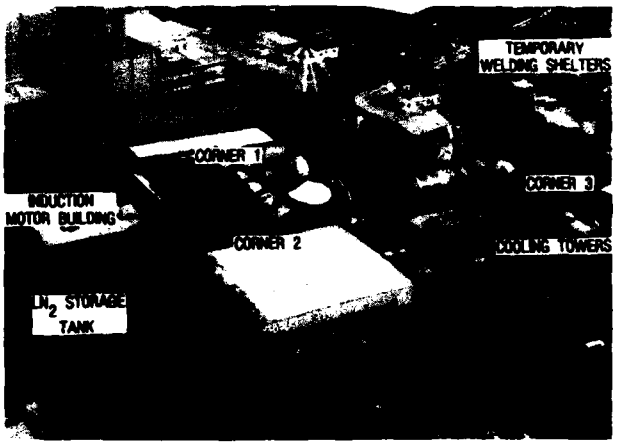

Fig. 21 Aerial view of NTF construction site (2/4/80).

5. CONCLUDING REMARKS

Construction is well underway on a major application of the cryogenic wind tunnel concept, the U.S. National Transonic Facility at the NASA Langley Research Center. This new tunnel is scheduled to become operational in 1982. Not only will it provide an order of magnitude increase in Reynolds number over existing U.S. tunnels, but because of the ability to vary pressure, Mach number, and temperature independently, it will also be able to perform the highly desirable research task of separating aeroelastic, compressibility, and viscous effect on the aerodynamic parameters being measured. It thus represents a significant step forward in fulfilling the requirements for new and improved research facilities in the field of transonic aerodynamics.

The new tunnel will have a closed return, fan-driven circuit with a 2.5 meter square slotted test section, and will be capable of operating at stagnation pressures up to 8.85 atmospheres. By virtue of its cryogenic feature, using cold nitrogen as the test gas, it will provide chord Reynolds numbers, based on a wing chord equal to 0.1 times the square root of the test section area, of 120 million at transonic speeds.

Although the cryogenic concept permits the achievement of high Reynolds numbers at relatively low energy consumption levels (compared to other high Reynolds number ground-test facility concepts) the overall consumption of energy is high and must be carefully managed. The NTF employs internal thermal insulation, a compact circuit design, extensive automation, and rapid data acquisition to combine high efficiency with high productivity and thus to minimize the consumption of liquid nitrogen which represents its main source of energy consumption.

6. REFERENCES

1. Heppe, Richard R.; O'Laughlin, B. D.; and Celniker, Leo: New Aeronautical Facilities - We Need Them Now. Astronaut. and Aeronaut., Vol. 6, No. 3, Mar. 1968, pp. 42-54.

2. Howe, John T., ed.: Some Fluid Mechanical Problems Related to Subsonic and Supersonic Aircraft. NASA SP-183, 1968.

3. Jones, J. Lloyd: Problems of Flow-Simulation in Wind Tunnels. AIAA 2nd Fluid and Plasma Dynamics Conference, San Francisco, CA., June 1969. AIAA Paper No. 69-660, June 1969.

4. Lukasiewicz, Julius: The Need for Developing a High Reynolds Number Transonic Wind Tunnel in the U.S. Astronaut. and Aeronaut., Vol. 9, No. 4, April 1971, pp. 64-70.

5. Transonic Aerodynamics. AGARD CP No. 35, 1968.

6. Facilities and Techniques for Aerodynamic Testing at Transonic Speeds and High Reynolds Number. AGARD CP No. 83, Aug. 1971.

7. The Need for Large Wind Tunnels in Europe. AGARD Advisory Report No. 60, December 1972.

8. Goodyer, Michael J.; and Kilgore, Robert A.: The High Reynolds Number Cryogenic Wind Tunnel. AIAA Paper No. 72-995, Sept. 1972. Also AIAA Journal, Vol. 11, No. 5, May 1973.

9. Margoulis, W.: A New Method of Testing Models in Wind Tunnels. NACA TN 52, August 1921.

10. Smelt, R.: Power Economy in High-Speed Wind Tunnels by Choice of Working Fluid and Temperature. Rep. No. Aero. 2081, Brit. R.A.E., Aug. 1945.

11. Nicks, Oran W.: The NTF as a National Facility. Proceedings of the Workshop on High Reynolds Number Research, Oct. 27-28, 1976. NASA CP-2009, 1977, pp. 19-25.

12. McKinney, Linwood W.; and Howell, Robert R.: The Characteristics of the Planned National Transonic Facility. Paper presented at the AIAA 9th Aerodynamic Testing Conference, Arlington, TX, June 7-9, 1976.

13. Howell, Robert R.; and McKinney, Linwood W.: The U. S. 2.5 Meter Cryogenic High Reynolds Number Tunnel. Paper presented at the 10th Congress of the International Council of the Aeronautical Sciences (ICAS), Ottawa, Canada, Oct. 3-9, 1976. Also NASA CP-2009, 1977, pp. 27-51.

14. Baals, Donald D.: Design Considerations of the National Transonic Facility. Advances in Engineering Science, Vol. 4, NASA CP-2001, Nov. 1-3, 1976, pp. 1583-1602.

15. Nicks, Oran W.; and McKinney, Linwood W.: Status and Operational Characteristics of the National Transonic Facility. Paper 78-770 presented at the AIAA 10th Aerodynamic Testing Conference, San Diego, CA, April 19-21, 1978.

16. Kilgore, Robert A.; Igoe, William B.; Adcock, Jerry B.; Hall, Robert M.; and Johnson, Charles B.: Full Scale Aircraft Simulation With Cryogenic Tunnels and Status of the National Transonic Facility. NASA TM 80085, April 1979.

17. Kilgore, Robert A.: Development of the Cryogenic Tunnel Concept and Application to the U. S. National Transonic Facility. Towards New Transonic Windtunnels, AGARD-AG-240, November 1979, pp. 2-1 to 2-27.

18. Howell, Robert R.: The National Transonic Facility: Status and Operational Planning. Paper presented at the AIAA 12th Aerodynamic Testing Conference, Denver, CO, March 18-20, 1980.

19. Polhamus, E. C.; Kilgore, R. A.; Adcock, J. B.; and Ray, E. J.: The Langley Cryogenic High Reynolds Number Wind-Tunnel Program. Astronaut. and Aeronaut., Oct. 1974.

20. Adcock, Jerry B.: Effect of LN_2 Injection Station Location on the Drive Fan Power and LN_2 Requirements of a Cryogenic Wind Tunnel. NASA TM X-74036, June 1977.

21. Dimmock, N. A.: The Development of a Simply Constructed Cascade Corner for Circular Cross-Section Ducts. N.G.T.E.M. 78, February 1950.

22. Küchemann, Dietrich; and Weber, Johanna: Aerodynamics of Propulsion. McGraw-Hill Book Co., Inc., 1953, pp. 274-278.

23. Barger, Raymond L.: Streamline Curvature Design Procedure for Subsonic and Transonic Ducts. NASA TN D-7368, December 1973.

24. Kilgore, Robert A.: Design Features and Operational Characteristics of the Langley 0.3-Meter Transonic Cryogenic Tunnel. NASA TN D-8304, December 1976.

25. Ray, Edward J.; Ladson, Charles L.; Adcock, Jerry B.; Lawing, Pierce L.; and Hall, Robert M.: Review of Design and Operational Characteristics of the 0.3-Meter Transonic Cryogenic Tunnel. NASA TM 80123, September 1979.

7. ACKNOWLEDGEMENT

I wish to express my appreciation to NASA for permission to present this lecture and to acknowledge the many contributions made towards its preparation by personnel at the Langley Research Center.

PROGRESS REPORT ON THE DOUGLAS AIRCRAFT COMPANY FOUR-FOOT CRYOGENIC WIND TUNNEL

by
J. D. Cadwell
Branch Chief
Wind Tunnel Test and Development
Aerodynamics Subdivision
Douglas Aircraft Company
McDonnell Douglas Corporation
3855 Lakewood Blvd.
Long Beach, Ca. 90846
USA

SUMMARY

The modification of the Douglas Aircraft four-foot trisonic wind tunnel to operate at cryogenic temperatures is nearing completion. This lecture will summarize the current status of the modification and will review the major areas that required work to convert an existing facility to one that can operate at cryogenic temperatures down to 180° Rankine (100° Kelvin).

Photographs showing the status of the modification at the end of February 1980 are included. In addition, the status of the development of the instrumentation and test techniques is also reviewed including model design, fabrication, and inspection techniques, force and moment, and pressure instrumentation, boundary layer transition detection methods, model angle of attack measurement, model pre-cooling evaluation, and selection of material for the verification model.

The current schedule of the tunnel checkout and calibration, and the development of instrumentation and test techniques is discussed as well as the verification test which will provide the data necessary to evaluate the performance of the modified four-foot tunnel at cryogenic temperatures for the Mach number range from 0.5 to 1.0.

INTRODUCTION

The Langley Research Center of NASA successfully demonstrated that the use of very cold gases as the test medium was not only feasible but that the available technology was prepared to meet the challenge of the cryogenic wind tunnel. The preliminary work at the Langley Research Center reviewed various tunnel concepts that could apply the cryogenic principles including a blowdown-to-atmosphere intermittent wind tunnel.

The Douglas Aircraft Company had considerable background on the need for high Reynolds number test capability and the high capital investment required to achieve the desired level of Reynolds number. A study of the application of cryogenic temperatures to the existing four-foot blowdown tunnel quickly indicated that significant Reynolds numbers could be obtained on a small model without increasing the dynamic pressure and loads on the model. Studies conducted in-house and by the Fluidyne Corporation further indicated that the existing tunnel could be modified so that operations could be conducted at temperatures very close to the boiling point of liquid nitrogen.

Management approval to proceed with the modification was given in August 1976. The successful operation at cryogenic temperatures of a one-foot pilot tunnel, 1-CWT, in May 1977 was the critical technical check point required to substantiate that the project was indeed feasible and practical.

The project proceeded from the pilot tunnel to the four-foot modification with in-house engineers doing the design and the DAC facilities group acting as the general contractor. Although the early tests in the 1-CWT pilot tunnel program answered a large percentage of the design questions, the tunnel has since been used to provide additional design information such as the steam injector to minimize the possibility of the condensed cloud touching down on adjoining property or on busy streets that are near the facility.

A parallel program has also been underway to develop instrumentation and test techniques required to take advantage of the high Reynolds number capability provided by the cryogenic temperatures. Although there are still many unanswered questions to be resolved the current test technique development program should provide the information necessary to conduct a successful verification test program.

THE MODIFICATION

The blowdown wind tunnel characteristic of short run times is the primary reason that an existing facility can be modified to operate at cryogenic temperatures. Figure 1 shows the effectiveness, for a short time period, that a thin layer of insulation will have on preventing the very cold temperature of the tunnel flow from significant heat transfer to the tunnel structure, that has an embrittlement temperature of -20°F. The net effect was that the majority of the tunnel primary structure would only require a thin layer of insulation which made the entire project feasible.

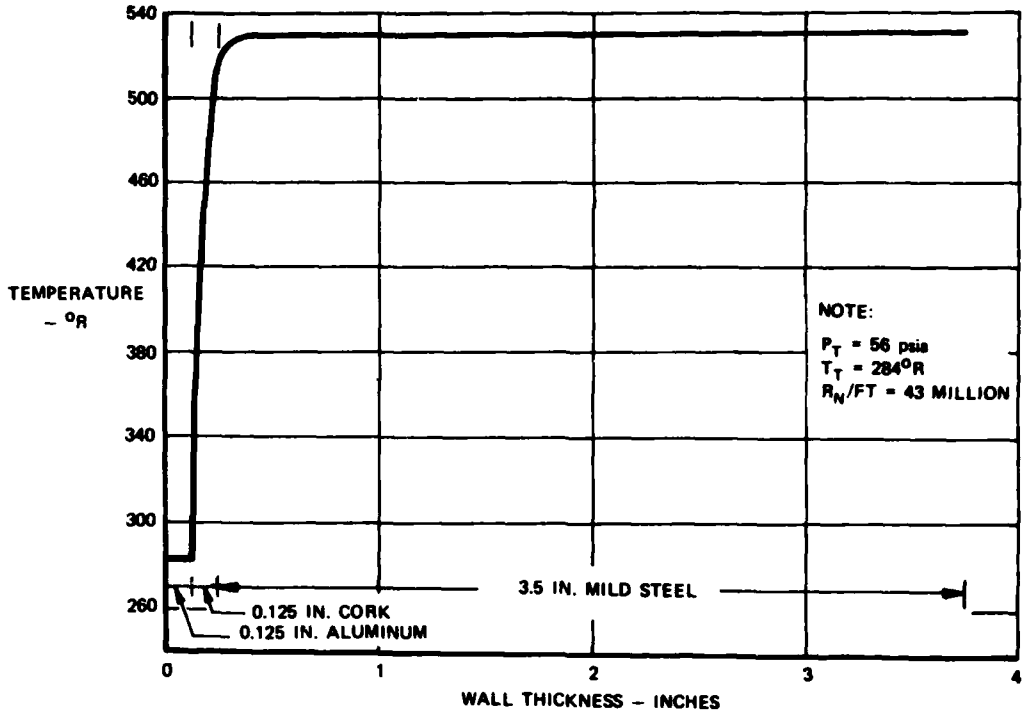

FIGURE 1. WALL TEMPERATURE DISTRIBUTION WITH INSULATING COVER

The major areas of modifications required to convert the tunnel to a cryogenic facility are shown below.

ITEM	REMARKS
1. Liquid nitrogen storage tank	40,000 gal capacity
2. Liquid nitrogen run tank	9,000 gal. capacity
3. Liquid nitrogen distribution system	Plumbing and control system for transferring LN_2 from storage tank, to run tank, to injection stations, and to model pre-cooling system
4. Axial flow control valve	Upgrade flow quality and increase run time
5. Liquid nitrogen injection chamber	60 ft x 6 ft dia. cryogenically compatible material Houses LN_2 injection system.
6. Relocate storage tanks, shutoff valves and feeder lines	Provide space for LN_2 run tank
7. Perforated plate in transition section from LN_2 injection chamber to stilling chamber	Prevent separation in wide angle diffuser
8. Rebuild settling chamber acoustic section with cryogenically compatible materials	Absorb noise generated upstream of stilling chamber
9. Replace test section walls	Use cryogenically compatible material with same hole geometry (normal holes), and porosity (22% open)
10. Reinforce muffler tower	Structural safety factor reduced as result of increased back pressure and loads due to cloud control doors at exit
11. Steam injection at muffler exit	Increase exhaust temperature to prevent touchdown of cloud
12. Install insulation throughout tunnel to protect structure	Prevent non-compatible materials from reaching embrittlement temperatures
13. Incorporate safety equipment	Guard against hazards that can result from reduced oxygen and/or cold temperature environment
14. Obtain cryogenically compatible tunnel calibration instrumentation	Update instrumentation as required
15. Modify control system to include temperature control	New requirement of cryogenic tunnel
16. Checkout modification and calibrate tunnel	Establish flow characteristics throughout temperature and pressure ranges
18. Conduct verification test	Establish data quality of cryogenic blowdown tunnel

MODIFICATION STATUS

The majority of hardware is completed and installed. The last major hardware item to be installed is the muffler steam injector and exit doors on the muffler tower. Figure 2 is an isometric sketch of the modified facility. Figures 3 through 12 show the status of the modification near the end of February 1980. At the time that this lecture is presented, the checkout of the facility should be underway. Figure 3 is a view of the 40,000 gallon LN_2 storage tank. Figure 4 shows the new arrangement of ducting the air from the storage tanks to the header tank just upstream of the control valve. Also shown are the two shutoff valves. The upright tank in Figure 5 is the run tank that transfers the LN_2 to the injection chamber at a flow rate up to 300 gallons per second at a pressure of 300 psia. Figure 6 shows the run tank fill line, in the foreground, and the line to the injection chamber. Figure 7 shows the new axial flow control valve installed and Figure 8 shows the LN_2 injection chamber in place. Figure 9 shows the control valves for the two LN_2 injection stations. Figure 10 shows workmen installing the acoustic panels in the stilling chamber. The man in the foreground is standing in the section where the honeycomb and fine mesh screens will be installed. Figure 11 shows the 1.29% DC-10 model installed in the test section for a spray nozzle pre-cooling evaluation. Figure 12 shows the muffler tower in the background before the installation of the exit flow control doors. In the left foreground is the steam injection system installation. The right foreground shows one of five air storage tanks. The air supply has a total capacity of 34,000 cubic feet at a pressure of 525 psia.

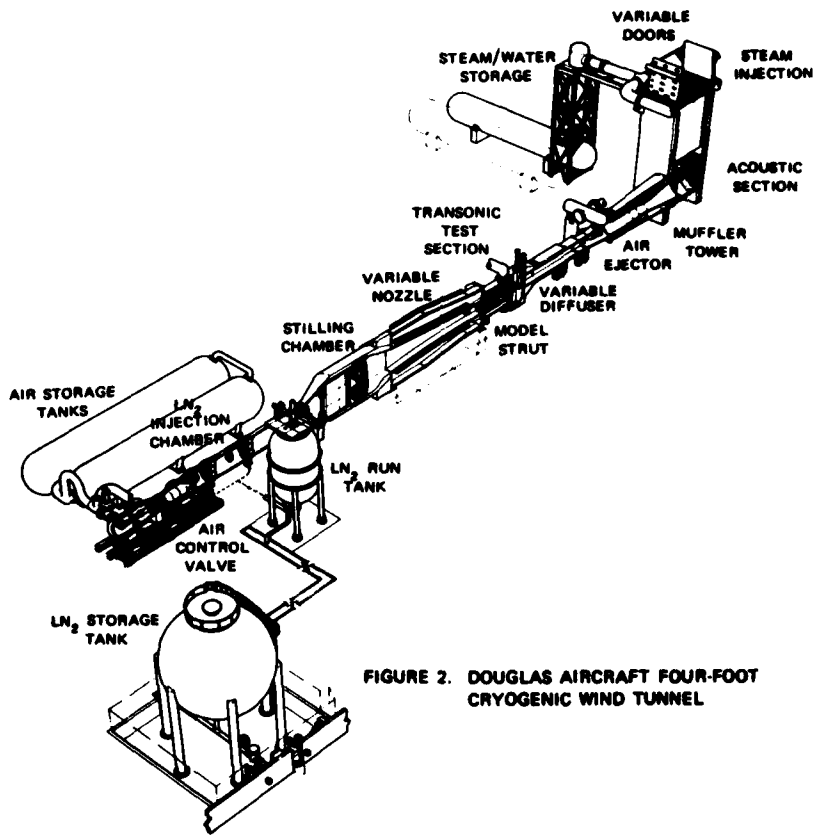

FIGURE 2. DOUGLAS AIRCRAFT FOUR-FOOT CRYOGENIC WIND TUNNEL

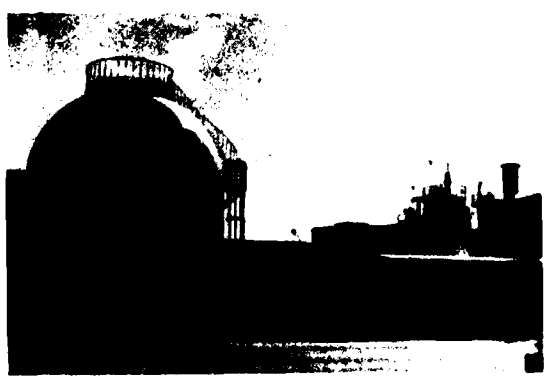

FIGURE 3. 40,000 GALLON LN_2 STORAGE TANK

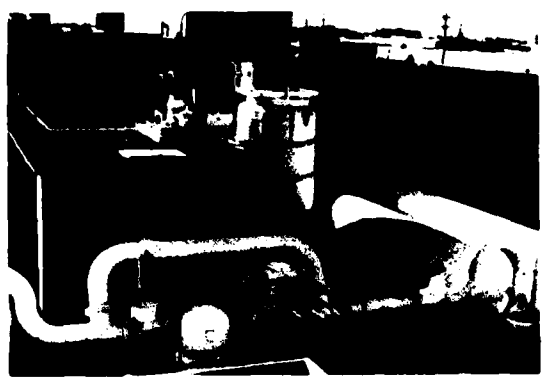

FIGURE 4. AIR SUPPLY PIPING TO TUNNEL AND 9,000 GALLON LN_2 RUN TANK

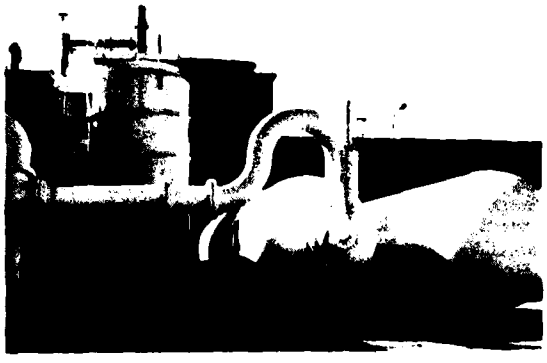

FIGURE 5. 9,000 GALLON LN_2 RUN TANK AND 2 AIR STORAGE TANKS

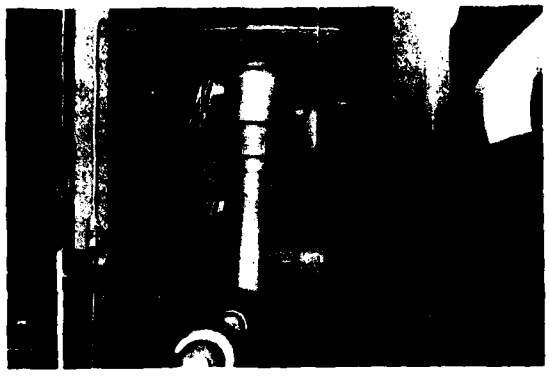

FIGURE 6. LN_2 LINES INTO AND OUT OF RUN TANK

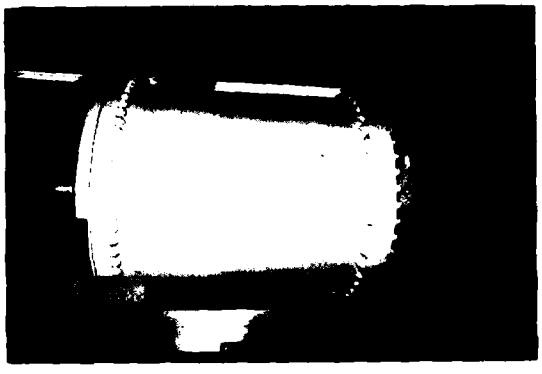

FIGURE 7. NEW AXIAL FLOW AIR CONTROL VALVE

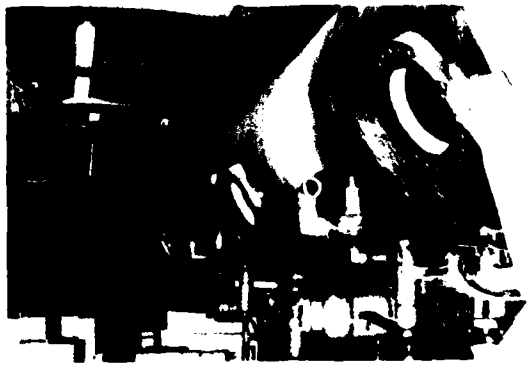

FIGURE 8. LN_2 INJECTION CHAMBER

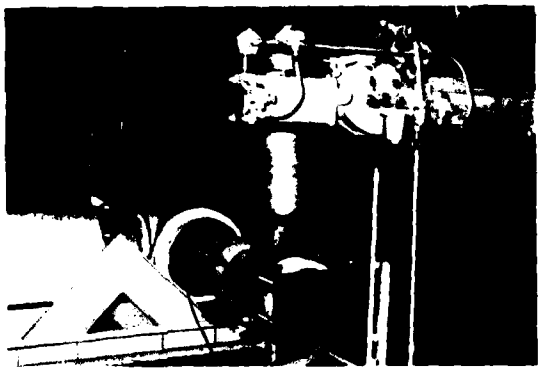

FIGURE 9. LN_2 CONTROL VALVES

FIGURE 10. ACOUSTIC PANELS BEING INSTALLED

FIGURE 11. DC-10 MODEL INSTALLED FOR PRE-COOLING TEST

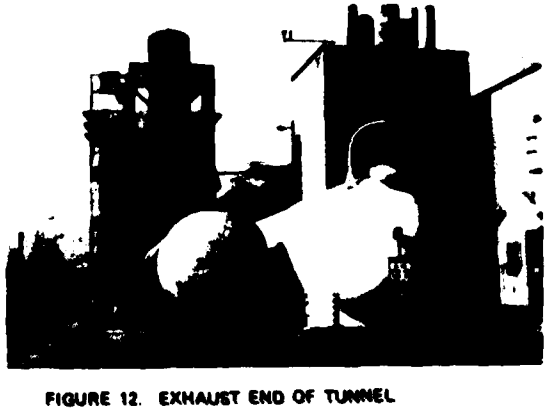

FIGURE 12. EXHAUST END OF TUNNEL

TEST TECHNIQUES & INSTRUMENTATION STATUS

The management approval to proceed with the cryogenic modification of the Douglas Aircraft Company four-foot blowdown wind tunnel also initiated the development of test techniques and instrumentation as well as the design and fabrication of models. The basic plan applied to all phases of the model program was to conduct analytical studies and then to check out the particular item in a cryogenic static test environment or to test it in the one-foot cryogenic pilot tunnel where actual test conditions could be simulated. The major items that required careful scrutiny before application to cryogenic testing are discussed in the following paragraphs.

MODEL DESIGN, FABRICATION, AND INSPECTION

The precision required in a high aspect ratio model sized for a four-foot wind tunnel represents a major challenge to the model technicians and inspectors. The results of early studies into this critical area indicated that major improvements in machinery and equipment, and in the working environment would be required. Work was accomplished before the end of 1978 to upgrade the working conditions by providing a temperature controlled environment, isolating machine foundations from ambient ground vibrations, adding new numerical control equipment, and providing a dedicated inspection area with accurate and stable coordinate inspection equipment. This equipment is now in service and is being used to make the cryogenic models that are required to develope instrumentation as well as to fabricate checkout and verification models.

STRAIN GAGE BALANCE

The decision was made early in the program to use existing internal strain gage balances and provide the necessary environmental control to keep the balance at a stable temperature. Satisfactory results have been obtained in the one-foot pilot tunnel (1-CWT) with the fuselage of a DC-10 model that will be used to verify the acceptability of data from the four-foot cryogenic tunnel (4-CWT). Improved versions of the balance heaters and the balance to sting interface heater will be checked in both the 1-CWT and the 4-CWT as part of other instrumentation checkout tests that will be discussed later in this report.

PRESSURE TRANSDUCERS

The two systems under consideration for measuring approximately 250 model static pressures are the conventional mechanical stepping modules and the new electronically scanned pressure sensor modules (ESP). The ESP system with individual transducers and multiplexer is the preferred system because of the short time required to record the pressure data. The system requires environmental control due to its sensitivity to temperature changes. Modified insitu calibration procedures that are necessary due to space limitations in the model should minimize the temperature sensitivity effects. Checkout of the ESP units will be made in both the 1-CWT and the 4-CWT tunnels under cryogenic conditions to establish that the system is ready for the verification test with the DC-10 model.

BOUNDARY LAYER TRANSITION DETECTION

The wide range of Reynolds numbers that will be encountered in the cryogenic tunnel establishes the requirement to be able to detect the point of boundary layer transition from laminar to turbulent. There are many techniques that have been used to detect transition. Hot film sensors, subminiature kulite transducers, and listening to and recording the rumble through pressure taps in the wing are all methods that have been used in the past and all will be considered for use in the cryogenic tunnel. The real trick is to select the method that can essentially be a part of the model and can be used throughout a test program to monitor the natural transition location or to determine if the artificial means used to fix its location is satisfactory. In order to establish the technique to be used on three dimensional models a two dimensional model (a planform sketch is shown in Figure 13) will be tested in the 1-CWT. The model includes 26 hot film senors distributed on the upper and lower surfaces, 13 Kulite transducers in the upper surface, and 12 static pressures in the upper surface, all of which will be used to detect the transition point.

ADDITIONAL INSTRUMENTATION - 2D MODEL

The model also includes 118 static pressures in the upper and lower surfaces to obtain spanwise distributions to check the two dimensionality of the flow across the span of the wing and chordwise distributions to obtain the section lift and pitching moment coefficients. Data from a traversing wake rake aft of the model with seven each static and total pressures, and temperature probes will be integrated to obtain the section drag coefficient.

The two dimensional model will also be instrumented with 47 thermocouples to measure the model surface temperature distributions. The correlation of the aerodynamic coefficients and the temperature distributions will be used to determine the acceptable temperature differential between the model wall and the air stream. A short segment of porous leading edge is installed in the model that will dispense dyed cryogenic fluid for observing surface flow visualization.

Tunnel instrumentation will include 18 static taps along the top wall to determine effects of changes to the boundary layer displacement thickness, 10 thermocouples along the top and bottom wall to monitor the time history of the test section wall temperatures, one Kulite pressure transducer in the top wall to check the boundary layer fluctuating pressure, and one hot-film/hot-wire probe mounted from the ceiling to measure free stream turbulence and temperature fluctuation levels.

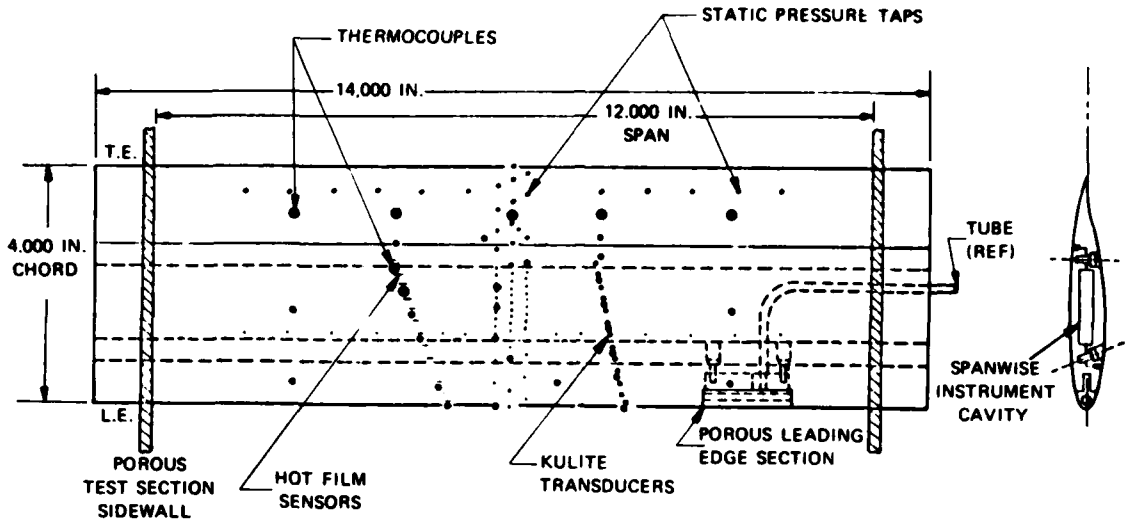

FIGURE 13. 2D TEST TECHNIQUE DEVELOPMENT MODEL

MODEL ANGLE OF ATTACK

The development of an accurate angle of attack system that measures the model attitude directly is mandatory as indicated in an earlier lecture on control of pertinent variables in a cryogenic blowdown wind tunnel. The "hot dog" effect caused from non-uniform cooling in the model support strut and sting essentially eliminates the conventional system of measuring the pod angle and correcting for sting and balance deflections due to aerodynamic loads on the model.

Three systems are currently being studied at the Douglas Aircraft Co. The first is the use of an accelerometer whose output is proportional to the sine of the angle and an on-board electrolytic bubble to indicate zero angle of attack. The second method is a polarization technique that incorporates two analyzer/detectors that sense the change in angle between a polarized light beam and the orientation of an analyzer/detector. The third method under evaluation is a laser system proposed by the Boeing Aircraft Company.

MODEL PRECOOLING & TRANSIENT SHIELD

The spray system that was selected for the model pre-cooling is currently being setup in the test section for checkout and evaluation. The transient shield to protect the model during tunnel start from warm air trapped between the valve and the test section will be evaluated using the two dimensional model in the 1-CWT. The results of the pre-cooling test and the transient shield check-out will be evaluated to determine if the systems are adequate or if a clamshell type enclosure is required to provide an adequate pre-cooling system and eliminate the need for a transient shield to protect the model during the tunnel start.

SELECTION OF MATERIAL

The selection of stainless steel or beryllium copper as the material to be used for the DC-10 verification model will depend upon the careful analysis of several tests that are to be conducted in the near future in both the 1-CWT and the 4-CWT. One of the tests is a checkout of the pre-cooling system using a stainless steel slab wing with a large number of thermocouples installed throughout the model. The main consideration in this test with regard to material selection will be the temperature uniformity that can be obtained with a stainless steel material and the spray nozzle type pre-cooling system. The improvement in temperature distribution can be significantly improved if the wing were made out of beryllium copper. Analysis of data from the two dimensional test in the 1-CWT will also be used to aid in the selection of the material to be used for the verification model. The principal input that will result from this 2-D test is the allowable tolerance on the deviation of model temperature from adiabatic wall conditions for acquisition of valid data in the 4-CWT. The third test that will provide insight into the selection of the material for the wing, fuselage, and empennage is an air-on test in the 4-CWT using the stainless steel slab wing where the time required to stabilize the model temperature distribution after the tunnel flow conditions have been set, and the change in that distribution as the model is pitched through an angle of attack range will be acquired and analyzed.

If the results of these tests indicate that the spray nozzle pre-cooling system and the transient shield appear adequate but that improvement in wing temperature distribution is necessary, then the selection of beryllium copper as the material for the wing, fuselage, empennage, and nacelles and pylons would be seriously considered, assuming of course that an acceptable Charpy Impact strength level can be obtained.

If the results indicate that a sophisticated model pre-cooling system such as a clamshell arrangement is required there is no need to give further consideration to the use of beryllium copper.

One alternative that is being considered, that could eliminate the need for a pre-cooling system, is to fabricate the model from composite materials which may have a low enough conductivity so that the heat transfer effects would be insignificant.

SCHEDULE

The current schedule for the completion of the facility modification, the checkout and calibration of the tunnel, and the development of test techniques is shown in Figure 14.

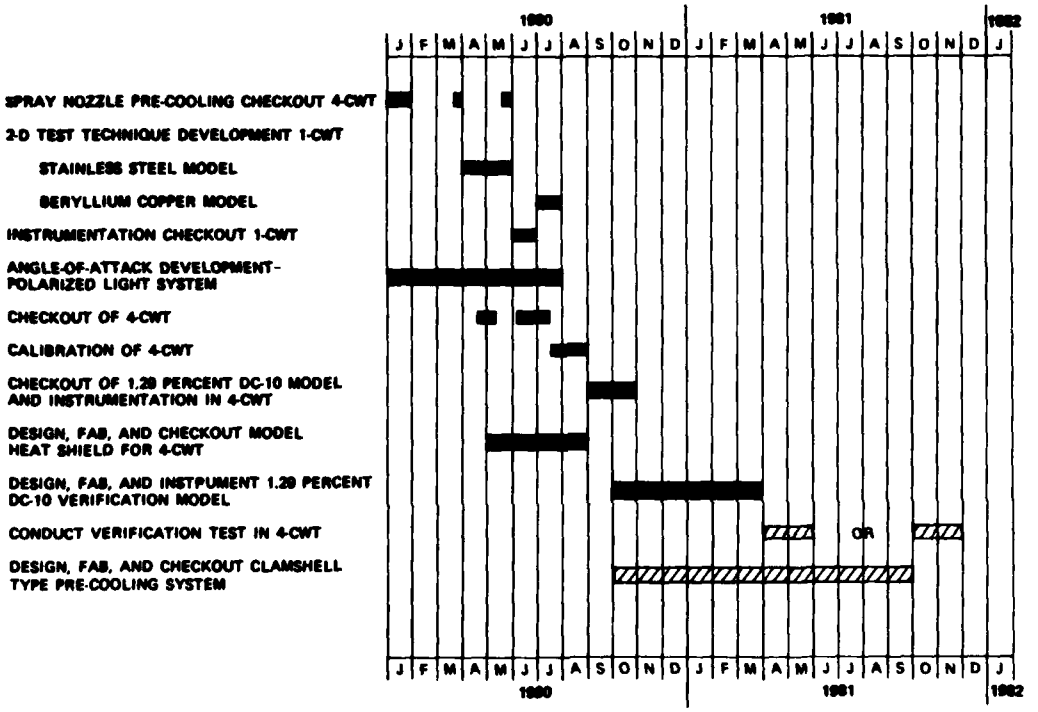

FIGURE 14. CURRENT CRYOGENIC DEVELOPMENT SCHEDULE

The pre-cooling checkout test will determine the error band within which the spray system can pre-cool the model over a range of desired temperatures and the temperature variation throughout a model that is fabricated of stainless steel. The analysis of the pre-cooling data, the heat transfer effects and thermal responses from the two dimensional test in the 1-CWT, the effectiveness of the transient shield also obtained from the two dimensional test in the 1-CWT, the thermal response of the stainless steel wing from the DC-10 model and the instrumentation checkout test in the 4-CWT will all be used to assess the adequacy of the spray nozzle pre-cooling system. At this point a trade-off study can be made to determine if a more sophisticated and efficient pre-cooling system would offset the capital expenditure of a clamshell type pre-cooling system.

The completion of the checkout of the DC-10 model and instrumentation in the 4-CWT is also a key milestone to be reached before the material selection for the final instrumented wing can be made. Once the wing material has been determined the design and fabrication of the model can be completed and the verification test can be conducted if the combination of spray nozzle pre-cooling and material selection has been demonstrated to be a satisfactory technique. If a sophisticated pre-cooling system is required, a delay in the verification test would be necessary to design, fabricate, install, and checkout the hardware.

ACKNOWLEDGEMENT

Dilworth, Secord, Meagher and Associates, LTD. (DSMA) of Toronto, Ontario, Canada has been granted an exclusive license for aspects of the tunnel design associated with the conversion of the Douglas Aircraft four-foot wind tunnel to operate at cryogenic temperatures.

A CRYOGENIC TRANSONIC INTERMITTENT TUNNEL PROJECT : THE INDUCED FLOW CRYOGENIC WIND TUNNEL T2 AT ONERA/CERT

R. Michel
Chief, Aerothermodynamics Department
ONERA, Centre d'Etudes et de Recherches de Toulouse
31055 - TOULOUSE, FRANCE

SUMMARY

This lecture presents the project for a new cryogenic intermittent tunnel, the induction driven tunnel T2 at ONERA/CERT, which uses high pressure air as a driving gas and nitrogen as a cooler.

A description of its main characteristics at ambient temperature operating is given at first. Then, the various aspects of its transformation for a low temperature operating are analysed : modifications of the circuit - thermal insulation technique - liquid nitrogen injection - regulation systems - cryogenic operating mode and expected performances.

RESUME

On présente le projet d'une nouvelle soufflerie cryogénique à rafales, la soufflerie à induction T2 de l'ONERA/CERT, qui utilise l'air à haute pression comme gaz moteur, et l'azote comme fluide réfrigérant.

On donne d'abord une description de ses principales caractéristiques dans le fonctionnement à température ambiante. On analyse ensuite les différents aspects de sa transformation pour un fonctionnement à basse température : modifications du circuit - technique d'isolation thermique - injection d'azote liquide- système de régulation - mode opératoire cryogénique et performances attendues.

1. INTRODUCTION

The solution selected by ONERA to provide itself with a cryogenic facility within reasonable delays and cost, is to adapt the existing transonic injector driven tunnel T2 for a short cryogenic runs operating.

This wind tunnel was installed and has been operating now at the ONERA Toulouse Research Center since 1975.

At that time AGARD considered a Large European High Reynolds Number Tunnel (LEHRT) which should permit to attain full scale Reynolds numbers by means of pressurization, and three main projects have been developped :

- The Ludwieg Tube, from DFVLR, Germany,
- The Evans Clean Tunnel, from RAE, Great Britain,
- The Injector Driven Tunnel, from ONERA, France.

With a run duration of 30 seconds (at maximum mass-flow),
a test section of 40 x 40 cm,
a Mach number from 0.3 to 1.1,
a stagnation pressure from 2 to 5 bars,
the T2 wind-tunnel represents about the one tenth scale pilot unit of the ONERA project for the Large European Wind Tunnel.

A description of its main characteristics at ambient temperature operating, is given in the first part of this paper.

The simple idea which led us to T2 cryogenic adaptation, was to combine a cryogenic operating with an induction one, in the hope that the small duration of the flow will only provide a small diminution of temperature of the circuit walls.

Systematic tests made on a small pilot facility, and described in a first paper[1], have confirmed that such a solution was feasible and have permitted to define the solutions to be hold for the cryogenic adaptation of the T2 wind tunnel. The various aspects of this adaptation, as well as the cryogenic operating mode and the expected performances, are analysed in the second part of this lecture.

2. THE WIND-TUNNEL MAIN CHARACTERISTICS AT AMBIENT TEMPERATURE OPERATING

2.1. Aerodynamic Circuit - Power Supply Facilities

T2 is a transonic closed return circuit wind-tunnel, which consists of the components shown in figure 1 :

- There is at first the stilling chamber, 1.8 by 1.8 meter cross-section, fitted out with honeycomb and grids, and surrounded by a cylindrical shell which supports the pressure forces,
- then the convergent, with a contraction ratio of 20, also contained in a conical shell,
- the test-section, 0.4 by 0.4 meter,equipped with solid walls for the results thereafter presented,
- it is ended with a second throat, which can be choked for Mach numbers above 0.6.

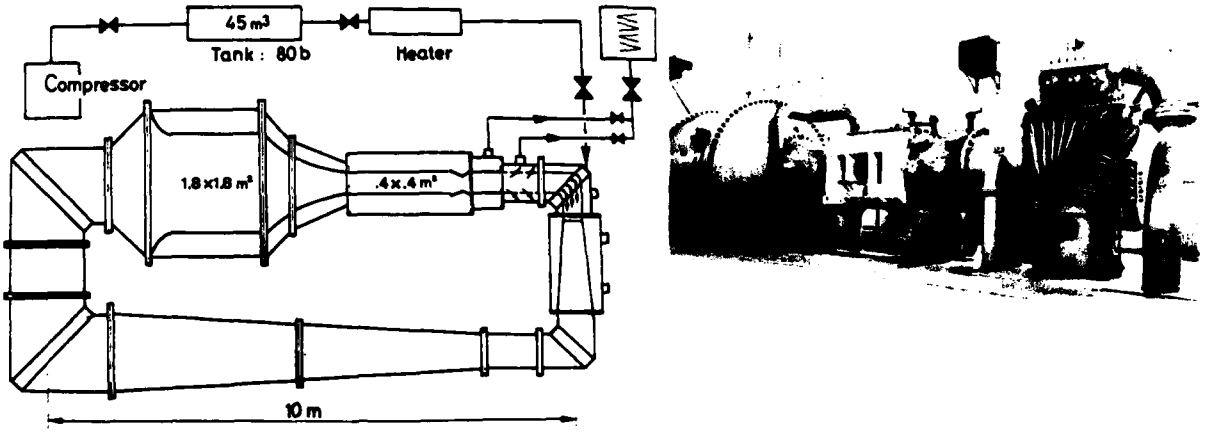

FIGURE 1 : Wind Tunnel T2 General Lay out.

T2 is an induction driven tunnel, and a first characteristic aspect is that the driving air injection is provided through the first corner turning vanes trailing edges. The injection involves seven two-dimensional jets which rapidly mix with the induced flow in a mixing chamber. So the emission of jet noise is located far from the test section, and essentially directed towards the return circuit, this being propitious to a damping of acoustic fluctuations.

The second typical aspect is that the flow removal is located just upstream of the injector. Taking advantage of the pressure level in the tunnel, it is simply performed through the porous walls of a rectangular cross section duct acting as a diffuser after the test section. The interest is that the injector has to drive only the difference between the mass flow in the test section and the removed mass-flow, also that the suction of the wall boundary layers reduces the total pressure loss of the circuit.

After the mixing chamber comes the second diffuser, which leads to about Mach number 0.3, and after it, the low velocity return circuit closing the tunnel.

The power supply facilities, also schematised in figure 1, include the following components :
- a compressor, providing about 0.5 kg/second mass flow at 80 bars,
- a tank of 45 m3 for the storage of compressed air,
- a heater for maintaining the injection total temperature near the ambiant,
- a pressure reducer provided with a regulation system insuring a constant injection pressure ; using a laminating concept, it generates a low noise level,
- exhaust pipes and valves, ended by a general valve and a sound-proof exit system.

2.2. - Multi-Injector Turn Vanes System

The choice of the injector parameters resulted from a thorough discussion of an injector drive system, based on the equations and parameters which were presented in paper 13, and which led to the choice of a reasonable compromise between high efficiency and aerodynamical or technological requirements.

As concerns the induced flow, a compromise between a velocity sufficiently high for having a good efficiency and the necessity to avoid supersonic flows development between the vanes, led us to choose an induced flow Mach number MI = 0.6.

As concerns the driving flow, the efficiency obviously increases with the jet pressure, but it is necessary on the other hand to limit the storage pressure at a reasonable value. The jet Mach number, 1.6, was therefore the result of another compromise.

The last parameter is λ, the injector exit to mixing cross section area ratio. It appeared very important to provide for its variation, in order to study its true influence on performances and flow qualities.

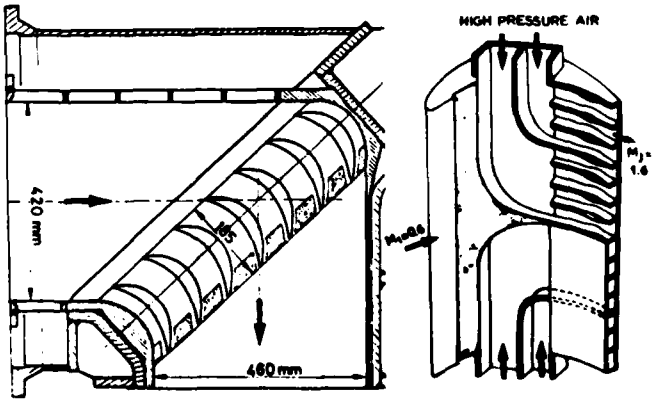

FIGURE 2 : Injector Corner System.

As shown in figure 2, the solution held for this variation, was to partition the inside of each vane so as to form 14 little nozzles giving the required Mach number 1.6, and to supply them with compressed air by groups of 3 or 4, separately.

2.3. Performances and Flow Qualities

Two main parameters influence directly the performances of the wind tunnel, as well as its flow qualities.

At first there is the area ratio between the mixing chamber and the driving gas injection sections, the value of which is very important for optimizations. Let us note that an interesting particular functionning can use the value of λ which realises the equality between jet and induced flow static pressures ; avoiding the formation of shock systems, this "adapted injection" has the advantage of reducing the jet noise.

The second important effect is that of the sonic throat, put at the rear of the test section. It influences mainly the flow qualities in preventing the jet noise from travelling upstream to the test section ; but it proved necessary to have a carefully shaped second throat, with a limited supersonic expansion, giving Mach number, say, not higher than 1.15. Then it was possible to limit the additional loss due to the second throat, and use it at test-section Mach numbers from 0.6 to 0.9.

Figure 3 is concerned with the drive system performances, that is, with the entrainment ratio defined as the ratio of the test section mass flow to the injected mass flow, and with the required jet to induced flow pressure ratio.

The influence of the area ratio λ has been studied, in varying the number of the injector drive nozzles. Finally a configuration with λ = 29 and the second throat choked has been retained for test section Mach numbers between 0.6 and 0.9.

It can be said that the performance is good, since we have an entrainment ratio of the order of 8 while the required pressure ratio is about 3.5.

Also is shown the influence of the area ratio : a smaller λ gives a decrease of the entrainment, but requires a lower pressure ratio.

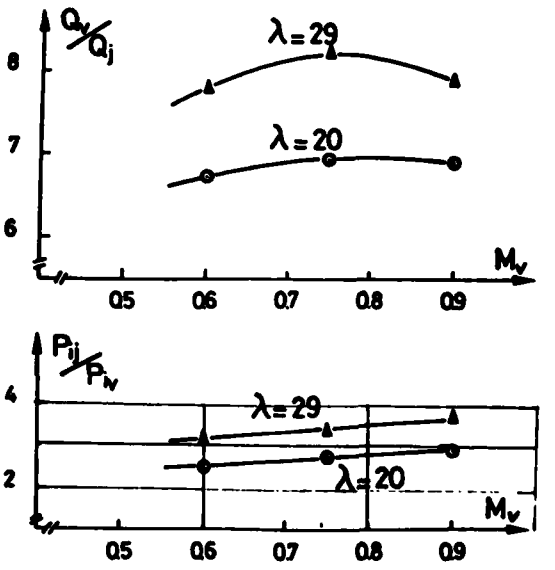

FIG. 3 : Drive System Performances.

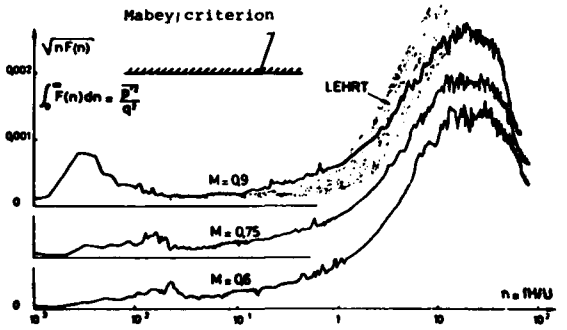

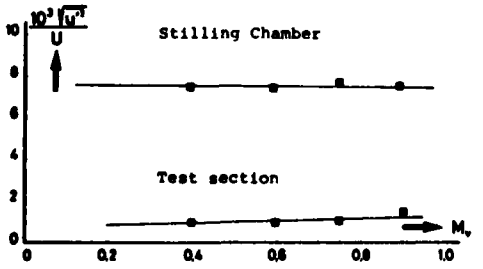

FIG. 4 : Pressure and Velocity Fluctuations.

Within the qualification tests requirements which were asked to the three candidate tunnels for LEHRT, we made a thorough analyzis of the T2 wind tunnel flow fluctuations.

Thanks to a carefully shaped second throat, and to an optimization of the area ratio and the jet nozzles configuration, it was possible to reduce considerably the fluctuations and obtain finally results, examples of which are shown on figure 4.

The pressure fluctuations spectra measured at the test section wall are given with the conventional coordinates, n and F, reduced frequency and reduced pressure fluctuation.

At high frequencies, the noticeable fluctuation increase obviously arises from the walls boundary layer noise. The level remains low up to a reduced frequency n = 1, that is in the frequency range where the flow fluctuations may have effect on the main phenomena (buffet, flutter...) to be studied in transonic aerodynamics.

Qualities obtained for the flow then appear compatible with the requirements which were asked at that time for the European Wind Tunnel. Stress is made of these requirements strictness : the required level is much more stringent than Mabey's criterion which is often used for normal wind tunnels.

Below is shown the longitudinal turbulence intensity measured in the stilling chamber and in the test section. Quite independent from Mach number, the turbulence remains at low levels, one thousands order in the test section.

2.4. Wind Tunnel Equipments

The wind tunnel T2 is used mostly as a research unit, devoted to point out and to specify the detailed characteristics of subsonic transonic flows, for example in elaborate studies which sould give the necessary elements for assessing theories and calculation methods of viscous and non viscous flows.

To that effect, the wind tunnel has been equiped with various measurements devices, especially with short response time probes. These are notably static and total pressure probes with incorporated Kulite transducers. Their response time is sufficiently short to allow a fast probe translation, and explore for example a boundary layer in a single 30 to 60 seconds run, with a good accuracy.

Detailed boundary layers and wakes probings are currently performed for steady and unsteady flows on two dimensional airfoils and swept wings.

Problems related with wall corrections have been particularly studied, and the T2 wind tunnel has been fitted with self-adaptive walls.

These are flexible solid walls, with a small thickness, which can be adjusted to take the shape that would have the model streamlines in unlimited flow.

For this, a measurement of the pressure and wall direction gives the two components of the flow velocity along the wall. A calculation of the external transonic flow field is joined, which allows to specify the conditions we should have at the wall in unlimited flow. Then the wind tunnel and the computer work simultaneously in an iterative process which leads to the shape of the unlimited flow streamlines.

A photograph of the adaptive walls installed in the T2 test section is shown figure 5 ; each wall is distorted by 16 hydraulic jacks, monitored by a micro computer.

Using a NACA 0012 airfoil, a systematic implementation study has been carried out. A good convergence towards the unlimited flow conditions could be realised, at various Mach numbers and pitch angles. The study underlined the capital influence of adaptation on measured transonic flow characteristics, shock wave location, drag and lift...

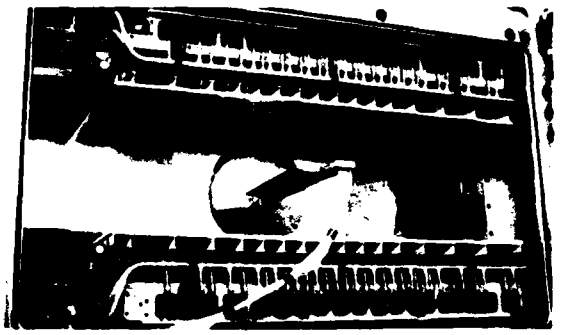

FIG. 5 : Self-Adaptive Walls.

3. CRYOGENIC ADAPTATION

Coming now to the cryogenization of the wind tunnel, let us recall the two main aspects of the solution, which were underlined with the tests made in the pilot unit T'2 :

- A very favourable influence, with respect to the driven gas mass flow rate, of a driving gas temperature superior to that of the driven flow ; i.e injection of driving air at room temperature and cooling of the flow with a quick supply of liquid nitrogen in the return circuit.
- A very good thermal protection of the metallic walls with a thin inner insulating coating. During the 30 to 40 seconds run, the metal remains at room temperature, while the surface temperature of the insulating material falls down very quickly to a value practically equal to the adiabatic wall temperature.

Modifications to be brought to the wind tunnel circuit resulted both from this cryogenic operating mode, and from the analysis of some safety requirements imposed by a circuit made in ordinary steel, for which a low temperature operating had not been originally foreseen.

Most of the circuit components remain in fact practically unchanged : the low velocity return circuit, the stilling chamber, the test section and the injector corner will be lined simply with an internal thermal insulator layer, with a thickness of 5 to 10 millimeters.

The components to be rebuilt are the following :

There is at first the part of the circuit which comes after the injector corner ; taking account of the informations given by the T'2 tests, we shall have the liquid nitrogen injection immediately after the injector corner, with a peripherical injector system. For safety reasons, it has been decided to change also the second diffuser and the second corner, and make them in stainless steel.

There is also the exhaust chamber, which has to work now at low temperature, with an exhausted mass flow rate practically doubled with respect to the ambiant temperature operating. Also will be described how it has to be equipped with a control system for regulating the tunnel pressure.

3.1. Thermal Insulation Technique

Some generalities about the requirements concerned with the insulating materials which can be appropriate to our problems are given at first :

- They must have a good compressive strength ; we have to run the tunnel up to 5 bars,
- Also a good fatigue strength to pressure load and temperature cycles is required ; the pressure will vary from atmospheric to several bars, the temperature from ambient to cryogenic at the beginning of each run, and conversely at the end, this in a few seconds.

We can distinguish the low velocity return circuit, and the high speed parts, where problems are somewhat different.

In the return circuit the velocity is sufficiently low to tolerate some surface roughness. We can find a material with a very low conductivity and a low heat capacity which insures a good thermal protection as well as a quick establishment of the surface temperature.

In the high speed parts, the heat transfer is higher and the wall temperature establishment is more rapid a priori, but a problem is to have limited friction losses and to insure good junctions, for example between walls and windows of the test section. The insulant must have a sufficiently smooth surface, and this can lead us to be a little less exigent about its thermal properties.

Using the heat transfer calculation method which was presented in the first paper[1], systematic calculations have been performed, in order to show in evidence the behaviour of internal insulants as function of their thermal properties.

Examples of results concerned with an insulant of a given thickness protecting the steel shell of the low velocity return circuit are shown in figure 6. On the left is shown the influence of thermal conductivity when keeping the heat capacity constant, on the right the influence of heat capacity with an assumed constant thermal conductivity.

The dotted line represents the flow temperature, assumed to fall down to 120°K in about 10 seconds. The wall temperature evolution is shown and the corresponding heat transfer is given below.

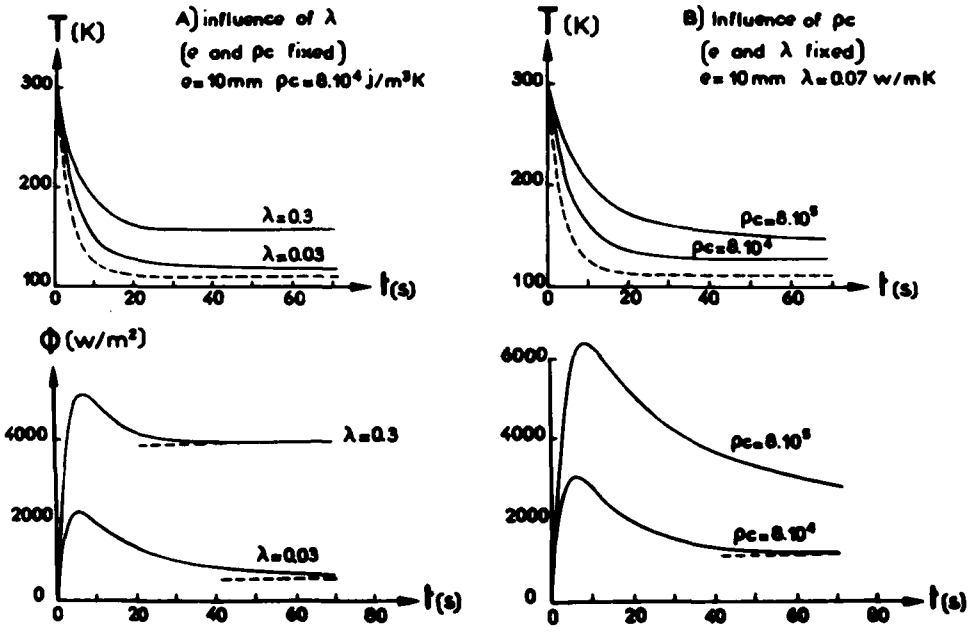

FIG. 6 : Internal Insulation. Wall Temperature and Heat Flux

Two main aspects of the internal insulation are underlined :

- Although the rigorous establishment to the adiabatic wall temperature should be obtained in an infinite time, there exists for the short flow duration considered, some kind of steady state regime, where the wall temperature and the heat flux attain and keep a practically constant value. For this first established regime it is observed that the wall temperature is all the more near the flow total temperature, and the heat flux all the less important, as the thermal conductivity is lower.
- But the time taken to attain this pseudo-established regime also depends on the thermal characteristics ; at fixed heat capacity it increases with a decreasing conductivity ; at fixed conductivity it also increases with an increasing heat capacity.

It is obvious that such calculations are very useful for choosing among various insulants a best compromise. Some materials which could be used in the T2 insulation are listed in the following table.

INSULATION	THERMAL CHARACTERISTICS AT 0°C			CAN BE USED FOR			OBSERVATIONS
	λ	ρC	a	LOW SPEED PARTS	HIGH SPEED PARTS	SPECIAL PARTS	
(Klegecell ((P.V.C. foam)	0.02	0.094	0.223	X	X		. Good thermal characteristics. . Failures under strong gradient.
(Special cork ((norcoat)	0.07	0.846	0.085		X		. Easy to set up. . Smooth surface.
(Polyuréthane foam	0.03	0.075	0.44	X		X	. Can be injected.
(Voltalef ((PTFCE)	0.06	1.890	0.03		X	X	. Expensive material.
(Teflon ((PTFE)	0.3	2.257	0.13			X	. Useful in a lot of cases but high conductivity.
(Polyuréthane (coating ((("Senotex"- (HB fuller)	0.13	1.410	0.10			X	. Thin layer protection.

3.2. Liquid Nitrogen Injection-Device

It has been shown by the tests performed in the pilot rig T'2 that a substantial improvement of the flow qualities are obtained when locating the nitrogen injection as far as possible upstream of the test section, and improving the vaporization process at injection.

Exactly as in T'2, the injection in T2 will be performed just after the driving air injector corner, in the chamber where the mixing between driving and driven flows in carried out.

A peripherical liquid nitrogen injection has been chosen. It is performed along two circle lines along which are distributed 16 spray nozzles supplied separately with liquid nitrogen (Figure 7).

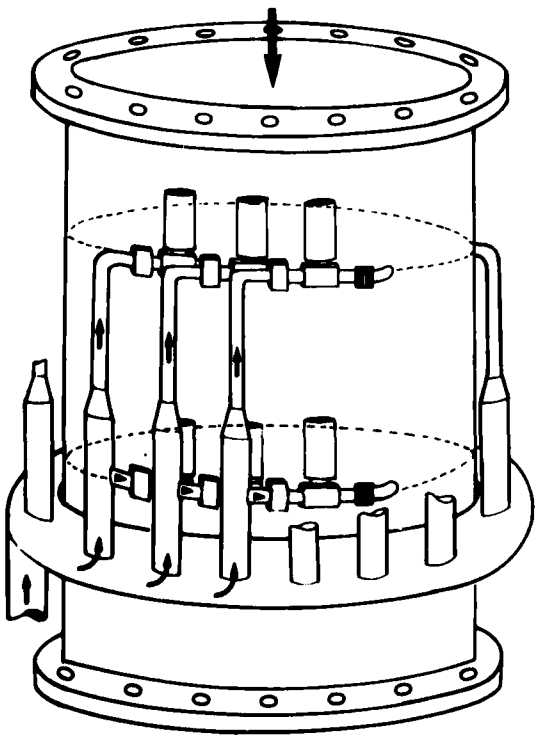

FIG. 7 : Pheripherical LN2 Injection Device.

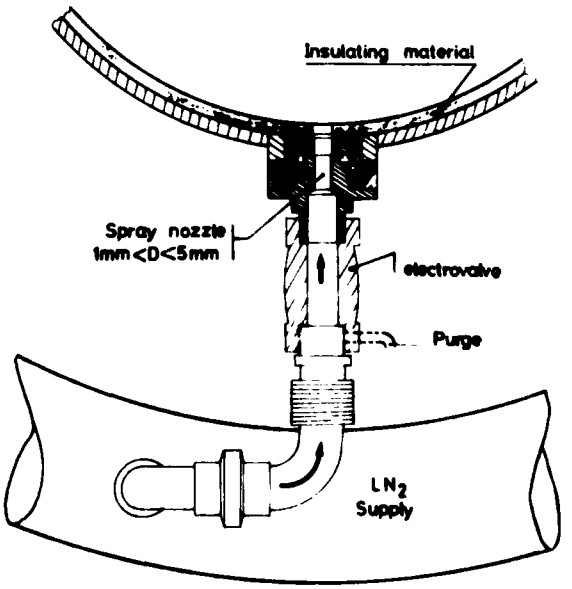

FIG. 8 : Injector Element.

Each of them can be open or closed by its own electrovalve and they have different diameters giving individual progressive mass flow rates. This permits to establish the laws to be chosen for the total nitrogen mass flow, for conveniently regulating the flow temperature during the run. The resolution is 1/1000 of the total nitrogen mass flow rate, this one being of 10 to 20 kg/second.

The whole system is isolated thermally from the external medium by means of an envelop surrounding the circuit component and filled with insulating balls.

Some details about each injector element are shown on figure 8.

For limiting the thermal losses, the internal wall of the nitrogen injection chamber will be coated with some adequate thermal insulating material. An insulating ring also separates the spray nozzle from the metallic shell.

Each individual electrovalve has its own purging pipe, permitting the injection device to be cooled up to here before the run ; the remaining metallic spray nozzle has a sufficiently small mass to be rapidly cooled by conduction at the beginning of the run.

Finally there is a flexible coupling connecting each injector with the nitrogen supply pipe.

Spray nozzles will have flat or axisymmetric jets, with a diameter of 1 to 5 millimeters.

A schematic diagram of the system which supplies the injectors with liquid nitrogen is shown in figure 9.

The storage tank is predicted to have a 20 m3 volume. It supplies a run tank with a 2 m3 volume, largely sufficient for two runs at maximum nitrogen consumption : the run tank is pressurised up to 18 bars, using gaseous nitrogen.

The injection is accomplished, as said previously, through 32 spray nozzles, each of one being controled by its own electrovalve.

The pipe between run tank and injectors has a 15 cm diameter, giving a low pressure loss. A flowmeter is located just after a safety valve permitting to stop the nitrogen supply. A pressure drop valve could be used in addition to the injectors electrovalves, for the nitrogen mass flow regulation.

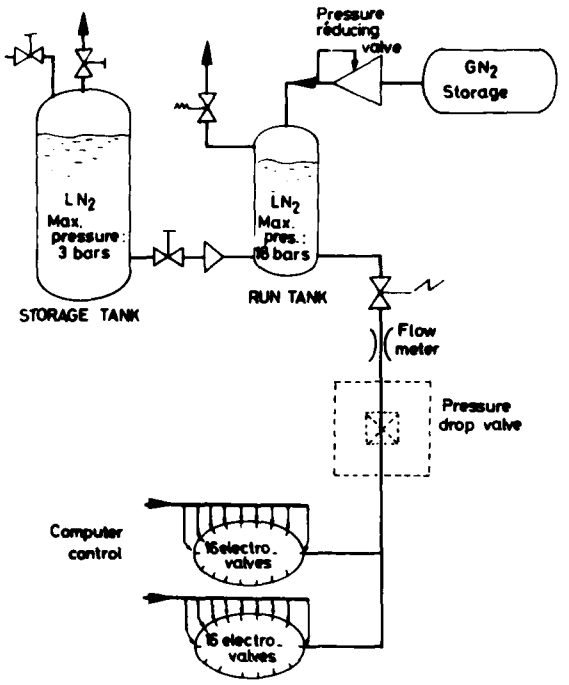

FIG. 9 : Liquid Nitrogen Supply System.

3.3. Exhaust System - Regulation Diagram

Figure 10 gives a sketch of the first diffuser, which is the component through which is exhausted a fluid quantity corresponding to the injected driving air and liquid nitrogen, and which is located just after the test section, between the second throat and the injector corner.

The exhaust is performed through porous bronze walls, of which the porosity has been chosen notably to avoid recirculation from the plenum chamber.

There are four exhaust pipes (30 cm diameter) gathered in a collector pipe, before separating the flow in two parts :

- A pipe taking the most important part of the mass flow : 3/4 of the total exhausted mass flow when its pre-positioning valve is completely open.
- A regulating pipe with a system of eight electrovalves giving a series of different and modulated mass flow rates and allowing to regulate the exhausted mass flow as function of the wanted flow conditions, mainly the test pressure.

Finally, a synthetic diagram summarizing the various regulation components which are involved in the tunnel control is shown in figure 11.

The three flow parameters are the Mach number and the total pressure and temperature.

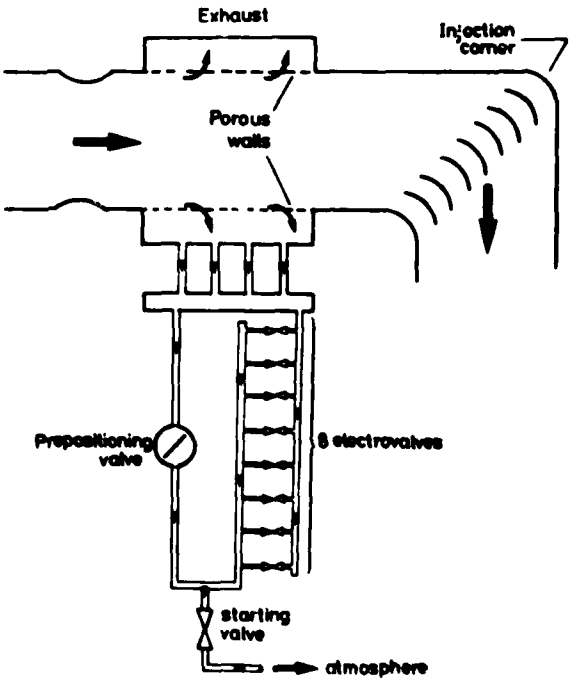

FIG. 10 : Exhaust System.

The Mach number is defined by the second throat area.

The total pressure and temperature have to be established at the wanted values and kept constant during the run by the control system.

The control system comprises three main components :

- The driving gas injection control, involving the pressure reducer which insures a regulated constant pressure by using a laminating concept for generating only a low noise level. This pressure reducer is followed by the multi vanes system which distributes the mass flow through the various corner vanes trailing edge nozzles.
- The liquid nitrogen control, involving adjustment of the run tank pressure and regulation of the nitrogen mass flow rate using the various spray nozzles electrovalves.

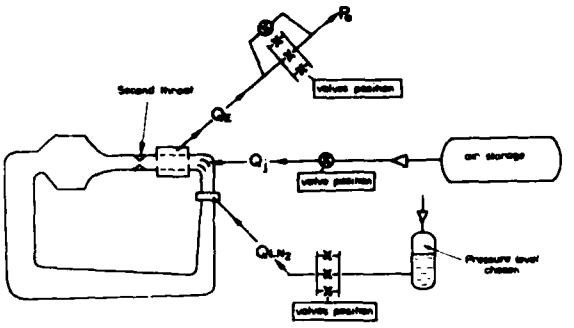

FIG. 11 : Tunnel Control Diagram.

- The exhausted flow control, with the main valve pre-positioning and the control of the regulating by-pass flow by the series of eight electrovalves.

3.4. Possible Operating Modes

It has been shown in paper 13[1], that the theoretical methods we developped for flow establishment calculations, could be controled very reasonably by the experiments carried out in the T'2 pilot unit. This gave us a very useful tool for predicting and optimizing the cryogenic operating mode to be hold for T2.

Figure 12 a represents the results of flow establishment calculations which correspond to a case in which : the driving gas injection mass flow Q_j being assumed to be established at its nominal value, the cooling is insured by a very fast liquid nitrogen process.

The dotted lines correspond to a nitrogen mass flow established instantaneously to its nominal value. We remember that this led in T'2 to an establishment of flow temperature in 6 to 8 seconds. As this establishment time is essentially proportional to the circuit length, we would have in T2 a much too long time, 20 to 25 seconds.

The solution for decreasing the temperature establishment time can be to have a liquid nitrogen mass flow overshoot at the beginning of the run. The calculation represented by the full lines in figure 12a, shows that it seems possible effectively to establish the flow temperature in not more than 8 to 10 seconds in T2, with a moderate and acceptable nitrogen over-flow.

A second type of operating which can be considered, consists in starting the run with a much lower flow Mach number, that is to say with a driving gas mass flow having at first a low value (Figure 12b).

The temperature is decreased by injecting at the same time a liquid nitrogen mass flow which cools the flow appreciably. Finally the driving gas and nitrogen flow rates are increased simultaneously and the flow establishes at the wanted pressure and Mach number.

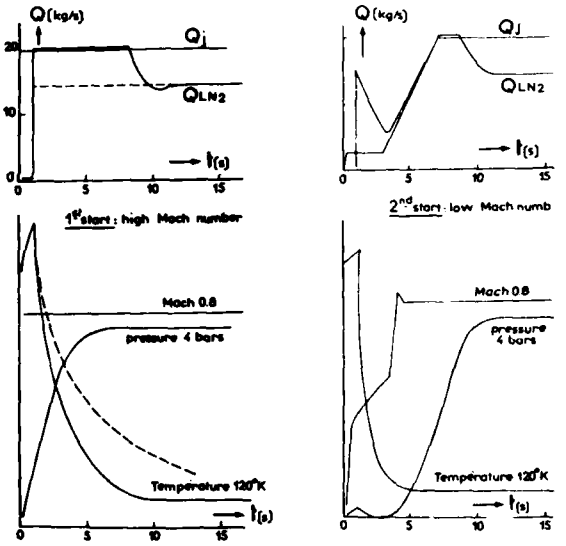

FIG. 12 : Possible Operating Modes.

This second type of operating may offer the advantage of involving a somewhat lower nitrogen consumption. Its main interest is to establish the temperature rapidly, while the other characteristics, especially the flow pressure, are established in a more progressive way.

3.5. Expected Performances and Corresponding Consumptions

The last two figures show the operating envelope extension that brings the T2 cryogenic adaptation, and the price which has to be paid for this extension.

It has been said that two-dimensional airfoils having a 10 cm chord are studied currently in T2 test section, thanks to its equipment with self-adaptive walls.

It does not seem that major problems will be encountered for also using self-adaptive walls at low flow temperatures ; the Reynolds number based on a 10 cm length is given in figure 13, as function of Mach number and stagnation pressure, at ambient operating and at 120°K.

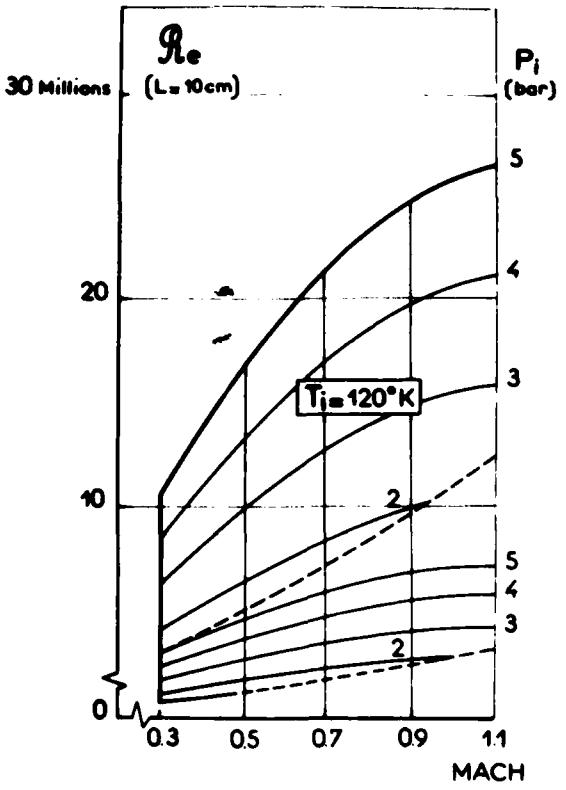

FIG. 13 : Operating Envelope.

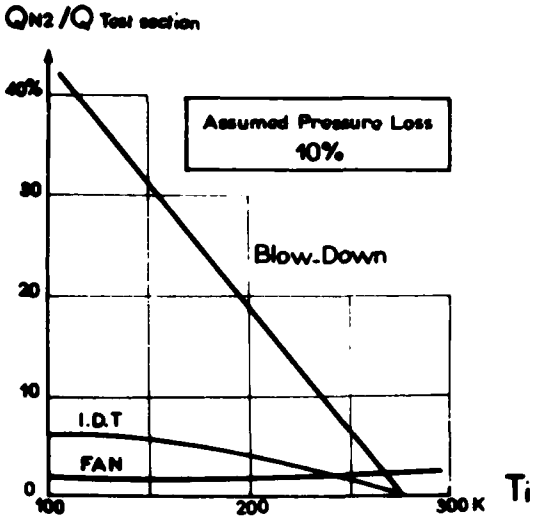

FIG. 14 : Compared Nitrogen Consumptions.

We could obtain in the transonic flow range a Reynolds number varying from 2 to more than 20 millions, an interesting performance for a wind tunnel which is yet a small facility.

The price to be paid is concerned mainly with the nitrogen consumption.

Taking for example the conditions :

Mach number 0.8 - total pressure 4 bars - total temperature 120°K, we reckon the nitrogen consumption to be about 15 kg/s in established flow (300 kg for 20 seconds) plus 20 kg/s during a 8 seconds flow establishment, which can give an overall consumption of 500 kg per run within the previously stated conditions.

Finally we compare in figure 14 the nitrogen consumption of the cryogenic induction driven tunnel, with the direct blow-down tunnel and with the continuous flow fan driven tunnel.

The conclusion is that the cryogenic induction driven tunnel stays in an honourable position between these two other solutions.

REFERENCES

1. Michel R. *The Development of a Cryogenic Wind Tunnel Driven by Induction : Flow Control and Instrumentation Studies in a Pilot Facility at ONERA/CERT.*
AGARD LECTURE SERIES, n° 111, CRYOGENIC WIND TUNNELS, May, June 1980, Paper 13.

AGARD is indebted to the US National Aeronautics and Space Administration for permission to reproduce this bibliography, previously published as NASA Technical Memorandum 80168.

Cryogenic Wind Tunnels - A Selected, Annotated Bibliography

Marie H. Tuttle and Robert A. Kilgore
Langley Research Center
Hampton, Virginia

National Aeronautics
and Space Administration

Scientific and Technical Information Branch

1979

INTRODUCTION

For the purpose of this bibliography, a cryogenic wind tunnel is defined as one which operates with test gas stagnation temperatures below 150 K. The intent is to list publications that might be useful to persons interested in building or using a cryogenic wind tunnel. Also included are some publications of historical interest that are directly related to key events in the evolution of the cryogenic wind tunnel. The arrangement is chronological by date of publication.

Considerable effort has been made to include the relevant literature. Some relevant papers have not been included due to the fact that they are not generally available. It is hoped that these papers will eventually be published in the open literature where their contribution will be available to all.

As is the case in any rapidly growing field, omissions will occur due to oversight. It is hoped that omissions of this type will be called to the attention of the compilers so that subsequent updated versions may be more nearly complete and, therefore, more useful.

There are several books, papers, and bibliographies that, although not dealing directly with cryogenic wind tunnels, have been found to be useful sources of information. These items have been added to the end of this bibliography as citations 118 through 124.

An author index is included at the back of this paper.

In many cases, abstracts used are from the NASA announcement bulletins "Scientific and Technical Aerospace Reports" (STAR) and "International Aerospace Abstracts" (IAA). In other cases, authors' abstracts were used. License was taken to modify or shorten abstracts, using only parts pertinent to the subject of the bibliography. If a paper has appeared in several forms, mention is made of this fact. Accession numbers, report numbers, and other identifying information are included in the citations in order to facilitate the filling of requests for specific items.

When requesting material from your library or other source, it is advisable to include the complete citation, omitting the abstract.

Availability sources of the different types of materials are given below:

Acquisition Number	Type of Material	Source
A xx-xxxxx	Published literature available from AIAA or in journals or conference, etc., as indicated.	American Institute of Aeronautics and Astronautics Technical Information Service 750 Third Avenue New York, NY 10017
B xx-xxxxx	Tech Briefs (NASA)	National Technical Information Service 5285 Port Royal Road Springfield, VA 22161
N xx-xxxxx	Report literature available from NTIS as shown in the citation.	National Technical Information Service 5285 Port Royal Road Springfield, VA 22161
Otherwise	Available from NASA, STIF.	NASA Scientific and Technical Information Facility P.O. Box 8757 B.W.I. Airport, MD 21240

A "#" after an acquisition number (A xx-xxxxx or N xx-xxxxx) indicates that the document is also available in microfiche form.

BIBLIOGRAPHY

1 *Margoulis, W.: Nouvelle Méthode d'essai de Modèles en Soufflerie Aerodynamiques. **(A New Method of Testing Models in Wind Tunnels.)** Comptes Rendus Acad. Sci. Vol. 171, 1920, pp. S997-999, Séance du 22 Nov. 1920.

This is a 2½ page short version (abstract), in French, of NACA TN-52. This was presented for W. Margoulis by M. L. Lecornu.

*NACA, Paris Office

2 *Margoulis, W.: **A New Method of Testing Models in Wind Tunnels.** NACA-TN-52, Aug. 1921.

This paper discusses the use of gases other than air and the use of non-ambient temperatures and pressures as ways of increasing test Reynolds number and reducing capital cost and drive power requirements for low speed wind tunnels. The use of carbonic acid gas (CO_2) is examined in detail.

*NACA, Paris Office

3 Smelt, R.: **Power Economy in High-Speed Wind Tunnels by Choice of Working Fluid and Temperature.** British R.A.E. Rep. no. Aero 2081, Aug. 1945.

The power required to operate a high-speed wind tunnel at fixed Mach number, Reynolds number, and pressure can be greatly reduced if instead of air at normal temperatures, other fluids or low temperatures are employed. If operation at normal temperatures is desired, best power economy is obtained by using certain fluorine compounds of high molecular weight. The value of γ for all these substances is low – about 1.15, compared with 1.4 for air. No substance is known which will permit substantial power reduction at normal temperature with $\gamma = 1.4$. If $\gamma = 1.4$ is essential – nothing definite can be said on this point – then power economy is best achieved by refrigeration. This is permissible down to a definite limiting temperature. For air the limit is 126° R, and the power there is only 7% of that at normal temperature. Use of nitrogen permits an operating temperature of 108° R, and the power required is 3.8% of that for air at normal temperatures.

4 Pankhurst, R. C.; and Holder, D. W.: **Power Economy by Reduction of Stagnation Temperature.** Wind Tunnel Technique, Sir Isaac Pitman and Sons, Ltd., London., 1952, pp. 45–47.

The advantages with respect to power economy of a reduction in stagnation temperature are noted. "Since refrigeration does not involve an increase in the stresses in the model, nor a departure from the conditions of dynamic similarity, it might appear to be a promising method of power economy. The practical difficulties involved would be considerable."

5 *Fowler, H. S.; and *Rush, C. K.: **Centrifugal Compressors–A Brief History and a Description of Some Current Research.** Quarterly Bulletin of the Division of Mechanical Engineering, National Research Council of Canada, Oct.–Dec., 1962, pp. 35–54. Also, Canadian Aeronautics and Space Journal, Jan. 1964, pp. 7–12. (N63-13998).

A brief account of the historical development of the centrifugal compressor shows a continued improvement until a peak was reached about 1955. After some years of neglect, interest is now reawakening in this field. Following a very short review of some aspects of compressor theory, two novel experimental approaches to the investigation of flow and efficiency in the compressor are described. The test rigs being used in these investigations in the Mechanical Engineering Division of NRC are illustrated. One of these rigs, the heat exchanger of which is cooled with liquid nitrogen, is of especial interest.

*National Research Council of Canada, Ottawa.

6 *Rush, C. K.: **A Low Temperature Centrifugal Compressor Test Rig** (Mechanical Engineering Report). National Research Council of Canada Rep. MD-48, NRC-7776, Nov. 1963. 57 pp. (N64-25199).

An examination of the requirements for dynamic similarity in centrifugal compressors demonstrates the possible advantages of using air at temperatures down to 100 K. A test rig capable of operating at low temperature is described. Test results for inlet conditions, ranging from room temperature to 125 K are presented. The predicted advantages of operating at low temperature are confirmed. However, the desired result that the performance should be identical at four different conditions of dynamic similarity was not achieved, although the differences are relatively small. Further examination of the results suggests that the differences are due to changes in geometry with changes in the test rig internal pressure.

*National Research Council of Canada, Ottawa

7 *Goodyer, M. J.; and **Kilgore, R. A.: **The High Reynolds Number Cryogenic Wind Tunnel.** AIAA paper 72-995, 7th Aerodynamic Testing Conference, Palo Alto, Calif., Sept. 13–15, 1972. Also, AIAA Journal, vol. 11, no. 5, May 1973, pp. 613–619. (A72-41581#).

Theoretical considerations indicate that cooling the wind-tunnel test gas to cryogenic temperatures will provide a large increase in test Reynolds number with no increase in dynamic pressure while reducing the tunnel drive-power requirements. Studies have been made to determine the expected variations of Reynolds number and other parameters over wide ranges of Mach number, pressure, and temperature with due regard to avoiding liquefaction and adverse real-gas effects. Practical operational procedures have been developed in a low-speed prototype cryogenic wind tunnel. Aerodynamic experiments in the facility have demonstrated the theoretically predicted variations in Reynolds number and drive power. Force and moment measurements on a wing model mounted on a water-jacketed strain-gage sting balance have demonstrated the feasibility of operation of such balances in a cryogenic environment.

*Univ. of Southampton, England
**NASA, Langley

8 *Jacobsen, R. T.; *Stewart, R. B.; *McCarty, R. D.; and *Hanley, H. J. M.: **Thermophysical Properties of Nitrogen**

from the Fusion Line to 3500 R (1944 K) for Pressures to 150,000 psia (10342 X 10^5 N/m^2). National Bureau of Standards, NBS TN-648, Dec. 1973. 162 pp. (N74-17637#. Contract NASA-MSC-T-1813A. (Available from U.S. Government Printing Office, Washington, D.C. 20402. Catalog #C13.46:648).

Tables of thermophysical properties of nitrogen are presented for temperatures from the fusion line to 3500 R for pressures to 3000 psia, and from the fusion line to 1500 R for pressures above 3000 psia to 150,000 psia. The tables include values of entropy, enthalpy, internal energy, density, specific volume, velocity of sound, specific heats (C_v and C_p), thermal conductivity, viscosity, thermal diffusivity, Prandtl number, and the dielectric constant for selected isobars. Additional tables are included for values of: $(\partial P/\partial V)_T$, $(\partial P/\partial T)_\rho$, $V(\partial H/\partial V)_\rho$, $(\partial P/\partial U)_v$, $V(\partial P/\partial V)_T$, and $(\partial V/\partial T)_\rho$, which have special utility in heat transfer calculations. Tables of selected isobars for the liquid and vapor phases, and for the saturated vapor and saturated liquid are included. An equation of state is presented for liquid and gaseous nitrogen for the temperature and pressure ranges of these tables. In the determination of the equation of state, all of the P-ρ-T (pressure-density-temperature) data available from the published literature were reviewed, and appropriate corrections made to bring experimental temperatures into accord with the International Practical Temperature Scale of 1968. The coefficients of the equation of state were determined by a weighted least squares fit to selected P-ρ-T data and simultaneously to C_v data determined by corresponding states analysis from oxygen data, and to data which defined the phase equilibrium criteria for the saturated liquid and saturated vapor. A vapor pressure equation, melting curve equation, and an equation to represent the ideal gas heat capacity of nitrogen are also presented. The equation of state is estimated to be accurate to within 0.5 percent in the liquid region, to within 0.1 percent for supercritical isotherms up to 15,000 psia, and to within 0.3 percent from 15,000 to 150,000 psia. The vapor pressure equation is accurate to within ±0.01 K between the triple point and the critical point.

*Nat. Bur. Stds., Boulder Labs., Boulder, Colorado 80302

9 *Kilgore, R. A.; *Adcock, J. B.; and *Ray, E. J.: **Flight Simulation Characteristics of the Langley High Reynolds Number Cryogenic Transonic Tunnel.** AIAA paper 74-80, 12th Aerospace Sciences Meeting, Washington, D.C., Jan. 30–Feb. 1, 1974. 9 pp. (A74-20761#).

The characteristics of the Langley 34 cm (13.5 in.) pilot cryogenic transonic pressure tunnel are described, and the results of initial tunnel operation are presented. Tests of a two-dimensional airfoil at a Mach number of 0.85 show identical pressure distributions for a chord Reynolds number of 8,600,000 obtained first at a stagnation pressure of 4.91 atmospheres at a stagnation temperature of +120° F and then at a stagnation pressure of 1.19 atmospheres at a stagnation temperature of -250° F

*NASA Langley

10 *Kilgore, Robert Ashworth **The Cryogenic Wind Tunnel for High Reynolds Number Testing.** Southampton Univ., U.K., Ph.D, Thesis. Feb. 1974. NASA TM X-70207. 230 pp. (N74-27722#, Available NTIS).

Experiments performed at the NASA Langley Research Center in a cryogenic low-speed continuous-flow tunnel and in a cryogenic transonic continuous-flow pressure tunnel have demonstrated the predicted changes in Reynolds number, drive power, and fan speed with temperature, while operating with nitrogen as the test gas. The experiments have also demonstrated that cooling to cryogenic temperatures by spraying liquid nitrogen directly into the tunnel circuit is practical and that tunnel temperature can be controlled within very close limits. Whereas most types of wind tunnels could operate with advantage at cryogenic temperatures, the continuous-flow fan-driven tunnel is particularly well suited to take full advantage of operating at these temperatures. A continuous-flow fan-driven cryogenic tunnel to satisfy current requirements for test Reynolds number can be constructed and operated using existing techniques. Both capital and operating costs appear acceptable.

*NASA, Langley

11 *Wilson, John F.; *Ware, George D.; and *Ramsey, James W., Jr.: **Pilot Cryo Tunnel: Attachments, Seals, and Insulation.** Presented at the ASCE National Structural Meeting, Cincinnati, Ohio, April 22–26, 1974. (Available STIF).

This paper describes tests performed in evaluation of flange attachments, seals, and the structural support insulation for a pilot cryogenic wind tunnel. The overall dimensions of the pilot tunnel are 9.9 meters long, 3.7 meters high, and 1.2 meters maximum diameter, with a 0.34 meter octagonal test section, and a 12/1 contraction ratio. The fan-driven closed circuit tunnel at NASA Langley Research Center was designed for operation at cryogenic nitrogen temperature and required knowledge of material behavior and performance in addition to that available from the literature. The design conditions for the tunnel are pressures up to 5 atmospheres (507 kPa) and temperatures from 78 K (-320° F) to 322 K (+120° F). The cold temperature, in conjunction with the pressure, required tests and studies in the following areas: Compatible bolting, adequate sealing, and effective insulating materials.

*NASA, Langley

12 *Ray, Edward J.; *Kilgore, Robert A.; *Adcock, Jerry B.; and *Davenport, Edwin E.: **Test Results From the Langley High Reynolds Number Cryogenic Transonic Tunnel.** AIAA paper 74-631, 8th Aerodynamic Testing Conference, Bethesda, Md., July 8–10, 1974. Also, Journal of Aircraft, vol. 12, no. 6, June 1975. pp. 539-544. (A74-35395#).

NASA has recently developed and proof tested a pilot cryogenic transonic pressure tunnel. In addition to providing an attractive method for obtaining high Reynolds number results at moderate aerodynamic loadings and tunnel power, this unique facility enables the independent determination of the effects of Reynolds number, Mach number, and aeroelasticity. The proof-of-concept experimental and theoretical studies are briefly reviewed. Experimental results are included which indicate pressure distributions for a

two-dimensional airfoil and strain-gage balance characteristics for a three-dimensional delta wing model.

*NASA, Langley

13 *Polhamus, E. C.; *Kilgore, R. A.; *Adcock, J. B., and *Ray, E. J. **The Langley Cryogenic High Reynolds Number Wind-Tunnel Program.** Astronautics and Aeronautics, vol. 12, no. 10, Oct. 1974, pp. 30-40. (A74-45305#).

A pilot version of a new type of transonic tunnel was placed in operation in the fall of 1973. In the tunnel the cryogenic method is used to obtain a high Reynolds number. The cryogenic concept employs low temperatures to increase the Reynolds number through reducing the viscous forces rather than increasing the inertia forces. The cryogenic approach offers the desired Reynolds-number increase with no increase in dynamic pressure, and therefore no increase in model loads. A series of aerodynamic experiments have been made in the pilot tunnel to confirm the cryogenic concept at transonic speeds. A brief description is given of the project for a large tunnel which has evolved from the investigations.

*NASA, Langley

14 *Kilgore, Robert A.; *Goodyer, Michael J., *Adcock, Jerry B., and *Davenport, Edwin E. **The Cryogenic Wind Tunnel Concept for High Reynolds Number Testing.** NASA-TN-D-7762, Nov. 1974. 96 pp. (N 75-12000#, Available NTIS).

Theoretical considerations indicate that cooling the wind-tunnel test gas to cryogenic temperatures will provide a large increase in Reynolds number with no increase in dynamic pressure while reducing the tunnel drive-power requirements. Studies were made to determine the expected variations of Reynolds number and other parameters over wide ranges of Mach number, pressure, and temperature, with due regard to avoiding liquefaction. Practical operational procedures were developed in a low-speed cryogenic tunnel. Aerodynamic experiments in the facility demonstrated the theoretically predicted variations in Reynolds number and drive power. The continuous-flow-fan-driven tunnel is shown to be particularly well suited to take full advantage of operating at cryogenic temperatures.

*NASA, Langley

15 *Kilgore, Robert A.; *Adcock, Jerry B.; and *Ray, Edward J. **Simulation of Flight Test Conditions in the Langley Pilot Transonic Cryogenic Tunnel.** NASA-TN-D-7811, Dec. 1974. 24 pp. (N75-12001#, Available NTIS).

The theory and advantages of the cryogenic tunnel concept are briefly reviewed. The unique ability to vary temperature independently of pressure and Mach number allows, in addition to large reductions in model loads and tunnel power, the independent determination of Reynolds number, Mach number, and aeroelastic effects on the aerodynamic characteristics of the model. Various combinations of Reynolds number and dynamic pressure are established to represent accurately flight variations of aeroelastic deformation with altitude changes. The consequences of the thermal and caloric imperfections of the test gas under cryogenic conditions were examined and found to be insignificant for operating pressures up to 5 atm. The characteristics of the Langley pilot transonic cryogenic tunnel are described and the results of initial tunnel operation are presented. Tests of a two-dimensional airfoil at a Mach number of 0.85 show identical pressure distributions for a chord Reynolds number of 8,600,000 obtained first at a stagnation pressure of 4.91 atm at a stagnation temperature of 322.0 K and then at a stagnation pressure of 1.19 atm at a stagnation temperature of 116.5 K.

*NASA, Langley

16 *Adcock, Jerry B.; *Kilgore, Robert A., and *Ray, Edward J. **Cryogenic Nitrogen as a Transonic Wind-Tunnel Test Gas.** AIAA Paper 75-143, 13th Aerospace Sciences Meeting, Pasadena, Calif. Jan. 20-22, 1975. 9 pp. (A75-18341#).

The test gas for the Langley Pilot Transonic Cryogenic Tunnel is nitrogen. Results from analytical and experimental studies that have verified cryogenic nitrogen as an acceptable test gas are reviewed. Real-gas isentropic and normal-shock flow solutions for nitrogen are compared to the ideal diatomic gas solutions. Experimental data demonstrate that for temperatures above the liquefaction boundaries there are no significant real-gas effects on two-dimensional airfoil pressure distributions. Results of studies to determine the minimum operating temperatures while avoiding appreciable effects due to liquefaction are included.

*NASA, Langley

17 *Reubush, David E. **The Effect of Reynolds Number on Boattail Drag.** AIAA paper 75-63, 13th Aerospace Sciences Meeting, Pasadena, Calif., Jan. 20-22, 1975. 7 pp. (A75-18286#).

An investigation has been conducted in the Langley pilot transonic cryogenic tunnel to determine the effects of varying Reynolds number on boattail drag at subsonic speeds. Six boattailed cone-cylinder nacelle models were tested with the jet exhaust simulated by a cylindrical sting. Reynolds number was varied from about 2.6 million to 132 million by changing model length and unit Reynolds number. Boattail pressure coefficient distributions show that increasing Reynolds number tends to make the pressure coefficients in the expansion region more negative and the pressure coefficients in the recompression region more positive. These two effects were compensating and as a result there was little or no effect of Reynolds number on the pressure drag of the isolated boattails.

*NASA, Langley

18 *Ray, Edward J., *Kilgore, Robert A., *Adcock, Jerry B., and *Davenport, Edwin E. **Analysis of Validation Tests of the Langley Pilot Transonic Cryogenic Tunnel.** NASA TN D-7828, Feb. 1975. 22 pp. (N75-16569#, Available NTIS).

A pilot transonic cryogenic pressure tunnel has recently been developed and proof tested at the NASA Langley Research Center. In addition to providing an attractive method for obtaining high Reynolds number results at moderate aerodynamic loadings and tunnel power, this unique tunnel allows the independent determination of the

effects of Reynolds number, Mach number, and dynamic pressure (aeroelasticity) on the aerodynamic characteristics of the model under test. The proof of concept experimental and theoretical studies are briefly reviewed. Experimental results obtained on both two- and three-dimensional models have substantiated that cryogenic test conditions can be set accurately and that cryogenic gaseous nitrogen is a valid test medium.

*NASA, Langley

19 *Kilgore, Robert A.; and *Kuhn, R. E.: **Recent Progress on New Facilities at the NASA Langley Research Center.** In AGARD CP-187, "Flight/Ground Testing Facilities Correlation," pp. 2–1 through 2–14. Presented at 46th Meeting of the Flight Mechanics Panel, Valloire, France, 9–13 June, 1975. (N76-25269#, Available NTIS).

A new fan-driven high Reynolds number transonic cryogenic tunnel is being planned for the United States. This tunnel, to be known as the National Transonic Facility, will take full advantage of the cryogenic concept to provide an order of magnitude increase in Reynolds number capability over existing tunnels. Based on theoretical studies and experience with the Langley 0.3-meter Transonic Cryogenic Tunnel, the cryogenic concept has been shown to offer many advantages with respect to the attainment of full-scale Reynolds number at reasonable levels of dynamic pressure in a ground-based facility. The unique modes of operation which are available only in a cryogenic tunnel make possible for the first time the separation of Mach number, Reynolds number, and aeroelastic effects. By reducing the drive power requirements to a level where a conventional fan drive system may be used, the cryogenic concept makes possible a tunnel with high productivity and run times sufficiently long to allow for all types of tests at reduced capital costs and, for equal amounts of testing, reduced total energy consumption in comparison with other tunnel concepts.

*NASA, Langley

20 *Hall, Robert M.: **Preliminary Study of the Minimum Temperatures for Valid Testing in a Cryogenic Wind Tunnel.** NASA-TM-X-72700, Aug. 1975. 125 pp. (N75-28078#, Available NTIS).

The minimum operating temperature which avoids real-gas effects, such as condensation, was determined at a Mach number of 0.85 for a 0.137-meter NACA 0012-64 airfoil mounted in the Langley 0.3-meter transonic cryogenic tunnel. For temperatures within 5 K of reservoir saturation and total pressures from 1.2 to 4.5 atmospheres, the pressure distributions over the airfoil are not altered by real-gas effects. This ability to test at total temperatures below those which avoid saturation over the airfoil allows an increase in Reynolds number capability of at least 17 percent for a constant tunnel total pressure. Similarly, 17 percent less total pressure is required to obtain a given Reynolds number.

*NASA, Langley

21 *Mabey, Dennis G.: **Some Remarks on the Design of Transonic Tunnels With Low Levels of Flow Unsteadiness.** NASA CR-2722, Aug. 1976, 19 pp. (N79-25039#, Available NTIS). (Based on a lecture given at Langley on Sept. 15, 1975.)

Flow unsteadiness in wind tunnels is defined and its importance for aerodynamic measurements outlined. The principal sources of flow unsteadiness in the circuit of a transonic wind tunnel are enumerated. Care must be taken to avoid flow separations, acoustic resonances and large scale turbulence. Some problems discussed are the elimination of diffuser separations, the aerodynamic design of coolers and the unsteadiness generated in ventilated working sections (both slotted and perforated).

*Royal Aircraft Establishment, Bedford, England, Structures Department

22 *Mabey, Dennis G.: **Some Remarks on Dynamic Aeroelastic Model Tests in Cryogenic Wind Tunnels.** Presented at NASA, Langley Research Center, Sept. 1975. NASA-CR-145029. 39 pp. (N76-78044, Available NTIS).

The application of cryogenic wind tunnels to dynamic aeroelastic model tests is the subject of this informal lecture and discussion. Emphasis is placed on buffet testing with a description of two semi-span models that could be tested in the 0.3-m transonic cryogenic tunnel to develop a buffet testing technique suitable for use at cryogenic temperatures.

*Royal Aircraft Establishment, Bedford, England, Structures Department

23 *Reubush, David E. **The Effect of Reynolds Number on the Boattail Drag of Two Wing-Body Configurations.** AIAA paper 75-1294, 11th AIAA and SAE Propulsion Conference, Anaheim, Calif., Sept. 29–Oct. 1, 1975. 8 pp. (A75-45681#).

An investigation has been conducted in the Langley 0.3-meter transonic cryogenic tunnel to determine the effects of varying Reynolds number on the boattail drag of wing-body configurations at subsonic speeds. Two boattailed cone-cylinder nacelle models were tested with a 60-deg delta wing at an angle of attack of 0 deg. Reynolds number, based on model length, was varied from about 2.5 million to 67 million. Even though the presence of the wing had large effects on the boattail pressure coefficients, the results of this investigation were similar to those previously found for a series of isolated boattails. Boattail pressure coefficients in the expansion region became more negative with increasing Reynolds number, while those in the recompression region became more positive. These two effects were compensating, and as a result, there was virtually no effect of Reynolds number on boattail pressure drag.

*NASA, Langley

24 *Hall, Robert M., and *Ray, Edward J.: **Investigation of Minimum Operating Temperatures for Cryogenic Wind Tunnels.** AIAA paper 76-89, 14th Aerospace Sciences Meeting, Wash., D.C., Jan. 26–28, 1976. Also, Journal of Aircraft, vol. 14, no. 6, June, 1977, pp. 560–564. (A76-18781#).

Total temperatures corresponding to the onset of condensation effects were determined for flow over a 0.137-m NACA 0012-64 airfoil mounted in the Langley 0.3-m transonic cryogenic wind tunnel. Tests were carried out at a total pressure range from 1.2 to 4.5 atm and at free-stream Mach numbers of 0.75, 0.85, and 0.95. No

condensation effects were found to occur until total temperatures were below those associated with free-stream saturation. Significant increases in Reynolds number may apparently be obtained by operation at wind tunnel temperatures below those associated with local saturation over the airfoil but above those where effects first occur. For the 0.85 and 0.95 Mach numbers the increase in Reynolds number was at least 15% over those achieved at local saturation conditions for the same pressure range.

*NASA, Langley

25 *Ludwieg, H.; Grauer-Carstensen, H.; and Lorenz-Mayer, W.: **The Ludwieg Tube—A Proposal for a High Reynolds Number Transonic Wind Tunnel.** In AGARD-CP-174, "Wind Tunnel Design and Testing Technology," pp. 3–1 through 3–11. March 1976. (N76-25216#, Available NTIS).

After a brief review of the historical development of the Large European High Reynolds Number Tunnel (LEHRT) and its specifications, the advantages and flexibility of a Ludwieg tube drive system are outlined. Special emphasis is given to the development of the boundary layer in the charge tube and its influence on the flow quality in the test section. The theoretical predictions of boundary layer growth are confirmed by experimental results. An improved prediction method for the turbulence in the test section is given. Means to affect the turbulence in order to meet the LEHRT requirements are outlined. After a short review of the development of cost estimates some options are discussed which promise significant reduction in construction costs without impairing performance. These solutions are the application of prestressed concrete for large parts of the construction, lowering the stagnation temperature by an amount of approximately 50° C, and operation at cryogenic temperatures.

*DFVLR, Goettingen (West Germany). Institute fuer Stroemungsmechanik

26 *Kilgore, Robert A.; *Adcock, Jerry B.; and *Ray, Edward J.: **The Cryogenic Transonic Wind Tunnel for High Reynolds Number Research.** In AGARD-CP-174, "Wind Tunnel Design and Testing Technology," Mar. 1976, pp. 1.1 through 1.20. (N76-25214, Available NTIS).

Based on theoretical studies and experience with a low speed cryogenic tunnel and with a transonic cryogenic tunnel, the cryogenic wind tunnel concept has been shown to offer many advantages with respect to the attainment of full scale Reynolds number at reasonable levels of dynamic pressure in a ground based facility. The unique modes of operation available in a pressurized cryogenic tunnel make possible for the first time the separation of Mach number, Reynolds number, and aeroelastic effects.

*NASA, Langley

27 *Haut, Richard C.; and **Adcock, Jerry B.: **Steady Normal Shock Wave Solution Tables of Parahydrogen for Total Temperatures from 30 K to 290 K and for Total Pressure from 1 Atm. to 10 Atm.** NASA TM X-73899, April 1976, 100 pp. (N76-23518#, Available NTIS).

The steady normal shock wave solutions of parahydrogen at various total pressures and total temperatures were numerically determined by iterating the upstream Mach number and by using a modified interval halving technique. The results obtained are compared with the ideal diatomic gas values and are presented in tabulated form.

*Old Dominion Univ., **NASA, Langley

28 *Haut, Richard C.; and **Adcock, Jerry B.: **Tables of Isentropic Expansions of Parahydrogen and Related Transport Properties for Total Temperatures from 25 K to 300 K and for Total Pressures from 1 Atm. to 10 Atm.** NASA-TM-X-72826, April 1976. 93 pp. (N76-22489#, Available NTIS).

The isentropic expansions of parahydrogen at various total pressures and total temperatures were numerically determined by iterating Mach number and by using a modified interval halving method. The calculated isentropic values and related properties are presented in tabulated form.

*Old Dominion Univ., **NASA, Langley

29 *Reubush, David E.; and *Putnam, Lawrence E.: **An Experimental and Analytical Investigation of Effect on Isolated Boattail Drag of Varying Reynolds Numbers up to 130,000,000.** NASA-TN-D-8210, May 1976. 85 pp. (N76-23171#, Available NTIS).

An investigation was conducted to determine whether large Reynolds number effects occur on isolated boattails. The investigation included an analytical study and tests in the Langley 0.3-meter transonic cryogenic tunnel. This investigation was conducted at an angle of attack of 0° at Mach numbers from 0.6 to 0.9 for Reynolds numbers up to 130×10^6. Results indicate that as the Reynolds number was increased, the boattail static pressure coefficients in the expansion region of the boattail became more negative whereas those in the recompression region became more positive. These two trends were compensating and, as a result, there was only a small effect (if any) of Reynolds number on boattail pressure drag.

*NASA, Langley

30 *McKinney, Linwood W.; and *Howell, Robert R.: **The Characteristics of the Planned National Transonic Facility.** 9th AIAA Aerodynamic Testing Conference, Arlington, Tex., June 7–9, 1976. (A76-38626, pp. 176–184) or (A76-38645#).

The National Transonic Facility is a high Reynolds number transonic wind tunnel designed to satisfy the research and development needs of NASA, DOD, and industry. The facility design incorporates the cryogenic approach to achieving high Reynolds numbers with manageable model loads. By using temperature as a test variable, a unique capability to clearly separate aeroelastic, Reynolds number, and Mach number effects will be possible. This capability will open new horizons in transonic aerodynamic research. The tunnel design including unique features and operating envelopes is described. A brief overview of the general operating arrangement and the schedule for facility construction is presented.

*NASA, Langley

31 *Kilgore, Robert A., and *Davenport, Edwin E. **Static Force Tests of a Sharp Leading Edge Delta-Wing Model at**

Ambient and Cryogenic Temperatures With a Description of the Apparatus Employed. NASA-TM-X-73901, June 1976. 50 pp. (N76-28159#, Available NTIS).

A sharp leading edge delta-wing model was tested through an angle-of-attack range at Mach numbers of 0.75, 0.80, and 0.85 at both ambient and cryogenic temperatures in the Langley 0.3-meter transonic cryogenic tunnel. Total pressure was varied with total temperature in order to hold test Reynolds number constant at a given Mach number. Agreement between the aerodynamic data obtained at ambient and cryogenic temperatures indicates that flows with leading-edge vortex effects are duplicated properly at cryogenic temperatures. The test results demonstrate that accurate aerodynamic data can be obtained by using conventional force-testing techniques if suitable measures are taken to minimize temperature gradients across the balance and to keep the balance at ambient (warm) temperatures during cryogenic operation of the tunnel.

*NASA, Langley

32 *Lambourne, N. C.: **Similarity Requirements for Flutter and Other Aeroelastic Models in a Cryogenic Wind Tunnel.** RAE-TM-Struct-888, June 1976. 13 pp. (N77-19083#, Available, NTIS).

A consideration of the requirements for aeroelastic similarity shows that the low working temperature of a cryogenic tunnel and an ability to vary temperature both have potential advantages in regard to the choice of suitable stiffness and density scales for an aeroelastic model. The advantages are incidental to the main purpose of a cryogenic tunnel, which is to achieve high Reynolds numbers.

*R.A.E. Farnborough, England

33 *Adcock, Jerry B.; and *Ogburn, Marilyn E.: **Power Calculations for Isentropic Compressions of Cryogenic Nitrogen.** NASA-TN-D-8389, Mar. 1977, 15 pp. (Formerly published as NASA-TM-X-73903, July 1976, N76-28516#). NASA-NSG-1010. (N77-20378#, Available NTIS).

A theoretical analysis has been made of the power required for isentropic compressions of cryogenic nitrogen in order to determine the extent that the drive power for cryogenic tunnels might be affected by real gas effects. The analysis covers temperatures from 80 to 310 K, pressures from 1.0 to 8.8 atm and fan pressure ratios from 1.025 to 1.200. The power required to compress cryogenic nitrogen was found to be lower than that required for an ideal diatomic gas by as much as 9.5 percent. Simple corrections to the ideal gas values were found to give accurate estimates of the real gas power values.

*NASA, Langley

34 *Hall, Robert M.: **Cryogenic Wind Tunnels: Unique Capabilities for the Aerodynamicist.** Presented at the 54th Annual Meeting of the Virginia Academy of Science, July 1976. NASA-TM-X-73920, 16 pp. (N76-27252#, Available NTIS).

The cryogenic wind-tunnel concept as a practical means for improving ground simulation of transonic flight conditions. The Langley 0.3-meter transonic cryogenic tunnel is operational, and the design of a cryogenic National Transonic Facility is undertaken. A review of some of the unique capabilities of cryogenic wind tunnels is presented. In particular, the advantages of having independent control of tunnel Mach number, total pressure, and total temperature are highlighted. This separate control over the three tunnel parameters will open new frontiers in Mach number, Reynolds number, aeroelastic, and model-tunnel interaction studies.

*NASA, Langley

35 *Reubush, David E.: **Effect of Reynolds Number on the Subsonic Boattail Drag of Several Wing-Body Configurations.** NASA TN-D-8238, July 1976, 84 pp. (N76-26157#, Available NTIS).

An investigation was conducted in a transonic cryogenic wind tunnel to determine the effect of varying Reynolds number on the boattail drag of several wing-body configurations. This study was made at 0 deg angle of attack at Mach numbers from 0.6 to 0.9 for Reynolds numbers up to 67 million (based on distance from the nose to the start of the boattail). Results indicate that as the Reynolds number was increased the boattail static pressure coefficients in the expansion region of the boattail became more negative while those in the recompression region became more positive. Results show that there was only a small effect of Reynolds number on boattail pressure drag.

*NASA, Langley

36 *Hall, Robert M.: **An Analysis of Data Related to the Minimum Temperatures for Valid Testing in Cryogenic Wind Tunnels Using Nitrogen as the Test Gas.** NASA-TM-X-73924, Aug. 1976, 110 pp. (N76-29269#, Available NTIS).

The minimum operating temperature which avoids adverse low temperature effects, such as condensation, has been determined at a free stream Mach number of 0.85 for flow over a 0.137 meter airfoil mounted at zero incidence in the Langley 0.3-meter transonic cryogenic tunnel. The onset of low temperature effects is established by comparing the pressure coefficient measured at a given orifice for a particular temperature with those measured at temperatures sufficiently above where low temperature effects might be expected to occur. The pressure distributions over the airfoil are presented in tabular form. In addition, the comparisons of the pressure coefficient as a function of total temperature are presented graphically for chord locations of 0, 25, 50, and 75 percent. Over the 1.2 to 4.5 atmosphere total pressure range investigated, low temperature effects are not detected until total temperatures are 2 K, or more, below free stream saturation temperatures.

*NASA, Langley

37 *Reubush, David E. **Experimental Investigation to Validate Use of Cryogenic Temperatures to Achieve High Reynolds Numbers in Boattail Pressure Testing.** NASA-TM-X-3396, Aug. 1976, 35 pp. (N76-30228#, Available NTIS).

An investigation has been conducted in the Langley 0.3-meter transonic cryogenic tunnel to validate the use of

cryogenic temperatures to achieve high Reynolds numbers in nozzle boattail pressure testing. Tests were conducted at 0 degree angle of attack and at Mach numbers of 0.60, 0.85, and 0.90 on two wing-body configurations with differing boattail geometries. Test data were obtained by using two different techniques, the cryogenic method and the conventional method, to obtain the same Reynolds number. Later, the test data obtained from the two techniques on boattail pressure coefficient distributions and pressure drag coefficients were compared; results from the comparisons show excellent repeatability for all test conditions and indicate no measurable errors when using cryogenic temperatures to achieve high Reynolds numbers for nozzle boattail pressure testing.

*NASA, Langley

38 Goethert, Bernhard H.. **Technical Evaluation Report on the Fluid Dynamics Panel Symposium on Wind Tunnel Design and Testing Techniques.** AGARD-AR-97, Aug. 1976, 23 pp. (N76-30236#, Available NTIS).

Advanced wind tunnel systems are discussed with emphasis on the impact of the cryogenic concept for high performance transonic wind tunnels. Topics covered include: cryogenic operation, adjustable walls, magnetic suspensions, and laser instrumentation.

39 *Haut, Richard C.; and **Adcock, Jerry B.. **Prandtl-Meyer Flow Tables for Parahydrogen at Total Temperatures from 30 K to 290 K and for Nitrogen at Total Temperatures from 100 K to 300 K at Total Pressures from 1 Atm. to 10 Atm.** NASA-TM-X-73932, Aug. 1976, 194 pp. (N76-30497#, Available NTIS).

The dependency of Mach number on the Prandtl-Meyer function was numerically determined by iterating the Prandtl-Meyer function and applying the Muller method to converge on the Mach number for flows in cryogenic parahydrogen and nitrogen at various total pressures and total temperatures. The results are compared with the ideal diatomic gas values and are presented in tabular form.

*Old Dominion Univ., **NASA, Langley

40 *Howell, Robert R., and *McKinney, Linwood W.. **The U.S. 2.5-Meter Cryogenic High Reynolds Number Tunnel.** ICAS paper 76-04, 10th ICAS Congress, Ottawa, Canada, Oct. 3–8, 1976. 12 pp. (A76-47353#).

The U.S. 2.5-Meter Cryogenic High Reynolds Number Tunnel is a fan-driven transonic wind tunnel scheduled for operation in 1981. It will operate at Mach numbers from 0.1 to 1.2, stagnation pressures from 1 to 9 bars, and stagnation temperatures from 352 to 80 Kelvin. The maximum Reynolds number capability will be 120 million at a Mach number of 1.0 based on a reference length of 0.25 meter. This paper describes the basis for the conceptual approach, the engineering design including unique features, and the performance operating envelopes for the tunnel.

*NASA, Langley

41 *Nicks, Oran W.. **The NTF As a National Facility.** In "High Reynolds Number Research," a workshop held at NASA, Langley, Oct. 27–28, 1976. N77-27139, pp. 19–51. (N77-27141#, Available NTIS).

Activities which led to the definition of the National Transonic Facility and the general agreements reached regarding its use and operations are reviewed. Topics discussed include: redefinition of test requirements, development of low cost options, consideration of a single transonic facility using existing hardware if feasible, facility concept recommendations, and acquisition schedule proposals.

*NASA, Langley

42 *Kilgore, Robert A.: **Cryogenic Wind-Tunnel Technology.** In "High Reynolds Number Research," a workshop held at NASA, Langley, Oct. 27–28, 1976. N77-27139, pp. 53–63. (N77-27142#, Available NTIS).

The cryogenic concept and the advantages it offers with respect to achieving full scale Reynolds number in a moderate size tunnel at reasonable levels of dynamic pressure are described. Aspects which must be considered during the development of a facility that uses cryogenic gaseous nitrogen as the test gases are examined. These include the properties of nitrogen, particularly at high pressure, isentropic expansion and normal shock flows in nitrogen, real gas ratios; and the problem of condensation. Sources of information on cryogenic technology are cited.

*NASA, Langley

43 *Gillespie, Vernon P.. **The Design of Models for Cryogenic Wind Tunnels.** In "High Reynolds Number Research," a workshop held at NASA, Langley, Oct. 27–28, 1976. N77-27139, pp. 73–79. (N77-27144#, Available NTIS).

Factors to be considered in the design and fabrication of models for transonic cryogenic wind tunnels operating at high pressures include high model loads imposed by the high operating pressures, the mechanical and thermodynamic properties of materials in low temperature environments, and the combination of aerodynamic loads with the thermal environment. Candidate materials are being investigated to establish criteria for cryogenic wind tunnel models and their installation. Data acquired from these tests will be provided to users of the National Transonic Facility.

*NASA, Langley

44 *Guarino, Joseph F.. **Instrumentation and Data Acquisition Systems.** In "High Reynolds Number Research," a workshop held at NASA, Langley, Oct. 27–28, 1976. N77-27139, pp. 81–101. (N77-27145#, Available NTIS).

A comprehensive and integrated measurement system was identified and a design and development effort initiated to meet the criteria imposed by the National Transonic Facility operating environment. Specific measurement areas receiving concentrated attention include: data acquisition, force measurement, pressure instrumentation, flow visualization techniques, model attitude and model deformation measurement, and temperature measurement. The NTF instrument complex will be centered around four 32-bit, 1-microsecond-cycle-time central processing units connected in a multipoint-distributed network configuration. The

principal activities to be supported by these computers are (1) data base management and processing; (2) research measurement data acquisition and display; (3) tunnel and model control; and (4) process monitoring and communication control. The distributed network approach was chosen to modularize the functional software into definable and implementable parts by the various groups involved in the design and to permit use of similar hardware configurations to improve reliability and maintainability.

*NASA, Langley

45 *Kilgore, Robert A.: **The Cryogenic Wind Tunnel.** In NASA-CP-2001, Advances in Engineering Science, Vol. 4, 1976, pp. 1565–1581. Presented at the 13th Annual Meeting of the Society of Engineering Science, Hampton, Va., Nov. 1–3, 1976. (N77-10368#, Available NTIS).

Based on theoretical studies and experience with a low speed cryogenic tunnel and with a 0.3-meter transonic cryogenic tunnel, the cryogenic wind tunnel concept is shown to offer many advantages with respect to the attainment of full scale Reynolds number at reasonable levels of dynamic pressure in a ground based facility. The unique modes of operation available in a pressurized cryogenic tunnel make possible for the first time the separation of Mach number, Reynolds number, and aeroelastic effects. By reducing the drive-power requirements to a level where a conventional fan drive system may be used, the cryogenic concept makes possible a tunnel with high productivity and run times sufficiently long to allow for all types of tests at reduced capital costs and, for equal amounts of testing, reduced total energy consumption in comparison with other tunnel concepts.

*NASA, Langley

46 *Baals, Donald D.: **Design Considerations of the National Transonic Facility.** In NASA-CP-2001, Advances in Engineering Science, vol. 4, 1976, pp. 1583–1602. Presented at the 13th Annual Meeting of the Society of Engineering Science, Hampton, Va., Nov. 1–3, 1976. (N77-10369#, Available NTIS).

The inability of existing wind tunnels to provide aerodynamic test data at transonic speeds and flight Reynolds numbers is examined. The proposed transonic facility is a high Reynolds number transonic wind tunnel designed to meet the research and development needs of industry, and the scientific community. The facility employs the cryogenic approach to achieve high transonic Reynolds numbers at acceptable model loads and tunnel power. By using temperature as a test variable, a unique capability to separate scale effects from model aeroelastic effects is provided. The performance envelope of the facility is shown to provide a ten fold increase in transonic Reynolds number capability compared to currently available facilities.

*George Washington Univ.

47 *Kilgore, Robert A.: **Design Features and Operational Characteristics of the Langley 0.3-Meter Transonic Cryogenic Tunnel.** NASA-TN-D-8304, Dec. 1976, 51 pp. (This document was previously published as NASA-TM-X-72012, 1974.) (N77-12071#, Available NTIS).

Experience with the Langley 0.3-meter transonic cryogenic tunnel, which is fan driven, indicated that such a tunnel presents no unusual design difficulties and is simple to operate. Purging, cooldown, and warmup times were acceptable and were predicted with good accuracy. Cooling with liquid nitrogen was practical over a wide range of operating conditions at power levels required for transonic testing, and good temperature distributions were obtained by using a simple liquid nitrogen injection system. To take full advantage of the unique Reynolds number capabilities of the 0.3-meter transonic tunnel, it was designed to accommodate test sections other than the original, octagonal, three dimensional test section. A 20- by 60-cm two dimensional test section was recently installed and is being calibrated. A two dimensional test section with self-streamlining walls and a test section incorporating a magnetic suspension and balance system are being considered.

*NASA, Langley

48 *Stallings, R. L., Jr., and *Lamb, M.: **A Simplified Method for Calculating Temperature Time Histories in Cryogenic Wind Tunnels.** NASA-TM-X-73949, Dec. 1976, 16 pp. (N77-13076#, Available NTIS).

Average temperature time history calculations of the test media and tunnel walls for cryogenic wind tunnels have been developed. Results are in general agreement with limited preliminary experimental measurements obtained in a 13.5-inch pilot cryogenic wind tunnel.

*NASA, Langley

49 *Adcock, Jerry B.: **Real-gas Effects Associated With One-Dimensional Transonic Flow of Cryogenic Nitrogen.** NASA-TN-D-8274, Dec. 1976. 272 pp. (N77-15345#, Available NTIS).

Real gas solutions for one-dimensional isentropic and normal-shock flows of nitrogen were obtained for a wide range of temperatures and pressures. These calculations are compared to ideal gas solutions and are presented in tables. For temperatures (300 K and below) and pressures (1 to 10 atm) that cover those anticipated for transonic cryogenic tunnels, the solutions are analyzed to obtain indications of the magnitude of inviscid flow simulation errors. For these ranges, the maximum deviation of the various isentropic and normal shock parameters from the ideal values is about 1 percent or less, which, for most wind tunnel investigations, would be insignificant.

*NASA, Langley

50 *Wagner, Bernhard, and *Schmidt, Wolfgang: **Theoretical Investigations of Real Gas Effects in Cryogenic Wind Tunnels, Final Report.** DS-FB-76/508, Dec. 1976, 82 pp. (N79-17820#, Available NTIS).

Real gas effects in cryogenic nitrogen flows were calculated using the Beattie-Bridgeman equation of state. The investigations include Prandtl-Meyer expansions, oblique shocks, transonic small perturbation theory, transonic flow past a NACA 0012 aerofoil and shock boundary layer interaction. The two last cases mentioned were treated with the aid of finite volume techniques.

*Dornier-System G.m.b.H., Friedrichshafen, West Germany Theoretical Aerodynamics Group

51 *Hartzuiker, J. P. **The Proposed Cryogenic European Transonic Wind Tunnel /ETW/.** Nederlandse Vereniging voor Luchtvaartechneik, Yearbook 1977, 1978, pp. 1.1–1.21. Based on a lecture presented to the Netherlands Association of Aeronautical Engineers, Jan. 20, 1977. (A79-17118#).

The proposed European Transonic Wind Tunnel is described: a cryogenic facility with test-section dimensions compatible with existing major European transonic facilities. Reynolds number based on mean aerodynamic chord lies between 25 million and 40 million. The advantages and drawbacks of cryogenic testing, as well as fundamental aspects of cryogenic aerodynamics, are discussed. Comparative estimates for capital and operating costs are presented.

*National Aerospace Laboratory, NLR

52 *Kilgore, Robert A., and *Adcock, Jerry, B. **Specific Cooling Capacity of Liquid Nitrogen.** NASA TM-X-74015, Feb. 1977, 19 pp. (N77-21261#, Available NTIS).

When cryogenic nitrogen wind tunnels are cooled by injecting liquid nitrogen directly into the tunnel, the specific cooling capacity of the nitrogen consists of the heat absorbed in warming and vaporizing the liquid plus the heat absorbed in warming the gaseous nitrogen to the tunnel stagnation temperature. The specific cooling capacity of nitrogen has been calculated for a simplified model based on this method of cooling by using a National Bureau of Standards program for the thermodynamic properties of nitrogen and the results fitted with a relatively simple equation having tunnel stagnation pressure and stagnation temperature as the independent variables. This report describes the assumed cooling process, describes the method used to calculate the specific cooling capacity of liquid nitrogen, gives the simple equation fitted to the calculated specific cooling capacity data, and presents in graphical form calculated values of the specific cooling capacity of nitrogen for stagnation temperatures from saturation to 350 K and stagnation pressures from 1 to 10 atmospheres.

*NASA, Langley

53 *Haut, Richard C. **Evaluation of Hydrogen as a Cryogenic Wind Tunnel Test Gas. Final Report.** NASA-CR-145186. April 1977. 159 pp. (Grant NGR-47-003-052). A synopsis of this report is contained in the Journal of Aircraft, Vol. 14, no. 12, Dec. 1977, pp. 1155–1156. (N77-24153#, Available NTIS).

The nondimensional ratios used to describe various flow situations in hydrogen were determined and compared with the corresponding ideal diatomic gas ratios. The results were used to examine different inviscid flow configurations. The relatively high value of the characteristic rotational temperature causes the behavior of hydrogen, under cryogenic conditions, to deviate substantially from the behavior of an ideal diatomic gas in the compressible flow regime. Therefore, if an ideal diatomic gas is to be modeled, cryogenic hydrogen is unacceptable as a wind tunnel gas in a compressible flow situation.

*Old Dominion Univ.

54 *Haut, Richard Carl. **Evaluation of Hydrogen as a Cryogenic Wind Tunnel Test Gas.** Ph.D. Thesis, 1977. Old Dominion Univ., 160 pp. (N78-12103, Available Univ. Microfilms, Order #77-17259).

A theoretical analysis of the properties of hydrogen was made to determine the suitability of hydrogen as a cryogenic wind tunnel test gas. By using cryogenic hydrogen a significant increase in the test Reynolds number is achieved without increasing the aerodynamic loads. Nondimensional ratios used to describe various flow situations in hydrogen determined that cryogenic hydrogen is unacceptable as a wind tunnel test gas in a compressible flow situation. At low Mach numbers, however, in the incompressible flow regime, cryogenic hydrogen is acceptable. Hydrogen properties and fan drive-power requirements related to a hydrogen wind tunnel were also examined.

*Old Dominion Univ., Norfolk, VA

55 *Voth, R. O., and *Strobridge, T. R. **Cryogenic Design and Safety Review—NASA-Langley Research Center 0.3-Meter Transonic Cryogenic Tunnel.** NASA-TM-74767, NBSIR-77-857, Apr. 1977, 28 pp. (N77-28143#, Available NTIS).

A cryogenic design and safety review of a 0.3-m transonic cryogenic tunnel is presented. The tunnel working fluid and coolant is nitrogen. The nitrogen, supplied as liquid, is exhausted as a low temperature gas. The tunnel and ancillary systems are generally well designed but several recommendations to improve the cryogenic systems are made. The cost of recovering the cold vent gas is compared to the cost of producing the required liquid nitrogen using a captive air separation plant. Although the economic analysis is preliminary, it shows that because of the periodic operation of the tunnel, a captive air separation plant has a lower annual operating cost than the vent gas recovery systems considered.

*National Bureau of Standards, Cryogenics Division, Inst. for Basic Standards, Boulder, Colo. 80302

56 *Wagner, Bernhard, and *Schmidt, Wolfgang Theoretische Untersuchungen zur Stoss-Grenzschicht-Wechselwirkung in kryogenem Stickstoff. **(Theoretical Investigations on the Shock Wave Boundary Layer Interaction in Cryogenic Nitrogen).** In Contributions on Transport Phenomena in Fluid Mechanics and Related Topics, Tech. Univ. Berlin, Apr. 12, 1977, pp. 277–287, (N77-12402#) or (A77-47972#). Also, Zeitschrift 'ur Flugwissenschaften und Weltraumforschung, vol. 2, No. 2, Mar.–Apr. 1978, pp. 81–88. (A78-34159). In German.

The basic effects of low temperatures close to liquefaction in cryogenic wind tunnels are studied theoretically for viscous compressible flow on the basis of shockwave-laminar boundary layer interaction. The full Navier Stokes equations in combination with the equations of state for a real gas and the material properties for low temperatures are solved by means of a finite volume method and MacCormacks time splitting technique. The results show relatively small deviations compared with the ideal gas case. The differences in the pressure distribution are mainly caused by real gas effects in the inviscid external flow field while the changes in the skin friction coefficient mainly depend on the different

viscosity characteristics and on the real gas effects in the temperature distribution.

*Dornier GmbH, Friedrichshafen, West Germany

57 *Adcock, Jerry B. **Effect of LN_2 Injection Station Location on the Drive Fan Power and LN_2 Requirements of a Cryogenic Wind Tunnel.** NASA-TM-X-74036, June 1977. 19 pp. (N77-27137#, Available NTIS).

A theoretical analysis comparing the fan power and coolant (LN_2) flow rates resulting from injection of the LN_2 either upstream or downstream of the drive fan of a closed circuit transonic cryogenic tunnel is presented. The analysis is restricted to steady state tunnel operation and to the condition that the tunnel walls are adiabatic. The stagnation pressure and temperature range of the tunnel is from 1.0 to 8.8 atm and from 300 K to liquefaction temperature, respectively. Calculations are made using real gas properties of nitrogen. Results show that the fan power and LN_2 flow rates are lower if the LN_2 is injected upstream of the fan. The lower fan inlet temperature resulting from injecting upstream of the fan has a greater influence on the power than does the additional mass flow going through the fan.

*NASA, Langley

58 *Wagner, B.; and *Schmidt, W. **Theoretical Investigation of Real Gas Effects in Cryogenic Windtunnels.** AIAA Paper 77-669, 10th Fluid and Plasmadynamics Conference, Albuquerque, N. Mex., June 27–28, 1977. 12 pp. (A77-37023#). Also, AIAA Journal, vol. 16, no. 6, June 1978, pp. 380–386.

Real gas effects in cryogenic nitrogen flows have been calculated using the Beattie-Bridgeman equation of state. The investigations include Prandtl-Meyer expansions, oblique shocks, transonic small perturbation theory, transonic flow past a NACA 0012 aerofoil and shock-boundary layer interaction. The two last cases mentioned have been treated with the aid of finite volume techniques. The results show some noticeable deviations from the behavior of an ideal gas not only at cryogenic conditions but also at normal temperatures and high pressures. The deviations remain very small within the operating range of cryogenic wind tunnels if suitable reference quantities are used. Only the friction coefficient exhibits some systematic variation of considerable amount.

*Dornier GmbH, Friedrichshafen, West Germany

59 *Lorenz-Meyer, W. Ueber einige Moelichkeiten zur Berechnung des aehnlichkeitsparameters kappa* bei Realen Gasen. DFVLR, In "Contribution to Steady and Unsteady Aerodynamics," Aug. 1977, N78-17004, pp. 189–201. (N78-17017#, Available NTIS). (In German).

For translation see NASA-TM-75222, **A Few Ways of Calculating the Similarity Parameter Kappa* for Real Gases.** 13 pp. (N78-14121#, Available NTIS).

In connection with the question on the applicability of test results obtained from cryogenic wind tunnels to the large-scale model the similarity parameter is referred to. A simple method is given for calculating the similarity parameter. From the numerical values obtained it can be deduced that nitrogen behaves practically like an ideal gas when it is close to the saturation point and in a pressure range up to 4 bar. The influence of this parameter on the pressure distribution of a supercritical profile confirms this finding.

*German Research & Test Center for Aerospace Travel

60 *Buongiorno, C. La Galleria Transonica Intermittente Criogenica per Gli Altissimi Numeri di Reynolds. **(Cryogenic Intermittent Transonic Wind Tunnel for Very High Reynolds Numbers).** Paper presented at the 4th National Congress of the Italian Association of Aeronautics, Milan, Italy, Sept. 19–23, 1977. 21 pp. (A78-49739), (In Italian).

The current status of U.S. and European studies on a very-high Reynolds-number transonic wind tunnel is reviewed and a tunnel to be used by the Italian Aerospace Industries is proposed in the form of a transonic wind tunnel that makes use of both blow-down and cryogenic technology. The proposed wind tunnel measures 1 x 1.2 m and has the following characteristics: Reynolds number–30 million, Mach number–0.8-1.2, total temperature–120 K, total pressure–520 KPa. Use of a sleeve valve significantly reduces turbulence intensity in the test section compared to the values normally obtained in a continuous wind tunnel. The air temperature is reduced to the desired stagnation temperature in an economical way through use of a regeneration heat exchanger. The relative low cost of the facility is given and its complementary use with the proposed European cooperative transonic wind tunnel is discussed.

*Roma, Universita, Rome, Italy

61 *Stollery, J. L., and **Murthy, A. V. **An Intermittent High-Reynolds-Number Wind Tunnel.** Aeronautical Quarterly, vol. 28, Nov. 1977, pp. 259–264. (A78-20193). Also, AIAA paper 78-766, 10th Aerodynamic Testing Conference, San Diego, Calif., Apr. 19–21, 1978, pp. 1–5, (A78-32327#). Also, 11th ICAS Congress, Lisbon, Portugal, Sept. 10–16, 1978, Proceedings, vol. 1, pp. 461–465. (A79-20116#).

The paper suggests a simple method of generating intermittent reservoir conditions for an intermittent, cryogenic wind tunnel. This can be done by operating some existing types of short-duration tunnels "in reverse." Two examples are considered (1) a modification of the Ludwieg Tube and (2) the Isentropic Light Piston Tunnel. The sizes of tunnels required to meet the European and American specifications for a high Reynolds number tunnel with a 10 second running time are given together with proposals for a more modest national or university facility with a one second test time.

*Cranfield Insti. of Tech., Cranfield, Beds., England
**National Aero. Lab., Bangalore, India

62 *Christophe, Jean: Genese du Projet de Soufflerie Transsonique Europeenne à Grand Nombre de Reynolds. **(Genesis of the European High-Reynolds-Number Transonic Wind Tunnel Project.)** Association Aeronautique et Astronautique de France, 14th Colloque d'Aerodynamique Appliquée, Toulouse, France, Nov. 7–9, 1977. Also, L'Aeronautique et l'Astronautique, no. 72, 1978, pp. 21–34. (In French). (A79-17769).

The proposed cryogenic wind tunnel project, which would involve cooperation by West Germany, France, the Netherlands, and the United Kingdom, is described. Reasons for performing high-Reynolds-number experiments are discussed, and examples of proposed problems and their analysis are examined. Reasons for selecting the cryogenic design are considered with attention to the history of the wind tunnel project and the performance of pilot-study wind tunnels.

*ONERA, 92320 Châtillon, France

63 *Faulmann, D.; *Prieur, J.; and *Vergnolle, J. F.: Essais Preliminaires sur une Installation Transsonique Fonctionnant par Rafales Cryogeniques. **(Preliminary Tests of a Transonic Installation Functioning With Cryogenic Gusts.)** Association Aéronautique et Astronautique de France, AAAF-NT-78-26, 15 pp. Presented at the 14th Colloque d' Aérodynamique Appliquée, Toulouse, Nov. 7, 8 and 9, 1977. (N79-23040#, Available NTIS and CEDOCAR, Paris). (In French).

To achieve in-flight Reynolds numbers, a preliminary system operative at low temperatures for a short period in a transonic wind tunnel is discussed and evaluated. Injection of liquid nitrogen at a point in the fluid circuit rapidly induces low temperatures for a test period on the order of 10 sec. This technique of increasing the Reynolds number without introducing severe instrumentation problems (as is the case with continuous cryogenic systems) permits adaptation of existing transonic wind tunnels to an extended Reynolds range. An induction system with primary air cooled to 80 K was also tried with negative results since it was not possible to reduce the main circulation temperature below 200 K.

*ONERA/CERT, Toulouse, France

64 *Christophe, J.: Projet de Soufflerie Transsonique Europeenne A Grand Nombre de Reynolds. **(Transonic European Wind Tunnel Project for High Reynolds Numbers.)** Association Aéronautique et Astronautique de France, AAAF-NT-78-01. Presented at the 14th Colloque d'Aérodynamique Appliquée, Toulouse, Nov. 7, 8, and 9, 1977. 34 pp. (N79-23118#, Available NTIS and CEDOCAR, Paris). (In French).

Work from 1968 to the final joint recommendation to build a cryogenic transonic high Reynolds number wind tunnel for European governments is discussed. Such a project is necessary since actual flight performance differs from low Reynolds number transonic wind tunnel results. Several alternatives were proposed and experimentally tried in pilot tests. The cryogenic solution was finally recommended as static pressure and power can be kept low for the same Reynolds number. The proposed wind tunnel is 1.95 x 1.65 sq m, with maximum pressure at 4.4 Bars, minimum temperature at 120 K, Mach number up to 1.35, and Reynolds number up to 40 million when working with nitrogen instead of air.

*ONERA, 92320 Châtillon, (France)

65 *Dupriez, F.: Similitude, Realisation, Identification et Instrumentation des Maquettes d'Essais. **(Similitude, Manufacturing, Identification, and Instrumentation of Test Models.)** Association Aéronautique et Astronautique de France, AAAF-NT-78-24, 38 pp. Presented at the 14th Colloque d'Aérodynamique Appliquée, Toulouse, Nov. 7, 8, and 9, 1977. (N79-23120#, Available NTIS and CEDOCAR, Paris). (In French).

Several aspects of present aircraft model technology are surveyed. Similitude and practical choice rules are discussed as well as identification and instrumentation techniques. Specifications and manufacturing are illustrated with several practical examples, such as use of high technology composite materials (carbon and boron fibers); increasing application of numerical control manufacturing techniques, the rapid development of microprocessor use, and adaptation to basic technological changes such as cryogenic wind tunnels.

*Univ. of Science & Technology, Lille, France

66 *Bazin, M.: Problemes de Construction de Maquettes pour les Souffleries à Grand Nombre de Reynolds. **(Construction Problems Specific to Models for High Reynolds Number Wind Tunnels.)** Association Aéronautique et Astronautique de France, AAAF-NT-78-02, 45 pp. Presented at the 14th Colloque d'Aérodynamique Appliquée, Toulouse, Nov. 7, 8, and 9, 1977. (N79-23124#, Available NTIS and CEDOCAR, Paris). (In French).

The state-of-the-art is surveyed for both pressurized and cryogenic wind tunnel alternatives. Materials, feasible dimensions, safety problems, cost, instrumentation, etc., are discussed by model construction experts. Feasibility is demonstrated, although an effort to reduce developing time is still necessary. Present limitations include balances and model supports. New methods or materials will be necessary to replace local gages in the case of cryogenic systems.

*ONERA, 92320, Châtillon, France

67 *Goodyer, M. J. **The 0.1M Subsonic Cryogenic Tunnel at the University of Southampton.** NASA-CR-145305, Jan. 1978, 43 pp. Grant NsG-7172. (N78-18086#, Available NTIS).

The design and performance of a low speed one atmosphere cryogenic wind tunnel is described. The tunnel is fan driven and operates over the temperature range 305 K to 77 K at Mach numbers up to 0.28. It is cooled by the injection and evaporation of liquid nitrogen in the circuit, and the usual test gas is nitrogen. The tunnel has a square test section 0.1m across and was built to allow, at low costs, the development of testing techniques and the development of instrumentation for use in cryogenic tunnels, and to exploit in general instrumentation work the unusually wide range of unit Reynolds number available in such tunnels. The tunnel was first used in the development of surface flow visualization techniques for use at cryogenic temperatures.

*Univ. of Southampton

68 *Ray, Edward J. **Langley's Two-Dimensional Research Facilities: Capabilities and Plans.** In "Advanced Technology Airfoil Research," Vol. 1, Part 1, Mar. 7-9, 1978, N79-20030, pp. 399-414. (N79-20055#, Available NTIS).

The current capabilities and the forthcoming plans for Langley's two-dimensional research facilities are described. The characteristics of the Langley facilities are discussed in

terms of Reynolds number, Mach number, and angle-of-attack capabilities. Comments are made with regard to the approaches which have been investigated to alleviate typical problem areas such as wall boundary effects. Because of the need for increased Reynolds number capability at high subsonic speeds, a considerable portion of the paper deals with a description of the 20 by 60 cm two-dimensional test section of the Langley 0.3-meter transonic cryogenic tunnel which is currently in the calibration and shakedown phase.

*NASA, Langley

69 *Ladson, Charles L.: **A New Airfoil Research Capability.** In "Advanced Technology Airfoil Research," vol. 1, Part 1, Mar. 7–9, 1978, N79-20030, pp. 425–432. (N79-20057#, Available NTIS).

The design and construction of a self-streamlining wall test section for the Langley 0.3-meter transonic cryogenic tunnel was included in the fiscal year 1978 construction of facilities budget for Langley Research Center. The design is based on the research being carried out by M. J. Goodyer at the University of Southampton, Southampton, England, and is supported by Langley Research Center. This paper presents a brief description of the project. Included are some of the design considerations, anticipated operational envelope, and sketches showing the detail design concepts. Some details of the proposed operational mode, safety aspects, and preliminary schedule are presented.

*NASA, Langley

70 *Nicks, Oran W., and *McKinney, Linwood W. **Status and Operational Characteristics of the National Transonic Facility.** AIAA paper 78-770, 10th Aerodynamic Testing Conference, San Diego, Calif., Apr. 19–21, 1978, Technical Papers. pp. 40–42. (A78-32331#).

This paper discusses the development and capabilities of the National Transonic Facility which is planned for operation in 1981. The fan-drive, cryogenic-pressurized, closed-return facility will have operating parameters of 0.1-1.2 Mach, 1-9 bars pressure, 78-340 K, 150 dB sound pressure, and ±0.001 rms turbulence intensity. These operating conditions have been selected on the basis of several current and future aircraft and space transportation systems. The facility will provide full-scale testing conditions for calculating subsonic drag, airloads, and stability and control information. Data for pre-test conditions, on-line information, and post-test analysis will be computer-processed.

*NASA, Langley

71 Inger, G. R.: **On the Simulation of Transonic Shock-Turbulent Boundary Layer Interactions in Cryogenic or Heavy Gas Wind Tunnels.** VPI-Aero-080, April 1978, 26 pp. Presented at 10th AIAA Aerodynamic Testing Conference. pp. 285–292. San Diego, Calif., Apr. 20, 1978. AIAA paper 78-808, (A78-32362#) or (N78-24501#, Available NTIS). Also Journal of Aircraft, vol. 16, no. 4, April 1979, pp. 284–287.

The role of the basic similitude parameters governing transonic normal shock-turbulent boundary layer interaction effects in cryogenic wind tunnel tests is studied theoretically for the non-separating case. Besides Mach and Reynolds number, these parameters are the wall to total temperatures ratio, specific heat ratio gamma, viscosity-temperature exponent and Prandtl number. The results show that lack of temperature ratio simulation has a significantly adverse effect on interactive skin friction and hence separation onset compared to the adiabatic free flight case; higher gamma's than air also may have some effect.

*VPI and State Univ. Blacksburg, Va.

72 *Hall, Robert M.: **Condensation and Its Growth Down the Test-Section of the Langley 0.3-M Transonic Cryogenic Tunnel.** AIAA paper 78-811, 10th Aerodynamic Testing Conference, San Diego, Calif., Apr. 19–21, 1978, Technical Papers. pp. 301–304, (A78-32365#).

Four total pressure probes were used to measure the growth of condensation down the test section of the Langley 0.3-m tunnel, and the condensation data were employed to verify a mathematical model which assumes condensation results from heterogeneous nucleation on preexisting seed particles. The onset of effects occurs throughout the test section at the same total temperature but the magnitude of the effects increases with increasing length down the test section. Condensation is important because it determines the minimum operating temperature of transonic cryogenic wind tunnels.

*NASA, Langley

73 *Hartzuiker, J. P., and *North, R. J. **The European Transonic Wind-Tunnel Project.** ICEC 7, Proceedings of the 7th Int. Cryogenic Engineering Conference, London, England, July 4–7, 1978, pp. 322–330. (A79-31021).

In 1978, four European nations agreed to cooperate in developing a large transonic high-Reynolds-number wind tunnel which would use cold nitrogen gas as the test medium. A test section size of 1.95 m x 1.65 m is envisaged. A continuous fan drive would provide runs with 10 periods of data acquisition, each lasting 10 sec, a typical day could yield four runs. Cryogenic engineering problems related to the construction of the wind tunnel are also considered.

*NLR, Amsterdam, Netherlands

74 *Michel, R., and *Faulmann, D. **Preliminary Tests in a Cryogenic Transonic Wind Tunnel Driven by Induction.** ONERA TP no. 1978-48E. Also, L'Recherche Aerospatiale, vol. 185, no. 4, July-Aug. 1978, pp. 205–207. (A79-15300#). (In French).

A problem associated with the use of the T2 injector-driven transonic wind tunnel is considered, and a procedure for obviating the problem is tested on the T2 pilot unit. The procedure, which combines a cryogenic test with an induction test, seeks to modify operating temperature characteristics. The ability of the procedure, which involves a short injection of liquid nitrogen, to reduce temperature in the walls and superficial areas, while maintaining high temperatures inside the walls, was examined. Some preliminary results are presented. The usefulness of external thermal insulation is indicated.

*ONERA-CERT, Toulouse, France

75 *Kell, D. M.: **A Surface Flow Visualization Technique for Use in Cryogenic Wind Tunnels.** Aeronautical Journal, vol. 82, no. 2, Nov. 1978, pp. 484–487, NSG-71-72, (A79-20795).

A method of surface flow visualization for use in cryogenic wind tunnels is described which requires injection of a cryogenic liquid onto the model while the tunnel is running. This necessitates the use of a substance that remains liquid over a large range of cryogenic wind tunnel operating temperatures. It is found that propane (C3H8) is a suitable substance. Experiments are conducted in a subsonic cryogenic wind tunnel to assess the practical application of liquid propane flow visualization. The propane is stored in a chamber cooled by liquid nitrogen and when required is pumped through pipes to a gallery inside the model and then out onto the surface through small holes. To color the liquid a suspension of pigment particles is used. Propane is supplied to the cooled chamber in gaseous form from a standard liquefied gas cylinder. The sequence of events is illustrated on a propane temperature-entropy diagram. The use of liquefied propane for flow visualization in a cryogenic tunnel operating at pressures up to 40 atm appears to be feasible. Illustrative examples are provided.

*British Aerospace, Production Engineering Dept., Weybridge, Surrey, England

76 Clausing, A. M.; Clark, C. L.; and *Mueller, M. H. **The Cryogenic Heat Transfer Tunnel—A New Tool for Convective Research.** Presented at the Winter Annual Meeting ASME, San Francisco, Calif., Dec. 10–15, 1978. pp. 73–78. (Research supported by Dept. of Energy.) (A79-24316#).

A novel heat transfer technique, the use of cryogenic temperatures for convective modeling, is used in this study in order to simultaneously obtain large Grashof and Reynolds numbers on a vertical cylinder. The research is motivated by the need to predict combined convective losses from large, high-temperature objects such as solar "power tower" receivers where the magnitudes of both the Grashof and Reynolds numbers are large. The cryogenic heat transfer tunnel provides an economical method of obtaining these large Grashof and Reynolds numbers with an appropriate and nearly constant Prandtl number, thus it is an excellent tool for study of convective heat transfer. Low-temperature modeling, a cryogenic testing facility, and a transient measurement technique are discussed.

*Illinois Univ.

77 *Bursik, Joseph W.; and **Hall, Robert M. **Metastable Sound Speed in Gas-Liquid Mixtures.** NASA-TM-78810, March 1979, 54 pp. (N79-20339#, Available NTIS).

A new method of calculating speed of sound for two-phase flow is presented. The new equation assumes no phase change during the propagation of an acoustic disturbance and assumes that only the total entropy of the mixture remains constant during the process. The new equation predicts single-phase values for the speed of sound in the limit of all gas or all liquid and agrees with available two-phase, air-water sound speed data. Other expressions used in the two-phase flow literature for calculating two-phase, metastable sound speed are reviewed and discussed. Comparisons are made between the new expression and several of the previous expressions--most notably a triply isentropic equation as used, among others, by Karplus and by Wallis. Appropriate differences are pointed out and a thermodynamic criterion is derived which must be satisfied in order for the triply isentropic expression to be thermodynamically consistent. This criterion is not satisfied for the cases examined, which included two-phase nitrogen, air-water, two-phase parahydrogen, and steam-water. Consequently, the new equation derived is found to be superior to the other equations reviewed.

*Rensselaer Polytechnic Institute
**NASA, Langley

78 *Hall, Robert M. **Onset of Condensation Effects With an NACA 0012-64 Airfoil Tested in the Langley 0.3-Meter Transonic Cryogenic Tunnel.** NASA-TP-1385, Apr. 1979. 72 pp. Formerly issued as NASA-TM-78666. (N79-22043#, Available NTIS).

A 0.137-meter NACA 0012-64 airfoil has been tested at a 0^{0} angle of attack in the nitrogen-gas Langley 0.3-meter transonic cryogenic tunnel at free-stream Mach numbers of 0.75, 0.85, and 0.95 over a total pressure range from 1.2 to 5.0 atmospheres. The onset of condensation effects as determined by varying stagnation temperature was found to correlate better with the amount of super-cooling in the free stream than it did with the supercooling in the region of maximum local Mach number over the airfoil. Effects in the pressure distribution over the airfoil were generally seen to appear over its entire length at nearly the same total temperature. Both observations suggest that heterogeneous nucleation does occur in the free stream. The present results are compared to calculations made by Sivier and data gathered by Goglia. The potential operational benefits realized from supercooling are presented in terms of increased Reynolds number capability at a given tunnel total pressure and reduced drive-fan power and liquid nitrogen consumption if Reynolds number is held constant. Depending on total pressure and free-stream Mach number, these three benefits are found to vary respectively from 8 to 19 percent, 12 to 24 percent, and 9 to 19 percent. An appendix is included which gives details of the data analysis and error estimates for the differences in pressure distributions.

*NASA, Langley

79 *Hottner, T. Anwendung der Tieftemperaturtechnik im strömungstechen Versuchswesen, **(The Application of Cryogenics in Experimental Aerodynamics).** Ingenieur-Archiv, vol. 47, no. 4, 1978, pp. 241–256. (A78-48982). (In German). For translation see NASA-TM-75385.

The application of cryogenics in wind tunnel design offers an increase in Reynolds number simulation at simultaneously reduced drive power for the wind tunnel compressor compared to a wind tunnel driven at normal temperatures. The price, however, is an additional cryogenic power. The report is concerned with the energetic aspect of cryotechnics in wind tunnel technique. With restriction only on cryogenic power due

to tunnel process-heat, the continuously running tunnel with closed circuit and the blow-down-storage tunnel are investigated. Finally, the possibility of reducing cryogenic power using heavy gases as test medium is discussed.

*Stuttgart, Universitaet, Stuttgart, West Germany

80 **First International Symposium on Cryogenic Wind Tunnels.** University of Southampton, England. April 3–5, 1979.

The first paper presented served as an introduction to the conference. The history of the development of cryogenic wind tunnels was given and suggestions made for future research to make tunnels of this kind even more valuable. Thirty-five additional papers were presented grouped under the following topics: Instrumentation, Cryogenic Tunnels with Magnetic Levitation, Liquid and Gaseous Nitrogen Flow Properties, Cryogenic Tunnel Technology, Tunnel Controls, Heat Transfer Topics, Model Design, and Reports on Tunnel Projects. Copies of this Symposium are available from Dr. M. J. Goodyer, Dept. of Aeronautics & Astronautics, The University, SO 95 NH, Southampton, Hampshire, U.K., Apr. 1979

81 *Goodyer, M. J.: **The Evolution of the Cryogenic Wind Tunnel.** Paper no. 1, 1st Int. Symp. on Cryogenic Wind Tunnels, Southampton, England, Apr. 3–5, 1979.

The main aim of this paper is to trace the key events in the emergence of the cryogenic wind tunnel, events which led therefore to this Symposium, to learn of its present state of development and to gain insight into the future pattern of evolution. A secondary aim is to attempt to influence evolution by drawing attention to areas of endeavour which are not receiving the degree of research effort which may be justified.

*Univ. of Southampton

82 *Bazin, Maurice; and Dubois, Maurice **Balance and Sting Design for Cryogenic Wind Tunnels.** Paper no. 2, 1st Int. Symp. on Cryogenic Wind Tunnels, Southampton, U.K., Apr. 3–5, 1979. ONERA-TP-1979-40. (A79-39089#).

The orientations and thoughts leading to the concept of balances and stings usable in the future European Transonic Wind Tunnel (ETW) are presented in this paper. They constitute the starting point of a national research program, integrated within the European program. The domain considered is that of ETW cryogenic runs of about 10 minutes, from 120 to 300 K, stagnation pressure 1 to 4.4 bar, Mach 0.2 to 1.35.

*ONERA, 92320, Châtillon, France

83 *Krogmann, Paul; and *Lorenz-Meyer, Wolfgang **Design and Testing of an Unheated Strain Gauge Balance Element for Cryogenic Temperatures.** Paper no. 3, 1st Int. Symp. on Cryo. Wind Tunnels, Southampton, U.K., Apr. 3–5, 1979.

In order to develop unheated strain gauge balances for use in cryogenic wind tunnels at low temperatures experiments were undertaken at DFVLR Göttingen on single-component elements which were made of different steels and were equipped with different types of strain gauges. Disappointingly bad results were obtained when unsuitable strain gauges were used on two identical elements of austenitic stainless steel. Subsequent experiments with another type of strain gauge on the same elements showed better but still poor results, which obviously have to be attributed to temperature dependent variations of the material properties. Finally, another element was manufactured of different steel. This element in connection with suitable strain gauges, so far has given most promising results.

*DFVLR, West Germany (FRG)

84 *Liousse, F.; *Calvet, P.; and *Giovannini, A. **Experimental Study of Thermoresistive Sensors Under Cryogenic Conditions.** Paper no. 4, 1st Int. Symp. on Cryogenic Wind Tunnels, Southampton, U.K., Apr. 3–5, 1979.

Thermoresistive sensors (commercially available "hot" wire or film type probes) are tested under steady and unsteady cryogenic flows in order to determine their aptitude to operate in cryogenic wind tunnels for instantaneous temperature and velocity measurements. Some specific devices have been designed. They consist of a small calibration tunnel performing controlled velocity variations and an electronic thermometer with a built-in circuit which permits in situ measurement of response time of the sensors.

*ONERA-CERT, Toulouse, France, Departement d'Etudes et de Recherches en Mécanique et Energétique des Systèmes

85 *Hartzuiker, J. P.; and *North, R. J.: **A Progress Report on the European Transonic Windtunnel Project.** Paper no. 5, 1st Int. Symp. on Cryogenic Wind Tunnels, Southampton, U.K., Apr. 3–5, 1979.

This paper was written about a year after the start of the Preliminary Design Phase of ETW. The organisational structure was established, the preliminary design of the pilot tunnel was finished and that of ETW was well under way. A substantial cryogenic technology programme had been initiated. Strong support was being given from many quarters to the work of the Technical Group. A further Memorandum of Understanding for the next Phase or Phases was under consideration and preparations were being made for a decision on the site. This all represented real progress towards the realisation of the European Transonic Windtunnel in the mid-1980's.

*(Technical Group, ETW), NLR, Amsterdam, Netherlands

86 *Nelander, Curt: **A Self-Contained Cryogenic Air Supply System for a Transonic Blow-Down Tunnel.** Paper no. 6, 1st Int. Symp. on Cryogenic Wind Tunnels, Southampton, U.K., Apr. 3–5, 1979

A high pressure air supply system can be used not only to feed a wind tunnel but also to reduce the total enthalpy of the gas. This can be done by various methods and to such an extent that cryogenic stagnation temperatures are achieved. The paper deals with some different methods which could be used to incorporate the cold-generating process into the wind tunnel run sequence. It is shown that with a huge low pressure air storage already on hand (as the case is at FFA)

the most attractive scheme should be to store the cold outlet air from the tunnel and to use this low enthalpy gas for cooling off the compressed air when the high pressure storage is recharged.

*Aeronautical Research Institute of Sweden (FFA)

87 *Ashcroft, D. H.; and *Emslie, K.: **A Cryogenic Transonic Blowdown Wind Tunnel Project.** Paper no. 7, 1st Int. Symp. on Cryogenic Wind Tunnels, Southampton, U.K., Apr. 3–5, 1979.

Combat aircraft operate within the range of serious scale effects and hence wind tunnel tests require full simulation of Reynolds number if seriously misleading results are to be avoided. Although there are many claims on the capital within the aircraft industry the provision of a high Reynolds number facility will produce cost effective returns. Means to achieve this are considered relative to capital and running costs. Long experience with a blowdown to atmosphere wind tunnel has been taken as the basis for a cryogenic version. Injection and evaporation of liquid nitrogen downstream of the airflow control valve will cool the test gas to flow across a previously cooled model. The test gas will be discarded, despite the high cost per run, because the alternatives which employ natural cooling processes, recirculation or energy saving would be much more costly to build. The major features of the project and potential performance are described. Comments are made on the key areas requiring experimental development work and on the program that will be undertaken to produce a successful facility.

*British Aerospace (Aircraft Group), Warton Division, Warton Aerodrome, Preston, PR4 1AX, Lancashire, England

88 *Hutt, G. R.; and *East, R. A.: **Preliminary Studies of a Free Piston Expander for an Intermittent Cryogenic Wind Tunnel.** Paper no. 8, 1st Int. Symp. on Cryogenic Wind Tunnels, Southampton, U.K., Apr. 3–5, 1979.

The purpose of the current work is to present preliminary experimental results of measurements of the tunnel stagnation temperatures which may be achieved in a small scale free piston device and to determine the effect of heat transfer from the tube on the uniformity of the conditions achieved. Results are presented of experiments using a small scale free piston expansion drive system proposed by Stollery and Murthy for an intermittent cryogenic wind tunnel. The feasibility of the proposed operating principle has been demonstrated and measurements of pressure and temperature during the expansion and run periods are compared with the predictions of a simple theoretical model.

*Univ. of Southampton, Dept. of Aeronautics & Astronautics, Hants, England

89 *Haldeman, Charles W.; **Kramer, Richard, A.; and ***Way, Peter **Developments at M.I.T. Related to Magnetic Model Suspension and Balance Systems for Large Scale Facilities.** Paper no. 9, 1st Int. Symp. on Cryogenic Wind Tunnels, Southampton, U.K., Apr. 3–5, 1979.

Magnetic model suspension and balance systems for wind tunnel use (1) have been designed, tested and used at M.I.T.'s Aerophysics Laboratory for over eighteen years. Despite this experience, which demonstrates the utility and durability of the magnetic model suspension and balance systems, no large-scale system has yet been constructed for use anywhere in the world. This appears to be principally due to the large capital cost of such a facility. This paper presents several attributes of magnetic balance systems which make them attractive for use in large-scale cryogenic facilities and reports on recent developments in model roll control and superconducting coil construction, which enhance system versatility and reduce the electrical power requirements.

*Research Associate, MIT, Department of Aeronautics and Astronautics, Associate Director, Aerophysics Laboratory, Cambridge, Massachusetts, U.S.A.

**Assistant Professor, Aeronautical Technology Arizona State University, Tempe, Arizona, U.S.A.

***Research Assistant, MIT, Department of Aeronautics and Astronautics, Cambridge, Massachusetts, U.S.A.

90 *Britcher, C. P.; *Goodyer, M. J.: **The Southampton University Magnetic Suspension/Cryogenic Wind Tunnel Facility.** Paper no. 10, 1st Int. Symp. on Cryogenic Wind Tunnels, Southampton, U.K., Apr. 3-5, 1979.

Scaling laws relating design parameters of magnetic suspension and balance systems to wind tunnel test conditions are identified. Reduction of test temperature is found to be the most attractive and powerful technique of reducing the cost of a magnetic suspension facility for specific test Reynolds Number and Mach Number requirements. Details of the adaption of a small, low-speed, fan driven cryogenic wind tunnel for use with a magnetic suspension and balance system are given. Aerodynamic data has been acquired from a model suspended in the new facility over a wide range of tunnel conditions. Temperature is shown to have a small effect on the magnetization of the model magnetic cores. Studies of the effect have begun.

*Univ. of Southampton, Dept. of A & A, The University, SO95 NH, Southampton, Hampshire, U.K.

91 *Kilgore, R. A.; *Igoe, William B.; *Adcock, Jerry B.; *Hall, Robert M.; and *Johnson, Charles B.: **Full-Scale Aircraft Simulation With Cryogenic Tunnels and Status of the National Transonic Facility.** Paper no. 11, 1st Int. Symp. on Cryogenic Wind Tunnels, Southampton, U.K., Apr. 3-5, 1979. NASA-TM-80085, 18 pp. (N79-26064#, Available NTIS).

Theoretical studies to determine the effect of thermal and caloric imperfections in cryogenic nitrogen on boundary layers indicate that in order to simulate nonadiabatic laminar or turbulent boundary layers in a cryogenic nitrogen wind tunnel, the flight enthalpy ratio, rather than the temperature ratio, should be reproduced. The absence of significant real-gas effects on both viscous and inviscid flows makes it unlikely that there will be large real-gas effects on the cryogenic tunnel simulation of shock boundary-layer interactions or other complex flow conditions encountered in flight. Experimental and theoretical studies on condensation effects to determine the minimum usable temperature indicate that under most circumstances free-stream Mach number rather than maximum local Mach number determines the onset of condensation effects. Progress is well underway

on a major application of the cryogenic wind-tunnel concept with the construction of the U.S. National Transonic Facility at the Langley Research Center. This new tunnel is scheduled to become operational by 1982. Not only will it provide an order of magnitude increase in Reynolds number capability over existing U.S. tunnels, but also, because of the ability to vary pressure, Mach number, and temperature independently, it will be able to perform the highly desirable research task of separating aeroelastic, compressibility, and viscous effects on the aerodynamic parameters being measured.

*NASA, Langley

92 *Edmundson, I. C. **The Generation of Cryogenic Temperatures by High Pressure Expansion,** Paper no. 12, 1st Int. Symp. on Cryogenic Wind Tunnels, Southampton, U.K., Apr. 3–5, 1979.

In designing an intermittent cryogenic tunnel it would seem logical to create the conditions intermittently. Stollery proposed that this could be done by using the expansion of a high pressure gas. A proposed scheme is explained. In the calculations an adiabatic, isentropic expansion was assumed. This paper reviews the available experimental evidence to examine this assumption. From the evidence presented, the deviations from an adiabatic, isentropic expansion has important implications for the design of this tunnel. Previous experimental work on the expansion of gases has shown that these deviations are significant. Experimental work is being carried out to assess a more realistic configuration.

*Cranfield Institute of Technology, College of Aeronautics

93 *Blanchard, A.; and *Faulmann, D.: **Progress Report on a Cryogenic Pilot Transonic Wind Tunnel Driven by Induction.** Paper no. 13, 1st Int. Symp. on Cryogenic Wind Tunnels, Southampton, U.K. Apr. 3–5, 1979.

A promising solution to increase the Reynolds number without producing too many technological problems seems to be provided by a short cryogenic operating run, in which the cooling is ensured by a quick injection of liquid nitrogen in the return leg circuit. A thin layer of internal thermal insulation allows a reduction of thermal losses and nitrogen consumption. This solution has been chosen for transforming existing wind tunnels, and in particular for the adaptation of T2 for cryogenic operation. In our present installation we are studying and resolving satisfactorily many problems connected with general cryogenic wind tunnel functioning. Many problems of low temperature operation must be solved through such fundamental studies before the error free realization of larger tunnels can be made.

*ONERA/CERT, Toulouse, France

94 *Luneau, James; *Rochas, Noël, and *Kirrmann, Clement: **Preliminary Study of the Injection Process of LN_2 in a Cryogenic Wind-Tunnel.** Paper no. 14, 1st Int. Symp. on Cryogenic Wind Tunnels, Southampton, U.K. Apr. 3–5, 1979.

The Ecole Nationale Supérieure de l'Aéronautique et de l'Espace (ENSAE) in collaboration with the Centre d'Essais Aéronautique de Toulouse (CEAT) has been studying a transonic cryogenic wind-tunnel. This wind-tunnel, which is now being built, is to be operational by the end of 1980. It has been conceived to study airfoils in the transonic field. To be sure that the liquid nitrogen has disappeared inside the test section, a study was made to determine the characteristics and the location of injectors able to maintain a monophasic, steady uniform flow in the test section. The theoretical study is being oriented towards modelling of breakup and coalescence phenomena. A small wind tunnel with a 60 mm x 120 mm test-section is now being built and will be used to study the influence of different parameters, such as injection velocity, gas flow velocity, and gas temperature. The final aim consists in validating a theoretical model of the diphasic flow, which should allow us to determine the optimal characteristics and position of the LN_2 injectors to be set in the ENSAE wind tunnel and other cryogenic wind tunnels of the future.

*Ecole Nationale Superieure de l'Aéronautique et d'l'Espace Aerodynamics Department

95 *Koppenwallner, G., and *Dankert, C. **The Homogeneous Nitrogen Condensation in Expansion Flows With ETW-Relevant Stagnation Conditions.** Paper no. 15, 1st Int. Symp. on Cryogenic Wind Tunnels, Southampton, U.K., Apr. 3–5, 1979.

The condensation in free jet expansions with stagnation conditions typical for transonic cryo-tunnels was studied. The results show the delay for condensation onset and the gas dynamic behaviour within the condensation regime. Although the experiments were performed in small scale nozzles, they nevertheless can be used to predict condensation delay in model flow fields.

*DFVLR – Institute für Experimentelle Strömungsmechanik Bunsenstrasse 10, 3400 Göttingen, West Germany (FRG)

96 *Younglove, B. A.: **Thermodynamic Properties of Nitrogen Gas From Sound Velocity Measurements.** Paper no. 16, 1st Int. Symp. on Cryogenic Wind Tunnels, Southampton, U.K., Apr. 3–5, 1979.

Thermodynamic properties of nitrogen gas have been calculated from 80 K to 350 K and at pressures to 10 bar from sound speed measurements and existing P-V-T data using multiproperty fitting techniques. These new data are intended to improve existing predictive capability of the equation of state in the low density region needed for use with the National Transonic Facility (NTF) now being built at the NASA–Langley Research Center.

*Thermophysical Properties Division, National Engineering Laboratory, National Bureau of Standards, Boulder, Colorado, U.S.A.

97 *Albone, C. M. **An Investigation Into the Real Gas Effects of Cryogenic Nitrogen in Inviscid Homentropic Flow.** Paper no. 17, 1st Int. Symp. on Cryogenic Wind Tunnels, Southampton, U.K., Apr. 3–5, 1979.

As a contribution to the investigation of the suitability of using cryogenic nitrogen as the test gas in a high Reynolds number transonic wind tunnel, a study is made of the real gas effects of nitrogen at low temperatures. The study, which is limited to inviscid, homentropic flow of a non-conducting gas, takes the form of an independent confirmation of results

by Kilgore, et al. The new contribution in this paper is that the use of a simplified equation of state enables an expression for enthalpy (and hence the terms in Bernoulli's equation) to be derived by analytic integration.

*Aerodynamics Department, RAE, Farnborough U.K.

98 *Inger, G. R.: **Transonic Shock-Boundary Layer Interactions in Cryogenic Wind Tunnels.** Paper no. 18, 1st Int. Symp. on Cryogenic Wind Tunnels, Southampton, U.K., Apr. 3–5, 1979.

Since the transonic aerodynamics of missiles and aircraft can be significantly influenced by shock wave – boundary layer interaction effects, these effects should be adequately simulated in cryogenic high Reynolds number wind tunnel experiments. In addition to flight Mach and Reynolds numbers which are simulated by design, there are four other interaction similitude parameters which may not be duplicated owing to the very low temperature – high pressure working fluid involved: wall to total temperature ratio T_w/T_t, specific heat ratio γ, viscosity temperature exponent ω and Prandtl number Pr. The first is deemed especially important since in some proposed short duration cryogenic transonic wind tunnels the model is at much higher temperature than T_t during the test. Moreover, the γ of cryogenic nitrogen can be larger (1.5–1.8) than air and thus influence the interaction; lower γ's are also of interest in heavy gas (Freon 12) facilities. This paper describes the application of an approximate non-asymptotic theory of weak normal shock nonseparating turbulent boundary layer interaction to the prediction of these heat transfer and real gas effects.

*Virginia Polytechnic Institute and State University, Blacksburg, VA USA

99 *Smith, David A.: **Development of a Test Procedure for Acoustically Dissipative Silencer Materials Used in Cryogenic Applications.** Paper no. 19, 1st Int. Symp. on Cryogenic Wind Tunnels, Southampton, U.K., Apr. 3–5, 1979.

The objective of the test procedure discussed is to guide selection of optimum mechanical properties of acoustically dissipative materials to be used in silencers for cryogenic applications. The items of primary concern are. erosion of materials due to grazing flow; fatigue of materials due to grazing flow and intense sound pressure levels; and thermal shock of materials due to cryogenic temperatures. The proposed test procedure quantifies the degradation of mechanical properties of acoustically dissipative materials intended for use in an intense acoustic field, with flow, at cryogenic temperatures.

*General Acoustics Corp., Los Angeles, Calif., U.S.A.

100 *North, R. J.: **The Cryogenic Technology Programme of the European Transonic Wind Tunnel Project.** Paper no. 20, 1st Int. Symp. on Cryogenic Wind Tunnels, Southampton, U.K., Apr., 3–5, 1979.

The ETW project is concerned with the design and feasibility of a proposed large new European transonic wind tunnel operating on the cryogenic principle. There are a number of problems to be solved in the design, construction and operation of such a tunnel. Amongst these problems are those of instrumentation, model design and construction, testing techniques, minimum operating temperature and so on. If it appears that there are basic difficulties in any of these areas the acceptability of the proposed tunnel to prospective users might be in doubt. Accordingly the Steering Committee of ETW has initiated a so-called cryogenic technology programme to examine these problems. A list of possible subjects of interest in a cryogenic technology programme is given. The present cryogenic technology programme is listed. A comparison of these lists shows that a combination of exchanges of information, an atmosphere of goodwill, and positive measures by the national representatives on the Steering Committee and by representatives of the aircraft industries has resulted in a program which covers a large part of the spectrum of interest.

*Technical Group, ETW, Amsterdam

101 *Haldeman, Charles W.: **Suggested Modification of Fog Flow Visualization for Use in Cryogenic Wind Tunnels.** Paper no. 21, 1st Int. Symp. on Cryogenic Wind Tunnels, Southampton, U.K., Apr. 3–5, 1979.

A mixture of liquid nitrogen and steam-bearing air has been used recently to produce flow visualization in a conventional subsonic wind tunnel. This note offers the suggestion that this technique might be modified to produce nitrogen "smoke" for flow visualization in cryogenic wind tunnels.

*Aerophysics, Lab., Massachusetts Institute of Technology, 77 Massachusetts Avenue, Cambridge, Mass. 02139

102 *Morel, J. P.; and **Mereau, P.: **Optimum Control of the European Transonic Wind Tunnel.** Paper no. 22, 1st Int. Symp. on Cryogenic Wind Tunnels, Southampton, U.K., Apr. 3–5, 1979.

Analyses of ETW operating costs have shown the large influence of liquid nitrogen consumption during transients. Optimisation of control for ETW is desirable; it involves a theoretical and experimental programme during preliminary design so that, by the time of ETW construction, theoretical models checked through experiments will help in the design of control architecture. Interfaces between control and other tasks will be examined thoroughly. A simplified model has shown the highly-coupled aspect of ETW flow dynamics. Optimum control of the tunnel parameters. Mach number, stagnation temperature, and stagnation pressure by use of the predictive algorithm IDCOM looks feasible based on some simulation on the simplified model. Preliminary results of the identification of Mach number process in the NLR HST shows that the validity of the use of the simplified model for control purposes looks promising in that field. More analysis is still required of test results obtained in the 1m x 1m DFVLR and ONERA/CERT T'2 wind tunnels. A general model with less restrictive assumptions is being implemented on a computer. It must be checked with simplified model results as well as with the experimental tests. By the end of this preliminary design phase it is expected that use of theoretical models, validated by basic experiments, will give a first definition of an ETW control architecture.

*Technical group, ETW

**Adersa-Gerbios, Velizy, France

103 *Balakrishna, S.; and **Thibodeaux, J. J.: **Modeling and Control of a LN_2-GN_2 Operated Closed Circuit Cryogenic Wind Tunnel.** Paper no. 23, 1st Int. Symp. on Cryogenic Wind Tunnels, Southampton, U.K., Apr. 3–5, 1979.

Full scale Reynolds number flow capability at transonic speeds has been successfully realized in wind tunnels by cooling the test gas to cryogenic temperatures. Gaseous nitrogen (GN_2) is an ideal cryogenic test medium because of its negligible thermal and calorific imperfections on isentropic expansion, and since it can be cooled efficiently by injected liquid nitrogen (LN_2) which evaporates into the test gas. Despite increased gas density, cryogenic operation of a closed circuit wind tunnel is associated with reduced fan power and no extra dynamic loads on the models. Further, a closed circuit cryogenic tunnel allows independent control of the tunnel flow parameters. Precise control of these parameters is an involved control problem in view of the non-linear and coupled nature of the tunnel responses. This paper aims at developing a simple lumped parameter multivariable control compatible mathematical model of a LN_2-GN_2 operated closed circuit cryogenic tunnel, and derive closed loop control laws with specific reference to the 0.3-m transonic cryogenic tunnel at the NASA Langley Research Center.

*Old Dominion University Research Foundation, Norfolk, VA 23508
**NASA, Langley

104 *Clausing, A. M.: **Experimental Studies of Forced, Natural and Combined Convective Heat Transfer at Cryogenic Temperatures.** Paper no. 24, 1st Int. Symp. on Cryogenic Wind Tunnels, Southampton, U.K., Apr. 3–5, 1979.

A novel heat transfer technique, the use of cryogenic temperatures for convective modeling, is used in this study to obtain significant increases in $\rho^2\beta/\mu^2$ and ρ/μ, in order to simultaneously obtain large Grashof and Reynolds numbers on a vertical cylinder. The research is motivated by the need to predict combined convective losses from large, high-temperature objects such as solar "power tower" receivers where the magnitudes of both the Grashof and Reynolds numbers are large. The cryogenic heat transfer tunnel provides an economical method of obtaining these large Grashof and Reynolds numbers with an appropriate and near constant Prandtl number; thus it is an excellent tool for study of convective heat transfer. Low-temperature modeling, a cryogenic testing facility, and a transient measurement technique are discussed.

*Univ. of Illinois

105 *Christophe, Jean; and *Francois, Gilbert: **Thermal Insulation of Pressurized Cryogenic Wind Tunnels.** Paper no. 25, 1st Int. Symp. on Cryogenic Wind Tunnels, Southampton, U.K., Apr. 3–5, 1979.

The transformation of existing wind tunnels for cryogenic operation requires an internal insulation to protect the walls, which usually are made of carbon steel, and are brittle at low temperatures. In order not to alter the shape of the aerodynamic circuit, a thin insulation is used that is efficient for a limited time only. A comparison of solutions with thick internal or external insulators allowed the study of the wall temperature evolution and of the energies implied during transient or permanent operations for long duration runs of several minutes to several tens of minutes. This paper presents a few remarks on the insulation of a wind tunnel with a view to its use down to 120 K. This fan driven wind tunnel, still under construction, will have a test section area of 0.15 x 0.35 m, a maximum stagnation pressure of 5 bars and a maximum velocity of Mach 1.0. Initially designed for operation at room temperature, it is now being modified for operation at cryogenic conditions. To this end, the main circuit is being built in stainless steel Z2CN 18-10 (the American 304 L). Provisions are planned for injection and evacuation of nitrogen and for thermal insulation.

*ONERA, 92320 Châtillon, France

106 *Green, J. E.; *Weeks, D. J.; and *Pugh, P. G. **Heat Transfer to Model or Test Section as a Source of Spurious Aerodynamic Effects in Transonic Wind Tunnels.** Paper no. 26, 1st Int. Symp. on Cryogenic Wind Tunnels, Southampton, U.K., Apr. 3–5, 1979.

For predictions of aerodynamic characteristics to be reliable, correct simulation of the thermal behaviour at full scale is essential. That is to say, the ratio of surface temperature to free-stream temperature may be expected to be just as important a parameter as Reynolds number in any flow in which boundary layer behaviour has a significant effect on the overall aerodynamics. The relative importance of Reynolds number and of heat transfer to the model is assessed in this paper on the basis of calculations of the flow over an aerofoil at subsonic and transonic speeds. The significance of heat transfer to the test-section walls is also assessed. Hence allowable temperature limits are suggested for both the model and the tunnel walls. The source of the results quoted here is a paper which was written in 1973 at the behest of the AGARD LaWs Group but given only limited circulation at that time. Whilst the theoretical methods used, particularly for the inviscid parts of the aerofoil calculations, have now been superseded by appreciably improved methods, there is no reason to suppose that the use of these later methods would significantly alter our main conclusions.

*Royal Aircraft Establishment (R.A.E.), England

107 *Mignosi, A.; and *Archambaud, J. P. **Prediction of Thermal Losses and Transient Flows in a Cryogenic Wind Tunnel.** Paper no. 27, 1st Int. Symp. on Cryogenic Wind Tunnels, Southampton, U.K., Apr. 3–5, 1979.

In parallel with the experimental studies developed in a cryogenic pilot wind-tunnel called T'2 which is induction driven, theoretical methods have been developed. This wind tunnel is used to give experimental data related with cryogenic problems. Prediction methods have been established to compute thermal losses, wind tunnel performances, and transient flows. These methods have been checked with experimental data and are used to predict and to optimize the wind tunnel flow. The contemplated application of these methods is a cryogenisation of our

induction driven wind tunnel T2 (test section 0.4 x 0.4 m) in which great values of Reynolds number could be obtained.

*ONERA/CERT Aerothermodynamics Department, Toulouse, France

108 *Ray, Edwards J.; *Ladson, Charles L.; *Adcock, Jerry B.; *Lawing, Pierce L.; and *Hall, Robert M.: **Review of Design and Operational Characteristics of the 0.3-Meter Transonic Cryogenic Tunnel.** Paper no. 28, 1st Int. Symp. on Cryogenic Wind Tunnels, Southampton, U.K., Apr. 3–5, 1979.

The past six years of operation with the NASA Langley 0.3-m transonic cryogenic tunnel (TCT) has shown that there are no insurmountable problems associated with cryogenic testing with gaseous nitrogen at transonic Mach numbers. The fundamentals of the concept have been validated both analytically and experimentally and the 0.3-m TCT, with its unique Reynolds number capability, has been used for a wide variety of aerodynamic tests. Techniques regarding real-gas effects have been developed and cryogenic tunnel conditions can be set and maintained accurately. It has been shown that cryogenic cooling by injecting nitrogen directly into the tunnel circuit imposes no problems with temperature distribution or dynamic response characteristics. Experience with the 0.3-m TCT has, however, indicated that there is a significant learning process associated with cryogenic, high Reynolds number testing. Many of the questions have already been answered; however, factors such as tunnel control, run logic, economics, instrumentation, and model technology present many new and challenging problems.

*NASA, Langley

109 *Richards, B. E.; *Wendt, J. F.: **Preliminary Design Study of a Regeneratively-Cooled Transonic Cryogenic Tunnel.** Paper no. 29, 1st Int. Symp. on Cryogenic Wind Tunnels, Southampton, U.K., Apr. 3–5, 1979.

The cost of liquid nitrogen dominates the operating expenses of a cryogenic tunnel, particularly in the high speed range. To reduce this cost, a number of short-duration designs have been studied; many of them will be discussed at this symposium. One idea which does not seem to have received serious attention is the regeneratively-cooled concept. The purpose of this short paper is to present the concept for constructive criticism.

*von Karman Inst. for Fluid Dynamics B-1640 Rhode Saint Genese, Belgium

110 *Lambourne, N. C.: **Synopsis of Similarity Requirements for Aeroelastic Models in Cryogenic Wind Tunnels.** Paper no. 30, 1st Int. Symp. on Cryogenic Wind Tunnels, Southampton, U.K., Apr. 3–5, 1979.

A consideration of the requirements for aeroelastic similarity shows the low working temperature of a cryogenic tunnel and an ability to vary temperature both have advantages in regard to the choice of suitable stiffness and density scales for an aeroelastic model. The advantages are incidental to the main purpose of a cryogenic tunnel, which is to achieve high Reynolds numbers.

*Dynamics Lab., RAE, Bedford

111 *Gravelle, Alain: **Aeroelastic Models for Cryogenic Wind Tunnels.** Paper no. 31, 1st Int. Symp. on Cryogenic Wind Tunnels, Southampton, U.K., Apr. 3–5, 1979. ONERA TP 1979-39, 1979. (A79-39088#).

The application of Mach and Froude similarity rules to cryogenic wind tunnel testing of aeroelastic models is examined. It is shown that when stagnation temperatures are low and can be varied over a wide range, it is possible to obtain reasonable values for static loads and Reynolds numbers with flutter models. The scaling of models of the Airbus A300B and the F1 fighter for testing in a S2-MA wind tunnel is discussed and compared with possible scalings of similar models for testing in a cryogenic facility.

*ONERA, 92320 Chatillon, France

112 *Ferris, Alice T. (Judy): **Cryogenic Wind Tunnel Force Instrumentation.** Paper no. 32, 1st Int. Symp. on Cryogenic Wind Tunnels, Southampton, U.K., Apr. 3–5, 1979.

A cryogenic wind tunnel imposes rather severe requirements on the measurement of aerodynamic forces and moments. Not only does the cryogenic environment present an unusual surrounding for the force balance, but also, because of the tunnel's high density capability, the magnitude of the load to be measured can be much greater than that of a conventional tunnel of the same size. Although pushing the state-of-the-art, initial studies indicate that one-piece, high-capacity strain-gage balances can be built to satisfy cryogenic requirements. This paper will outline the work that has been accomplished at Langley Research Center while investigating the effects of the cryogenic environment on one-piece multicomponent strain-gage balances, with particular emphasis on cryogenic balances for use in the National Transonic Facility (NTF), a 2.5-meter cryogenic facility that is being constructed at the National Aeronautics and Space Administration (NASA), Langley Research Center (LaRC), Hampton, VA. The NTF is scheduled to begin operation in mid-1982. One-piece multicomponent strain-gage balances have been designed to meet the requirements imposed by the cryogenic environment. These balances are a result of extensive studies in the areas of design, balance materials, strain gages (including application techniques), and cryogenic calibration. The laboratory results indicate that these balances will yield reliable, repeatable, and predictable data from 340 K to 77 K under steady-state conditions. Work is continuing in a number of areas to reduce the effect of the cryogenic environment even further where possible and to study the problems associated with thermal control that may be needed to eliminate thermal gradients.

*NASA, Langley

113 *Hill, Eugene G.: **The Proposed Boeing Supersonic Wind Tunnel High Reynolds Number Insert.** Paper no. 33, 1st Int. Symp. on Cryogenic Wind Tunnels, Southampton, U.K., Apr. 3–5, 1979.

Modification of the infrequently used Boeing Supersonic Wind Tunnel (BSWT) to provide high Reynolds number testing capabilities has been under study since 1974. Operating the modified four foot tunnel at cryogenic temperatures produces full scale Reynolds number with approximately 0.02 scale models. Current plans are to

continue a low budget circuit development effort and to monitor progress in cryogenic wind tunnel testing technology. Non-cryogenic circuit development studies are scheduled for completion by the end of 1979. Subsequently, cryogenic circuit development studies in the 0.10 scale BSWT/BHRT pilot facility will continue during 1980. Limited studies are continuing to define the modifications required to convert the Boeing Supersonic Wind Tunnel into a high Reynolds number tunnel, BHRT. Many of the non-cryogenic modification have been defined. Studies concerning cryogenic operations will begin late in 1979.

*Senior Engineer, Boeing Company

114 *Cadwell, J. D.: **Design, Fabrication, and Instrumentation Preparation of a Verification Model for the Douglas Aircraft Four Foot Cryogenic Wind Tunnel (4-CWT).** Paper no. 34, 1st Int. Symp. on Cryogenic Wind Tunnels, Southampton, U.K., Apr. 3–5, 1979.

The advent of the cryogenic work at the NASA Langley Research Center presented the technique that would allow the McDonnell Douglas Corporation to obtain a high Reynolds number transonic facility with reasonable dynamic pressures for a moderate capital expenditure. Although NASA had a continuous flow cryogenic pilot tunnel in operation, the blowdown concept had not been checked experimentally. Prior to approval of the capital expenditure an inhouse study was accomplished and verified in an independent feasibility study accomplished by the Fluidyne Corporation. Management approval to proceed with the modification of the existing four foot transonic tunnel to a four foot cryogenic tunnel (4-CWT) was given in mid 1976. The purpose of this report is to review the work accomplished to date on the design, fabrication, and instrumentation of the DC-10 model to be used in the verification test of the McDonnell Douglas four foot Cryogenic Transonic Wind Tunnel.

*Douglas Aircraft Co., McDonnell Douglas Corp.

115 *Aldrich, J. F. L.: **Progress Report on the Douglas Four-Foot Cryogenic Wind Tunnel.** Paper no. 35, 1st Int. Symp. on Cryogenic Wind Tunnels, Southampton, U.K., Apr. 3–5, 1979.

The Douglas design effort toward a cryogenic operating mode of their intermittent 4-foot wind tunnel began in August 1976 under the leadership of NASA Langley. The preliminary study had concluded that it was feasible, that the cost was reasonable for the Reynolds number gain, but that certain scaled tests should be conducted to minimize risks. The experimental program conducted is summarized. The design of the modifications on the 4-Foot Cryogenic Wind Tunnel (4CWT) began with the completion of the 1-Foot Cryogenic Wind Tunnel (1CWT) design and continued in parallel with the experimental program. About 85 percent of the design has been completed. Approximately 165 drawings have been released. The remaining design work includes stings, calibration equipment, control sensor installation and interconnections to operating console and computer. The majority of the supplier-fabricated items have been delivered. Modifications and installation work by the contractors is expected to be completed in August, at which time prerun checkout of the tunnel subsystems will begin and build up to check runs of the total system at ambient and cryogenic temperatures about October.

*Douglas Aircraft Co.; McDonnell Douglas Corp., Long Beach, CA

116 *Clark, P. J. F.; and **Morel, J. P.: **Circuit Optimization Study for the European Transonic Wind Tunnel.** Paper no. 36, 1st Int. Symp. on Cryogenic Wind Tunnels, Southampton, U.K., Apr. 3–5, 1979.

An Airline Optimization Study defines the most economical circuit configuration for the European Transonic Wind Tunnel (ETW) based on the combination of capital and operating costs consistent with flow quality, test spectrum and operational flexibility requirements. This study included investigations of the sensitivity of the optimum configuration to variations in the factors which affect the cost of the various components or cost elements over a reasonable range.

*DSMA International Inc., Toronto, Canada
**(Technical Group, ETW)

117 *Hall, Robert M.: **Onset of Condensation Effects as Detected by Total Pressure Probes in the Langley 0.3-Meter Transonic Cryogenic Tunnel.** 51 pp. NASA-TN-80072, May 1979. (N79-27094#).

Total pressure probes mounted in the test section of the Langley 0.3-meter transonic cryogenic tunnel are used to detect the onset of condensation effects for free-stream Mach numbers of 0.50, 0.75, 0.85, and 0.95 and for total pressures between one and five atmospheres. The amount of supercooling is found to be about 3 K and suggests that condensation is occurring on pre-existing liquid nitrogen droplets resulting from incomplete evaporation of the liquid nitrogen injected to cool the tunnel. The liquid nitrogen injection process presently being used for the 0.3-m tunnel results in a wide spectrum of droplet sizes being injected into the flow. Since the relatively larger droplets take much more time to evaporate than the more numerous smaller droplets, the larger ones reach the test section first as the tunnel operating temperature is reduced. However, condensation effects in the test section are not immediately measurable because there is not a sufficient number of the larger droplets to have an influence on the thermodynamics of the flow.

*NASA, Langley

★ ★ ★ ★ ★

The following citations, while not dealing directly with cryogenic wind tunnels, have been found to be useful sources of information.

★ ★ ★ ★ ★

118 Pankhurst, R. C.; and Holder, D. W.: **Wind Tunnel Technique.** Sir Isaac Pitman and Sons, Ltd. London, 1965.

This book is an attempt to satisfy the need which the authors felt to exist for a coherent account of modern wind-tunnel practice written in the form of a critical resume rather than as a textbook which starts from first principles. It

is intended primarily for graduates entering the field of experimental aerodynamics since it is felt that, although having a good knowledge of the theory, they may in many cases have had little opportunity of becoming familiar with experimental practice. It is hoped that the work may also be of value as a reference book for the research worker and for the model-testing personnel of aircraft firms. The scope of the book is best judged from the Contents and from the forward references to the remainder of the text given in Chapter 1. For this reprint (1965) we have been able to correct known misprints and other errors (particularly the omission of the chord/span ratio from equations (3)–(5) on p. 238) but have not introduced fresh material. The only substantial alteration occurs in Chapter VIII, where the drag correction ascribed to wall-induced inclination of the lift vector has been deleted in cases of two-dimensional flow.

119 Barron, Randall F.: **Cryogenic Systems.** McGraw-Hill, New York, 1966. (McGraw-Hill series in mechanical engineering).

The objective of this book is to present an introduction to the engineering aspects and challenges of cryogenics. Emphasis is placed on the design and analysis of systems used to produce, maintain, and utilize low temperatures. The text is an outgrowth of class notes and lecture material associated with a course in cryogenic systems taught at Ohio State University and is slanted primarily toward senior mechanical engineering students, although the text is arranged so that it may be used by an engineer unfamiliar with cryogenic techniques when he is called upon to assist in the design of a system for low temperatures. The required background for the student includes a knowledge of the basic engineering sciences—thermodynamics, heat transfer, fluid flow, and mechanics of solids. Because a book must always have a finite number of pages, not all topics in cryogenics are covered, but it is hoped that a student will have a firm foundation in cryogenics after studying this text. The text is intended for a one-semester undergraduate course in cryogenic systems. Books for additional reading are suggested at the end of each chapter.

120 *Scurlock, R. G.: **Low Temperature Behaviour of Solids: An Introduction.** 1966. Routledge and Kegan Paul, Ltd, London. Dover Publications, Inc., New York.

This book provides an elementary introduction to the behaviour of solids, at temperatures ranging down from room temperature. It is directed at the level of the second or third year undergraduate student in science and engineering, and provides a concise account of some of the more important properties of the solid state. A strict mathematical approach is avoided, and discussion is limited to qualitative, order of magnitude, explanations of low temperature behaviour.

*University of Southampton

121 *Reed, William E.: **Cryogenic Refrigeration, Vol. 2. A Bibliography With Abstracts.** Progress Rep. 1973–Oct. 1977, NTIS/PS-78/1261/3, Dec. 1978. 236 pp. (N79-16144#, Available NTIS).

Cryogenic cooling of electronic equipment, infrared equipment, cryogenic storage vessels, magnetohydrodynamic generators, and superconducting magnets, coils, rotating machinery, and transmission lines is reported. Marine refrigeration of liquefied natural gas, cryogenic heat pipes, cryogenic heat transfer, and space applications are studied. Methods investigated include adiabatic demagnetization, electrocaloric effect, Joule-Thompson effect, thermoelectric cooling, and Crayton, Claude, Gifford-McMahon, Sterling, and Vuilleumier cycles. This updated bibliography contains 229 abstracts, none of which are new entries to the previous edition.

*NTIS

122 *Reed, William E.: **Cryogenic Refrigeration, Vol. 3. A Bibliography With Abstracts.** Progress Rep., Nov. 1977–Nov. 1978. 84 p. (N79-16145#, Available NTIS).

Cryogenic cooling of electronic equipment, infrared equipment, cryogenic storage vessels, magnetohydrodynamic generators, and superconducting magnets, coils, rotating machinery, and transmission lines is reported. Marine refrigeration of liquefied natural gas, cryogenic heat pipes, cryogenic heat transfer, and space applications are studied. Methods investigated include adiabatic demagnetization, electrocaloric effect, Joule-Thomson effect, thermoelectric cooling, and Crayton, Claude, Gifford-McMahon, Sterling, and Vuilleumier cycles. This updated bibliography contains 77 abstracts, all of which are new entries to the previous edition.

*NTIS

123 *Corruccini, Robert J., and *Gniewek, John J.: **Specific Heats and Enthalpies of Technical Solids at Low Temperatures – A Compilation From the Literature.** (311 refs.) NBS Monograph 21, Oct. 1960. (N63-81125, Available from STIF).

Tables are given of the specific heat, c_p, and the enthalpy of 28 metals, 3 alloys, 8 other inorganic substances, and 8 organic substances in the temperature range, 1 to 300 K.

*Nat. Bur. Stds.

124 *Jacobs, R. B.: **Liquid Requirements for the Cool-Down of Cryogenic Equipment.** Advances in Cryogenic Engineering, Vol. 8, 1963, pp. 529–535. Presented at the Cryogenic Engineering Conference, Los Angeles, Calif., Aug. 1962.

It is frequently necessary to estimate the amounts of cryogenic liquid required to cool cryogenic equipment to its operating condition. The purpose of this paper is three-fold (1) to derive relations for making these estimates, (2) to compute the cool-down requirements for the commonly used liquids (helium, hydrogen, nitrogen, and oxygen) with some commonly used materials (stainless steel, copper, and aluminum), and (3) to present the results of the computations in a readily usable graphical form.

*CEL National Bureau of Standards, Boulder, Colorado

125 *Lin, Shih-Chun: **An Experimental Study of Gasdynamical Turbulence.** California Univ., San Diego. Ph.D. Thesis, 1972, 230 pp. (N73-19280, Available Univ. Microfilms, Order No. 72-24634).

A nearly homogeneous grid turbulence field with large-amplitude temperature fluctuations is investigated experimentally. In order to generate a nearly homogeneous flow field with large temperature fluctuations in the laboratory, a 21' x 21' variable density, subsonic wind tunnel with the capability of generating Reynolds number per inch up to 3.5 x 10,000 when operated at ambient temperatures and up to 3.0 x 10^5 when operated at 100 K by the direct injection of liquid nitrogen has been designed and developed. The details of the design and the discussion of the tunnel performance are presented. A nearly homogeneous turbulence field with large amplitude temperature fluctuations is generated in the 21' x 21' test section by rapid mixing of 64 hot and cold air streams behind a specially constructed grid. Electrical heating power up to 300 kW is applied to generate initial hot and cold stream temperature ratios up to 1.6 at a mean velocity of about 11 m/sec. Due to icing problems, the liquid nitrogen mode of operation has been postponed.

*Univ. of California, San Diego, CA, U.S.A.

126 *Adcock, J. B.: **The Cryogenic Wind Tunnel Concept.** (Presented during The House Authorization Subcommittee Hearings on the OAST FY '75 Budget). NASA-TM-80504, Mar. 1974, 13 pp. (X80-70012#, Available from STIF to NASA only).

*NASA, Langley Research Center, Hampton, Va. 23665, U.S.A.

127 *Zapata, Ricardo N.; *Humphris, Robert R.; and *Henderson, Karl C.: **Experimental Feasibility Study of the Application of Magnetic Suspension Techniques to Large-Scale Aerodynamic Test Facilities.** 8th AIAA Aerodynamic Testing Conference, Bethesda, Md., July 8–10, 1974, AIAA Paper 74-615, 11 pp. (A74-35383#). This was also published as NASA-CR-146,761, 1975, 10 pp. (N80-11102#), Available NTIS).

Based on the premises that magnetic suspension techniques can play a useful role in large-scale aerodynamic testing and that superconductor technology offers the only practical hope for building large-scale magnetic suspensions, an all-superconductor three-component magnetic suspension and balance facility was built as a prototype and was tested successfully. Quantitative extrapolations of design and performance characteristics of this prototype system to larger systems compatible with existing and planned high Reynolds number facilities have been made and show that this experimental technique should be particularly attractive when used in conjunction with large cryogenic wind tunnels.

Note: Similar information is contained in AGARD-CP-174 (N76-25213#), and in NASA-CR-2565 (N75-28025).

*Univ. of Virginia, Charlottesville, Va., U.S.A.

Grants NGR-47-005-029, NGR-47-005-110, NGR-47-005-112, and NSG-1010.

128 *Osborne, B. P., Jr.; and **Nicks, O. W. (Co-chairmen): **National Transonic Facility: Report of the 1974 National Aeronautical Facilities Subpanel to the Aeronautics Panel, AACB.** Aeronautics and Astronautics Coordinating Board, Washington D.C., U.S.A. Report. May 1975, 63 pp. (N79-79161#, Available NTIS).

At its 69th meeting, the Aeronautics and Astronautics Coordinating Board (AACB) authorized the Aeronautics Panel to proceed with a review of national aeronautics facilities. The specific Terms of Reference are set forth in Attachment A. The members of the 1974 National Aeronautics Facilities Subpanel constituted by the Aeronautics Panel are identified in Attachment B. Prior to the first meeting of the subpanel, the Cochairmen of the AACB Aeronautics Panel agreed to modify the Terms of Reference to eliminate consideration by this subpanel of the USAF Aeropropulsion System Test Facility (ASTF) and the NASA/Ames 40 x 80 foot tunnel modifications. Hence, this report is concerned only with a review of the High Reynolds Number Tunnel (HIRT) and the Transonic Research Tunnel (TRT) and related requirements.

*U.S. Dept. of Defense

**NASA, Langley Research Center, Hampton, Va. 23665, U.S.A.

129 *Rao, D. M.: **Wind Tunnel Design Studies.** Final Report (June '75 through May '76). Old Dominion Univ., TR-76-T11; NASA CR-148,149, May 1976, 31 pp. (N76-25156#, Available NTIS).

This report describes work performed at Langley Research Center in support of the National Transonic Facility Project Office. The report is in three parts: estimation of aerodynamic losses in the tunnel circuit, 2nd-turn model studies, and proposed circuit modification for LN_2 economy and shell cost savings. The report emphasizes the basic motivation behind the problems studied, and gives the main results and conclusions obtained. A more detailed presentation of the experimental data and analysis is deferred to a subsequent document.

*Old Dominion University, Norfolk, Va. 23508, U.S.A.

NASA Grant No. NSG 1135

130 *Wagner, B., and *Schmidt, W.: **Theoretical Studies on the Shock Wave-Boundary Layer Interaction in Cryogenic Nitrogen.** Rept. No. ESA-TT-498, pp. 419-436, March 1979. This is an English translation of the 1977 German report previously announced as N79-12402. (N79-31569#, Available NTIS).

The basic effects of low temperatures close to liquefaction in cryogenic wind tunnels were studied theoretically for viscous compressible flow on the basis of shock wave-laminar boundary layer interaction. The full Navier-Stokes equations in combination with the equations of state for a real gas and the material properties for low temperatures were solved by means of a finite volume method and MacCormack's time splitting technique. Results show relatively small deviations compared with the ideal gas case. The differences in the pressure distribution are caused

mainly by real gas effects in the inviscid external flow field while the changes in the skin friction coefficients depend mainly on the different viscosity characteristics and on the real gas effects in the temperature distribution.

*Dornier GmbH, Theoretical Aerodynamics Dept., Postfach 1420, 7990 Friedrichshafen, West Germany

Note: The original German report is no. 56 in the main part of this bibliography.

131 *Bazin, Maurice: **Construction Problems for High Reynolds Number Wind Tunnel Models.** Presented at the 14th Colloq d'Aerodyn. Appl. de l'Assoc. Aeron. et Astron. de France, Toulouse 7–9 Nov. 1977. European Space Agency, Paris, France Rep. No. ESA-TT-564, June 1979. 50 pp. This is the English translation of ONERA-NT-1978-6. (N80-12101#, Available NTIS).

Design structures, problems of definition, and materials for high Reynolds number wind tunnel models are discussed. Models for force and pressure distributions, air intakes, jet simulation, and dynamic flutter are considered. It is shown that deformations in operation under the effect of aerodynamic and thermal loads require new measuring techniques and the adaptation of the capacity, thermal protection, and calibration methods of the balance. The mechanical strength of the supports, in particular the risk of divergence, and the dynamic behavior of the mountings are the most severe limitations in the use of pressurized wind tunnels. Thermal problems are added in a cryogenic environment. The development of pressure measurement methods and instruments is considered.

*O.N.E.R.A., 92320 Châtillon, France

Note: The original French report is no. 66 in the main part of this bibliography.

132 *Michel, R.; and *Fauldmann, D.: **Preliminary Tests in a Cryogenic Wind Tunnel Driven by Induction.** ONERA-TP-1978-48E, July 1978, 9 pp. Translated into English from La Recherche Aerospatiale, Bulletin Bimestriel (Paris) No. 1978–4, July–Aug. 1978, pp. 205–207. A79-15300#. (N80-12019#, Available NTIS).

A 1/4 scale cryogenic operation pilot wind tunnel test for higher Reynolds number was performed to verify a liquid nitrogen injection fast cooling process. The cryogenic operation was combined with an induction driven operation in the hope that the short flow duration will give rise to a decrease in the wall and model surface temperature only, avoiding some technological problems. Operation temperatures down to 100 K were obtained. Thin layers of wall insulation are shown to be efficient in containing nitrogen consumption. It is concluded that the simplicity of implementation makes the process promising for adapting existing wind tunnels to cryogenic operation.

*O.N.E.R.A.–CERT, Toulouse, France

Note: The original French report is no. 74 in the main part of this bibliography.

133 *Hartzuiker, J. P.; and *North, R. J.: **The European Transonic Windtunnel (ETW) for High Reynolds-Number Testing.** Presented at the 11th Congress of ICAS, Lisbon, 11–16 Sept., 1978. Rep. No. TG-ETW/D2, Sept. 1978, 9 pp. (To be published and will be announced in "International Aerospace Abstracts.")

A joint project of four nations (France, Germany, The Netherlands, and U.K.) to define, and later to construct, a new European high-Reynolds-number transonic windtunnel using cold nitrogen gas as the test medium is described. The concept of windtunnel testing at cryogenic temperatures is discussed and a brief description of the proposed tunnel, as it is envisaged at present, is given.

*J. P. Hartzuiker and R. J. North, Technical Group ETW, c/o National Aerospace Laboratory NLR, Anthony Fokkerweg 2, 1059 CM Amsterdam, The Netherlands

134 *Ray, Edward J.; *Ladson, Charles L.; *Adcock, Jerry B.; *Lawing, Pierce L.; and *Hall, Robert M.: **Review of Design and Operational Characteristics of the 0.3-Meter Transonic Cryogenic Tunnel.** NASA TM-80123, Sept. 1979, 56 pp. Also presented at the 1st Int. Symp. on Cryogenic Wind Tunnels, Southampton, England, Apr. 3–5, 1979. (No. 108 in the main part of this bibliography.) (N79-32159#, Available NTIS).

The past 6 years of operation with the NASA Langley 0.3-m transonic cryogenic tunnel (TCT) show that there are no insurmountable problems associated with cryogenic testing with gaseous nitrogen at transonic Mach numbers. The fundamentals of the concept were validated both analytically and experimentally and the 0.3-m TCT, with its unique Reynolds number capability, was used for a wide variety of aerodynamic tests. Techniques regarding real-gas effects were developed and cryogenic tunnel conditions can be set and maintained accurately. Cryogenic cooling by injecting liquid nitrogen directly into the tunnel circuit imposes no problems with temperature distribution or dynamic response characteristics. Experience with the 0.3-m TCT, indicates that there is a significant learning process associated with cryogenic, high Reynolds number testing. Many of the questions have already been answered, however, factors such as tunnel control, run logic, economics, instrumentation, and model technology present many new and challenging problems.

*NASA, Langley Research Center, Hampton, Va. 23665, U.S.A.

135 *Albone, C. M.: **An Investigation into the Real Gas Effects of Cryogenic Nitrogen in Inviscid Homentropic Flow.** R.A.E.TM Aero 1805, May 1979, 17 pp.

As a contribution to the investigation of the suitability of using cryogenic nitrogen as the test gas in a high Reynolds number transonic wind-tunnel, a study is made here of the real gas effects of nitrogen at low temperatures. The study, which is limited to inviscid, homentropic flow of a non-conducting gas, takes the form of an independent confirmation of results by Kilgore, et al. A recent paper by Wagner and Schmidt on this subject employs a different equation of state from that used here and their investigations cover more than just homentropic flow. The new contribution in this Memorandum is that the use of a simplified equation of state enables an expression for enthalpy (and, hence, the terms in Bernoulli's equation) to be derived by analytic integration.

*Royal Aircraft Establishment, Farnborough, Hants, UK.

Note: A shortened varsion of this Memorandum (no. 97 in the main part of this bibliography) was presented at the First International Symposium on Cryogenic Wind-Tunnels at Southampton University 3–5 April 1979.

136 *Goodyer, M. J.: **Cryogenic Wind Tunnel Activities at the University of Southampton.** NASA-CR-159144, Sept. 1979, 10 pp. (N80-10231#, Available NTIS).

The characteristics and behavior of a 0.3-m transonic cryogenic wind tunnel are discussed. The wide band of usable Reynolds numbers is analyzed along with a flow visualization technique using propane. The combination of magnetic suspension with the cryogenic wind tunnel is described. An outline of the circuit showing the locations of the magnet system and the features of the tunnel are presented.

*Southampton Univ., Southampton SO9 5NH, UK

NASA Grant No. NSG-7523

137 *Tuttle, Marie H.; and *Kilgore, Robert A.: **Cryogenic Wind Tunnels—A Selected, Annotated Bibliography.** NASA TM-80168, October 1979, 30 pp. (N79-33221#, Available NTIS).

The design and characteristics of cryogenic wind tunnels are discussed in the 124 publications included in this bibliography. Evaluations of cryogenic fluids used as wind tunnel test gases and tests performed in the cryogenic wind tunnels are reported.

*NASA, Langley Research Center, Hampton, Va. 23665, U.S.A.

Note: This is the main bibliography of which the present collection is a supplement.

138 *Kilgore, Robert A.: **Development of the Cryogenic Tunnel Concept and Application to the U.S. National Transonic Facility.** Paper No. 2 in AGARDograph No. 240, "Towards New Transonic Windtunnels," Nov. 1979, 27 pp.

N80-19139#

Based on theoretical studies and experience with a low-speed fan-driven tunnel and with a pressurized transonic tunnel, the cryogenic wind-tunnel concept has been shown to offer many advantages with respect to the attainment of full-scale Reynolds number at reasonable levels of dynamic pressure in a ground-based facility. The unique modes of operation available in a pressurized cryogenic tunnel make possible for the first time the separation of Mach number, Reynolds number, and aeroelastic effects. By reducing the drive-power requirements to a level where a conventional fan-drive system may be used, the cryogenic concept makes possible a tunnel with high productivity and run times sufficiently long to allow for all types of tests at reduced capital costs and, for equal amounts of testing, reduced total energy consumption in comparison with other tunnel concepts. A new fan-driven high Reynolds number transonic cryogenic tunnel is now under construction in the United States at the NASA Langley Research Center. The tunnel, to be known as the National Transonic Facility (NTF), will have a 2.5 by 2.5-m test section and will be capable to operating from ambient to cryogenic temperatures at stagnation pressures up to 8.8 atm. By taking full advantage of the cryogenic concept, the NTF will provide an order of magnitude increase in Reynolds number capability over existing tunnels in the United States.

*NASA, Langley Research Center, Hampton, Va. 23665, U.S.A.

139 *Hartzuiker, J. P., **Christophe, Jr., ***Lorenz-Meyer, W., and ****Pugh, P. G. **The Cryogenic Windtunnel; Another Option for the European Transonic Facility.** Paper No. 3 in AGARDograph No. 240, "Toward New Transonic Windtunnels," Nov. 1979, 15 pp.

N80-19140#

A new option for the proposed European transonic windtunnel is described: a cryogenic facility with test section dimensions compatible with existing major European transonic facilities. The tunnel performance is to the functional specification of the LaWs Group (Reynolds number based on mean aerodynamic chord variable between 25×10^6 and 40×10^6). The advantages and drawbacks of cryogenic testing as well as fundamental aspects of cryogenic aerodynamics are discussed. Comparative estimates for capital and operating costs are presented.

*National Aerospace Laboratory (NLR) Amsterdam, The Netherlands

**O.N.E.R.A., 92320 Châtillon, France

***DFVLR, Institut für Experimentelle Strömungsmechanik Bunsenstrausse 10, 3400 Gottingen, West Germany (FRG)

****Royal Aircraft Establishment, Bedford, UK

140 *Balakrishna, S.: **Synthesis of a Control Model for a Liquid Nitrogen Cooled, Closed Circuit, Cryogenic Nitrogen Wind Tunnel and its Validation.** Progress Rept., period ending Sept. 1979. NASA CR-162, 508, Nov. 1979, 142 pp. (N80-13058#, Available NTIS).

The details of the efforts to synthesize a control-compatible multivariable model of a liquid nitrogen cooled, gaseous nitrogen operated, closed circuit, cryogenic pressure tunnel are presented. The synthesized model was transformed into a real-time cryogenic tunnel simulator, and this model is validated by comparing the model responses to the actual tunnel responses of the 0.3-m transonic cryogenic tunnel using the quasi-steady-state and the transient responses of the model and the tunnel. The global nature of the simple, explicit, lumped multivariable model of a closed circuit cryogenic tunnel is demonstrated.

*Old Dominion University, Norfolk, Va. 23508

NASA Grant No. NSG-1503

141 *Younglove, Ben; and *McCarty, R. D.: **Thermodynamic Properties of Nitrogen Gas Derived from Measurements of Sound Speed.** NASA RP-1051, Dec. 1979, 5 pp., NBSIR-79-1611, (N80-14257#, Available NTIS).

A virial equation of state for nitrogen has been determined by use of newly measured speed-of-sound data and existing pressure-density-temperature data in a multiproperty-fitting technique. The experimental data taken were chosen to optimize the equation of state for a pressure range of 0 to 10 atm and for a temperature range of 60 to 350 K. Comparisons are made for thermodynamic properties calculated both from the new equation and from existing equations of state.

*Thermophysical Properties Division, National Engineering Lab, National Bureau of Standards, Boulder, Co. 80302, U.S.A.

Funded by NASA, Langley Research Center

142 *Johnson, W. G., Jr.; and *Igoe, W. B.: **Aerodynamic Characteristics at Low Reynolds Numbers of Several Heat-Exchanger Configurations for Wind Tunnel Use.** NASA TM-80188, Dec. 1979, 54 pp. (N80-14046#, Available NTIS).

In response to design requirements of the National Transonic Facility, aerodynamic tests were conducted to determine the pressure-drop, flow-uniformity, and turbulence characteristics of various heat-exchanger configurations as a function of Reynolds number. Data were obtained in air with an indraft flow apparatus operated at ambient temperature and pressure. The unit Reynolds number of the tests varied from about 0.06 x 10 to 6th power to about 1.3 x 10 to 6th power per meter. The test models were designed to represent segments of full-scale tube bundles and included bundles of round tubes with plate fins in both staggered and inline tube arrays, round tubes with spiral fins, elliptical tubes with plate fins, and an inline grouping of tubes with segmented fins.

*NASA, Langley Research Center, Hampton, Va. 23665, U.S.A.

143 *Adcock, Jerry B.; and *Johnson, Charles B.: **A Theoretical Analysis of Simulated Transonic Boundary Layers in Cryogenic-Nitrogen Wind Tunnels.** NASA TP-1631, March 1980, 37 pp. (Available NTIS). N80-19131 #

A theoretical analysis has been made to determine the real-gas effects on simulation of transonic boundary layers in wind tunnels with cryogenic nitrogen as the test gas. The analysis included laminar and turbulent flat-plate boundary layers and turbulent boundary layers on a two-dimensional airfoil. The results indicate that boundary layers in such wind tunnels should not be substantially different from ideal-gas boundary layers at standard conditions. At a pressure of 9.0 atm, two separate effects produce deviations of real-gas values from ideal-gas values which are in the opposite direction from deviations at 1.0 atm and are of the same insignificant order of magnitude. Results also show that nonadiabatic boundary layers should be adequately simulated if the enthalpy ratio is the correlating parameter rather than the temperature ratio.

*NASA, Langley Research Center, Hampton, Va. 23665, U.S.A.

144 *Howell, Robert R. **The National Transonic Facility: Status and Operational Planning.** Presented at the AIAA 11th Aerodynamic Testing Conference, Denver, Colorado, March 18–20, 1980. AIAA paper 80-0415, 9 pp.

The construction of the National Transonic Facility is advancing on schedule toward a target completion date in 1982. Several residual concerns remain which may emerge as problems in the operation of the facility. Among these are thermal stress constraints which may limit the rate at which temperatures can be changed, seal performance in a dynamic cryogenic environment which may result in undesirable internal flow leaks, and inadequate understanding of the detailed tunnel flow process which could result in inefficient process controls. The current design affords the capability of dealing with all of these concerns if they become problems. The outstanding instrument need is for a real time model surface deformation measurement system. A program for the development of this instrument system is underway. The user access to the National Transonic Facility has been addressed and a plan developed which will allow any qualified user access to the facility. The use of the NTF by organizations outside of NASA is encouraged. A practical look at the occupancy cost and the cost of liquid nitrogen for high Reynolds number tests indicates that operating costs should not be an inhibiting factor in the use of the NTF.

*NASA, Langley Research Center, Hampton, Va. 23665, U.S.A.

145 *Thibodeaux, Jerry J.; and **Balakrishna, S. **Automatic Control of NASA Langley's 0.3-Meter Cryogenic Test Facility.** Presented at the AIAA 11th Aerodynamic Testing Conference, Denver, Colorado, March 18–20, 1980. AIAA paper 80-0416, 15 pp.

Experience during the past 6 years of operation of the 0.3-meter transonic cryogenic tunnel at the NASA Langley Research Center has shown that there are problems associated with efficient operation and control of cryogenic tunnels using manual control schemes. This is due to the high degree of process crosscoupling between the independent control variables (temperature, pressure, and fan drive speed) and the desired test condition (Mach number and Reynolds number). One problem has been the inability to maintain long term accurate control of the test parameters. Additionally, the time required to change from one test condition to another has proven to be excessively long and much less efficient than desirable in terms of liquid nitrogen and electrical power usage. For these reasons, studies have been undertaken to: (1) develop and validate a mathematical model of the 0.3-meter cryogenic tunnel process, (2) utilize this model in a hybrid computer simulation to design temperature and pressure feedback control laws, and (3) evaluate the adequacy of these control schemes by analysis of closed-loop experimental data. This paper will present the results of these studies.

*NASA, Langley Research Center, Hampton, Va. 23665, U.S.A.
**Old Dominion Univ., Norfolk, Va. 23508, U.S.A.

146 *Johnson, Charles B.: **A Study of Nonadiabatic Boundary-Layer Stabilization Time in a Cryogenic Tunnel for Typical Wing and Fuselage Models.** Presented at the AIAA 11th Aerodynamic Testing Conference, Denver, Colorado, March 18–20, 1980. AIAA paper 80-0417, 9 pp.

A theoretical study has been made of the time varying effect of nonadiabatic wall conditions on boundary layer properties for a two-dimensional wing section and an axisymmetric body of revolution typical of a fuselage. The wing section and body of revolution are representative of the root chord and fuselage of what is considered to be a typical size transport model for the National Transonic Facility. The transient analysis was made at a Mach number of 0.85, for stagnation pressures of 2, 6, and 9 atmospheres at several cryogenic values of total temperature for a solid wing and for

three different fuselage skin thickness configurations. The analysis considered wing and fuselage sections made from stainless steel, beryllium copper, and aluminum. Examples are presented that may be used to determine the time required to reach an adiabatic condition after a change in total temperature.

*NASA, Langley Research Center, Hampton, Va. 23665, U.S.A.

147 *Balakrishna, S.: **Automatic Control of a Liquid Nitrogen Cooled, Closed-Circuit, Cryogenic Pressure Tunnel.** Progress Report for the period Oct. 1979–March 1980. Submitted by the Old Dominion University Research Foundation, Norfolk, Va., March 1980, 97 pp.

This report details the control analysis phase of the project "Modeling and Control of Transonic Cryogenic Wind Tunnels," sponsored by NASA/Langley Research Center (LaRC). The contents of this document complement the modeling phase activity which has been reported as "Synthesis of a Control Model for a Liquid Nitrogen Cooled Closed Circuit Cryogenic Nitrogen Wind Tunnel and its Validation" (no. 140 in this compilation). This document reports the details of control law design, proof of its adequacy, microprocessor compatible software design, and electronic hardware realization and its successful performance on the 0.3-m transonic cryogenic tunnel at NASA/LaRC.

*Old Dominion University, Norfolk, Va. 23508, U.S.A.

NASA Grant No. NSG-1503

148 Goodyer, M. J. (Lecture Series Director): **Cryogenic Wind Tunnels; AGARD/VKI Lecture Series 111.** Presented May 19–23, 1980, at Rhode-Saint-Genese, Belgium; and May 27–30, 1980, at NASA, Langley Research Center, Hampton, Va., U.S.A.

This Lecture Series is designed for engineers, including those experienced with conventional wind tunnels, wishing to acquire in a concentrated form the principles and practice of cryogenic wind tunnels. The emphasis is on the unfamiliar facets of technology which must be applied, and on solutions to special problems which arise from the exploitation of a low temperature test gas. Lectures provide up-to-date information on the aerodynamic and mechanical design of continuous and intermittent cryogenic wind tunnels and their models, and on techniques for controlling test parameters. Design information includes properties of materials, the storage and handling of cryogenic liquids, insulation systems for pipelines and tunnel circuits, and safety requirements. Solutions are included for the special requirements of instrumentation systems for plant, tunnel, and model. The physical processes will be described which determine the lower limits of operating temperature. The four major cryogenic wind tunnel projects for aeronautical testing are also described. Two of these being in the U.S.A. and two in Europe.

Note: The Series was sponsored by the Fluid Dynamics Panel of AGARD and implemented by the von Karman Institute. Nineteen papers were presented and are listed immediately following this entry.

149 *Goodyer, M. J.: **Introduction to the Principles of Cryogenic Wind Tunnels with Outlines of Potential Applications.** Presented as Paper No. 1 at the AGARD/VKI Lecture Series 111, May 19-23, 1980–Rhode-Saint-Genese, Belgium, May 27–30, 1980, Hampton Va., U.S.A.

*The University of Southampton, Southampton, SO9 5NH, U.K., Department of Aeronautics & Astronautics

150 *Scurlock, R. G.: **Cryogenic Engineering I.** Presented as Paper No. 2 at the AGARD/VKI Lecture Series III, May 19–23, 1980–Rhode-Saint-Genese, Belgium, May 27–30, 1980, Hampton, Va., U.S.A.

Subjects covered in this lecture include Basic properties of liquid nitrogen, oxygen, and air. Control of heat fluxes, insulation techniques, and low-loss storage.

*Univ. of Southampton, Southampton SO9 5NH, U.K., Department of Physics

151 *Scurlock, R. G.: **Cryogenic Engineering II.** Presented as Paper No. 3 at the AGARD/VKI Lecture Series 111, May 19–23, 1980–Rhode-Saint-Genese, Belgium, May 27–30, 1980, Hampton, Va., U.S.A.

Subjects covered in this lecture include. Thermal properties of commercial materials. Instrumentation including thermometry, flow, and pressure. Avoidance of two-phase flow.

*Univ. of Southampton, Southampton SO9 5NH, U.K., Department of Physics

152 *Wigley, D. A.: **Properties of Materials I.** Presented as Paper No. 4 at the AGARD/VKI Lecture Series No. III, May 19–23, 1980–Rhode-Saint-Genese, Belgium; May 27–30, 1980–Hampton, Va., U.S.A.

Subjects covered in this lecture include: The effect of temperature on the mechanical and physical properties of metals, including strength and toughness. Failure mechanism, influence of cracks and flaws, and fracture toughness.

*Department of Mechanical Engineering, Univ. of Southampton, Southampton SO9 5NH, U.K.

153 *Hall, Robert M.: **Real-Gas Effects I–Simulation of Ideal Gas Flow by Cryogenic Nitrogen and Other Selected Gases.** Presented as Paper No. 5 at the AGARD/VKI Lecture Series III, May 19–23, 1980–Rhode-Saint-Genese, Belgium, May 27–30, 1980, Hampton, Va., U.S.A.

The thermodynamic properties of nitrogen gas do not thermodynamically approximate an ideal, diatomic gas at cryogenic temperatures. Choice of a suitable equation of state to model its behavior is discussed and the equation of Beattie and Bridgeman is selected as best meeting the needs for cryogenic wind tunnel use. The real-gas behavior of nitrogen gas is compared to an ideal, diatomic gas for the following flow processes: isentropic expansions, normal shocks, boundary layers, and shock wave-boundary layer interactions. The only differences in predicted pressure ratio between nitrogen and an ideal gas that may limit the minimum operating temperatures of transonic cryogenic wind tunnels seem to occur at total pressures approaching 9 atmospheres and total temperatures 10 K below the

corresponding saturation temperature, where the differences approach 1 percent for both isentropic expansions and normal shocks. Several alternative cryogenic test gases—air, helium, and hydrogen—are also analyzed. Differences in air from an ideal, diatomic gas are similar in magnitude to those of nitrogen and should present no difficulty. However, differences for helium and hydrogen are over an order of magnitude greater than those for nitrogen or air. It is concluded that helium and hydrogen would not approximate the compressible flow of an ideal, diatomic gas.

*NASA, Langley Research Center, Hampton, Va. 23665, U.S.A.

154 *Wigley, D. A.: **Properties of Materials II.** Presented as Paper No. 6 at the AGARD/VKI Lecture Series III, May 19–23, 1980–Rhode-Saint-Genese, Belgium; May 27–30, Hampton, Va., U.S.A.

Subjects covered in this lecture include: The effect of temperature on the mechanical and physical properties of non-metals, including glasses, polymers, and composites. Sources of information.

*Department of Mechanical Engineering, Univ. of Southampton, Southampton SO9 5NH, U.K.

155 *Hall, Robert M.: **Real-Gas Effects II—Influence of Condensation on Minimum Operating Temperatures of Cryogenic Wind Tunnels.** Presented as Paper No. 7 at the AGARD/VKI Lecture Series III, May 19–23, 1980–Rhode-Saint-Genese, Belgium, May 27–30, 1980–Hampton, Va., U.S.A.

Minimum operating temperatures of cryogenic wind tunnels are limited by real-gas effects. In particular, condensation effects are responsible for the minimum operating temperatures at total pressures up to about 9 atmospheres. The present paper reviews the two primary modes of condensation—homogeneous nucleation and heterogeneous nucleation—and the conditions with which either may limit minimum operating temperatures. Previous hypersonic and supersonic condensation data are reviewed as are data taken in the nitrogen-gas, Langley 0.3-Meter transonic cryogenic tunnel (TCT). Analysis of data in the 0.3-m TCT suggests that the onset of homogeneous nucleation may be approximated by an analysis by Sivier and that the onset of heterogeneous nucleation is only apparent just below free-stream saturation. Extension of the results from the 0.3-m TCT to other nitrogen-gas cryogenic tunnels is discussed and is shown to depend on length scales, purity of the liquid nitrogen injected for cooling, number of particulates in the flow, and the extent to which the injected liquid nitrogen is evaporated. On the basis of previous data, hybrid air-nitrogen tunnels are expected to realize little, if any, supercooling.

*NASA, Langley Research Center, Hampton, Va. 23665, U.S.A.

156 *Scurlock, R. G.: **Cryogenic Engineering III.** Presented as Paper No. 8 at the AGARD/VKI Lecture Series III, May 19–23, 1980–Rhode-Saint-Genese, Belgium; May 27–30, 1980, Hampton, Va., U.S.A.

Subjects covered in this lecture include: Handling and transfer of liquid nitrogen. Cooldown and thermal cycling problems. Safety, including asphyxia, cold burns, explosions, and fire hazards.

*Department of Physics, Univ. of Southampton, Southampton SO9 5NH, U.K.

157 *Kilgore, Robert A.: **Model Design and Instrumentation Experiences With Continuous-Flow Cryogenic Tunnels.** Presented as Paper No. 9 at the AGARD/VKI Lecture Series III, May 19–23, 1980–Rhode-Saint-Genese, Belgium; May 27–30, 1980, Hampton, Va., U.S.A.

The development of wind tunnels that can be operated at cryogenic temperatures has placed several new demands on our ability to build and instrument wind tunnel models. Some of the experiences at the NASA Langley Research Center relative to the design and instrumentation of models for continous-flow cryogenic wind tunnels are reviewed in this lecture.

*NASA, Langley Research Center, Hampton, Va. 23665, U.S.A.

158 *Cadwell, J. D.: **Model Design and Instrumentation for Intermittent Tunnels.** Presented as Paper No. 10 at the AGARD/VKI Lecture Series III, May 19–23, 1980–Rhode-Saint-Genese, Belgium; May 27–30, 1980, Hampton, Va., U.S.A.

The concept of a blowdown-to-atmosphere cryogenic wind tunnel was successfully proven when the Douglas Aircraft Company one-foot tunnel first operated cryogenically on May 20, 1977. Since that time a continuing effort has been underway at Douglas to develop the technology required to design, fabricate, and instrument a model that can withstand the hostile environment of a cryogenic flow without sacrificing the acceptable accuracy that can be obtained at conventional temperatures, i.e., 10° C to 65° C. This report summarizes the current state of this technology with a review of the many aspects of the design and instrumentation of a model for a blowdown-to-atmosphere cryogenic wind tunnel. Also included is a discussion of the model conditioning required before a run in order to minimize the time for the model to stabilize at the adiabatic wall temperature, the model reheat system required after a run when model changes are to be made, and the humidity control of the test section and surrounding area in order to prevent frost from forming on the cold model.

*Wind-Tunnel Test and Development, Aerodynamics Subdivision, Douglas Aircraft Co., 3855 Lakewood Boulevard, Long Beach, Ca. 90846, U.S.A.

159 *Kilgore, Robert A.: **Selection and Application of Instrumentation for Calibration and Control of a Continuous-Flow Cryogenic Tunnel.** Presented as Paper No. 11 at the AGARD/VKI Lecture Series III, May 19–23, 1980–Rhode-Saint-Genese, Belgium, May 27–30, Hampton, Va., U.S.A.

This lecture describes those aspects of selection and application of calibration and control instrumentation that

are influenced by the extremes in the temperature environment to be found in cryogenic tunnels. A description is given of the instrumentation and data acquisition system used in the Langley 0.3-m transonic cryogenic tunnel along with typical calibration data obtained in a 20- by 60-cm two-dimensional test section.

*NASA, Langley Research Center, Hampton, Va. 23665, U.S.A.

160 *Cadwell, J. D.: **Calibration of a Blowdown-to-Atmosphere Cryogenic Wind Tunnel.** Presented as Paper No. 12 at the AGARD/VKI Lecture Series III, May 19–23, 1980–Rhode-Saint-Genese, Belgium; May 27–30, 1980, Hampton, Va., U.S.A.

The modification of the existing four-foot trisonic wind tunnel at the Douglas Aircraft Company to a cryogenic facility required considerable change to the existing tunnel internals. When the tunnel comes back on-line early in 1980 a complete tunnel calibration will be made following a shakedown and checkout of the modified facility. The calibration procedure to determine the quality and characteristics of the tunnel airflow of the modified facility at conventional temperatures and at cryogenic temperatures is described. Instrumentation to measure the axial and lateral pressure and temperature variations as a function of Mach number and Reynolds number are reviewed as in the instrumentation to be used in determining the flow angularity and turbulence levels. The variation in tunnel flow parameters that result from the change in displacement thickness due to heat transfer between the warm wall and the cold airflow is also discussed.

*Wind Tunnel Test and Development, Aerodynamics Subdivision, Douglas Aircraft Co., 3855 Lakewood Boulevard, Long Beach, Ca. 90846, U.S.A.

161 *Michel, R.: **The Development of a Cryogenic Wind-Tunnel Driven by Induction.** Presented as Paper No. 13 at the AGARD/VKI Lecture Series III, May 19–23, 1980 -Rhode-Saint Genese, Belgium; May 27–30, 1980, Hampton, Va., U.S.A.

This lecture describes flow control and instrumentation studies in a pilot facility (T'2) at ONERA/CERT.

*Aerothermodynamics Dept., ONERA-CERT, 2 Avenue Edouard Belin, B.P. No. 4025, 31055 Toulouse Cedex, France

162 *Kilgore, Robert A.: **Experience in the Control of a Continuous Flow Cryogenic Tunnel.** Presented as Paper No. 14 at the AGARD/VKI Lecture Series III, May 19–23, 1980–Rhode-Saint-Genese, Belgium; May 27–30, 1980, Hampton, Va., U.S.A.

The economical operation of liquid nitrogen cooled cryogenic tunnels is critically dependent on fast and accurate control of the tunnel variables. In this lecture, the control problem of a continuous flow fan driven cryogenic tunnel has been addressed, firstly by developing a lumped multivariable mathematical model of a tunnel and validating the model by reconciling the responses of the Langley 0.3-m transonic cryogenic tunnel to the responses of the mathematical model on a simulator. Finally, the development of laws for the closed loop control of the tunnel pressure and temperature and the successful implementation of a control system for the 0.3-m transonic cryogenic tunnel based on these laws are presented. An accuracy of ±0.25 K in temperature and ±0.017 atm in pressure in the tunnel control has been achieved.

*NASA, Langley Research Center, Hampton, Va. 23665, U.S.A.

163 *Cadwell, J. D.: **The Control of Pressure, Temperature and Mach Number in a Blowdown-to-Atmosphere Cryogenic Wind Tunnel.** Presented as Paper No. 15 at the AGARD/VKI Lecture Series III, May 19–23, 1980–Rhode-Saint-Genese, Belgium, May 27–30, 1980, Hampton, Va., U.S.A.

The transonic section of the Douglas Aircraft Company four-foot blowdown-to-atmosphere wind tunnel was placed in operation in March 1962. The tunnel control system that evolved and was in operation prior to the shutdown for modification is discussed as a starting point since one of the modification objectives is to be able to operate the tunnel in a conventional mode as well as at cryogenic temperatures. The modifications to the basic system to include the control of tunnel total temperature down to 100 K is described. The effects that the injection of large quantities of liquid nitrogen on the pressure control system is shown. The critical timing of the tunnel start considers the opening of the pressure control valve and the initiation of the liquid nitrogen into the airstream which can result in either a varying test section temperature distribution during a blow or reheating the precooled model. The evaluation of a shield to protect the precooled model during the tunnel start when the airstream is changing temperature from warm to the planned operating condition is presented.

*Wind Tunnel Test and Development, Aerodynamics Subdivision, Douglas Aircraft Co., 3855 Long Beach, Ca. 90846, U.S.A.

164 *Igoe, William B.: **Characteristics and Status of the U.S. National Transonic Facility.** Presented as Paper No. 16 at the AGARD/VKI Lecture Series III, May 19–23, 1980–Rhode-Saint-Genese, Belgium; May 27–30, 1980, Hampton, Va., U.S.A.

The U.S. National Transonic Facility (NTF), a major application of the cryogenic wind tunnel concept, is under construction at the NASA Langley Research Center and is scheduled to become operational in 1982. It will have a closed return fan-driven circuit with a 2.5-meter square slotted test section, be pressurized up to 8.85 atmospheres, and provide chord Reynolds numbers of 120 million based on a chord of 0.25 meter at transonic speeds using cold nitrogen as the test gas. Many of the design features of the NTF, as well as the status of its construction, are presented in this lecture.

*NASA, Langley Research Center, Hampton, Va. 23665, U.S.A.

165 *Cadwell, J. D.: **Progress Reports on the Douglas Aircraft Company Four-Foot Cryogenic Wind Tunnel.** Presented as Paper No. 17 at the AGARD/VKI Lecture Series

III, May 19–23, 1980–Rhode-Saint-Genese, Belgium; May 27–30, 1980, Hampton, Va., U.S.A.

The McDonnell Douglas Corporation approved the modification of the existing Douglas Aircraft Company four-foot trisonic wind tunnel to a cryogenic facility in mid 1976. The successful operation of the one-foot pilot tunnel in May 1977 gave the final technical approval to proceed with the four-foot tunnel modification program. This lecture gives an update on the progress of the modification. In addition, a review of the test technique development program that will provide the technology necessary to conduct the production type testing required for the design of new or derivative type aircraft programs is presented.

*Wind Tunnel Test and Development, Aerodynamics Subdivision, Douglas Aircraft Company, 3855 Lakewood, Boulevard, Long Beach, Ca. 90846, U.S.A.

166 *Michel, R.: **A Cryogenic Transonic Intermittent Tunnel Project: The Induced-Flow Cryogenic Wind-Tunnel T2 at ONERA/CERT.** Presented as Paper No. 18 at the AGARD/VKI Lecture Series III, May 19–23, 1980–Rhode-Saint-Genese, Belgium; May 27–30, 1980, Hampton, Va., U.S.A.

*Aerothermodynamics Dept., ONERA-CERT, 2, Avenue Edouard Belin, B.P. No. 4025, 31055 Toulouse Cedex, France

167 *Hartzuiker, J. P.: **The European Transonic Wind Tunnel.** Presented as Paper No. 19 at the AGARD/VKI Lecture Series III, May 19–23, 1980–Rhode-Saint-Genese, Belgium; May 27–30, 1980, Hampton, Va., U.S.A.

This lecture summarizes the present situation concerning ETW: Aerodynamics, performance, design, mode handling, nitrogen systems, controls, etc. . . . A short description is presented of the pilot tunnel, PETW, which is now under construction. Finally, the program on model design and instrumentation is described. Attention is paid especially to the cryogenic aspects of ETW.

*Technical Group, European Transonic Wind Tunnel–ETU, c/o National Aerospace Lab.–NLR, Anthony Fokkerweg 2, 1059 CM Amsterdam, The Netherlands

AUTHOR INDEX

Entry

Entry

Entry

REPORT DOCUMENTATION PAGE

1. Recipient's Reference	2. Originator's Reference	3. Further Reference	4. Security Classification of Document
	AGARD-LS-111	ISBN 92-835-1360-6	UNCLASSIFIED

5. Originator Advisory Group for Aerospace Research and Development
North Atlantic Treaty Organization
7 rue Ancelle, 92200 Neuilly sur Seine, France

6. Title CRYOGENIC WIND TUNNELS

7. Presented on 19–23 May 1980 at the von Kármán Institute, Rhode-Saint-Genèse, Belgium and 27–30 May 1980 at NASA Langley Research Center, Virginia, USA.

8. Author(s)/Editor(s)	9. Date
Various	July 1980
10. Author's/Editor's Address	**11. Pages**
Various	280

12. Distribution Statement This document is distributed in accordance with AGARD policies and regulations, which are outlined on the Outside Back Covers of all AGARD publications.

13. Keywords/Descriptors

Wind tunnels	Model tests
Cryogenics	Safety engineering
Design criteria	Fluid dynamics
Low temperature tests	

14. Abstract

For aeronautical research the advantages of the cryogenic wind tunnel lie mainly in the practical attainment of full scale values of Reynolds number, and in the case of pressurised cryogenic tunnels the means to separate Mach and Reynolds number effects from aeroelastic effects.

This Lecture series is designed for engineers, including those experienced with conventional wind tunnels, wishing to acquire in a concentrated form the principles and practices of cryogenic wind tunnels. The emphasis is on the unfamiliar facets of technology which must be applied, and on solutions to special problems which arise from the exploitation of a low temperature test gas. The Lectures provide up-to-date information on the aerodynamic and mechanical design of continuous and intermittent cryogenic wind tunnels and their models, and on techniques for controlling test parameters. Design information includes properties of materials, the storage and handling of cryogenic liquids, insulation systems for pipelines and tunnel circuits, and safety requirements. Solutions are included for the special requirements of instrumentation systems for plant, tunnel and model. The physical processes are described which determine the lower limits of operating temperature.

The material in this publication was assembled to support a Lecture Series under the sponsorship of the Fluid Dynamics Panel, the Consultant and Exchange Programme of AGARD and the von Kármán Institute for Fluid Dynamics.

AGARD Lecture Series No.111
Advisory Group for Aerospace Research and Development, NATO
CRYOGENIC WIND TUNNELS
Published July 1980
280 pages

For aeronautical research the advantages of the cryogenic wind tunnel lie mainly in the practical attainment of full scale values of Reynolds number, and in the case of pressurised cryogenic tunnels the means to separate Mach and Reynolds number effects from aeroelastic effects.

This Lecture Series is designed for engineers, including those experienced with conventional wind tunnels,

P.T.O.

AGARD-LS-111

Wind tunnels
Cryogenics
Design criteria
Low temperature tests
Model tests
Safety engineering
Fluid dynamics

AGARD Lecture Series No.111
Advisory Group for Aerospace Research and Development, NATO
CRYOGENIC WIND TUNNELS
Published July 1980
280 pages

For aeronautical research the advantages of the cryogenic wind tunnel lie mainly in the practical attainment of full scale values of Reynolds number, and in the case of pressurised cryogenic tunnels the means to separate Mach and Reynolds number effects from aeroelastic effects.

This Lecture Series is designed for engineers, including those experienced with conventional wind tunnels,

P.T.O.

AGARD-LS-111

Wind tunnels
Cryogenics
Design criteria
Low temperature tests
Model tests
Safety engineering
Fluid dynamics

AGARD Lecture Series No.111
Advisory Group for Aerospace Research and Development, NATO
CRYOGENIC WIND TUNNELS
Published July 1980
280 pages

For aeronautical research the advantages of the cryogenic wind tunnel lie mainly in the practical attainment of full scale values of Reynolds number, and in the case of pressurised cryogenic tunnels the means to separate Mach and Reynolds number effects from aeroelastic effects.

This Lecture Series is designed for engineers, including those experienced with conventional wind tunnels,

P.T.O.

AGARD-LS-111

Wind tunnels
Cryogenics
Design criteria
Low temperature tests
Model tests
Safety engineering
Fluid dynamics

AGARD Lecture Series No.111
Advisory Group for Aerospace Research and Development, NATO
CRYOGENIC WIND TUNNELS
Published July 1980
280 pages

For aeronautical research the advantages of the cryogenic wind tunnel lie mainly in the practical attainment of full scale values of Reynolds number, and in the case of pressurised cryogenic tunnels the means to separate Mach and Reynolds number effects from aeroelastic effects.

This Lecture Series is designed for engineers, including those experienced with conventional wind tunnels,

P.T.O.

AGARD-LS-111

Wind tunnels
Cryogenics
Design criteria
Low temperature tests
Model tests
Safety engineering
Fluid dynamics

wishing to acquire in a concentrated form the principles and practice of cryogenic wind tunnels. The emphasis is on the unfamiliar facets of technology which must be applied, and on solutions to special problems which arise from the exploitation of a low temperature test gas. The Lectures provide up-to-date information on the aerodynamic and mechanical design of continuous and intermittent cryogenic wind tunnels and their models, and on techniques for controlling test parameters. Design information includes properties of materials, the storage and handling of cryogenic liquids, insulation systems for pipelines and tunnel circuits, and safety requirements. Solutions are included for the special requirements of instrumentation systems for plant, tunnel and model. The physical processes are described which determine the lower limits of operating temperature.

The material in this publication was assembled to support a Lecture Series under the sponsorship of the Fluid Dynamics Panel, the Consultant and Exchange Programme of AGARD and the von Kármán Institute for Fluid Dynamics presented on: 19–23 May 1980 at the von Kármán Institute, Rhode-Saint-Genèse, Belgium and 27–30 May 1980 at NASA Langley Research Center, Virginia, USA.

ISBN 92-835-1360-6

wishing to acquire in a concentrated form the principles and practice of cryogenic wind tunnels. The emphasis is on the unfamiliar facets of technology which must be applied, and on solutions to special problems which arise from the exploitation of a low temperature test gas. The Lectures provide up-to-date information on the aerodynamic and mechanical design of continuous and intermittent cryogenic wind tunnels and their models, and on techniques for controlling test parameters. Design information includes properties of materials, the storage and handling of cryogenic liquids, insulation systems for pipelines and tunnel circuits, and safety requirements. Solutions are included for the special requirements of instrumentation systems for plant, tunnel and model. The physical processes are described which determine the lower limits of operating temperature.

The material in this publication was assembled to support a Lecture Series under the sponsorship of the Fluid Dynamics Panel, the Consultant and Exchange Programme of AGARD and the von Kármán Institute for Fluid Dynamics presented on: 19–23 May 1980 at the von Kármán Institute, Rhode-Saint-Genèse, Belgium and 27–30 May 1980 at NASA Langley Research Center, Virginia, USA.

ISBN 92-835-1360-6

wishing to acquire in a concentrated form the principles and practice of cryogenic wind tunnels. The emphasis is on the unfamiliar facets of technology which must be applied, and on solutions to special problems which arise from the exploitation of a low temperature test gas. The Lectures provide up-to-date information on the aerodynamic and mechanical design of continuous and intermittent cryogenic wind tunnels and their models, and on techniques for controlling test parameters. Design information includes properties of materials, the storage and handling of cryogenic liquids, insulation systems for pipelines and tunnel circuits, and safety requirements. Solutions are included for the special requirements of instrumentation systems for plant, tunnel and model. The physical processes are described which determine the lower limits of operating temperature.

The material in this publication was assembled to support a Lecture Series under the sponsorship of the Fluid Dynamics Panel, the Consultant and Exchange Programme of AGARD and the von Kármán Institute for Fluid Dynamics presented on: 19–23 May 1980 at the von Kármán Institute, Rhode-Saint-Genèse, Belgium and 27–30 May 1980 at NASA Langley Research Center, Virginia, USA.

ISBN 92-835-1360-6

wishing to acquire in a concentrated form the principles and practice of cryogenic wind tunnels. The emphasis is on the unfamiliar facets of technology which must be applied, and on solutions to special problems which arise from the exploitation of a low temperature test gas. The Lectures provide up-to-date information on the aerodynamic and mechanical design of continuous and intermittent cryogenic wind tunnels and their models, and on techniques for controlling test parameters. Design information includes properties of materials, the storage and handling of cryogenic liquids, insulation systems for pipelines and tunnel circuits, and safety requirements. Solutions are included for the special requirements of instrumentation systems for plant, tunnel and model. The physical processes are described which determine the lower limits of operating temperature.

The material in this publication was assembled to support a Lecture Series under the sponsorship of the Fluid Dynamics Panel, the Consultant and Exchange Programme of AGARD and the von Kármán Institute for Fluid Dynamics presented on: 19–23 May 1980 at the von Kármán Institute, Rhode-Saint-Genèse, Belgium and 27–30 May 1980 at NASA Langley Research Center, Virginia, USA.

ISBN 92-835-1360-6

AGARD
NATO OTAN
7 RUE ANCELLE · 92200 NEUILLY-SUR-SEINE
FRANCE
Telephone 745.08.10 · Telex 610176

DISTRIBUTION OF UNCLASSIFIED AGARD PUBLICATIONS

AGARD does NOT hold stocks of AGARD publications at the above address for general distribution. Initial distribution of AGARD publications is made to AGARD Member Nations through the following National Distribution Centres. Further copies are sometimes available from these Centres, but if not may be purchased in Microfiche or Photocopy form from the Purchase Agencies listed below.

NATIONAL DISTRIBUTION CENTRES

BELGIUM
Coordonnateur AGARD – VSL
Etat-Major de la Force Aérienne
Quartier Reine Elisabeth
Rue d'Evere, 1140 Bruxelles

CANADA
Defence Science Information Services
Department of National Defence
Ottawa, Ontario K1A OK2

DENMARK
Danish Defence Research Board
Østerbrogades Kaserne
Copenhagen Ø

FRANCE
O.N.E.R.A. (Direction)
29 Avenue de la Division Leclerc
92320 Châtillon sous Bagneux

GERMANY
Zentralstelle für Luft- und Raumfahrt-
dokumentation und -information
c/o Fachinformationszentrum Energie,
Physik, Mathematik GmbH
Kernforschungszentrum
7514 Eggenstein-Leopoldshafen 2

GREECE
Hellenic Air Force General Staff
Research and Development Directorate
Holargos, Athens

ICELAND
Director of Aviation
c/o Flugrad
Reykjavik

ITALY
Aeronautica Militare
Ufficio del Delegato Nazionale all'AGARD
3, Piazzale Adenauer
Roma/EUR

LUXEMBOURG
See Belgium

NETHERLANDS
Netherlands Delegation to AGARD
National Aerospace Laboratory, NLR
P.O. Box 126
2600 A.C. Delft

NORWAY
Norwegian Defence Research Establishment
Main Library
P.O. Box 25
N-2007 Kjeller

PORTUGAL
Direcção do Serviço de Material
da Forca Aerea
Rua da Escola Politécnica 42
Lisboa
Attn: AGARD National Delegate

TURKEY
Department of Research and Development (ARGE)
Ministry of National Defence, Ankara

UNITED KINGDOM
Defence Research Information Centre
Station Square House
St. Mary Cray
Orpington, Kent BR5 3RE

UNITED STATES
National Aeronautics and Space Administration (NASA)
Langley Field, Virginia 23365
Attn: Report Distribution and Storage Unit

THE UNITED STATES NATIONAL DISTRIBUTION CENTRE (NASA) DOES NOT HOLD STOCKS OF AGARD PUBLICATIONS, AND APPLICATIONS FOR COPIES SHOULD BE MADE DIRECT TO THE NATIONAL TECHNICAL INFORMATION SERVICE (NTIS) AT THE ADDRESS BELOW.

PURCHASE AGENCIES

Microfiche or Photocopy
National Technical
Information Service (NTIS)
5285 Port Royal Road
Springfield
Virginia 22161, USA

Microfiche
Space Documentation Service
European Space Agency
10, rue Mario Nikis
75015 Paris, France

Microfiche
Technology Reports
Centre (DTI)
Station Square House
St. Mary Cray
Orpington, Kent BR5 3RF
England

Requests for microfiche or photocopies of AGARD documents should include the AGARD serial number, title, author or editor, and publication date. Requests to NTIS should include the NASA accession report number. Full bibliographical references and abstracts of AGARD publications are given in the following journals:

Scientific and Technical Aerospace Reports (STAR)
published by NASA Scientific and Technical
Information Facility
Post Office Box 8757
Baltimore/Washington International Airport
Maryland 21240, USA

Government Reports Announcements (GRA)
published by the National Technical
Information Services, Springfield
Virginia 22161, USA

Printed by Technical Editing and Reproduction Ltd
Harford House, 7–9 Charlotte St, London W1P 1HD

ISBN 92-835-1360-6